SOVIET PHYSICS

JETP

A translation of the Journal of Experimental and Theoretical Physics of the USSR.

SOVIET PHYSICS JETP VOL. 35(8) NO. 5, pp. 743-921 MAY, 1959

WORK OF FORMATION OF AN ELASTIC TWIN IN CALCITE

I. V. OBREIMOV and V. I. STARTSEV

Khar' kov Institute for Mechanization of Agriculture; Moscow Engineering-Physical Institute

Submitted to JETP editor June 7, 1958

J. Exptl. Theoret. Phys. (U.S.S.R.) **35**, 1065-1073 (November, 1958)

The linear dimensions and shape of an elastic twin in calcite, produced under the action of a concentrated load, have been measured. The linear dimensions are proportional to the load, and the area of the twin surface is proportional to the work done by the deforming stress.

1. STATEMENT OF THE PROBLEM

CRYSTALS of the mineral calcite belong to the trigonal class. They possess a highly perfected cleavage. A calcite crystal bounded by cleavage planes has the shape of a rhombohedron whose three obtuse angles about the three-fold symmetry axis are equal to 101°52′ (Fig. 1). A calcite crystal is shown in profile in Fig. 2. It has long been known (even in the days of Huygens[1]) that under a tangential stress, as indicated in Figs. 1 and 2, a calcite crystal shifts into a twinned configuration (see Figs. 2 and 3). The plane EGHK is the boundary separating the two crystals, parent and twin. The latter is the mirror image of the parent crystal in the plane EGHK. The angle AEA_1 (Fig. 2) is 38°04′; half of this angle is equal to 19°02′.

Kelvin has suggested that mechanical twinning proceeds as follows (see Fig. 2): The crystal has two states of stable equilibrium. At first, under the action of the tangential stress, the angle A′ approaches a right angle, then attains the value 90°, after which the crystal switches over into the symmetrical twinned configuration.

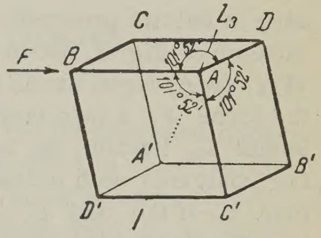

FIG. 1. A rhombohedron of calcite, bounded by cleavage planes.

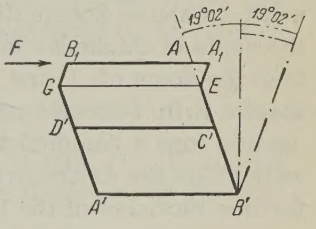

FIG. 2. Calcite rhombohedron, profile view. The upper part of the crystal is brought to the twinned configuration by the load F; GE is the twinning plane, A_1 is the new position of point A after twinning.

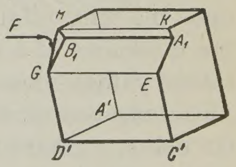

FIG. 3. The twinned calcite crystal. GHKE is the twinning plane, A_1B_1 is the new position of the edge AB of Fig. 1 after twinning.

Voigt[2] measured the tangential stress at which the twinning transformation occurs in a calcite crystal and obtained the figures 3200 and 7500 g/mm^2; these are very low values, which give angle changes of 4.4′ for the first figure and 10.4′ for the second, and for which the deformation is within the limits of Hooke's law. This fact is common to all types of crystal rupture: rupture occurs at stresses that are several orders lower than those which follows from any theory.

As is known, Garber[1,3] found a way out of this contradiction. The point is that mechanical twin-

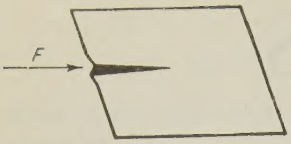

FIG. 4. Elastic twin (according to Garber[1]).

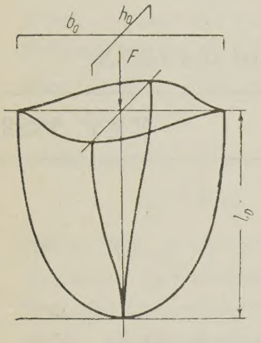

FIG. 5. Diagram of an elastic twin. l – coordinate in the direction of the length, l_0 – total length of the twin, b/2 – coordinate in the direction of the breadth, b_0 – total width of the twin, h/2 – coordinate in the direction of the thickness, h_0 – maximum thickness of the twin.

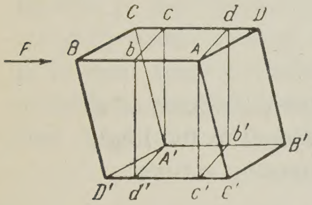

FIG. 6. Preparation of the rhombohedron of calcite, depicted in Fig. 1, for the experiment.

ning in calcite proceeds not according to the scheme of Fig. 2, but in the following manner (Fig. 4): At first, at the point of application of the force F, a twin lamella is formed, whose length l_0, breadth b_0 and thickness h_0 grow (or contract) with increasing (or decreasing) load F. If the load F is removed, then the twin lamella disappears entirely. The shape of an elastic twin, obtained on the basis of the present work, is shown schematically in Fig. 5, in which the scale of thickness is taken three orders larger than the scale of l and b. This formation, called elastic twin, becomes under a sufficiently large applied load a residual twin — a twin lamella, which fills the entire crystal and which, upon further increase of the load F, grows in breadth in an irreversible manner. Upon removal of the load, h and b do not decrease. Garber[4] measured the tangential stress necessary to increase the thickness of a residual twin lamella and obtained values from 50 to 400 g/mm^2 (reference 5). As to any measured values that characterize elastic twins, we have no corresponding figures. The object of the present work is to obtain the values that characterize an elastic twin.

2. ARRANGEMENT AND OBJECT OF THE EXPERIMENT

We prepared a calcite crystal for experiment in the following manner:

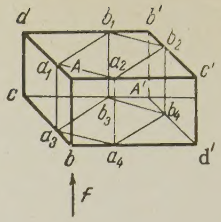

FIG. 7. Further preparation of the calcite prism bcA'd' – Adb'c', depicted in Fig. 6, for the experiment.

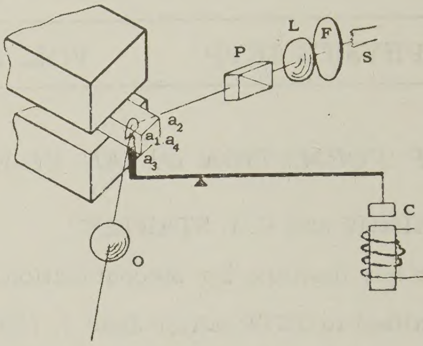

FIG. 8. Diagram of the apparatus. The crystal $a_1a_2a_4a_3$ is held in the vise. A piece of soft iron C is attracted to the electromagnet and through the lever provides a localized load on the calcite crystal. S) light source, F) filter, L) lens, P) polarizer, O) objective which projects the image of the twin onto a photographic plate.

(1) The facets CBD'A' and ADB'C' were cut away with a fine cutter on a milling machine to form the two faces cbd'A' and dAb'c', perpendicular to the edge BA (Fig. 6). These faces were ground and polished. (After further working, the crystal was clamped with the face dAb'c' on the underside of the upper stage of a press, the pressure being exerted by balls of various diameters on the lower face cbd'A'.)

(2) The dihedral corners b'dA and b'c'A were cut off by planes parallel to the edges c'd' and cd and perpendicular to the major diagonal dc' (Fig. 7). These planes too were ground and polished. The crystal was illuminated through one of these and the elastic twin was observed through the other. Finally, the dihedral corners Ab and A'b' (Fig. 7) were cut away. The parallelopiped $a_1b_1b_2a_2a_3b_3b_4a_4$ obtained became the object of further experiments. The specimen was clamped in a vise so that the face $a_1a_2a_3a_4$ was on the bottom (Fig. 8). The pressure was produced by a punch, the end of which was rounded off in the form of a hemisphere. The pressure was brought to bear by a lever of the first order. The force on the end of the lever was produced by the soft iron core C, which was drawn into a solenoid. The force was determined from the current, and in reality from the position of the slide of the rheostat that regulated the current. The twinned petal was illuminated by a beam of parallel light (an automobile lamp at the principal

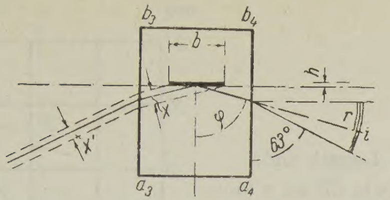

FIG. 9. Construction by means of which Eq. (5) is demonstrated. $a_3b_3a_4b_4$ is the calcite crystal and the heavy segment is the twin lamella, b) its breadth, h) its thickness, i) the angle of incidence, r) the angle of refraction, φ) the angle of incidence of the beam on the twin lamella; $\varphi = 90° - r$, X') the apparent breadth of the twin.

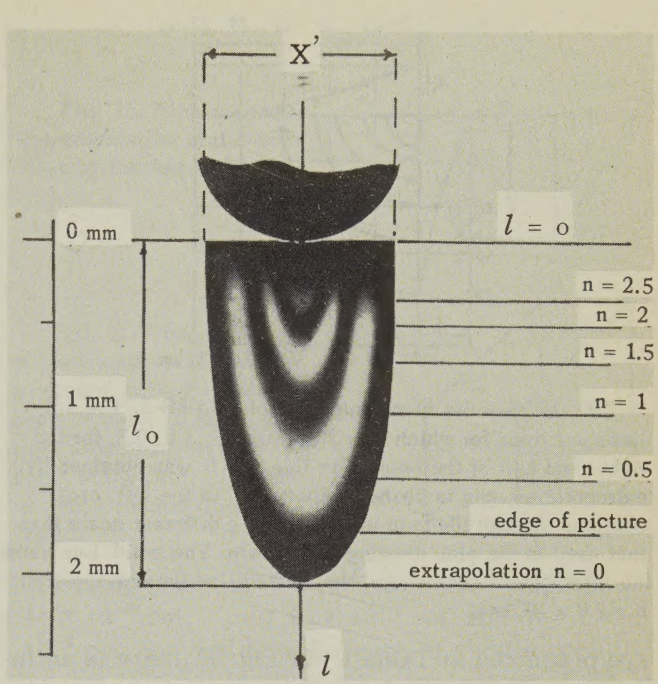

FIG. 10. Photograph of elastic twin 8B-3. The scale of measurement is shown at the left. Designation is given at the right above the lines. The figure has been cut out of a photograph, and its external contour has been extrapolated. Above, the spherical tip of the steel plunger is indicated.

focus of the lens L with principal focal distance f ~ 20 cm.). The light passed through an interference filter F, which transmitted the wavelength $\lambda = 5.88 \times 10^{-5}$ cm; the angle of incidence was 27°. Experiment and calculations have shown[6] that with normal incidence of light on a twin lamella, there must be no reflected light observed at all. The optimum reflection is at the 27° angle of incidence chosen by us. The image of the elastic twin was projected onto a photographic plate by means of the objective lens of a binocular microscope (or examined directly by eye). On account of the double refraction in calcite, two images of the petal were obtained. The extraordinary-beam image was eliminated by the Nicol prism P, and observations were conducted with the ordinary beam. We have assumed that the indices of refraction μ_0 and μ_e for the ordinary and extraordinary beams respectively are equal to:[7]

$$\mu_0 = 1.658; \ \mu_e = 1.486. \tag{1}$$

With the angle of incidence at 27°, the angle of refraction for the ordinary beam is 15°53′ and the beam is incident on the twin at the angle φ (Fig. 9).

$$b_0 = X'2\mu_0 \cos r / \sin 2i = 3.945X', \tag{2}$$

The image of the twin was covered with interference fringes, through which it was possible to determine the thickness of the twin according to the formula

$$2\mu h \cos \psi = n\lambda, \tag{3}$$

where h is the thickness of the twin, ψ the angle of refraction, μ the index of refraction of the twin, n the number of the interference fringe, and λ the wavelength of the light, equal to 5.88×10^{-5} cm.

With regard to the quantities μ and ψ, it must be borne in mind that inside the twin the position of the optical axis is different than in the parent crystal and the beam which is extraordinary inside the twin undergoes total internal reflection. Thus, inside the twin we have $\mu = \mu_0$; ψ is equal to the angle of incidence, and Eq. (3) yields:

$$h = n \cdot 5.88 \cdot 10^{-5} / 1.658 \cdot 0.2737 \ = n \cdot 1.30 \cdot 10^{-4} \text{ cm}, \tag{4}$$

where n is the number of the interference fringe.

The shape of elastic twin 8B-3 is shown in Fig. 10. The length of the twin l_0 is given by direct measurement. The width of the twin b_0 is seen in projection. To obtain the true width of the twin, it is necessary to multiply its apparent width (X′ in Fig. 10) by the amount indicated in the following formula:

$$b_0 = X'2\mu_0 \cos r / \sin 2i = 3.945X', \tag{5}$$

which is clear from Fig. 9, if Eqs. (1), (2) and (4) are taken into account. The thickness of the twin is given by Eq. (4).

3. SHAPE AND DIMENSIONS OF AN ELASTIC TWIN

From Fig. 10 it is seen that the length l_0 and breadth b_0 of an elastic twin are in essence quantities of the same order, while its thickness is three orders smaller, Schematically, the shape of the twin is given in Fig. 5, in which the scale of thickness is magnified 1000 times. Figure 11 shows two cross sections of elastic twin 8B-3; l_0 and b_0 are given in millimeters and the thickness h_0 in microns. The results of measurement of twin 8B-3

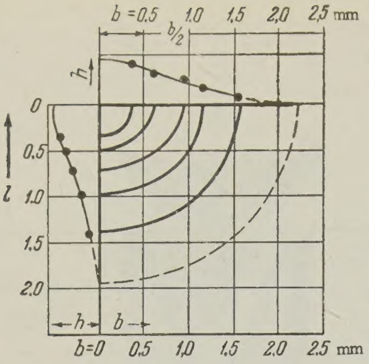

FIG. 11. Results of measurement of twin 8B-3. The solid lines are lines for which n = 2.5, 2.0, 1.5, 1.0, 0.5, for the right-hand half of the twin. The line n = 0 was obtained by extrapolation, and is dashed. Above and to the left, cross sections through the twin are shown in a different scale than that used in the plan drawing of the twin. The solid line shows the interpolated contour and the dashed line the extrapolated. $h = 2.0 \times 10^{-3}$mm.

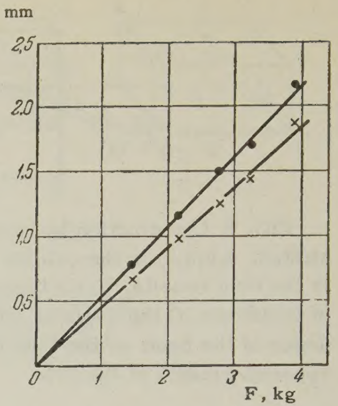

FIG. 12. Length and breadth of twin 6R as a function of load. ●) values of b_0, ×) values of l_0.

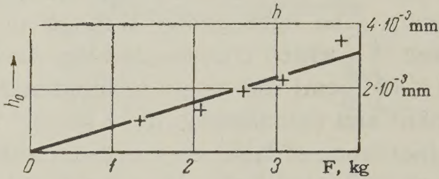

FIG. 13. Thickness h_0 of twin 8B as a function the load.

are presented in Table I. In Fig. 11 there is an indeterminacy which always occurs in the measurement of small thicknesses by an interference method, namely in gaging the point where n = 0. We did this by a very unreliable method for want of a better one. Experience in the investigation of optical contacts[8] has shown that the location of the spot with thickness h = 0 can be determined as follows: The distance from the middle of the band n = 0.5 to the "border" (a very indefinite concept) of the interference picture is measured. The vanishing point of the interference is assumed to be at a like distance beyond the "border" of the interference picture.

We possessed three calcite crystals, Nos. 6, 7, and 8. Crystals 6 and 7, were colorless, cleaved easily upon twinning by Baumgauer's method, and had mosaic cleavage planes. Crystal No. 8 was of light yellow color (probably due to $FeCO_3$ dissolved in it) was very perfect and twinned softly and easily. The results of measurements analagous to those presented in Table I are given in Figs. 12 and 13. In Fig. 12 the load F is plotted along the abscissa while the ordinates of b_0 are marked by dots and those of l_0 by crosses. It is seen that the length and breadth of an elastic twin are proportional to the load as has been noted by Garber.[1] In Fig. 13 the value of h is given as a function of F. This last quantity is also seen to be proportional to the load. Thus, under the influence of a concentrated load, an elastic twin changes its dimensions but retains its shape.

Figures 14 and 15 show the results of measurements made at different points of crystals Nos. 6,

TABLE I. Dimensions of twin 8B-3:
$l_0 = 1.95$ mm; $b_0 = 2.44$ mm;
$h_0 = 1.95 \times 10^{-4}$ cm. Load F = 2.58 kg.

n	X'	l, mm	b, mm	$h \cdot 10^{-4}$, cm
3.0	0	0	0	$h_0 = 1.95$
2,5	0.11	0,34	0.45	1.63
2.0	0.15	0,48	0.60	1,30
1,5	0.23	0,72	0,93	0,98
1,0	0.29	0,98	1,14	0,65
0.5	0.36	1,40	1,47	0,33
0*	0,52*	$l_0=1.95$*	$b_0=2.44$*	0*

*Extrapolated

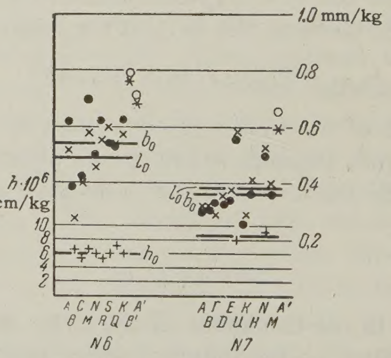

FIG. 14. Results of experiments on crystals No. 6 and 7. Values of the quantities dl_0/df and $db/_0/dF$ (in mm/kg) and values of dh_0/dF (in cm/kg × 10^6) are plotted along the ordinate. The average value of each of these quantities is given as a heavy line for each of the specimens. Measurements for a single experiment are plotted on one vertical, below which the number for the experiment is denoted by a letter. o) breadth b_0, 1 mm diameter ball; ●) breadth b_0, 1.8 mm diameter ball; *) length l_0, 1 mm diameter ball; ×) length l_0, 1.8 mm diameter ball; +) thickness h_0 (in the other scale).

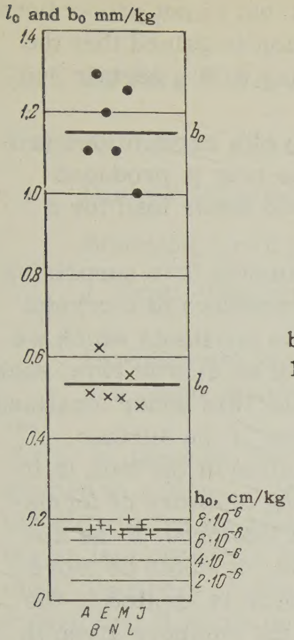

FIG. 15. The same as Fig. 14, but for crystal No. 8. Ball diameter 1.8 mm.

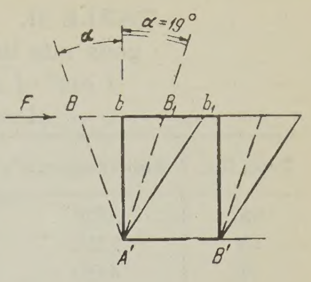

FIG. 16. Illustration for the calculation of the work done by the force F.

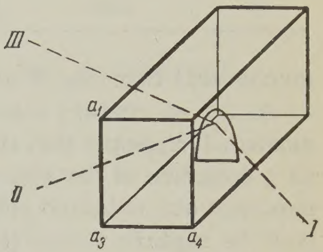

FIG. 17. Observation of cracks associated with an elastic twin. I) incident beam of light, II) beam of light reflected from the plane of the twin, III) beam of light reflected from the cracks.

7, and 8. The abscissa represents the number of the experiment, and the ordinate the values of l_0, b_0, and h_0 which the twinned petal assumes under an absolute load of 1 kg. Using these data and also the data of Figs. 12 and 13, we can measure the work of the force F. As an example, we have from Table I a load F of 2.58 kg. = 2.54×10^6 dynes. The thickness of the twin is 1.95×10^{-4} cm. As is evident from Fig. 16, the distance over which the plunger is displaced is

$$bb_1 = h \cdot 2 \tan 19° = 0.688 \cdot 1.95 \cdot 10^{-4} \text{ cm} = 1.34 \cdot 10^{-4} \text{ cm}.$$

Hence, the work done by the plunger is equal to

$$A = {}^1/_2 F \cdot \overline{bb}_1 = 340 \text{ ergs}.$$

This energy can go either into production of elastic tension in the elastic twin and its surroundings, or into formation of the surface of the twin. The area of our twin is $\pi l_0 b_0 / 2$, and its two surfaces amount to $S = \pi l_0 b_0 = 1.42 \times 10^{-1}$ cm²:

$$A/s = 2400 \text{ ergs/cm}^2.$$

The corresponding work of formation of one surface comes to 1200 ergs/cm². We can show that the elastic energy of the deformed twin and its surroundings is two orders smaller than this value.

Let us make a very rough calculation: We replace the twinned petal by a platelet having the shape of a parallelopiped of height l_0, breadth $2b_0$ and thickness h_0. Under the action of the load F, the height is shortened by an amount Δl, where $\Delta l = l_0 F / E b_0 h_0$, and E is Young's modulus. The work of compression of such a parallelopiped is equal to $\Delta l^2 E b_0 h_0 / 2 l_0$. In place of $1/E$ we use the coefficient s_{11}. For calcite, $s_{11} = 11.3 \times 10^{-13}$ in the cgs system. As also in the foregoing example, having taken $\Delta l = bl_1 = 1.34 \times 10^{-4}$ cm, $b_0 = 2.44 \times 10^{-1}$ cm, $l_0 = 1.95 \times 10^{-1}$ cm, and $h = 1.95 \times 10^{-4}$ cm, we find that the work of elastic compression is equal in all to 2.9 ergs instead of 340 ergs. Thus it is found that the entire work of the force F is in the surface layer of the twin.

It is necessary to note that this energy is very large (the surface tension of water is equal to 70 ergs/cm²). If one imagines the boundary of the twin and parent crystal as closely contiguous, then such values of surface energy seem impossible. This value does appear possible, however, if one imagines that the boundary of the twin and parent crystal is stepped and that these little steps constitute a break in the cleavage plane. It can happen that one of the faces of the elastic twin is a crystallographic twin plane in which case the energy calculated by us applies to one of the surfaces of the twin. It can happen that both surfaces are not crystallographic planes and then the energy we calculated applies to both sides of the twin.

Direct observation confirms that near the surface of an elastic twin there is a break of continuity. Specifically, if we illuminate the twin, as usual, with beam I (Fig. 17) and place our eye or the objective of a microscope in the reflected beam II, we see the interference pattern shown in Fig. 10. If, however, we sight in the direction III, then we again see light reflected from the elastic twin, which indicates the presence of a crack or cracks close to the surface of the elastic twin. We are planning a detailed investigation of this phenomenon.

4. BREAKDOWN OF CRYSTALS

There are two types of crystal breakdown: (1) rupture along a cleavage plane with a break in continuity; (2) various types of "slip," to which

TABLE II. The work which goes into the formation of 1 cm^2 of surface of an elastic twin

Twin No.	Work (Ergs/cm^2)	Twin No.	Work (Ergs/cm^2)
6K	3720	8A	2670
6S	5160	8B	2400
7U	4450	8L	2890
7N	6400	8β	2400

mechanical twinning is also related.

As far as rupture along a cleavage plane is concerned, it appears that if the rupture stress is taken as a measure of the stability of a crystal, no fixed numbers are obtained and the stability depends on how the rupture stress is applied. If, however, the specific work necessary for the formation of a new surface is taken as the measure of stability, this work does not depend on how the rupture proceeds and it can be called an invariant of the breakdown.

At first glance, the breakdown of a crystal by rupture and by slip have nothing in common with each other, but more and more observations indicate that, in order for the shearing action to become possible, a break in continuity is necessary and rupture is essential. In fact, in the case of optical contact of two polished optical surfaces,[8] slip of these surfaces is not possible: it is necessary for them to first break away from one another, after which they can shift. This pertains to all forms of optical contact.[9] In reference 10 it is shown that the initial stage of plastic deformation in rock salt is by ultramicroscopic cracks which manifest themselves as Tyndall cones.[4] In numerous papers by Likhtman and Rebinder (e.g., reference 11), the effect of surface-active substances on plastic deformation is demonstrated. It has been directly demonstrated how surface-active substances affect the formation of cracks and how cracks initiate shears.[3] Finally, in the present work it is shown that the start of mechanical twinning in calcite is the formation of a new surface and that the specific work for the formation of this surface is an invariant quantity, characteristic of the material.*

5. CERTAIN DETAILS OF THE PHENOMENON

It should be noted that not all the experiments go as smoothly as described in the preceeding sections. Cases occur where the length of the twin depends linearly on the load, but is not proportional to the load, i.e., an impression is gained that the elastic twin is formed starting with a certain requisite initial load.

In some cases application of a certain load produces no twin at first, but the twin is produced after the crystal has remained under load for a while.

We feel that in our experiments it is surprising and noteworthy that in the breakdown of a crystal it is possible to obtain certain constants which we call invariants. In the case of an elastic twin, such invariants are the shape of the twin under localized load and the work of formation of the surface.

Finally, the work of formation of the twin is itself very large. In calculating the work of formation of the twin, we regarded the force F as applied to the border of the twin. It would be more correct to assume that the force is applied to the center of the twin. Then all the numbers given in Figs. 14 and 15 must be reduced by a factor of two, and with them also the amounts of work presented in Table II. A direct measurement of the work must settle this question.

---

*The major role which cracks in the cleavage plane play in plastic slip and twinning has already been indicated repeatedly by R. I. Garber in earlier communications.

[1] R. I. Garber, Dissertation, Alma Ata, 1942.

[2] W. Voigt, Wiedem. Ann. **67**, 201 (1899).

[3] R. I. Garber, J. Exptl. Theoret. Phys. (U.S.S.R.) **17**, 1 (1947).

[4] R. I. Garber, Dokl. Akad. Nauk SSSR **57**, 555 (1947).

[5] R. I. Garber, J. Exptl. Theoret. Phys. (U.S.S.R.) **16**, 923 (1946).

[6] G. B. Rais, Dokl. Akad. Nauk SSSR **106**, 841 (1956).

[7] Ia. G. Dorfman and S. E. Frish, Сб. физических констант (Collection of Physical Constants), ONTI (1937).

[8] I. V. Obreimov and E. S. Trekhov, J. Exptl. Theoret. Phys. (U.S.S.R.) **32**, 185 (1957), Soviet Phys. JETP **5**, 235 (1957).

[9] J. W. Obreimoff, Proc. Roy. Soc. **A127**, 290 (1930).

[10] Garber, Obreimov, and Poliakov, Dokl. Akad. Nauk SSSR **108**, 425 (1956), Soviet Phys. "Doklady" **1**, 314 (1956).

[11] Rebinder, Likhtman and Kachanova, Dokl. Akad. Nauk SSSR **111**, 1278 (1956).

Translated by R. Eisner
232

SOVIET PHYSICS JETP VOLUME 35(8), NUMBER 5 MAY, 1959

THE EFFECT OF NEUTRINO RECOIL IN THE BETA DECAY OF He^6

J. CSIKAI and A. SZALAY

Nuclear Physics Institute, Hungarian Academy of Sciences, Debrecen, Hungary

Submitted to JETP editor November 21, 1957

J. Exptl. Theoret. Phys. (U.S.S.R.) **35**, 1074-75 (November, 1958)

Experiments are described on neutrino recoil effects from the β decay of He^6 as observed in a cloud chamber.

THE β decay of He^6 has not previously been studied in a cloud chamber, most likely owing to the difficulties presented by the task of introducing an isotope whose half-life is 0.8 sec into the cloud chamber. A few years ago we became convinced that it would be worthwhile to overcome these technicalities, because this β decay is most convenient from the point of view of the neutrino problem. The process $He^6 \rightarrow Li^6 + \beta + \nu + 3.6$ Mev has a wide spectrum of decay energies uncontaminated by γ radiation, and the daughter nucleus (Li^6) has the smallest mass of all radioactive isotopes (with the exception of He^3). It may acquire a large recoil energy (maximum 1.405 ev) and we were hoping that its track could be detected in a cloud chamber filled with hydrogen at low pressure. By the simultaneous determination of the momentum and energy of the β particle and daughter nucleus in the same elementary act we can obtain the missing momentum and energy carried off by the neutrino.

The cloud-chamber method is more convenient than the electronic method utilized by a number of authors[1,2] because it not only permits the observation of single atomic processes but also the precise measurement of angular correlations.

A cloud chamber with a rubber membrane was built working well when filled with hydrogen at 200 mm Hg and water and alcohol vapor. Figure 1 shows how the problem of introducing He^6 into the chamber was solved. A few seconds before expansion the 4C (Po + Be) source was introduced pneumatically into the vicinity of the weakly emitting powder [approximately 5 g of $Be(OH)_2$], placed in a box made out of porous filter paper and located inside the cloud chamber. An elastic rubber bag separated the volume of this vessel from the pneumatic compressor. Immediately (0.3 sec) prior to expansion the neutron source was pneumatically swept past the shielding layer. The same air shock would stretch the rubber bag forcing the He^6 liberated from the $Be(OH)_2$ powder to enter the chamber through the porous wall.

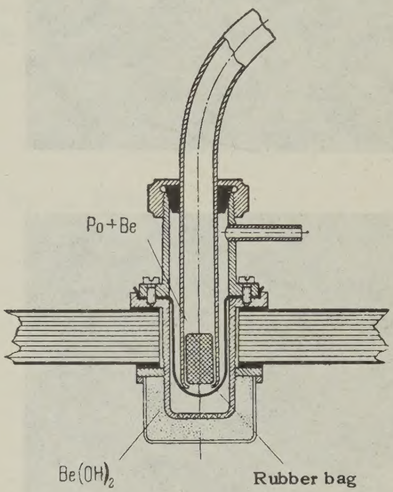

FIG. 1. Setup for the introduction of He^6 into the cloud chamber.

As can be seen from a few typical examples of our photographs (Figs. 2a, b, c), our expectations were fulfilled. The track of the recoil nucleus is clearly visible. Its direction is usually not directly opposite to that of the β particle: they form an obtuse angle, i.e., it is clearly seen that a certain amount of momentum is missing. In an analogous manner, in the photographs (Figs. 3a, b) in which the ions diffused prior to expansion, the effect of the neutrino manifests itself in the fact that the energy and momentum of the recoil nucleus are smaller or larger than what would have been expected from the energy of the β particle alone.

We obtained a total of more than 2000 stereo photographs, among which there were 120 tracks good enough for a quantitative analysis. The complete energy-momentum balance for the transition can be obtained if the curvature of the β track in a magnetic field and the angle between the β particle and the recoil nucleus are measured.

Figure 4 shows the electron-neutrino angular

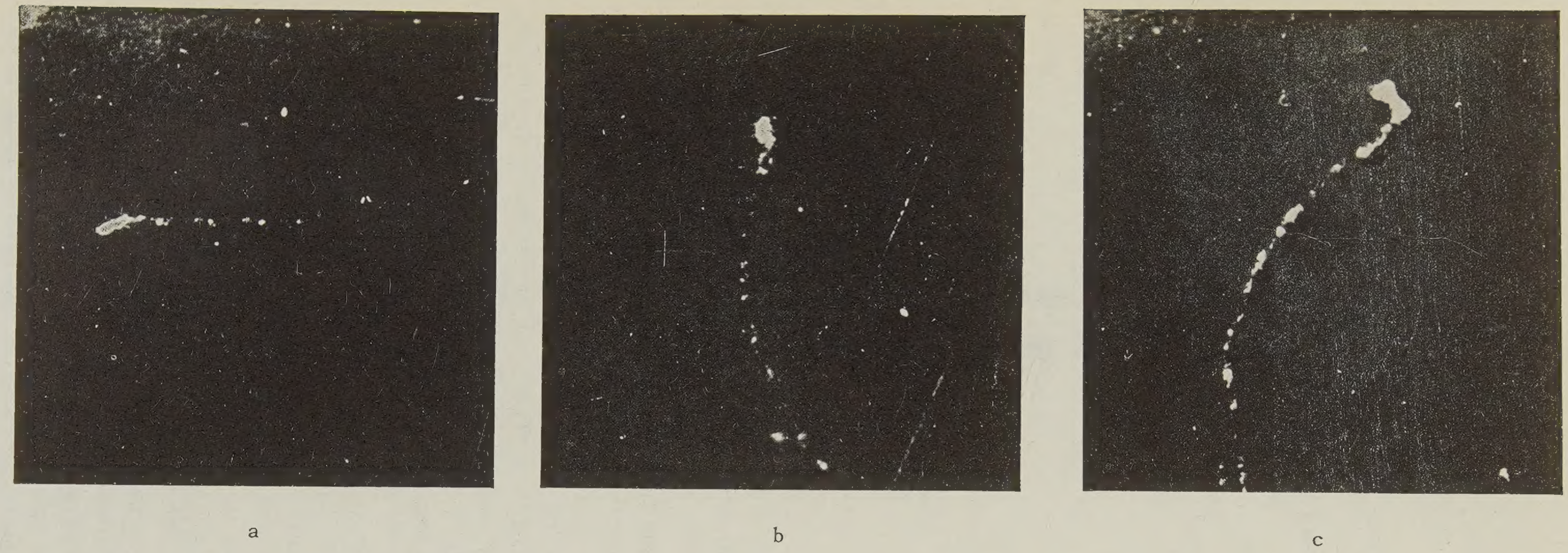

FIG. 2. a, b, c, Cloud chamber photographs of the β decay of He^6 (acute angle between the electron and recoil nucleus tracks).

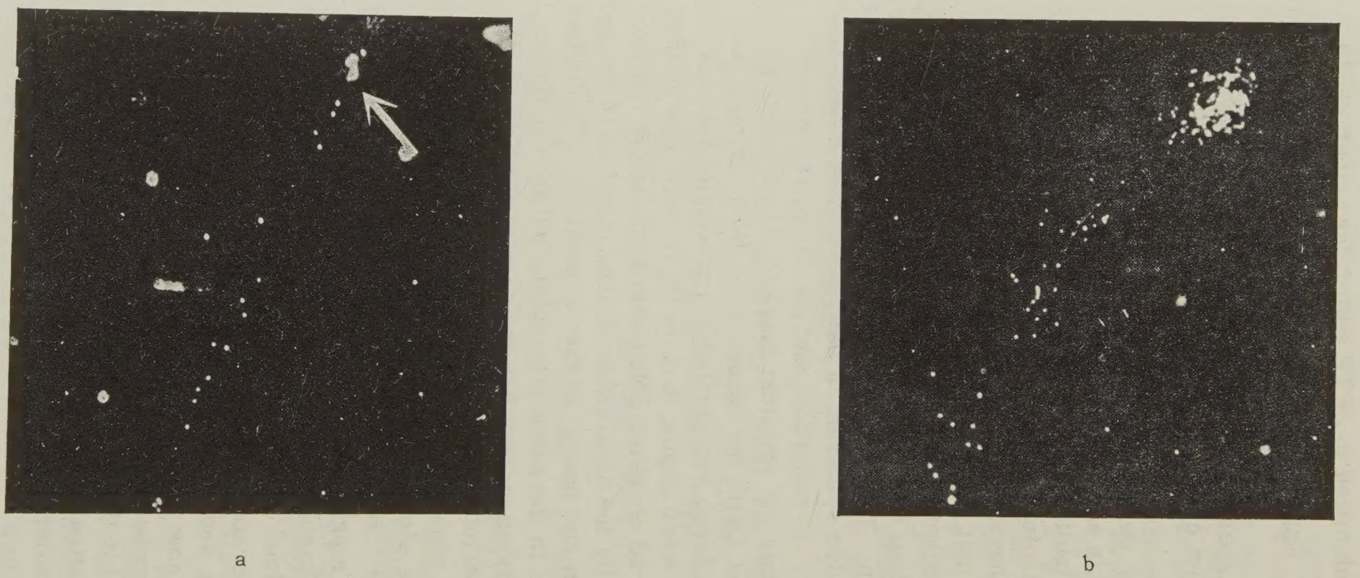

FIG. 3. a, b. Cloud chamber photographs of the β decay of He^6 (the energy, i.e., the number of drops in the track of the recoil nucleus, is in contradiction with the energy of the β particle).

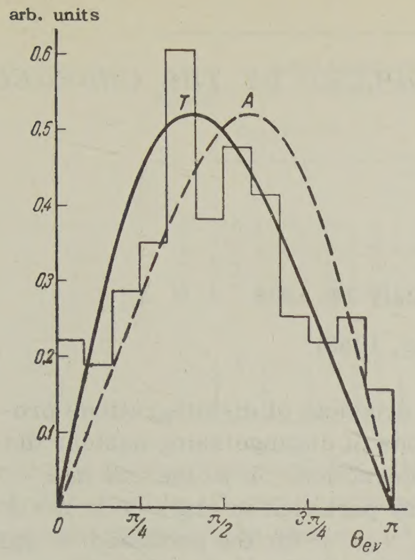

FIG. 4. Electron-neutrino angular correlation from 120 measured tracks in the β decay of He^6. T and A are the theoretical curves for tensor ($\alpha = 1/3$) and axial-vector ($\alpha = -1/3$) interactions respectively. v/c = 0.92.

correlation for the 120 measured tracks; statistical errors are still large, owing to the small number of events. A comparison of the distribution with the theoretical calculations of De Groot and Tolhoek[2] shows good agreement with the curve calculated on the assumption of tensor interaction for the β decay (the other curve refers to the axial vector interaction).

We hope soon to be able to confirm this result with a larger number of measured tracks.

---

[1] J. S. Allen and W. K. Jentschke, Phys. Rev. 89, 902 (1953). B. M. Rustad and S. L. Ruby, Phys. Rev. 97, 991 (1955).

[2] S. R. De Groot and H. A. Tolhoek, Physica 16, 456 (1950).

Translated by A. Bincer
233

SOVIET PHYSICS JETP VOLUME 35(8), NUMBER 5 MAY, 1959

INVESTIGATION OF NUCLEAR DISINTEGRATIONS PRODUCED BY THE CHARGED COMPONENT OF COSMIC RADIATION

G. V. KHRIMIAN

Physics Institute, Academy of Sciences, Armenian S.S.R.

Submitted to JETP editor December 30, 1957; resubmitted July 14, 1958

J. Exptl. Theoret. Phys. (U.S.S.R.) 35, 1076-1082 (November, 1958)

Results are presented of a mass-spectrometer study of the products of disintegrations produced by the charged component of cosmic radiation. Methods of distinguishing nuclear disintegrations from showers originating in electromagnetic interactions of μ mesons are indicated. The differential momentum spectrum of secondary particles in stars with $n > 2$ has been measured. It has been found that the ratio $N(\pi^+)/N(\pi^-)$ for the produced π mesons is equal to 1.18 ± 0.23 in the momentum range 0.12 to 0.9 Bev/c, and that the π mesons constitute $53 \pm 5\%$ of the secondary particles with momentum ≥ 1 Bev/c. The ratio of charged to neutral star producing particles of ~ 30 Bev is equal to 1.2 ± 0.16.

In a hodoscope study of the secondaries of stars produced by charged particles a difficulty is encountered due to the considerable background of showers originating in electromagnetic interactions of μ mesons. The majority of investigators limit therefore their experiments either to the stars produced by neutral particles[1-4] or to the large stars $(m \geq 2,\ n \geq 5)$* produced by charged particles.[5] In the latter case, smaller stars, which constitute $\sim 50\%$ of all events produced by charged particles, are disregarded.

In the present work, data are given on secondaries observed in large $(m \geq 2,\ n \geq 5)$ and small $(m \geq 2,\ n < 5;\ n = 1,\ n > 2)$ stars produced by the charged component of cosmic radiation.

The measurements were carried out using the Alikhanian-Alikhanov magnetic mass-spectrometer at 3250 m above sea level (Aragats). The hodoscope, placed above the magnet, detected nuclear disintegrations in the targets A, B, C, D, E, F placed between the counter trays. The nature of secondaries was studied by means of the mass spectrometer. The instrument and the method of selection of particles by the magnetic field have been described in reference 5. The thickness of the targets and absorbers, and their position in the instrument, are given in Table I.

In this article we discuss only the stars in which the angle between the primary trajectory and the vertical was not greater than 35°. According to Camerini et al.,[6] the fraction of such stars amounts to $\sim 75\%$ of all stars produced by charged particles. The distribution of the secondaries of large stars $(m \geq 2,\ n \geq 5)$ with respect to the direction of motion (the angle with the primary trajectory) in the plane perpendicular to the magnetic deviation is shown in Fig. 1. Data obtained by Camerini[6] by means of emulsions are included in the figure. It follows that our apparatus located with a large efficiency particles emitted at an angle $\leq 35°$ which, according to reference 6, amount to $\sim 90\%$ of all secondaries.

SEPARATION OF NUCLEAR DISINTEGRATIONS AND SHOWERS INITIATED BY μ MESONS

All observed stars were divided into groups according to the number of secondaries and their range in the targets (Table II). To determine the groups that did not contain showers initiated by μ mesons, we studied the passage of the secondaries of a given group through the absorbers (Table II).* For this purpose we used the results of the third series of measurements, in which the total thickness of absorbers is 2.5 times larger than the nuclear-interaction mean free path.

It follows from the data that the stars with five and more secondaries, at least two of which pass through the next target [i.e., stars of the type $(m \geq 2,\ n \geq 5)$], represent nuclear disintegra-

---

*Stars observed by means of a hodoscope are characterized by the numbers m and n, where m is the number of trays (separated by targets) traversed by at least two particles of the star, and n is the observed number of secondary star particles (multiplicity).

*For comparison, data on the passage of secondary nuclear-active particles produced by neutrons are given at the end of the table.

TABLE I

Series	Lead target, cm						Absorber, cm					
	A	B	C	D	E	F	1	2	3	4	5	6
Graphite												
1	0	7	6	5	4	3	4	9	4	3.6	3.9	1Pb + 9Cu
2	0	7	6	0	0	0	4	9	4	2	2	1Pb + 9Cu
7	7	6	5	0	0	0	4	8	4	2	2	11Cu
11	7	6	5	0	0	0	4	8	4	2	3Pb+0.6Cu	11Cu
Copper												
3	8	7	6	5	4	3	3.6	8.26	4.26	3.1	4 or 2.6 + 1 Pb	12 or 9.25 + 1 Pb

tions produced by charged particles. All stars of this type, observed in all series of measurements, were regarded therefore as such.

The remaining groups $(m \geq 2,\ n < 5$ and $m = 1,\ n > 2)$ contain both electronic showers initiated by μ mesons and nuclear disintegrations. In these, only the stars in which the secondaries underwent nuclear interactions in the absorbers were accepted as nuclear events. In order to exclude completely the μ mesons that produce showers both in the targets and in the absorbers of the instrument, we studied the passage of μ mesons through the lead and graphite absorbers.

Showers initiated by μ mesons. All single particles with momentum $p \geq 1$ Bev/c which passed through all the targets (25 cm Pb) without an interaction were assumed to be μ mesons, since the fraction of nuclear-active particles among such particles amounts to ~2% only.* Data on the passage of μ mesons through the absorbers of the apparatus as well as on the passage of secondary particles of large and small stars through the absorbers, are given in Table III.

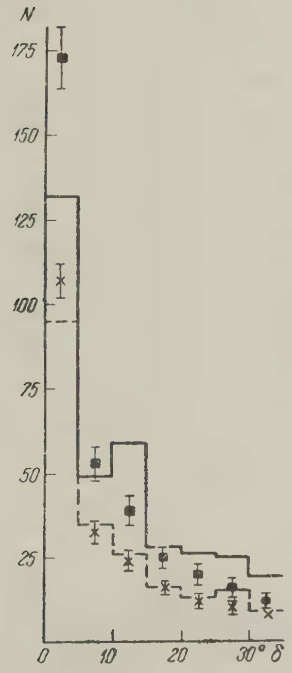

FIG. 1. Direction distribution of secondary particles (with respect to the primary). Solid curve represents all particles produced in large stars, dashed – positive particles with $p \geq 10^9$ ev/c and all negative particles (i.e. shower particles); ×) ■ data of Camerini et.al., renormalized to the area.

It follows from the table that: (1) interactions of the type b, c, d, e, and f originate in the majority of cases in electromagnetic interactions of charged particles, and it is therefore impossible to distinguish nuclear-active particles from μ mesons; (2) stars of the type g $(m \geq 2,\ n \geq 2)$, large-angle scattering events (h), and stopping of particles not due to ionization losses (i) involve nuclear-active particles only. The stars, in which the secondaries underwent interactions of the type g, h, and i in the absorbers were considered therefore as nuclear disintegration.†

NATURE AND MOMENTUM SPECTRUM OF SECONDARY PARTICLES

We observed 135 particles with mass $M \leq 1300\ m_e$ in nuclear disintegrations with $n > 2$ in the momentum range from 0.12 to 0.9 Bev/c. The upper mass limit of the particles was estimated from their momentum and minimum range. The minimum range was defined as the absorber thickness traversed by the particle without a visible interaction. The mass distribution of the particles is given in Table IV. Of the 135 particles, 73 were positive and 62 negative, i.e., the ratio of positive to negative mesons produced in lead by charged particles equals 1.18 ± 0.23. The result

---

*According to references 7 and 8, the fraction of nuclear-active particles amounts to ~10% of the total flux at 3200 m altitude. Of these, not more than 20% can traverse 25 cm Pb without an interaction.

†Interactions of the type g, h, and i involving μ mesons (~1%) are explained by the presence of ~2% protons among the "μ mesons," half of which should, according to data of Table III, undergo interactions of the type g, h, and i.

TABLE II*

Type of star	Passage of secondaries through absorbers					
	No interaction	Weak interaction**	Nuclear interactions			Total
			scattering $> 2 \langle\vartheta\rangle$	stopping (not due to ionization)	star $m \geqslant 2$, $n > 2$	
$m = 1$, $n > 2$, $\delta < 5°$	184	16	5	6	—	211
$m = 1$, $n > 2$, $5 \leqslant \delta < 9°$	3	2	1	—	—	6
$m = 1$, $n > 2$, $\delta \geqslant 9°$	4	—	—	1	—	5
$m \geqslant 2$, $n < 5$	21	3	7	10	1	42
$m \geqslant 2$, $n \geqslant 5$	7	2	8	19	16	52
Neutron-produced stars	4	—	18			22

*δ) angle of emission of secondary particles with respect to the direction of the primary, $\langle\vartheta\rangle$) mean angle of multiple scattering.

**Discharges in two adjacent counters in two consecutive trays or three discharges in one tray, and stars $m = 1$, $n > 2$; $m \geq 2$, $n = 2$.

TABLE IV

Upper mass limit		$M \leqslant 1300 m_e$	$M \leqslant 900 m_e$	$M \leqslant 500 m_e$
Number of particles	N^+	73	44	12
	N^-	62	39	12

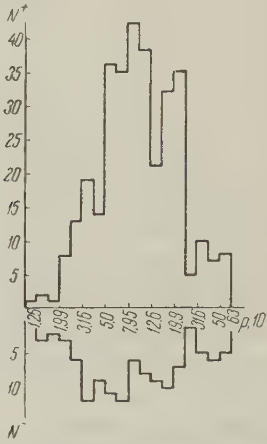

FIG. 2. Differential momentum spectrum of secondaries in large stars ($m \geq 2$, $n \geq 5$).

obtained refers to π^+ and π^- mesons since of the 135 particles selected by the momentum-minimum range method, the masses of 83 particles are clearly less than that of the K•meson, and K mesons cannot constitute more than 20% of the remaining 52 particles.[9,10]

The differential momentum spectrum of secondary particles produced in large stars ($m \geq 2$, $n \geq 5$) is shown in Fig. 2. The spectra may be represented by a function $N(p) \sim p^{-\gamma}$, where $\gamma = 1.48 \pm 0.14$ for negative particles in the momentum range ≥ 0.4 Bev/c, and $\gamma = 2.04 \pm 0.19$ for positive particles of ≥ 1 Bev/c.*

TABLE III

Passage through the absorbers**	Type of particles*					
	μ-mesons		Secondaries in small stars		Secondaries in large stars	
	N	N, %	N	N, %	N	N, %
a	316	72	513	85	18	36
b	45	10.3			1	
c	31	7.1			3	
d_1	10	2.3			2	
d_2 ($m = 1$, $n = 2$)	11	2.5			3	
e ($m = 1$, $n > 2$)	6	1.4	17	2.8	2	5.3
f ($m = 2$, $n = 2$)	13	3	12	2	2	
g ($m \geqslant 2$, $n > 2$)	3	0.7	14	2.3	13	17.3
h	2	0.5	16	2.7	7	9.3
i	—	—	32	5.3	24	32
Total	437	100	604	100	75	100

*Data of the first series or measurements. N) number of particles.

**a) no interaction; b) two adjacent discharges in a tray; c) two non-adjacent discharges in a tray; d) two adjacent discharges in two non-consecutive trays; d_2, e, f, g) stars of various types; h) scattering at an angle greater than twice the mean multiple scattering angle; i) stopping.

442 particles, among them 115 negative, were observed in the momentum range from 0.12 to 6.3 Bev/c. In the range ≥ 1 Bev/c the ratio of positive to negative particles is 156 : 51, i.e. $N_\pi / N_s = 0.5$ to 0.6 (N_π is the number of π mesons and N_s is the number of particles with momentum ≥ 1 Bev/c.).

The differential momentum spectrum of 407 secondary particles in the momentum range from 0.12 to 6.3 Bev/c produced in small stars ($m \geq 2$,

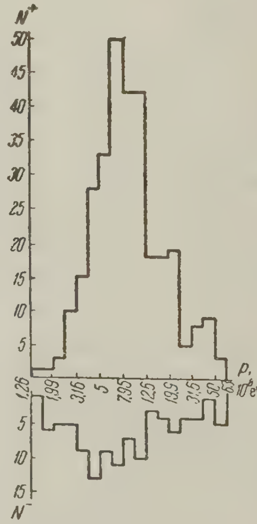

FIG. 3. Differential momentum spectrum of secondaries in small stars ($m = 1$, $n > 2$; $m \geq 2$, $n < 5$).

---

*The exponent γ was determined by the method of least squares, taking into account the statistical weight of the experimental points. In determining the spectrum of positive particles, ionization losses in the target were neglected.

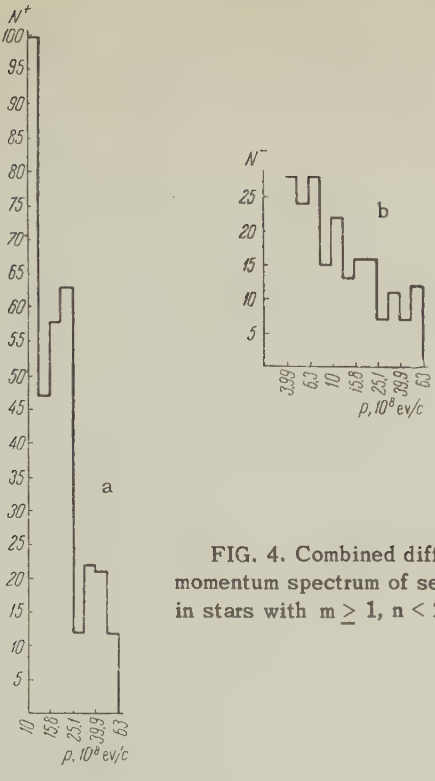

FIG. 4. Combined differential momentum spectrum of secondaries in stars with $m \geq 1$, $n < 2$.

$n < 5$; $m = 1$, $n > 2$) is shown in Fig. 3. The spectrum of negative particles in the momentum range from 0.4 to 6.3 Bev/c may be described by a function $N(p) \sim p^{-1.61 \pm 0.16}$, while the spectrum of positive particles with $p \geq 1$ Bec/c is of the form $N \sim p^{-2.2 \pm 0.2}$. The ratio of positive to negative particles in the range ≥ 1 Bev/c is 122 : 37, i.e., $N_\pi / N_s \sim 0.5$.

The combined differential momentum spectrum of secondary particles produced in all observed nuclear disintegrations with $n > 2$ (the spectrum of positive particles in the momentum range ≥ 1 Bev/c and of negative particles in the range ≥ 0.4 Bev/c) is shown in Fig. 4a and 4b. The spectra were corrected for secondaries in small stars, which did not interact in the absorbers and were excluded according to the selection rules for small stars. The correction was determined from a study of the passage of secondary particles of large stars ($m \geq 2$, $n \geq 5$) produced by charged particles, and of particles produced by the neutral component.

RATIO OF CHARGED TO NEUTRAL STAR-PRODUCING PARTICLES AND THEIR ENERGY

The energy of primary particles producing large stars ($m \geq 2$, $n \geq 5$) amounts to ~30 Bev.[5] This value was estimated from the angular distribution of penetrating particles.

The interactions of secondary particles of a known momentum in the lead absorbers of the array (series 3, Table I) were used for an estimate of the minimum energy of primary particles producing small stars, ($m \geq 2$, $n < 5$; $m = 1$, $n > 2$). Nineteen such stars were observed. It was found that the minimum momentum of the particles which produced them was ≥ 3 Bev/c.

For the determination of the ratio of neutral to charged star-producing particles of ~ 30 Bev, in the seventh and eleventh series of measurements we studied large stars ($m \geq 2$, $n \geq 5$) produced both by the charged and the neutral component. Out of 238 stars, 83 were produced by neutral particles (N_n^0).* Among the remaining 155 stars, there were stars of the type $N_n^1 + N_n^2$, which cannot be distinguished from proton-produced stars N_p because of fast secondaries (with range $R >$ 8 cm Pb). If we consider the stars produced by primary particles arriving within the angle of 35° then the number of stars N_p^1† with one secondary emitted at an angle $\leq 35°$ with respect to the primary amounts to ~ 12% of $N_p^0 + N_n^1$. If the direction of the primaries is arbitrary, then

$$N_p^1 \sim 0.3\,(N_p^0 + N_n^1).$$

If we consider therefore the stars having not more than one fast secondary ($N_p^0 + N_p^1$; $N_n^0 + N_n^1$), the ratio of star producing protons N_p to star-producing neutrons N_n of ~ 30 Bev in cosmic radiation at 3250 m altitude is equal to 1.2 ± 0.16.

In conclusion, the author wishes to express his gratitude to his supervisor A. I. Alikhanian, and to A. V. Khrimian, T. L. Asatiani, and V. Sh. Kamalian who helped in the course of the work.

---

[1] Alikhanian, Daion, and Kharitonov, J. Exptl. Theoret. Phys. (U.S.S.R.) **19**, 739 (1949).

[2] A. V. Khrimian, Dokl. Akad. Nauk SSSR **85**, 75 (1952); V. Sh. Kamalian, and A. I. Alikhanian, Dokl. Akad. Nauk SSSR **97**, 425 (1954).

[3] A. T. Dadaian and G. Merzon, Dokl. Akad. Nauk SSSR **86**, 259 (1952).

[4] Kocharian, Saakian, Aivazian, Kirakosian, and Aleksanian, Izv. Akad. Nauk ArmSSR **19**, 598 (1955).

[5] T. L. Asatiani and G. V. Khrimian, J. Exptl. Theoret. Phys. (U.S.S.R.) **33**, 561 (1957), Soviet Phys. JETP **6**, 437 (1958).

---

*N_n^k – number of neutron-produced stars with multiplicity k.

†We determined the number of stars with two fast particles ($R > 8$ cm Pb) in the upper hemisphere $N_p^1 + N_n^2$. It was assumed that all these stars were produced by charged particles, i.e. $N_p^1 \gg N_n^2$ and that $N_p^1/N_n^1 = N_p^0/N_n^0$.

[6] Powell, Camerini, et al. Usp. Fiz. Nauk **40**, 76 (1950).

[7] Alikhanian, Alikhanov, Morozov, Muskhelishvili, and Khrimian, J. Exptl. Theoret. Phys. (U.S.S.R.) **18**, 673 (1948).

[8] N. M. Kocharian, Doctoral Dissertation, Phys. Inst. Armenian S.S.R., 1954.

[9] Alikhanian, Shostakovich, Dadaian, Fedorov, and Deriagin, J. Exptl. Theoret. Phys. **31**, 955 (1956), Soviet Phys. JETP **4**, 817 (1957).

[10] Alikhanov, Eliseev, Kamalian, Liubimov, and Khrimian. J. Exptl. Theoret. Phys. (U.S.S.R.) (in print).

Translated by H. Kasha
234

SOVIET PHYSICS JETP VOLUME 35(8), NUMBER 5 MAY, 1959

EFFECT OF UNIFORM COMPRESSION ON THE OSCILLATION OF THE MAGNETIC SUSCEPTIBILITY OF BISMUTH AT LOW TEMPERATURES

N. V. BRANDT and V. A. VENTTSEL'

Moscow State University

Submitted to JETP editor January 24, 1958; resubmitted August 5, 1958

J. Exptl. Theoret. Phys. (U.S.S.R.) 35, 1083-1087 (November, 1958)

The influence of approximately 1000 atmospheres of hydrostatic pressure on the oscillation of the magnetic susceptibility of bismuth in magnetic fields up to 13,000 oersteds has been investigated at 4.2° to 1.6°K. The character of variation of the effective mass tensor, the Fermi energy E_0, the Dingle factor, and the electron concentration have been estimated by means of Landau's equations. Suggestions are made regarding the nature of the electron energy spectrum in bismuth.

IN earlier papers[1-3] concerning the influence of pressure on the galvanomagnetic properties of bismuth it was suggested that it might be possible to observe an appreciable pressure effect on the quantum oscillations of the magnetic susceptibility of metals in a magnetic field H at low temperatures, even under not very high pressures. Such an investigation would make it possible to determine the character of deformation of the effective mass tensor in compressed Bi, and would provide an interesting comparison with experimental and theoretical work studying the effect of pressure on the de Haas-van Alphen effect.[1-6]

Measurements were obtained for the three principal orientations of very pure Bi single crystals. The samples were fastened in a special holder inside a magnetically isotropic pressure vessel (Fig. 1),[4] which was joined to the suspension of a torsion balance. Pressures were produced by the method of Lazarev and Kan.[7] However, for the purpose of improving the uniformity of the pressure, aqueous solutions of ethyl alcohol were used instead of water, thus greatly reducing the nonuniform stresses in compressed samples and approximating uniform compression.[8] Pressures were measured according to the elongation of the vessel by means of a simple indicator consisting of two narrow flat springs welded on the vessel at two different heights.

For each sample we recorded the relation between the moment of the forces C acting on the sample in a static magnetic field and the magnetic field direction in a plane perpendicular to the axis of suspension, as well as the dependence of C on the field strength for different directions of the sample at the temperatures 4.2° and 1.6°K. All of these measurements were performed before the samples were subjected to pressure, then under hydrostatic pressure of about 1000 atmos, and finally after release of the pressure. Excellent reproducibility of the results was obtained when the procedure was repeated, which was done four times in some instances. Figure 2 shows some curves of $C/H^2 = \Delta\chi \cdot \sin\psi \cdot \cos\psi$ as a function of $1/H$, where $\Delta\chi$ is the anisotropy of the magnetic susceptibility and ψ is the angle between the principal axis and the magnetic field. The figure shows that a pressure of about 1000 atmos reduces the amplitude of oscillation by about 30%, with the effect increasing somewhat when $\psi \to 0$ and H is reduced; the oscillation frequency E_0/β is also reduced (see Landau's equations in reference 9). Figure 3 shows the change of oscillation frequency under compression as ψ is varied.

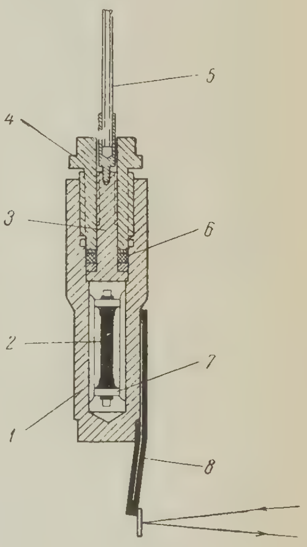

FIG. 1. Construction of pressure vessel: 1) shell; 2) sample; 3) mushroom-shaped pin; 4) cap; 5) glass rod; 6) gaskets; 7) sample holder; 8) pressure indicator with mirror.

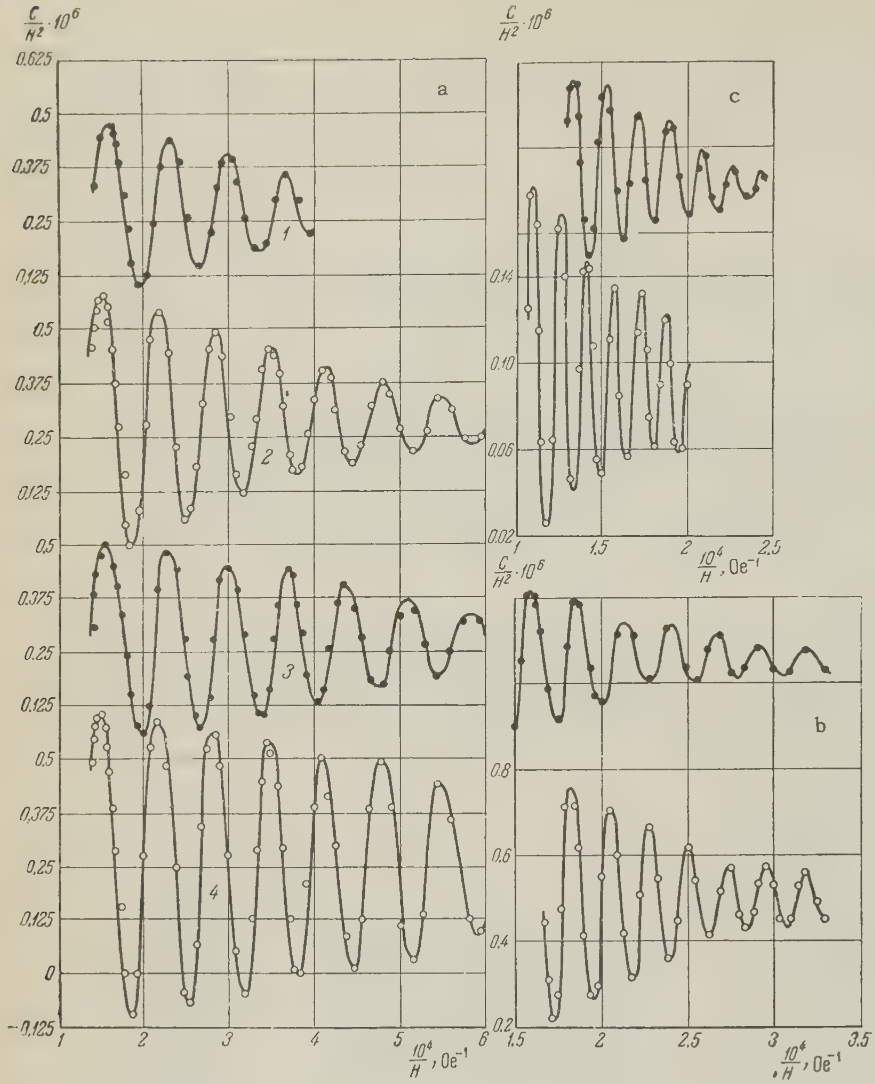

FIG. 2. Anisotropy of the susceptibility of bismuth (with the principal and binary axes perpendicular to the axis of suspension) as a function of magnetic field strength: ○) p = 0, ●) p = 1000 atmos: a) $\psi = 76°$, curves 1 and 2 – T = 4.2°K; curves 3 and 4 – T = 1.6°K; b) $\psi = 170°$, T = 1.6°K; c) $\psi = 175°$, T = 1.6°K.

Curve 1, which is for a sample not under pressure, is a good fit of measurements obtained after pressure was released one or more times. Curves a and b were plotted from the equations used in reference 9. For the two other orientations of the sample we also observed good agreement between the experimental dependence of E_0/β on ψ and the theoretical curves. In addition, the variation of E_0/β under pressure was in qualitative agreement with the data shown in Fig. 4.

Our results are thus in good agreement with Shoenberg's three-ellipsoid model of the Fermi surface for electrons. Since E_0/β is proportional to the extremal area S_m of a section of the Fermi surface cut by a plane perpendicular to the magnetic field direction,[10] we can conclude from Fig. 4 that the deformation of the Fermi surface for bismuth under pressure is not uniform.[4]

It was also found that the change of oscillation phase $\Delta\chi$ under 1000 atmos does not exceed ±10°, and that the change of the anisotropy $\Delta\chi_0$ of the constant part of the magnetic susceptibility is ±2%.

A calculation shows that $\Delta\chi_0 = \chi_\perp - \chi_\|$ for bismuth at the temperature of liquid helium corresponds to the anisotropy of the effective mass tensor for the group of electrons which produce the de Haas–van Alphen effect, but that the calculated absolute values of $\chi_\perp$ and $\chi_\|$ differ from the observed values by an amount of the order of 0.8×10^{-6} emu. Using this fact and assuming that the rotation angle of the Fermi surface ellipsoids does not change under hydrostatic pressure by more than 1 to 2%, we can use Landau's equations to determine the character of the changes in the effective masses m_1, m_2, m_3, and m_4 (in the coordinate system associated with the principal axes of the bismuth lattice) and m_1', m_2' and m_3' (in the coordinate system associated with the principal axes of the ellipsoid), the Fermi energy E_0, the electron concentration n, and the Dingle factor x under uniform pressure (see the table; at p = 0 the data are Shoenberg's[9] and our own; the

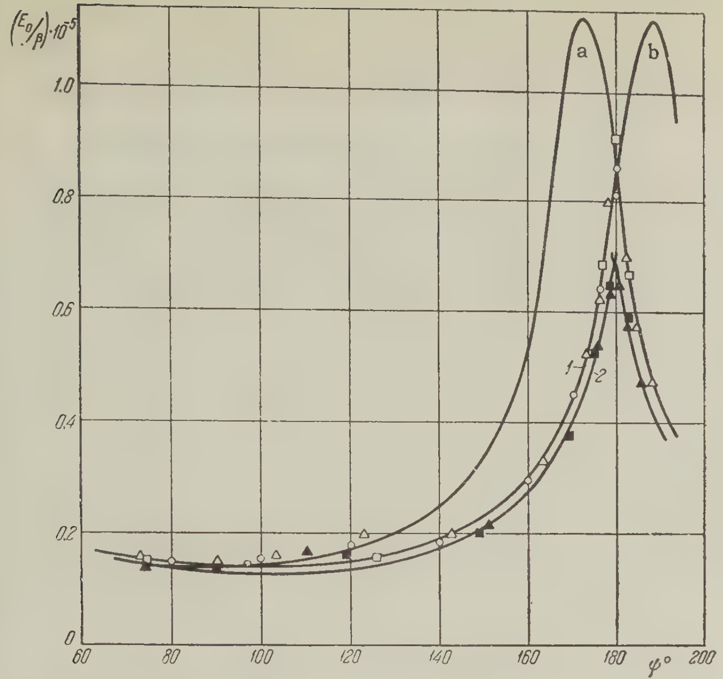

FIG. 3. $E_0/\beta \approx S_m$ for bismuth (principal and binary axes perpendicular to the axis of suspension) as a function of the angle ψ. ⊙) p = 0, △) p_1 removed, ▲) $p_2 \sim 100$ atmos, □) p_2 removed, ■) $p_3 \sim 1000$ atmos.

masses are given in units of the electron mass m_0).

	p = 0	p = 1000 atmos	Relative change under pressure, in %
$m_1 \cdot 10^3$	2.4	1.8±0.2	—25±10
m_2	2.5	2.55±0.12	2±5
m_3	0.05	0.056±0.003	12±5
m_4	—0.25	—0.255±0.012	2±5
$m'_1 \cdot 10^3$	2.4	1.8±0.2	—25±10
m'_2	2.53	2.58±0.12	2±5
m'_3	0.025	0.03±0.001	20±5
$E_0 \cdot 10^{14}$erg	2.81±0.07	2.68±0.07	—5±5
$\frac{E_0}{k}$, °K	204±5	194±5	—5±5
$n \cdot 10^5$	1.42±0.07	1.275±0.075	—10±10
x, °K	1.7±0.1	2.18±0.05	28±10

The good qualitative agreement of the variation of n under pressure with the data in references 1 to 3 is evidence that in bismuth there exists only one electron group corresponding to the Jones-Shoenberg model, and that the character of the deformation of its Fermi surface agrees with the basic ideas of Jones,[11] who considers bismuth to be a metal with an irregular structure. On the basis of this model we may assume that bismuth can contain two groups of holes whose Fermi surfaces are surfaces of revolution located at the corners of the Brillouin zone. One type of holes is represented by one such surface while the second type of holes is represented by two surfaces which transform into each other under rotation around the binary axis.

FIG. 4. Relative variation $\Delta S_m/S_m$ at ≈ 1000 atmos.

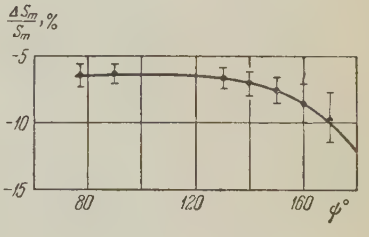

It is quite possible that one group of holes with a nearly spherical Fermi surface, effective mass ~ 0.002 m_0 and Fermi energy ~ 14×10^{-12} erg is associated with the isotropic part of the magnetic susceptibility (0.8×10^{-6}) and that the other group is associated with a large value of the linear term in the specific heat of bismuth.[12] It is of interest that cyclotron resonance experiments have revealed holes with the mass ~ 0.0015 m_0.[13]

In conclusion we wish to thank N. E. Alekseevskii and A. A. Abrikosov for their interest and for valuable comments on the results, Master Technician S. G. Obruchnikov for excellent shop work, and Iu. V. Erofeev for assistance with the measurements.

---

[1] N. B. Brandt, Dissertation, Moscow State University, 1954.

[2] N. E. Alekseevskii and N. B. Brandt, J. Exptl. Theoret. Phys. (U.S.S.R.) **28**, 379 (1955), Soviet Phys. JETP **1**, 384 (1955).

[3] Alekseevskii, Brandt, and Kostina, Izv. Akad. Nauk SSSR, Ser. Fiz. **21**, 790 (1957) [Columbia Tech. Transl. **21**, 792 (1957)].

[4] Berkin, Dmitrenko, and Lazarev, J. Exptl. Theoret. Phys. (U.S.S.R.) **31**, 538 (1956), Soviet Phys. JETP **4**, 432 (1957); **35**, 328 (1958).

[5] Dmitrenko, Verkin, and Lazarev, J. Exptl.

Theoret. Phys. (U.S.S.R.) **33**, 287 (1957), Soviet Phys. JETP **6**, 223 (1958).

[6] A. M. Kosevich, J. Exptl. Theoret. Phys. (U.S.S.R.) **35**, 249 (1958), Soviet Phys. JETP **8**, 171 (1959).

[7] B. G. Lazarev and L. S. Kan, J. Exptl. Theoret. Phys. (U.S.S.R.) **14**, 470 (1944).

[8] N. B. Brandt and A. K. Tomashik, **Приборы и техника эксперимента** (Instruments and Measurement Engineering) **2**, 113 (1958); **Журнал общей химии** (J. Gen. Chem.) (in press).

[9] D. Shoenberg, Phil. Trans. Roy. Soc. (London) **A245**, 1 (1952); Proc. Roy. Soc. (London) **A170**, 341 (1939).

[10] I. M. Lifshitz and A. M. Kosevich, Dokl. Akad. Nauk SSSR **96**, 963 (1954); J. Exptl. Theoret. Phys. (U.S.S.R.) **29**, 730 (1955), Soviet Phys. JETP **2**, 636 (1956).

[11] H. Jones, Proc. Roy. Soc. (London) **A144**, 225 (1934); **A147**, 396 (1934).

[12] P. G. Strelkov and I. N. Kalinkina, J. Exptl. Theoret. Phys. (U.S.S.R.) **34**, 616 (1958), Soviet Phys. JETP **7**, 426 (1958).

[13] Galt, Yager, Merritt, Cetlin, and Dail, Phys. Rev. **100**, 748 (1955).

Translated by I. Emin
235

SOVIET PHYSICS JETP VOLUME 35(8), NUMBER 5 MAY, 1959

MEASUREMENT OF COSMIC-RAY INTENSITY IN THE STRATOSPHERE AT VARIOUS ALTITUDES AND LATITUDES

A. N. CHARAKHCH'IAN and T. N. CHARAKHCH'IAN

P. N. Lebedev Physics Institute, Academy of Sciences, U.S.S.R.; Institute of Nuclear Physics, Moscow State University

Submitted to JETP editor May 12, 1958

J. Exptl. Theoret. Phys. (U.S.S.R.) **35**, 1088-1102 (November, 1958)

We present the results of measurement of the altitude dependence of particles of various ranges contained in the soft component of cosmic rays at latitudes 51° and 31°. The altitude dependence of electrons of a given energy is computed from the energy spectrum of the μ-meson production in the atmosphere. The results of the calculations are in good agreement with the results of measurements made at a latitude of 31°. This indicates that the overwhelming majority of the soft-component particles are electrons generated by μ mesons at the indicated latitude. An analysis of the experimental and calculated data for 51° indicates the existence of an excess of electrons with ranges less than two or three g/cm^2. This phenomenon, which is most pronounced at 51°, is most probably due to gamma quanta emitted in the atmosphere in inelastic neutron-evaporation reactions. The energy flux carried away by these surplus short-range electrons is approximately 10% of the total energy flux of the electron component at this latitude.

The cosmic-ray energy flux has been evaluated at latitudes of 2°, 31°, and 51°. Based on these data, and also on data concerning the cosmic-ray particle intensity at the top of the atmosphere at 51° and 31°, an expression has been derived for the energy spectrum of the primary particles. A new value of 0.48 ± 0.04 particles/min-cm^2-sterad has been obtained for the primary cosmic-ray particle flux $(N_p + N_\alpha)$ at the equator (2°).

In spite of the sufficiently numerous measurements made in the upper layers of the atmosphere, no exact data have been obtained as yet on the absolute intensity of the cosmic radiation in the stratosphere. There is poor agreement between the measured values for the total and penetrating radiation in the vertical direction obtained by various authors using Geiger-counter telescopes.

Our own observations show that the discrepancies in the data on the total intensity are due essentially to failure to account for the absorption of particles in the counter and telescope walls. Depending on the type of counter employed, and also depending on the number of counters in the telescopes, the effective wall thickness fluctuates from 0.4 g/cm^2 (reference 1) to 6.0 g/cm^2 (reference 2). The measurements of Pomerantz[3] and Schein,[2] pertaining to latitudes from 52 to 55°, have been made with telescopes with walls 4.2 and 60 g/cm^2 thick, respectively. The values obtained by Pomerantz and Schein are 30 and ~ 40% lower than ours, obtained at 51° with a telescope having an effective counter wall thickness of 0.4 g/cm^2. Such a difference, obtained at the indicated wall thickness, is readily explained from the point of view of the data on the particle-range spectrum in the stratosphere, cited in reference 1.

In the upper layers of the atmosphere, the intensity of the proton component of cosmic radiation becomes commensurate with that of the μ-meson component. Under these conditions it becomes difficult to obtain with the aid of a telescope exact data on the flux of penetrating particles. Upon passing through the telescope absorber (usually 8 to 15 cm of lead), protons with energies less than 2 or 3 Bev form "stars" essentially without penetrating particles. Such protons do not pass through the absorber and do not produce the required coincidence in the telescope. This reduces the measured value of the penetrating-particle flux. On the other hand, the intensity of the penetrating particles may appear to be too high, owing to the presence of high energy protons. The latter is connected with the fact that the aperture ratio of the telescope is higher for protons, and these generate a noticeable number of penetrating particles in the telescope absorber. Because of the indicated apparatus effects, which depend on the energy spectrum of the protons, high-altitude measurements made at different latitudes cannot be compared with each other correctly. A. N. Charakhch'ian[4] overcame these difficulties by separating the single penetrating particles, which pass through the telescope absorber without interaction, from the particles that generate electron-nuclear showers in the telescope absorber. The absolute number of the electron-nuclear showers generated in the telescope absorber (10 cm of lead) was determined from the measured altitude dependence of the showers and from the geometric cross section of the nuclear interaction between the primary cosmic particles in lead. The total intensity of the penetrating components at various altitudes was obtained by adding the measured number of single particles to the number of showers. This led to data that are closer to the exact values of the absolute flux of penetrating particles in the upper layers of the atmosphere at various latitudes.

An important role is played in measurements in the atmosphere by the so-called "side" showers. The measured number of these showers depends on the multiplicity of the selected coincidences, and also on the amount of substance surrounding the telescope in the instrument. To exclude the influence of such showers, additional counters were placed on both sides of the telescope to measure the coincidences produced by the single particles passing through the telescope as well as the coincidences produced by the particles of the side showers.

CALCULATION OF THE INTENSITY OF THE ELECTRON COMPONENT

The calculations are based on the generally accepted premise that the electron-photon component of cosmic radiation in the stratosphere is produced by charged and neutral π mesons, which decay in accordance with the following schemes:

$$\pi^{\pm} \rightarrow \mu^{\pm} + \nu,\ \mu^{\pm} \rightarrow e^{\pm} + 2\nu \text{ and } \pi^{0} \rightarrow 2\gamma.$$

The $\pi^{\pm}$ and π^{0} mesons are produced in the atmosphere by nuclear interactions between high-energy nuclei (in excess of 1.5 Bev).

We used in the calculations the corresponding data from the theory of electromagnetic cascade processes, data on the energy spectrum of the generation of μ mesons in the atmosphere at 51° and 31°, and data on the altitude of the nuclear component that generates the electron-nuclear showers.

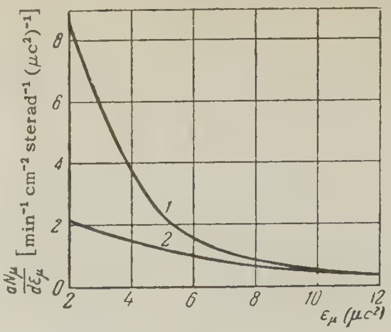

FIG. 1. Energy spectra for the generation of μ mesons in the atmosphere: 1) for 51° latitude; 2) for 31° latitude.

1. A substantial role is played in the calculations by cascades produced by the primary electrons or photons of low energies, on the order of the critical energy for air. We used for this energy range the cascade curves calculated by Ivanenko.[5] For electrons and photons with energies greater than 3×10^{8} ev, the calculations were made with Belen'kii's formulas.[6]

In comparing the calculated data with experiment, it was necessary to estimate the role of the Coulomb scattering of the shower electrons in the atmosphere. We used for this purpose the values of the mean shower-electron deviation angles from reference 7. The angular distribution was assumed to be Gaussian.

The energy spectra for the generation of μ mesons in the stratosphere at 51° and 31° were investigated in references 8 and 9. The resultant spectra of the generated μ mesons are shown in Fig. 1, where the abscissa is the μ-meson energy in μc^2 units, and the ordinate represents the number of μ mesons. For μ-meson energies greater than $10\,\mu c^2$, the spectrum dependence is given by $200/\epsilon$ (references 2 and 6).

3. The variation of the generating component at 31° with altitude was taken to obey the absorption law for nucleons with energies greater than 1.5 Bev, which follows from Grigorov's calculations[10] of the altitude dependence of the nucleon component for 31°. The absorption law selected is quite close to actual one, since Grigorov's results are in good agreement with the experimental data on the absorption of protons with energies greater than 3 Bev in the atmosphere.[11] For primary particles that are sensitive to the earth's magnetic field between latitudes of 51 and 31°, the law of absorption of the generating component was taken in the form $\exp\{-x/b\beta_0\}$, where x is the amount of matter from the top of the atmosphere and $\beta_0 = 120\ \text{g/cm}^2$.

The spectra of the photons generated by π^0 mesons were calculated under the assumption that they are the same as the spectra for the $\pi^{\pm}$ mesons. The primary energy spectrum of electrons at dif-

TABLE I. Calculated values of $M_{\pi 0}$ and M_μ ($\text{min}^{-1}\ \text{cm}^{-2}\ \text{sterad}^{-1}$) for 31° latitude

Electron energy, E′, Mev	$E' > 0$		$E' > 6$		$E' > 26$		$\frac{M_{\pi^0}(>0) - M_{\pi^0}(>6)}{M_{\pi^0}(>0) - M_{\pi^0}(>26)}$	$\frac{M_\mu(>0) - M_\mu(>6)}{M_\mu(>0) - M_\mu(>26)}$
Amount of matter from the top of the atmosphere, t units	M_{π^0}	M_μ	M_{π^0}	M_μ	M_{π^0}	M_μ		
1.4	3,3	2,89	2.52	2.24	1.86	1.67	0.54	0.53
3.0	7.76	3.89	5.56	2,85	3.74	1,91	0.53	0.53
4.6	9.7	3.67	6.92	2.61	4.42	1.65	0.53	0,52
6,2	9,6	3,17	6,68	2.22	4.18	1,36	0,54	0.53
7,8	8.64	2.54	5.68	1.75	3.44	1.08	0.57	0.54
9,8	6,37	1,85	4.27	1.28	2.53	0.79	0.54	0,54
12,2	4.22	1,25	2,78	0,86	1.63	0.52	0.55	0.53
14.6	2.58	0.88	1.64	0.58	0.99	0.35	0.59	0,57

TABLE II. Calculated values of $M_{\pi 0}$ and M_μ ($\text{min}^{-1}\ \text{cm}^{-2}\ \text{sterad}^{-1}$) for the latitude difference (51°—31°)

Electron energy, E′, Mev	$E' > 0$		$E' > 6$		$E' > 26$		$\frac{M_{\pi^0}(>0) - M_{\pi^0}(>6)}{M_{\pi^0}(>0) - M_{\pi^0}(>26)}$	$\frac{M_\mu(>0) - M_\mu(>6)}{M_\mu(>0) - M_\mu(>26)}$
Amount of matter from the top of the atmosphere, t units	M_{π^0}	M_μ	M_{π^0}	M_μ	M_{π^0}	M_μ		
1.4	3,10	3,06	2.36	2,42	1,66	1,74	0,51	0.49
3,0	4,86	3,17	3.57	2,33	2,34	1.46	0.51	0.49
4.6	4,49	2.77	3,18	2.01	1,90	1,24	0.51	0,50
6,2	3.33	1,88	2.28	1,26	1.30	0,74	0.52	0,51
7.8	2,34	1,09	1.48	0,74	0,85	0,43	0,57	0.53
9.8	1,29	0.55	0.62	0.28	0,50	0,21	0.57	0.51
12.2	0.68	0.25	0.45	0,17	0.26	0,10	0.55	0.53
14,6	0,38	0,13	0.26	0.08	0,14	0,05	0.57	0,56

TABLE III

Al, g/cm²	E, Mev	Al, g/cm²	E, Mev
0,4	1.2	2.0	5,8
0.9	2.6	6.6	25,0
1.2	3.3	11,4	45,0

ferent altitudes was calculated from the spectrum of the decay electrons of a μ meson at rest, with allowance for the energy distribution of the decaying μ mesons over the altitude.[8]

Experimental data on the intensity of the soft component at 31° are best reconciled with the calculated data if the ratio of the energy carried by the π^0 mesons to that carried by the $\pi^\pm$ mesons is taken as $k = 0.4$.

Tables I and II list some of the results of the calculations. Here $M_{\pi 0}$ and M_μ are the intensities of the electrons obtained by decay of π^0 and μ mesons, respectively. The data in the last columns of the tables characterize the variation with pressure of the energy spectra of the electrons with energies less than 26 Mev.

We thus draw the following conclusions from the calculations: (1) The number of electrons formed by decay of π^0 mesons exceeds the number of electrons due to decay of μ mesons at practically all altitudes. (2) The energy spectra of low-energy electrons (< 26 Mev) are practically the same for both latitudes and depend little on the pressure.

It follows from a calculation of the Coulomb scattering of the electrons in the atmosphere that as the altitude increases the energy spectrum of the electrons becomes richer in low-energy electrons. This circumstance offers the most probable explanation for the fact, noted in reference 1, that the soft-component particle-range spectrum softens with increasing observation altitude.

The calculated energy spectrum of the electrons in the atmosphere differs from the Tamm-Belen'kii equilibrium electron spectrum lies essentially in the low-energy region. The relative number of electrons with energies less than 20 Mev near the maximum intensity in the atmosphere is approximately 25% less than the relative number of electrons of the same energy as given by the Tamm-Belen'kii equilibrium spectrum.

Table III gives the dependence of the effective electron range on the electron energy, obtained on the basis of experiments on the absorption of electrons in aluminum.[12]

APPARATUS

The number of charged particles with ranges from 1.2 to 2.0, from 2.0 to 6.6, and from 6.6 to 11.4 g/cm^2 in a vertical direction at latitudes 51° and 31° were measured simultaneously with three telescopes in an instrument with suitable absorbers. The right corner of Fig. 2 shows the placement of the counters in the first telescope, which measures the number of particles in the range interval from 1.2 to 2.0 g/cm^2 of glass. The telescope comprised counters 1 and 2, the coincidence of which produced the control pulse. Three counters in group 3, connected in parallel, were so arranged that single particles passing through telescopes 1 and 2 traversed the effective regions of counters 3. To measure the side showers, the particles of which produce double coincidences, telescopes 1 and 2 were surrounded on both sides by the parallel-connected counters of group 4.

The electronic circuitry described in reference 4 was used to transmit, for each of the telescopes in the instrument, radio signals of the following coincidences: (a) $1 + 2 - (3, 4)$ — coincidences of discharges in telescope counters 1 and 2, when no discharges occur in the remaining counters, including those in group 3. These coincidences are evidence that the particle has passed through less than five counter walls but more than three walls. (b) $1 + 2 + 3 - (4)$ — coincidences of discharges in counters 1, 2, 3 without discharges in counters 4 (these coincidences correspond to the registration of single particles). (c) $1 + 2 + 4 - 3$ and $1 + 2 + 3 + 4$ — coincidences in which counters 4 operated, and which were due essentially to side showers.

The thickness of one wall in counters 1, 2, or 3 is 1.2 mm of glass in the radial direction. Assuming the particles travel along the chords, the effective counter of thickness is increased by approximately 20%. Thus, three counter walls correspond to 1.2 g/cm^2, and five walls correspond to 2 g/cm^2. In the second telescope, where a 3-mm aluminum plate was placed between counters 1 and 2 and a 14 mm aluminum plate was placed between counters 2 and 3, the coincidences $1 + 2 - (3, 4)$ corresponded to the number of particles with ranges in the interval from 2.0 to 6.6 g/cm^2 of aluminum. In the third telescope, 20 mm of aluminum was placed between counters 1 and 2 and 14 mm of aluminum between counters 2 and 3. The coincidences $1 + 2 - (3, 4)$ corresponded there to the number of particles with ranges in the interval from 6.6 to 10.4 g/cm^2 of aluminum. The effective length of counters 1, 2 and 4 was 190 mm and that of the counters of group 3 was 300 mm. The inside diameter was 20 mm in all counters. The distance between centers of counters 1 and 2 was 150 mm. The telescopes were calibrated, with an accuracy of approximately 1.5%, against the measured intensity of the hard component on the surface of the earth at 51°. This intensity is 0.46 particles/min-cm^2-sterad with a 10-cm lead absorber. In the processing of the measurement results, allowance was made for the increased aperture of the telescopes with altitude. At an altitude corresponding to a pressure of 40 g/cm^2, this increase (above sea level) amounts to 10%. Measurements at 51° were taken on April 1, 1952, and on May 29 and September 4, 1954. The measurements at 31° were made on August 6, 12, and 30, 1955.

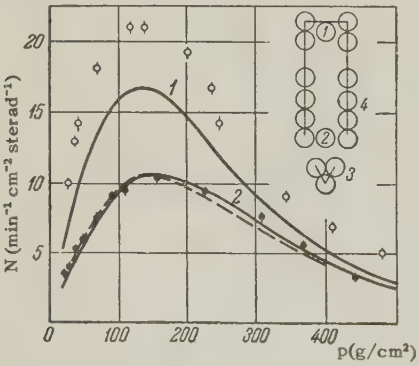

FIG. 2. Altitude dependence of the number of particles of the soft component with ranges more than 1.2 g/cm^2 of glass: o) experimental data at 51°, •) experimental data at 31°. Solid curves — calculated electron component: 1) for 51°; 2) for 31°. Dotted curve — results of calculation with allowance for the Coulomb scattering of electrons in the atmosphere at 31°.

MEASUREMENT RESULTS

The results of the measurement of the total intensity of the particles are best presented in the form of two plots, one of the intensity of the penetrating particles, and one of the intensity of the

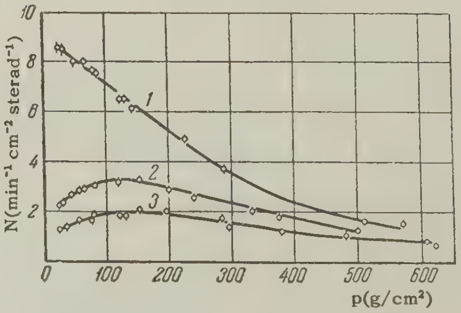

FIG. 3. Altitude dependence of the intensity of penetrating particles (with a 10 cm lead absorber) at the following geomagnetic latitudes: 1) 51°, 2) 31°, 3) 2°.

so-called soft component, obtained by subtracting the number of penetrating particles from the total number of particles. This makes it possible to separate, as a first approximation, the electronic from the non-electronic components. The altitude dependence of the intensity of the penetrating particles (for a 10-cm lead absorber), taken from reference 4 for altitudes 51°, 31° and 2°, is shown in Fig. 3. The corresponding variation of the intensity of the soft-component particles (with ranges greater than 1.2 g/cm^2 of aluminum) with altitude is represented by the dots of Fig. 2 for 51° and 31°. The smooth curves represent the calculated values (the abscissa indicates the atmospheric pressure in g/cm^2, and the ordinate the number of particles). As can be seen from Fig. 2, the measurement results obtained at 31° are in good agreement with the calculated data. At 51°, the measured intensity of the soft-component particles exceeds the calculated value. However, with only these measurements of the total intensity of the soft-component particles it is difficult to explain the discrepancy between the calculated data for electrons and the measured intensities of the soft-component particles.

Figure 4 shows, for the 31° latitude, the altitude dependence of the number of particles with ranges from 1.2 to 2.0, from 2.0 to 6.6, and from 6.6 to 11.4 g/cm^2 of aluminum and of particles with ranges greater than 11.4 g/cm^2 of aluminum and less than 114 g/cm^2 of lead. The dots indicate the measured results and the smooth curve the calculated values. Disregarding certain discrepancies between the experimental and calculated data for particles with ranges from 1.2 to 2.0 g/cm^2 of aluminum (the meaning of which will be explained below), a comparison of the measures and calculated results, shown in Fig. 4, leads to the conclusion that the theory explains the generation of the electron component in the atmosphere rather well not only qualitatively, but also quantitatively, and that at 31° the soft-component particles in cosmic radiation consist for the most part of electrons.

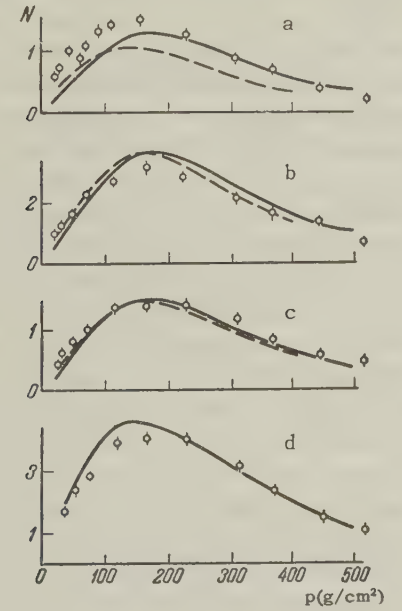

FIG. 4. Altitude dependence of the number of particles (min^{-1} cm^{-2} sterad^{-1}) of the soft-component at 31° for particles with the following ranges: a) from 1.2 to 2.0, b) from 2.0 to 6.6, c) from 6.6 to 11.4 g/cm^2 of aluminum, d) from 11.4 g/cm^2 of aluminum to 114 g/cm^2 of lead; ●) experimental data. Solid curves – calculated results, dotted curves – calculated results with allowance for the Coulomb scattering of electrons in the atmosphere.

Since the measured intensity of the soft-component particles at 31° agrees with the expected intensity for the electrons generated by the π mesons, the excess soft-component particles observed at 51° must be attributed essentially to phenomena caused by primary particles with energies less than 7 Bev (for protons). It is therefore advisable to subtract the 31° data from the measured data obtained at 51°. As a result we obtain the variation with altitude of the difference of the soft-component particle intensity, $N_S^p = N_S^{51°} - N_S^{31°}$. The dots on Fig. 5 show these relations for the same range intervals as for the 31° latitude, while the smooth curves show the results of the calculations. We see that the excess noted above in the total number of soft-component particles at 51° is due essentially to short-range particles (see curve 5a) and to particles with relatively large ranges $R > 11.4$ g/cm^2.

The discrepancey between the measured and

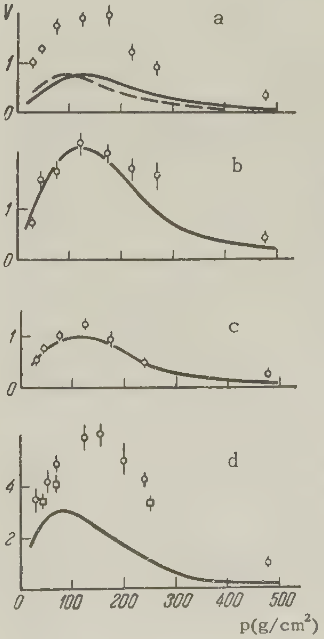

FIG. 5. Variation with altitude of the number of particles $N_s^p = N_s^{51°} - N_s^{31°}$ (min^{-1} cm^{-2} sterad^{-1}) of the soft component, generated by the primary particles with a critical energy less than 7 Bev (for protons), for particles having the following ranges: a) from 1.2 to 2.0, b) from 2.0 to 6.6, c) from 6.6 to 11.4 g/cm^{-2} of aluminum and d) from 11.4 g/cm^2 of aluminum to 114 g/cm^2 of lead. o) experimental data. Dotted curves – calculation with allowance for the Coulomb scattering of electrons in the atmosphere; solid curves – results of calculations.

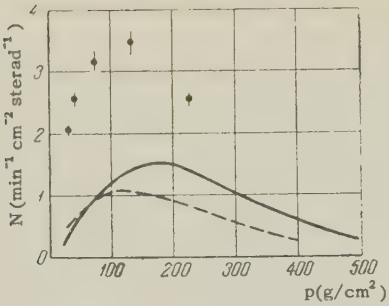

FIG. 6. Variation with altitude of the number of the soft-component particles with ranges in the interval from 0.4 to 0.9 g/cm^2 of glass at a latitude of 51°. ●) experimental data. Solid curve – results of calculation; dotted curve – result of calculations with allowance for the Coulomb scattering of electrons in the atmosphere.

computed values for ranges above 11.4 g/cm^2 of aluminum is attributed to the noticeable number of slow protons, with ranges from 11.4 g/cm^2 of aluminum to 114 g/cm^2 of lead, contained among the particles in this interval. These protons produce an increased ionization (by a factor from 1.5 to 3 times). Rapoport,[13] who measured the ionization spectrum of particles in the stratosphere at 51° latitude with the aid of a pulse ionization chamber, determined the intensity of particles that have this increased ionization. The small squares in Fig. 5d represent the sum of our calculated electron intensity and the intensity obtained by Rapoport for the protons. Consequently, taking into account the intensities of the protons of the corresponding ranges, the measured and calculated results for electrons with ranges more than 11.4 g/cm^2 of aluminum are in satisfactory agreement at 51°, too.

At short ranges, a discrepancy between the calculated and experimental data is found not only for 1.2 to 2.0 g/cm^2 of aluminum, but to an even greater extent for 0.4 to 0.9 g/cm^2 of aluminum. Figure 6 shows the experimental points corresponding to the intensity of particles with ranges from 0.4 to 0.9 g/cm^2 of aluminum at the latitude of 51° (reference 1), and the calculated curve of electron intensity for the same range interval. The assumed existence of a noticeable number of protons among the short-range particles in the above two range intervals contradicts the known data on the excess ionization produced in the stratosphere by the slow protons.[13] In addition, on the basis of the work cited above, Rapoport has concluded that more than 80% of the particles with ranges close to those considered here are light particles (electrons).

A striking fact is that the latitude effect of short-range electrons is large at great depths. At a depth of 500 g/cm^2 this latitude effect, between 51° and 31°, is close to 2. Not a single component of cosmic radiation, with the exception of the star-producing component, has a latitude effect of such order of magnitude at great depths. This suggests that a noticeable portion of the short-range electrons is due to the star-producing component or most readily to its principal portion, the neutrons.

No electrons or photons of low energy are produced in stars generated directly by fast neutrons. However, evaporation neutrons produced in stars are capable of producing hard gamma quanta during nuclear reactions in the atmosphere. At the present time there are no exhaustive data on the hard quanta emitted in reactions between neutrons and nitrogen or oxygen for the entire energy spectrum of the neutrons. Data are available for 14.1-Mev neutrons, for which the cross section of the inelastic reaction with nitrogen amounts to approximately 30% of the total cross section.[14] Since neutrons lose a small fraction of their energy (~ 15%) in elastic reactions, and since hard gamma quanta carry away about half the kinetic energy of the incident neutron in inelastic reactions,[15,16] neutrons with energies from 5 to 15 Mev give up a substantial portion of their energy to gamma quanta as they pass through the atmosphere.

It appears therefore that the excess intensity of short-range electrons obtained by us at 51°, particularly in the region of medium altitudes, is essentially due to the above mechanism of radiation of hard gamma quanta. At the present time it is impossible to give a quantitative estimate of the role of the above phenomenon in the generation of short-range electrons in the atmosphere. Nevertheless, we can attempt to answer the following question: does the intensity of the neutrons generated in the atmosphere seem reasonable if it is assumed that all the energy carried by the excess short-range electrons is due to gamma quanta from neutron reactions in the atmosphere?

From the area under the excess-intensity curve of the short-range electrons, the energy carried away by these electrons is ~ 1.5 Bev min^{-1} cm^{-2} sterad^{-1} (amounting to approximately 10% of the total energy of the electron component). It is reasonable to assume that the average energy of the gamma quanta radiated during neutron reactions in the atmosphere amounts to approximately 5 Mev. To obtain the above 1.5 Bev min^{-1} cm^{-2} sterad^{-1}, we must assume that 300 evaporation neutrons are generated on the average in one min-cm^2-sterad in the entire atmosphere at a latitude of 51°. We can start with the assumption that in the entire atmosphere an intensity equilibrium is established between the evaporation neutrons and the thermal neutrons. Assuming that approximately 30% of the neutrons are absorbed after inelastic nuclear reactions (for example, in reactions $N^{14}(n\alpha)B^{11}$ etc.[16]), the expected number of thermal neutrons in the atmosphere is 200 neutrons (cm^{-2} min^{-1} $sterad^{-1}$).

According to measurement data,[17] the intensity of thermal neutrons in the entire atmosphere at a 51° is 135 neutrons (cm^{-2} min^{-1} $sterad^{-1}$), which is close enough to the value obtained above. This is another argument in favor of the neutron origin of the considerable portion of the excess short-range electrons observed by us.

SPECTRUM OF PRIMARY COSMIC RADIATION

The expressions found in the literature for the spectrum of primary particles are contradictory in that respect, that the spectra obtained in investigations based on the measurement of the intensity of primary particles at different latitudes give for the primary cosmic-ray energy flux a value that is two or three times greater than that obtained experimentally. On the other hand, the spectrum obtained in reference 8 gives for the primary-particle flux values that are 1.5 or 2 times less than would follow from references 19 and 20.

It seems to us that these contradictions are due to the inaccuracy of experimental data used to obtain the primary-particle spectrum. When measuring the particle intensities with the aid of rockets, the backward flux of low energy particles and the showers produced in the rocket housing increase artificially the value of the flux of the primary particles. The lower the latitude at which the measurements are performed, the more do these secondary effects manifest themselves in the experimental results. It is therefore necessary to assume that the authors who made the rocket measurements used exaggerated values of the particle flux to obtain the spectrum of the primary particles, particularly at the equatorial latitude. The data used in reference 18 on the cosmic-ray energy flux at various latitudes are not sufficiently accurate. In particular, owing to the lack of data on the intensity of the electron and μ-meson component, the value of the energy carried away by the neutrino in the decay of μ mesons at various latitudes remains undetermined.

The investigations reported below on the energy spectrum of primary cosmic particles are based on data of the altitude dependence of the electrons studied in this investigation, and also on data on the altitude dependence of the μ-meson and nucleon components, reported in references 8 and 10 for 51°, 31° and 2°. In addition, we used in this work the values of the cosmic-ray intensity on the top of the atmosphere, obtained for 51° and 31°.

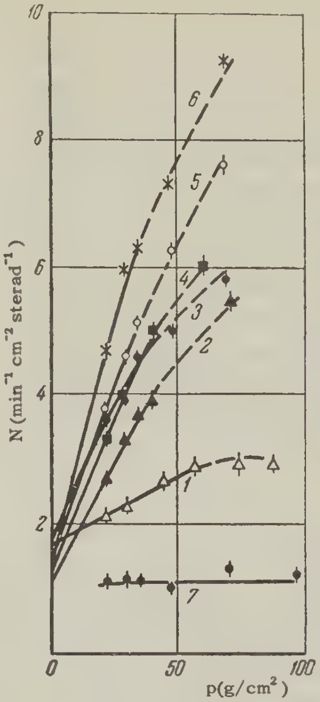

FIG. 7. Variation with altitude at 31°: 1) number of penetrating particles; 2 and 3) number of identical particles with ranges greater than 3 and 10 mm lead; 4, 5, and 6) number of single particles with ranges greater than 11.4, 6.6, and 2.0 g/cm² of aluminum, respectively; 7) number of side showers, obtained when measuring (with a telescope) single particles with ranges greater than 2.0 g/cm² glass.

PRIMARY FLUX OF COSMIC RADIATION AT 31°

In the measurements described above we also obtained data on the intensity of single particles with ranges greater than 2.0, 6.6, and 11.4 g/cm^2 of glass and aluminum, and also with ranges greater than 3 and 10 mm of lead. The results of these measurements, made at low pressures, are shown in Fig. 7, where the ordinates are the measured intensities of single particles and the abscissas the pressure in g/cm^2.

Let us examine the particle intensities obtained by extrapolation of these variations with altitude to the top of the atmosphere. As can be seen from Fig. 7, the straight lines (each of which passes through three measured points on curves 2, 3, 4, 5, and 6) intersect the ordinate axis within an intensity range from 1.2 to 1.9 particles (min^{-1} cm^{-2} $sterad^{-1}$).* Curve 1 of Fig. 7, representing the intensity of the penetrating particles, is based on the data of reference 4. The average value of the flux of primary particles is 1.5 ± 0.1 particles. It is somewhat smaller than the values obtained in reference 21 (1.8 particles) and in reference 22 (2.0 particles). The above error for the particle intensity corresponds to the mean squared deviation from these extrapolations.

---

*Henceforth we shall omit the dimensions min^{-1} cm^{-2} $sterad^{-1}$.

In the measurements we also obtained data on the intensity of the side showers registered with the telescope. The results of one of the measurements are given in Fig. 7 (curve 7). This curve represents the altitude dependence of the intensity of the side showers, obtained when measuring single particles with ranges greater than 2.0 g/cm^2. As can be seen from the diagram, to us the intensity of the showers is almost constant in the pressure range of interest. It is therefore quite likely that the number of showers remains constant to the top of the atmosphere. Under the conditions of our experiments, this gives 1.1 particles, leading to an increase of approximately 60% in the flux of the primary particles.

ENERGY OF PRIMARY COSMIC RADIATION

The energy carried away by the primary cosmic radiation has been determined in the following manner. Knowing the altitude dependence of the intensity of the electron and μ-meson components, we determined the energy carried away by the $\pi^\pm$ and π^0 mesons in the atmosphere. The energy liberated in the atmosphere by slow nucleons[10] is then added to the found π-meson energy.

The initial data for the determination of the energy flux carried away by the π mesons in the atmosphere are the data on the electron component. By calculating the area under the curve of the intensity of the soft component in the altitude interval from the top of the atmosphere to sea level, and multiplying this area by the ionization losses of the electrons in air (2.15×10^6 ev-g^{-1}-cm^{-2}), we find that the energy carried by the electrons with ranges more than 1.2 g/cm^2 of glass amounts to 8.2 ± 0.16 Bev at 31°. On the basis of the calculations performed, this energy must be increased by 25% because of the electrons with ranges greater than 1.2 g/cm^2. Thus, the energy liberated by the electrons in the atmosphere at 31° amounts to 10.2 ± 0.2 Bev.

For the 2° latitude, there are no direct data on the composition of the soft-component particles. Nevertheless, it is quite likely that at this latitude, as at 31°, the predominant portion of the soft component is made up of electrons. When evaluating the electron energy at 2° from the data of reference 23, the area under the soft-component intensity curve is reduced by 8% (because the side showers have not been excluded in the measurements made at 2°) and is increased by 25% (on account of the electrons with ranges less than 1.2 g/cm^2). After introducing these corrections, the electron energy liberated in the atmosphere at 2° latitude becomes 6.10 ± 0.2 Bev.

It was shown above that at 51° the soft component contains a noticeable number of slow protons. In addition, a considerable portion of the electrons with ranges less than 2 or 3 g/cm^2 is generated not by π mesons, but by gamma quanta emitted upon interaction of the evaporation neutrons in the atmosphere.* The energy of the electron-photon component, due to π mesons at 51°, is therefore best determined from the calculations. These yield a value of 13.5 Bev.

Starting with the known π-meson decay schemes ($\pi^\pm \rightarrow \mu^\pm + \nu$, $\mu^\pm \rightarrow e^\pm + 2\nu$, and $\pi^0 \rightarrow 2\nu$) it is possible to obtain a relation between the energy of the electron component and the energy carried by the π mesons in the atmosphere. The energy transferred to the electron component in the process of decay of charged π-mesons is

$$ {}^1/_3\left(\frac{m_\mu}{m_\pi}E_{\pi\pm} - E_{\mu\,\text{ion}}\right), $$

where $E_{\pi^\pm}$ is the energy carried by the $\pi^\pm$ mesons; $E_{\mu\,\text{ion}}$ is the energy lost by the μ mesons to ionization in the atmosphere and in the soil; m_μ and m_π are the rest masses of the μ and π mesons. Adding to this energy the energy E_{π^0} of the neutral π mesons, we obtain for the energy of the electron component in the atmosphere

$$ E_e = {}^1/_3\left(\frac{m_\mu}{m_\pi}E_\pi - E_{\mu\,\text{ion}}\right) + E_{\pi^0}. $$

After suitable transformations, we obtain for the total energy of the $\pi^\pm$ and π^0 mesons, at $m_\mu/m_\pi = 0.78$:

$$ E_{\pi\pm} + E_{\pi^0} = \frac{1+k}{0.26+k}\left(E_e + {}^1/_3\,E_{\mu\,\text{ion}}\right), \qquad (1) $$

where k is the ratio $E_{\pi^0}/E_{\pi^\pm}$.

The energy lost by the μ mesons to ionization in the atmosphere at 51°, 31°, and 2° was determined from the areas under the corresponding penetrating-particle intensity curves (Fig. 3), with correction for the intensity of the protons, the variation with altitude of which was determined from the variation with altitude of the electron-nuclear showers.[21] The energy carried by the mesons at sea level was taken to be 2.0 Bev.

The value of the ratio $k = E_{\pi^0}/E_{\pi^\pm}$ in formula (1) has not been established experimentally with sufficient accuracy. According to the data of the

---

*These two sources of soft-component particles are naturally also present at 31° latitude. But the contribution of such particles to the soft component, compared with the number of electrons due to generation of π mesons in the atmosphere, is much less at 31° than at 51°.

TABLE IV

Geomagnetic latitude	2°	31°	51°
Energy flux *carried by π mesons, $E_{\pi^\pm} + E_{\pi^0}$	15.5±0.5	24.8±0.5	32.5±0.5
Energy consumed in nuclear disintegration, E_{nuc}.	3.2±0.3	5.6±0.4	22.5±1.2
Energy lost to ionization by primary cosmic particles, E_p	0.4±0.04	0.5±0.05	1.7±0.2
Total flux of energy of cosmic radiation $E_\pi + E_{\pi^0} + E_{\text{nuc}} + E_p$	19.1±0.6	30.9±0.6	56.7±1.3
Flux of primary particles $N_p + N_\alpha$, $\text{min}^{-1}\ \text{cm}^{-2}\ \text{sterad}^{-1}$	9.0	1.5±0.1	0.48±0.04

*The energy is given in $\text{Bev-min}^{-1}\text{-cm}^{-2}\text{-sterad}^{-1}$.

present work, this ratio in the stratosphere at 31° is 0.4, and at any rate not greater than 0.5. We assume $k = 0.4$ regardless of the latitude. The inaccuracy admitted in the value of k cannot influence the results substantially. Thus, for example, the total energy $E_{\pi^\pm} + E_{\pi^0}$ will be only 7% greater at $k = 0.4$ than at $k = 0.5$, and 8% less when $k = 0.3$.

Inserting into expression (1) the values of E_e and $E_{\mu\,\text{ion}}$ for the corresponding latitudes, we obtain the total energy carried by the charged and neutral π mesons at geomagnetic latitudes of 51°, 31°, and 2°. These data are given in the first line of Table IV.

In the generation of the electron component in the atmosphere, a certain role is played by the π and μ mesons, which come from the decay of K mesons. In this case the fraction of the energy that goes to the neutrino will be greater compared with the fraction of the neutrino energy accounted for by formula (1), the latter being obtained under the assumption that all the charged mesons are formed directly in nuclear interactions. However this hardly affects our results, as can be seen from the following example. We can assume, for example, for a latitude of 2°, that the energy carried away by the charged K mesons amounts to 0.25 of the total energy of the charged π and K mesons, and that the neutral to charged π meson energy ratio is 0.5. Then, in the decay of a K meson into a π meson and two neutrinos, when the energy carried away by the neutrino is maximum, the energy flux of the cosmic radiation at 2° increases by only 5%.

The second line of the table gives the energies E_{nuc} going into nuclear disintegration, as given in reference 10. The value of E_{nuc} cited for 51° is increased by 30%, owing to the need for considering that approximately 20% of the global flux of charged particles at this latitude is due to nuclear disintegration. The third line of the table gives the energy lost to ionization by primary particles. The values of the total energy liberated in the atmosphere by cosmic radiation are given in the fourth line. The fifth line gives data on the flux of primary particles (for 51°, in accordance with reference 21). The errors in the table are statistical. The value for 2°, which will be discussed below, was obtained in the present work.

EMPIRICAL EXPRESSION FOR THE ENERGY SPECTRUM OF THE PRIMARY PARTICLES

With data on hand on the flux of energy of cosmic radiation at 51°, 31°, and 2°, and with a definite assumption made regarding the α particle to proton intensity ratio in the primary radiation, it is possible to find the energy spectrum of the primary particles. At the present time there is no agreement on primary-proton to α-particle intensity ratio. However, the available experimental data do not contradict the opinion that the fraction of the particles in the total flux is independent of the latitude.

For primary particles with energies that are not too low, it is advisable to use first a power-type spectrum of the type $\epsilon^{-\bar{\gamma}}$, where $\bar{\gamma}$ is a constant. In this case the relation between the energy flux U_p and the intensity $N_p(>\epsilon_p)$ of the primary protons has the simple form

$$U_p = N_p(>\varepsilon_p)\,\frac{\bar{\gamma}-1}{\bar{\gamma}-2}\,\varepsilon_p, \tag{2}$$

where ϵ_p is the kinetic energy of the protons.

It follows from Eq. (2) that if the values of U_p and ϵ_p are specified, the value of the flux $N_p(>\epsilon_p)$ will increase with increasing $\bar{\gamma}$. The experimental data lead to the assumption that $\bar{\gamma} \le 3.0$. Taking $\bar{\gamma} = 3.0$ we find an upper limit for the intensity $N_p\ (>\epsilon_p)$.

For the 2° latitude, the flux of the cosmic-ray energy is 19.1 ± 0.6 Bev. The energy flux carried by the protons is accordingly 13.3 Bev. Inserting this value for U_p and a value of 14 Bev for ϵ_p into Eq. (2), we find that $N_p^{2°}$ (> 14) ≤ 0.48 protons. Performing analogous operations for the 31° latitude, we find that $N_p^{31°}$ (> 7) ≤ 1.6 protons. Measurements of the intensity of primary particles at these latitudes should give results that are in agreement with the preceding inequalities. From this point of view, our value of the total intensity of the primary particles at 31° appears sensible.

We obtain the flux of the primary protons at 2° with the aid of relation (2), which we apply to the 2° and 31° latitudes:

$$N_p^{2°}(>\varepsilon_p^{2°}) = (U_p^{2°}/U_p^{31°})(\varepsilon_p^{31°}/\varepsilon_p^{2°})N_p^{31°}(>\varepsilon_p^{31°}), \qquad (3)$$

where $\epsilon_p^{2°} = 14.0$ Bev and $\epsilon_p^{31°} = 7.0$ Bev.

We assume that $U_p^{2°}/U_p^{31°}$ equals the corresponding ratio of the fluxes of the total energy of the cosmic radiation, and that $N_p^{31°}$ amount to 85% of the total flux of primary particles. Inserting these values into (3) we find that $N_p^{2°}$ (14) = 0.41 ± 0.03 protons. Accordingly, the total flux of the primary particles $N_p + N_\alpha$ will be 0.48 ± 0.04 particles at 2°.

With the aid of a power-law energy spectrum it is possible to obtain the ratio

$$(\varepsilon_p^{31°}/\varepsilon_p^{2°})^{\bar{\gamma}-2} = U_p^{31°}/U_p^{2°},$$

from which we get $\bar{\gamma} - 2 = 0.7 \pm 0.05$.

It is preferable to represent the general empirical expression for a primary-particle integral energy spectrum that satisfies the experimental data at the three latitudes, 51°, 31°, and 2°, in the following form

$$N_p(>\varepsilon_p) = \frac{A_p}{(\varepsilon_p+2)^{\gamma-1}} - \frac{A_p'}{(\varepsilon_p+2)^{2\gamma-1}};$$
$$N_\alpha(>\varepsilon_\alpha) = \frac{A_\alpha}{(\varepsilon_\alpha+5)^{\gamma'-1}} - \frac{A_\alpha'}{(\varepsilon_\alpha+5)^{2\gamma'-1}}. \qquad (4)$$

Here the first expression is for protons and the second for α particles, while ϵ_p and ϵ_α are the kinetic energies of the primary protons and the primary α particles, in Bev. The other quantities in the right halves of the equations are constant, including γ and γ'. The terms 2 and 5 in Eq. (4) are so chosen as to make the ratio $(\epsilon_\alpha + 5)/(\epsilon_p + 2)$ independent of ϵ_α and ϵ_p. This ratio is equal to 2, accurate to within 3 or 4%, for $\epsilon_p > 1.5$ and accordingly $\epsilon_\alpha > 2.2$ Bev (values of the critical energies at 51°). If $\gamma = \gamma'$, the integral spectra of the protons and α particles will be similar, and the fraction of the α particles will be independent of the latitude. The constants A_p, A_p' for N_p $(> \epsilon_p)$ and A_α, A_α' for N_α $(> \epsilon_\alpha)$ in Eq. (4) are chosen such as to make the value of the primary-particle flux at 51°, for definite values of the index γ, equal to none particles,[21] with 85% of this value pertaining to protons and 15% to α particles. This value of the flux of primary particles at 51° is quite accurate and has been well confirmed in supplementary experiments performed by us at this latitude.

TABLE V

Geomatic latitude	Exponent	Flux of primary cosmic-radition energy (Bev-min^{-1} cm^{-2}-sterad^{-1})	Intensity of primary cosmic particles (min^{-1} cm^{-2} sterad^{-1})
2°	2.8	28.7	0.70
	3.0	18.6	0.50
	3.2	12.4	0.38
	Experiment	19.1±0.6	0.48±0.04
31°	2.8	43.2	1.96
	3.0	31.0	1.60
	3.2	23.2	1.30
	Experiment	30.8±0.6	1.5±0.1
51°	2.8	69.5	9.0
	3.0	58.3	9.0
	3.2	51.0	9.0
	Experiment	56.7±1.3	9.0

With the aid of the spectra (4), we calculated the energy fluxes at 51°, 31°, and 2° and the intensities of the primary cosmic particles at 31° and 2° for values of γ of 2.8, 3.0, and 3.2. These data are given in Table V. The third column of the table gives the values of the total energy carried by the primary protons, α particles, and particles with charge $Z \geq 3$ (the energy flux carried by the particles with charge $Z \geq 3$ has been estimated to be approximately 20% of the energy flux carried by the α particles). The fourth column gives the values of the flux of primary particles $N_p + N_\alpha$. The table gives also experimental data for the corresponding latitudes, taken from Table IV. As can be seen from Table V, a good description of the experimental data is obtained when the index is $\gamma = 3.0$. For $\gamma = 3.0$, the spectra (4), written with the numerical values of the constants, become

$$N_p(>\varepsilon_p) = 110/(\varepsilon_p+2)^{\gamma-1} - 700/(\varepsilon_p+2)^{2\gamma-1},$$
$$50 > \varepsilon_p \geqslant 1.5;$$
$$N_\alpha(>\varepsilon_\alpha) = 80/(\varepsilon_\alpha+5)^{\gamma-1} - 4\cdot 10^3/(\varepsilon_\alpha+5)^{2\gamma-1}, \qquad (5)$$
$$100 > \varepsilon_\alpha \geqslant 2.2,$$

where $\gamma = 3.0^{-0.05}_{+0.07}$. The second terms in (5) decrease rapidly with increasing proton and α-particle energies. For $\epsilon_p = 1.5$ Bev and $\epsilon_\alpha = 2.2$ Bev;

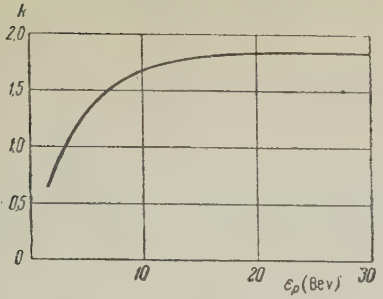

FIG. 8. Dependence of the exponent k on the energy ε for an integral spectrum of primary particles of the type const/ε^k.

the second terms amount to 15% of the first terms. When $\epsilon_p = 4$ Bev and $\epsilon_\alpha = 6.6$ Bev, the second terms diminish by a factor of 6.

Naturally, high-energy primary particles are not effective in our experiments. Only one-third of the flux of cosmic-ray energy at 2° is due to primary particles with energies greater than 50 Bev (for protons). The foregoing energy spectrum (5) cited above is therefore apparently effective up to primary-proton energies of 30 to 50 Bev. We remark that the spectra (5) are equivalent to a power relation of the type const/ϵ^k, where the exponent k is a function of the energy ϵ. The dependence of k on ϵ is illustrated in Fig. 8. It is seen from this diagram that k(ϵ) varies rapidly at first and, at energies of 10 to 20 Bev, reaches values of 1.7 to 1.8, usually obtained in extensive atmospheric showers.

The authors express their deep gratitude to Prof. S. N. Vernov for interest in the work and for a discussion of the results, and also to I. P. Ivanenko for valuable advice on the computations performed.

---

[1] Ageshin, Charkhch'ian, and Charakhch'ian, Izv. Akad. Nauk SSSR, Ser. Fiz. 19, 533 (1955), [Columbia Techn. Transl. 19, 478 (1955)].

[2] M. Vidale and M. Schein, Phys. Rev. 81, 1065 (1951).

[3] M. A. Pomerantz, Phys. Rev. 75, 69 (1949).

[4] A. N. Charakhch'ian, Dissertation, Phys. Inst. Acad. Sci. U.S.S.R., 1952.

[5] I. P. Ivanenko, J. Exptl. Theoret. Phys. (U.S.S.R.) 33, 135 (1957), Soviet Phys. JETP 6, 105 (1958).

[6] S. Z. Belen'kii, Лавинные процессы в космических лучах (Cascade Processes in Cosmic Rays), Gostekhizdat, 1948, p. 101.

[7] S. Z. Belen'kii, ibid. p. 150.

[8] P. N. Ageshin and T. N. Charakhch'ian, Вестник МГУ (Bull. Moscow State Univ.) 2, 77 (1956).

[9] V. F. Tulinov, J. Exptl. Theoret. Phys. (U.S.S.R.) 33, 1163 (1957), Soviet Phys. JETP 6, 894 (1958).

[10] N. L. Grigorov, Usp. Fiz. Nauk 58, 599 (1956).

[11] Vernov, Kulikov, and Charakhch'ian, Izv. Akad. Nauk SSSR, Ser. Fiz. 17, 13 (1953).

[12] Johns, Cunningham, and Katz, Phys. Rev. 83, 952 (1951). F. L. Hereford and C. P. Swann, Phys. Rev. 78, 727 (1950).

[13] I. D. Rapoport, Izv. Akad. Nauk SSSR, Ser. Fiz. 19, 519 (1955) [Columbia Techn. Transl. 19, 466 (1955)].

[14] J. R. Smith, Phys. Rev. 95, 730 (1954).

[15] Scherrer, Thens, and Faust, Phys. Rev. 91, 1476 (1953).

[16] F. Ajzenberg and L. Lauritsen, Revs. Modern Phys. 27, 132 (1955).

[17] C. L. Yuan, Phys. Rev. 81, 175 (1951).

[18] G. Nier, Physics of Cosmic Rays, (Russ. Transl) IIL, 1954, p 251.

[19] Winckler, Stok, Dwight, and Sabin, Phys. Rev. 79, 656 (1950).

[20] I. A. Van Allen and S. F. Singer, Phys. Rev. 78, 819 (1950); 80, 116 (1950).

[21] S. N. Vernov and A. N. Charakhch'ian, Dokl. Akad. Nauk SSSR 91, 487 (1953).

[22] K. I. Alekseeva and N. L. Grigorov, Dokl. Akad. Nauk SSSR 115, 259 (1957), Soviet Phys. "Doklady" 2, 317 (1957).

[23] Vernov, Kulikov, and Charakhch'ian, Dokl. Akad. Nauk SSSR, 85, 525 (1952).

Translated by J. G. Adashko
236

SOVIET PHYSICS JETP VOLUME 35(8), NUMBER 5 MAY, 1959

A RADIOCHEMICAL STUDY OF THE (*p*, *pxn*), (*p*, *4pxn*), AND (*p*, *5pxn*) REACTIONS

T. V. MALYSHEVA and I. P. ALIMARIN

Institute of Geochemistry and Analytical Chemistry, Academy of Sciences, U.S.S.R.

Submitted to JETP editor May 17, 1958

J. Exptl. Theoret. Phys. (U.S.S.R.) **35**, 1103-1112 (November, 1958)

A radiochemical investigation of the isotopes of bismuth, mercury, and gold produced in the disintegration of bismuth by 660-Mev protons has been carried out. A method for quantitative determination of the radio isotopes, based on L radiation, is proposed for isotopes that have undergone elementary capture. The half-life of Hg^{193} (4 hr) and the E capture in the gold isomer Au^{193m} have been determined by successive extraction of the daughter fraction. The dependence of the yields of the reactions (p, pxn), (p, 4pxn) and (p, 5pxn) on the number of neutrons emitted leads to certain conclusions regarding the mechanism of disintegration of complex nuclei by high-energy protons.

INTRODUCTION

THE reactions (p, pxn), (p, 4pxn), and (p, 5pxn) take place when complex nuclei interact with high-energy protons. The target employed to study these reactions can be an element with only one stable isotope. In the case of medium nuclei, these reactions have been studied for the interaction between protons of various energies with cobalt (60, 100, 170, 240, 370 Mev),[1,2] yttrium (240 Mev),[3] cesium,[4] and tantalum (340 Mev).[5] Whenever several isotopes of the same element could be separated, it was observed that the yield of the (p, 4pxn) and (p, 5pxn) reactions tends to increase as x increases to the maximum, while the yield of the reaction (p, pxn) decreases.

As to heavy nuclei, a study was made of the disintegration of uranium and thorium by 340-Mev protons.[6] The same dependence is observed for these reactions as for light nuclei, but the situation is masked here by the competing fission process, particularly in the case of uranium. The disintegration of bismuth was studied by bombarding it with 375- and 450-Mev,[7] 480-Mev,[8,9] and 660-Mev protons.[9] But in none of these investigations were the yields of more than two or three isotopes of the same element determined. This is explained by the complexity of the decay schemes of heavy nuclei, and also by the lack of a satisfactory procedure for counting the radio isotopes that decay via E capture.

In reference 7, which deals with disintegration of bismuth, the yields of the radio isotopes that disintegrate by E capture have not been corrected for the efficiency of the counting apparatus. In other papers, the count of the radioactivity of the isotopes experiencing capture of an orbital electron, was determined from the K radiation[9] or from the K and L radiation.[8] In either case, to calculate the absolute yields of the above radio isotopes it is necessary to know not only the decay schemes, but also the ratio of the L capture to the K capture, and to take into account the contribution of the soft gamma radiation, the wavelength of which is comparable with that of the K radiation.

It is known[10] that the probability of L capture increases with diminishing transition energy and with increasing forbiddenness of the transition. Theoretical calculations, however, yield a single-valued solution only for the allowed transitions. Since the probability of L_{II} capture in an allowed transition is small, and no L_{III} capture has been observed at all, the ratio of the probabilities of L capture (λ_L) to those of K capture (λ_K) is given by[11]

$$\frac{\lambda_L}{\lambda_K} \sim \frac{\lambda_{L_1}}{\lambda_K} = \left(\frac{W_0 + W_{L_1}}{W_0 + W_K}\right)\frac{g_{L_1}^2}{g_K^2},$$

where g_i is the wave function, W_0 the transition energy, W_i the transition of the i-th level. When $W_0 \gg W_K$ and $W_0 \gg W_{L_1}$, $\lambda_{L_1}/\lambda_K \sim g_{L_1}^2/g_K^2$.

The ratio $g_{L_1}^2/g_K^2$ for allowed transitions, calculated by Rose and Jackson,[12] increases smoothly with increasing mass number and reaches a value of 0.18 for heavy nuclei. At the same time, the experimental L/K capture ratio has a great variety of values for neighboring elements and in some cases, particularly in the range of heavy nuclei, becomes greater than unity.

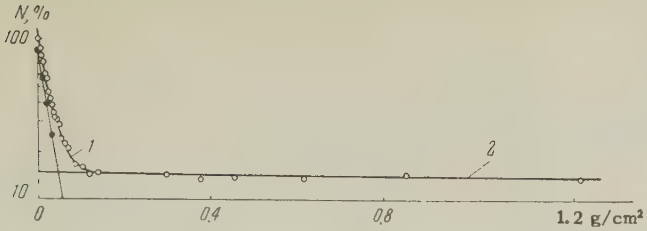

FIG. 1. Absorption curve for electromagnetic radiation from Re^{186} in aluminum: 1) L radiation; 2) gamma background (N is the number of counts as percentage of the initial count).

It follows from the above that at the present time there are not enough theoretical and experimental data on the contribution of L capture in the case of forbidden transitions.

SETUP OF THE EXPERIMENT

In this investigation we studied the reactions (p, pxn), (p, 4pxn) and (p, 5pxn) with radioisotopes of gold, mercury, and bismuth, obtained by disintegrating bismuth with 660-Mev protons. For this purpose, spectrally pure metallic bismuth in quantities of 0.5 or 1 g was irradiated in the internal beam of the synchrocyclotron of the Joint Institute for Nuclear Research. After irradiation, the bismuth was dissolved in concentrated nitric acid and the gold, mercury, and bismuth were separated on suitable isotope carriers. The radioisotopes were identified by their half-lives, by the radiation energy, and by the genetic bonds. The proton current was determined[13] from the yield of the reaction $Al^{27}(p, 3pn)Na^{24}$.

Counting Procedure

To avoid substantial errors due to the indeterminacy in the L/K capture ratio, we determined the activity of the radioisotopes experiencing E capture from their L radiation. This method is effective because K capture is accompanied not only by K radiation but also by L radiation of almost the same intensity. The number of secondary x-ray L quanta that accompany the K capture, can be calculated from the following formula[14]

$$n_L = \omega_K \left(\frac{N_{K_\alpha}}{N_K}\right) + a_K \frac{2(K-LL)+(K-LX)}{\Sigma e_{\text{Auger}}},$$

where ω_K is the fluorescent yield, N_{K_α}/N_k is the ratio of the intensity of the K_α radiation to the intensity of all the K rays, a_K is the number of Auger K electrons, and (K – LX) is the partial yield of the Auger electrons.

The number of secondary L quanta amounts to 80% in the range studied (Z = 80). If the ratio L/K capture ratio is assumed to be unity, the total number of L quanta per decay due to E capture amounts to 0.9. Even at very large deviations of L/K from the chosen value, the error in the estimate of the total number of decays deos not exceed 10%.

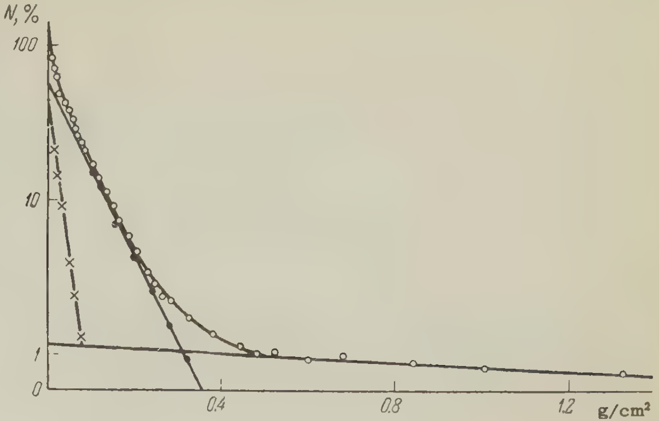

FIG. 2 o) absorption curve of total radiation from Re^{186} in aluminum; ×) L radiation; ●) beta component; solid line – gamma background.

The detector employed was a standard argon-filled TM-20 end counter which transmitted the K radiation and the soft gamma quanta (0.1 to 0.05 Mev) with almost no absorption (efficiency 0.5%), and which recorded x-rays with an efficiency of 20%. The counter efficiency was calculated from the formula

$$Q = 1 - e^{-\mu d},$$

where d is the thickness of the gas layer of the counter in g/cm^2 and μ is the mass absorption coefficient, found from the tables compiled by Allen.[15] In addition to calculating the efficiency, the counts corresponding to the activity of the radioisotope experiencing E capture were corrected for the following factors: (1) absorption of radiation in the counter window, in the air gap, and in the covering of the sample; (2) self-absorption in the source material; (3) background of hard gamma quanta (determined with the aid of a lead absorber); (4) L-fluorescence yield (according to Burhop's data[16]); (5) number of x-ray L quanta and electrons due to internal conversion (using the decay schemes listed in Table III below. The conversion coefficients were determined from the tables of Sliv and Band[17] and Dranitsina.[18]

The sources used to verify the proposed procedure were the radioisotopes Cu^{64} (K_α radiation of wavelength 1.65 A, close to that of the L radiation from the heavy elements) and Re^{186} (L_α with λ = 1.43 A). The number of E captures or β decays per disintegrating atom of either isotope is found in the literature. We first measured the

TABLE I

Isotope	X-ray wavelength, A	Literature data		Data of present investigation	
		Number of beta decays, %	Number of E captures, %	Number of beta decays, %	Number of E captures, %
$_{29}Cu^{64}$	K_α, $\lambda = 1.65$	58	42 [19]	59	41
$_{75}Re^{186}$	L_α, $\lambda = 1.43$	91	9 [20]	93	7
		95	5 [21]		

total activity with a standard end counter and then deflected the charged particles in the magnetic field and registered only the electromagnetic radiation.

An investigation of the absorption of the radiation from Re in aluminum with the magnetic field on (Fig. 1) and off (Fig. 2) has shown that the absorption curves contain none of the component corresponding to K radiation from tungsten, i.e., the A capture is registered only because of the L radiation. The measurement results listed in Table I are in good agreement with literature data. The accuracy of the method amounts to 20 or 30%, without allowance for the error with which the decay scheme is determined.

Determination of the Half-Life of Hg^{193}

In many cases there were no accurate half-lives available for the mercury radioisotopes. Thus, Seaborg's table[22] lists several values for Hg^{193} (10 hours, 14.5 hours, 29.0 hours, and 5 hours) and none for Hg^{194}. To determine the unknown half-lives we used the Neuman and Perlman method,[23] whereby the daughter fractions are separated from the mother substance at equal time intervals, corresponding approximately to the expected half-life of the mother element. If $N_1\lambda_1$ is the activity of the daughter material and k is the counting efficiency of the daughter material, then

$$kN_1\lambda_1 = N_2\lambda_2 \frac{T_2}{T_2 - T_1} (e^{-\lambda_2\tau} - e^{-\lambda_1\tau}),$$

where $N_2\lambda_2$ is the activity of the daughter material and τ is the growth time. When τ = const, the activity of the daughter substance is proportional to the rate of decay of the mother substance at the start of the period.

To determine more exactly the half-life of Hg^{193}, the daughter gold fractions were separated from the mercury every three hours. The component with half-life of 16 hours belonging to Au^{193}, was separated in the decay curves for gold. The rate of decrease in activity of this component was used to determine the half-life of Hg^{193}, which was found to be four hours (Fig. 3).

To prove that the half-life obtained pertains to the ground state of Hg^{193} and not to the isomer Hg^{193m}, we plotted the theoretical curve for the growth of Au^{193} (T = 16 hr) from Hg^{193} (T = 4 hr), shown in Fig. 1. The data obtained in several experiments are in good agreement with the theoretical values.

E Capture of the Au^{193m} Isomer

It follows from the above that the isomer Hg^{193m} (T = 12 hr), if it is formed at all in the disintegration of bismuth, decays via E capture into the isomer Au^{193m} (T = 3.8 sec), which is directly converted, also by capture of an orbital electron, into the isomer Pt^{193m} (T = 3.8 days), bypassing the ground state of gold (Fig. 5). Indications that the transition $Au^{193m} \rightarrow Pt^{193m}$ is possible are found in the paper by Brunner.[24]

To observe the activity of Hg^{193m}, the daughter platinum was separated from the mercury fraction every four hours. To exclude the influence of the mass-191 chain, the mercury was separated from the bismuth every 12 hours after the termination

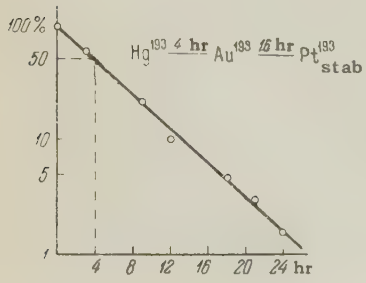

FIG. 3. Radiochemical yield of daughter activity of Au^{193} as a function of time.

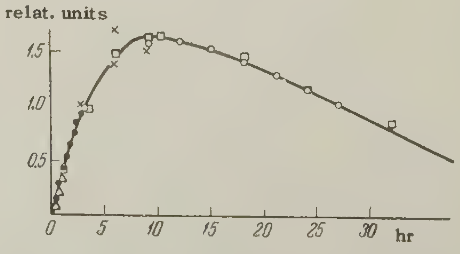

FIG. 4. Growth curve of daughter activity of Au^{193} as a function of time: □) theoretical curve; △, ●, ○, ×) experimental data.

TABLE II

Nucleus	Gamma-transition energy, Mev[26]	Conversion-coefficient ratio, L_{II}/L_{III}[27]	Conversion-coefficient α_{av} (ref. 18)	Transition probability (relative units)
Au^{193m}	0.0324	0.65	17 250	0.03
Au^{195m}	0.0569	1	3 000	0.3
Au^{197m}	0.13	2.5	28	1

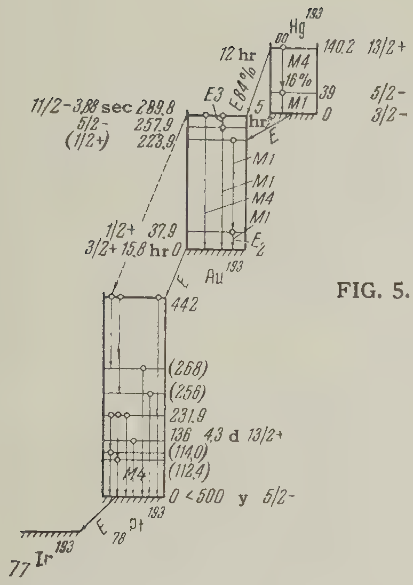

FIG. 5. Decay scheme of Hg^{193}.

of the radiation. From the change of the activity of the platinum (half-life 3.5 days) we found the half-life of Hg^{193m} to be approximately 12 hours. Attempts at observing the three-day activity in the platinum fraction separated from the daughter gold were not successful.

Let us see whether the existence of this transition contradicts the fundamental theoretical premises. The probability of transition of the excited nuclear state for gamma radiation depends on the multipole order of the transition, on the energy of the gamma rays, and on the wave functions of the nuclear states participating in the transition. For specific calculations of the probabilities of the gamma transitions it is necessary to specify some nuclear model. In our case we can consider radiation from an individual proton, moving in the constant field produced by other particles contained in the nucleus. The probability of the electrical 2^L transition can then be expressed by the following Weisskopf formula[25]

$$T_{(EL)} = \frac{4.4\,(L+1)}{L\,[(2L+1)!!]^2}\left(\frac{3}{L+3}\right)^2\left(\frac{\hbar\omega}{197\text{Mev}}\right)^{2L+1}$$

$$\times\, a^{2L} S\,(j_i, L_{jf})\cdot 10^{21}\ \text{sec}^{-1},$$

Where L is the multipole order, $a = 1.45 \times 10^{-13} A^{1/3}$ cm, S is a statistical factor, and $\hbar\omega$ is the gamma-quantum energy in Mev. The resultant transition probability is corrected for the internal conversion of the gamma radiation:

$$T_{(EL)\,(\text{corr})} = T_{(EL)}\,(1+\alpha),$$

where α is the internal-conversion coefficient.

It must be noted that the theoretical calculations are rough and cannot be expected to be able to represent exact transitions in actual nuclei. They can serve, however, as the starting point for the interpretation of the experimental results.

We have estimated the probabilities of the gamma transitions from the 11/2 level to the 5/2 level for Au^{193m}, Au^{195m}, and Au^{197m}. The initial calculated results are listed in Table II.

As can be seen from the results, the probability of radiation transition diminishes rapidly from Au^{197m} to Au^{193}. According to the data of Gillion et al.,[28] the probability of decay by isomer transition diminishes also for Hg^{193m}, Hg^{195m}, and Hg^{197m} (in a ratio of 0.16 : 0.5 : 1). At the same time, the probability of E capture increases with increasing neutron deficit of the isotope, i.e., the capture/emission ratio can be rather large for the nucleus considered.

The above data make it possible to conclude that a $Au^{193m} \rightarrow Pt^{193m}$ transition exists and has an intensity of at least 90% (within the limits of experimental accuracy).

Half-Life of Hg^{194}

To observe the activity due to Hg^{194}, the daughter gold was separated from the mercury fraction at various time intervals (from 20 minutes to 20 hours). The 40-hour activity belonging to Au^{194} was found in none of the separated daughter fractions. The mercury was separated from the bismuth within 45 minutes to one hour after the completion of the irradiation. Consequently, the half-life of Hg^{194} is either large or else is less than ten minutes. The latter is not likely, since the Weisskopf mass formula predicts for the $Hg^{194} \rightarrow Au^{194}$ transition an energy less than 80 kev.

A prolonged measurement of the activity of the mercury fraction (on the order of one year) yielded for the long-lived activity a half-life of 130 days.

TABLE III

Isotope	Type of decay	Half-life		$\sigma \cdot 10^{-27}$ cm²	Decay schemes used, references
		From tables of references 18 and 19	Our data		
$_{79}Au^{191}$	E	3 hr	4 hr	40	[28]
Au^{192}	E, β^+	4,2 »			
Au^{193}	E	15.8 »	16 »	16	[31]
Au^{194}	E, β^+	40 »	39 »	12	[32]
Au^{195}	E	185 d	180 d	1.8	
$_{80}Hg^{190}$	E	90 min	1 hr	12	[33]
Hg^{191}	E	57 »			
Hg^{192}	E, β^+	5,7 hr	5,6 »	22	[28]
Hg^{193m}	E, IT	12 »	11 »	8.3	[33,24]
Hg^{193}	E	5 »	4 »	20	[31,34]
Hg^{194}	E	130 d	130 d	27	[33]
Hg^{195m}	E, IT	40 hr	39 hr	6	[24]
Hg^{195}	E	9.5 »	11 »	12	[32,35]
Hg^{197m}	E, IT	24 »	—	—	—
Hg^{197}	E	65 »	66 »	7	[35]
$_{83}Bi^{201}$	E	2 »	2 »	4	[33]
Bi^{202}	E	95 min		8	[33]
Bi^{203}	E	12 hr	10 »	9	[33,22]
Bi^{204}	E	12 »		21	[33]
Bi^{205}	E	14.5 d	14.5 d	22	[36]
Bi^{206}	E	6,4 »	6.3 »	25	[37]

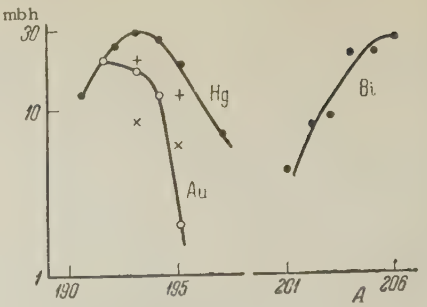

FIG. 6. Dependence of the cross section for the production of radioisotopes of gold, mercury, and bismuth on the mass number, at a proton energy of 660 Mev: +) yield of mercury radioisotopes in the ground state; ×) the same in the isomer state; ●) total yield of radioisotopes of mercury and bismuth; ○) yield of gold radioisotopes.

This result is in good agreement with the data of Brunner et al.[29] who ascribed the 130-day mercury activity to the mass 194.

During the course of the investigation, we developed chemical procedures that ensure a most exact determination of the separation time of the daughter and mother fractions.* The mercury was separated from the gold by extraction of gold chloride with diethyl ether with subsequent precipitation of the gold with sulfite. The platinum was separated from the mercury and the gold by extraction of chloride complexes of mercury and gold with ethyl acetate, while the platinum remaining in the water film was precipitated with formic acid. Chemical procedures described in reference 30 were used to separate the gold, mercury, and the bismuth from the irradiated bismuth.

DISCUSSION OF THE RESULTS

As a result of the investigation we identified approximately 20 radioisotopes of gold, mercury, and bismuth, produced through (p, pxn), (p, 4pxn), and (p, 5pxn) reactions in the disintegration of bismuth by 660-Mev protons. We also calculated the cross sections for the production of these isotopes. The results are listed in Table III.

The yields of the radioisotopes Hg^{192}, Hg^{193}, Hg^{193m}, Hg^{195}, Bi^{201}, and Bi^{203} have been calculated from the yield of the daughter fractions of platinum, gold and lead. The isomer-pair Hg^{193}/Hg^{193m} and Hg^{195}/Hg^{195m} yield ratio was found to be equal to 2.5. For comparison, we measured the Hg^{193}/Hg^{193m} ratio at a lower bombarding-proton energy. The ratio increases to 8 at a proton energy of 220 Mev, indicating that when the irradiation energy is increased, the yield of the isomer in the higher spin state (Hg^{193m}, spin $^{13}/_{2}$) is greater than the yield of the isomer in the lower spin state (Hg^{193}, spin $^{3}/_{2}$). The results are in good agreement with the data of Hicks and Gilbert.[38]

The dependence of the cross section for the production of the identified isotopes on the mass-number is shown for each element in Fig. 6. As can be seen from the diagram, the course of the curves for mercury and gold, produced via reactions (p, 4pxn) and (p, 5pxn) differs from the curve for bismuth [reaction (p, pxn)]: while the yields of the radioisotopes of gold and mercury increase with the neutron deficit of the isotope and go through a maximum in the case of mercury, the opposite is observed for the bismuth radioisotopes.

To interpret the data obtained it is necessary to consider the mechanism of interaction of high energy particles with complex nuclei. According to the model proposed by Serber,[39] the interaction between a fast proton and a nucleus proceeds in two stages. First the colliding proton knocks out from the nucleus a few fast particles, from essentially neutrons and protons, leaving the remainder of the nucleus in an excited state, which is then deexcited by evaporation of neutrons, protons, and α particles.

The nuclear cascade was first calculated by Goldberger[40] by the Monte Carlo method, and then by a few other authors. The quantitative calculations are laborious and require the use of electronic computers. The calculations show that when 660-Mev protons interact with a bismuth nucleus,

---

*L. V. Filatova helped with the chemical operations.

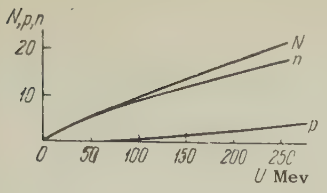

FIG. 7. Number of evaporated particles as a function of the excitation energy U: N) total number of nucleons, n) neutrons, p) protons.

of two fast protons and two fast neutrons are emitted on the average from the latter.[41]

The evaporation of the excited nucleus is satisfactorily explained with the aid of nuclear thermodynamics. In our case, without introducing a substantial error, we can consider the evaporation of neutrons and protons only. Then, according to the simplest variants of nuclear statistical theory, the total number of evaporated nucleons can be calculated with the aid of the following equations:[9]

$$-\frac{\partial U}{\partial (n+p)} = \frac{\Gamma_n (E_n + 2T) + \Gamma_p (V_p + E_p + 2T)}{\Gamma_n + \Gamma_p},$$

$$\frac{\Gamma_p}{\Gamma_n} = \left(1 + \frac{V_p}{T}\right) e^{-\frac{V_p}{T}} \frac{Z}{A - Z},$$

where U is the excitation energy of the nucleus, γ_n and γ_p are the widths of the energy levels of the neutrons and protons (proportional to the emission probability), E_x is the particle binding energy in the nucleus ($E_p = E_n = 7.5$ Mev), A is the mass number, C is the nuclear charge, E_p is the height of the Coulomb barrier for protons (8 Mev), and T is the temperature of the nucleus ($0.22\sqrt{U}$).

The calculated dependence of the total number of evaporated particles N, the number of the neutrons n, and the number of protons p on the excitation energy is shown in Fig. 7. If the knock-out component contains two protons and two neutrons, the evaporation involves, two protons and seven to eleven neutrons in the case of gold, and two protons and six to thirteen neutrons in the case of mercury. The greatest yield, according to our measurements, is obtained with the radioisotope Hg^{193} (two protons and eleven neutrons are evaporated), corresponding to a most probable value of excitation energy of 150 Mev. This value may be somewhat too high, if the yield of the radioisotopes of thallium, which were not investigated in this work, is greater than that of the mercury radioisotopes. The most probable excitation energy is then reduced to 100 or 110 Mev.

When bismuth nuclei are formed, there is emitted from the nucleus one proton that can be attributed with full justification to the knock-out component. In this case neutrons alone will be evaporated from the nucleus and, according to Fig. 7, the most probable excitation energy should not exceed 50 Mev.

Our experimental results are in good agreement with the theoretical calculations of Jackson.[42] The cross sections he calculated for the disintegration of elements with A ~ 200 by 400-Mev protons are shown in Figs. 8A and 8B, which also show, for comparison, our experimental data.

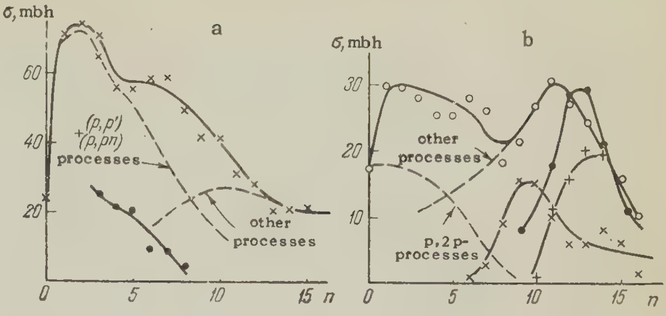

FIG. 8. Cross sections for disintegration as a function of the number of emitted neutrons n and the number of protons p: a) for p = 1 (× – calculated values, ● – experimental values for Bi); b) for p = 2 (○ – calculated values, ● – experimental data for Hg) and for p = 3 (× – calculated values, + – experimental data for gold).

It is seen from Fig. 8 that the curve for the bismuth isotopes is similar to the theoretical curve, and that the knock-out mechanism is decisive for the (p, pxn) reaction. The discrepancy in the absolute values of the yields of the (p, pxn) reaction can apparently be ascribed to the fact that our experimental data have been obtained at a higher proton energy.

The dependence of the yields of the reactions (p, 4pxn) and (p, 5pxn) (Fig. 8B) is in good agreement with the theoretical data for 2p and 3p. This fact can be readily explained by the circumstance that when he calculated the evaporating process, Jackson[42] neglected the evaporation of protons, while it is seen from Fig. 7 that on the average 10 to 12 evaporated neutrons are associated with two evaporated protons. It follows from the comparison of the theoretical and experimental values that the evaporation process plays the decisive role in the formation of radioisotopes of mercury and gold and dictates the character of the dependence of the radioisotope yields on the mass number.

The same characteristic features of the reactions (p, pxn), (p, 4pxn), and (p, 5pxn) are also observed in the disintegration of elements of medium atomic weights,[1–5] since the difference in the yields of neighboring isotopes of the same element increase with diminishing Z of the irradiated nucleus and with diminishing energy of the incident protons.

It can thus be concluded that in the disintegration of complicated nuclei by high-energy protons, the distribution of the residual nuclei is caused by the following interaction mechanisms: (1) during the course of the reactions (p, 4pxn) and (p, 5pxn), the decisive process is evaporation and the yield of the radioisotopes increases with increasing neutron deficit and goes through a maximum; (2) the (p, pxn) reactions occur when a small excitation energy is transferred to the nucleus, the emission of a large number of neutrons is difficult, and consequently the yield of the radioisotopes diminishes with increasing neutron deficit.

---

[1] E. Belmont and J. M. Miller, Phys. Rev. **95**, 1554 (1954).

[2] G. D. Wagner and E. O. Wiig, Phys. Rev. **96**, 1100 (1954).

[3] A. A. Caretto Jr. and E. O. Wiig, Phys. Rev. **103**, 236 (1956).

[4] R. W. Fink and E. O. Wiig, Phys. Rev. **94**, 1357 (1954).

[5] W. E. Nervik and G. T. Seaborg, Phys. Rev. **97**, 1092 (1955).

[6] M. Lindner and R. H. Osborne, Phys. Rev. **103**, 378 (1956).

[7] W. E. Bennett, Phys. Rev. **94**, 997 (1954).

[8] Vinogradov, Alimarin, Baranov, Lavrukhina, Baranova (Malysheva), and Pavlotskaia, Session of Acad. Sci. (U.S.S.R.) on Peaceful Use of Atomic Energy, Meeting of Div. of Chem. Sciences, 1955 (Translation publ. by U. S. Dept. of Commerce).

[9] Murin, Preobrazhenskii, Iutlandov, and Iakimov, ibid., 1955.

[10] R. Marshak, Phys. Rev. **61**, 431 (1942).

[11] Beta- and Gamma-Ray Spectroscopy, ed. K. Sigbahn, Amsterdam, 1955, p 289.

[12] M. Rose and J. Jackson, Phys. Rev. **76**, 1540 (1949).

[13] Fridlander, Hudis, and Wolfgang, Phys. Rev. **99**, 263 (1955).

[14] B. Robinson and R. Fink, Revs. Modern Phys. **27**, 424 (1955).

[15] S. Allen, Handbook of Chemistry and Physics, 1952.

[16] E. Burhop, The Auger Effect, Cambridge Univ. Press, Cambridge, 1952.

[17] L. A. Sliv and I. M. Band **Таблицы коэффициентов внутренней конверсии гамма-излучения** (Table of Gamma-Ray Internal-Conversion Coefficients, Part 1, The K Shell), Acad. Sci. Press, M-L, 1957.

[18] G. F. Drantsina, **Коэффициенты внутренней конверсии на L_{I}, L_{II}, L_{III} подоболочках** (Coefficients of Internal Conversions on L_{I}, L_{II}, and L_{III} Subshells), Acad. Sci. Press, M-L, 1957.

[19] E. Plassmann and F. Scott, Phys. Rev. **84m**, 156 (1951).

[20] R. Steffen, Phys. Rev. **82**, 827 (1951).

[21] F. Metzger, and R. Hill, Phys. Rev. **82**, 546 (1951).

[22] Seaborg, Perlman, and Hollander, Tables of Isotopes. IIL, Moscow, 1956 [Transl. from Revs. Modern Phys. **25**, 469 (1953)].

[23] H. Neuman and J. Perlman, Phys. Rev. **78**, 191 (1950).

[24] Brunner, Guhl, Halter, and Huber, Helv. Phys. Acta **28**, 85 (1955).

[25] Beta- and Gamma-Ray Spectroscopy, ed. K. Siegbahn, Amsterdam, 1955, p. 373.

[26] G. Wilkinson, Phys. Rev. **79**, 1014 (1950).

[27] J. Mihelich, Phys. Rev. **96**, 1450 (1954).

[28] Gillion, Gopalakrishnan, de-Shalit, and Mihelich, Phys. Rev. **93**, 124 (1954).

[29] Brunner, Guhl, Halter, and Leisi, Helv. Phys. Acta **28**, 475 (1955).

[30] A. K. Larukhina, Doctoral Dissertation, Geochem. Inst., Moscow, 1955.

[31] G. Ewan, Canad. J. Phys. **35**, 672 (1957).

[32] Steffen, Huber, and Humbel, Helv. Phys. Acta **22**, 167 (1949).

[33] B. S. Dzhelepov and L. K. Peker, **Схемы распада радиоактивных изотопов** (Decay Schemes of Radioactive Isotopes) Acad. Sci. Press, M-L, 1957.

[34] Brunner, Halter, and Perdrisai, Helv. Phys. Acta **30**, 270 (1957).

[35] Joly, Brunner, Halter, and Huber, Helv. Phys. Acta **28**, 403 (1955).

[36] Schmorak, Stockendal, McDonnell, and Bergstrom, Nucl. Phys. **2**, 193 (1956).

[37] D. Alburger and M. Pryce, Phys. Rev. **95**, 1482 (1954).

[38] J. H. Hicks and R. Gilbert, Phys. Rev. **100**, 1286 (1955).

[39] R. Serber, Phys. Rev. **72**, 1114 (1947).

[40] M. Goldberger, Phys. Rev. **74**, 1269 (1948).

[41] Metropolis, Turkevich, Miller, Bivins, Stoom, and Friedlander, BNL-2998, 1957.

[42] J. Jackson, Canad. J. Phys. **35**, 21 (1957).

Translated by J. G. Adashko
237

APPLICATION OF MAGNETIC SLITS FOR FORMING CIRCULAR CHARGED-PARTICLE TRAJECTORIES

V. M. KEL'MAN, V. A. KOLIUNOV, and M. V. KARPOV

Leningrad Physico-Technical Institute, Academy of Sciences, U.S.S.R.

Submitted to JETP editor May 16, 1958

J. Exptl. Theoret. Phys. (U.S.S.R.) 35, 1113-1115 (November, 1958)

An electron-optical system is proposed for forming circular charged-particle trajectories; the system consists of magnetic slits arranged in a circle. The strength of the magnetic field in this system increases rapidly with distance from the axis, but there is no vertical defocusing. A system of this type can be used in an accelerator with a fixed guide field. An experimental investigation has been made of the first circuit of an electron beam in a system of this kind.

IN the present note we consider an electron-optical system for forming circular charged-particle trajectories by means of a magnetic field which increases rapidly toward the periphery of the systems; this field does not cause vertical defocusing.

The system consists of magnetic slits,* located at equal intervals about the periphery of a circle. The fields in adjacent slits are in opposite directions. Regardless of the field direction each slit deflects charged particles toward the axis of the system; with appropriate choice of magnetic field and particle vector velocity the particle will describe a trajectory which is essentially circular.

In order to simplify the analysis we replace the slit system by an equivalent system; the equivalent system consists of linear conductors in which the direction of current flow alternates as one goes around the circle (Fig. 1).

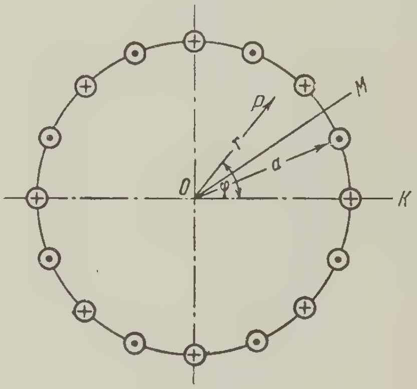

FIG. 1

In this system the vector potential is:

$$\frac{m}{e}\ddot{x} = -\frac{\partial Q}{\partial x}, \quad \frac{m}{e}\ddot{y} = -\frac{\partial Q}{\partial y},$$

$$Q = \frac{e}{2m}A^2$$

Here I is the current in each conductor; r is the distance from the system axis O to the point P at which the vector potential is computed; φ is the polar angle, measured from a line OK which passes through the system axis O and one of the conductors; a is the distance from the axis to the conductor and 2n is the number of conductors.

Because the vector potential is independent of z this coordinate is cyclical. Hence the generalized momentum component P_z is a constant:

$$P_z = \frac{\partial L}{\partial \dot{z}} = m\dot{z} + \frac{e}{c}A = m\dot{z}_0 + \frac{e}{c}A_0 = \text{const},$$

where

$$L = \frac{m}{2}(\dot{x}^2 + \dot{y}^2 + \dot{z}^2) + \frac{e}{c}A\dot{z}$$

is the Lagrangian. In a plane OM which passes through O and midway between any two neighboring conductors the vector potential vanishes. If the particle starts at any one of these planes with $\dot{z}_0 = 0$, in passing through any other of these planes its velocity component $\dot{z}$ will always be zero. Between any of the planes OM the particle is deflected upward and then downward (we assume that the conductors are oriented vertically); however, since these deflections are equal, the particle oscillates about a plane perpendicular to the axis. The projection of the particle motion on this plane is described by the equation (in Cartesian coordinates)

---

*By "magnetic slit" is meant an electron-optical deflection element which consists of two magnetic poles of opposite sign (elongated in one direction); in contrast with an ordinary deflection magnet, an electron is affected by the "fringing field" rather than the field in the gap itself. If the electrons which enter the field of a magnetic slit move in a direction which is perpendicular to the long dimension of the poles the trajectories are characterized by displacement in this direction and deflection in the direction of the magnetic slit.[1-3]

$$\frac{m}{e}\ddot{x} = -\frac{\partial Q}{\partial x}, \quad \frac{m}{e}\ddot{y} = -\frac{\partial Q}{\partial y},$$

$$Q = \frac{e}{2m}A^2$$

and can be represented by a rubber-sheet model in which small balls move under the influence of gravitational forces.[4]

The profile of the rubber-sheet model consists of a number of elevated points (equal to the number of conductors) located in a circle. The height of the profile h is proportional to Q. It is apparent that conditions can be found for which a small ball will roll along the inner sides of the slopes, describing a trajectory which is almost circular. Because of frictional effects, however, only one complete circuit can be achieved. Nevertheless, this is sufficient to demonstrate the essential nature of the particle motion. We also note that a system of conductors in which the current flows in the same direction can also be used to confine charged particles. However, in a system of this kind it would be difficult to avoid loss of particles in the vertical directions.

An experimental device has been built to check the analysis given above (Fig. 2). The deflection elements are magnetic slits, since these provide considerably stronger magnetic fields than can be achieved with current-carrying conductors. The fields in adjacent slits are in opposite directions. In order to provide vertical focusing, the poles 1 which form the magnetic slits are concave in shape; although it would not defocus the beam, a system of straight magnetic slits would not produce focusing in the vertical direction. Each pole has a coil 2 of 200 turns. The chamber 3 is barrel-shaped and is provided with observation windows 4. Inside the chamber there is an electron gun 5 and a fluorescent screen 6. The electron gun forms a cylindrical beam with a divergence angle of 3°. It can be rotated about axis 7 and displaced over a small range. The screen can be moved around the axis of the system.

An investigation was made of the shape of the electron beam when the following parameters were varied: magnetic field strength, electron energy, position of the electron gun, and starting direction of the beam. At appropriate values of these parameters the electron beam is deflected in alternate directions by the magnetic slits, forming a complete circle.

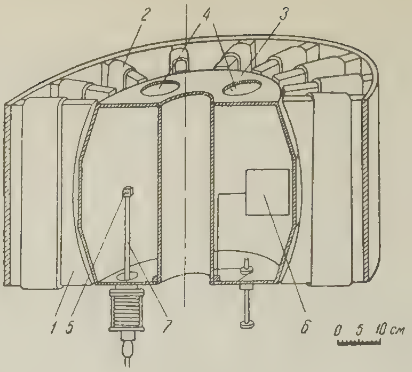

FIG. 2

An examination of the displacement of the luminous spot on the screen when the latter is moved shows that the electrons describe a spatial trajectory characterized by periodic radial and vertical oscillations, which are superimposed on a circle. With 16 poles and with the gun 4 to 5 cm from the poles the amplitude of the radial oscillations is approximately 2 cm and the amplitude of the vertical oscillations is approximately 5 cm. Under these conditions the electron energy is 5 kv and the current in the windings, which is a strong function of the distance between the gun and the poles, is 5 to 10 amps. The width of the image, which is a slightly curved band, varies between 1 and 3 mm, depending on the position of the screen. The image height is 10 to 20 mm. Similar results are obtained with 32 poles, although the oscillation amplitude is somewhat smaller.

Thus it would appear that a system consisting of magnetic slits arranged in a circle can provide a charged-particle trajectory that is almost circular.

Because the strength of the magnetic field increases rapidly with increasing distance from the axis of the system and because there are no vertical defocusing forces, a system of this kind can be used in an accelerator with a fixed (also variable) magnetic guide field. The charged particles in such a system can be accelerated by an induction scheme or by a variable electric field.

---

[1] Baranovskii, Kaminskii and Kel'man, J. Tech. Phys. (U.S.S.R.) **25**, 610 (1955).

[2] Baranovskii, Kaminskii and Kel'man, J. Tech. Phys. (U.S.S.R.) **25**, 1954 (1955).

[3] V. N. Kel'man and I. V. Rodnikova, J. Exptl. Theoret. Phys. (U.S.S.R.) **21**, 1364 (1951).

[4] Kel'man, Kaminskii and Iavor, J. Tech. Phys. (U.S.S.R.) **24**, 1410 (1954).

Translated by H. Lashinsky
238

SOVIET PHYSICS JETP VOLUME 35(8), NUMBER 5 MAY, 1959

CYCLIC ACCELERATION OF PARTICLES IN HIGH-FREQUENCY FIELDS*

V. I. VEKSLER and L. M. KOVRIZHNYKH

P. N. Lebedev Physics Institute, Academy of Sciences, U.S.S.R.

Submitted to JETP editor, May 21, 1958

J. Exptl. Theoret. Phys. (U.S.S.R.) 35, 1116-1118 (November, 1958)

The feasibility of using high-frequency fields for controlling the motion of particles in cyclic accelerators is indicated.

IN 1947 one of us directed attention to the possibility of cyclic acceleration of charged particles in rapidly varying magnetic fields. The basic idea of an accelerator of this kind is described below.

If a constant or slowly-varying (in time) magnetic field acts over sectors, rather than over an entire circular area, at an appropriate field value (the same in all sectors) a particle with constant energy will move along a curve which is a closed polygon with rounded vertices.

Instead of a fixed magnetic field or a slowly varying magnetic field, we can use a rapidly varying field; if the time in which the particle traverses one sector is a multiple of the period of the magnetic field, the particle will enter each magnetic sector at a time such that the field in the sector is at the desired value. The sectors can be rectangular wave guides with closed ends. A traveling-wave circular accelerator has also been considered.

Calculations carried out by Burshtein and Kolomenskii[1] indicated, however, that the variants cited above would not provide stable motion.

We wish to point out the possibility of cyclical acceleration by a rapidly varying electromagnetic field. As in the above examples, this field must act as a guide field.

The characteristic feature of the method proposed below is that the particle is not in the high-frequency electromagnetic field for a fraction of a period, as above, but rather for a large number of periods, or even for the entire time of acceleration. Consider the motion of a particle in a field produced by a plane standing wave $E_y = E_0 \cos kx \times \sin \omega t$ and $H_z = -H_0 \sin kx \cos \omega t$ where E_0 and H_0 are the amplitudes of the electric and magnetic fields respectively. Integrating the appropriate equations of motion we have

$$\frac{d}{dt} m\dot{x} = \frac{e^2}{mc^2} \frac{E_0 H_0}{2k} \sin 2kx \cos^2 \omega t. \tag{1}$$

Thus, on a particle in the field of a standing wave there is exerted a force which tends to localize the particle at the nodes of the electric field.* If we now assume that the nodal surface is a cylinder, it is easily shown that the particle will be confined by the varying field, executing oscillations about some closed orbit.

As an example, we consider the motion of a particle in a coaxial cylindrical resonator in which an axially symmetric TM mode is excited (the axis of the resonator is taken as the z axis). We are not concerned with the acceleration mechanism and shall consider only the stability of a particle with given energy.

We have the following equations of motion

$$\begin{gathered} \frac{d}{dt} m\dot{r} = mr\dot{\theta}^2 + eE_r - \frac{e}{c}\dot{z}H_0, \\ \frac{d}{dt} mr^2\dot{\theta} = 0, \quad \frac{d}{dt} m\dot{z} = eE_z + \frac{e}{c}\dot{r}H_\theta, \end{gathered} \tag{2}$$

where

$$\begin{gathered} E_r = \frac{h}{\lambda} A_0 r^{-1/2} \cos \lambda (r - a) \sin hz \sin \omega t, \\ E_z = - A_0 r^{-1/2} \sin \lambda (r - a) \cos hz \sin \omega t, \\ H_\theta = \frac{k}{\lambda} A_0 r^{-1/2} \cos \lambda (r - a) \cos hz \cos \omega t, \\ \lambda = n\pi/(b - a), \quad h = m\pi/d, \quad k^2 = \omega^2/c^2 = h^2 + \lambda^2, \end{gathered}$$

a and b are the major and minor radii of the cylinder and d is the height. It is assumed that $\lambda r \gg 1$ and that the asymptotic expressions for the Bessel functions can be used.

In the general case the solution of these equations is extremely complicated; however, as an illustrative example, we may consider the case in which $n = 2$ and $m = 0$. Assuming that $r = R_0 + \rho$ where $R_0 = (a + b)/2$ and that $\rho/R_0 \ll 1$, to first order in ρ/R_0 we have:

---

*This work was carried out in 1956.

*The problem of trapping particles in high-frequency fields has been considered by Gaponov and Miller.[2]

$$\frac{d}{dt} m\dot{\rho} = m(R_0 + \rho)\dot{\theta}^2 + \frac{eH_0}{c}\dot{z}\cos k\rho\cos\omega t,$$

$$mR_0(R_0 + 2\rho)\dot{\theta} = M_0, \tag{3}$$

$$\frac{d}{dt} m\dot{z} = eE_0 \sin k\rho \sin \omega t - \frac{eH_0}{c}\dot{\rho}\cos k\rho\cos\omega t,$$

where $E_0 = H_0 = A_0 R_0^{-1/2}$. Whence we obtain the equation for ρ:

$$\frac{d}{dt} m\dot{\rho} = \frac{M_0^2}{mR_0^3} - \frac{3M_0^2}{mR_0^4}\rho - \frac{e^2}{mc^2}\frac{E_0 H_0}{2k}\sin 2k\rho\cos^2\omega t. \tag{4}$$

Assuming now that $eE_0 < km_0c^2$, $k\rho \ll 1$ and $p_0^2 \ll p_H^2$, as is the case for large radii, we have

$$d^2\rho/d\tau^2 + p_H^2\rho\cos^2\tau = p_0^2 R_0, \tag{5}$$

where

$$\tau = \omega t,\ \ p_0 = \omega_0/\omega,\ \ p_H = \omega_H/\omega,$$

$$\omega_0 = M_0/mR_0^2,\ \ \omega_H = eH_0/mc.$$

Equation (5) is the Mathieu equation which, as is well known, has stable solutions. By choosing an appropriate frequency ω and high-frequency field E_0 we can achieve operation in a given stability region. Under these conditions, a particle moving along the circle will oscillate about $\bar{\rho} \sim 2R_0(p_0/p_H)^2$.

As the energy increases the representative point is shifted toward the origin of the stability diagram. Thus, if we do not operate in the first stability region, leaving other considerations aside, the maximum energy is determined by the value of p_H which obtains at the boundary of a given stability region. The motion of a particle in a system of this kind is reminiscent, in some respects, of motion in a strong-focusing accelerator.

In the example considered above we have not considered stability in the z direction. However, by appropriate choice of mode and resonator shape it is also possible to achieve vertical stability.*

An interesting feature of the mechanism considered here is the fact that the force is independent of the sign of the charge; thus a system of this type could be used for confining quasi-neutral bunches. In turn, this makes possible the use of a radiation acceleration method[3] for cyclic acceleration of quasi-neutral bunches.

---

[1] E. L. Burshtein and A. A. Kolomenskii, Reports of the Institute of Physics, Academy of Sciences, USSR (1947).

[2] A. V. Gaponov and M. A. Miller, J. Exptl. Theoret. Physics (U.S.S.R.) **34**, 242 (1958), Soviet Phys. JETP **7**, 168 (1958).

[3] V. I. Veksler, Proceedings of the CERN Symposium on High-Energy Accelerators, I. Geneva 1956.

Translated by H. Lashinsky
239

---

*By absence of stability here we mean that a state of neutral equilibrium obtains.

SOVIET PHYSICS JETP VOLUME 35(8), NUMBER 5 MAY, 1959

CROSS SECTIONS FOR THE CAPTURE OF SLOW ELECTRONS BY O_2 AND H_2O MOLECULES AND MOLECULES OF HALOGEN COMPOUNDS

I. S. BUCHEL'NIKOVA

Institute of Chemical Physics, Academy of Sciences, U.S.S.R.

Submitted to JETP editor, May 22, 1958; resubmitted July 21, 1958

J. Exptl. Theoret. Phys. (U.S.S.R.) 35, 1119-1130 (November, 1958)

Using a nearly-monoenergetic electron beam and the single-collision method, cross sections have been measured for the capture of slow electrons by the molecules SF_6, CCl_4, CF_3I, CCl_2F_2, BCl_3, HCl, and HBr; capture cross section for electrons with energies of several electron volts by O_2 and H_2O have also been measured. The width of the electron energy distribution was 0.2 to 0.3 ev; the energy was measured with an accuracy of 0.01 to 0.02 ev. The following values were found for the maximum cross sections: SF_6, 5.7×10^{-16} cm^2; CCl_4, 1.3×10^{-16} cm^2; CF_3I, 7.8×10^{-17} cm^2; CCl_2F_2, 5.4×10^{-17} cm^2; BCl_3, 2.8×10^{-17} cm^2; HBr, 5.8×10^{-17} cm^2; HCl, 3.9×10^{-18} cm^2; H_2O, 4.8×10^{-18} cm^2; O_2, 1.3×10^{-18} cm^2. It is found that the appearance potential for O^- in O_2 is 4.63 ± 0.04 ev; the appearance potential for H^- in H_2O is 5.45 ± 0.09 ev.

In the present work we report on measurements of the cross sections for capture of slow electrons by SF_6, CCl_4, CF_3I, CCl_2F_2, BCl_3, HCl, HBr and the capture of electrons with energies of several electron volts by O_2 and H_2O. The measurements were carried out by the single-collision method, using a nearly-monoenergetic electron beam. The method of measurement is as follows.[1] A beam of electrons, which is collimated by a honeycomb diaphragm (divergence angle of 2°) and a magnetic field of 15 to 20 oersteds enters an equipotential region through a system of grids and then strikes a collector. Ions which are formed in the equipotential region are collected by a cylindrical electrode. To eliminate the effect of the cathode voltage drop on electron energy the cathode is heated by pulses and the electrons are extracted during the time in which heater current does not flow. In the path of the electron beam there is a diaphragm which is at a potential greater than the space-charge potential of the beam (1 to 1.5 volts). Only electrons with energies greater than this value pass through the diaphragm. The electron current is approximately (1 to 3) $\times 10^{-8}$ amp, with a beam cross-sectional area of approximately 3 cm^2, so that space charge effects are negligibly small.

The energy distribution of the electron beam which passes through the diaphragm is exponential, with a sharp cut-off on the low-energy side; the width of the distribution is approximately 1 ev. By employing a nearly-monoenergetic beam[2] it is possible to reduce the width to 0.2 or 0.3 ev. The logarithm of the ion current for the monoenergetic component is found to be a linear function of the retarding potential; hence it may be assumed that the distribution in the monoenergetic component is exponential.

Provision is made for compensation of the contact potentials of the diaphragms and grids which define the equipotential region. The elements of the system are gold-plated in order to achieve stable contact potentials. By careful compensation of the contact potentials and avoidance of distortion of the electric fields in the equipotential region it is possible to determine the energy with an accuracy of the order of 0.02 ev.

The magnetic field makes it impossible for scattered electrons to reach the ion collector. Since the divergence angle of the electron beam is 2°, a beam of 15 to 20 oersteds is sufficient to eliminate scattering. Because of the small field the radii for ions with masses greater than 20 atomic mass units is greater than the radius of the ion collector; however, most of the ions strike the collector. By introducing corrections for the instrument geometry it is possible to determine the ion collection with an accuracy of the order of several percent.

Because the divergence angle of the beam is small, it is possible to determine the length of the electron path in the equipotential region with good accuracy. It should be noted that the solenoid which produces the magnetic field is positioned in such a way that increasing the field to 30 or 40 oersteds does not increase the number of electrons which pass through the diaphragm. Thus, there is no change in the effective divergence angle of the electron beam, or the path length, when the magnetic field is turned on.

The ion and electron currents are measured with electrometer amplifiers. The gas pressure is measured with an ionization gage which is calibrated against a McLeod gage for the gas being studied.

The measurements are carried out in the 0 to 1 ev and 0 to 3 ev electron-energy ranges. In the first case the ion and electron collectors are at zero potential with respect to the cathode and the current of scattered electrons is negligibly small. In the measurements in the energy region up to 3 ev, the collector potential is maintained at +4 volts and the scattered-electron current can be important. It is possible to estimate the current of scattered electrons from the current at the ion collector. In this case, the cross sections is calculated by subtracting the scattered-electron current from the current at the ion collector. It has been found that the cross-section values obtained in experiments without scattering and the values computed from the collector current (subtracting the scattered-electron component) are in agreement within the accuracy of the measurements. The capture cross section is computed from the formula

$$\sigma = \frac{I_i/\eta\xi}{(I_e/\beta)\cdot 3.55\cdot 10^{16}\cdot 273\,(\chi p/T)\,\lambda L},$$

where I_i is the ion current, I_e is the electron current, p is the gas pressure shown by the ionization gauge, χ is the conversion coefficient for converting the reading on the ionization gauge to the true pressure, T is the temperature of the operating region, L is the length of the operating region, β is a correction for interception of ions by the grids which shield the ion collector, ξ is a correction for ion loss, and λ is a correction introduced to average over paths of electrons which move at different angles. The total error in the corrections is approximately 20 to 25%.

In those cases in which the width of the capture region is smaller than or comparable with the width of the electron energy distribution the distribution is taken into account in computing the cross sections. Let I(V) be the observed dependence of ion current on accelerating potential and $N_e(U)\,dU$ the number of electrons with energies between U and U + dU; in the present case $N_e(U) = N_0 \exp\{-U/kT\}$ and E = U + V is the total electron energy. Then

$$I(V) = \int_0^\infty A\sigma(E)\, N_0 e^{-U/kT}\, dU,$$

where $A = 969.15 \times 10^{16}\, \eta\xi\chi p\lambda L/\beta t$. Converting to the variable E, we have

$$I(V) = AN_0 e^{V/kT} \int_V^\infty \sigma(E)\, e^{-E/kT}\, dE$$

and

$$I'(V) = AN_0 \left[\frac{1}{kT} e^{V/kT} \int_V^\infty \sigma(E)\, e^{-E/kT}\, dE - \sigma(V)\right],$$

whence

$$\sigma(V) = \frac{I(V) - kTI'(V)}{AN_0 kT}.$$

The quantity

$$N_0 kT = \int_0^\infty N_0 e^{-U/kT}\, dU$$

is the total electron current. Determining the effective value of kT from the slope of the function $\log I_e = f(-V)$, finding I′(V) by graphical differentiation of I(V), we can ascertain the true dependence of cross section on electron energy.

The cross-section curves for a given molecule, obtained in different experiments, were averaged over the points. The mean-square error for each point is less than 15 to 20%.

1. SF_6, CCl_4 and CF_3I. If the width of the capture region is much smaller than the width of the electron energy distribution the ion-current curve should be similar to the distribution curve and the displacement of the ion current peak with respect to the distribution peak characterizes the energy at which capture takes place. In an earlier report[3] it was shown that these curves are, in fact, similar for SF_6 and CCl_4; hence the width of the capture region in these cases is several hundred

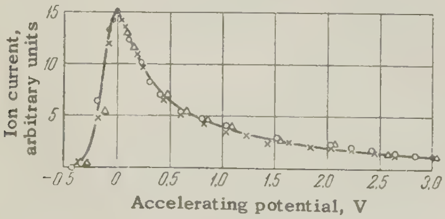

FIG. 1. Negative ion current in SF_6.

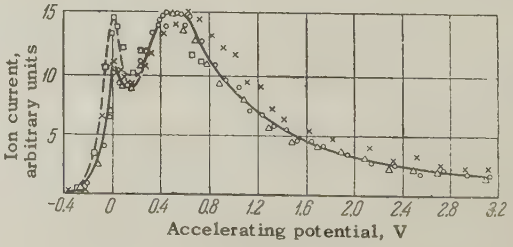

FIG. 2. Negative ion current in CCl_4.

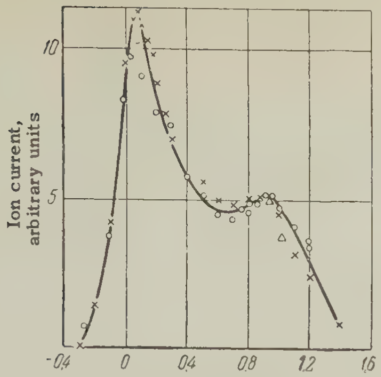

FIG. 3. Negative ion current in CF_3I.

electron volts. The displacements of the peaks are 0 ± 0.01 ev for SF_6 and 0.02 ± 0.01 ev for CCl_4. In CF_3I it is also found that the ion current curve is similar to the distribution curve and that the ion current peak is displaced with respect to the distribution maximum by 0.05 ± 0.01 ev (average of four measurements).

Figures 1 to 3 show the ion current as a function of accelerating potential for SF_6, CCl_4 and CF_3I. In each figure are shown the data of three different experiments. The ion current is given in arbitrary units and is adjusted to obtain coincidence of the peaks obtained in different experiments. The energy scale is given with respect to the position of the first ion-current peak.

It has been shown by mass-spectrometer studies[4,5] that in SF_6 the ions SF_6^-, SF_5^-, and F^- are formed in this energy region. According to the data reported in reference 4 the SF_6^- current is shifted with respect to the electron peak by 0.1 ev; the width of the region in which SF_5^- is formed is approximately 1 ev. The ratio of the maximum SF_6^- current to the maximum SF_5^- current is approximately 25. The F^- current is approximately 100 times smaller than the SF_5^- current.

Thus, the curve shown in Fig. 1 represents the total current for SF_6^-, SF_5^- and F^-. The current at the maximum is mainly the SF_6^- current. It is apparent from Fig. 1 that when the acceleration potential is greater than 1.5 volts the current does not change very much as the electron energy is varied. Since the F^- current is very small, it is reasonable to assume that the collector current in this region is due to scattered electrons. To compute the cross section the current of scattered electrons was taken equal to two units on the scale in Fig. 1.

Figure 2 shows the ion current curve for CCl_4. The data obtained in the different experiments are consistent, with the exception of a discrepancy in the region of the first peak. The discrepancy is explained by the fact that Curve 1 (dotted) was taken at zero collector potential. In this case the width of the electron energy distribution is considerably smaller than in the other experiments. The discrepancy in this region is not important as far as a determination of the cross sections is concerned since these cross sections are determined by measurements at zero collector potential.

A number of workers have observed the formation of negative ions in CCl_4.[6-10] The appearance potentials for these ions are as follows:

Ion	Appearance Potential, ev		Probability	
Cl^-	0.2 [8],	~ 0 [10]	$CCl_4 + e \rightarrow CCl_3 + Cl^-$	(1)
Cl_2^-	—	0.8	$CCl_4 + e \rightarrow CCl_2 + Cl_2^-$	(2)
CCl_3^-	—	1.4	$CCl_4 + e \rightarrow Cl + CCl_3^-$	(3)

According to the data of reference 10 the Cl_2^- peak is approximately 45 times smaller than the Cl^- peak while the CCl_3^- peak is approximately 450 times smaller than the Cl^- peak. For this reason the second maximum observed on the curve in the present work cannot be attributed to Cl_2^- or CCl_3^-. It is apparently explained by the process given in (1), with the transition to another potential curve of the intermediate ion CCl_4^-. The second maximum has also been observed in reference 9, in which a Lozier apparatus was used. The fact that this maximum has not been observed by other workers is explained by the large width of their energy distributions. Actually, it has been found[8] that the appearance potential for negative ions is 0.2 ev while the ion current peak is at 1.7 ev; whence it follows that the width of the energy distribution in these experiments was not smaller than 2 or 3 ev. It is natural that the first and second maxima would not be resolved under these conditions.

As is apparent from Fig. 2, the ion current becomes relatively insensitive to energy at electron energies greater than 2 ev. In computing the cross section it was assumed that the current due to scattered electrons was equal to 3 units on the scale in Fig. 2.

A curve showing the dependence of ion current on accelerating potential for CF_3I is shown in Fig. 3. The formation of negative ions in CF_3I has been studied earlier in reference 11 to 13. The following appearance potentials were found:

Ion	Appearance Potential, ev			Probability	
F^-	1.5 ± 0.2 [13];	3.6 ± 0.3 [12],	~ 0 [11]	$CF_3J + e \rightarrow CF_2J + F^-$	(4)
J^-	~ 0	~ 0	~ 0	$CF_3J + e \rightarrow CF_3 + J^-$	(5)

In this case the I^- current at 0 ev is 10 times larger than the F^- current. Thus, there is little

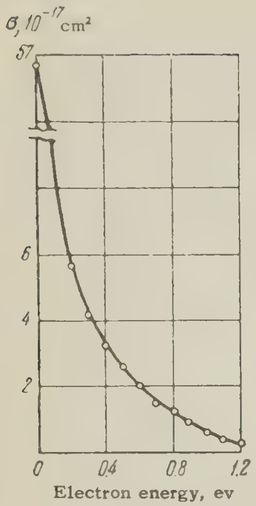

FIG. 4. Electron capture cross sections in the molecule SF_6.

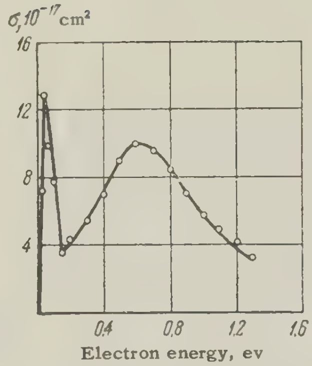

FIG. 5. Electron capture cross sections in the molecule CCl_4.

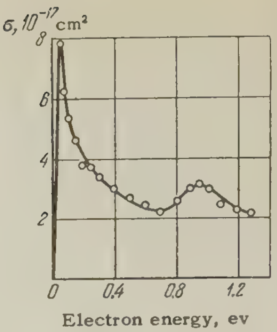

FIG. 6. Electron capture cross sections in the molecule CF_3I.

doubt that the narrow maximum at 0.05 ev is due to the process in (4). The origin of the second maximum is not clear. It arises either as a result of (4) with transition to another potential curve of CF_3I, or by virtue of the process in (5). The curve shown in Fig. 3 was taken at zero collector potentials since the current due to scattered electrons was negligibly small.

Figures 4 to 6 show the capture cross sections σ as functions of electron energy for SF_6, CCl_4 and CF_3I. In computing the cross section in the energy region 0 to 0.2 ev only the data obtained in experiments with zero collector potential were used.

2. CCl_2F_2. Figure 7 shows the ion current as a function of accelerating potential for CCl_2F_2. In this same figure the dashed curve denotes the electron energy distribution. The shape of the beginning of the ion current curve is similar to the distribution curve. This indicates that the cross section increases from zero to maximum in an energy region which is small compared with the distribution width. The curve has a flat maximum which is 0.12 volts wide. The beginning of the maximum is shifted with respect to the electron energy peak by 0.07 ± 0.01 volts (average of six measurements). There are no reliable data on the formation of negative ions in CCl_2F_2 so that the observed effects could not be interpreted.

A curve showing the capture cross section as a function of electron energy is given in Fig. 8.

3. BCl_3. A curve for the negative ion current in BCl_3 is shown in Fig. 9. The initial part of the curve is again similar to the electron curve (dashed). The curve has a flat maximum 0.2 volts wide. The beginning of the maximum is shifted with respect to the peak in the electron distribution by 0.23 ± 0.01 ev (average of six measurements). The dependence of capture cross section on electron energy is given in Fig. 10. The formation of Cl^- at electron energies close to zero has been observed by a mass-spectrometer measurement in BCl_3.[14] The authors, however, think it is possible that the Cl^- ions are formed because of HCl impurities. The present results indicate that the negative ions in BCl_3 are in fact a result of the reaction $BCl_3 + e \rightarrow BCl_2 + Cl^-$, since the maximum in the negative ion current in HCl oc-

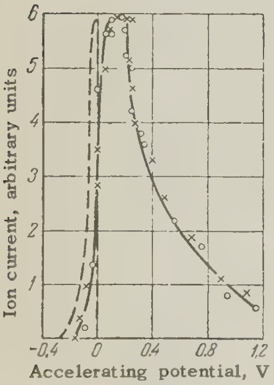

FIG. 7. Negative ion current in CCl_2F_2.

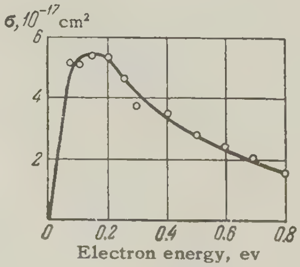

FIG. 8. Electron capture cross sections in the molecule CCl_2F_2.

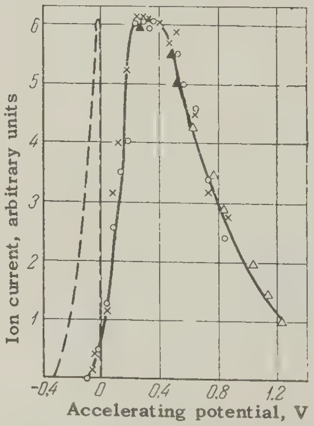

FIG. 9. Negative ion in BCl_3.

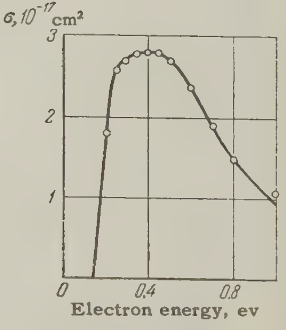

FIG. 10. Electron capture cross sections in the molecule BCl_3.

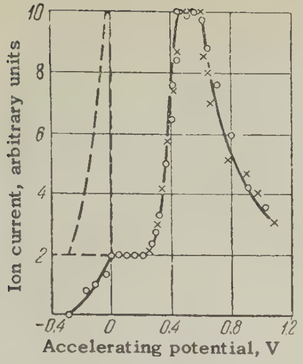

FIG. 11. Negative ion current in HCl.

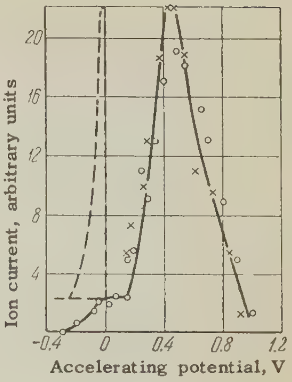

FIG. 12. Negative ion current in HBr.

curs at an electron energy of 0.05 ev and the HCl capture cross section is of an order of magnitude smaller than that observed for BCl_3.

4. HCl and HBr. The ion current curves for HCl and HBr are given in Figs. 11 and 12. In these cases scattering is important even at zero collector potentials since the initial part of the ion current curve (up to 0.25 volts for HCl and up to 0.15 volts for HBr) is determined by the scattered electrons. The curve showing the increase in ion current in these cases is similar to the electron energy distribution curves. The ion current curves have flat maxima. The shift of the beginning of the maximum with respect to the distribution peak for HCl is 0.46 ± 0.02 volts (average of six measurements); in HBr this shift is 0.43 ± 0.01 volts (average of four measurements). The width of the maximum in HCl is 0.15 volts; in HBr it is several hundredths of a volt.

The appearance potentials for Cl^- in HCl and Br^- in HBr in this energy region have been determined by mass-spectrometer methods. The following results were obtained:

Ion	Appearance Potential, ev	Probability
Br^-	0.6 ± 0.3 [10]	$HBr + e \rightarrow H + Br^-$
Cl^-	0.8 ± 0.3 [16]; 0.4 [10]; 0.66 ± 0.02 [15]	$HCl + e \rightarrow H + Cl^-$

The value 0.66 ± 0.02 ev was found by Fox for the shift in the Cl^- peak with respect to the SF_6^- peak in a mass-spectrometer investigation of the negative ions in HCl, using a nearly-monoenergetic electron beam. Since the SF_6^- peak occurs at zero electron energy, the shift in the Cl^- peak with respect to the SF_6^- peak should be the same as the shift in the Cl^- peak with respect to the electron peak. However, in the present case a flat maximum is observed; the maximum extends from 0.46 ± 0.02 ev to 0.62 ± 0.01 ev. The discrepancy may be explained by the difference in the shape of the energy distribution in the present experiments as compared with those in the Fox experiments. Since the distribution in the Fox experiments did not have a sharp cut-off, the ion current peak may be in the middle or at an extremity of the region in which the capture cross section is not strongly affected by energy. The width of the distribution in the Fox experiments (approximately 0.5 ev) was larger than the width of this region whereas in the present case approximately 60% of the electrons have energies within an interval of 0.1 ev and the total width of the distribution is 0.25 to 0.30 ev. The distribution has a sharp edge on the low energy side so that the beginning of the ion peak should coincide with the beginning of the region in which the cross section is not a strong function of energy.

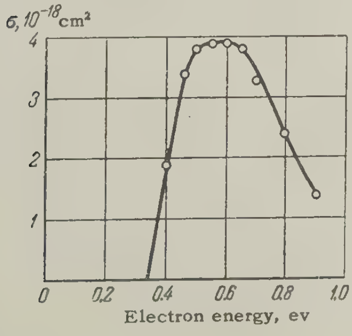

FIG. 13. Electron capture cross sections in the molecule HCl.

Curves showing the dependence of capture cross section on electron energy are given in Figs. 13 and 14. The capture probability and the electron sticking coefficient for HCl have been measured earlier by diffusion methods.[17,18] An estimate of the capture cross section on the basis of the data reported in reference 17 shows that the cross section at the maximum is of the order of 10^{-18} cm²; this result is in good agreement with the value obtained in the present work, 4×10^{-18} cm².

5. O_2 and H_2O. These measurements were

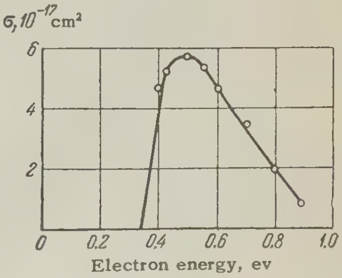

FIG. 14. Electron capture cross sections in the molecule HBr.

carried out in the electron energy ranges 0 to 8 ev for O_2 and 0 to 10 ev for H_2O. It has been shown by mass-spectrometer measurements that the following processes occur in this energy region:

Process	Appearance Potential, ev	
$O_2 + e \rightarrow O + O^-$	4.7 ± 0.1 [8,19,20]	(6)
$H_2O + e \rightarrow H^- + OH$	5.6 ± 0.5 [21,22]	(7)
$H^- + OH$	(maximum at 7.1 ev)	(8)
$O^- + 2H$	7.5 ± 0.3	

In the present case the appearance potentials are determined from the ion current curve. Under these conditions the electron energies are given by the accelerating potential. The zero of the energy scale is established by compensation of the contact potentials of the grids which define the equipotential region and is verified by the position of the peak in the electron energy distribution. It is found that the position of the peak in the distribution does not depart from $V = 0$ by more than 0.02 or 0.03 ev.

Although a nearly-monoenergetic electron beam is used, in determining the appearance potentials one must take account of the width of the electron energy distribution. This procedure is carried out as follows.[23] As has been indicated above, the dependence of ion current on accelerating potential is of the form

$$I(V) = \int_0^\infty A\sigma(E) N_0 e^{-U/kT}\, dU = N_0 \int_0^\infty p(E)\, e^{-U/kT} dU,$$

where $p(E)$ is the capture probability. Let the appearance potential be A. Then for $E < A$, $p(E) = 0$. We assume that when $E > A$,

$$p(E) = a(E - A)^n.$$

Considering the cases $n = 1$ and $n = 2$ we find for the first case:

$$d \ln I_i / dV = 1/kT \text{ for } V \leqslant A;$$

$$d \ln I_i / dV = 1/(kT + V - A) \text{ for } V > A.$$

In the second case:

$$d \ln I_i / dV = 1/kT \text{ for } V \leqslant A;$$

$$d \ln I_i / dV = 2(V - A + kT)/[k^2T^2 + (V - A + kT)^2] \text{ for } V > A.$$

Thus, assuming a linear or quadratic dependence of electron capture probability on energy, the function $\ln I_i = f(V)$ is a straight line with slope $1/kT$ up to the point $V = A$, at which the accelerating voltage is equal to the appearance potential. For $V > A$, $\ln I_i$ is some other curve. The appearance potential can be found by determining the point at which the transition from the straight line to the other curve takes place.

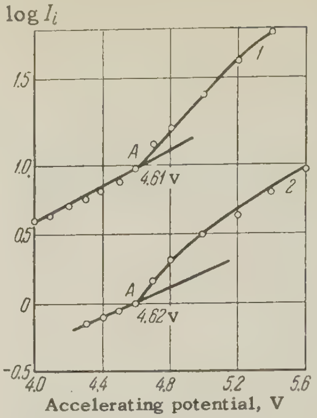

FIG. 15. The quantity $\ln I_i = f(v)$ as a function of accelerating potential for O_2. 1) total ion current 2) current of the monoenergetic component.

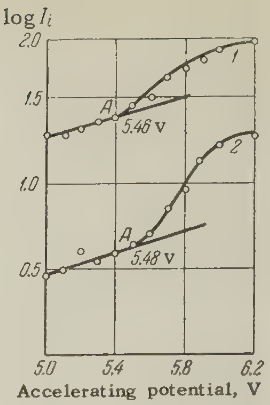

FIG. 16. The quantity $\ln I_i = f(v)$ as a function of accelerating potential for H_2O. 1) total ion current 2) current of the monoenergetic component.

Figures 15 and 16 show the dependence of the logarithms of ion current on accelerating potential. It is apparent from the figures that the initial part of the function $\ln I_i$ is actually a linear function of V. The appearance potential is determined from the transition point between the linear segment and the curvilinear segment (A on the figures). It was found that the appearance potential for O^- in O_2 is 4.63 ± 0.04 ev (average of fifteen measurements); the appearance potential for H^- in H_2O is 5.45 ± 0.09 ev (average of nine measurements). It should be noted that the uncertainty in the given energy scale appears in the spread of the appearance potentials.

The appearance potential for O^- is frequently used as a standard for calibrating energy scales in determining the appearance potentials for negative ions. However, the available data are not consistent. Thus, in the work reported by Lozier[24] it was found that $A(O^-)$ is 4.8 ev. McDowell and Warren,[25] taking the appearance potential of O^- in CO as 9.3 ev, found $A(O^-)$ to be 4.9 ± 0.1 ev. The most reliable value of $A(O^-)$ has been obtained by Marriott and Craggs[8] using a Lozier apparatus. Calibrating the energy scale by the appearance potential of the O_2^+ ion, 12.19 ev, these workers found that $A(O^-) = 4.7 \pm 0.1$ ev. The value found by us for the O^- appearance potential, 4.63 ± 0.04 ev, is in good agreement with the value 4.7 ± 0.1 ev, which was obtained with better accuracy. It should be emphasized that in the present case the appearance potential is determined on an absolute scale without reference to any standard.

In computing the capture cross section the current due to scattered electrons was subtracted from the ion collector current; this electron current was taken equal to the collector current at at accelerating potential smaller than the appearance potential. In O_2 the scattered-electron current was 1 or 2%; in H_2O it was 5 to 10%. The presence of an electron energy distribution was taken into account only in the initial part of the curve. Since the width of the capture region is large compared with the width of the distribution in the region far from the appearance potential, taking account of the distribution will not affect the results to any great extent. It should be noted that in spite of the magnetic field all the H^- and O^- ions must strike the collector since, according to the data in the literature, the kinetic energy of these ions is greater than 1.5 ev.[21,24]

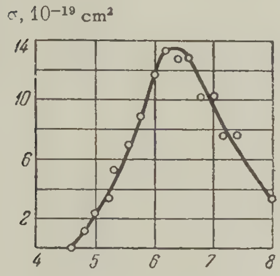

FIG. 17. Electron capture cross section in the molecule O_2.

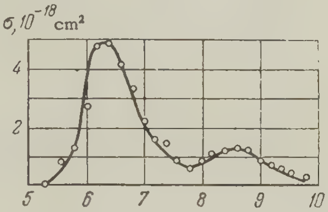

FIG. 18. Electron capture cross section in the molecule H_2O.

Curves showing the dependence of capture cross section on electron energy for O_2 and H_2O are given in Figs. 17 and 18. In O_2 the cross section peak occurs at an energy of 6.2 ev, $\sigma_{max} = (1.3 \pm 0.2) \times 10^{-18}$ cm^2 (average of seven measurements). In H_2O the first peak occurs at $\epsilon = 6.4$ ev, $\sigma_{max} = (4.8 \pm 1.5) \times 10^{-18}$ cm^2; the second peak occurs at $\epsilon = 8.6$ ev, $\sigma_{max} = (1.3 \pm 0.1) \times 10^{-18}$ cm^2 (average of eight measurements).

The second peak on the H_2O curve is apparently due to the formation of excited H_2O^-, which dissociates into H^- and OH. It should be noted that at electron energies greater than 7.5 ev the H^- current is somewhat high because of O^-, although, according to the data of reference 21, the maximum O^- current is approximately four times smaller than the H^- current.

The value of the capture cross section for O_2 at the peak has recently been determined by the single-collision method.[26] The measurements were carried out in a Lozier apparatus, using a magnetic field of approximately 200 oersteds. The capture cross section was determined from the ionization cross section for O_2 or Ar by a comparison of the positive and negative ion currents. Since no measures were taken to avoid the effects of space charge, the cross section determined in this way depends on electron current. Furthermore, a dependence of cross section on pressure and magnetic field was observed as a result of changes in scattering and changes in the electron path length with changes in p and H. To avoid these errors the curves showing the dependence of σ^- on I_e, p and H were extrapolated to the zero values. In making the calculations the values of σ^+ determined in refereces 27 and 28 were used.

The measurements show that the capture cross section at the peak is $(2.25 \pm 0.3) \times 10^{-18}$ cm^2 (average of four measurements). Taking account of the errors pointed out above and possible errors in the values of σ^+ it may be assumed that this value is in agreement with the value found in the present work $(1.3 \pm 0.2) \times 10^{-18}$ cm^2.

6. The table below lists the values of the electron capture cross sections at the peaks and the electron energies at which the peaks occur.

A tendency toward increased cross section with increased molecular complexity can be discerned. It is characteristic that in all the molecules containing halogens which have been investigated the capture cross section increases sharply in the region of the appearance potential. All the molecules which contain halogens have a capture region whose width is approximately several tenths of an electron volt at electron energies of the order of tenths of an

Molecule	Cross section at the first maximum, cm²	Electron energy at the first maximum, ev	Cross section at the second maximum, cm²	Electron energy at the second maximum, ev	Relative dielectric strength*
SF_6	$5.7 \cdot 10^{-16}$	0.00	—	~0.1 [4]	2.3—2.5 [29]
CCl_4	$1.3 \cdot 10^{-16}$	0.02	$1.0 \cdot 10^{-16}$	0.6	6.3 [29]
CF_3J	$7.8 \cdot 10^{-17}$	0.05	$3.2 \cdot 10^{-17}$	0.9	—
CCl_2F_2	$5.4 \cdot 10^{-17}$	0.15			2.4—2.5 [29]
BCl_3	$2.8 \cdot 10^{-17}$	0.4			—
HBr	$5.8 \cdot 10^{-17}$	0.5			2.2 [30]
HCl	$3.9 \cdot 10^{-18}$	0.6			1.5 [30]
H_2O	$4.8 \cdot 10^{-18}$	6.4	$1.3 \cdot 10^{-18}$	.8.6	—
O_2	$1.3 \cdot 10^{-18}$	6.2			—

*With respect to $N_2 = 1$.

electron volt. Further, the more complicated molecules (SF_6, CCl_4 and CF_3I) have a capture region whose width is of the order of hundredths of an electron volt at electron energies of the same order of magnitude. O_2 and H_2O capture electrons with energies of several electron volts and the width of the capture region is also several electron volts.

The observed capture reactions can be explained in terms of rotational (hundredths of electron volts) or vibrational (tenths of electron volts) excitation of the molecule upon collision with the electron and subsequent capture of the electron. As has been shown theoretically[31,32] and experimentally,[33,34] in the molecules H_2 and N_2 the excitation cross sections for the vibrational and rotational levels increase sharply in the threshold energy region (hundredths of electron volts for rotational levels and tenths of electron volts for vibrational levels). The same dependence of capture cross section on electron energy near the appearance potential has been observed in the present case. Capture of this type can be interpreted by the intersection of the potential curve for the negative ion with the potential curve of the neutral ion at a point corresponding to an excited level. In O_2 and H_2O the potential curve for the negative ion lies considerably above the curve for the molecule so that this transition requires an energy of the order of several electron volts.

It is interesting to consider the SF_2^- ion. This ion is apparently an excited ion and the excitation energy, which exceeds the S-F binding energy, is distributed in the different vibrational and rotational degrees of freedom.[4]

A determination of the capture cross sections for slow electrons is of great interest in connection with the dielectric strength of gases. It may be assumed[29,35,36] that a higher dielectric strength is to be associated with a lower value of the Townsend coefficient α. Obviously the coefficient α is reduced with increasing electron capture.

The last column of the table lists values for relative dielectric strength. It is evident from the table that there is some correlation between the values of the capture cross section and the dielectric strength. Complete agreement is not to be expected since the measured cross sections (aside from SF_6) are cross sections for dissociative capture. At high pressures triple collisions are of greatest importance. In this case the capture probability can increase by virtue of stabilization of the molecular ion.

At low pressures, if the greater part of the unstable molecular ions decay with electron detachment, the capture probability with stabilization may increase many fold. On the other hand, if the molecular ions dissociate completely an increase in pressure will have essentially no effect on the capture probability. It is possible that this is the case in HCl and HBr. The cross section for dissociative capture in HBr is larger than the capture cross section in HCl and the dielectric strength in HBr is also greater than the dielectric strength of HCl. The increase in capture cross section, which is characteristic of increasing molecular complexity, may explain the increase in dielectric strength with increasing molecular weight of the gas which has been frequently observed.

I wish to thank V. L. Tal'roze for his interest in the work and valuable comments.

---

[1] N. S. Buchel'nikova, **Приборы и техника эксперимента** (Instruments and Measurement Engg.) 6, (1958).

[2] Fox, Hickam, Grove, and Kjeldaas, Rev. Sci. Instr. **26**, 1101 (1955).

[3] N. S. Buchel'nikova, J. Exptl. Theoret. Phys. (U.S.S.R.) **34**, 519 (1958), Soviet Phys. JETP **7**, 358 (1958).

[4] W. Hickam and R. Fox, J. Chem. Phys. **25**, 642 (1956).

[5] A. J. Ahearn and N. Hanney, J. Chem. Phys. **21**, 119 (1953).

[6] R. Baker and J. Tate, Phys. Rev. **53**, 683 (1938).

[7] Craggs, McDowell, and Warren, Trans. Faraday Soc. **48**, 1093 (1952).

[8] J. Marriott and J. Craggs, Electr. Res. Assoc. Rep. L/T308, (1954).

[9] Marriott, Thurburn, and Craggs, Proc. Phys. Soc. (London) **B67**, 437 (1954).

[10] Reese, Dibeler, and Mohler, J. Res. NBS **57**, 367 (1956).

[11] J. Marriott, Electr. Res. Assoc. Rep. L/T301 (1953).

[12] Dibeler, Reese, and Mohler, J. Res. NBS **57**, 113 (1956).

[13] J. Marriott and J. Craggs, J. Electronics **1**, 405 (1956).

[14] J. Marriott and J. Craggs, J. Electronics **3**, 194 (1957).

[15] R. Fox, J. Chem. Phys. **26**, 1281 (1957).

[16] H. Gutbier and H. Neuert, Z. Naturforsch **9a**, 335 (1954).

[17] R. Healey and J. Read, The Behavior of Slow Electrons in Gases, Sydney 1941.

[18] N. Bradbury, Phys. Rev. **45**, 287 (1934).

[19] H. D. Hagstrum, J. Chem. Phys. **23**, 1178 (1955).

[20] R. Thorburn, Appl. Mass. Spectr. Conf. Rep., London Inst. Petroleum 1954.

[21] Mann, Hustrulid and Tate, Phys. Rev. **58**, 340 (1940).

[22] K. Laidler, J. Chem. Phys. **22**, 1740 (1954).

[23] R. E. Honig, J. Chem. Phys. **16**, 105 (1948).

[24] W. Lozier, Phys. Rev. **46**, 268 (1934).

[25] C. A. McDowell and J. Warren, Disc. Far. Soc. **10**, 53 (1951).

[26] Craggs, Thorburn, and Tozer, Proc. Roy. Soc. (London) **240A**, 473 (1957).

[27] J. T. Tate and P. T. Smith, Phys. Rev. **39**, 270 (1932).

[28] P. T. Smith, Phys. Rev. **36**, 1293 (1930).

[29] B. M. Gokhberg and E. I. Zandberg, Dokl. Akad. Nauk SSSR **53**, 515 (1946).

[30] C. Kowalenko, J. Phys. U.S.S.R. **3**, 455 (1940).

[31] Ta-You Wu, Phys. Rev. **71**, 111 (1947).

[32] E. Gerjuoy and S. Stein, Phys. Rev. **97**, 1671 (1955).

[33] J. Anderson and L. Goldstein, Phys. Rev. **102**, 388 (1956).

[34] R. Haas, Z. Physik **148**, 177 (1957).

[35] Warren, Hopwood, and Craggs, Proc. Phys. Soc. (London) **B63**, 180 (1950).

[36] Warren, Marriott, and Craggs, Nature **171**, 514 (1953).

Translated by H. Lashinsky
240

SOVIET PHYSICS JETP VOLUME 35(8), NUMBER 5 MAY, 1959

MEASUREMENT OF THE POLARIZATION OF NEGATIVE μ-MESONS IN CARBON, OXYGEN, MAGNESIUM, SULPHUR, ZINC, CADMIUM AND LEAD MESIC ATOMS

A. E. IGNATENKO, L. B. EGOROV, B. KHALUPA, and D. CHULTEM

Joint Institute for Nuclear Research

Submitted to JETP editor May 31, 1958

J. Exptl. Theoret. Phys. (U.S.S.R.) **35**, 1131-1134 (November, 1958)

Angular distributions of electrons from the decays of μ mesons in C, O, Mg, S, Zn, Cd, and Pb mesic atoms were measured using scintillation counters. The μ-meson polarization was determined from the results of these measurements. The polarization amounts to $(19 \pm 7)\%$ in Mg, Zn, Cd, and Pb mesic atoms, and to $(15 \pm 4)\%$ in C, O, and S mesic atoms. Depolarization of μ mesons in substances with zero nuclear spin is explained as due mainly to the spin-orbit interaction in the mesic atom formation process, and due in part to the action of the magnetic field of the atomic electron shell on the μ meson during its lifetime in the K orbit.

1. INTRODUCTION

It is known that in the process of slowing down, negative μ mesons first form mesic atoms and then undergo nuclear capture. The capture process may be described by the reaction $\mu^- + p \rightarrow n + \nu$. The study of the angular distribution of neutrons produced in the capture of μ^- mesons in liquid hydrogen provides a method for the determination of the form of the weak μ-meson-nucleon interaction.[1,2] However, experiments[3] on the polarization of μ^- mesons in liquid hydrogen indicate that this method is not useful, owing to the total depolarization of the μ^- mesons. A theoretical discussion of the capture of polarized μ^- mesons by light nuclei shows[2] that measurement of the angular distribution of neutrons with energies near the upper end of the spectrum may provide a means of determining the interaction form. The neutron angular distribution is given by the formula

$$W(\theta) = 1 + a\beta\gamma\cos\theta, \qquad (1)$$

where β is the asymmetry coefficient whose magnitude and sign depend on the interaction form, θ is the angle between the direction of emission of the neutron and the μ^- meson spin, a is a coefficient which depends on the degree of polarization of the μ^- meson in the mesic atom, and γ is a coefficient that depends on the depolarization of the neutrons inside the nucleus.

It follows from Eq. (1) that an experiment on the neutron angular distribution should be preceded by experiments on μ^--meson polarization in mesic atoms and on neutron depolarization in nuclear matter. The present work is devoted to the study of the μ^--meson polarization in various substances.

2. MAIN THEORETICAL ASSUMPTIONS

We start from the following assumptions about the depolarization mechanism of μ^--mesons which are being slowed down and stopped in matter. It follows from the work of Ford and Mullin[4] and Bincer[5] that in the slowing down of μ mesons no depolarization occurs prior to their capture into a mesic atom orbit. In the process of mesic atom formation depolarization is possible due to the fine structure, and due to the action of the magnetic fields of the atomic electron shell and the atomic nucleus. Depolarization due to the spin-orbit interaction will occur if the lifetime τ_{life} of the μ^- meson in a given $l \neq 0$ level is longer that the time τ_{flip} necessary for the μ-meson spin to flip under the action of the magnetic field created by the orbital motion. The lifetime τ_{life} can be calculated from the formula given by Fermi and Teller.[6] The time τ_{flip} can be estimated from the relation $\tau_{\text{flip}}\Delta E \sim h$ where ΔE is the separation of the fine structure levels in mesic atoms.[7] It turns out that τ_{life} is larger than τ_{flip} by several orders of magnitude. Depolarization due to the action of the magnetic fields of the electronic shell and of the nucleus will be negligible in the process of the meson reaching the K orbit. In fact, for this case one has $\tau_{\text{life}} < \tau'_{\text{flip}}$, where $\tau'_{\text{flip}} = h/\Delta E'$ ($\Delta E'$ is the separation of the hyperfine structure levels).

It can therefore be said that in the process of formation of mesic atoms depolarization proceeds mainly due to the fine and hyperfine structure interactions. After the μ^- meson reaches the K orbit, where it remains until its decay or nuclear capture, depolarization may be caused by the magnetic field of the electronic shell (I. M. Shmushkevich, private communication).

Depolarization due to the hyperfine structure can be avoided by employing materials with zero nuclear spin. Depolarization due to the field of the electronic shell cannot be avoided in this manner, since the mesic atom formation process is always accompanied by a rearrangement of the electronic shell of the capturing atom (owing to the change in the effective charge of the nucleus by one unit). Consequently, in the stopping of μ^- mesons in such materials the main sources of depolarization will apparently be the spin-orbit interaction and the interaction between the magnetic field of the electronic shell and that of the μ^- meson during its lifetime in the K orbit.

Starting from these assumptions, we measured the polarization of μ^- mesons in a number of substances, 85 to 95% of which were composed of atoms with zero nuclear spin, namely C, O, Mg, S, Zn, Cd, and Pb.

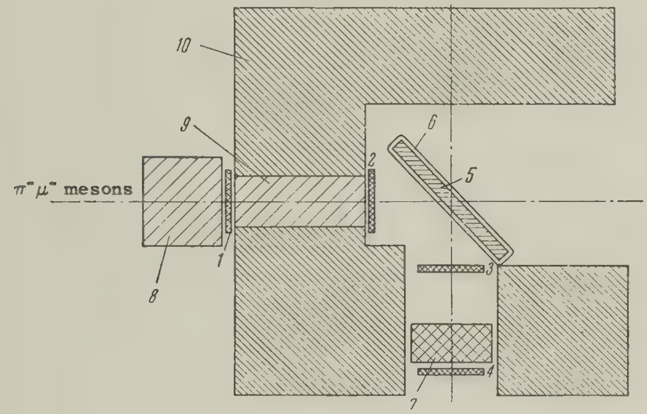

1, 2, 3, 4) scintillation counters; 5) target; 6) magnetizing coil; 7) paraffin filter; 8, 9) aluminum filters; 10) lead shield.

3. THE EXPERIMENT

The polarization of the μ^- mesons was studied by measuring the anisotropy in the angular distribution of the decay electrons. The experimental arrangement was the same as that used previously.[3] The π and μ mesons were slowed down by aluminum filters. The μ^- mesons, after traversing the filters, were stopped in a target made of the substance under investigation. The targets measured 15 × 15 cm and were 2 to 6 g/cm² thick. The angle between the target and the "axis" of the meson beam was 45°. The target was wrapped in a copper wire coil which served to create the magnetic field necessary to make the μ mesons precess. Our previously published work[3] gives a detailed description of the experimental conditions, the scintillation counters, and the electronic apparatus. In the present experiments the polyethylene filter between counters 3 and 4 was 4 to 8 g/cm² thick.

For carbon, oxygen, magnesium, and sulphur the asymetry coefficient a in the decay electron angular distribution $I(\theta) = 1 + a\cos\theta$ was determined from the dependence of the number of electrons observed on the intensity of the magnetic field H surrounding the target. For zinc, cadmium, and lead the quantity a was determined from the number of electrons obtained when the field value was $H_{\max}$ and $H_{\min}$, corresponding to the maximum and minimum intensity of electrons in the precession curve calculated from the expression

$$I(H) = \int_{t_1}^{t_2} e^{-t/\tau}\left[1 + a\cos(2\pi ft + \theta_0)\right] dt,$$

taking into account the delay time t_1, the "gate" width $t_2 - t_1$, and the lifetime τ of μ^- mesons.[8,9]

The "gate" width was approximately equal to τ in the C, O, Mg, and S experiments and 2τ to 3τ in the Zn, Cd, and Pb experiments. The ratio $t_1/(t_2 - t_1)$ was approximately 0.3 in all experiments. In the carbon experiments, for example, the counting speed at H = 0 was 120 electrons per minute, while in the lead experiments it was about 8 electrons per minute. The background level amounted to 3 counts per minute and was independent of the field H. The background was taken as half the sum of the electron detector counts obtained without the target and magnetizing coil and the counts obtained with the coil but without the target.

As a result of the experiments, values of the asymmetry coefficient a were obtained for electrons which traversed more than $x = x_1 + \frac{1}{2}x_2 + x_3$ g/cm² (here x_1 is the thickness of the filter between counters 3 and 4, x_2 is the target thickness, and x_3 is the thickness of the scintillation counters in the electron detector). Then, using the data[10] on the energy dependence of the asymmetry in $\mu^+ - e^+$ decay, we obtained values for a_0, the asymmetry coefficient for the integrated spectrum, i.e., for x = 0. The values of a_0 are listed in the second column of the table.

The listed values of a_0 were corrected for the delay time, "gate" width, μ^--meson decay, and the solid angle of the electron detector. The indicated errors are standard statistical deviations.

Substance	$-a_0$	Polarization P, %
C	0.040±0.005	14±4
$O(H_2)$	0.043±0.005	15±4
Mg	0.058±0.008	20±5
S	0.042±0.006	15±4
Zn	0.056±0.011	19±7
Cd	0.055±0.012	19±7
Pb	0.054±0.013	19±7

4. DISCUSSION OF RESULTS

On the assumption of invariance under CP, the magnitude of the polarization P_- of μ^--mesons in mesic atoms can be obtained from the equality $a_0^-/P_- = a_0^+/P_+$, where a_0^- and a_0^+ are the asymmetry coefficients for the μ^-- and μ^+-mesons respectively and P_+ is the degree of polarization of μ^+-mesons before decay. Let us assume that the degree of polarization of μ^+-meson beams obtained from internal targets in synchrocyclotrons is independent of the energy of the accelerated protons.[10] If the μ^--meson beam we used is taken to have the same degree of polarization as the μ^+-meson beams, then P_- can be obtained from the inequality[11] $3a_0 \leq P \leq 4a_0$. Values of P obtained in this manner are listed in the third column of the table. Only errors in the quantity a_0 were taken into account in this calculation. As can be seen from the table the polarization amounts to (19 ± 7)% in magnesium, zinc, cadmium, and lead mesic atoms, and (15 ± 4)% in carbon, oxygen, and sulphur mesic atoms. From a comparison of the maximum polarizations observed for μ^- and μ^+ mesons we conclude that μ^- mesons are depolarized to a larger extent. The strong depolarization of μ^- mesons can be explained by the factors mentioned earlier.

The question arises whether it is possible to restore in some manner the polarization of μ mesons in mesic atoms. Clearly, there is no simple way to eliminate the depolarization due to the spin-orbit interaction. The depolarization due to the action of the electronic shell can, apparently, be eliminated. Placing the target in a longitudinal magnetic field of ~ 10,000 Oe should result in a "partial restoration" of the polarization due to the decoupling of the electronic shell and the μ^- meson.

In conclusion, the authors consider it their duty to thank Prof. B. Pontecorvo for a number of valuable comments. The authors also take this opportunity to thank S. S. Gershtein, V. B. Beliaev, and B. N. Zakharev for discussion of the results and continued interest in this work.

---

[1] Shapiro, Dolinskii, and Blokhintsev, Dokl. Akad. Nauk SSSR **116**, 946 (1957), Soviet Phys. "Doklady" **2**, 475 (1957).

[2] B. L. Ioffe, J. Exptl. Theoret. Phys. (U.S.S.R.) **33**, 308 (1957), Soviet Phys. JETP **6**, 240 (1958).

[3] Ignatenko, Yegorov, Khalupa and Chultem, J. Exptl. Theoret. Phys. (U.S.S.R.) **35**, 894 (1958), Soviet Phys. JETP **8**, 621 (1959).

[4] G. W. Ford and C. J. Mullin, Phys. Rev. **108**, 477 (1957).

[5] A. M. Bincer, Phys. Rev. **107**, 1434 (1957).

[6] E. Fermi and E. Teller, Phys. Rev. **72**, 399 (1947).

[7] R. E. Marshak, Meson Physics, ch. 5, N. Y. 1952.

[8] Garwin, Lederman, and Weinrich, Phys. Rev. **105**, 1415 (1957).

[9] Sens, Swanson, Telegdi, and Yovanovitch, Phys. Rev. **107**, 1464 (1957).

[10] Mukhin, Ozerov, and Pontecorvo, J. Exptl. Theoret. Phys. (U.S.S.R.) **35**, 340 (1958), Soviet Phys. JETP **8**, 237 (1959).

[11] H. Öberall, Nuovo cimento **6**, 533 (1957).

Translated by A. M. Bincer
241

SOVIET PHYSICS JEPT VOLUME 35(8), NUMBER 5 MAY, 1959

RADIOCHEMICAL STUDY OF THE PHOTOFISSION OF Th^{232}

I. A. VASIL' EV and K. A. PETRZHAK

Leningrad Technological Institute

Submitted to JETP editor June 2, 1958

J. Exptl. Theoret. Phys. (U.S.S.R.) **35**, 1135-1140 (November, 1958)

Twelve types of fragments from the photofission of Th^{232} at a peak bremsstrahlung energy of 10 Mev were identified by a radiochemical method. The dependence of the fission product yield on the mass number was determined. The dependence of the peak-to-valley ratio of the Th^{232} and U^{238} photofission yield curves on the peak bremsstrahlung energy was determined in the energy range from 8 to 14 Mev. Results of calculations by Fong's method relating to the photofission of thorium and uranium are presented.

THE photofission of heavy nuclei at low excitation energies provides several important items of information on nuclear properties. The items investigated are the photofission thresholds, the differential cross sections, the distribution of fission fragments in mass, energy and charge, the average number of neutrons per fission and, finally, the angular anisotropy in the distribution of fission fragments.

The overall picture of the mass distribution of fission fragments enables us to determine the most probable type of fission, the dependence of the symmetric fission on excitation energy, the mean number of neutrons per fission, and also the role played by the shell structure in the yield of the primary fission products and the role played by the collective oscillations of nuclear matter at low excitation energies. From published work it can be seen that the mass distribution of fission fragments depends on the structure of the nucleus undergoing fission and on the type and energy of the particles producing fission.

At the present time there are two papers devoted to the experimental study of the mass distribution of the products of photofission of Th^{232}. Hiller and Martin[1] identified thirteen fragments by a radiochemical method and used the data so obtained to plot the dependence of the yields on the mass number for the photofission of Th^{232} at a bremsstrahlung peak energy of 69 Mev. In Avdonin and Petrzhak's paper[2] the determination of the mass distribution of fission products was not the main problem, and at a maximum γ-quantum energy of 12 Mev essentially only the position of the minimum has been determined for the photofission of Th^{232}.

However, photofission at low excitation energies has a number of advantages over other forms of fission. Only in the case of photofission is it possible to observe the fission of the nucleus under investigation, since the absorption of a γ quantum does not change its charge and mass. Low excitation energy also eliminates the indefiniteness in the mass and in the charge of the nucleus undergoing fission, since at such energies the emission of nucleons before fission is energetically impossible. The study of the characteristics of photofission near the threshhold and below the threshhold permits us to elucidate the nature of spontaneous fission. For example, spontaneous fission may be regarded as a special case of photofission at a γ-quantum energy equal to zero. It therefore appeared to be of interest to study in greater detail the shape of the yield curve for the photofission of Th^{232} at low excitation energies.

The literature already contains a number of papers[3-5] on the low energy photofission of U^{238}, To be able to compare the yield curves for thorium and uranium, the peak bremsstrahlung energy for the study of Th^{232} was therefore taken to be 10 Mev. The work was carried out with the betatron of the Leningrad Technological Institute, with a maximum energy of 15 Mev. To obtain greater fission-fragment activities, the samples were irradiated inside the betatron accelerating chamber. The accelerated electrons were stopped directly in the substance of the sample undergoing irradiation, and this increased the betatron-radiation utilization factor. The fraction of fissions produced by electrons is assumed to be insignificant in view of the small interaction cross section for the electron and of the large surface density of the sample in the direction of the electron beam (of the order of 10 g/cm^2). The number of fissions induced by the neutrons produced in the sample itself and in the surrounding materials by fission or by the photonuclear effect can be estimated from the known neutron cross sections and geometrical conditions. In our case they were calculated to be less than 0.2% of the total effect for thorium and uranium. This question has been investigated experimentally by Richter and Coryell[4] and by Schmitt and Duffield.[6] Their results also lead to the conclusion that the number of fissions due to neutrons is less than 1%.

The sample for irradiation was prepared by pressing baked thorium oxide (in the case when uranium was irradiated it was prepared from uranium oxides). The weight of the sample was 0.5 to 1.0 gm. The time of irradiation was usually ~ 10 hours.

The energy of the betatron radiation was calibrated by making use of the known values for the thresholds of photonuclear reactions in a number of elements. In the course of the work the constancy of the calibration was checked by means of the threshold of the reaction $Cu^{63}(\gamma; n) Cu^{62}$. The stability of the energy during irradiation was monitored by a voltage induced in a loop situated in the magnetic field of the betatron. The error in the determination of the peak bremsstrahlung energy is estimated to be ± 0.3 Mev. The constancy of the radiation intensity was monitored by means of an ionization chamber.

The irradiated sample was dissolved in acid and a certain amount of isotopic carriers was added to the solution so obtained. Usually from two to five fission fragments were separated out from a mixture of products after one irradiation. The methods described in reference 7 were taken as the basis for the chemical procedures for the separation and the radiochemical purification of fission products. Certain changes were introduced into them associated with the necessity of opening up the irradiated oxide samples, and of separating the fragments from thorium. At the end of the radiochemical operations the carrier was precipitated for quantitative analysis. The preparation for β counting was made by transferring this precipitate onto a disk of filter paper.

The β activity of the preparations was measured by an end counter for several half-lives. The decay curves for each element were analyzed and the fact that the resultant activity belonged to the isotope under investigation was established by means of the half-life.

Twelve different kinds of fragments were separated in the course of the work. Fission fragments with different mass numbers from 83 to 143 and having short half-lives were selected. Relative activities of the fission products were determined, i.e., one fission fragment was chosen as a standard and was separated in each experiment, and the intensity of the β radiation of the others was determined relative to the intensity for the standard one. Ce^{143} was chosen as the standard. The relative activity for each kind of fission fragment was determined by taking the average of the results of from 2 to 6 irradiations.

To convert from the relative activity to the relative yield for a pair of fission fragments it is necessary to know the efficiency of the end counter for the β radiation from these fragments. To obtain the required conversion coefficients, uranium samples were irradiated under similar conditions. The same fission fragments were separated from the fission products of U^{238}, as in the case of thorium, and their relative activities were found. By utilizing data available in the literature[3,4] on the photofission of U^{238} at 10 Mev, we determined the coefficients needed for the conversion from relative activity to relative yields. These coefficients were then used to obtain the relative yields for the photofission of Th^{232}.

Along with determining the yield curve for the photofission of Th^{232} at 10 Mev, we also investigated, for both thorium and uranium, the dependence on the bremsstrahlung peak energy in the energy range from 8 to 14 Mev of the ratio of the most probable type of fission to symmetric fission. For this purpose three fragment elements (silver, cadmium, and cerium) were separated from samples irradiated at different energies. The relative yields of Ag^{113}, Cd^{115} and Cd^{117} determined the position of the minimum of the yield curve, while the yield of Ce^{143} corresponded within experimental error to the maximum yield. Experiments on the determination of the peak-to-valley ratio carried out at the peak energy of 10 Mev demonstrated good reproducibility of the results. We found it therefore possible to determine this ratio at other energies by means of a single irradiation.

The results of determining yields for the photofission of Th^{232} at 10 Mev are given in Table I. In this table column 3 gives the yields of the fission products relative to the yield of Ce^{143}. We assumed that the total yields of the fragments shown in the table are equal to the total yield of the chain of a given mass number. An examination of the independent yields of the subsequent members of the chain shows that this assumption holds with a high degree of accuracy.

In the fission process to each mass number indicated in the table there corresponds a com-

TABLE I. Yields of products of photofission of Th^{232} at a maximum bremsstrahlung energy of 10 Mev

Separated fragment	Half-life, hours	Yield relative to Ce^{143}		Yield in % normalized to 200%	
		Value	% error	Value	% error
1	2	3		4	
Br^{83}	2.4	0.187	25	1.8	0.44
Sr^{91}	9.7	0.597	16	5.7	0.91
Zr^{97}	17.0	0.244	22	2.3	0.51
Mo^{99}	68.3	0.119	18	1.1	0.2
Ag^{113}	5.3	0.007	24	0.066	0.016
Cd^{115}	53	0.0034	26	0.032	0.008
Cd^{117}	2.83	0.0039	30	0.037	0.011
Sb^{129}	4.2	0.052	48	0.50	0.25
J^{133}	20.5	0.45	40	4.3	1.7
Ba^{139}	1.43	0.53	15	5.0	0.75
Ba^{140}	306	0.808	21	7.7	1.5
Ce^{143}	33.0	1.0	—	9.5	—

plementary "mirror-point" fragment, which has the same yield. To determine its mass it is necessary to know the mean number of neutrons emitted per fission. By making different assumptions with respect to the mean number of neutrons we found that the fundamental and the mirror points fit a smooth curve best when $\nu = 3$ (Fig. 1). By equating the area bounded by the smooth curve of relative yields to 200% we obtained the values for the absolute yields of the fission products under investigation. The absolute yields are given in column 4.

The large values of the errors in Table I is explained in the following manner. In view of the low activities of the products of low energy photofission of Th^{232}, the error in the relative activities obtained directly from experiment was about 6% in the neighborhood of the peaks and about 10 to 12% in the neighborhood of the minimum. The larger errors for Sb^{129} and I^{133} are due to the poor reproducibility of results in the former case and to the difficulty in analyzing the complex decay curve and to the extrapolation error in the latter case. Our method of calibrating the counting apparatus requires us to take into account the error in the determination of relative activities in the photofission of U^{238} and the error in the relative yields taken from references 3 and 4. The error introduced through the normalization of the area bounded by the smooth yield curve to 200% is insignificant and was not taken into account in our work.

Figure 1 shows three curves of the dependence on the mass number of the fission product yields. The main characteristics of these curves are given in Table II.

From a comparison of the yield curves for the

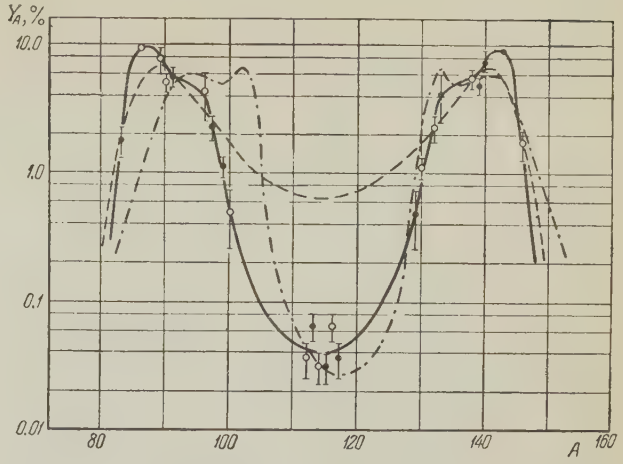

FIG. 1. The dependence of fission product yields on the mass number. Solid curve gives the results of the present work for the photofission of Th^{232} at 10 Mev: ● are the basic points, ○ are the mirror points; the dotted curve corresponds to the photofission of Th^{232} at 69 Mev;[1] the dot-dashed curve corresponds to the photofission of U^{238} at 10 Mev.[3,4]

photofission of Th^{232} and U^{238} at 10 Mev it may be seen that the peak for the light fragments in the thorium curve is noticeably displaced towards lower mass numbers compared to the same peak in the case of uranium. At the same time the positions of the heavy fragment peaks almost coincide. Such a distribution of fission-product yields of thorium and of uranium agrees well with the mechanism of fission proposed by Hill[8] and determined by the nuclear shell effect and by the principal role played by the heavy fragment.

In the neighborhood of mass numbers 133 and 96 on the yield curve for the photofission of Th^{232} higher yields are observed compared to the smooth decrease of the yields from the peak towards the minimum. In the heavy fragment peak this region coincides with the region of mass numbers where "fine structure" is observed in the photofission of U^{238}. This enables us to make the hypothesis that

TABLE II. Principal characteristics of the yield curves for the photofission of Th^{232} and U^{238}

Parameters of the yield curves	Th^{232} (γ_{10}; f) present work	Th^{232} (γ_{69}; f) from reference 1	U^{238} (γ_{10}; f) from references 3 and 4
Position of the heavy fragment peak	140	139	138
Position of the light fragment peak	89	90	97
Maximum yield	9.5%	6.8%	6.0%
Half-width of peak	8	11	12–13
Peak-to-valley ratio	250	10	215

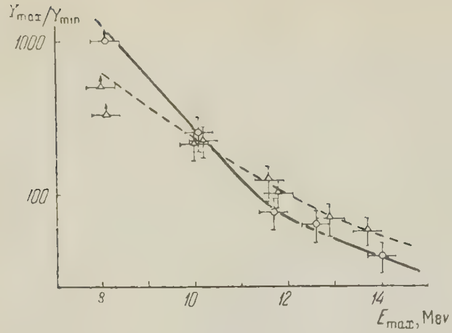

FIG. 2. Dependence of the peak-to-valley ratio on the maximum bremsstrahlung energy for photofission of: solid curve – Th^{232}, dotted curve – U^{238}.

the higher yields in the photofission of Th^{232} are associated with the preferred formation among the primary fission products of nuclei with a closed shell ($N = 82$).

A comparison of the yield curves[1] for the photofission of Th^{232} at 10 Mev and at 69 Mev shows that in this case the positions of the peaks almost coincide. However, in the former case the half width of the peak of the yield curve is less and the value of the maximum yield is greater than in the latter case. Thus the peak of the yield curve becomes wider and lower as the excitation energy of the nucleus undergoing fission is raised, while the proportion of symmetric fissions increases. The width of the peak also increases as the mass number of the nucleus undergoing fission is increased.

The peak-to-valley ratio is one of the basic characteristics of the dependence of the fission product yield on the mass number and is specially investigated in a number of papers.[3,5,9,10]. In our work this ratio is determined for the first time for the photofission of Th^{232} in the region of low excitation energies and it is shown that the variation of this ratio in the range from 8 to 14 Mev for the peak bremsstrahlung spectrum energies is more pronounced for thorium than for uranium. Figure 2 shows the variation of this ratio with energy. The results of the present work are in good agreement with the number 80 obtained for the photofission of thorium at 12 Mev.[2]

In Fong's last paper[11] a new method was proposed for calculating the yield curve theoretically. We considered it to be of interest to utilize this method to calculate the yield curves theoretically for the photofission of thorium and of uranium. Unfortunately, final results have not been obtained due to the lack of precise values for the nuclear masses of Th^{232} and U^{238}. As a result of these calculations we have obtained only the differences in the maximum excitation energies for a given type of fission and for symmetric fission [formula (46) of reference 11]. The dependence of this difference on the ratio of the masses of primary fission fragments enables us to show in general outline the shape of the yield curves and the position of the peaks on these curves.

The results obtained by us for the photofission of Th^{232} and U^{238} agree well with the experimental data both with respect to the shape of the curves and also with respect to the position of the maxima. Thus, the position of the maxima of the theoretically calculated curve for Th^{232} is at mass numbers 89 and 140, while for U^{238} the corresponding values are 97 and 138. The calculated curve for the photofission of U^{238} has "fine structure" at mass number 132.

---

[1] D. M. Hiller and D. S. Martin, Phys. Rev. **90**, 581 (1953). D. M. Hiller, Iowa State Coll. J. of Sci. 29, 428 (1955).

[2] V. P. Avdonin and K. A. Petrzhak, Тр. Ленинградского технологического института (Trans. Leningrad Technological Inst.) **40**, 5 (1957).

[3] R. A. Schmitt and N. Sugarman, Phys. Rev. **95**, 1260 (1954).

[4] H. G. Richter and C. D. Coryell, Phys. Rev. **95**, 1550 (1954).

[5] Katz, Kavanach, Cameron, Bailey, and Spinks, Phys. Rev. **99**, 98 (1955).

[6] R. A. Schmitt and R. B. Duffield, Phys. Rev. **105**, 1277 (1957).

[7] Nat. Nucl. Energy Series, Plutonium Project Record, vol. 9, div. IV.

[8] R. D. Hill, Phys. Rev. **98**, 1272 (1955).

[9] Turkevich, Niday, and Tompkins, Phys. Rev. **89**, 552 (1953).

[10] Fowler, Jones, and Paehler, Phys. Rev. **88**, 71 (1952).

[11] P. Fong, Phys. Rev. **102**, 434 (1956).

Translated by G. Volkoff
242

SOVIET PHYSICS JETP VOLUME 35(8), NUMBER 5 MAY, 1959

KINETIC EQUATIONS FOR A SYSTEM OF PARTICLES INTERACTING WITH LATTICE VIBRATIONS

Iu. L. KLIMONTOVICH and S. V. TEMKO

Moscow State University

Submitted to JETP editor March 3, 1958; resubmitted July 3, 1958

J. Exptl. Theoret. Phys. (U.S.S.R.) **35**, 1141-1147 (November, 1958)

A derivation is given of the kinetic equations for the distribution functions of electrons and vibrations of a crystalline lattice. In the spatially homogeneous case, the equation for the distribution function of the electrons is identical to the kinetic equation in Bloch's theory of electric conductivity. An equation is obtained for the lattice vibrations, and expressions have been found for the frequency and the damping decrement of these vibrations.

IN the present paper, the method of Bogoliubov[1,2] has been applied to the derivation of the kinetic equations for the electron and the oscillations of a crystalline lattice. Several very interesting researches, devoted to the theory of superconductivity, have recently been reported. On the one hand there are the researches of Bardeen, Cooper, and Schrieffer,[3] and on the other, the new method in the theory of superconductivity developed by Bogoliubov.[4] In this connection, there is interest in the study of the kinetic equations for systems of electrons interacting with the lattice vibrations. However, for the purpose of finding a simpler approach to the description of nonequilibrium processes in solids, we limit ourselves in the present note only to the approximation leading to the Bloch theory, and do not take up the question of superconductivity. We note that, in recently published works,[5,6] a derivation has been given of the quantum kinetic equation for electrons interacting with lattice vibrations, in the spatially homogeneous case. This equation is identical to the well-known equation of Bloch theory. The approximate kinetic equations have been obtained by us both for electrons and also for the oscillators of the crystalline lattice in the homogeneous case. Initially, the equations were obtained for the distribution functions of the electrons and the oscillators of the lattice in the classical approximation; these have the form of the Fokker-Planck equations in phase space. Then a derivation was given of the kinetic equations for the corresponding inhomogeneous quantum distribution functions.

Following Fröhlich, we shall write the Hamiltonian function for the system of electrons interacting with the lattice vibrations of a crystal in the form

$$H_{\mathrm{F}} = \sum_{(1\leqslant i\leqslant N)} \frac{\mathbf{p}_i^2}{2m} + \frac{c}{\sqrt{N}} \sum_{(1\leqslant i\leqslant N)} \int \delta(\mathbf{q}-\mathbf{q}_i)\,\mathrm{div}_{\mathbf{q}} \sum_{\mathbf{k}} (\mathbf{Q}_{\mathbf{k}}^{(1)} \tag{1}$$

$$\times \sin \mathbf{k}\cdot\mathbf{q} + \mathbf{Q}_{\mathbf{k}}^{(2)} \cos \mathbf{k}\cdot\mathbf{q})\,d\mathbf{q} + \sum_{\mathbf{k}} \sum_{j=1}^{2} (\mathbf{P}_{\mathbf{k}}^{(j)^2}/2M + M\omega_{\kappa}^2 \mathbf{Q}_{\mathbf{k}}^{(j)^2}/2).$$

Here N is the number of electrons, c is the interaction constant, which has the dimensions of energy; M is the mass of the ions; $\mathbf{Q}_{\mathbf{k}}^{(j)}$, $\mathbf{P}_{\mathbf{k}}^{(j)}$ are the coordinates and the momenta of the lattice oscillators; j = 1, 2; $\omega_{\mathbf{k}} = ks$ is the vibration frequency with wave number k; s is the sound velocity without consideration of the interaction between the electrons and the lattice vibrations of the crystal. Making use of the Hamiltonian (1), we obtained the equations of motion for the electrons and for the oscillators of the lattice. Desiring to set up the kinetic equations for the distribution functions of the electrons and the waves of the crystalline lattice, we introduce the distribution functions of the coordinates and momenta of all the electrons and oscillators of the lattice of the crystal. This distribution function can be normalized since the event, that the coordinates and momenta of the electrons and lattice oscillators have any values at all, is certain. By virtue of the Hamilton equations for the distribution function f thus introduced, the equation

$$\frac{\partial f}{\partial t} + \sum_i \frac{\mathbf{p}_i}{m} \frac{\partial f}{\partial \mathbf{q}_i} + \sum_{\mathbf{k},j} \left(\frac{\mathbf{P}_{\mathbf{k}}^{(j)}}{M} \frac{\partial f}{\partial \mathbf{Q}_{\mathbf{k}}^{(j)}} - M\omega_{\mathbf{k}}^2 Q_{\mathbf{k}}^{(j)} \frac{\partial f}{\partial \mathbf{P}_{\mathbf{k}}^{(j)}} \right)$$

$$\times \frac{c}{\sqrt{N}} \sum_{\mathbf{k},j,i} (\mathbf{Q}_{\mathbf{k}}^{(j)}\cdot\mathbf{k}) \begin{matrix} \sin \mathbf{k}\cdot\mathbf{q}_i \\ \cos \mathbf{k}\cdot\mathbf{q}_i \end{matrix} \mathbf{k} \frac{\partial f}{\partial \mathbf{p}_i}$$

$$- \frac{c}{\sqrt{N}} \sum_{\mathbf{k},j,i} \begin{matrix} \cos \mathbf{k}\cdot\mathbf{q}_i \\ -\sin \mathbf{k}\cdot\mathbf{q}_i \end{matrix} \mathbf{k} \frac{\partial f}{\partial \mathbf{P}_{\mathbf{k}}^{(j)}} = 0 \tag{2}$$

is obtained. Here and below, the upper function refers to the term with $j = 1$, while the lower refers to $j = 2$. From this equation we can, by integration, obtain a chain of equations for the corresponding distribution functions. We have limited ourselves to the consideration of the equation only for the first distribution functions of the electrons and lattice oscillators $f_1(\mathbf{q}, \mathbf{p};\ t)\, F_1(\mathbf{Q}_\mathbf{k}^{(j)}, \mathbf{P}_\mathbf{k}^{(j)};\ t)$, and only for one mixed second distribution function $\Phi_2(\mathbf{q}\cdot\mathbf{p};\ \mathbf{Q}_\mathbf{k}^{(j)}, \mathbf{P}_\mathbf{k}^{(j)};\ t)$. For brevity, we shall not write out the expansion here. (Where possible, we shall omit the arguments of the distribution functions in what follows.) To obtain a closed set of approximate equations according to the work of Bogoliubov and Gurov,^{2} we have made use of the following approximations of the second distribution functions:

$$\Phi_2(\mathbf{q}, \mathbf{p};\ \mathbf{Q}_\mathbf{k}, \mathbf{P}_\mathbf{k};\ t) = f_1(\mathbf{q}, \mathbf{p};\ t)\, F_1(\mathbf{Q}_\mathbf{k}, \mathbf{P}_\mathbf{k};\ t) + g(\mathbf{q}, \mathbf{p};\ \mathbf{Q}_\mathbf{k}, \mathbf{P}_\mathbf{k};\ t),$$

where g is the correlation function that governs the interaction of the electrons with the lattice vibrations. The third distribution functions are represented in the form of products of the corresponding first distribution functions. Here the interaction between the electrons and the lattice vibrations is assumed to be weak, and we can therefore regard the function of the correlation deviation g to be small in comparison with the products of the first distribution functions. In the approximation under consideration, the equations for f_1, F_1 and g take on the following forms:

$$\frac{\partial f_1}{\partial t} + \frac{\mathbf{p}}{m}\frac{\partial f_1}{\partial \mathbf{q}} + \frac{c}{\sqrt{N}}\sum_{j,\mathbf{k}}\int (\mathbf{Q}_\mathbf{k}^{(j)}\cdot\mathbf{k}) \begin{matrix}\sin \mathbf{k}\cdot\mathbf{q}\\ \cdot\\ \cos \mathbf{k}\cdot\mathbf{q}\end{matrix} F_1(\mathbf{Q}_\mathbf{k}, \mathbf{P}_\mathbf{k};\ t) \tag{3}$$

$$\times\, d\mathbf{Q}_\mathbf{k} d\mathbf{P}_\mathbf{k}\, \mathbf{k}\frac{\partial f_1}{\partial \mathbf{p}} = -\frac{c}{\sqrt{N}}\sum_{j,\mathbf{k}}\int (\mathbf{k}\cdot\mathbf{Q}_\mathbf{k}^{(j)}) \begin{matrix}\sin \mathbf{k}\cdot\mathbf{q}\\ \\ \cos \mathbf{k}\cdot\mathbf{q}\end{matrix}\, \mathbf{k}\frac{\partial g}{\partial \mathbf{p}}\, d\mathbf{Q}_\mathbf{k} d\mathbf{P}_\mathbf{k};$$

$$\frac{\partial F_1}{\partial t} + \sum_j\left(\frac{\mathbf{P}_\mathbf{k}^{(j)}}{M}\frac{\partial F_1}{\partial \mathbf{Q}_\mathbf{k}^{(j)}} - M\omega_\mathbf{k}^2\mathbf{Q}_\mathbf{k}^{(j)}\frac{\partial F_1}{\partial \mathbf{P}_\mathbf{k}^{(j)}}\right)$$

$$-\frac{c}{\sqrt{N}}\frac{1}{v}\sum_j\int \begin{matrix}\cos \mathbf{k}\cdot\mathbf{q}\\ \\ -\sin \mathbf{k}\cdot\mathbf{q}\end{matrix} f_1(\mathbf{q};\ \mathbf{p};\ t)\, d\mathbf{q}\, d\mathbf{p}\, \mathbf{k}\frac{\partial F_1}{\partial \mathbf{P}_\mathbf{k}^{(j)}}$$

$$= \frac{c}{\sqrt{N}}\frac{1}{v}\sum_j\int \begin{matrix}\cos \mathbf{k}\cdot\mathbf{q}\\ \\ -\sin \mathbf{k}\cdot\mathbf{q}\end{matrix} \mathbf{k}\frac{\partial g}{\partial \mathbf{P}_\mathbf{k}^{(j)}}\, d\mathbf{q}\, d\mathbf{p};\quad v = V/N; \tag{4}$$

$$\frac{\partial g}{\partial t} + \frac{\mathbf{p}}{m}\frac{\partial g}{\partial \mathbf{q}} + \sum_j\left(\frac{\mathbf{P}_\mathbf{k}^{(j)}}{M}\frac{\partial g}{\partial \mathbf{Q}_\mathbf{k}^{(j)}} - M\omega_k^2\mathbf{Q}_\mathbf{k}^{(j)}\frac{\partial g}{\partial \mathbf{P}_\mathbf{k}^{(j)}}\right)$$

$$= \frac{c}{\sqrt{N}}\sum_j \begin{matrix}\cos \mathbf{k}\cdot\mathbf{q}\\ \\ -\sin \mathbf{k}\cdot\mathbf{q}\end{matrix} \mathbf{k}\frac{\partial F_1}{\partial \mathbf{P}_\mathbf{k}^{(j)}} f_1 - \frac{c}{\sqrt{N}}\sum_j (\mathbf{k}Q_\mathbf{k}^{(j)}) \begin{matrix}\sin \mathbf{k}\cdot\mathbf{q}\\ \\ \cos \mathbf{k}\cdot\mathbf{q}\end{matrix} \mathbf{k}\frac{\partial f_1}{\partial \mathbf{p}} F_1. \tag{5}$$

If, with the aid of Eq. (5), we express the function g in terms of the first distribution function f_1, F_1 and substitute the expressions thus obtained in Eqs. (3) and (4), then we can get a set of equations for f_1 and F_1, which serve for the description of random processes in the crystalline lattice with account of the previous history. General consideration of such a type of processes was carried out by Khinchin.^{7} However, the solutions of these equations will naturally depend not only on the initial values of the functions f_1, F_1, but also on the initial values of the correlation function g. Inasmuch as the initial value of g is usually unknown, we are obliged to consider the system of approximate kinetic equations for the functions f_1 and F_1, the solutions of which must depend only on the initial values of the functions f_1 and F_1. Such a system of approximate equations is valid only over time intervals that exceed the correlation time. This corresponds to the fact that, in the solution of the equation for g, the time dependence of the correlation function is determined by specifying the first functions f_1 and F_1 at this same instant of time.

Wishing to obtain from such a system of equations for f_1 and F_1 a separate approximate equation for the electron distribution function f_1 with accuracy up to c^2, we assume that at the initial instant the lattice vibrations are in equilibrium, while the states of the electrons depart little from the equilibrium state. In this case we must, by way of the initial distribution of the oscillators of the lattice, substitute in Eq. (5) the solution of the equation for F_1 at $c = 0$; this has the following form:

$$F_1^{(0)} = B\exp\left\{-\sum_j (\mathbf{P}_\mathbf{k}^{(j)2}/M + M\omega_k^2\mathbf{Q}_\mathbf{k}^{(j)2})/2\varkappa T\right\}.$$

In transforming the left side of the equation for the function f_1, (by virtue of the required accuracy) we require a more detailed solution of the equation for F_1, namely

$$F_1 = F_1^{(0)}(\mathbf{Q}_\mathbf{k}^{(j)0}, \mathbf{P}_\mathbf{k}^{(j)0};\ t_0) + \frac{c}{\sqrt{N}}\frac{1}{v}$$

$$\times \sum_{l=1}^{2}\int_0^{t-t_0}\int \begin{matrix}\cos \mathbf{k}\cdot\mathbf{q}\\ \\ -\sin \mathbf{k}\cdot\mathbf{q}\end{matrix} f_1(\mathbf{q}, \mathbf{p};\ t-\theta)\, d\mathbf{q}\, d\mathbf{p}\left(\mathbf{k}\frac{\partial F_1^{(0)}}{\partial \mathbf{P}_\mathbf{k}^{(l)}}\right)_0 d\theta. \tag{6}$$

Here

$$\mathbf{Q}_\mathbf{k}^{(j)0} = \mathbf{Q}_\mathbf{k}^{(j)}\cos\omega_\mathbf{k}\theta - \frac{\mathbf{P}_\mathbf{k}^{(j)}}{M\omega_k}\sin\omega_k\theta,$$

$$\mathbf{P}_\mathbf{k}^{(j)0} = M\omega_k\mathbf{Q}_\mathbf{k}^{(j)}\sin\omega_k\theta + \mathbf{P}_\mathbf{k}^{(j)}\cos\omega_k\theta,$$

$(\ldots)_0$ means that $\mathbf{Q}_\mathbf{k}^{(j)0}, \mathbf{P}_\mathbf{k}^{(j)0}$ must be substituted for $\mathbf{Q}_\mathbf{k}^{(j)}, \mathbf{P}_\mathbf{k}^{(j)}$ after differentiation. After the elimination of the functions F_1 and g from Eq. (3), we obtain the kinetic equation for the distribution function of the electrons, interacting with the lattice vibrations of the crystal, in the form of the Fokker-Planck equation in phase space:[8]

$$\frac{\partial f_1}{\partial t} + \frac{\mathbf{p}}{m}\frac{\partial f_1}{\partial \mathbf{q}} - \frac{c^2}{4\pi M s^2}\Delta_{\mathbf{q}}$$

$$\times \int\limits_{|\mathbf{q}-\mathbf{q}'|\leqslant s(t-t_0)} \frac{\frac{\partial}{\partial \mathbf{q}'} f_1(\mathbf{q}', \mathbf{p}'; t - |\mathbf{q}-\mathbf{q}'|/s)}{|\mathbf{q}-\mathbf{q}'|} d\mathbf{q}' d\mathbf{p}' \frac{\partial f_1}{\partial \mathbf{p}}$$

$$= \frac{\partial}{\partial \mathbf{p}} B(s; \mathbf{p}) \frac{\partial}{\partial \mathbf{p}} f_1(\mathbf{q}, \mathbf{p}; t) + \frac{\partial}{\partial \mathbf{p}} \mathbf{A}(s; \mathbf{p}) f_1(\mathbf{q}, \mathbf{p}; t). \quad (7)$$

Here A and B are the Fokker-Planck coefficients for the given system:

$$B(s, \mathbf{p}) = \frac{c^2 \varkappa T v}{8\pi^2 M s^2} \int \delta\left(\omega_k - \frac{\mathbf{k}\cdot\mathbf{p}}{m}\right) \mathbf{k}^2 d\mathbf{k},$$

$$\mathbf{A}(s; \mathbf{p}) = \frac{c^2 v}{8\pi^2 M s^2} \int \omega_k \mathbf{k} \delta\left(\omega_k - \frac{\mathbf{k}\cdot\mathbf{p}}{m}\right) d\mathbf{k}.$$

We note that the coefficients of "diffusion" and "friction" in Eq. (7) are different from zero only upon satisfaction of the radiation condition. It is natural that, in the classical approximation, the Fokker-Planck coefficients A and B diverge for large wave numbers k. However, we can break off the integration over k at some value $k_{\max}$ which can be chosen from the Debye temperature Θ: $k_{\max} = \kappa\Theta/\hbar s$; κ is the Boltzmann constant. After integration over k, the coefficients A and B take the following form:

$$A^{\alpha} = \frac{c^2 m v}{4\pi M s^2 p}\left(\frac{\varkappa\theta}{\hbar s}\right) D(x); \quad B^{\alpha\beta} = \frac{c^2 m \varkappa T v}{4\pi M s^2 p}\left(\frac{\varkappa\theta}{\hbar s}\right) D(x),$$

where

$$D(x) = \frac{1}{x^4}\int_0^x \frac{y^4 dy}{e^y - 1}, \quad x \doteq \frac{\Theta}{T}.$$

In the equilibrium case, Eq. (7) is satisfied by the Maxwell distribution. The region of integration on the left side of Eq. (7) is bounded by the condition $|\mathbf{q}-\mathbf{q}'| \leq s(t-t_0)$. This limitation of the integration over $\mathbf{q}'$ arises from the fact that the problem is considered when, at the initial moment $t = t_0$, the distribution functions of the electrons and the oscillators of the lattice are given. Therefore, the only electrons that can have an effect on the change of the function f_1 at the point $\mathbf{q}$ and time $t > t_0$ are those removed from $\mathbf{q}$ by the distance $|\mathbf{q}-\mathbf{q}'| \leq s(t-t_0)$, since in this case the electrons interact only through vibrations of the crystalline lattice.

The approximate kinetic equation for the distribution function of the oscillators of the lattice is similarly constructed. Only now we must consider the initial distribution of the electrons at equilibrium. On the other hand, the initial state of the lattice vibrations here must be assumed to differ slightly from the equilibrium state. As a result, the equation for the distribution function F_1 has the form:

$$\frac{\partial F_1}{\partial t} + \sum_j \frac{\mathbf{P}_{\mathbf{k}}^{(j)}}{M}\frac{\partial F_1}{\partial \mathbf{Q}_{\mathbf{k}}^{(j)}} - \sum_j \left\{ M\Omega_k^2 \mathbf{Q}_{\mathbf{k}}^{(j)} \right.$$

$$\left. + \frac{c^2}{M\omega_k} \operatorname{Re} I_2 \left(\mathbf{k}\frac{\partial}{\partial \mathbf{Q}_{\mathbf{k}}^{(j)}}\right)\mathbf{k} \right\} \frac{\partial F_1}{\partial \mathbf{P}_{\mathbf{k}}^{(j)}}$$

$$+ \sum_j \int\int_0^{t-t_0} U^{(j)}(\mathbf{Q}_{\mathbf{k}}'; t-\theta)\, d\theta\, d\mathbf{Q}_{\mathbf{k}}'\cdot\mathbf{k} \frac{\partial F_1}{\partial \mathbf{P}_{\mathbf{k}}^{(j)}}$$

$$= c^2 \sum_j \left\{ \operatorname{Im} I_2 \mathbf{k} \frac{\partial}{\partial \mathbf{P}_{\mathbf{k}}^{(j)}} \mathbf{k} \frac{\partial F_1}{\partial \mathbf{P}_{\mathbf{k}}^{(j)}} + \operatorname{Im} I_1 \mathbf{k} \frac{\partial}{\partial \mathbf{P}_{\mathbf{k}}^{(j)}} \left(\frac{\mathbf{k}\cdot\mathbf{P}_{\mathbf{k}}^{(j)}}{M\omega_k}\right) F_1 \right\}. \quad (8)$$

Here

$$\Omega_k^2 = \omega_k^2 + (c^2 k^2/M) \operatorname{Re} I_1;$$

$$I_1 = \int \frac{\mathbf{k}\frac{\partial f_1^{(0)}}{\partial \mathbf{p}} d\mathbf{p}}{(\mathbf{k}\cdot\mathbf{p}/m) - \omega_k}; \quad I_2 = \int \frac{f_1^{(0)} d\mathbf{p}}{(\mathbf{k}\cdot\mathbf{p}/m) - \omega_k};$$

$$U^{(j)} = -c^2 \int (\mathbf{k}\cdot\mathbf{Q}_{\mathbf{k}}^{(j)\prime}) F_1(\mathbf{Q}_{\mathbf{k}}', \mathbf{P}_{\mathbf{k}}', t-\theta)\, \mathbf{k}\frac{\partial f_1^{(0)}}{\partial \mathbf{p}}$$

$$\times \sin\frac{\mathbf{k}\cdot\mathbf{p}}{m}\theta \cdot d\mathbf{p}\, d\mathbf{P}_{\mathbf{k}}';$$

$f_1^{(0)}$ is the equilibrium distribution function of the conduction electrons. In the case of thermal equilibrium, $F_1^{(0)}$ does not make the right side of Eq. (8) vanish. Because of the presence of the interaction, the stationary distribution of the waves of the lattice, by virtue of Eq. (6), takes the form $F_1(Q_{\mathbf{k}}, P_{\mathbf{k}}) = F_1^{(0)}(Q_{\mathbf{k}}, P_{\mathbf{k}}) + c^2 F_1^{(1)}(Q_{\mathbf{k}}, P_{\mathbf{k}})$, which agrees with the assumption of Peierls.[9]

Upon the derivation of the quantum kinetic equation for electrons and phonons, we start out from the equation for the quantum distribution function (the density matrix in the mixed representation) in the form set forth by Wigner. As a Hamiltonian, we again use Eq. (1). In the self-consistent approximation for the quantum distribution function of the conduction electrons f_1, we find:

$$\frac{\partial f_1}{\partial t} + \frac{\mathbf{p}}{m}\frac{\partial f_1}{\partial \mathbf{q}} + \frac{ic^2}{4\pi s^2 M\hbar}\frac{1}{(2\pi)^3}\Delta_{\mathbf{q}}$$

$$\times \int \left[\frac{f_1\left(\mathbf{q}', \mathbf{p}'; t - \left|\mathbf{q}-\mathbf{q}'-\frac{1}{2}\hbar\tau\right| / s\right)}{\left|\mathbf{q}-\mathbf{q}'-\frac{1}{2}\hbar\tau\right|} \right.$$

$$\left. - \frac{f_1(\mathbf{q}', \mathbf{p}'; t - |\mathbf{q}-\mathbf{q}'+\hbar\tau/2|/s)}{|\mathbf{q}-\mathbf{q}'+\hbar\tau/2|} \right]$$

$$\times e^{i\tau(\eta-\mathbf{p})} f_1(\mathbf{q}, \boldsymbol{\eta}; t)\, d\tau\, d\boldsymbol{\eta}\, d\mathbf{p}' d\mathbf{q}' = 0. \quad (9)$$

The region of integration over $\mathbf{q}'$ in this equation is limited by the condition $|\mathbf{q}-\mathbf{q}' \pm \hbar\tau/2| \leq s(t-t_0)$, where the upper sign refers to the first, and the lower, to the second, integral. For $F_1^{(0)}$ we have used the expression for the quantum distribution function of oscillators obtained in reference 10. Account of correlation permits us to compute the change in the distribution function f_1 at the expense of the "collision" of electrons with the lattice waves, which can be represented in the form of a set of three expressions. The first of these is similar to the diffusion term in Eq. (7) and can be written in the form

$$\frac{\pi c^2}{s^2\hbar MN}\sum_{\mathbf{k}}\varkappa T_{\mathbf{k}}\Big\{\delta\Big(\frac{p^2}{2m}-\frac{(\mathbf{p}+\hbar\mathbf{k})^2}{2m}-\hbar\omega_{\mathbf{k}}\Big)$$

$$\times\Big[f_1(\mathbf{p}+\hbar\mathbf{k},\,\mathbf{q};\,t)-f_1(\mathbf{p},\,\mathbf{q};\,t)\Big]$$

$$+\,\delta\Big(\frac{p^2}{2m}-\frac{(\mathbf{p}+\hbar\mathbf{k})^2}{2m}+\hbar\omega_{\mathbf{k}}\Big)[f_1(\mathbf{p}+\hbar\mathbf{k},\,\mathbf{q};\,t)-f_1(\mathbf{p},\,\mathbf{q};\,t)]\Big\},$$

where

$$\varkappa T_{\mathbf{k}}=\frac{1}{2}\hbar\omega_{\mathbf{k}}+\frac{\hbar\omega_k}{\exp\{\hbar\omega_k/\varkappa T\}-1};$$

the second is similar to the term of systematic friction and has the form

$$\frac{\pi c^2}{s^2\hbar MN}\sum_{\mathbf{k}}\frac{\hbar\omega_k}{2}\Big\{\delta\Big(\frac{p^2}{2m}-\frac{(\mathbf{p}+\hbar\mathbf{k})^2}{2m}+\hbar\omega_k\Big)$$

$$\times\Big[f_1(\mathbf{p}+\hbar\mathbf{k},\,\mathbf{q};\,t)+f_1(\mathbf{p},\,\mathbf{q};\,t)\Big]$$

$$-\,\delta\Big(\frac{p^2}{2m}-\frac{(\mathbf{p}+\hbar\mathbf{k})^2}{2m}-\hbar\omega_k\Big)[f_1(\mathbf{p}+\hbar\mathbf{k},\,\mathbf{q};\,t)+f_1(\mathbf{p},\,\mathbf{q};\,t)]\Big\};$$

while the third is due to exchange effects and has no classical analogue:

$$\frac{c^2}{vs^2\hbar MN(2\pi)^3}\sum_{\mathbf{k}}\iint_0^\infty\omega_k\sin\omega_k\theta\sin\mathbf{k}\Big(\mathbf{q}-\mathbf{q}'-\frac{\boldsymbol{\eta}}{m}\theta\Big)$$

$$\times\Big[\delta\Big(\boldsymbol{\eta}-\mathbf{p}+\frac{\hbar\mathbf{k}}{2}\Big)-\delta\Big(\boldsymbol{\eta}-\mathbf{p}-\frac{\hbar\mathbf{k}}{2}\Big)\Big]f_1$$

$$\times\Bigg(\frac{\mathbf{q}+\mathbf{q}'-\frac{\boldsymbol{\eta}}{m}\theta}{2}+\frac{\hbar\boldsymbol{\tau}}{4},\;\boldsymbol{\pi}';t\Bigg)f_1\Bigg(\frac{\mathbf{q}+\mathbf{q}'-\frac{\boldsymbol{\eta}}{m}\theta}{2}-\frac{\hbar\boldsymbol{\tau}}{4},\boldsymbol{\pi}'';t\Bigg)$$

$$\times\exp\Big\{i\Big(\mathbf{q}-\mathbf{q}'-\frac{\boldsymbol{\eta}}{m}\theta\Big)\frac{\pi'-\pi''}{\hbar}$$

$$+\,i\tau\Big(\frac{\pi'+\pi''}{2}-\boldsymbol{\eta}\Big)\Big\}\,d\theta\,d\mathbf{q}'\,d\boldsymbol{\pi}'\,d\boldsymbol{\pi}''\,d\boldsymbol{\tau}\,d\boldsymbol{\eta}.$$

Joining these together, after substitution in the right side of Eq. (9), we find the quantum kinetic equation for the electrons in the inhomogeneous case. For a homogeneous distribution, the exchange term is materially simplified, and the equation for the distribution function of the electrons takes the following form:

$$\frac{\partial w(p;t)}{\partial t}=\frac{\pi c^2}{s^2\hbar MN}\sum_{\mathbf{k}}\Big\{\delta\Big(\frac{p^2}{2m}-\frac{(\mathbf{p}+\hbar\mathbf{k})^2}{2m}-\hbar\omega_k\Big)\Big[\overline{N}_{\hbar\omega_k}w$$

$$\times(\mathbf{p}+\hbar\mathbf{k})(1-w(\mathbf{p}))-(\overline{N}_{\hbar\omega_k}+\hbar\omega_k)\,w(\mathbf{p})\,(1-w(\mathbf{p}+\hbar\mathbf{k}))\Big]$$

$$+\,\delta\Big(\frac{p^2}{2m}-\frac{(\mathbf{p}+\hbar\mathbf{k})^2}{2m}+\hbar\omega_k\Big)[(\overline{N}_{\hbar\omega_k}+\hbar\omega_k)\,w(\mathbf{p}+\hbar\mathbf{k})$$

$$\times(1-w(\mathbf{p}))-\overline{N}_{\hbar\omega k}w(\mathbf{p})\,(1-w(\mathbf{p}+\hbar\mathbf{k}))]\Big\}. \tag{10}$$

Here

$$\overline{N}_{\hbar\omega k}=\hbar\omega_k(e^{\hbar\omega k/\varkappa T}-1)^{-1};\; w(\mathbf{p};\,t)=\frac{(2\pi\hbar)^3}{v}f_1(\mathbf{p};\,t).$$

This equation is identical with the well known equation of Bloch theory.[9,11] Relative to the quantum kinetic equation for the distribution function of the phonons F_1, we note that it preserves the form of Eq. (8), with this one difference, that the expressions for the potential (8) and for the integrals I_1 and I_2 are changed. From Eq. (8) we get the averaged equation of the vibrations of the crystalline lattice, which, for a homogeneous distribution of electrons, has the following form:

$$\ddot{\overline{\mathbf{Q}}}{}_{\mathbf{k}}^{(j)}+2\gamma_k\dot{\overline{\mathbf{Q}}}{}_{\mathbf{k}}^{(j)}+\Omega_k^2\overline{\mathbf{Q}}{}_{\mathbf{k}}^{(j)}=0, \tag{11}$$

where

$$\overline{\mathbf{Q}}{}_k^{(j)}=\int\mathbf{Q}_{\mathbf{k}}^{(j)}F_1d\mathbf{Q}_{\mathbf{k}}^{(j)}d\mathbf{P}_{\mathbf{k}}^{(j)};\;2\gamma_k=\frac{c^2k^2}{M\omega_k}\operatorname{Im}I_1.$$

In the case of complete Fermi degeneracy for the electrons, the frequency of the characteristic vibrations $\Omega_{\mathbf{k}}$ and the damping decrement $\gamma_{\mathbf{k}}$ of the lattice waves are easily computed:

$$\Omega_k^2=\omega_k^2-\frac{3c^2m}{p_0^2M}k^2;\;\gamma_k=\frac{3}{8}\pi\Big(\frac{c}{\varepsilon_0}\Big)^2\frac{p_0}{M}k, \tag{12}$$

where ϵ_0, p_0 are the limiting values of the energy and momentum for the Fermi distribution.

The value for $\Omega_{\mathbf{k}}$ corresponds to the expression obtained in the work of Fröhlich.[12] For the estimate of the value of the damping $\gamma_{\mathbf{k}}$, we can use, for example, the tabulated data for (c/ϵ_0) given by Bethe and Sommerfeld.[9]

We note that in a number of cases it is not possible to obtain separate equations for f_1, F_1 from the approximate (in the sense given above) system of equations for the distribution functions of the electrons and waves of the crystalline lattice. We must then solve simultaneously the set of equations for these functions. In our treatment, we started from the Hamiltonian of Fröhlich, in which neither the periodic field of the ions nor the interaction between the phonons and the Coulombic interaction between the conduction electrons were considered. Employing the results of the present note, we hope in the future to consider more accurate kinetic equations for the electrons and the vibrations of the crystalline lattice.

In conclusion, we wish to express our gratitude to Academician N. N. Bogoliubov and D. N. Zubarev for discussion of the present research.

---

[1] N. N. Bogoliubov, Проблемы динамической теории в статистической физике (Problems of Dynamical Theory in Statistical Physics) Gostekhizdat, 1946.

[2] N. N. Bogoliubov and K. P. Gurov, J. Exptl. Theoret. Phys. (U.S.S.R.) **17**, 614 (1947).

[3] Bardeen, Cooper, and Schrieffer, Phys. Rev. **106**, 162 (1957).

[4] N. N. Bogoliubov, J. Exptl. Theoret. Phys. (U.S.S,R.) **34**, 58 (1958), Soviet Phys. JETP **7**, **41** (1958).

[5] H. Mori, Progr. Theoret. Phys. **9**, 473 (1953).

[6] R. N. Gurzhi, J. Exptl. Theoret. Phys. (U.S.S.R.) **33**, 451 (1957), Soviet Phys. JETP **6**, 352 (1958).

[7] A. Ia. Khinchin, Usp. Mat. Nauk **5**, 42 (1938).

[8] S. Chandrasekhar, Revs. Modern Phys. **15**, 1 (1943).

[9] H. Bethe and A. Sommerfeld, *Elektronentheorie der Metale Hand. Physik*. B 24/2, 2 Aufl. Berlin, 1933 (Russ. Transl.).

[10] Iu. L. Klimontovich, Dokl. Akad. Nauk SSSR **108**, 1033 (1955), Soviet Phys. "Doklady" **1**, 383 (1955).

[11] L. D. Landau and A. S. Kompaneets, Электропроводность металлов (*Electric Conductivity of Metals*) (DNTVU, 1935).

[12] H. Fröhlich, Proc. Roy. Soc. **A215**, 291 (1952).

Translated by R. T. Beyer
243

SOVIET PHYSICS JETP VOLUME 35(8), NUMBER 5 MAY, 1959

INTERACTION BETWEEN OUTER AND INNER ELECTRONS IN FERROMAGNETIC TRANSITION METALS

Iu. A. IZIUMOV

Ural' State University

Submitted to JETP editor April 7, 1958

J. Exptl. Theoret. Phys. (U.S.S.R.) 35, 1148-1154 (November, 1958)

The interaction between 4s and 3d electrons in transition metals is investigated. It is shown that the dynamical part of the interaction manifests itself in the interaction between Fermi and Bose elementary excitations. At low temperatures elastic collision between these excitations predominate, whereas at high temperatures transition processes begin to play an important part. The magnetization is calculated as a function of temperature and field strength.

1. During recent years increased interest has been shown in the transition metals, but agreement still has not been reached regarding the electron interactions that produce the ferromagnetic state of these metals. It is therefore necessary to analyze these interactions carefully in every model of the transition metals. The so-called s-d exchange model developed by Vonsovskii and his coworkers[1,2] is based on the assumption that electrons of the unfilled 3d shell play an important part in transition metals in addition to the 4s valence electrons. A strong exchange interaction with a positive exchange integral leads to complete ordering of the 3d electron spins, that is, to ferromagnetism. The 4s electrons are collectively responsible for transfer phenomena in a crystal.

This electron system has a mixed spectrum with Bose and Fermi branches. The Bose branch is associated with the 3d electrons which provide the elementary excitations called "ferromagnons" (or "spin waves") while the Fermi branch is associated with the 4s electrons which provide the elementary excitations that we call "conduction electrons."

The Hamiltonian of weakly-excited electron states in the s-d model can be represented as follows:

$$\hat{\mathscr{H}} = E_0 + \hat{H}_0 + \hat{H}_1; \tag{1}$$

$$\hat{H}_0 = \sideset{}{'}\sum_{\mathbf{k}\sigma} \varepsilon_{\mathbf{k}}^{\sigma} a_{\mathbf{k}\sigma}^{+} a_{\mathbf{k}\sigma} + \sideset{}{'}\sum_{\mathbf{g}} \varepsilon_{\mathbf{g}} b_{\mathbf{g}}^{+} b_{\mathbf{g}}; \tag{1a}$$

$$\hat{H}_1 = N^{-1/2} \sideset{}{'}\sum_{\mathbf{k}_1\mathbf{k}_2\mathbf{g}} J(\mathbf{k}_1\mathbf{k}_2)\,\delta(\mathbf{k}_2 - \mathbf{k}_1 + \mathbf{g})\,[a_{\mathbf{k}_1(+)} a_{\mathbf{k}_2(-)}^{+} b_{\mathbf{g}}^{+} - a_{\mathbf{k}_1(+)}^{+} a_{\mathbf{k}_2(-)} b_{\mathbf{g}}]$$
$$+ \frac{1}{N} \sideset{}{'}\sum_{\mathbf{k}_1\mathbf{k}_2\mathbf{g}_1\mathbf{g}_2} J(\mathbf{k}_1\mathbf{k}_2)\,\delta(\mathbf{k}_2 - \mathbf{k}_1 + \mathbf{g}_1 - \mathbf{g}_2)\,[a_{\mathbf{k}_1(-)}^{+} a_{\mathbf{k}_2(-)} b_{\mathbf{g}_2}^{+} b_{\mathbf{g}_1} - a_{\mathbf{k}_1(+)}^{+} a_{\mathbf{k}_2(+)} b_{\mathbf{g}_2}^{+} b_{\mathbf{g}_1}]. \tag{1b}$$

Here $a_{\mathbf{k}}$ and $a_{\mathbf{k}}^{+}$ are the Fermi second-quantization operators with the signs + and − denoting the spin projection (in the ground state of a 3d electron the spin projection is denoted by −); $b_{\mathbf{g}}$ and $b_{\mathbf{g}}^{+}$ are Bose operators; **k** and **g** are the quasi-momentum of a conduction electron and of a ferromagnon, respectively; $J(\mathbf{k}_1\mathbf{k}_2)$ is the s-d exchange integral.

The Hamiltonian (1) was obtained by Vonsovskii and Turov.[2] The following expressions were obtained for conduction electron energies:

$$\varepsilon_{\mathbf{k}}^{-} = -\alpha + \hbar^2 k^2/2m_{-};\quad \varepsilon_{\mathbf{k}}^{+} = \alpha + \hbar^2 k^2/2m_{+}, \tag{2}$$

where m_- and m_+ are the effective electron masses with the respective spin directions and α is the coupling constant of s and d electrons, which is determined by expanding the s-d exchange integral in powers of the quasi-momenta (for a cubic crystal):

$$J(\mathbf{k}_1\mathbf{k}_2) = 2\alpha - \gamma\,[(ak_1)^2 + (ak_2)^2] + \ldots \tag{3}$$

The terms in (1) have the following significance: E_0 is the constant energy of the 3d electrons with completely ordered spins; H_0 is the combined energy of all elementary excitations (conduction electrons and ferromagnons); H_1 represents the energy of interaction between the latter.

The complete Hamiltonian of the electron system must contain two more terms, one of which will describe the interaction between ferromagnons while the other describes the interaction between conduction electrons. However, as Dyson[3] has shown, the interaction between spin waves (ferromagnons) in a ferromagnet is very small and can be neglected at temperatures up to one-fourth of the Curie temperature.

Neglect of the interaction between conduction electrons does not have the same rigorous justification, but it can be assumed that the interaction between the original 4s electrons is partly taken into account self-consistently in the effective masses of the conduction electrons.

Thus the interaction between 4s and 3d electrons is manifested in two different ways. The conduction electron spectrum is altered [Eq. (2) includes the s-d interaction parameters]. This can be called the static part of the interaction, which leads to the 4s-electron magnetization noted by Vonsovskii.

Equation (1b) describes the dynamical interaction of 4s and 3d electrons by means of the interaction between conduction electrons and ferromagnons. The term of $\hat{H}_1$ which contains three operators describes transitions between these elementary excitations, while the term with four operators describes elastic collisions between these same excitations. In the present work these interactions will be taken into account in the thermodynamic function of the system.

2. We limit ourselves to low temperatures (not above one-fourth the Curie point) and use the perturbation theory of statistical mechanics with $\hat{H}_1$ as a perturbation.[4] The free energy is obtained from

$$e^{-\beta F} = \mathrm{Sp}\, e^{-\beta \hat{H}}, \tag{4}$$

where $\beta = 1/kT$. We obtain the following expansion of the trace in powers of $\hat{H}_1$:

$$\mathrm{Sp}\, e^{-\beta(\hat{H}_0+\hat{H}_1)} = \mathrm{Sp}\, e^{-\beta\hat{H}_0} + \beta \sum_{k=1}^{\infty} \frac{(-1)^k}{k}$$
$$\times \int_0^{\beta}\int_0^{\lambda_1}\int_0^{\lambda_{k-2}} d\lambda_1 \ldots d\lambda_{k-1}\, \mathrm{Sp}\, [e^{-\beta\hat{H}_0}\hat{H}_1(\lambda_1)\ldots\hat{H}_1(\lambda_{k-1})\hat{H}_1], \tag{5}$$

where

$$\hat{H}_1(\lambda) = e^{\lambda\hat{H}_0}\hat{H}_1 e^{-\lambda\hat{H}_0}. \tag{6}$$

When the free energy F is expanded in powers of the small parameter $\sim H_1/H_0$

$$F = F_0 + F_1 + F_2 + \ldots,$$

we obtain from (4) and (5), to second order terms,

$$F_0 = -\beta^{-1}\ln \mathrm{Sp}\, e^{-\beta\hat{H}_0};\ F_1 = \langle\hat{H}_1\rangle_\beta; \tag{7}$$

$$F_2 = {}^1/_2\left\{\beta\langle\hat{H}_1\rangle_\beta^2 - \int_0^\beta d\lambda\,\langle\hat{H}_1(\lambda)\hat{H}_1\rangle_\beta\right\}, \tag{8}$$

$<\ldots>$ denotes averaging over the statistical assembly with the Hamiltonian $\hat{H}_0$. A direct calculation by means of (6) shows that the $\hat{H}_1 \to \hat{H}_1(\lambda)$ transition corresponds to the following substitution of operators:

$$a_k \to a_k e^{-\lambda\varepsilon_k},\ a_k^+ \to a_k^+ e^{\lambda\varepsilon_k},\ b_g \to b_g e^{-\lambda\varepsilon_g},\ b_g^+ \to b_g^+ e^{\lambda\varepsilon_g}.$$

In calculating various average values we use the following expressions, which can also be derived by direct calculation:

$$\langle b_{g_1}^+ b_{g_2}\rangle_\beta = \delta(g_1 - g_2) f_f(g_1) = \delta(g_1 - g_2)[\exp\{\beta\varepsilon_{g_1}\} - 1]^{-1}; \tag{9}$$

$$\langle a_{k_1(+)}^+ a_{k_2(+)}\rangle_\beta = \delta(k_1 - k_2) f_e^+(k_1)$$
$$= \delta(k_1 - k_2)[\exp\{\beta(\varepsilon_{k_1}^+ - \xi)\} + 1]^{-1}, \tag{10}$$

where ξ denotes the chemical potential of the electrons and is determined from the conservation of the number of 4s electrons:

$$\sum_k [f_e^+(k) + f_e^-(k)] = N_s. \tag{11}$$

The following results are now obtained from a calculation of (7) and (8):

$$F_0 = N_s\xi - \beta^{-1}\sum_k [\ln(1 + \exp\{-\beta(\varepsilon_k^+ - \xi)\})$$
$$+ \ln(1 + \exp\{-\beta(\varepsilon_k^- - \xi)\})] + \beta^{-1}\sum_g \ln(1 - \exp\{-\beta\varepsilon_g\}); \tag{12}$$

$$F_1 = \frac{1}{N}\sum_g f_f(g)\sum_k J(kk)[f_e^-(k) - f_e^+(k)]; \tag{13}$$

$$F_2^{(3)} = \frac{1}{2N}\sum_{kg} J^2(k, k-g)\left\{\frac{\exp\{-\beta(\varepsilon_{k-g}^- - \varepsilon_k^+ + \varepsilon_g)\} - 1}{\varepsilon_{k-g}^- - \varepsilon_k^+ + \varepsilon_g} f_e^+\right.$$
$$\times (k)(1 - f_e^-(k-g))(1 + f_f(g))$$
$$\left. - \frac{\exp\{\beta(\varepsilon_{k-g}^- - \varepsilon_k^+ + \varepsilon_g)\} - 1}{\varepsilon_{k-g}^- - \varepsilon_k^+ + \varepsilon_g} f_e^-(k-g)(1 - f_e^+(k)) f_f(g)\right\}. \tag{14}$$

We note that the first approximation of the three-operator terms vanishes in virtue of the properties of the operators b_g and b_g^+, so that $F_2^{(3)}$ is the first nonvanishing correction from the three-operator terms in $\hat{H}_1$ which describe transitions. This corresponds formally to the second approximation in the perturbation theory. F_1 is the first approximation correction from the four-operator terms in $\hat{H}_1$.

3. We shall now calculate the magnetization $M = \partial F/\partial H$. In a magnetic field directed along the axis of spontaneous magnetization the energy is

changed by the amount

$$\Delta H = -N\mu_0 H + 2\mu_0 H \sum_{g} n_g + \mu_0 H \sum_{k} (n_k^+ - n_k^-),$$

after which the distribution functions $f_e(\mathbf{k})$ and $f_f(\mathbf{g})$ will depend on the magnetic field. For the zero approximation of the magnetization we obtain

$$M_d^0 = N\mu_0 \left\{1 - \frac{2}{N} \sum_{g} f_f(g)\right\}; \tag{15}$$

$$M_s^0 = \mu_0 \sum_{k} [f_e^-(k) - f_e^+(k)]. \tag{16}$$

Instead of immediately calculating the next approximation of the magnetization we shall first calculate the free energy corrections F_1 and $F_2^{(3)}$. We note that (11), (13), and (16) possess the same structure and can be calculated by the same method. In these expressions we pass from summation over k to integration. Integrating by parts, we distinguish the derivative of the distribution function in the integrand and regard it as the nucleus of an integral operator which is approximated by

$$-\frac{d}{dx}(e^{x-\beta\xi} + 1)^{-1} = \delta(x - \beta\xi)\left(1 + \frac{\pi^2}{6}\frac{d^2}{dx^2} + \ldots\right), \tag{17}$$

since $\beta\xi$ is much larger than unity. After calculation of the integrals the results can be represented conveniently by means of the notation

$$X_{s,p}^{\pm} = \left(\frac{m_-}{m}\right)^p \left(1 + \frac{\alpha + \mu_0 H}{\xi}\right)^s \pm \left(\frac{m_+}{m}\right)^p \left(1 - \frac{\alpha + \mu_0 H}{\xi}\right)^s, \tag{18}$$

where m is the electron mass. From (11) we obtain the chemical potential of the conduction electrons in the magnetic field:

$$\xi = \xi_0 \left[\frac{1}{2} X^{+}_{3/2,\,3/2} + \frac{\pi^2}{16}\left(\frac{kT}{\xi_0}\right)^2 X^{+}_{-1/2,\,3/2}\right]^{-2/3}; \quad \xi_0 = \frac{\hbar^2}{2m}(3\pi^2 n_s^0)^{2/3}. \tag{19}$$

n_s^0 is the number of 4s electrons per unit volume. Since $(kT/\xi_0)^2 < 10^{-4}$ we can neglect the dependence of ξ on temperature. In the same approximation we obtain for (16) and (13):

$$M_s^0 = N_s \mu_0 X^{-}_{3/2,\,3/2} (X^{+}_{3/2,\,3/2})^{-1}; \tag{20}$$

$$F_1 = \frac{1}{N} \sum_{g} f_f(g) \cdot 2N_s \left\{\alpha X^{-}_{3/2,\,3/2} (X^{+}_{3/2,\,3/2})^{-1} - \gamma\left(\frac{2ma^2\xi_0}{\hbar^2}\right)\frac{3}{10} X^{-}_{5/2,\,5/2}\left(\frac{1}{2} X^{+}_{3/2,\,3/2}\right)^{-5/3}\right\}. \tag{21}$$

We cannot calculate (14) to the same order of approximation; a number of supplementary approximations are required. We neglect the energy and momentum of the ferromagnons if they are of the same order as the energy and momentum of electrons, since the principal contribution to the sums comes from terms with small ferromagnon momenta and large electron momenta (on the order of the Fermi momentum). Separating the summations over $\mathbf{k}$ and $\mathbf{g}$, we integrate over $\mathbf{k}$ using the approximation (17) and obtain

$$F_2 = -\frac{1}{N} \sum_{g} f_f(g) \cdot 3N_s \frac{\alpha^2}{\xi_0} \frac{kT}{\alpha} \tanh\frac{\alpha}{kT}\left(1 - \frac{\mu_0 H}{kT}\right). \tag{22}$$

In order to make the meaning of the final result clearer we neglect the difference between the effective electron masses in (19), (20) and (21), letting $m_- = m_+ = m$, $\gamma = 0$. Since α and $\mu_0 H \ll \xi$, we assume

$$X_{s,p}^{+} \approx 2; \quad X_{s,p}^{-} \approx 2s(\alpha + \mu_0 H)/\xi_0; \quad \xi = \xi_0.$$

The total correction to the free energy due to the interaction between conduction electrons and ferromagnons is given by

$$F_1 + F_2 = \frac{1}{N} \sum_{g} f_f(g) \cdot 3N_s \frac{\alpha^2}{\xi_0} D(H), \tag{23}$$

$$D(H) = 1 + \frac{\mu_0 H}{\alpha} - \frac{kT}{\alpha} \tanh\frac{\alpha}{kT}\left(1 - \frac{\mu_0 H}{kT}\right).$$

We shall now calculate the magnetization. In the given approximations the magnetization of s electrons is, according to (20),

$$M_s^0 = 3N_s\mu_0\alpha/2\xi_0 + 3N_s\mu_0^2 H/2\xi_0 \tag{24}$$

where the second term is the paramagnetic (Pauli) magnetization of the electron gas, while the first (constant) term results from magnetization of the 4s-electron gas by 3d electrons, the s-d exchange field being the equivalent of an effective magnetic field $H_{\text{eff}} = \alpha/\mu_0$. If we assume that α is of the order of 5×10^{-15} erg, then H_{eff} is of the order of 10^6 oersteds, so that the 4s electrons will contribute considerably to the spontaneous magnetization of metals. Using (15), (23), and (24) we obtain an expression for the total magnetization in terms of the 3d-electron magnetization:

$$M = \left(1 + \frac{3}{2}\frac{N_s}{N}\frac{\alpha}{\xi_0}\right) M_d^0 + \frac{3}{2} N_s \mu_0 \frac{\alpha}{\xi_0} \left\{\frac{\mu_0 H}{\alpha} - \left(1 - \frac{M_d^0}{N\mu_0}\right)\tanh\frac{\alpha}{kT} + D(H)\frac{\alpha}{\mu_0}\frac{\partial}{\partial H}\left(\frac{M_d^0}{N\mu_0}\right)\right\}. \tag{25}$$

Since M_d^0 is the magnetization of 3d electrons in the absence of an s-d interaction, the first term in this expression represents the usual spontaneous magnetization of ferromagnetic 3d electrons and of the fraction of the 4s electrons which is magnetized by the s-d exchange field. Thus this term describes ideal ferromagnetism with the average number of electrons per lattice site given by $1 + (3N_s/2N)\alpha/\xi_0$. The second term in (25) provides a correction to the magnetization resulting from the dynamical interaction of 4s electrons and ferromagnons.

M_d^0 can be calculated from (15) if the dispersion law for ferromagnons is known. If we assume the usual result of spin-wave theory, which gives $\epsilon_g \sim Jg^2$, the derivative, with respect to the field, of the resulting expression for M_d^0 will diverge at $H = 0$, and we obtain a diverging expression for the magnetization (25). The reason for such singularities in the theory of magnetism has frequently been discussed (see reference 5, for example), and evidently lies in the fact that in such instances a decisive part is played by magnetic interactions which are not taken into account by the Bloch spin-wave theory. We shall assume that as a result of the magnetic interaction there is required a certain activation energy ΔE of a spin-wave with zero quasi-momentum, so that

$$\varepsilon_g = \Delta E + J(ag)^2.$$

The calculation of ΔE does not enter into our problem, but we can state immediately that it must be small, being of the order of the anisotropy energy. It is easily found that

$$\frac{1}{N}\sum_g f_f(g) = \frac{1}{(2\sqrt{\pi})^3}\left(\frac{kT}{J}\right)^{3/2} Z_{3/2}\left(\frac{\Delta E + 2\mu_0 H}{kT}\right),$$

where

$$Z_{3/2}(x) = \sum_{n=1}^{\infty} n^{-3/2} e^{-xn}$$

$$= 2.61 - 3.54x^{1/2} + 1.46x - 0.104x^2 + \dots$$

This last expression was obtained by Robinson[6] and converges rapidly for $x \leq 1$. Keeping only the first two terms in the expansion, we obtain

$$M_d^0 = N_{\mu_0}\left\{1 - 0.1174\left(\frac{kT}{J}\right)^{3/2}\left[1 - 1.36\left(\frac{\Delta E + 2\mu_0 H}{kT}\right)^{1/2} + 0.56\left(\frac{\Delta E + 2\mu_0 H}{kT}\right) - \dots\right]\right\}, \quad (26)$$

which is applicable to not too low temperatures, where $(\Delta E + 2\mu_0 H) < kT$. Eqs. (25) and (26) give the dependence of the magnetization on temperature and field. Let us consider two limiting cases:

(a) $\alpha \ll kT$, weak s-d coupling, high temperature; $D(H) \approx \mu_0 H/\alpha \ll 1$. We see that the first and second approximation corrections to the free energy cancel each other to a considerable extent and disappear entirely in the absence of a magnetic field. We obtain for the spontaneous magnetization:

$$M = \left(1 + \frac{3}{2}\frac{N_s}{N}\frac{\alpha}{\xi_0}\right) M_d^0 - 0.1174\frac{3N_s\mu_0\alpha^2}{2\xi_0 J^{3/2}}(kT)^{1/2}. \quad (27)$$

(b) $\alpha \gg kT$, strong s-d coupling, low temperature; $D(H) \approx 1 + 2\mu_0 H/\alpha$. In this case the first and second approximation corrections to the free energy, which depend on the field, are equal, but the first approximation correction, which corresponds to elastic collisions, is predominant in their constant parts. The spontaneous magnetization is given by

$$M = \left(1 + \frac{3}{2}\frac{N_s}{N}\frac{\alpha}{\xi_0}\right) M_d^0 + 0.159\frac{3N_s\mu_0\alpha^2}{2\xi_0 J^{3/2}(\Delta E)^{1/2}} kT. \quad (28)$$

Except for the notation this agrees with the expression obtained in references 7 and 8, where only elastic collisions were taken into account. We have now determined the range of applicability of this result.

Despite the fact that the correction terms in (27) and (28) contain the factors $(kT/J)^{1/2}$ and (kT/J), which at low temperatures decrease more slowly than the term containing $(kT/J)^{3/2}$ in M_d^0, they remain smaller than the latter in the given temperature range because of their small coefficients. By means of the values given above it can easily be shown that the second term in (28) does not exceed 10% of the first term.

Thus of the two types of dynamic interaction between 3d and 4s electrons elastic collisions between ferromagnons and conduction electrons dominate at low temperatures, while at higher temperatures transition processes begin to play a part. These two temperature regions are separated by the temperature $\theta = \alpha/k$. Since our calculation is valid in the temperature range from a few degrees to ~ 200° the possibility of including transition processes in this region depends on the magnitude of the s-d exchange integral.

I take this opportunity to thank E. A. Turov for his interest and Professor S. V. Vonsovskii for a discussion of the results.

---

[1] S. V. Vonsovskii, J. Exptl. Theoret. Phys. (U.S.S.R.) **16**, 981 (1946).

[2] S. V. Vonsovskii and E. A. Turov, J. Exptl. Theoret. Phys. (U.S.S.R.) **24**, 419 (1953).

[3] F. Dyson, Phys. Rev. **102**, 1217 (1956).

[4] S. Nakajima, Advances in Phys. **4**, 363 (1955).

[5] R. Kubo, Phys. Rev. **87**, 568 (1952).

[6] J. E. Robinson, Phys. Rev. **83**, 678 (1951).

[7] E. A. Turov, J. Exptl. Theoret. Phys. (U.S.S.R.) **25**, 352 (1953).

[8] A. A. Berdyshev and Iu. A. Iziumov, Физика металлов и металловедение (Physics of Metals and Metal Research) **5**, 552 (1957).

Translated by I. Emin
244

SOVIET PHYSICS JETP VOLUME 35 (8), NUMBER 5 MAY, 1959

LOW-FREQUENCY OSCILLATIONS OF A PLASMA IN A MAGNETIC FIELD

K. N. STEPANOV

Physico-Technical Institute, Academy of Sciences, Ukrainian S.S.R.

Submitted to JETP editor April 30, 1958

J. Exptl. Theoret. Phys. (U.S.S.R.) 35, 1155-1160 (November, 1958)

The low-frequency electron-ion longitudinal oscillations in a plasma confined by a magnetic field are considered.

It is well known that a plasma is capable of two kinds of oscillations: high-frequency electronic oscillations, and low-frequency oscillations in which both electrons and ions take part. The theory of the low-frequency oscillations has been developed by Tonks and Langmuir,[1] Gordeev[2] and others. In the present paper we consider the low-frequency longitudinal oscillations of an unbounded plasma which is confined by a fixed, uniform, magnetic field.

1. DISPERSION EQUATION

We consider small oscillations of a plasma consisting of electrons and singly charged ions. It will be assumed that the oscillation frequency is high so that the collision integrals can be neglected in the kinetic equations which describe deviations in the electron (ion) distribution functions from the equilibrium values. Suppose that at time $t = 0$ we turn off the external effect which causes the plasma to deviate from the equilibrium state. After a sufficiently long period of time t the Fourier component of the electric field intensity will be proportional to $\exp\{-i\omega t - \gamma t\}$ where the frequency ω and the damping factor γ are determined from a dispersion equation of the form

$$An'^4 + Bn'^2 + C = 0, \quad n' = kc/\omega',$$

where $\omega' = \omega - i\gamma$ and $\mathbf{k}$ is the propagation vector. Expressions for the coefficients A and B and C are given in reference 3. If the individual terms which appear in A are much larger than $|B/n'^2|$ and $|C/n'^4|$ an approximate solution of the dispersion equation can be obtained by setting $A = 0$. The equation $A = 0$ is the dispersion equation for oscillations characterized by curl $\mathbf{E} \approx 0$ (longitudinal plasma oscillations). Thus, we have

$$A(\omega', k) = 1 + K_e + K_i = 0, \tag{1}$$

where[3,4] (α = e, i)

$$K_\alpha = \frac{1}{k^2 a_\alpha^2} + \frac{i\omega'}{k^2 a_\alpha^2 \omega_H^\alpha} \exp(-\mu_\alpha \sin^2\theta)$$
$$\times \int_0^\infty \exp\left(-\frac{1}{2}\mu_\alpha \cos^2\theta\varphi^2 + \frac{i\omega'}{\omega_H^\alpha}\varphi + \mu_\alpha \sin^2\theta\cos\varphi\right) d\varphi, \tag{2}$$
$$a_\alpha = (T_\alpha/4\pi e^2 n_0)^{1/2}, \quad \Omega_\alpha = (4\pi e^2 n_0/m_\alpha)^{1/2},$$
$$\mu_\alpha = (k a_\alpha \Omega_\alpha/\omega_H^\alpha)^2, \quad v_T^\alpha = (T_\alpha/m_\alpha)^{1/2}, \quad a_\alpha\Omega_\alpha = v_T^\alpha.$$

Here θ is the angle between the direction of the external magnetic field $\mathbf{H}_0$ and the propagation vector $\mathbf{k}$, $\omega_H^\alpha = eH_0/mc$ is the gyromagnetic frequency for a particle of mass m_α and charge e (the subscript α = e refers to electrons, α = i refers to ions) T_α is the temperature of the gas of particles of type α and n_0 is the equilibrium electron density.

The quantity K_α can also be given in the form

$$K_\alpha = \frac{1}{k^2 a_\alpha^2} \tag{3}$$
$$- \frac{1}{k^2 a_\alpha^2} e^{-\mu_\alpha \sin^2\theta} \sum_{n=-\infty}^{\infty} I_n(\mu_\alpha \sin^2\theta) \frac{z_0^\alpha}{\sqrt{\pi}} \int_C \frac{e^{-t^2}}{z_n^\alpha - t} dt,$$
$$z_n^\alpha = (\omega' - n\omega_H^\alpha)/\sqrt{2}\, k v_T^\alpha \cos\theta,$$

where I_n is a Bessel function of imaginary argument. The integration over t in Eq. (3) is taken over the path C which goes along the real axis from $-\infty$ to $+\infty$, going around the singularities $t = z_n^\alpha$ from below for $\cos\theta > 0$ and from above for $\cos\theta < 0$. Below, it is assumed that $\cos\theta > 0$.

Equation (3) for K_α is obtained from Eq. (2) by expanding $\exp(+\mu_\alpha \sin^2\theta\cos\varphi)$ in Eq. (2) in powers of $e^{i\varphi}$ and using the relation following between the integrals over the contour C, which appear in Eq. (3), and the probability integral:[5]

$$\frac{1}{\sqrt{\pi}} \int_C \frac{e^{-t^2}}{z - t} dt = -i\sqrt{\pi} e^{-z^2}\left(1 + \frac{2i}{\sqrt{\pi}} \int_0^z e^{t^2} dt\right). \tag{4}$$

2. INVESTIGATION OF THE DISPERSION EQUATION

The dispersion equation (1) is extremely complicated and can be solved only in certain limiting cases. If the phase velocity of the oscillations $V_{ph} = \omega/k$ is much larger than the mean thermal velocity of the electrons v_T^e in Eq. (1) K_i can be neglected compared with K_e. The resulting dispersion equation $1 + K_e = 0$ describes the high-frequency oscillations of the plasma. This equation has been investigated in detail in reference 6 and 7. Below, we study the oscillations for which

$$v_T^i \ll V_{ph} = \omega / k \ll v_T^e \qquad (5)$$

(low-frequency oscillations) in three different cases: weak magnetic field, $\omega_H^e \ll kv_T^e$; strong magnetic field, $\omega_H^i \gg kv_T^i$; the intermediate case, in which $\omega_H^e \gg kv_T^e$ and $\omega_H^i \ll kv_T^i$.

In order to investigate Eq. (1) we use the asymptotic expression for the integral in (4) (large values of z)

$$\frac{1}{\sqrt{\pi}}\int\limits_C \frac{e^{-t^2}}{z-t}\,dt \sim \frac{1}{z} + \frac{1}{2z^3} + \frac{3}{4z^5} + \ldots - i\sqrt{\pi}e^{-z^2}, \qquad (6)$$
$$|\operatorname{Re} z| \gg 1, \quad \operatorname{Im} z \ll 1.$$

At small values of z the function in (4) is conveniently expanded in powers of z, in which case

$$\frac{1}{\sqrt{\pi}}\int\limits_C \frac{e^{-t^2}}{z-t}\,dt = -i\sqrt{\pi} + O(z), \quad |z| \ll 1. \qquad (7)$$

(a) Suppose $\omega_H^e \ll kv_T^e$ (weak magnetic field). Then the following inequality holds: $\omega_H^i \ll kv_T^i$. Expanding $\cos\varphi$ in Eq. (2) in powers of φ and taking account of the inequality in (5), we have

$$K_e = \frac{1 + i\sqrt{\pi}z_e + \ldots}{k^2 a_e^2}, \quad z_e = \omega'/\sqrt{2}kv_T^e, \quad |z_e| \ll 1; \qquad (8)$$

$$K_i = -\frac{1}{k^2 a_i^2}\left(\frac{1}{2z_i^2} + \frac{3}{4z_i^4} + \cdots\right), \quad z_i = \omega'/\sqrt{2}kv_T^i, \quad |z_i| \gg 1. \qquad (9)$$

Substituting Eqs. (8) and (9) in Eq. (1) and solving for ω', we have

$$\omega^2 = \omega_0^2 + 3k^2 v_T^{i2}, \quad \omega_0 = \Omega_i k a_e (1 + k^2 a_e^2)^{-1/2}, \qquad (10)$$

$$\gamma = \gamma_0 = \sqrt{\frac{\pi m_e}{8 m_i}}\,\frac{\Omega_i k a_e}{(1 + k^2 a_e^2)^2}. \qquad (11)$$

The frequency equation (10) (for $v_T^i \to 0$) was given by Tonks and Langmuir.[1] The correction $3k^2 v_T^{i2}$ which takes account of the thermal spread in the ion velocities and the damping term (11), were given by Gordeev.[2] The introduction of a magnetic field results in the appearance of an additional small term in the expression for ω^2:

$$\omega_H^{i2} \sin^2\theta \cdot k^2 a_e^2 / (1 + k^2 a_e^2).$$

The condition $|z_e| \ll 1$, which must be satisfied if (8) is to hold, is always satisfied since $(m_e/m_i)^{1/2} \ll 1$. The condition of applicability for the expansion in (9), $|z_i| \gg 1$, can be used if

$$T_e \gg T_i, \qquad (12)$$

i.e., the plasma must be highly non-isothermal. If this is not the case the low-frequency oscillations are highly damped: $\gamma \sim \omega_0$. According to Eqs. (10) and (11) the damping factor is small compared with the frequency $\gamma/\omega \sim (m_e/m_i)^{1/2}$. The damping factor (11) is due to the "remote" collective interactions of the particles. The plasma oscillations also are damped by "local" collisions.

(b) Intermediate case. Suppose now that the following inequalities hold: $(\omega_H^e)^2 \gg (kv_T^e)^2$ and $\omega_H^{i2} \ll k^2 v_T^{i2}$ or

$$1 \ll (\omega_H^e / kv_T^e)^2 \ll m_i T_i / m_e T_e. \qquad (13)$$

Because the ratio m_i/m_e is very large (approximately 10^3 to 10^5) there are values of ω_H^e/kv_T^e (even when $T_i \ll T_e$) for which the inequality in (13) is satisfied.

If the condition in (13) is satisfied, we can use the earlier expression for K_i (9). In computing K_e, we assume that because of (13) $\mu_e \ll 1$. Hence, from Eq. (3) we find, (assuming that $|z_0^e| \ll 1$ for values of θ far from $\pi/2$)

$$K_e \approx (1 + i\sqrt{\pi}z_0^e) / k^2 a_e^2. \qquad (14)$$

Substituting Eqs. (9) and (14) in Eq. (1), we obtain the earlier expression for the frequency (10), and the damping term

$$\gamma = \gamma_0 / |\cos\theta|. \qquad (15)$$

As θ increases the damping term also increases. However, when θ approaches $\pi/2$, Eqs. (10) and (15) no longer hold since these equations were obtained under the condition that $|z_0^e| \ll 1$, which is satisfied only when $|\pi/2 - \theta| \gg (m_e/m_i)^{1/2}$.

We assume now that $|z_n^e| \gg 1$ $(n = 0, \pm 1, \pm 2)$. Then, by virtue of Eq. (6) we have

$$K_e = -\frac{\Omega_e^2\cos^2\theta}{\omega'^2} - \frac{\Omega_e^2\sin^2\theta}{\omega'^2-\omega_H^{e2}} - \frac{3k^2v_T^{e2}\Omega_e^2}{\omega'^4}$$

$$\times\left[\cos^4\theta + \frac{6-3u_e+u_e^2}{3(1-u_e)^3}\cos^2\theta\sin^2\theta + \frac{\sin^4\theta}{(1-u_e)(1-4u_e)}\right] \tag{16}$$

$$+ i\sqrt{\frac{\pi}{2}}\frac{\omega'}{k^2a_e^2\Omega_e|\cos\theta|}\sum_{n=-\infty}^{\infty}\frac{\mu_e^{|n|}\sin^{2|n|}\theta}{|n|!\,2^{|n|}}e^{-z_n^2},\quad u_e = (\omega_H^e/\omega')^2.$$

Substituting Eqs. (9) and (16) in Eq. (1) and neglecting the thermal corrections we have

$$1 - \frac{\Omega_e^2\cos^2\theta}{\omega^2} - \frac{\Omega_e^2\sin^2\theta}{\omega^2-\omega_H^{e2}} - \frac{\Omega_i^2}{\omega^2} = 0. \tag{17}$$

Neglecting the last term in Eq. (17) for values of θ far from π 2, we find the resonance frequencies of the electron plasma oscillations in the "hydrodynamic" approximation:

$$\omega_{1,2}^2 = \omega_\pm^2 = \frac{1}{2}(\Omega_e^2+\omega_H^{e2}) \pm \frac{1}{2}\left[\left(\Omega_e^2+\omega_H^{e2}\right)^2 - 4\Omega_e^2\omega_H^{e2}\cos^2\theta\right]^{1/2} \tag{18}$$

When $\theta \to \pi/2$

$$\omega_1^2 = \Omega_e^2 + \omega_H^{e2};\quad \omega_2^2 = \Omega_e^2\omega_H^{e2}\cos^2\theta/(\Omega_e^2+\omega_H^{e2}). \tag{19}$$

Equation (19) for ω_2 applies if $|\pi/2-\theta|^2 \gg m_e/m_i$. If, however, $|\pi/2-\theta|^2 < m_e/m_i$, from Eq. (17) we have

$$\omega_2^2 = \widetilde{\omega}^2 = (\Omega_e^2\cos^2\theta + \Omega_i^2)/(1+\Omega_e^2/\omega_H^{e2}). \tag{20}$$

Taking account of the correction terms in Eqs. (9) and (16), we find the frequency and the damping term

$$\omega_2 = \widetilde{\omega}(1+\widetilde{\varepsilon}),\ |\widetilde{\varepsilon}| \ll 1, \tag{21}$$

$$\widetilde{\varepsilon} = \frac{1}{2(1+\Omega_e^2/\omega_H^{e2})}\left\{-\frac{\widetilde{\omega}^2\Omega_e^2}{\omega_H^{e4}} + \frac{3k^2v_T^{i2}\Omega_i^2}{\widetilde{\omega}^4}\right.$$
$$\left. + 3k^2v_T^{e2}\Omega_e^2\left(\frac{\cos^4\theta}{\widetilde{\omega}^4} - \frac{\cos^2\theta}{3\widetilde{\omega}^2\omega_H^{e2}} + \frac{1}{4\omega_H^{e4}}\right)\right\}, \tag{22}$$

$$\gamma = \sqrt{\frac{\pi}{8}}\frac{\widetilde{\omega}^2}{1+\Omega_e^2/\omega_H^{e2}}\left\{\frac{\exp(-\omega_2^2/2k^2v_T^{e2}\cos^2\theta)}{k^3a_e^3\Omega_e|\cos\theta|}\right.$$
$$\left. + \frac{\exp(-\omega_2^2/2k^2v_T^{i2})}{k^3a_i^3\Omega_i}\right\}. \tag{23}$$

The inequalities $|z_i| \gg 1$, $|z_0^e| \gg 1$, $|\widetilde{\epsilon}| \ll 1$, and $\gamma_2 \ll \widetilde{\omega}$ are satisfied if $ka_e \ll 1$ and $ka_i \ll 1$.

(c) In the strong field case, when $\omega_H^i \gg kv_T^i$ and $\omega_H^e \gg k_T^e$, when $|z_0^e| \ll 1$ we can use Eq. (14) for K_e; when $|z_n| \gg 1$ we can use Eq. (16) for K_i (in Eq. (16) we replace T_e by T_i and m_e by m_i). Equation (1) then assumes the form

$$1 + \frac{1}{k^2a_e^2} - \frac{\Omega_i^2\cos^2\theta}{\omega'^2} - \frac{\Omega_i^2\sin^2\theta}{\omega'^2-\omega_H^{i2}} - \frac{3k^2v_T^{i2}\Omega_i^2}{\omega^4}$$

$$\times\left\{\cos^4\theta + \cos^2\theta\sin^2\theta\,\frac{6-3u_i+u_i^2}{3(1-u_i)^3} + \frac{\sin^4\theta}{(1-u_i)(1-4u_i)}\right\} \tag{24}$$

$$+ i\sqrt{\frac{\pi}{2}}\frac{\omega'}{k^3a_e^3\Omega_e|\cos\theta|} = 0,\quad u_i = (\omega_H^i/\omega)^2.$$

From Eq. (24) we find the resonance frequencies $\omega_{1,2}$ of the electron-ion oscillations in a strong magnetic field:

$$\omega_{1,2} = \widetilde{\omega}_\pm(1+\widetilde{\varepsilon}_\pm),\quad |\widetilde{\varepsilon}_\pm| \ll 1, \tag{25}$$

where

$$\widetilde{\omega}_\pm^2 = \frac{1}{2}(\omega_0^2+\omega_H^{i2}) \pm \frac{1}{2}\{(\omega_0^2+\omega_H^{i2})^2 - 4\omega_0^2\omega_H^{i2}\cos^2\theta\}^{1/2} \tag{26}$$

are the resonance frequencies when the thermal motion of the ions is neglected; $\widetilde{\epsilon}_\pm$ determines the corrections for ω_1 and ω_2 due to the thermal motion of the ions

$$\widetilde{\varepsilon}_\pm = \frac{3k^2v_T^{i2}}{2\widetilde{\omega}_\pm^2[\cos^2\theta + \sin^2\theta\,\widetilde{\omega}_\pm^4/(\widetilde{\omega}_\pm^2-\omega_H^{i2})^2]}$$
$$\times\left[\cos^4\theta + \frac{6-3u_\pm+u_\pm^2}{3(1-u_\pm)^3}\cos^2\theta\sin^2\theta + \frac{\sin^4\theta}{(1-u_\pm)(1-4u_\pm)}\right], \tag{27}$$

$$u_\pm = \left(\frac{\omega_H^i}{\widetilde{\omega}_\pm}\right)^2.$$

The damping factor corresponding to the frequencies $\omega_{1,2}$ is

$$\gamma_{1,2} = \sqrt{\frac{\pi}{8}}\frac{\widetilde{\omega}_\pm^4}{k^3a_e^3|\cos\theta|[\cos^2\theta + \sin^2\theta\,\widetilde{\omega}_\pm^4/(\widetilde{\omega}_\pm^2-\omega_H^{i2})^2]\Omega_e\Omega_i^2}. \tag{28}$$

Eqs. (24) and (28) apply if the inequalities $|z_n^i| \gg 1$ and $|z_0^e| \ll 1$ hold. The inequality $|z_0^i| \gg 1$ is satisfied for values of θ far from $\pi/2$ and if the plasma is highly non-isothermal, $T_e \gg T_i$. The condition $|z_n^i| \gg 1$ $(n = 1, 2, \ldots)$ holds if $\widetilde{\omega}_+$ is not close to $n\omega_H^i$. The inequality $|z_0^e| \ll 1$ is always satisfied for values of θ which are not close to $\pi/2$ and $\omega_H^i < \omega_0$ because $m_e \ll m_i$. If, however, $\omega_H^i > kv_T^e$, the inequality $|z_0^e| \ll 1$ is satisfied only for one of the solutions of Eqs. (25) to (28), $\omega = \omega_0\cos\theta$, $\gamma = \gamma_0\cos\theta$.

As $\theta \to 0$, one of the solutions of Eq. (25), $\omega_1 \approx \widetilde{\omega}_+$, approaches the expression given in (10) while the other $\omega_2 \approx \widetilde{\omega}_-$ approaches ω_H^i However, at small values of θ Eqs. (25) to (28) for ω_2 and γ_2 do not apply since the condition $|z_1^i| \gg 1$ does not hold at values of θ close to 0. If at small values of θ the inequality $|\omega_1' - \omega_H^i| \gg kv_T^i$ does not hold when $\omega_1 \approx \widetilde{\omega}_+$, Eq. (27) (thermal frequency correction) and Eq. (28) (damping) are not correct. When $|\widetilde{\omega} - \omega_H^i| \ll kv_T^i$, the integral $\int \frac{e^{-t^2}dt}{z_1^i - t} \approx -i\pi$. Thus we find

$$\omega_1 = \frac{\Omega_i k a_e}{\sqrt{1 + k^2 a_e^2}} \approx \omega_H^i, \quad \gamma_1 = \gamma_0 + \frac{1}{2}\sqrt{\frac{\pi T_e}{8T_i}}\,\theta^2 \Omega_i k a_e. \qquad (29)$$

If, at some value of θ, not close to $\pi/2$ it turns out $\widetilde{\omega}_+ \approx 2\omega_H^i$, then the inequality $|z_2^i| \gg 1$ no longer holds and consequently Eq. (27) for $\widetilde{\varepsilon}_+$ is no longer valid. If $|\widetilde{\omega}_+ - 2\omega_H^i| \ll kv_T^i \cos\theta$, the integral which contains z_2^i in (3) is approximately equal to $-i\pi$ and gives additional damping at frequency ω_1. The additional damping also obtains in the general case when $|\omega_+ - m\omega_H^i| < kv_T^i \times \cos\theta$ $(m = 2, 3, \ldots)$

$$\gamma_1 = \sqrt{\frac{\pi}{8}}\,\frac{m^4}{|\cos^3\theta|\,[1 + (m^2 - 1)^{-2} m^4 \operatorname{tg}^2\theta]}$$

$$\times \left\{\frac{\omega_H^{i4}}{\Omega_i^2 \Omega_e k^2 a_e^3} + \frac{\sin^{2m}\theta\, k v_T^i}{2^m m!}\left(\frac{k v_T^i}{\omega_H^i}\right)^{2m-4} \exp\left(-z_m^{i2}\right)\right\}, \qquad (30)$$

$$z_m^i = (\omega_1 - m\omega_H^i) / (\sqrt{2}\, k v_T^i \cos\theta).$$

The inequality $\gamma_1 \ll \omega_1$ for $m = 3, 4$ is always satisfied for any value of θ excluding $\theta \sim \pi/2$ since $kv_T^i \ll \omega_H^i$. When $m = 2$ this inequality is satisfied for small values of θ.

For $\theta \rightarrow \pi/2$, from Eq. (25) we find

$$\omega_1^2 \approx \widetilde{\omega}_+^2 = \omega_H^{i2} + \omega_0^2. \qquad (31)$$

Eq. (31) is valid if the inequality $|z_0^e| \ll 1$ is satisfied, i.e., if

$$\pi/2 - \theta|^2 \gg (\omega_H^i / k v_T^e)^2 + m_e / m_i,$$

from which it follows that Eq. (31) does not apply in the narrow region of angles about $\pi/2$.

We now assume that $|z_n^e| \gg 1$ and $|z_n^i| \gg 1$. In this case (16) applies for K_e and K_i. At values of θ far from $\pi/2$ K_i is small as compared with K_e and can be neglected. In this case, using Eq. (1) we obtain the results given in references 6 and 7. If, however, $\theta \sim \pi/2$, assuming that $\omega \ll \omega_H^e$, from the dispersion equation we find $\omega_{1,2} \approx \Omega_\pm$, where

$$\Omega_\pm^2 = \frac{1}{2(1 + \Omega_e^2/\omega_H^{e2})}\{\omega_H^{i2} + \Omega_i^2 + \Omega_e^2\cos^2\theta \qquad (32)$$

$$\pm [(\omega_H^{i2} + \Omega_i^2 + \Omega_e^2\cos^2\theta)^2 - 4(1 + \Omega_e^2/\omega_H^{e2})\,\Omega_e^2\omega_H^{i2}\cos^2\theta]^{1/2}\}.$$

The damping of waves with frequencies given by (32) turns out to be small (exponential factor).

In conclusion we may note that if the conditions

$$|K_i| \gg |B_0/n'^2|, \quad |K_i| \gg |C_0/n'^4|, \qquad (33)$$

are satisfied, when $H_0 \neq 0$ we can approximately isolate the low-frequency longitudinal oscillations; these conditions are satisfied in cases (b) and (c) if

$$k^2c^2 \gg \Omega_i^2.$$

(In case (c) it is assumed that $\widetilde{\omega}_\pm \sim \omega_0 \sim \omega_H^i$ and $\Omega_\pm \sim \Omega_i$).

---

[1] L. Tonks and I. Langmuir, Phys. Rev. **33**, 195 (1929).

[2] G. V. Gordeev, J. Exptl. Theoret. Phys. (U.S.S.R.) **27**, 19 (1954).

[3] K. N. Stepanov, J. Exptl. Theoret. Phys. (U.S.S.R.) **34**, 1292 (1958), Soviet Phys. JETP **7**, 892 (1958).

[4] G. V. Gordeev, J. Exptl. Theoret. Phys. (U.S.S.R.) **23**, 660 (1952).

[5] Faddeeva and Terent'ev, **Таблицы значений интеграла вероятностей от комплексного аргумента** (Tables of Values of the Probability Integral for Complex Argument) Gostekhizdat, Mos. 1954.

[6] B. N. Gershman, J. Exptl. Theoret. Phys. (U.S.S.R.) **24**, 659 (1953).

[7] A. G. Sitenko and K. N. Stepanov, J. Exptl. Theoret. Phys. (U.S.S.R.) **31**, 642 (1956), Soviet Phys. JETP **4**, 512 (1957).

Translated by H. Lashinsky
245

SOVIET PHYSICS JETP VOLUME 35(8), NUMBER 5 MAY, 1959

ON THE PRECISION OF QUANTUM MECHANICAL MEAN VALUES COMPUTED BY THE VARIATIONAL METHOD

V. M. BUIMISTROV

Physics Institute, Academy of Sciences, Ukrainian S.S.R.

Submitted to JETP editor May 5, 1958

J. Exptl. Theoret. Phys. (U.S.S.R.) 35, 1161-1164 (November, 1958)

Kato[1] and Temple[2] have given a method for estimating the accuracy of approximate eigenvalues for a linear self-adjoint operator. We show that it is also possible to estimate the accuracy of calculated quantum-mechanical mean values of certain functions of the coordinates.

KATO[1] and Temple[2] have given a method for estimating the accuracy with which the variational method yields the eigenvalues of a linear self-adjoint operator. Relying on Kato's results, we give a method of evaluating how accurate is a calculation of the quantum mechanical average of certain functions $F(q)$, where q is the set of coordinates describing the system.

Let H be a linear self-adjoint operator, λ_n its eigenvalues and φ_n its eigenfunctions, which form a complete orthonormal system. Let us assume that the interval (α, β) contains one and only one eigenvalue (λ_p) of the operator H:

$$\begin{aligned}(\lambda_n-\alpha)(\lambda_n-\beta) &\geqslant 0, \quad n \neq p;\\ (\lambda_p-\alpha)(\lambda_p-\beta) &< 0, \quad n=p.\end{aligned} \tag{1}$$

Let ψ_p be an approximation to the function φ_p and expand it in a series of the φ_n: $\psi_p = \Sigma a_n \varphi_n$. If, now, we multiply the first of the inequalities (1) by $|a_n|^2$ and sum over all $n \neq p$ we obtain

$$\sum_{n\neq p}|a_n|^2\lambda_n - (\alpha+\beta)\sum_{n\neq p}|a_n|^2\lambda_n + \alpha\beta\sum_{n\neq p}|a_n|^2 \geqslant 0. \tag{2}$$

It is not difficult to see that

$$\overline{H} \equiv (\psi_p, H\psi_p) = \sum_n |a_n|^2\lambda_n, \quad (H\psi_p, H\psi_p) = \sum_n |a_n|^2\lambda_n^2, \quad \sum_n |a_n|^2 = 1,$$

if the trial function ψ_p is normalized. Adding the term with $n = p$ to each sum in (2) and solving for this term, we get

$$-|a_p|^2(\lambda_p-\alpha)(\lambda_p-\beta) + \varepsilon^2 + (\overline{H}-\alpha)(\overline{H}-\beta) \geqslant 0, \quad \varepsilon^2 = (H\psi_p, H\psi_p) - \overline{H}^2. \tag{3}$$

Identical transformations with the use of the second of the inequalities (1) leads to

$$1 - |a_p|^2 \leqslant \frac{\varepsilon^2 + (\overline{H}-\lambda_p)(\overline{H}+\lambda_p-\alpha-\beta)}{(\lambda_p-\alpha)(\beta-\lambda_p)} \equiv R_p. \tag{4}$$

In order that the interval (α, β) contain the lowest eigenvalue λ_0, it is necessary to take $\alpha = -\infty$, $\beta = \lambda_1$. Then (4) becomes

$$1 - |a_0|^2 \leqslant (\overline{H}-\lambda_0)/(\lambda_1-\lambda_0). \tag{5}$$

We note that if the interval (α, β) does not contain any eigenvalues of H, then the first of the inequalities (1) holds for all n. Multiplying it by $|a_n|^2$ and summing over all n, we obtain $\epsilon^2 + (\overline{H}-\alpha)(\overline{H}-\beta) \geq 0$. Taking $\alpha = \lambda_0$ and $\overline{H} < \beta < \lambda_1$, we obtain the following lower limit for λ_0:

$$\overline{H} - \varepsilon^2/(\beta-\overline{H}) \leqslant \lambda_0. \tag{6}$$

The derivation given above for formulas (4), (5), and (6) has been carried out for a discrete spectrum, but it holds as well when the operator H has a mixed spectrum, with discrete and continuous parts. The inequalities (4) to (6) are derived by a somewhat different method in reference 1.

Given a function $F(q)$, let us evaluate the absolute magnitude of the difference between the true value $\overline{F}_T = (\varphi_p, F\varphi_p)$ of its quantum mechanical average and the approximate value $\overline{F}_A = (\psi_p, F\psi_p)$. The Buniakovski-Schwarz inequality gives

$$\begin{aligned}|\overline{F}_T - \overline{F}_A| &= \left|\int F(|\varphi_p|-|\psi_p|)(|\varphi_p|+|\psi_p|)\,dq\right|\\ &\leqslant \left[\int |F|^2(|\varphi_p|+|\psi_p|)^2\,dq \cdot \int(|\varphi_p|-|\psi_p|)^2\,dq\right]^{1/2}.\end{aligned} \tag{7}$$

Consider first the integral

$$\int(|\varphi_p|-|\psi_p|)^2\,dq = 2\left(1-\int|\varphi_p||\psi_p|\,dq\right).$$

From the inequalities (4), $1 - |\int \psi_p^* \varphi_p\, dq|^2 \leq R_p$, and $\left|\int \psi_p^* \varphi_p \, dq\right| \leq \int |\psi_p| \, |\varphi_p| \, dq$, it immediately follows that

$$\int (|\varphi_p| - |\psi_p|)^2 \, dq \leqslant 2S_p, \quad S_p \equiv 1 - \sqrt{1 - R_p}. \tag{8}$$

We write the second factor in (7) in the form

$$\int |F|^2 (|\varphi_p| + |\psi_p|)^2 \, dq = 4 \int |F|^2 |\psi_p|^2 \, dq$$
$$+ 4 \int |F|^2 |\psi_p| (|\varphi_p| - |\psi_p|) \, dq + \int |F|^2 (|\varphi_p| - |\psi_p|)^2 \, dq.$$

Application of the Buniakovski-Schwarz inequality and inequality (8) then leads to the formula

$$\int |F|^2 (|\varphi_p| + |\psi_p|)^2 \, dq \leqslant 4 \, \overline{|F|^2}^p + 4 \left(\overline{|F|^4}^p \cdot 2S_p\right)^{1/2}$$
$$+ \int |F|^2 (|\varphi_p| - |\psi_p|)^2 \, dq, \tag{9}$$
$$\overline{\varphi}^p = \int \varphi \, |\psi_p|^2 \, dq.$$

When $|F|$ is bounded, so that $|F|^2 < B$ for all q, we finally obtain

$$|\overline{F}_T - \overline{F}_A| \leqslant \left[2S_p \left(4 \, \overline{|F|^2}^p + 4 \sqrt{2S_p \, \overline{|F|^4}^p} + 2BS_p\right)\right]^{1/2}. \tag{10}$$

If, on the other hand, $|F|$ increases without limit for sufficiently large q, while $|\varphi_p|^2$ decreases, we can break up the configuration space into two parts I and II, so that $|F|^2 < B$ in the region I and

$$\int_{(II)} |F|^2 (|\varphi_p|^2 + |\psi_p|^2) \, dq \ll \overline{|F|^2}^p$$

because the wave function decreases rapidly. Then

$$\int |F|^2 (|\varphi_p| - |\psi_p|)^2 \, dq \leqslant 2BS_p + \int_{(II)} |F|^2 (|\varphi_p|^2 + |\psi_p|^2) \, dq$$

and we obtain (10) once more.

Similar formulas can be derived for quantum mechanical transition probabilities.

Let φ_n be the real function, ψ an approximation to φ_n. Let us evaluate

$$|(\varphi_m, F\varphi_n) - (\psi_m, F\psi_n)|$$
$$= \left|\int \delta_m F \psi_n \, dq + \int \psi_m F \delta_n \, dq + \int \delta_m F \delta_n \, dq\right|, \tag{11}$$
$$\delta_n = \varphi_n - \psi_n.$$

Assuming that $|F|^2 < B$ for all q, and noting that $\int \delta_n^2 \, dq \leq 2S_n$ ($\int \varphi_n \psi_n \, dq$ is taken to be positive), the Buniakovski-Schwarz inequality gives

$$|(\varphi_m, F\varphi_n) - (\psi_m, F\psi_n)| \leqslant \left(2S_m \, \overline{|F|^2}^n\right)^{1/2}$$
$$+ \left(2S_n \, \overline{|F|^2}^m\right)^{1/2} + 2 (BS_m S_n)^{1/2}. \tag{12}$$

If $|F|$ increases without limit at large q, then we break up the configuration space into two parts, region I where $|F|^2 < B$, and region II in which

$$\int_{(II)} (\psi_m^2 + \varphi_m^2) |F|^2 \, dq \ll \overline{|F|^2}^m,$$

We then obtain (12) once more.

If, in (12), we take $m = n$, we obtain a new inequality for the mean which is sometimes more convenient than the inequality (10).

It is not difficult to see that the right hand sides of (10) and (12) go to zero as the approximation ψ approaches the exact function φ, i.e., for a sufficiently close approximation to φ the estimates here obtained become as accurate as desired.

In applying the above formulas, it is of course not necessary that the approximation ψ be obtained by a straight variational method. It could be obtained by some other approximation procedure (e.g., perturbation theory); the inequalities will then give an estimate of the accuracy of this method. If the energy levels are sufficiently well known, the formulas (10) and (12) can, for example, be used to obtain an estimate of the accuracy of the quantum mechanical calculations of the diamagnetic susceptibility or of transition probabilities in atoms or molecules.

Let us estimate, for example, the accuracy of the calculation of the diamagnetic susceptibility of the helium atom. It is sufficient to consider only the calculation of the mean square radius $\overline{r^2}$. Following Hylleras,[3] we take our approximate ground state wave function to be

$$\psi = Ae^{-sk/2} (1 + 0.08uk + 0.01 \, t^2 k^2),$$
$$s = r_1 + r_2, \quad t = r_1 - r_2, \quad u = r_{12} = |\mathbf{r}_1 - \mathbf{r}_2|, \quad k = 3.63,$$

where $\mathbf{r}_1$ and $\mathbf{r}_2$ are the radius vectors to the first and second electrons. With this approximation, $\overline{H} = -2.9024$ atomic units; experimentally, the first and second energy levels are $\lambda_0 = -2.9035$ and $\lambda_1 = -2.175$ atomic units.

In applying the inequality (10), we break up the configuration space $\mathbf{r}_1, \mathbf{r}_2$ into region I: $\mathbf{r}_1 < 10$ and II: $\mathbf{r}_1 > 10$ atomic units. An estimate of the integral $\int |F|^2 (|\varphi_p|^2 + |\psi_p|^2) \, dq$ [neglected in deriving (10)] over the region II shows that this integral is one-millionth of the part retained. Substituting (5) in (8) and (8) in (10), we obtain $|\bar{F}_T - \bar{F}_A|/|\bar{F}_A| < 0.2$. The diamagnetic susceptibility calculated with the approximation ψ differs from the measured value by less than 1%, which does not disagree with our estimate of the accuracy of the variational method.

We take this opportunity to express our thanks to Prof. S. I. Pekar, M. F. Deigen, E. I. Rashba, and the other members of the Theoretical Seminar at the Institute of Physics, and also to V. Iu. Fedorchenko who carried out the calculations.

[1] T. Kato, Japan. J. Phys. **4**, 334 (1949).

[2] G. Temple, Proc. Roy. Soc. (London) **211A**, 204 (1952).

[3] H. Bethe, Квантовая механика простейших систем (Quantum Mechanics of Simplest Systems) ONTI, Moscow-Leningrad, 1935, page 120.

Translated by R. Krotkov
246

SOVIET PHYSICS JETP VOLUME 35(8), NUMBER 5 MAY, 1959

EXCHANGE EFFECTS IN STRIPPING REACTIONS

V. G. NEUDACHIN

Scientific Research Institute of Nuclear Physics, Moscow State University

Submitted to JETP editor May 9, 1958

J. Exptl. Theoret. Phys. (U.S.S.R.) **35**, 1165-1170 (November, 1958)

Formulas for the differential cross sections of the stripping reactions (d, p) and (d, n) have been obtained in the Born approximation, with inclusion of effects of the antisymmetry of the total wave function. The most important case, that of the shell configurations j^{n-1} for the initial nucleus and j^n for the final nucleus, has been considered.

1. GENERAL THEORY

It has been shown in a number of papers that in particular cases of calculations of stripping reaction cross-sections the antisymmetrization of the total wave function can affect the results of the calculations to an important extent.[1] Calculations on stripping reactions with inclusion of the antisymmetrization have not been carried out, however, unless one counts the work of French, which is of a preliminary nature.

We shall use the results of the general theory of scattering.[2,3] We first carry through a treatment without antisymmetrization. We assign the numbers 0 and 1 to the proton and neutron in the deuteron; V(01) is the interaction between them. The interaction of the proton with the other nucleons of the nucleus is described by an averaged potential V(0ξ), taken, for example, from the optical model. Then the wave function is determined from the equation

$$\Psi^{(+)} = \Phi + (1/a^{(\pm)}) V(01)\Phi, \quad a^{(\pm)} = E \pm i\varepsilon - H, \tag{1}$$

where H is the total Hamiltonian of the system, and Φ is the wave function of the initial state [reaction (p, d)].

The antisymmetrization is performed by the application of an operator A (whose concrete form will be given below):

$$\overline{\Psi}^{(+)} = A\Psi^{(+)} = A\Phi + (1/a^{(\pm)}) AV\Phi. \tag{2}$$

To obtain the expression for the reaction amplitude in the Born approximation, we replace 1/a by 1/a′(01), using the fact that[3]

$$1/a = \{1/a'(01)\}[1 + \{H'(01)/a\}],$$

where a′(01) is the Green's function of the final system,[2] and $H_{\text{fin}} = H - H'(01)$ is its Hamiltonian.

The reaction amplitude is given by the second term in Eq. (2), that is,

$$AV\Phi / a'(01). \tag{3}$$

Thus our task reduces to the calculation, in Born approximation with distorted waves for the protons and deuterons, of the matrix element

$$\int \Psi^{*}_{\text{fin}}(2, 3, \ldots, n)\, \Psi^{*}_{\mathbf{k}_d}(0,1)\, AV\, \Psi_{\text{int}}(1, 2 \ldots n) \times \Psi_{\mathbf{k}_p}(0)\, d\mathbf{r}_0 \ldots d\mathbf{r}_n, \tag{4}$$

where Ψ_{fin} is the wave function of the final nucleus, Ψ_{init} is that of the initial nucleus, $\Psi_{\mathbf{K}_p}$ is the wave function of the proton in the field of the initial nucleus, and $\Psi_{\mathbf{K}_d}$ is that of the deuteron. The antisymmetrization operator A is defined in the following way:

$$AV\Psi_{\text{int}}(1, 2 \ldots n)\Psi_{\mathbf{k}_p}(0) = \frac{1}{\sqrt{n+1}} \sum_{i \neq j} (-1)^{n+1-i} V(i, j) \times \Psi_{\text{int}}(0, 1 \ldots i-1, i+1, \ldots n)\Psi_{\mathbf{k}_p}(i). \tag{5}$$

The normalization factor in this case is found from the requirement of conservation of flux. The antisymmetrization procedure used in Eq. (5) was indicated by Racah in reference 4, where the antisymmetrization was carried out for the wave function of the shell configuration $l^n l'$.

2. CALCULATION WITH WAVE FUNCTIONS OF THE SHELL THEORY

We shall suppose that

$$\Psi_{\text{int}} = |j^n \alpha_1\rangle, \quad \Psi_{\text{fin}} = |j^{n-1} \alpha_2\rangle,$$

where α is the set of quantum numbers necessary for unique specification of a state. Using Racah's technique,[4,5] with the expression (5) for the operator A, we work out the matrix element (4):

$$\begin{aligned} I &= 2I_1 + (n-1)\,2I_2 + 2\,(n-1)\,(n-2)\,I_3;\\ I_1 &\sim \langle \mathbf{k}_d S_d\,(12)\,|\,V\,(12)\,|\,j\,(1)\,\mathbf{k}_p s_p\,(2)\rangle;\\ I_2 &\sim \sum_{\alpha_3\alpha_4} \langle \mathbf{k}_d S_d\,(12),\ j\,(3)\,|\,V\,(13)\,|\ j^2\alpha_4\,(12)\,\mathbf{k}_p s_p\,(3)\rangle\\ &\quad\times \langle j^n\alpha_1\,|\,j^{n-2}\alpha_3;\ j^2\alpha_4\rangle\,\langle j^{n-1}\alpha_2\,|\,j^{n-2}\alpha_3\rangle;\\ I_3 &\sim \sum_{\alpha_6\alpha_5\alpha_7\alpha_8} \langle j^2\alpha_8\,(12)\,|\,V\,(12)\,|\,j\,(1)\,\mathbf{k}_p s_p\,(2)\rangle\,\langle \mathbf{k}_d S_d\,(34)\,|\,j^2\alpha_6\,(34)\rangle\\ &\quad\times \langle j^n\alpha_1\,|\,j^{n-2}\alpha_5;\ j^2\alpha_6\rangle\,\langle j^{n-1}\alpha_2\,|\,j^{n-3}\alpha_7;\ j^2\alpha_8\rangle\,\langle j^{n-2}\alpha_5\,|\,j^{n-3}\alpha_7\rangle. \end{aligned} \tag{6}$$

Here $<j^n\,|\,j^{n-1}>$ and so on are fractional parentage coefficients. Thus the calculation of the differential cross-section reduces to the calculation of I_1^2, I_2^2, I_1I_2, etc.

In carrying out the sums of products of Clebsch-Gordan coefficients over magnetic quantum numbers we have used the effective graphic method of Levinson.[6] We thus arrive at the following formulas (the expressions for the interference terms are not presented here):

$$\begin{aligned} I_1^2 &= \frac{[J_1]\,[S_d]}{4\pi\,[s]}\,\left(C^{1/2\ 1/2\ 0}_{1/2\,-1/2\ 0}\right)^2 \left(C^{T_2\tau T_1}_{M_{\tau_2}\,-1/2\,M_{\tau_1}}\right)^2\\ &\quad\times \langle j^n\alpha_1\,|\,j^{n-1}\alpha_2\rangle\,D_l^2\,(\mathbf{k}_p-\mathbf{k}_d),\\ D_l\,(\mathbf{k}_p-\mathbf{k}_d) &= 4\pi\varphi_l\,(R)\,[h_l^{(1)}\,(\varkappa R)]^{-1}\\ &\quad\times \frac{\hbar^2\,(8\pi\alpha)^{1/2}}{M}\int\limits_R^\infty h_l^{(1)}\,(\varkappa r)\,j_l\,(|\,\mathbf{k}_p-\mathbf{k}_d\,|\,r)\,r^2\,dr. \end{aligned} \tag{7}$$

Here α is the reciprocal of the deuteron radius; $\varphi_l(R)$ is the amplitude of the wave function of a bound nucleon at the surface of the nucleus; $h_l^{(1)}(x)$ is the spherical Hankel function of the first kind; $j_l(x)$ is the spherical Bessel function; κ is the imaginary wave number of a bound nucleon; R is the radius of the "edge" of the nucleus; $[J_1] = 2J_1 + 1$, etc.; and $C^{j_1j_2j_3}_{m_1m_2m_3}$ are Clebsch-Gordan coefficients.

$$\begin{aligned} I_2^5 &= (4\pi)^2\,[J_1]\,[J_2]\,[j]^3\,[l]\,\left(C^{T_1\tau T_2}_{M\tau_1\ 1/2\,M\tau_2}\right)^2 \sum [a]\,[b] \begin{Bmatrix} l & s & j\\ l & s & j\\ L_4 & S_4 & J_4 \end{Bmatrix} \sqrt{[S_4]\,[J_4]}\ [L_4]\,[L_0]\,\langle j^n\alpha_1\,|\,j^{n-2}\alpha_3;\ j^2\alpha_4\rangle\,\langle j^{n-1}\alpha_2\,|\,j^{n-2}\alpha_3\rangle\,\hat{C}^{LL'a}_{000}\\ &\quad\times \hat{C}^{l_2l_2'a}_{000}\,\hat{C}^{lLL_0}_{000}\,\hat{C}^{lkL_0}_{000}\,\hat{C}^{kl_2l}_{000} \begin{Bmatrix} L_4 & l & l\\ k & L_0 & l_2 \end{Bmatrix} E_{\mathbf{k}_d\mathbf{k}_p}\,(l,\,k,\,l_2,\,L)\,\sqrt{[S_4']\,[J_4']}\ [L_4']\,[L_0'] \begin{Bmatrix} l & s & j\\ l & s & j\\ L_4' & S_4' & J_4' \end{Bmatrix} \langle j^n\alpha_1\,|\,j^{n-2}\alpha_3';\ j^2\alpha_4'\rangle\\ &\quad\times \langle j^{n-1}\alpha_2\,|\,j^{n-2}\alpha_3'\rangle\,\hat{C}^{lk'L_0'}_{000}\,\hat{C}^{lk'L_0'}_{000}\,\hat{C}^{k'l_2'l}_{000} \begin{Bmatrix} L_4' & l & l\\ k' & L_0' & l_2' \end{Bmatrix} E^*_{\mathbf{k}_d\mathbf{k}_p}\,(l,\,k',\,l_2',\,L')\,(-1)^{\rho_{22}} \begin{bmatrix} L_0' & L' & a & l_2'\\ l & L & l_2 & L_4'\\ b & l & L_0 & L_4 \end{bmatrix} \begin{Bmatrix} J_4 & L_4 & S_d\\ L_4' & J_4' & b \end{Bmatrix}\\ &\quad\times \begin{Bmatrix} J_3 & J_4 & J_1\\ J_4' & J_3' & b \end{Bmatrix} \begin{Bmatrix} J_3 & j & J_2\\ j & J_3' & b \end{Bmatrix} \begin{Bmatrix} l & j & s\\ j & l & b \end{Bmatrix} P_a\,(\cos\theta). \end{aligned} \tag{8}$$

Here S_d is the spin of the deuteron, s that of the nucleon; $\rho_{22} = J_1 + J_2 + l + s + l_2 + L + a$; the summation is taken over all indices except l, s, j, S_d, α_1, α_2 [α = (J, T, seniority)]. We also make use of the facts that $S_4 = S_4' = S_d = 1$, $T_4 = T_4' = T_d = 0$, $J_4 + T_4$ is even, $L_4 + S_4 + T_4$ is odd;

$$\begin{Bmatrix} j_1 & j_2 & j_3\\ j_4 & j_5 & j_6 \end{Bmatrix} = (-1)^{j_1+j_2+j_4+j_5}\,W\,(j_1j_2j_5j_4;\ j_3j_6),$$

W is a Racah coefficient; $\begin{Bmatrix} j_1 & j_2 & j_3\\ l_1 & l_2 & l_3\\ k_1 & k_2 & k_3 \end{Bmatrix}$ is a 9j symbol[7,8];

$\begin{bmatrix} j_1 & j_2 & j_3 & j_4\\ l_1 & l_2 & l_3 & l_4\\ k_1 & k_2 & k_3 & k_4 \end{bmatrix}$ is a 12j symbol of the second kind[8];

$$\begin{bmatrix} j_1 & j_2 & j_3 & j_4\\ l_1 & l_2 & l_3 & l_4\\ k_1 & k_2 & k_3 & k_4 \end{bmatrix} = \sum_x (-1)^f\,[x] \begin{Bmatrix} j_1 & k_1 & x\\ k_2 & j_2 & l_1 \end{Bmatrix} \begin{Bmatrix} j_2 & k_2 & x\\ k_3 & j_3 & l_2 \end{Bmatrix} \begin{Bmatrix} j_3 & k_3 & x\\ k_4 & j_4 & l_3 \end{Bmatrix} \begin{Bmatrix} j_4 & k_4 & x\\ k_1 & j_1 & l_4 \end{Bmatrix},$$

f is the sum of all the parameters of the 12j symbol;

$$\hat{C}^{l_1l_2l_3}_{000} = \sqrt{[l_1]\,[l_2]\,/\,4\pi\,[l_3]}\ C^{l_1l_2l_3}_{000};$$

θ is the angle between $\mathbf{k}_d$ and $1/2\,\mathbf{k}_d - \mathbf{k}_p$;

$$E_{\mathbf{k}_d,\,\mathbf{k}_p}\,(l,\,k,\,l_2,\,L) = V_0 i^{l_2-L} \iint\limits_R^\infty f_k\,(r_1,\,r_2)\,j_{l_2}\!\left(\frac{1}{2}\,k_d r_2\right) j_L\left(\left|\frac{1}{2}\,\mathbf{k}_d-\mathbf{k}_p\right| r_1\right) \varphi_l^2\,(r_1)\ \varphi_l\,(r_2)\,r_1^2r_2^2\,dr_1\,dr_2,$$

where $\varphi_l(r)$ is the radial part of the wave number of a bound nucleon with the orbital angular momentum l; $f_k(r_1, r_2)$ is defined in terms of the internal wave function of the deuteron

$$\chi_d(\mathbf{r}_1-\mathbf{r}_2)=\sum_k f_k(r_1, r_2)[k]P_k(\cos\omega_{12}),$$

in particular[1,9]

$$e^{-\alpha r_{12}}/r_{12}=\alpha\sum_k[k]j_k(i\alpha r_1)h_k^{(1)}(i\alpha r_2)P_k(\cos\omega_{12})$$

for $\mathbf{r}_1<\mathbf{r}_2$; $V_0=4\pi\hbar^2 M\alpha$ [the interaction potential of the nucleons is taken in the form $V_0\delta(\mathbf{r}_1-\mathbf{r}_2)$].

$$\begin{gathered}I_3^2=\frac{1}{4\pi}\left(C_{M_{T_1}\,{}^1\!/_2\,M_{T_2}}^{T_1\tau T_2}\right)^2[J_1][J_2][j][T_1]\sum C_{j^{n-2}\alpha_6;\,j^2\alpha_8}^{j^n_{\alpha_1}}\\
\times C_{j^{n-3}\alpha_7;\,j^2\alpha_5}^{j^{n-1}\alpha_2}C_{j^{n-3}\alpha_7}^{j^{n-2}\alpha_6}\left\{\begin{matrix}T_2 & T_1 & \tau\\ \tau & T_5 & T_7\end{matrix}\right\}\left\{\begin{matrix}T_2 & T_1 & \tau\\ \tau & T_5' & T_7'\end{matrix}\right\}[T_5]^{1/2}[T_5']^{1/2}\\
\times(-1)^{2T_1+1+T_7+T_7'}\hat{C}_{000}^{l\,l\,L_5}\hat{C}_{000}^{L_5 l\,l_p}\hat{C}_{000}^{l\,l\,L_5'}\hat{C}_{000}^{L_5' l\,l_p'}\\
\times\hat{C}_{000}^{l_p l_p' a}\hat{C}_{000}^{L_8 L_8' a}\sqrt{[J_6][J_6'][J_8][J_8'][J_5][J_5'][S_5][S_5'][l_p][l_p']}\\
\times(-1)^{\rho_{33}}\left\{\begin{matrix}L_8 & J_8 & S_8\\ J_8' & L_8' & a\end{matrix}\right\}\left\{\begin{matrix}J_8 & J_6 & J_1\\ J_6' & J_8' & a\end{matrix}\right\}\left\{\begin{matrix}J_6' & J_2 & b\\ J_5' & j & J_7'\end{matrix}\right\}\left\{\begin{matrix}J_6 & J_2 & c\\ J_5 & j & J_7\end{matrix}\right\}\left\{\begin{matrix}j & l & s\\ J_5' & L_5' & S_5'\\ b & l_p' & s\end{matrix}\right\}\\
\times\left\{\begin{matrix}j & l & s\\ J_5 & L_5 & S_5\\ c & l_p & s\end{matrix}\right\}\left\{\begin{matrix}J_6 & c & J_2\\ b & J_6' & a\end{matrix}\right\}\left\{\begin{matrix}c & l_p & s\\ l_p' & b & a\end{matrix}\right\}P_a(\cos\gamma)A_{\mathbf{k}_d}(l^2, L_8)\\
\times A_{\mathbf{k}_d}^*(l^2, L_8')B_{\mathbf{k}_p}(l, l_p)B_{\mathbf{k}_p}^*(l, l_p')+\text{comp. conj.}\end{gathered}\tag{9}$$

where

$$A_{\mathbf{k}_d}(l^2, L_8)=4\pi i^{-L_8}\int_R^\infty j_{L_8}(k_dR)Y_{L_8, M_8}^*(\mathbf{R}_d)\chi_d(\mathbf{r})$$

$$\times\Psi_{l^2L_8M_8}(\mathbf{r}_1\mathbf{r}_2)\,d\mathbf{r}_1d\mathbf{r}_2,\quad \mathbf{R}_d=\frac{\mathbf{r}_1+\mathbf{r}_2}{2},\quad \mathbf{r}=\mathbf{r}_1-\mathbf{r}_2;$$

$$B_{\mathbf{k}_p}(l, l_p)=4\pi i^{l_p}V_0\int_R^\infty\varphi_l^3(r)j_{l_p}(k_pr)r^2dr;$$

$\rho_{33}=J_1+J_2-s+1+b+c+J_7+J_7'$; in the summation we use the facts that $S_8=S_d=1$, $T_8=T_d=0$, J_8+T_8 is odd, $L_8+S_8+T_8$ is odd; γ is the angle between $\mathbf{k}_p$ and $\mathbf{k}_d$.

$$\frac{d\sigma}{d\Omega}=\frac{M_pM_d}{4\pi^2\hbar^4}\frac{k_p}{k_d}\frac{1}{[J_2][S_d]}\frac{n}{2}I^2,\tag{10}$$

for the reaction A(d, p)A + 1.

The calculation of the radial integrals B, D, and E is simple in principle. We can make an estimate of the integrals A if we extend the integration over the entire region and use oscillator wave functions for the bound nucleons, which makes it possible to use a simple transformation to separate the motion of the center of mass of two nucleons from their relative motion.[10] For the integrals B, D, and E it is natural to use as the wave functions of the bound nucleon the functions $h_l^{(1)}(\kappa r)$. They are normalized in the following way:[11] $[\varphi_l(R)/h_l^{(1)}(\kappa R)]h_l^{(1)}(\kappa r)$; $\varphi_l(R)$ is the amplitude of the single-particle wave function at the surface of the nucleus. The Wigner limit for the reduced width corresponds to the value of $\varphi_l(R)$ given by:[12] $R^3[\varphi_l(R)]^2/2=1$.

The usual theory of stripping involves only one radial integral $D_{\mathbf{k}_d, \mathbf{k}_p}(l)$, and its absolute value does not affect the angular distribution. Use of plane waves in the crudest sort of calculation gives for the particles topping the barrier an increase of the radial integral by a factor of five to seven, in the case of reactions with light nuclei.[11,13] The facts show,[14] however, that the relative values of the absolute cross-sections for cases of capture of nucleons with different values of l are well reproduced by the expression $D^2(l)$.

Our results involve a large number of radial integrals, so that the crudeness with which they are estimated makes the results, generally speaking, rather indefinite. Nevertheless the fact noted above allows us to hope that for each series of integrals the dependences on k, L, l_p, and so on are given correctly, so that in the calculation of angular distributions we can try to confine ourselves to the two unknown constant coefficients of I_2 and I_3, with a crude preliminary estimate of their order of magnitude.

The calculation of the expressions containing spherical functions can be carried out more simply by directing the z axis along one of the momenta, for example $\frac{1}{2}\mathbf{k}_d-\mathbf{k}_p$, or $\mathbf{k}_d$, etc., depending on the particular term.

3. CONCLUDING REMARKS

The cases that are the simplest and most interesting to analyze occur when one or two of the three terms in the expression (6) for the matrix element vanish. If n = 1, there remains only I_1, and we arrive at the usual formulas of the theory of stripping. If n = 2, the term in I_3 vanishes. If we consider the inverse process, the proton is incident on an odd-odd nucleus with two nucleons outside a closed shell. The structure of the expression (6) for the amplitude I_2 shows that I_2 is the reaction amplitude for the process of "knocking out" of a deuteron from the nucleus by the proton, which is itself bound in the final state. I_3^2 corresponds to the process of "heavy particle stripping,"[15,16] although it is not a complete expression for the squared amplitude of this process. In this case the angular distribution will have a maximum in the backward hemisphere. I_2^2 will evidently not have this peculiarity, since the "knocking out" of a particle is as a rule associated with a maximum in the forward part of the angular distribution. This argument agrees qualitatively with the angular distribution[17] of the protons from the reaction $B^{10}(dp)B^{11*}(J^* = \frac{1}{2}-)$, which is mainly due to a term of the type I_2^2. In fact, in a case in which $J_{fin} = J_1$ cannot be obtained by vector composition of $J_{init} = J_2$ and j, $I_1 = 0$, i.e., ordinary "stripping" is "forbidden" in the shell theory. There remain the terms in I_2 and I_3. An example of this latter type occurs in the reaction $B^{10}(n,d)Be^{9*}$ with formation of the Be^9 in the first excited state $J^* = \frac{1}{2}-$.

For the calculation of the cross-section of the reaction $B^{10}(d,p)B^{11*}$ mentioned above, the final formulas must be changed somewhat, since the final nucleus is described by the configuration j^6j', $j = {}^3\!/_2-$, $j' = {}^1\!/_2-$.

In conclusion the writer expresses his gratitude to K. A. Ter-Martirosian for a discussion of the statement of the problem.

---

[1] A. P. French, Phys. Rev. **107**, 1655 (1957). Kammuri, Nakasima, and Takagi, Prog. Theor. Phys. **17**, 306 (1957).

[2] B. A. Lippmann, Phys. Rev. **102**, 264 (1956).

[3] G. Takeda and K. M. Watson, Phys. Rev. **97**, 1336 (1955).

[4] G. Racah, Phys. Rev. **63**, 367 (1943).

[5] G. Racah, Phys. Rev. **62**, 438 (1942). A. R. Edmonds and B. H. Flowers, Proc. Roy. Soc. **A214**, 515 (1952).

[6] I. B. Levinson, Тр. физ.-техн. ин-та АН ЛитССР (Trans. Phys.-Tech. Inst. Acad. Sci. Lithuanian S.S.R.) **2**, 17, 31 (1957); Тр. АН ЛитССР (Trans. Acad. Sci. Lithuanian S.S.R.) **B4**, 3 (1957).

[7] A. de-Shalit, Phys. Rev. **91**, 1479 (1953). Arima, Horie and Tanabe, Prog. Theor. Phys. **11**, 143 (1954). H. Jahn and J. Hope, Phys. Rev. **93**, 318 (1954).

[8] I. B. Levinson and V. V. Vanagas, **Оптика и спектроскопия** (Optics and Spectroscopy) **2**, 10 (1957).

[9] W. Swiatecki, Proc. Roy. Soc. **A205**, 238 (1951).

[10] I. Talmi, Helv. Phys. Acta **25**, 185 (1952).

[11] W. Tobocman and M. H. Kalos, Phys. Rev. **97**, 132 (1955).

[12] A. M. Lane, Proc. Phys. Soc. **A66**, 977 (1953).

[13] K. Standing, Phys. Rev. **101**, 152 (1956).

[14] J. Holt and T. Marsham, Proc. Phys. Soc. **A66**, 1032 (1953).

[15] T. Fulton and G. E. Owen, Phys. Rev. **108**, 789 (1957).

[16] L. Madansky and G. E. Owen, Phys. Rev. **99**, 1608 (1955).

[17] N. Evans and W. Parkinson, Proc. Phys. Soc. A67, 684 (1954).

Translated by W. H. Furry
247

ENERGY LOSSES OF AN ELECTRON IN A MEDIUM WITH SPATIAL DISPERSION

V. M. AGRANOVICH and A. A. RUKHADZE

Submitted to JETP editor, June 10, 1958

J. Exptl. Theoret. Phys. (U.S.S.R.) 35, 1171-1174 (November, 1958)

A general formula is obtained for the energy losses of an electron moving in an arbitrary anisotropic medium characterized by spatial dispersion. It is shown that in the nonrelativistic case the total energy losses in an isotropic medium do not change when spatial dispersion of the medium is taken into account; however, the losses due to excitation of longitudinal waves do change in the general case. It is also shown that when spatial dispersion is taken into consideration the Cerenkov radiation at a frequency ω is distributed over several cones. The intensity of this radiation is calculated.

1. Ginzburg[1] has recently analyzed the propagation of electromagnetic waves in media with spatial dispersion. It is especially important to take account of this dispersion at frequencies close to resonances in the medium. The optical properties of a medium in the neighborhood of resonances has been considered in greater detail by Pekar[2] and the present authors.[3] It is also of interest to study effects that arise if one considers the influence of spatial dispersion on the energy losses of an electron which moves in a medium.

Suppose that an electron with velocity **v** moves in an anisotropic medium characterized by an arbitrary spatial dispersion. Maxwell's equations for this case are written as follows:

$$\operatorname{div}\mathbf{H} = 0, \quad \operatorname{curl}\mathbf{E} = -\frac{1}{c}\frac{\partial \mathbf{H}}{\partial t},$$

$$\operatorname{div}\mathbf{D} = 4\pi e\delta(\mathbf{r} - \mathbf{v}t), \operatorname{curl}\mathbf{H} = \frac{1}{c}\frac{\partial \mathbf{D}}{\partial t} + \frac{4\pi}{c}e\mathbf{v}\delta(\mathbf{r} - \mathbf{v}t),$$

$$\mathbf{D} = \int \hat{\varepsilon}(\omega, \mathbf{q})\,\mathbf{E}_q\, e^{i(\mathbf{q}\cdot\mathbf{r} - \omega t)}\, d\mathbf{q}. \qquad (1)$$

Taking Fourier components of **E**, **D**, and **H** we have

$$\mathbf{E}(\mathbf{r}, t) = -\frac{ie^2}{2\pi^2 c^2}\int (\mathbf{q}\cdot\mathbf{v})\left\{q^2\hat{\eta} - \frac{(\mathbf{q}\cdot\mathbf{v})^2}{c^2}\hat{\varepsilon}(\mathbf{q}\cdot\mathbf{v}, \mathbf{q})\right\}^{-1}\mathbf{v}e^{i\mathbf{q}\cdot(\mathbf{r}-\mathbf{v}t)}d\mathbf{q}, \qquad (2)$$

where $\hat{\eta}$ is a projection tensor in which $\eta_{ik} = \delta_{ik} - q_i q_k/q^2$.

The energy losses of an electron moving through a medium are determined by the work of the retarding force that acts on the electron; these forces arise by virtue of the field set up by the electron itself. Substituting the field at the electron, i.e., at the point $\mathbf{r} = \mathbf{v}t$, and using the identity

$$\left\{q^2\hat{\eta} - \frac{(\mathbf{q}\cdot\mathbf{v})^2}{c^2}\hat{\varepsilon}(\mathbf{q}\cdot\mathbf{v}, \mathbf{q})\right\}^{-1}\mathbf{v} \equiv \hat{b}^{-1}\mathbf{v} + \frac{(\mathbf{q}, \hat{b}^{-1})^2\,\hat{b}^{-1}\mathbf{q}}{1 - (\mathbf{q}, \hat{b}^{-1}\mathbf{q})},$$

where

$$\hat{b} = q^2 - (\mathbf{q}\cdot\mathbf{v})^2/c^2\hat{\varepsilon}(\mathbf{q}\cdot\mathbf{v}, \mathbf{q}),$$

we find the following expression for the loss per unit path length:

$$F = -\frac{ie^2}{2\pi^2 vc^2}\int (\mathbf{q}\cdot\mathbf{v})\frac{|(\mathbf{v}, \hat{b}^{-1}\mathbf{q})|^2 - (\mathbf{v}, \hat{b}^{-1}\mathbf{v})(\mathbf{q}, \hat{b}^{-1}\mathbf{q}) + (\mathbf{v}, \hat{b}^{-1}\mathbf{v})}{1 - (\mathbf{q}, \hat{b}^{-1}\mathbf{q})}d\mathbf{q}. \qquad (3)$$

This is the energy loss of an electron which moves in an anisotropic medium with arbitrary spatial dispersion and is a generalization of the corresponding formulas given, for example, in the review paper by Bolotovskii.[4]

2. In the nonrelativistic approximation Eq. (3) is simplified and assumes the following form:

$$F = -\frac{ie^2}{2\pi^2 v}\int \frac{(\mathbf{q}\cdot\mathbf{v})}{(\mathbf{q}, \hat{\varepsilon}\mathbf{q})}d\mathbf{q}. \qquad (4)$$

As an example we may consider the case of an isotropic non-gyrotropic medium with arbitrary spatial dispersion. The dielectric-constant tensor is then

$$\varepsilon_{ik}(\mathbf{q}\cdot\mathbf{v}, \mathbf{q}) = \varepsilon_0(\mathbf{q}\cdot\mathbf{v}, \mathbf{q})\,\delta_{ik} + \varepsilon_1(\mathbf{q}\cdot\mathbf{v}, \mathbf{q})\,q_i q_k/q^2. \qquad (5)$$

We take the z axis in the direction of **v** and introduce the notation $k = \sqrt{q_x^2 + q_y^2}$, $\omega = q_y^2 v$. Equation (4) becomes*

$$F = \frac{ie^2}{\pi}\int_{-\infty}^{+\infty}\int_0^{k_0}\frac{\omega d\omega\, kdk}{\bar{\varepsilon}(\omega, k^2 + \omega^2/v^2)(v^2k^2 + \omega^2)}, \qquad (6)$$

where

$$\bar{\varepsilon} \equiv (\mathbf{q}, \hat{\varepsilon}\mathbf{q})/q^2 = \varepsilon_0 + \varepsilon_1. \qquad (7)$$

Assuming that the complex dielectric constant

---

*The upper limit k_0 in the integration over k is determined by the condition of applicability of the macroscopic analysis (cf. reference 5, §84).

$\bar{\epsilon}(\omega,\ k^2+\omega^2/v^2)$ has no poles in the upper half-plane, we have from Eq. (6)

$$F = \frac{e^2}{v^2}\int_0^{ik_0v} \omega d\omega\,[1 - 1/\bar{\varepsilon}(\omega, 0)]. \tag{8}$$

Since $\epsilon_1(\omega, 0) = 0$ (cf. reference 1) and $\bar{\epsilon}(\omega, 0) = \epsilon_0(\omega, 0)$ is the dielectric susceptibility when spatial dispersion is not taken into account, we may conclude that in the nonrelativistic approximation spatial dispersion does not effect the total energy loss of an electron which moves in an isotropic medium. Equation (8) has been investigated in detail in reference 5. It should be noted, however, that while the total energy loss is not changed when spatial dispersion is considered, there can be a change in the energy lost by excitation of longitudinal waves. As follows from Eq. (6), the losses due to excitation of the longitudinal waves are determined by the zeroes of the quantity $\bar{\epsilon}(\omega,\ k^2+\omega^2/v^2)$ which, when spatial dispersion is introduced, lead to poles at frequencies $\omega_n = \pm\omega_n(k^2)$. Hence, the loss due to excitation of longitudinal waves (with spatial dispersion) is given by the following expression, which also applies in the relativistic case:

$$F_{\text{long}} = \frac{e^2}{2}\sum_n \int_0^{k_0^2} \omega_n(x)\,dx / [v^2x + \omega_n^2(x)]\, \frac{d}{d\omega_n}\bar{\varepsilon}$$
$$\times \left[\omega_n(x), x + \frac{\omega_n^2(x)}{v^2}\right]. \tag{9}$$

According to reference 3, the dielectric-constant tensor associated with one of the resonant absorption frequencies of the medium (assuming spatial dispersion in an isotropic, non-gyrotropic medium) is:

$$\varepsilon_{ik}(\omega, \mathbf{q}) = \frac{\omega^2 - \alpha q^2 - \beta}{\omega^2 - \alpha q^2 - \beta + \omega_0^2}\,\delta_{ik} - \frac{\alpha_1 q_i q_k}{\omega^2 - \alpha q^2 - \beta + \omega_0^2}, \tag{10}$$

where the quantities α and α_1 characterize the spatial dispersion of the medium. In this case the zeroes of the quantity $\bar{\epsilon}(\omega,\ k^2+\omega^2/v^2)$ determine two poles at frequencies:

$$\omega_{1,2}(k^2) = \pm\left[\frac{(\alpha+\alpha_1)k^2+\beta}{1-(\alpha+\alpha_1)v^{-2}}\right]^{1/2}. \tag{11}$$

Using Eqs. (7) and (10), we obtain from Eq. (9) the loss due to excitation of longitudinal waves, on the basis of the model considered in reference 3

$$F_{\text{long}} = \frac{\omega_0^2}{v^2}e^2 \ln\frac{k_0 v}{\sqrt{\beta}} - \frac{\alpha_1 e^2 k_0^2}{2(v^2-\alpha-\alpha_1)}. \tag{12}$$

This expression differs by the presence of the second term from the energy loss in a medium in which spatial dispersion is neglected.

Since α and α_1 are approximately $(d/\lambda_0)^2 v_{\text{el}}^2$ where v_{el} is the velocity of an electron in an atom ($v_{\text{el}} \sim 10^8$ cm/sec), $d \sim 10^{-8}$ cm is the lattice constant, $k_0 \sim 1/d$, when $v > v_{\text{el}}$ the ratio of the second term to the first term in Eq. (12) is a small quantity $(d/\lambda_0)^2 \sim 10^{-6}$. This estimate indicates that if we take account of the spatial dispersion, there is practically no change in the amount of energy lost by a moving electron in the excitation of longitudinal waves. This result is to be expected because spatial dispersion is important only near resonant frequencies of the medium $[\epsilon_0(\omega, 0) \to \infty]$ while the frequency region associated with longitudinal waves is very far from these resonance frequencies.

3. For an isotropic non-gyrotropic medium, we have from Eq. (5)*

$$\hat{b}^{-1} = \frac{1}{q^2 - c^{-2}(\mathbf{q}\cdot\mathbf{v})^2\,\bar{\varepsilon}}\;\frac{q^2 - c^{-2}(\mathbf{q}\cdot\mathbf{v})^2\varepsilon_0 - c^{-2}(\mathbf{q}\cdot\mathbf{v})^2\varepsilon_1\hat{\eta}}{q^2 - c^{-2}(\mathbf{q}\cdot\mathbf{v})^2\varepsilon_0}. \tag{13}$$

Hence, in the relativistic case, using Eq. (3) we find the following expression for the total energy loss:

$$F = -\frac{ie^2}{\pi}\int_{-\infty}^{+\infty}\omega d\omega \int_0^{k_0} kdk$$
$$\times \frac{[v^{-2} - c^{-2}\bar{\varepsilon}(\omega, k^2+\omega^2/v^2) + \omega^2\varepsilon_1(\omega, k^2+\omega^2/c^2)/(v^2k^2+\omega^2)c^2]}{\bar{\varepsilon}(\omega, k^2+\omega^2/v^2)\{k^2+\omega^2[v^{-2} - c^{-2}\varepsilon_0(\omega, k^2+\omega^2/v^2)]\}}. \tag{14}$$

If spatial dispersion is neglected, the quantity ϵ_1 vanishes and $\bar{\epsilon}$ becomes $\epsilon_0(\omega, 0)$, so that Eq. (14) becomes the well-known expression for loss in an isotropic medium in which spatial dispersion is neglected (cf. references 4 and 5).

Since Cerenkov radiation losses are determined by the zeroes of the expression in the curly brackets in the denominator of Eq. (14), we may conclude that these losses are centered in frequency regions in which $v > c/n_i(\omega)$, where the $n_i(\omega)$ are defined by the equation

$$n^2 = \varepsilon_0(\omega, n^2\omega^2/c^2). \tag{15}$$

If spatial dispersion is neglected, Eq. (15) has a single root $n^2 = \epsilon_0(\omega, 0)$. When spatial dispersion is taken into account, in general, Eq. (15) has several roots $n_i = n_i(\omega)$. If θ is the angle between the direction of motion of the electron and the radiation direction, since $\cos\theta_i = c/vn_i(\omega)$, we find that the Cerenkov radiation at frequency ω is distributed over several cones with aperture angles θ_i. It is easy to show that the intensity of the Cerenkov radiation in the frequency interval ω, $\omega + d\omega$ is given by the following expression:

---

*To verify the identity in (13) we recall that $\hat{\eta}^2 = \hat{\eta}$.

$$dF = \frac{e^2}{c^2} \sum_i \frac{1 - c^2/v^2 n_i^2(\omega)}{|\, 1 - (d/dn_i^2)\, \varepsilon_0(\omega, n_i^2\omega^2/c^2)\,|}\, \omega d\omega. \qquad (16)$$

Since spatial dispersion is important close to the absorption poles of the medium, the new Cerenkov radiation cones will, in general, correspond to a frequency region close to a resonance frequency of the medium. Thus the transmission of Cerenkov radiation is difficult because of absorption; to observe this effect experimentally, it would be necessary to use very thin film. The situation is simplified in optically-active media in which, according to reference 1, the frequency regions in which the new solutions appear are rather broad, so that absorption effects are not important.

In conclusion the authors wish to thank V. L. Ginzburg for his continued interest in this work and valuable discussions.

[1] V. L. Ginzburg, J. Exptl. Theoret. Phys. (U.S.S.R.) **34**, 1593 (1958), Soviet Phys. JETP **7**, 1096 (1958).

[2] S. I. Pekar, J. Exptl. Theoret. Phys. (U.S.S.R.) 33, 1022 (1957), Soviet Phys. JETP **6**, 785 (1958).

[3] V. M. Agranovich and A. A. Rukadze, J. Exptl. Theoret. Phys. (U.S.S.R.) 35, 982 (1958), Soviet Phys. JETP 8, 685 (1959).

[4] B. N. Bolotovskii, Usp. Fiz. Nauk 62, 201 (1957).

[5] Landau and Lifshitz, Electrodynamics of Continuous Media, Gostekhizdat Mos. 1957.

Translated by H. Lashinsky
248

SOVIET PHYSICS JETP VOLUME 35(8), NUMBER 5 MAY, 1959

A CONTRIBUTION TO THE THEORY OF DOMAIN WALLS IN FERROELECTRICS

V. A. ZHIRNOV

P. N. Lebedev Physics Institute, Academy of Sciences, U.S.S.R.

Submitted to JETP editor May 19, 1958; resubmitted June 30, 1958

J. Exptl. Theoret. Phys. (U.S.S.R.) **35**, 1175-1180 (November, 1958)

Transition regions in the 180° and 90° boundaries of ferroelectric domains in barium titanate are considered. The equilibrium variation of the spontaneous-polarization vector is deduced from the condition of minimum thermodynamic potential. Explicit expressions are obtained for the thickness and surface energy of the domain boundaries, and numerical estimates are made. The 180° domain boundary in Rochelle salt crystals is discussed.

NUMEROUS experiments performed by different investigators[1,2] have shown that in the domain structures of single crystals of barium titanate the directions of spontaneous polarization in neighboring domains form angles of 180° or 90°, which we shall call 180° and 90° domains. Little[1] concluded from optical observations that the thickness of the transition region between 180° domains is of the order of the lattice constant ($d = 4 \times 10^{-8}$ cm), whereas for 90° domains it is 5×10^{-5} cm. She also noted the dominant generation and growth of 90° domains and the relatively greater ease with which 90° boundaries are moved by external mechanical stresses. This latter effect is evidently the result of lower surface energy of 90° boundaries compared with 180° boundaries.

It may be of interest to obtain quantitative results for the thicknesses of transition layers and surface energies of 180° and 90° domain walls. We shall use the method suggested by Landau and Lifshitz[3] for investigation of the domain structure of ferromagnets. The variation of polarization in an intermediate region is determined under thermodynamic equilibrium in the absence of an external field, and explicit expressions are obtained for the thickness of the transition layer and for the surface energy density which plays a part as the "coefficient of surface tension" of domain walls.

We shall obtain the contributions to the thermodynamic potential which are associated with the anisotropy energy, elastic energy, and electrostriction for cubically symmetrical barium titanate near the Curie point. In a transition region, an essentail part is also played by the energy associated with nonuniform distribution of the polarization vector $\mathbf{P}$:

$$\frac{\varkappa}{2}[(\nabla P_x)^2 + (\nabla P_y)^2 + (\nabla P_z)^2].$$

This expression can reasonably be used so long as the thickness of the transition layer is considerably greater than the lattice constant. The thermodynamic potential in the transition layer is thus given by

$$\begin{aligned}\Phi = \Phi_0 &+ \frac{\varkappa}{2}[(\nabla P_x)^2 + (\nabla P_y)^2 + (\nabla P_z)^2] \\ &+ \alpha(P_x^2 + P_y^2 + P_z^2) + \frac{\beta_1}{2}(P_x^4 + P_y^4 + P_z^4) \\ &+ \beta_2(P_x^2P_y^2 + P_x^2P_z^2 + P_y^2P_z^2) + \frac{c_{11}}{2}(u_{xx}^2 + u_{yy}^2 + u_{zz}^2) \\ &+ c_{12}(u_{xx}u_{yy} + u_{xx}u_{zz} + u_{yy}u_{zz}) + \frac{c_{44}}{2}(u_{xy}^2 + u_{xz}^2 + u_{yz}^2) \\ &+ q_{11}(u_{xx}P_x^2 + u_{yy}P_y^2 + u_{zz}P_z^2) \\ &+ q_{12}[u_{xx}(P_y^2 + P_z^2) + u_{yy}(P_x^2 + P_z^2) \\ &+ u_{zz}(P_x^2 + P_y^2)] + 2q_{44}(u_{xy}P_xP_y + u_{xz}P_xP_z + u_{yz}P_yP_z),\end{aligned} \quad (1)$$

where u_{ik} is the deformation tensor. The parameter κ can be evaluated by assuming that the energy $(\kappa/2)(\nabla P)^2$ is of the order of the exchange energy αP^2 far from the transition point if $\mathbf{P}$ varies essentially only at distances of the order of the lattice constant d. Then the lower limit of κ is given by $\kappa \sim |\alpha(0)|d^2$, where $\alpha(T) = 3.8 \times 10^{-5}(T - \Theta)$. A reasonable range of values is $\kappa \sim 3 \times 10^{-15}$ to 3×10^{-16} cm^2.

In the theory of domain structure the essential difference between ferroelectrics and ferromagnets is provided by two factors. The exchange interaction in ferromagnets results in a constant absolute value of the magnetization so that the only change which occurs is a continuous rotation of the direction of magnetization in the intermediate region. In the case of ferroelectrics we must take into account the fact that the absolute value of the spontaneous polarization in the intermediate region can change from the very beginning.

It must be remembered, however, that in any real ferroelectric crystal the conductivity is different from zero. Therefore free charges can generally accumulate on crystal boundaries or domain walls. For this reason a flat ferroelectric in a condenser cannot be divided into domains.[4] For the 180° and 90° domains of interest here, assuming equal magnitude of the polarization throughout both domains, we can have the condition $\operatorname{div} \mathbf{P} = 0$. Therefore the absence of free charges on domain walls, that is, $\operatorname{div} \mathbf{D} = 0$, is consistent with zero value of the electric field $\mathbf{E}$, as is required for equilibrium when conduction occurs. We shall consider this case.

Let us consider the 180° domain wall of a $BaTiO_3$ single crystal when, for example, the polarization of neighboring domains is parallel and antiparallel to the z axis and the separating wall is in the (100) crystallographic plane. Then $\operatorname{div} \mathbf{P} = 0$ leads to $P_x = 0$. Furthermore, since the interior of each domain can be regarded as unstressed all components of the stress tensor $\sigma_{ik} = -\partial\Phi/\partial u_{ik}$ will be zero far from the transition layer, that is, for $x = \pm\infty$.

The deformation tensor in the interior of the domains is then given by

$$u_{xx} = u_{yy} = \mu P_0^2, \;\; u_{zz} = \rho P_0^2, \;\; u_{xy} = u_{xz} = u_{yz} = 0,$$

where the measurements of Caspari and Merz[5] give the following values of the constants: $\mu = -10.5 \times 10^6$ cm^4/coulomb^2 and $\rho = 24.0 \times 10^6$ cm^4/coulomb^2. Since the polarization distribution in the transition layer depends only on x the deformation tensor also can depend only on x; therefore u_{yy}, u_{zz}, and u_{yz} remain constant and equal to their boundary values. The other deformation components are determined from the equilibrium equations of an elastic body, $\partial\sigma_{ik}/\partial x_k = 0$, which in our case become

$$\sigma_{xx} = 0, \quad \sigma_{xy} = 0, \quad \sigma_{xz} = 0.$$

We thus obtain

$$u_{xx} = \mu P_0^2 - (q_{12}/c_{11})(P_y^2 + P_z^2 - P_0^2), \quad u_{xy} = u_{xz} = 0,$$

and all components of the deformation tensor in the transition layer satisfy St. Venant's continuity conditions.

Inserting the deformations into (1), we obtain the variable part of the thermodynamic potential in the form

$$\Phi = \Phi_0 + \frac{\varkappa}{2}[(\nabla P_y)^2 + (\nabla P_z)^2]$$
$$+ \frac{a}{2} P_y^2 + \frac{b}{2} P_z^2 + \frac{c}{4}(P_y^4 + P_z^4) + \frac{d}{2} P_y^2 P_z^2,$$
$$a/2 = \alpha + [q_{11}\mu + q_{12}\rho - (q_{12}c_{12}/c_{11})(\rho + \mu)] P_0^2,$$
$$b/2 = \alpha + [q_{11}\rho + q_{12}\mu - (q_{12}c_{12}/c_{11})(\rho + \mu)] P_0^2,$$
$$c/2 = \beta_1 - q_{12}^2/c_{11}, \quad d/2 = \beta_2 - q_{12}^2/c_{11}.$$

On the basis of Devonshire's results[6] we can assume the following values of the constants:

$a \approx 1.5 \times 10^{-2}$, $b \approx -5.6 \times 10^{-2}$,
$c \approx 1.5 \times 10^{8}$ cm^4/coulomb^2,
$d \approx -5 \times 10^{7}$ cm^4/coulomb^2.

Near the Curie point, where and only where an expansion of the thermodynamic potential is valid, the temperature-dependent coefficient $\alpha = 3.8 \times 10^{-5}(T - \Theta)$ gives a small contribution to the coefficients a and b, which are entirely determined by electrostriction and have opposite signs, with b essentially negative. All of this is true only for the transition layer, since within a domain $P_y = 0$, $|P_z| = P_0$ and in the expression

$$\frac{b}{2} P_z^2 = \alpha P_0^2 + \left[q_{11}\rho + q_{12}\mu - q_{12}\frac{c_{12}}{c_{11}}(\rho + \mu)\right] P_0^4$$

the coefficient of P_0^2 vanishes at the Curie point, which is in accordance with the phenomenological theory.

The condition of thermodynamic equilibrium, which is the minimization of $\int \Phi(P_y, P_z)\,dV$, reduces to the equations

$$\varkappa P_y'' = aP_y + cP_y^3 + dP_y P_z^2, \;\; \varkappa P_z'' = bP_z + cP_z^3 + dP_z P_y^2,$$

which must be supplemented by the following boundary conditions at $x \doteq -\infty$:

$$P_y' = P_z' = 0, \;\; P_y = 0, \;\; P_z = -P_0.$$

Besides the "trivial" solution $P_y = 0$, $P_z = -P_0$, which represents uniform polarization in the absence of domain walls, there exists an exact solution representing the presence of a transition layer and satisfying the boundary conditions

$$P_y = 0, \;\; P_z = P_0 \tanh(x/\delta),$$

where $P_0^2 = |b|/c$ determines the equilibrium polarization within the domains and $\delta = P_0^{-1}\sqrt{2\kappa/c}$ determines the effective size of a transition region for 180° domains. When d is sufficiently small to be neglected by comparison with c, the equations are separable and the solution is unique. In the general case the proof of uniqueness requires further examination.

We note that the foregoing solution differs essentially from the solution for a 180° transition region in the case of ferromagnetism:[3]

$$M_y = M_0 \sin\theta, \;\; M_z = M_0 \cos\theta, \sinh(\varkappa/\delta) = D\cot\theta.$$

This is associated with the fact that the spin exchange energy gives an "infinitely" larger contribution (10^5 times larger) to the thermodynamic potential than the elastic energy and higher terms of the expansion. This insures a constant absolute value of the magnetic moment in the transition region. Therefore in the ferromagnetic case the original set of equations is highly degenerate, with $a = b$, $c = 0$, so that its first integral gives the required solution.

The solution for $BaTiO_3$ gives $\delta \approx 2 \times 10^{-7}$ – 5×10^{-8} cm for the thickness of 180° domain walls, which is several times the lattice constant, and thus agrees with experimental results.[1]

We can also obtain an expression for the excess surface energy associated with the existence of a 180° domain wall:

$$\sigma = \int_{-\infty}^{\infty} (\Phi - \Phi_0)\, dx = {}^4/_3 P_0^3 \sqrt{2\varkappa c} \approx 10 \text{ erg/cm}^2.$$

This agrees with the value given by Merz.[7]

We shall now consider a 90° domain wall of barium titanate in the (101) plane with the polarization in neighboring domains directed along the z and x axes, respectively. For ease of calculation we shall turn the coordinate system around the y axis through $\pi/4$ so that the domain wall will lie in the plane $x = 0$. The notation will now refer to the new coordinate system. The condition $\operatorname{div} \mathbf{P} = 0$ now reduces to conservation of the component normal to the wall, $P_x = P_0/\sqrt{2}$; thus all variations, as in the case of the 180° layer, will be associated with the dependence of P_y and P_z on x. The previous method is used to determine the components of the deformation tensor in the 90° layer. These components satisfy St. Venant's continuity condition and are given by

$$u_{xx} = [(c_{44}(\mu + \rho) - c_{12}\mu - q_{44}) P_0^2 - 2q_{12}P_y^2$$
$$- (q_{11} + q_{12} - 2q_{44}) P_z^2] (c_{11} + c_{12} + 2c_{44})^{-1},$$
$$u_{yy} = \mu P_0^2, \quad u_{zz} = \frac{\mu + \rho}{2} P_0^2, \quad u_{xy} = -\sqrt{2}\frac{q_{44}}{c_{44}} P_0 P_y,$$
$$u_{xz} = \frac{q_{12} - q_{11}}{c_{11} - c_{12}} \frac{P_0}{\sqrt{2}} P_z, \quad u_{yz} = 0.$$

The variable part of the thermodynamic potential can be written as

$$\Phi = \Phi_0 + \frac{\varkappa}{2} [(\nabla P_y)^2 + (\nabla P_z)^2]$$
$$+ \frac{a_1}{2} P_y^2 + \frac{b_1}{2} P_z^2 + \frac{c_1}{4} P_y^4 + \frac{c_2}{4} P_z^4 + \frac{d_1}{2} P_y^2 P_z^2,$$

with the condition for the minimum given by the equations

$$\varkappa P_y'' = a_1 P_y + c_1 P_y^3 + d_1 P_y P_z^2,$$
$$\varkappa P_z'' = b_1 P_z + c_2 P_z^3 + d_2 P_z P_y^2.$$

The only solution which satisfies the boundary conditions $P_y' = P_y = 0$, $P_z' = 0$, $P_z = P_0/\sqrt{2}$ at $x = -\infty$ is given by

$$P_y = 0, \qquad P_z = -\frac{P_0}{\sqrt{2}} \tanh \frac{x}{\delta_1},$$

where

$$P_0^2 = 2|b|/c_2; \quad \delta_1 = (2/P_0)\sqrt{\varkappa/c_2}.$$

A numerical estimate gives

$$c_2 = \beta_1 + \beta_2 - (q_{11} - q_{12} - 2q_{44})^2 / (c_{11} + c_{12} + 2c_{44})$$
$$\approx 10^7 \text{ cm}^4/\text{coulomb}^2,$$

from which we obtain $\delta_1 \sim 10^{-6}$ to 5×10^{-7} cm, which is one order of magnitude larger than for the 180° case. The disagreement with the experimental value $\delta_1 \sim 10^{-5}$ cm may result from the fact that the 90° domains observed in reference 1 were comparable in size with the thickness of the transition layer, in which case the crystal cannot be regarded as unstressed inside a domain.

For the surface energy of a 90° transition layer of barium titanate we obtain the expression

$$\sigma_1 = {}^2/_3 \sqrt{\varkappa c_2} P_0^3.$$

For this case an estimate gives $\sigma_1 \approx 2$ to 4 erg/cm^2. Comparison with 180° domains shows that in the 90° transition layer a change of the polarization vector is favored energetically since the minimum absolute value is $P_x = P_0/\sqrt{2}$ rather than zero. This evidently accounts for the ease with which 90° domain boundaries are produced and moved.

We shall now consider a 180° domain wall in the actually observable case of a Rochelle salt single crystal where the polarization in neighboring domains is directed parallel and antiparallel to the y axis and all changes occur along the z axis. As previously, the condition $\operatorname{div} \mathbf{P} = 0$ reduces to the relation $P_x = 0$. The thermodynamic potential will receive contributions from the energy of nonuniform polarization, anisotropy, elastic energy (taking account of the orthorhombic symmetry), linear piezoelectric effect, and quadratic electrostrictive effect:

$$\Phi = \Phi_0 + \frac{\varkappa_1}{2} (\nabla P_y)^2 + \frac{\varkappa_2}{2} (\nabla P_z)^2 + \alpha_2 P_y^2 + \alpha_3 P_z^2$$
$$+ \frac{\beta_2}{2} P_y^4 + \frac{\beta_3}{2} P_z^4 + \frac{1}{2} (c_{11} u_{xx}^2 + c_{22} u_{yy}^2 + c_{33} u_{zz}^2$$
$$+ c_{44} u_{yz}^2 + c_{55} u_{xz}^2 + c_{66} u_{xy}^2) + c_{12} u_{xx} u_{yy} + c_{13} u_{xx} u_{zz}$$
$$+ c_{23} u_{yy} u_{zz} - h_{14} u_{yz} P_x - h_{25} u_{xz} P_y - h_{36} u_{xy} P_z$$
$$+ (q_{12} P_y^2 + q_{13} P_z^2) u_{xx} + (q_{22} P_y^2 + q_{23} P_z^2) u_{yy}$$
$$+ (q_{23} P_y^2 + q_{33} P_z^2) u_{zz} + 2q_{44} P_y P_z u_{yz}.$$

In the absence of an external electric field the stress tensor σ_{ik} is given by $\sigma_{ik} = -\partial\Phi/\partial u_{ik}$. If the crystal can be regarded as unstressed inside the domains the deformations are determined from the equations $\sigma_{ik} = 0$, $P_x = P_y = 0$, $P_z = \pm P_0$ with $x = \pm\infty$ and are found to be

$$u_{xx}=\rho P_0^2,\ u_{xz}=0,\ u_{yy}=\mu P_0^2,\ u_{yz}=0,$$

$$u_{zz}=\lambda P_0^2,\ u_{xy}=\pm h_{36}P_0/c_{66},$$

where the constants ρ, μ, λ are solutions of the equations

$$c_{i1}\rho+c_{i2}\mu+c_{i3}\lambda=-q_{i3}\ (i=1,2,3).$$

In the transition layer, as previously, u_{yy}, u_{zz} and u_{yz} retain their boundary values, and the other components of u_{ik} are obtained from the equilibrium equations $\sigma_{1i}=0$:

$$u_{xx}=-\left(\frac{c_{12}}{c_{11}}\mu+\frac{c_{13}}{c_{11}}\lambda\right)P_0^2-\frac{q_{12}}{c_{11}}P_y^2-\frac{q_{13}}{c_{11}}P_z^2,$$

$$u_{xz}=\frac{h_{25}}{c_{55}}P_y,\quad u_{xy}=\frac{h_{36}}{c_{66}}P_z.$$

These deformations give the following form to the variable part of the thermodynamic potential:

$$\Phi=\Phi_0+\frac{\varkappa_1}{2}(\nabla P_y)^2+\frac{\varkappa_2}{2}(\nabla P_z)^2$$

$$+\frac{A}{2}P_y^2+\frac{B}{2}P_z^2+\frac{C}{4}P_y^4+\frac{D}{4}P_z^4+\frac{F}{2}P_y^2P_z^2,$$

$$\frac{A}{2}=\alpha_2-\frac{h_{25}^2}{2c_{25}}+\left[\lambda q_{23}+\left(\mu-\frac{c_{12}}{c_{11}}\mu-\frac{c_{13}}{c_{11}}\lambda\right)q_{12}\right]P_0^2,$$

$$\frac{B}{2}=\alpha_3-\frac{h_{36}^2}{2c_{66}}+\left[\lambda q_{33}+\mu q_{23}-\left(\frac{c_{12}}{c_{11}}\mu+\frac{c_{13}}{c_{11}}\lambda\right)q_{13}\right]P_0^2,$$

$$\frac{C}{2}=\beta_2-q_{12}^2/c_{11},\ \frac{D}{2}=\beta_3-q_{13}^2/c_{11},\ F=-q_{12}q_{13}/c_{11}.$$

The minimum of $\int\Phi\,dV$ reduces to the equations

$$\varkappa_2P_y''=AP_y+CP_y^3+FP_yP_z^2,\ \varkappa_3P_z''=BP_z+DP_z^3+FP_y^2P_z,$$

with one solution that satisfies the boundary conditions $P_y'=P_y=0$, $P_z'=0$, $P_z=-P_0$ when $x=-\infty$:

$$P_y=0;\ P_z=P_0\tanh\frac{x}{\delta};\quad \delta=\frac{1}{P_0}\sqrt{\frac{2\varkappa_3}{D}}.$$

For the density of the surface energy associated with a domain wall in Rochelle salt we obtain

$$\sigma={}^4/_3\sqrt{\varkappa_3D}P_0^3. \tag{2}$$

It is known[8] that at T = 0°C

$$P_0=2.5\cdot10^{-7}\ \text{coulomb/cm}^2,\quad \alpha_3=-2\cdot10^{-2},$$

$$\beta_3=3.3\cdot10^{11}\ \text{cm}^4/\text{coulomb}^2,\quad q_{13}\sim90,$$

and at T = 20°C

$$P_0=1.4\cdot10^{-7}\ \text{coulomb/cm}^2,\quad \alpha_3=-8\cdot10^{-2},$$

$$\beta_3=4\cdot10^{11}\ \text{cm}^4/\text{coulomb}^2,\quad q_{13}\sim150.$$

In addition, using the values $\kappa\sim d^2\sim10^{-14}\ \text{cm}^2$, $c_{11}=4\times10^{-8}\ \text{coulomb}^2/\text{cm}^4$, we obtain

at $T=0°\text{C}$: $\delta\simeq1.2\cdot10^{-7}$ cm, $\sigma\sim6\cdot10^{-2}\ \text{erg/cm}^2$;
at $T=20°\text{C}$: $\delta\simeq2.2\cdot10^{-6}$ cm, $\sigma\sim1.2\cdot10^{-2}\ \text{erg/cm}^2$.

These values agree with the results of reference 8, where, however, electrostriction is not taken into account consistently and the deformations do not satisfy the St. Venant's compatibility conditions.

The given values of the surface energy of domain boundaries in ferroelectrics enable us to investigate different domain configurations corresponding to the minimum thermodynamic potential.

In conclusion the author wishes to thank Prof. V. L. Ginzburg and I. E. Dzialoshinskii for valuable suggestions and fruitful discussions.

---

[1] E. A. Little, Phys. Rev. **98**, 978 (1955).

[2] W. J. Merz, Phys. Rev. **88**, 421 (1952); A. von Hippel, Revs. Modern Phys. **22**, 221 (1950).

[3] L. D. Landau and E. M. Lifshitz, Physik. Z. Sowjetunion **8**, 153 (1935).

[4] V. L. Ginzburg, J. Exptl. Theoret. Phys. (U.S.S.R.) **15**, 739 (1945).

[5] M. E. Caspari and W. J. Merz, Phys. Rev. **80**, 1082 (1950).

[6] A. F. Devonshire, Phil. Mag. **40**, 1040 (1949).

[7] W. J. Merz, Phys. Rev. **95**, 690 (1954).

[8] T. Mitsui and J. Furuichi, Phys. Rev. **90**, 193 (1953).

Translated by I. Emin
249

SOVIET PHYSICS JETP VOLUME 35(8), NUMBER 5 MAY, 1959

THE ACCELERATION OF COSMIC RAYS IN A FLUCTUATING MAGNETIC FIELD

V. M. BIAKOV and R. G. AVALOV

Submitted to JETP editor May 19, 1958; resubmitted July 18, 1958

J. Exptl. Theoret. Phys. (U.S.S.R.) **35**, 1181-1184 (November, 1958)

A mechanism for the acceleration of cosmic rays is examined which involves their passage through regions of fluctuating magnetic field in the galaxy or the atmospheres of certain types of stars. During the passage of a stream of particles through a region of fluctuating magnetic field the spread of the particles in energy is increased, and a systematic acceleration occurs. Estimates show that the mechanism considered here may be more effective than the Fermi acceleration mechanism.

1. In the present paper we consider the acceleration of cosmic-ray particles by magnetic fields that vary with time. Such fields accompany turbulent motions of the interstellar medium, and also the atmospheric motions in certain types of stars. In an ideally-conducting magnetized medium (such as cosmic space) the magnetic lines of force are attached to the matter, so that a change of the density means at the same time a change of the magnetic field.

In the interstellar medium the hydrodynamic velocities are as a rule never small in comparison with the speed of sound. Under these conditions velocity fluctuations bring about large fluctuations of the density, and we can expect also large fluctuations of the magnetic field.

We may consider two possibilities for the state of the magnetic field: it is either increasing on the average on account of the turbulent motion of the magnetized medium, or it is stationary (or relatively slowly changing), so that basically the only changes are fluctuations.

The acceleration of cosmic rays in a magnetic field that is increasing because of the turbulent motions of the interstellar gas has been studied by Logunov and Terletskii,[1] and acceleration by magnetohydrodynamic waves in a spiral arm of the galaxy has been studied by Davis.[2]

Here we shall start with the second possibility and examine the acceleration of charged particles occurring on account of fluctuations of the magnetic field.

Charged particles moving in a fluctuating magnetic field will sometimes get into regions where the field is increasing, and at other times into regions where it is falling off, with corresponding increases and decreases of their energy. It is obvious that as a result of fluctuations in the numbers of positive and negative changes of energy experienced by individual particles, some of the particles will be accelerated and will acquire considerable energies under suitable conditions. Generally speaking, in addition to this spread in particle energies there will also occur a systematic increase of the energy of the particles. On certain assumptions, which are indicated below, this acceleration mechanism can be more effective than the mechanism proposed by Fermi.[3]

2. Let us estimate the order of magnitude of the effect to be expected.

The change of the energy of a particle of charge e moving in a fluctuating magnetic field depends on the rate of change of the field with time and on its degree of homogeneity in space. If the momentum p of the particle satisfies the condition

$$p \ll (e/c) H^2 / |\operatorname{grad} H|, \tag{1}$$

its motion takes place along a spiral trajectory, which is characterized by the magnitude of the momentum and the angle ϑ between the direction of the momentum and that of the magnetic field intensity vector H (c is the speed of light).

In interstellar space, with field intensities $\leq 10^{-5}$ oersteds, for particles with energies corresponding to the main mass of the cosmic radiation, the condition (1) is as a rule well satisfied within the limits of a single fluctuation region. In this case, since the change of the field in the time of a single turn around the spiral is negligible, we can base the calculation of the change in the particle's energy on the condition of conservation of the adiabatic invariant

$$p^2 \sin^2 \vartheta / H = p_1^2 \sin^2 \vartheta_1 / H_1. \tag{2}$$

The index 1 is affixed to quantities taken at the time of entrance of the particle into the field region in question.

The changing magnetic field changes only the component of the particle's momentum perpendicular to the field; the momentum component parallel to the field remains unchanged during the motion:

$$p\cos\vartheta = p_1\cos\vartheta_1. \qquad (3)$$

For a nonrelativistic particle this equation means that the speed of the motion along the field, $v\cos\vartheta$, is constant, and the time t of passage of the particle through a region of linear dimension l is given by

$$t = l\,/\,v\cos\vartheta. \qquad (4)$$

At relativistic energies, for which the speed of the particle is of the order of that of light, $v\cos\vartheta$ does not remain constant, and we can use the relation (4) as an approximate one for small changes of the energy of the particle.

Equations (2) and (3) lead to

$$\Delta p^2 = p^2 - p_1^2 = p_1^2\sin^2\vartheta_1(H\,/\,H_1 - 1),$$
$$\Delta p = p - p_1 = p_1\left[\sqrt{1+\sin^2\vartheta_1(H\,/\,H_1-1)} - 1\right],$$
$$(\Delta p)^2 = p_1^2[\sin^2\vartheta_1(H\,/\,H_1 - 1)$$
$$-2(\sqrt{1+\sin^2\vartheta_1(H\,/\,H_1-1)}-1)] = \Delta p^2 - 2p_1\Delta p.$$

We shall consider only small changes of the magnetic field, for which Δp and $(\Delta p)^2$ can be represented in the forms:

$$\Delta p = \frac{p_1}{2}\sin^2\vartheta_1\left(\frac{H}{H_1}-1\right) - \frac{p_1}{8}\sin^4\vartheta_1\left(\frac{H}{H_1}-1\right)^2,$$
$$(\Delta p)^2 = \frac{1}{4}p_1^2\sin^4\vartheta_1\left(\frac{H}{H_1}-1\right)^2. \qquad (5)$$

At the boundaries of the fluctuating regions or "clouds," which are evidently determined by shock waves,[4,5] the strong field gradients can cause scattering of the particles, which destroys the correlation between values of the angle ϑ in different regions of the medium. We shall assume that this scattering preserves the isotropic character of the cosmic-ray flux.

The rate of acceleration can be characterized by the average values of the quantities

$$\frac{dp}{dt} = \frac{v}{l}\Delta p, \quad \frac{dp^2}{dt} = \frac{v}{l}\Delta p^2,$$

which, in the absence of correlation between the values of v/l and Δp (or Δp^2), can be written in the form

$$\frac{\overline{dp}}{dt} = \frac{\bar{v}}{l}\overline{\Delta p}, \qquad \frac{\overline{dp^2}}{dt} = \frac{\bar{v}}{l}\overline{\Delta p^2}. \qquad (6)$$

Here the average distance between fluctuations is taken to be of the order of magnitude of the average dimensions of the fluctuations themselves, and $\overline{\Delta p}$ and $\overline{\Delta p^2}$ denote the average changes of the momentum and of its square on passage of the particle through a single fluctuation.

The averaging has to be carried out over all possible values of the angles of entrance, or, what is the same thing in view of relation (4), over all values of the time of flight through a fluctuation region, and also over all times of entrance t_1. If 2τ is the period of variation of the field (see below), the averaging process gives

$$\overline{\Delta p^2} = \frac{l}{2v\tau}p^2J_1, \quad \overline{\Delta p} = \frac{l}{4v\tau}pJ_1 - \frac{1}{16}\frac{l}{v\tau}pJ_2,$$
$$\overline{(\Delta p)^2} = \frac{l}{8v\tau}p^2J_2 = \overline{\Delta p^2} - 2p\overline{\Delta p},$$

where

$$J_1 = \int\limits_0^{2\tau}dt_1\int\limits_{l/v}^{\infty}\left[1-\left(\frac{l}{vt}\right)^2\right]\frac{dt}{t^2}\left[\frac{H(t+t_1)}{H(t_1)}-1\right],$$
$$J_2 = \int\limits_0^{2\tau}dt_1\int\limits_{l/v}^{\infty}\left[1-\left(\frac{l}{vt}\right)^2\right]^2\frac{dt}{t^2}\left[\frac{H(t+t_1)}{H(t_1)}-1\right]^2.$$

Choosing the origin for counting the time so that at time zero the value of the field strength was a minimum, we can write:

$$0\leqslant t\leqslant\tau \qquad H = H_{\min}[1+nt/\tau],$$
$$\tau\leqslant t\leqslant 2\tau \qquad H = H_{\min}[1+n(2\tau-t)/\tau],$$

where

$$\frac{n}{\tau} = \frac{1}{H_{\min}}\left\langle\frac{dH}{dt}\right\rangle_{\text{av}}, \qquad n = \frac{H_{\max}-H_{\min}}{H_{\min}}.$$

If we assume that the average time τ for variation of the magnetic field is given in order of magnitude by l/V, where V is the speed of the turbulent motions, then for sufficiently fast particles $l/v\tau = V/v \ll 1$. Calculating the integrals with neglect of terms of the order $l/v\tau$ and of higher-order terms, and assuming that $n^2/(1+n) \ll 3$, we have

$$J_1 = n^2/2(1+n), \quad J_2 = 2J_1,$$
$$\overline{\Delta p^2} = \frac{1}{4}\frac{n^2}{1+n}\frac{l}{v\tau}p^2 = \frac{1}{4}\frac{n^2}{1+n}\frac{V}{c}p^2,$$
$$\overline{\Delta p} = \frac{1}{16}\frac{n^2}{1+n}\frac{V}{c}p, \quad \overline{(\Delta p)^2} = \frac{1}{8}\frac{n^2}{1+n}\frac{V}{c}p^2. \qquad (7)$$

The comparatively large values of $\overline{\Delta p}$ and $\overline{(\Delta p)^2}$ are due to the possibility of taking independent averages in the formulas (6). The existence of correlations between the angles leads to a lowering of the rate of the acceleration.[2]

3. Let us compare the effectiveness of this mechanism of acceleration with that of the Fermi acceleration mechanism.[3] According to Fermi, in the relativistic case the average rate of increase of the energy of a particle is

$$\left(\frac{\overline{dE}}{dt}\right)_{\text{F}} = \frac{v}{l}\left(\frac{V}{c}\right)^2E,$$

(E is the total energy of the particle), whereas according to Eqs. (6), (7)

$$\left(\frac{\overline{dE}}{dt}\right) = \frac{1}{16}\frac{n^2}{1+n}\frac{v}{l}\frac{V}{c}E. \qquad (8)$$

From this we have

$$\left(\frac{\overline{dE}}{dt}\right) \Big/ \left(\frac{\overline{dE}}{dt}\right)_{\mathrm{F}} = \frac{1}{16}\,\frac{n^2}{1+n}\,\frac{c}{V}\,.$$

Since for the interstellar medium $V \leq 100$ km/sec, already for $n > 0.1$ the fluctuational changes of the field can play an important part in the acceleration of particles.

We have not given detailed consideration to effects associated with the passage of particles through the boundaries of the fluctuation regions. Reflection of particles from these boundaries, and also possible anisotropy of the flux can, generally speaking, reduce the acceleration below the above estimates. Nevertheless the data at present available clearly indicate that these effects are not so large that our estimate needs to be changed greatly. We hope later on to examine this question in more detail.*

Let us estimate the average value of the magnetic field fluctuation that can be expected in a magnetized turbulent medium. This can be done if we assume, following Batchelor,[5] that the average energy density of the magnetic field is of the same order of magnitude as the energy of the smallest turbulent eddies. Then the magnetic effects manifest themselves only in the domains of the smallest eddies, and can be neglected for the larger eddies.

Neglecting also the influence of viscous forces, we get for the average value of the fractional density fluctuation the expression

$$\Delta\rho / \rho = (V / u)^2,$$

where u is the speed of sound and ρ is the mean density. If we assume that the compressions and rarefactions of the gas occur isotropically, then $H \sim \alpha\rho^{2/3}$, and

$$\Delta H / H = {}^2/_3\,(V / u)^2.$$

As we mentioned above, speeds of the interstellar gas, small in comparison with the speed of sound, are never of common occurrence. Therefore we can expect considerable fluctuations of the magnetic field strength.

In conclusion we remark that the mechanism considered here may turn out to be important in treating the acceleration of cosmic rays in the expanding shells of supernovas and novas, where in a number of cases the Fermi mechanism gives a retardation.[6]

The writers express their deep gratitude to K. A. Ter-Martirosian for the exceptional amount of attention and support that he has given to this work, and also thank S. B. Pikel'ner and I. S. Shklovskii for helpful discussions.

---

*The writers are grateful to E. L. Feinberg for calling their attention to the possible importance of these effects.

[1] A. A. Logunov and Ia. P. Terletskii, Izv. Akad. Nauk SSSR, Ser. Fiz. **17**, 119 (1953).

[2] L. Davis, Phys. Rev. **101**, 351 (1956).

[3] E. Fermi, Phys. Rev. **75**, 1169 (1949).

[4] Gas. Dynamics of Cosmic Clouds, North-Holland Publ. Co. 1955.

[5] Problems of Cosmic Aerodynamics (Russ. Transl.), IIL 1953.

[6] V. L. Ginzburg, S. B. Pikel'ner and I. S. Shklovskii, Астрономич. журн. (Astronomy Journal) **36**, 503 (1955).

Translated by W. H. Furry
250

SOVIET PHYSICS JETP VOLUME 35(8), NUMBER 5 MAY, 1959

HYDRODYNAMIC THEORY OF MULTIPLE PRODUCTION OF PARTICLES IN COLLISIONS BETWEEN FAST NUCLEONS AND NUCLEI

G. A. MILEKHIN

P. N. Lebedev Physics Institute, Academy of Sciences, U.S.S.R.

Submitted to JETP editor May 25, 1958

J. Exptl. Theoret. Phys. (U.S.S.R.) 35, 1185-1197 (November, 1958)

The three-dimensional hydrodynamic problem of the dispersion of the particles emitted in the collision between a nucleon and a nucleus has been solved by a method which is different from, and more exact than, that applied in references 1 and 2. The distributions of the energy, the angles, and of the transverse momenta are investigated with the aid of the solution obtained. The error in the final formulae is ~20%.

1. INTRODUCTION

THE hydrodynamic theory of multiple production of mesons in the collision of high energy particles was developed in a paper by Landau.[1] In view of the great mathematical complexity of this theory, the author confined himself to an approximate theory in which the final formulae have only logarithmic accuracy and describe only collisions between identical particles. Better accuracy is needed for a comparison of theory and experiment. Furthermore it is necessary to generalize the results for the case of collisions between a nucleon and a nucleus, since these are usually observed in experiment.

In the investigation of the collision process between a nucleon and a nucleus one usually uses the tube model,[3] i.e., it is assumed that the nucleon interacts only with the nuclear matter inside a tube which it cuts out of the nucleus during the collision. In the present paper we restrict ourselves to the case where the ratio n of the tube length over the linear dimension of the nucleon, which is approximately equal to the number of nucleons in the tube, does not exceed 3.7.

Belen'kii and the author[4] solved the first part of the problem: the determination of the total number of particles N_0 formed during the collision of the nucleon with the nucleus. They obtained the formula $N_0 = k(n+1)E_0^{1/4}$, where E_0 is the energy of the primary nucleon in the laboratory system, and k is a constant factor.

In the present paper we investigate the distribution of the secondary particles over the angles, the energies, and the transverse momenta. Since the energy, the transverse momentum, and the angle under which it is emitted are determined by the components of the 4-velocity of the particle, our problem is to find the distribution of the particles in velocity space. The symmetry properties of the distribution were discussed in reference 5, where it was shown that the distribution should, in some special coordinate system close to the center of mass system, be symmetric with respect to the plane perpendicular to the direction of motion of the colliding particles. Apart from this it must, of course, have cylindrical symmetry.

According to the hydrodynamic theory, the motion of the system after the collision is governed by the relativistic hydrodynamic equations for the ideal liquid:

$$\partial T_i^k / \partial x^k = 0, \quad T_{ik} = (p+\varepsilon) u_i u_k + p g_{ik}, \tag{1}$$

where p is the pressure, ϵ the energy density, u^i the 4-velocity of the medium, and g_{ik} the metric tensor with components $-g_{00} = g_{11} = g_{22} = g_{33} = 1$, $g_{ik} = 0$ for $i \neq k$. For the equation of state we take the equation of state of the extremely relativistic medium $p = \epsilon/3$.

Below we shall use a system of units in which the Planck constant $\hbar$, the Boltzmann constant, and the velocity of light are equal to unity.

2. ONE-DIMENSIONAL STAGE OF THE EXPANSION OF THE SYSTEM

Owing to the Lorentz contraction of the colliding particles the first stage of the motion of the system after the collision will be approximately one-dimensional. In this case we can make a special change of variables, proposed by Khalatnikov,[6] which brings the nonlinear equations (1) into the form

$$3\partial^2\chi / \partial\eta^2 - \partial^2\chi / \partial y^2 - 2\partial\chi / \partial y = 0, \tag{2}$$

where $\eta = \tan^{-1} v$, $y = \ln(T/T_0)$, v and T are the velocity and the temperature of the medium, and T_0 is the initial temperature. The coordinate x and the time t are connected with the potential χ through the relations

$$x = e^{-y}\left(\frac{\partial\chi}{\partial y}\sinh\eta - \frac{\partial\chi}{\partial\eta}\cosh\eta\right); \quad (3)$$

$$t = e^{-y}\left(\frac{\partial\chi}{\partial y}\cosh\eta - \frac{\partial\chi}{\partial\eta}\sinh\eta\right). \quad (4)$$

The stage of one-dimensional motion was discussed in references 2 and 5 for the case $n < 3.7$. It is convenient to use a coordinate system in which the colliding particles have oppositely equal velocities. As a consequence of the discontinuities in the initial conditions the motion of the medium cannot be described by a single analytic formula. We have to do with three regions. Bordering on the vacuum we have the region of traveling waves, whose entropy is very small towards the end of the one-dimensional stage, but which carry a significant part of the energy.[2,7] The main part of the entropy is contained in the region of the so-called nontrivial solution, which is enclosed by traveling waves on both sides. In the following we shall be mainly interested in this region.

According to reference 5, the solution of Eq. (2) in this region is of the form

$$\chi = \frac{\sqrt{3}}{2}\left(l - t_0\frac{\partial}{\partial\eta}\right)e^{y}\int_{\eta/\sqrt{3}}^{y} e^{-2y'} I_0\left(\sqrt{y'^2 - \frac{\eta^2}{3}}\right)dy' + \frac{\sqrt{3}}{2}t_0\frac{\partial}{\partial\eta}\int_{\eta/\sqrt{3}}^{y} e^{-y'} I_0\left(\sqrt{y'^2 - \frac{\eta^2}{3}}\right)dy', \quad (5)$$

where $l = \frac{1}{4}(n+1)d$, $t_0 = \frac{3}{4}(n-1)d$, and d is the "length" of the Lorentz contracted nucleon. Replacing the Bessel function I_0 by its asymptotic expression, we may write this solution, by (3) and (4), in the form

$$3y = -\ln\frac{t^2 - x^2}{\Delta^2} + \left(\ln\frac{t+x}{\Delta}\ln\frac{t-x}{\Delta}\right)^{1/2}; \quad (6)$$

$$\eta = \frac{1}{2}\ln\frac{t+x}{t-x} \quad \text{or } v = \frac{x}{t}, \quad (7)$$

where $\Delta = l/\sqrt{6\pi|y|}$.

We find the distribution function of the entropy with respect to the velocities $dS/d\eta$ in the one-dimensional stage, using (5). Here we must remember that the different volume elements of the nuclear matter decay into the various particles at different time instants. We therefore require the distribution function $dS/d\eta$ not for a given time instant $t = \text{const}$, but on some surface $t = t(x)$. We assume that this surface is space-like.* We can then choose a coordinate system t', x' such that the derivative dt'/dx' is zero at an arbitrary given point of this surface. In this coordinate system the usual formula $dS = su^{0\prime}dx'$ is valid in the neighborhood of the given point, where s is the density of the entropy. Transforming back to the original coordinates, we obtain

$$dS = su^0dx - su^1dt. \quad (8)$$

Going over, using (3) and (4), to the independent variables η, y, we write (8) in the form:

$$dS = -s_0e^{2y}\left(\frac{\partial\psi}{\partial\eta}dy + \frac{1}{3}\frac{\partial\psi}{\partial y}d\eta\right), \quad (9)$$

where $\psi = \partial\chi/\partial y - \chi$, and s_0 is the initial density of the entropy. The derivatives appearing in this expression are equal to

$$\frac{\partial\psi}{\partial y} = \frac{\sqrt{3}}{2}e^{-y}\left(l\frac{\partial}{\partial y} - t_0\frac{\partial}{\partial\eta} - l\right)I_0\left(\sqrt{y^2 - \frac{\eta^2}{3}}\right), \quad (10)$$

$$\frac{\partial\psi}{\partial\eta} = \frac{\sqrt{3}}{2}e^{-y}\left(l\frac{\partial}{\partial\eta} - \frac{1}{3}t_0\frac{\partial}{\partial y} - \frac{1}{3}t_0\right)I_0\left(\sqrt{y^2 - \frac{\eta^2}{3}}\right). \quad (11)$$

If the temperature of the medium drops to the critical value T_k already in the one-dimensional phase, the distribution of the entropy over the velocity is given by the formula

$$\frac{dS}{d\eta} = -\frac{1}{3}s_0e^{2y_k}\frac{\partial\psi(\eta, y_k)}{\partial y_k} \approx \frac{S_0}{\sqrt{6\pi|y_k|}}\exp\left\{\frac{\eta^2}{6y_k}\right\}, \quad (12)$$

where $y_k = \ln(T_k/T_0)$, and S_0 is the total entropy. This case may arise in the collision of two heavy nuclei with low energies, when the number of secondary particles is large (so that hydrodynamics applies), but the initial temperature is small; then the three-dimensional stage cannot develop.

Thus the so-called quasi-one-dimensional approximation[8] amounts to the assumption that formula (12) gives the final solution to the problem even for high energies of the colliding particles. The distribution of the secondary particles over the transverse momenta is in this approximation completely determined by the thermal motion of decay.[9]

The present paper is mainly devoted to the investigation of the three-dimensional stage of the motion of the medium. We use an essentially different approach from that of references 1 and 2.

3. THREE-DIMENSIONAL STAGE

As our system has boundaries in the transverse direction, the matter flow will not be strictly one-dimensional, and the deviation from unidimensionality will increase as time goes on. At $t \sim a$ ($a = 1/\mu$ is the initial radius of the system, μ is the mass of the π meson) the matter flow will be essentially three-dimensional. The general pic-

---

*The following calculations will justify this assumption.

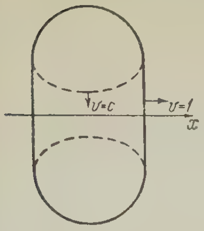

FIG. 1. Illustration of the three-dimensional expansion at the time instant $t \sim a$. The dotted line represents the boundary between the regions of one-dimensional and three-dimensional flow, x is the direction of motion of the colliding particles.

ture of the three-dimensional motion is the following. At the initial moment the temperature at $r = a$ drops suddenly from T_0 to zero, i.e., a sharp discontinuity arises. This discontinuity subsequently splits into two weak discontinuities bounding the region of three-dimensional matter flow. At the borderline with the vacuum the velocity of the medium is equal to the velocity of light, and the boundary between the regions of one-dimensional and three-dimensional flow, like every weak perturbation, moves with the velocity of sound $c = 1/\sqrt{3}$ with respect to the medium. For those elements of the medium which were in the one-dimensional stage, the region of three-dimensional flow is enclosed between the limits $r = a - ct$ and $r = a + t$. For the elements moving along the x axis (in the case of nucleon-nucleon collisions everywhere, with $x \neq 0$), this region has smaller dimensions (Fig. 1), owing to the Lorentz transformation of the transverse components of the velocity (or the time). The instant of time when the region of three-dimensional flow reaches the axis of the system can be called by convention the end of the one-dimensional stage. According to what has been said above, the end of the one-dimensional stage occurs sooner for the slow elements of the medium than for the fast ones.

Because of the cylindrical symmetry of the problem and because of the relation $u^i u_i = -1$, only two of the components u^i are independent. It is convenient to introduce new variables η, ξ, which automatically satisfy the above-mentioned conditions:

$$u^0 = \cosh\eta \, \cosh\xi, \; u^1 = \sinh\eta \, \cosh\xi,$$

$$u^2 = \sinh\xi \cos\varphi, \; u^3 = \sinh\xi \sin\varphi.$$

Here $\tanh\xi$ is the radial velocity in the coordinate system moving with the medium along the direction of the x axis.

We make use of the following circumstance in solving the three-dimensional problem. According to (7), $v = x/t$ in the one-dimensional stage, i.e., each element of the medium moves with almost constant velocity, as a quasi-inertial system. It is natural to expect the radial dispersion of the medium not to change the quasi-inertial character of the motion along the x axis, i.e., $v_x \approx x/t$ also in the region of three-dimensional flow. The discussion of the three-dimensional stage is therefore greatly simplified by eliminating the velocity $v_x = x/t$ through a transition to a suitable (curvilinear) coordinate system. This leads to the following coordinates:

$$\omega = \tanh^{-1}(x/t), \; t' = \sqrt{t^2 - x^2}.$$

The coordinate lines $\omega = \text{const}$ in the x, t plane are straight lines $x/t = \tanh\omega$. Hence the trajectories of the points with coordinates $\omega = \text{const}$ coincide with the trajectories of those elements of the medium moving as inertial systems. The variable t' is the proper time of such elements.

We introduce polar coordinates r, φ in the plane perpendicular to the x axis.

We can use the formulae of general relativity to write down the equations of motion in the new coordinates. The generalization of equation (1) to the case of curvilinear coordinates is:[10]

$$\frac{1}{\sqrt{-g}} \frac{\partial(\sqrt{-g}T_i^k)}{\partial x^k} = \frac{1}{2} \frac{\partial g_{kl}}{\partial x^i} T^{kl}. \tag{13}$$

In the transition from the coordinates x^i to the new coordinates $x^{i'}$, the tensor quantities transform according to the law $u^{i'} = (\partial x^{i'}/\partial x^k) u^k$ etc. With our choice of coordinates $x^{i'}$ ($x^{0'} = t'$, $x^{1'} = \omega$, $x^{2'} = r$, $x^{3'} = \varphi$) the metric tensor and the 4-velocity have the form

$$g'_{00} = -1, \; g'_{11} = t'^2, \; g'_{22} = 1, \; g'_{33} = r^2; \; g_{ik} = 0 \text{ when } i \neq k$$

$$u^{0'} = \cosh\eta' \cosh\xi, \; u^{1'} = \frac{1}{t'} \sinh\eta' \cosh\xi,$$

$$u^{2'} = \sinh\xi, \; u^{3'} = 0,$$

where $\eta' = \eta - \omega$.

It is hardly possible to solve (13) exactly. We use an approximate method, whose main features will be explained in the example of one-dimensional flow. It is convenient for this purpose to rewrite Eq. (13) in a form which is solved for the derivatives $\partial y/\partial x^i$:

$$\frac{\partial y}{\partial x^i} = \frac{1}{3} \frac{u_i}{\sqrt{-g}} \frac{\partial(\sqrt{-g}u^k)}{\partial x^k} - u^k \left(\frac{\partial u_i}{\partial x^k} - \frac{1}{2} u^l \frac{\partial g_{kl}}{\partial x^i} \right). \tag{14}$$

We convince ourselves of the equivalence of Eqs. (13) and (14) by "projecting" them on the direction of u^i and on the direction perpendicular to u^i. In the one-dimensional case the equations (14) have the form

$$\frac{\partial y}{\partial \omega} = -\frac{1}{3} \sinh 2\eta' \left(1 + \frac{\partial\eta'}{\partial\omega}\right) - \frac{1}{3}(\cosh 2\eta' + 2) t' \frac{\partial\eta'}{\partial t'}; \tag{15}$$

$$t' \frac{\partial y}{\partial t'} = \frac{1}{3}(\cosh 2\eta' - 2)\left(1 + \frac{\partial\eta'}{\partial\omega}\right) + \frac{1}{3} \sinh 2\eta' \cdot t' \frac{\partial\eta'}{\partial t'}. \tag{16}$$

The following assumption, which will be justified below, is essential for the whole approximate method of solution:*

$$t'\partial\eta'/\partial t',\ \partial\eta'/\partial\omega \ll 1.$$

With this assumption, (15) and (16) take the form

$$\partial y/\partial\omega = -{}^1/_3 \sinh 2\eta'; \tag{17}$$

$$t'\partial y/\partial t' = {}^1/_3 (\cosh 2\eta' - 2). \tag{18}$$

Eliminating η' from (17) and (18), we obtain

$$(3t'\partial y/\partial t' + 2)^2 - 9\,(\partial y/\partial\omega)^2 = 1. \tag{19}$$

The general solution of this equation is, as is easily seen,

$$y = {}^1/_3 [(\cosh 2\alpha - 2) \ln (t'/\beta) - \omega \sinh 2\alpha], \tag{20}$$

where α and β are arbitrary constants. We note that the general solution (20), together with the relation $\eta' = \alpha$, is at the same time the exact solution of (15) and (16). A special case of this solution is the traveling wave which is obtained by setting $\tanh \alpha = 1/\sqrt{3}$. In our coordinate system the velocity of the medium $\tanh \eta'$ changes thus from zero in the center of the system to the velocity of sound in the region of traveling waves.

It is customary to use the boundary conditions to obtain the solution of the problem from the general integral. However, we cannot do this, as our approximation is, as is seen from the following, an asymptotic one, which is valid only for large t'. We therefore use the asymptotic formula (6), which in our variables has the form

$$y = {}^1/_3 (\sqrt{\tau^2 - \omega^2} - 2\tau), \tag{21}$$

where $\tau = \ln (t'/\Delta)$. This expression satisfies Eq. (19) and is therefore the required solution. It is obtained from (20) by setting

$$\beta = \Delta,\ \tanh 2\alpha = \omega/\tau. \tag{22}$$

Substituting (21) in (17) or (18), we obtain $\eta' = \alpha$. The derivatives $\partial\eta'/\partial\omega$, $\partial\eta'/\partial\tau$ are of order $1/\tau$; they can thus indeed be neglected for $\tau \gg 1$. Hence the velocity of the medium $\tanh \eta'$ is a slowly varying function of ω and τ, and its magnitude does not exceed the velocity of sound. These properties are the mathematical expression of the fact that the flow along the x axis is quasi-inertial.

The boundary between the regions of one-dimensional and three-dimensional flow is given by a surface on which the derivatives of the hydrodynamic quantities are discontinuous, i.e., by the characteristic surface of Eq. (13). We can find the differential equation determining the characteristic surface $\Sigma\,(x^i) = 0$ by the usual method[11] from the requirement that it be impossible to determine all derivatives of first order from the equations of motion (13) by fixing the initial values on this surface. Some cumbersome calculations, which we shall not repeat here, lead to

$$2\left(u^k \frac{\partial\Sigma}{\partial x^k}\right)^2 - g^{ik}\frac{\partial\Sigma}{\partial x^i}\frac{\partial\Sigma}{\partial x^k} = 0. \tag{23}$$

The physical meaning of this equation is that the characteristic surface always moves with the velocity of sound with respect to the medium.

With the help of (23) we determine the equation for the boundary between the regions of one-dimensional and three-dimensional flow. Noting that $\xi = 0$, $\eta' = \alpha$ on this boundary, we obtain

$$2\left(\cosh\alpha\frac{\partial\Sigma}{\partial t'} + \frac{\sinh\alpha}{t'}\frac{\partial\Sigma}{\partial\omega}\right)^2 + \left(\frac{\partial\Sigma}{\partial t'}\right)^2 - \left(\frac{1}{t'}\frac{\partial\Sigma}{\partial\omega}\right)^2 - \left(\frac{\partial\Sigma}{\partial r}\right)^2 = 0. \tag{24}$$

Dividing (24) by $(\partial\Sigma/\partial r)^2$, we obtain an equation for $r = r\,(\omega, t')$:

$$2\left(\cosh\alpha\frac{\partial r}{\partial t'} + \frac{\sinh\alpha}{t'}\frac{\partial r}{\partial\omega}\right)^2 + \left(\frac{\partial r}{\partial t'}\right)^2 - \left(\frac{1}{t'}\frac{\partial r}{\partial\omega}\right)^2 = 1. \tag{25}$$

We seek a solution of this equation in the form $r = r\,(t')$. Then (25) takes the form

$$dr/dt' = \pm (\cosh 2\alpha + 2)^{-1/2}. \tag{26}$$

With neglect of the derivatives of α we obtain a solution which satisfies the initial conditions:

$$r = a - t'/\sqrt{\cosh 2\alpha + 2}. \tag{27}$$

We turn to the discussion of the region of three-dimensional motion of the medium. We make the substitution

$$y = y_1 + y_2, \tag{28}$$

where y_1 is the value of y in the absence of transverse dispersion, i.e., the solution of the one-dimensional problem obtained earlier. The variable y_2 is therefore responsible for an additional lowering of the temperature as a consequence of the radial motion of the medium. Corresponding to (28) we also transform the components of the energy-momentum tensor: $T_{ik} = e^{4y_1} I_{ik}$. Then (13) takes the form

$$\frac{\partial(\sqrt{-g}\,I_i^k)}{\partial x^k} + \left(4g_{il}\frac{\partial y_1}{\partial x^k} - {}^1/_2\frac{\partial g_{kl}}{\partial x^i}\right)\sqrt{-g}\,I^{kl} = 0. \tag{29}$$

For the derivatives of y_1 we have to substitute the expressions (17) and (18), in which we replace η' by the known function α. The boundary conditions for Eq. (29) have the form on the surface $r = a - t' / \sqrt{\cosh 2\alpha + 2}$:

---

*This corresponds to neglecting the derivatives of the slowly varying function f in reference 1.

$$y_2 = 0,\ \xi = 0,\ \eta' = \alpha. \tag{30}$$

After the substitution (28) the variable ω clearly enters into the equations of motion (29) and into the boundary conditions (30) only through the slowly varying function α, whose derivatives can be neglected, as was shown earlier. We can therefore regard α as a parameter, and look for the solution in the form

$$y_2 = y_2(t', r, \alpha), \quad \xi = \xi(t', r, \alpha), \quad \eta' = \eta'(t', r, \alpha).$$

We thus obtain the important result that we have separated the variables in the problem of the three-dimensional motion of the medium in the asymptotic approximation, which, as a consequence, lowers the number of independent variables from three to two. We note that this result is exact in the region of traveling waves, since the derivatives of α are strictly zero in this region.

We expand the required functions in a series in powers of α. Since α is an odd function of x, the expansions of y_2 and ξ contain only even powers of α, and the expansion of η', only odd powers of α. The main part of the entropy is concentrated in the region where $\omega \sim 1$. In this region, according to (22), $\alpha \sim 1/\tau$, i.e., α is an asymptotically small quantity. We therefore confine ourselves to the linear approximation in α, i.e., we require the solution in the form

$$y_2 = y_2(r, t'),\ \xi = \xi(r, t'),\ \eta' = \alpha f(r, t').$$

4. AVERAGING OF THE HYDRODYNAMIC QUANTITIES OVER THE RADIUS

A consequence of the equations of motion is the conservation law for the entropy, which, in curvilinear coordinates, has the form

$$\frac{1}{\sqrt{-g}} \frac{\partial(\sqrt{-g}\, su^k)}{\partial x^k} = 0. \tag{31}$$

After the substitution $s_2e^{3y_1}$ according to (28), we can write Eq. (31) in our approximation as

$$\frac{\partial(rs_2u^{0'})}{\partial t'} + \frac{\partial(rs_2u^{2'})}{\partial r} = 0. \tag{32}$$

The conservation law for the quantity $\int s_2u^{0'} r\, dr$ follows from this equation. It implies that the amount of entropy enclosed in the interval $d\omega$ is the same as that in the absence of the transverse dispersion, which means it is given by the formula

$$\frac{dS}{d\omega} = -s_0e^{2y_1}\left(\frac{\partial\psi}{\partial\eta_1}\frac{dy_1}{d\omega} + {}^1\!/_3\frac{\partial\psi}{\partial y_1}\frac{d\eta_1}{d\omega}\right), \tag{33}$$

where η_1 is the value of η in the absence of the transverse dispersion. Since the derivative $d\eta/d\omega$ is asymptotically equal to zero, the same formula describes the distribution $dS/d\eta$ in the three-dimensional stage. Formula (33) can approximately be written in a form analogous to (12):

$$\frac{1}{S_0}\frac{dS}{d\omega} = \frac{\exp(\eta^2/6y_1)}{\sqrt{6\pi|y_1|}}. \tag{34}$$

The temperature of the elements in the interval $d\omega$ with different coordinates r reaches the critical value T_k at different time instants. The values of $y_1 = y_k - y_2$ which have to be substituted in (34) in order to find the distribution of the produced particles with respect to η are therefore different for different elements. However, this difference is small. Estimates show that the decay of the elements of the medium occurs at $t' \sim a$. At that time the system is still quite uniform in the transverse direction, and $y_2 \sim 1$. In view of the weak dependence of (34) on y_1 we can therefore neglect this difference in the calculation of the distribution function $dS/d\eta$. We shall assume that all elements of the medium with the same coordinate ω decay simultaneously when their average temperature reaches the critical value. We restrict ourselves to the computation of this average value of the temperature.

In the calculation of the distribution function for the produced particles with respect to the transverse components of the velocity we must take account of the thermal motion of the particles, which is superposed on the hydrodynamic motion in a given volume element. The thermal motion of the particles plays indeed a fundamental role, so that the radial component of the hydrodynamic 4-velocity is small at the instant $t' \sim a$, and $u^2 \sim 1$. For each plane $\omega = \text{const}$ we can therefore take a value for the hydrodynamic radial velocity which is averaged over the radius.

Below we shall estimate the accuracy of the results obtained in this approximation.

To find the average values of the hydrodynamic quantities, we make use of the conservation laws in the integral form, which refer to finite, instead of infinitesimal, elements of the medium. These laws were also used in reference 1 in the investigation of the three-dimensional stage of the motion of the medium. However, our separation of variables gives the possibility to obtain more accurate results. We integrate Eq. (29) over the radius in the region of three-dimensional flow, i.e., from $r = a - ct'$ to $r = a + t'$ for $t' < \sqrt{3}\, a$, and from $r = 0$ to $r = a + t'$ for $t' > \sqrt{3}\, a$. Replacing all hydrodynamic quantities under the integral sign by their average values and taking these outside the integral, we obtain a system of ordinary differential equations for the mean values of the hydrodynamic quantities. These equations were solved numerically. The results of the numerical calculation of the hydrodynamic quantities averaged over the area of the transverse cross section are shown in Fig. 2.

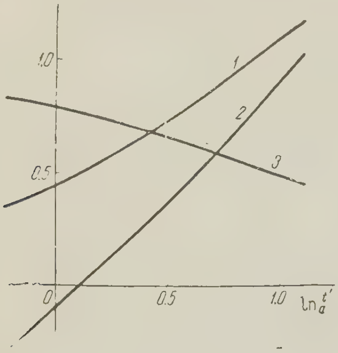

FIG. 2. Curve 1) y_2; curve 2) $\ln\overline{\sinh\xi}$; curve 3) $f = \overline{\eta'}/\alpha$.

5. DISTRIBUTION OF THE PARTICLES IN VELOCITY SPACE

As mentioned earlier, the distribution of the particles with respect to the transverse components of the velocity depends essentially on the thermal motion of the particles. We retain the notation ξ for the hydrodynamic velocity, and denote the radial component of the actual 4-velocity of the particles by $\sinh\zeta$. We write the required distribution function $F(\eta, \zeta)$ in the form

$$F(\eta,\ \zeta) = N_0 F_1(\eta) F_2(\eta,\ \zeta). \qquad (35)$$

The quantity $N_0 F_1(\eta)\,d\eta$ is the total number of particles in the interval $d\eta$, and the function $F_2(\eta, \zeta)$ gives the distribution of the particles with respect to the variable ζ for a given η. The functions $F_1(\eta) = N_0^{-1}dN/d\eta$ and $F_2(\eta, \zeta)$ must, of course, be normalized:

$$\int_{-\infty}^{\infty} F_1(\eta)\,d\eta = 1; \qquad \int_{0}^{\infty} F_2(\eta,\ \zeta)\,d\zeta = 1. \qquad ($$

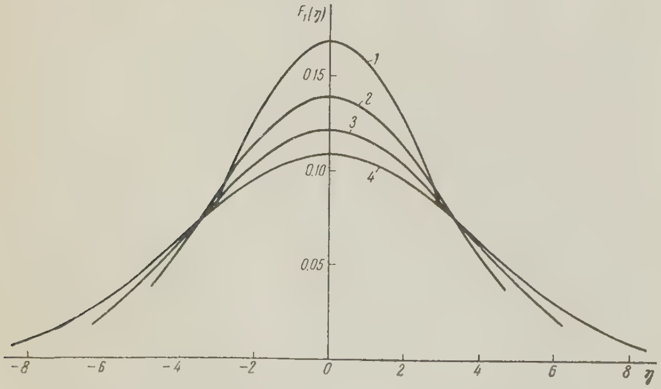

FIG. 3. Function $F_1(\eta)$ for $n = 1$. The initial energy E_0 is equal to: 1) 10^{12} ev, 2) 10^{14} ev, 3) 10^{16} ev, 4) 10^{18} ev.

The function $F_1(\eta)$ is computed with the help of formula (33) and the curves in Fig. 2. Figures 3 and 4 show the results of the calculation for $T_k = \mu$. According to (34), $F_1(\eta)$ can approximately be represented by a Gauss function. We therefore approximate the function $F_1(\eta)$ in the center of mass system by a Gauss function with parameter L:

$$F_1(\eta) = (2\pi L)^{-1/2}\exp(-\eta^2/2L); \qquad (37)$$

$$L = 0.56\ln\frac{E_0}{M} + 1.6\ln\frac{2}{n+1} + 1.6. \qquad (38)$$

where M is the mass of the nucleon.

Formulae (37) and (38) give an approximation to the curves in Figs. 3 and 4, with an error not exceeding 10%.

We turn to the computation of the function $F_2(\eta, \zeta)$. The thermal motion of the particles at the moment of breakup of the element into separate particles may be described by the formulae for the ideal gas. In the rest system of the element of the medium the distribution of the particles in momentum space is known to have the form

$$dN = A\frac{dp'_x\,dp'_y\,dp'_z}{\exp(E'/T) \pm 1}, \qquad (39)$$

where the plus sign refers to Fermi statistics, and the minus sign to Bose statistics. The factor A is determined from the normalization condition on the function F_2. We introduce a coordinate system in which the element moves along the z axis with the velocity $v_z = \tanh\xi$. Energy and momentum are then transformed in the following way:

$$E' = E\cosh\xi - p_z\sinh\xi;$$

$$p'_z = p_z\cosh\xi - E\sinh\xi;\quad p'_x = p_x;\quad p'_y = p_y.$$

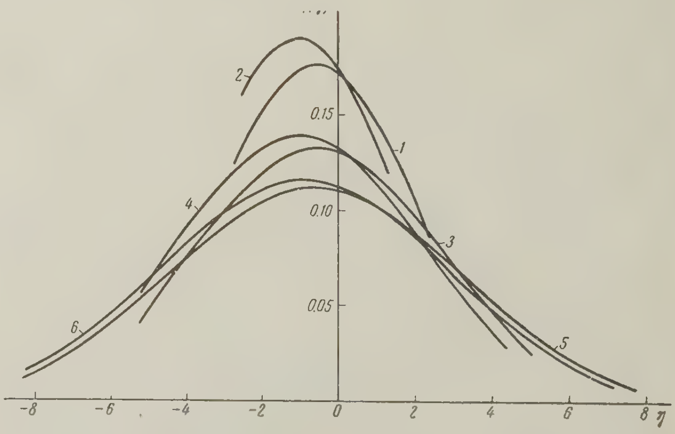

FIG. 4. Function $F_1(\eta)$ for the collision of a nucleon with the tube in the system of oppositely equal velocities of the colliding particles. n = 2 for curves 1, 3, and 5; n = 3.7 for curves 2, 4, and 6. E_0 is equal to: 1, 2) 10^{12} ev, 3, 4) 10^{15} ev, and 5, 6) 10^{18} ev.

Formula (39) takes the form

$$dN = A\left(\cosh\xi - \frac{p_z}{E}\sinh\xi\right)$$
$$\times\left[\exp\left(\frac{E\cosh\xi - p_z\sinh\xi}{T}\right)\pm 1\right]^{-1} dp_x dp_y dp_z. \tag{40}$$

Changing to cylindrical coordinates in momentum space and integrating over the azimuthal angle and the component p_x, we obtain

$$F_2(\eta,\zeta) = 4\pi A m^3 \sinh\zeta\cosh\zeta \sum_{n=1}^{\infty}(\mp)^{n-1}\Big\{\cosh\xi\cosh\zeta K_1$$
$$\times\left(n\frac{m}{T}\cosh\xi\cosh\zeta\right) I_0\left(n\frac{m}{T}\sinh\xi\sinh\zeta\right)$$
$$-\sinh\xi\sinh\zeta\, K_0\left(n\frac{m}{T}\cosh\xi\cosh\zeta\right)$$
$$\times I_1\left(n\frac{m}{T}\sinh\xi\sinh\zeta\right)\Big\}. \tag{41}$$

In the integration we expanded the denominator of the expression under the integral sign into a series in powers of $\exp\{-(E\cosh\xi - p_z\sinh\xi)/T\}$ and applied the relations

$$K_m(\lambda) = \int_0^{\infty} e^{-\lambda\cosh t}\cosh(mt)\,dt;\quad I_m(\lambda)$$
$$= \frac{1}{2\pi}\int_0^{2\pi} e^{\lambda\cos\theta}\cos(m\theta)\,d\theta.$$

Integrating (39) over all momentum space we similarly obtain an expression for A:

$$\frac{1}{A} = 4\pi m^2 T\sum_{n=1}^{\infty}(\mp)^{n-1}\frac{K_2(nm/T)}{n}. \tag{42}$$

Figure 6 shows the distribution functions with respect to the transverse momenta $(\mu/N_0)\,dN/dp_\perp = F_2/\cosh\xi$ for Bose particles for $T_k = \mu$ and various values of the parameter ξ.

The hydrodynamic transverse velocity ξ at the moment of break-up is with good accuracy ($\sim 10\%$) given by the approximate formula

$$\sinh\xi = 0.53\left(\frac{n+1}{2}\right)^{0.4}\left(\frac{E_0}{M}\right)^{1/14} e^{-\eta^2/6L}. \tag{43}$$

It follows from this formula that the transverse momenta of the fast particles should on the average be smaller than the transverse momenta of the slow particles. At energies of 10^{12} to 10^{13} ev the difference between them is, however, very small. Only at energies of order 10^{15} to 10^{18} ev do the transverse momenta of the fastest particles become significantly smaller (by a factor of ½ or ⅓) than those of the other particles.

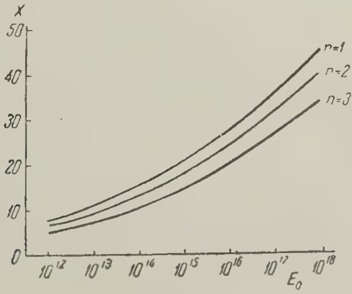

FIG. 5

6. DISTRIBUTION OF THE PARTICLES WITH RESPECT TO THE ANGLES, ENERGIES, AND TRANSVERSE MOMENTA

After the determination of the function $F(\eta,\xi)$, we find the distribution of the particles with respect to the angles, energies, and transverse momenta with the help of the formula

$$\tan\theta = \frac{\tanh\zeta}{\sinh\eta},\quad E = \mu\cosh\eta\cosh\zeta,\quad p_\perp = \mu\sinh\zeta.$$

Figure 6 shows that for the overwhelming majority of the particles $p_\perp > \mu$, i.e., $\tanh\zeta$ is rather close to unity. The angular distribution of the particles is therefore quite accurately given by the relations

$$\frac{1}{N_0}\frac{dN}{d\eta} = F_1(\eta) = \frac{\exp(-\eta^2/2L)}{\sqrt{2\pi L}}, \tag{44}$$

$$\tan\theta = 1/\sinh\eta. \tag{45}$$

In going over to the laboratory system we change η in formula (45) to $\eta + \eta_c$, where $V_c = \tanh\eta_c$ is the velocity of the center of mass system with respect to the laboratory system. Since η_c is a big quantity, we can write

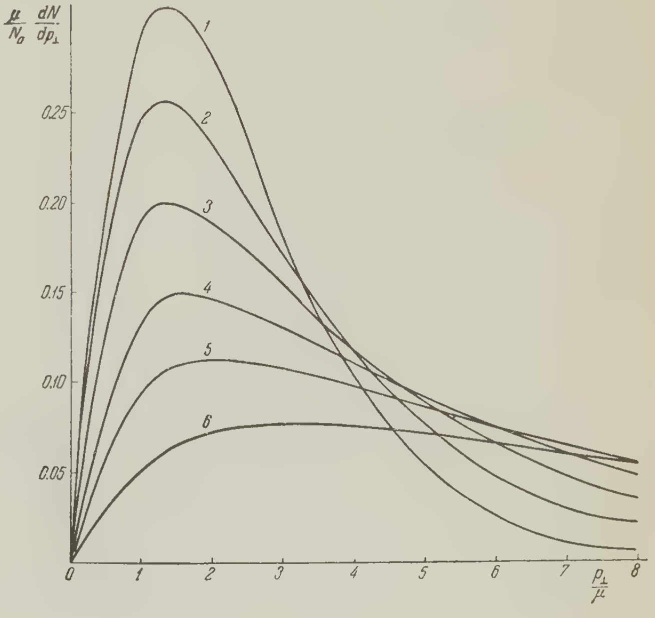

FIG. 6. Values of sinh ξ: 1) 0; 2) 0.5; 3) 1; 4) 1.5; 5) 2; 6) 3.

$$\vartheta / 2 = \exp(-\eta - \gamma_c). \qquad (46)$$

Formulae (44) and (45) give a more anisotropic distribution than the corresponding formulae of Landau.

A very sensitive characteristic of the angular distribution is the quantity $X = x/x_1$ introduced by Kaplon and Ritson,[12] where $x = \vartheta_{3/4}\ \vartheta_{1/4}$, and $\vartheta_{1/4}$ and $\vartheta_{3/4}$ are the angles within which ¼ and ¾ of all particles are, respectively, emitted; x_1 is the analogous quantity for the case of an isotropic distribution in the center-of-mass system.

To find the distribution of the particles over the transverse momenta, we have to compute the integral

$$\int_{-\infty}^{\infty} F(\eta, \zeta)\, d\eta = \frac{1}{N_0}\frac{dN}{d\zeta}.$$

The factor $\exp(-\eta^2/6L)$ in formula (43) is significant in the region $\eta \gtrsim \sqrt{L}$, where only a small fraction of the particles is to be found. The required distribution can therefore with good accuracy be written in the form

$$\frac{1}{N_0}\frac{dN}{d\zeta} = F_2(0, \zeta), \quad p_\perp = \mu \sinh \xi. \qquad (47)$$

For the determination of the energy distribution we have to integrate the function $F(\eta, \xi)$ over the surface $E = \text{const}$ in velocity space. We shall not concern ourselves with this distribution in detail. We remark only that since the transverse momenta of all particles are of the same order, the energy of the particles can approximately be written as

$$E \approx (\overline{p}_\perp^2 + \mu^2)^{1/2} \cosh \eta, \qquad (48)$$

where $\overline{p}_\perp$ is the average value of the transverse momentum of the particles. Formulae (44) and (48) determine the order of manitude of the energy distribution of the particles.

We estimate the accuracy of the formulae obtained. Formula (9), which describes the distribution of the entropy with respect to the velocities in the one-dimensional state, is exact. In the investigation of the three-dimensional stage we made use of the asymptotic approximation, i.e., we neglected quantities of order $1/\tau$. In order to estimate the effect of this neglect on $F_1(\eta)$, it is convenient to consider the conservation law for the entropy (31). The most significant of the terms discarded in equation (32) has the order of magnitude $\partial(\alpha - \eta')/\partial\omega \approx (1 - f)/2\tau$. The inclusion of this term leads to a change of 5 to 7% in the entropy enclosed in the interval $d\omega$, which also gives a measure for the error. Replacing all hydrodynamic quantities by their averages over the area of the transverse cross section entails a further approximation. The corresponding error was estimated in the following fashion. The region of three-dimensional flow was subdivided into three sections with respect to the radius, and the averaging was then done over these sections separately. The more exact solution obtained in this way was used to calculate the function $F_1(\eta)$ for the energies 10^{12} ev and 10^{15} ev. The result agrees with that obtained earlier within ~ 10% of error.

Despite the very approximate character of the treatment of the three-dimensional stage of the motion of the medium, the accuracy of the computed function $F_1(\eta)$ appears to be rather good (~ 10 to 15%). The physical reason for this is that the elements of the medium move almost inertially along the x axis at the moment of transition to the three-dimensional stage. As a consequence, the distribution of the entropy with respect to the velocities $dS/d\eta$ is mainly determined by the one-dimensional stage of motion.

Analogous estimates yield ~ 20 to 25% as the accuracy for $F_2(\eta, \xi)$. In this case the effect of the three-dimensional stage is small also on account of the great role played by the thermal motion of the particles. We note that the transverse hydrodynamic velocity increases slowly with increasing energy, whereas the role of the thermal motion becomes less significant. The accuracy of the calculation of $F_2(\eta, \xi)$ is therefore the better, the lower the initial energy, in contradistinction to the situation in the case of $F_1(\eta)$.

In conclusion we remark on the following interesting point. It is seen from Figs. 3, 4, and 6 that the functions $F_1(\eta)$ and $F_2(\eta, \xi)$ depend very weakly on the energy of the primary nucleon. According to (38) and (43),

$$L \sim \ln(E_0 / M), \quad \sinh \xi \sim E_0^{1/14}.$$

At the same time the initial width of the disk changes by three orders of magnitude when the energy is increased from 10^{12} ev to 10^{18} ev. This points to a very weak dependence of the results on the initial conditions. We may therefore suppose that, for $n > 3.7$, the distribution over energies and angles is described by formulae which are not very different from those obtained above. One should also expect that the quantum effects,[13] which are strongest at the initial moment, do not change our results significantly.

The author is very obligated to the late S. Z. Belen'kii. The author thanks E. L. Feinberg for valuable advice and L. V. Pariiska and N. E. Nikulina for doing the numerical calculations.

[1] L. D. Landau, Izv. Akad. Nauk SSSR, Ser. Fiz. **17**, 51 (1953).

[2] Amai, Fukuda, Iso, and Sato, Progr. Theor. Phys. **17**, 241 (1957).

[3] I. L. Rozental' and D. S. Chernavskii, Usp. Fiz. Nauk **52**, 185 (1954).

[4] S. Z. Belen'kii and G. A. Milekhin, J. Exptl. Theoret. Phys. (U.S.S.R.) **29**, 20 (1955), Soviet Phys. JETP **2**, 14 (1956).

[5] G. A. Milekhin, J. Exptl. Theoret. Phys. (U.S.S.R.) **35**, 978 (1958), Soviet Phys. JETP **8**, 000 (1959).

[6] I. M. Khalatnikov, J. Exptl. Theoret. Phys. (U.S.S.R.) **26**, 529 (1954).

[7] N. M. Gerasimova and D. S. Chernavskii, J. Exptl. Theoret. Phys. (U.S.S.R.) **29**, 372 (1955), Soviet Phys. JETP **2**, 344 (1956).

[8] I. L. Rozental', J. Exptl. Theoret. Phys. (U.S.S.R.) **31**, 278 (1956), Soviet Phys. JETP **4**, 217 (1957).

[9] G. A. Milekhin and I. L. Rozental', J. Exptl. Theoret. Phys. (U.S.S.R.) **33**, 197 (1957), Soviet Phys. JETP **6**, 154 (1958).

[10] L. D. Landau and E. M. Lifshitz, **Теория поля** (Field Theory), GTTI, M.-L., 1948. [Engl. Transl. Addison Wesley, 1951.]

[11] V. I. Smirnov, **Курс высшей математики** (Course of Higher Mathematics), GTTI, M., 1957.

[12] M. F. Kaplon and D. M. Ritson, Phys. Rev. **88**, 386 (1952).

[13] D. I. Blokhintsev, J. Exptl. Theoret. Phys. (U.S.S.R.) **32**, 350 (1957), Soviet Phys. JETP **5**, 286 (1957).

Translated by R. Lipperheide
251

CORRELATION ENERGY OF AN INHOMOGENEOUS ELECTRON GAS

D. A. KIRZHNITS

P. N. Lebedev Physics Institute, Academy of Sciences, U.S.S.R.

Submitted to JETP editor May 21, 1958

J. Exptl. Theoret. Phys. (U.S.S.R.) 35, 1198-1208 (November, 1958)

The influence of a non-uniform distribution of particles on the electron correlation energy is investigated. It is found that this influence is so large that the corresponding expressions obtained on the basis of the uniform distribution model[1,2] are not valid for real systems. The principal part of the correlation energy of the electrons in the crystalline lattice (without consideration of interaction with the vibrations of the latter) has been found for high pressures, low temperatures, and large values of the nuclear charge. Estimates are given for the correlation energy of uncompressed matter.

1. INTRODUCTION

It is well known that in polyelectronic systems a very important role is assigned to long range (many particle) correlations. In the most systematic form these correlations were studied in the recent work of Gell-Mann and Brueckner[2] (see also reference 3), where the correlation energy of the electron gas was found in the region of high compressions and low temperatures.

It is necessary, however, to emphasize that calculations of electron correlations are usually carried out with the use of a uniform model which greatly simplifies the real situation. In this model the nuclei (or ions) are replaced by a uniformly distributed positive background which guarantees the neutrality of the system as a whole. Such an approach completely ignores the atomistic structure of the positive charge: on the one hand the inhomogeneity of the charge distribution associated, for example, with the crystalline structure of the material is not taken into account, and on the other hand considerations of processes with participation of phonons and also electron-nuclear and nuclear correlations are left out.

The present work is devoted to consideration of the first of the enumerated factors, i.e., it contains the generalization of the results of Gell-Mann and Brueckner in the case of a non-uniform (but specified) distribution of the nuclei. The self-consistent potential $\Phi(\mathbf{x})$ corresponding to this situation, and the limiting Fermi momentum of the electron $p_0(\mathbf{x}) = [2M(E_0 - \Phi(\mathbf{x})]^{1/2}$ are functions of the coordinates (E_0 is the limiting energy). As will be shown below, the electron correlation energy reveals an extraordinarily strong sensitivity to the presence of non-uniformities. Even in the regions of high compressions, where the distribution of electrons is non-uniform only in small degree, a radical departure takes place from the results contained in reference 2.

Consideration of the rest of the factors mentioned above (in the first place, the lattice vibrations) can also lead to a significant contribution to the correlation energy of the crystalline body. The role of nuclear and electron-nuclear correlations is especially important in the plasma state where the radius and energy of the correlation are determined not by the electronic but by the nuclear mass and charge. These questions, however, require special consideration.

The anomalous sensitivity just mentioned of the correlation toward non-uniformity of the system has a simple physical explanation and is accounted for in the final analysis by the fact that the principal contribution to the correlation energy is made by a narrow strip of phase space adjoining the Fermi surface. It is easy to find the latter from the uniform case: according to references 1 and 2, the principal term of the correlation energy has the form

$$\delta E = -\frac{\Omega e^2}{16\pi^7\hbar^3 a_0}\int\limits_{p_D}^{\infty}\frac{d\mathbf{q}}{q^4}\int\frac{d\mathbf{p}_1 d\mathbf{p}_2}{q^2+\mathbf{q}(\mathbf{p}_1+\mathbf{p}_2)}$$

with the conditions $p_{1,2} < p_0$, $|\mathbf{p}_{1,2} + \mathbf{q}| > p_0$. Here Ω is the volume of the system, $p_D = (\hbar p_0/a_0)^{1/2}$ is the Debye momentum, a_0 is the Bohr radius. If the condition

$$\hbar/a_0 p_0 \ll 1, \tag{I}$$

is satisfied then the region of integration over $p_{1,2}$ in the foregoing equation is actually narrow:

$|p_{1,2} - p_0| \sim p_D \ll p_0$.

On the other hand, as was emphasized in reference 4, diffusion of the momentum distribution close to the Fermi surface is inevitably connected with the non-uniformity of the system, even if the system is a step function in the energy representation (the degenerate case). We introduce the characteristic "length of the non-uniformity" l over which p_0 changes by a significant amount, and which is determined by the average value of $p_0/\nabla p_0$. Then, from the indeterminancy principle, we obtain the following expression for the diffusion referred to:

$$\delta p \sim (\hbar / l p_0)^{1/2} p_0.$$

The quantum fluctuations in potential energy in the stationary state must be identical in magnitude; that is, $p_0 \delta p/M \sim p_0^2 \delta x/lM$, whence, with the help of $\delta p \delta x \sim \hbar$, the desired quantity is obtained. At some distance from the Fermi surface, this dispersion of the momentum is shown to be small, since there the distribution did not depend on the momentum; however, in the vicinity of p_0 an intermingling of filled and unfilled regions takes place and the form of the distribution in the vicinity of $|p - p_0| \sim \delta p$ is changed significantly (for details see reference 4). Upon satisfaction of the quasi-classical condition

$$\hbar / l p_0 \ll 1 \qquad \text{(II)}$$

this diffusion occupies the narrow band $\delta p \ll p_0$.

It is important that fulfillment of the condition (II) is not at all sufficient that the non-uniformity have only a slight effect on the result. More stringent conditions must be satisfied: the magnitude of the quantum diffusion δp must be much less than the width of the effective region of integration, i.e., in our case, p_D.

For clarification of the possibility of satisfying this condition, let us consider the case of strongly compressed matter where (see Sec. 4)

$$p_0(x) \sim (\hbar Z^{1/3} / R)(1 + (RZ^{1/3} / a_0) f(x/R) + \ldots),$$

and the case of uncompressed matter with a large nuclear charge Z, where[5]

$$p_0(x) \sim (\hbar Z^{2/3} / a_0) \varphi(xZ^{1/3} / a_0).$$

Here R is the radius of the neutral cell, x is the distance from its center (this distribution is repeated periodically throughout the other cells), f and φ are slowly varying functions. In both cases, the conditions (I) and (II) are satisfied and the "length of non-uniformity" l has the form*

$$l \sim a_0 Z^{-1/3}.$$

It then follows that the condition $\delta p/p_D \ll 1$ is not only not satisfied, but for heavy nuclei the opposite condition

$$\delta p/p_D \sim (a_0/l)^{1/2} \sim Z^{1/6} > 1,$$

is satisfied; this also testifies to the inapplicability of the uniform model. In what follows we shall for simplicity limit ourselves to ascertaining the asymptotic form of the energy correlation for $Z \to \infty$, i.e., in addition to conditions (I) and (II), we shall consider the condition

$$\delta p/p_D \sim (\hbar p_0/l p_D^2)^{1/2} \gg 1 \qquad \text{(III)}$$

to be satisfied. In the case of compressed matter in addition to (II) a more stringent condition $\hbar/lp_D \ll 1$ is satisfied; however, for uncompressed matter, $\hbar/lp_D \sim 1$.

Finally, we note that the correlation energy is highly sensitive with respect to the temperature inasmuch as the latter, as also the non-uniformity, leads to a diffusion of the Fermi distribution. The limit below which we can use the relations for a degenerate gas is determined not by the temperature of the degeneracy $kT_0 \sim p_0^2/2M$ but by the quantity $p_0 p_D/M \ll kT_0$. In this case it follows from condition (III) that in all regions of degeneracy δp exceeds the width of the temperature diffusion and the effect of non-uniformity considered above takes the place.

We used atomic units: $e = \hbar = M = 1$.

2. PRELIMINARY REMARKS

We proceed to a consideration of other complications associated with the transition to the non-uniform case. In the non-uniform case it is necessary to define more clearly the actual meaning of the correlation interaction. We shall consider as a correlation† that part of the interaction which is not taken into account in the Hartree-Fock approximation (HFA) and appears apart from the mean (self-consistent) interaction. The total energy of the system in the HFA has the form (ρ is the density of electrons, ρ_n is the density of nuclei)

---

*We note that in the case of strongly compressed matter ($RZ^{1/2}/a_0 < 1$, the pressure $P \gtrsim 10^8 \times Z^{10/3}$ atmos), in addition to the expression for l written here, there are other parameters of the dimensions of length (the radius of the cell R and also various combinations of R and l). However, these parameters are connected with derivatives (or, what amounts to the same thing, with commutators[4]) of higher order than the first and upon satisfaction of condition (II) they play a relatively unimportant role. An estimate shows that their role is significant only in the region $RZ^{2/3}/a_0 < 1$, $P \lesssim 10^8 Z^5$ atmos, which is relativistic for heavy atoms and is considered neither in reference 4 or in the present research.

†Strictly speaking, we are talking about the so called strong correlation which appears in addition to the exchange correlation.

$$E = {}^3/_{10}(3\pi^2)^{2/3}\int \rho^{5/3}\,dx - {}^3/_4(3/\pi)^{1/3}\int \rho^{4/3}\,dx + \frac{1}{2}\int\frac{dx\,dx'}{|x-x'|} \tag{2.1}$$
$$\times(\rho(x)\rho(x') - 2Z\rho(x)\rho_n(x') + Z^2\rho_n(x)\rho_n(x')) + \Delta E.$$

Here we have, respectively, the kinetic energy of the electrons, their exchange energy, the potential energy of interactions of the electrons with each other and with nuclei, and the energy of interaction of the nuclei. The last term, ΔE, corresponds to the specific quantum corrections[6] associated with a non-uniform system,* and upon satisfaction of the condition (II) reduces to the small quantity

$$({}^1/_{72})\int[(\nabla\rho)^2/\rho]\,dx.$$

In the uniform case, Eq. (2.1) reduces to the first two terms wherein, upon satisfaction of the condition (I), the exchange term plays a small role. In view of this fact we can consider the electrons to be free in the case considered in the HFA. Therefore, we can compute the energy of the electron correlation with the help of perturbation theory, expanding in a series of the Coulomb interaction and throwing away the first correction, which was already considered in the HFA. This was precisely the treatment of the problem given in reference 2.

In the non-uniform case the HFA must appear as the zeroth approximation while the perturbation is the difference between the Coulombic and the self-consistent interaction of the electrons. Such an approach to the calculation of correlation effects was assumed in the work of Møller and Plesset.[7] As the perturbation Hamiltonian in this method one must choose the expression

$$\hat{H}' = {}^1/_2\sum_{ij}{}' |x_i - x_j|^{-1} - \sum_j\int\bar{\psi}_{0j}(\xi)\,|x_i - \xi|^{-1}(1-\hat{P})\,\psi_{0j}(\xi)\,d\xi$$
$$+ {}^1/_2\sum_{ij}{}'[M(0_i0_j,\ 0_i0_j) - M(0_i0_j,\ 0_j0_i)], \tag{2.2}$$

where ψ_{0j} are single-particle wave functions of the fundamental configuration with energy ϵ_{0j},

$$\hat{P}\psi_\alpha(\xi)\,\psi_\beta(x) \equiv \psi_\beta(\xi)\,\psi_\alpha(x),$$

$$M(\alpha\beta,\gamma\delta) \equiv \int\bar{\psi}_\alpha(\xi)\,\bar{\psi}_\beta(\eta)\,|\xi-\eta|^{-1}\,\psi_\gamma(\xi)\,\psi_\delta(\eta)\,d\xi\,d\eta.$$

The unperturbed wave function of the system Ψ_0 for the fundamental configuration is a determinant constructed from the functions ψ_{0j} while for the perturbed configurations the index 0 is replaced by n, n′, etc. The third term is introduced in (2.2) in order that the first-order correction to the energy $\delta_1 E = (\Psi_0 H' \Psi_0)$ vanish, since in HFA the energy is equal to the mean value of the exact Hamiltonian.

For computation of the corrections of higher order, it is necessary to know the matrix elements of H' and the corresponding perturbation energy. A not very difficult calculation yields

$$(\Psi_n H' \Psi_{n'}) = \frac{1}{4}\sum_{ij}{}'\sum_{kl}{}'[M(n_in_j,\ n'_kn'_l)$$
$$- M(n_in_j,\ n'_ln'_k)]\,\Delta(n_in'_k,\ n_jn'_l)\,S(n_in'_k,\ n_jn'_l), \tag{2.3}$$

where Δ is a matrix which is diagonal for all states except $n_in_jn'_kn'_l$;

$$S = s^{n_i}_{n'_k}\, s^{n_j}_{n'_l}\, s^{n_i}_{n'_l}\, s^{n_j}_{n'_k},$$
$$s^{n_i}_{n'_k} = 1 - \delta_{n_in'_k}\sum_\alpha \delta_{n_i0_\alpha}\sum_\beta \delta_{n'_k0_\beta}. \tag{2.4}$$

Each term of the sum (2.3) corresponds to the transition of a pair of particles from the states n_in_j to $n'_kn'_l$. The factor S (2.4) forbids such transitions when the initial and final states of the particle are identical while they both belong to the fundamental configuration. In the other cases, S = 1 and (2.3) is identical with the matrix element of only a single Coulomb interaction. To find the chief term of the correlation energy we must sum only "platform" diagrams (see below) for which S = 1. Therefore, in actuality, in the present work the expansion is simply carried out over the Coulomb interaction.

So far as the perturbation energy is concerned, it is equal to

$$E_{n'} - E_n = \sum_i(\varepsilon_{n'_i} - \varepsilon_{n_i}).$$

This is connected with the fact that all the perturbed states correspond to one and the same Hamiltonian (self-consistency is obtained only within the framework of the fundamental configuration).

Corrections to the energy are computed according to the general formulas of perturbation theory. In particular, for the second-order correction we have

$$\delta_2 E = {}^1/_2\sum_{ij}{}'\sum_{nn'}{}'' \frac{|M(0_i0_j,\ nn')|^2 - M(0_i0_j,\ n'n)\,M(nn',\ 0_i0_j)}{\varepsilon_{0i} + \varepsilon_{0j} - \varepsilon_n - \varepsilon_{n'}}. \tag{2.5}$$

Here the double prime on the sum denotes summation only over those states n, n′, no one of which is a part of the fundamental configuration. This condition follows from the properties of the matrix S.

---

*The non-uniformity in Eq. (2.1) also appears in trivial form because of the dependence of ρ on the coordinates in the remaining terms of (2.1).

Out of all of the diagrams of higher order in reference 2 there were considered only the diagrams of the "platform" type in which in the interaction each particle either becomes excited, i.e., transfers from a region inside the Fermi sphere to a region outside of it, or conversely, gives up its excitation i.e., executes the opposite transition. An example of such a diagram of third order is pictured in Fig. 1, where the solid lines indicate the normal, and dotted lines the perturbed states of the particle; q is the momentum transferred. In diagrams of such type to each act of the interaction there corresponds the denominator q^2. In the diagrams not yet considered there are nodes with momentum transfers with the order of p_0, as a consequence of which the contribution of these diagrams is small. For the same reason we can omit the exchange parts of the platform diagrams (the corresponding arrangement of particles in the final state).

In the non-uniform case we must also consider only platform diagrams since the divergences at the lower limit become stronger, being linear instead of logarithmic (Sec. 3). Therefore, the decisive role of these diagrams becomes still clearer.

In the uniform case there is a logarithmic situation in which one of the two terms of the same type dominates over the other because of the large logarithmic factor. Therefore, the principal term of the energy was slightly sensitive relative to a choice of cumulative diagrams. In the non-uniform case, because of the linear character of the divergence, a correct choice of the diagrams is necessary even for calculation of the principal term.

We note further that the contribution of the exchange effects to the wave functions and the energy of the electrons is unimportant upon fulfillment of conditions (I) and (II). Thus, we can use these quantities in the Hartree approximation.

From what was said above, it follows that the only complication connected with consideration of non-uniformity in essence consists of the replacement of the wave functions and the energy of the free electrons by the corresponding quantities computed with account of non-uniformity.

3. QUALITATIVE CONSIDERATION

For a clarification of the aforementioned effects associated with consideration of non-uniformity, let us first consider the simplified expression for the correlation energy in which the summation of the diagrams of higher order is replaced by cutting off the integral over the momentum transfer in the diagram of second order by a quantity of the order of the Debye momentum p_D. In other words, a screened Coulomb interaction is introduced from the very beginning. A rigorous analysis (Sec. 4) confirms the possibility of such an approach and shows that the non-uniformity has practically no effect on the cut-off momentum.

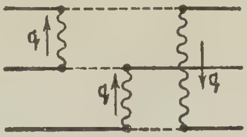

FIG. 1

The expression for the correlation energy of the second order has the form (C (2.5); the exchange diagrams are neglected):

$$\delta_2 E = {}^1\!/_2 \sum_{ij}{}' \sum_{nn'}{}'' \left| M(0_i 0_j, nn') \right|^2 / (\varepsilon_{0i} + \varepsilon_{0j} - \varepsilon_n - \varepsilon_{n'}). \quad (3.1)$$

It is appropriate to show the transition to the operator representation (3.1). With this aim let us express the matrix element in (3.1) in explicit form. We group the wave functions with the same indices and introduce into consideration the density matrix[6]

$$\rho(x, x') = \Sigma \bar{\psi}(x') \psi(x) = \theta_-(\hat{H}_x - E_0)\,\delta(x - x'),$$

which arises from summation over i, j in (3.1). Here the sum runs over the occupied states, the sum over the unoccupied states (summation over n, n′) is equal to

$$\delta(x - x') - \rho(x, x') = \theta_+(\hat{H}_x - E_0)\,\delta(x - x').$$

Here

$$\theta_\pm(a) = {}^1\!/_2 (1 \pm a/|a|),$$

$\hat{H}_x$ is the Hamiltonian of the Hartree approximation which acts on the variables x.

We can represent the energy denominator in the form

$$-{}^1\!/_2 \int_{-\infty}^{\infty} \exp\{-|t|(\varepsilon_n + \varepsilon_{n'} - \varepsilon_{0i} - \varepsilon_{0j})\}\,dt$$

and replace each ϵ in this equation by the Hamiltonian acting on the corresponding wave function in the density matrix. Introducing the notation

$$N_\pm(\mathrm{x}, \mathrm{y}) = \exp(\pm |t| \hat{H}_x)\,\theta_\mp(\hat{H}_x - E_0)\,\delta(x - y),$$

we get for (3.1)

$$\delta_2 E = -\int_{-\infty}^{\infty} dt \int \frac{d\mathrm{x}_1 d\mathrm{x}_2 d\mathrm{x}_3 d\mathrm{x}_4}{|\mathrm{x}_1 - \mathrm{x}_2|\,|\mathrm{x}_3 - \mathrm{x}_4|}$$

$$\times N_+(\mathrm{x}_1\mathrm{x}_3)\,N_+(\mathrm{x}_2\mathrm{x}_4)\,N_-(\mathrm{x}_3\mathrm{x}_1)\,N_-(\mathrm{x}_4\mathrm{x}_2).$$

It is expedient to transform to the momentum representation

$$N_\pm(\mathbf{x}, \mathbf{y}) = \int d\mathbf{p} \exp(i\mathbf{p}(\mathbf{x}-\mathbf{y}))\,\mu_\pm(\mathbf{x}, \mathbf{p}),$$

hence

$$\mu_\pm(\mathbf{x}, \mathbf{p}) = \langle \exp(\pm|t|\hat{H})\,\theta_\mp(\hat{H}-E_0)\rangle_\mathbf{p}. \qquad (3.2)$$

Here and below

$$\langle\hat{a}\rangle_\mathbf{p} = \exp(-i\mathbf{p}\cdot\mathbf{x})\,\hat{a}\exp(i\mathbf{p}\cdot\mathbf{x}),$$

where $\hat{a}$ is an arbitrary operator. This yields

$$\delta E = -(4\pi^4)^{-1}\int\limits_{-\infty}^{\infty} dt\int d\mathbf{x}\prod_1^3 d\mathbf{z}_i\int\prod_1^2 (d\mathbf{p}_i d\mathbf{q}_i d\mathbf{k}_i/k_i^2)\mu_+ \times(\mathbf{x}, \mathbf{p}_1)\,\mu_-(\mathbf{x}+\mathbf{z}_1, \mathbf{p}_1+\mathbf{q}_1) \qquad (3.3)$$

$$\times\mu_+(\mathbf{x}+\mathbf{z}_2, \mathbf{p}_2)\,\mu_-(\mathbf{x}+\mathbf{z}_3, \mathbf{p}_2+\mathbf{q}_2)\exp\{i[\mathbf{z}_1(\mathbf{k}_2+\mathbf{q}_1) + \mathbf{z}_2(\mathbf{q}_2-\mathbf{k}_2)-\mathbf{z}_3(\mathbf{q}_2+\mathbf{k}_1)]\}.$$

In this case, q_i must vary from p_D to ∞.

Limiting ourselves in this section to the case $lp_D \gg 1$, we can neglect the contributions of z_i to the arguments $\mu_\pm$. Actually, because of the presence of the exponent in (3.3), $z_i < p_D^{-1} \ll l$. This permits us to carry out a series of integrations and we obtain the formula*

$$\delta E = -(32\pi^7)^{-1}\int\limits_{-\infty}^{\infty} dt\int d\mathbf{x}\int d\mathbf{p}_1 d\mathbf{p}_2\int\limits_{p_D}^{\infty}\frac{d\mathbf{q}}{q^4} \qquad (3.4)$$

$$\times\mu_+(\mathbf{x}, \mathbf{p}_1)\,\mu_-(\mathbf{x}, \mathbf{p}_1+\mathbf{q})\,\mu_+(\mathbf{x}, \mathbf{p}_2)\,\mu_-(\mathbf{x}, \mathbf{p}_2-\mathbf{q}).$$

For the transition to the uniform case it suffices to say that $\hat{H} = \hat{p}^2/2$, which gives

$$\mu_\pm(\mathbf{x}, \mathbf{p}) = \exp(\pm|t|p^2/2)\,\theta_\mp(p^2/2-E_0), \qquad (3.5)$$

and we return to the equation for δE given in Sec. 1.

We note that the condition $lp_D \gg 1$ permits us to make use of the law of conservation of momentum (Fig. 2). Actually, the momentum acquired by the particle from the external field consists, as is easy to verify, of a quantity of the order of $1/l$ which is small in comparison with the momentum of transfer p_D.

In this section, we limit ourselves to a qualitative estimate of δE based on the results set forth in the introduction.

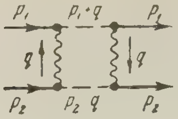

FIG. 2

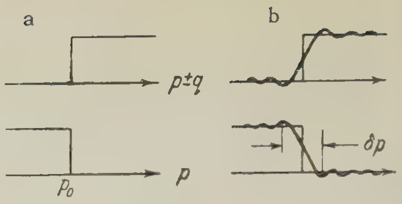

FIG. 3

We designate by Δp the width of the effective region of momentum space close to the Fermi surface which makes a significant contribution to (3.4). According to (3.2) and (3.4), this quantity is determined by the fact that the particle with momentum $\mathbf{p}_i$ and energy $E < E_0$, acquiring the momentum $\pm\mathbf{q}$ in the interaction, undergoes a transition to a state with momentum $\mathbf{p}_i \pm \mathbf{q}$ and energy $E > E_0$. Integration over t in (3.4) gives the energy gap $\Delta E \sim \Delta(p^2/2) \sim p_0\Delta p$. With consideration of $\int d\mathbf{p} \sim p_0^2\Delta p$, $p_0 \sim \rho^{1/2}$, we obtain

$$\delta E \sim -\int\rho dx\int\limits_{p_D}\frac{dq}{q^4}\,\Delta p. \qquad (3.6)$$

In the uniform case, the width Δp is determined by the conditions $p_i < p_0$, $|\mathbf{p}_i \pm \mathbf{q}| > p_0$, whence $\Delta p \sim q$ and $\delta E \sim -\Omega\rho\ln p_0$.

However, in the non-uniform case, when a scattering of the momentum $\delta p \sim (p_0/l)^{1/2}$ takes place in the state with given energy (Sec. 1), the effective width Δp can depend materially on δp. Upon satisfying the condition (III) $(\delta p \gg p_D)$ the width Δp becomes identical with δp. In this case, (3.6) yields

$$\delta E \sim -\int dx\rho\delta p/p_D \sim -\Omega\rho/l^{1/2}. \qquad (3.7)$$

Thus, upon consideration of the non-uniformity, the divergence is strengthened, becoming linear instead of logarithmic. This is associated with the fact that the effective range of integration over the momentum in the uniform case tends to zero along with q, while in the non-uniform case it remains finite.

The estimates obtained for the quantity Δp are illustrated in Fig. 3, where the distribution functions over the momentum are plotted for energies less than E_0 (lower curve) and above E_0 (upper curve). Curves a and b correspond to the uniform and non-uniform cases, respectively.

4. CONSIDERATION OF DIAGRAMS OF HIGHER ORDER

In this section we calculate exactly the principal term of the correlation energy by means of summation of the platform diagrams of higher orders. The method used is a direct generalization of the non-uniform case, the method of Gell-Mann and Brueckner,[2] and operates under conditions (I) to (III) (Sec. 1). We note that in reference 2 a condition was obtained which directly contradicts (III); correspondingly, the results obtained below and the results of reference 2 refer to different limiting cases.

---

*The apparent locality of the expression (3.4) in the coordinates is connected with the uniformity of the system at distances of the order of correlation radius $1/p_D$. Actually, as is seen from (3.3), the region $|\mathbf{x}-\mathbf{x}_0| \sim 1/p_D$ makes a contribution to the density of the correlation of the energy at the point $\mathbf{x}_0$.

Let us first consider the case $lp_D \gg 1$ (at the correlation radius the distribution is uniform). For the "propagator function" $F_q(t)$ introduced in reference 2 we must choose in this case the expression:*

$$F_q(t) = (2\pi)^3 \sum_{n,m} \exp[|t|(E_n - E_m)]\,\theta_-(E_n - E_0)\,\theta_+(E_m - E_0)$$
$$\times \int d\xi \bar{\psi}_n(x+\xi)\,\psi_n(x)\,\psi_m(x-\xi)\,\bar{\psi}_m(x)\exp(i\mathbf{q}\cdot\xi),$$

where ψ and E are the wave function and the energy in the external field. Making use of (3.2) we can put this expression in operator form:

$$F_q(t) = \int d\mathbf{p}\,\mu_+(\mathbf{x}, \mathbf{p})\,\mu_-(\mathbf{x}, \mathbf{p}+\mathbf{q}). \tag{4.1}$$

In the uniform case, (4.1) undergoes a transition, in accord with (3.5), to the corresponding expression of Gell-Mann and Brueckner:[2]

$$F_q(t) = \int d\mathbf{p}\exp(-|t|(q^2/2 + \mathbf{p}\cdot\mathbf{q})) \tag{4.2}$$

with the conditions $p < p_0$, $|\mathbf{p}+\mathbf{q}| > p_0$. The difference between (4.1) and (4.2) thus consists only in the substitution of the Hamiltonian of the free particles $\hat{p}^2/2$ by the complete Hamiltonian† $\hat{H} = \frac{1}{2}(\hat{p}^2 - p_0^2(\mathbf{x})) + E_0$.

In complete correspondence with reference 2, the sum of the platform diagrams has the form

$$\delta E = -(32\pi^4)^{-1}\int d\mathbf{x}\int d\mathbf{q}\int_{-\infty}^{\infty} du \sum_{n=2}^{\infty} A^n/n, \tag{4.3}$$

where $A = 4p_0\varphi_q(u)/\pi q^2$ and

$$\varphi_q(u) = (1/4\pi p_0)\int_{-\infty}^{\infty} e^{itu}F_q(t)\,dt. \tag{4.4}$$

The sum in Eq. (4.3) is expressed in finite form and is equal to $A - \ln(1-A)$. In this case, the integral (4.3) no longer diverges at the lower limit and is cut off at $q \sim (\varphi p_0)^{1/2}$.

In the calculation of $\varphi_q(u)$ the chief difficulty consists in finding the quantity μ which is a function of the Hamiltonian, which itself represents the sum of two non-commuting operators — the kinetic and the potential energy. As was shown in reference 4, to obtain an expression which is valid close to the Fermi surface, we must limit ourselves to a consideration of the first commutator of the operators shown and to all its powers. This gives for the arbitrary function f

$$\langle f(\hat{p}^2 - p_0^2)\rangle_\rho = \frac{1-is}{\sqrt{2\pi}}\int_{-\infty}^{\infty} e^{i\tau^2 s} f(p^2 - p_0^2 + 2\tau(|\mathbf{p}\nabla p_0^2|)^{1/2})\,d\tau, \tag{4.5}$$

where $s = \mathbf{p}\nabla p_0^2/|\mathbf{p}\nabla p_0^2|$. This expression is valid everywhere except for the extremely narrow (and therefore unimportant) region close to the Fermi surface $|p - p_0| \sim 1/l$.

Applying this equation to (3.2) and making use of (3.1) and (4.4), we obtain the following expression for $\varphi_q(u)$ (after some simple calculations*):

$$\varphi_q(u) \equiv \varphi(\lambda) = 1 + \pi\lambda^2 - 2\sqrt{\pi}(\cos\lambda^2\cdot S(\lambda) - \sin\lambda^2\cdot C(\lambda))$$
$$- 4\sqrt{2\pi}\lambda^2\int_0^\lambda[\sin x^2\cdot S(x) + \cos x^2\cdot C(x)]\,dx, \tag{4.6}$$
$$\lambda = u/(2p_0|\nabla p_0^2|)^{1/2},$$

where C and S are the Fresnel integrals. The quantity $\varphi(\lambda)$ is a monotonically decreasing function of λ, and for small λ has the form $1 - \sqrt{2\pi}\,\lambda$, while for large values of λ it has the form $4/\lambda^4$.

Substitution of (4.6) in (4.3) gives

$$\delta E = -\frac{2\sqrt{2}}{3\pi^{7/2}} I\int d\mathbf{x}\,p_0^2|\nabla p_0^2|^{1/2},$$

where

$$I = \int_0^\infty \varphi^{3/2}(\lambda)\,d\lambda = 0.286.$$

The correlation energy δE, as a functional of the density ρ, has the form

$$\delta E = -0.118\int(\rho|\nabla\rho|)^{1/2}\,d\mathbf{x}. \tag{4.7}$$

A correspondence of this expression to the qualitative equation (3.7) is evident. We note that the principal contribution to (4.3) is given by the region $\lambda \sim 1$; therefore, the effective cutoff radius $q \sim p_0^{1/2}$ is identical with the Debye radius.

For a strongly compressed lattice we can, in finding $\rho(x)$, make use of the Thomas-Fermi model (see reference 5)

$$(3\pi^2\rho)^{1/3} = 2(E_0 + Z/x - \int\rho(\mathbf{x}')|\mathbf{x} - \mathbf{x}'|^{-1}\,d\mathbf{x}'),$$

whence

$$\rho = (3Z/4\pi R^3)\{1 + (16Z/3\pi^2)^{1/3}R(\xi^2/2 + \xi^{-1} - 3/2) + \cdots\}, \tag{4.8}$$

---

*Strictly speaking, this quantity is not a propagator function in the ordinary sense and corresponds to the diagram of Fig. 4. In terms of field theory, there corresponds to it the

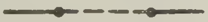

FIG. 4

expression $\bar{\psi}\Gamma G\Gamma\psi$ where ψ encompasses the occupied states, Γ is the vertex part with momentum transfer q, G is the Green's function of the electron. Furthermore, in reference 2 and below, a purely expotential dependence of $F_q(t)$ on the time is assumed.

†The validity of the expression (4.1) also follows from comparison with the formulas of perturbation theory [see for example, (3.4)].

*The condition (III) permits us to replace $\mathbf{p}+\mathbf{q}$ by $\mathbf{p}$ in the argument of the function μ_- (4.1).

where $\xi = x/R$, R is the radius of the neutral cell. Substitution of this expression in (4.7) gives (N is the total number of particles)*

$$\delta E = -0.106\, NZ^{1/6}.$$

The most important term not considered here is the exchange energy of second order which has a magnitude of the order of 0.02 N (See reference 2). The ratio of (4.9) to the total compressed matter is equal to $2.87\,\mathrm{N}\,\rho^{2/3}$ and is a small quantity.

We proceed to find the contribution of the correlation to the equation of state of the material. The corresponding correction to the pressure is determined by the equation

$$\delta P = -\,\partial(\delta E)/\partial V = (\rho^2/N)\,\partial(\delta E)/\partial\rho.$$

In view of the fact that the principal term δE does not depend on the ρ, it is necessary to make use of the following terms of an expansion of the type of the second term of (4.8). This gives

$$\delta P \sim Z^{5/6}\rho^{3/2}. \qquad (4.10)$$

The ratio of δP to the principal term in the pressure is equal to $1.92\,\rho^{5/3}$, which is always very small.

We note that the model frequently used in calculations of the equation of state, in which the neutral cell is considered independent of the rest of the material, gives an incorrect value of the correlation contribution to the pressure. The fact is that at high compression, when the dimensions of the lattice R becomes smaller than $1/p_D$ (while the latter quantity, being of the order of $\sqrt{R}$, falls off more slowly than R), distant correlations are not taken into account in this model.

We proceed to the case $lp_D \sim 1$. In this case, we can introduce only symbolic expressions for δE, obtained by replacing the sum in (4.3) by the quantities†

$$\sum_{n=2}^{\infty}\langle(4p_0\varphi(\lambda)/\pi\Delta)^n\rangle_q/n. \qquad (4.11)$$

Here the operator Δ^{-1} acts on all subsequent factors, while in the uniform case and in the case considered above, only the result of the effect of Δ^{-1} on $\exp(i\mathbf{q}\cdot\mathbf{x})$ was important.

The case under consideration corresponds to uncompressed material with large Z. The expressions (4.7) to (4.10) obtained above are applicable here only qualitatively. So far as electron correlation in metals is concerned, we must emphasize the impossibility of separate consideration of conduction electrons and ionic electrons, since the correlation radius in a real metal is of the order of the distance between nuclei. Therefore, strong correlation coupling will take place between the conduction electrons and the ionic electrons. In view of the fact that the number of the latter is large in comparison with the number of conduction electrons, we must consider that these correlations play a more important role that the correlations between the conduction electrons. Therefore, although the conduction electrons also form a more uniform distribution than the ionic electrons, the uniform model is inapplicable in this case also.

For an isolated atom we can obtain the dependence of δE on Z; and Eqs. (4.9) ($lp_D \gg 1$) and (4.14) ($lp_D \ll 1$; see below) lead to the same result

$$\delta E \sim Z^{7/6},. \qquad (4.12)$$

naturally with a small coefficient. Thus, for large Z, the contribution of the correlation to the energy of the atom is small (principal energy term $\sim Z^{7/3}$). It is also actually small for z.

In the case $lp_D \ll 1$, Eq. (4.11) can be materially simplified, since the first term in it will play the fundamental role. Introducing the expression $\psi(u, x) \equiv 4p_0(x)\,\varphi(\lambda(x))/\pi$, we have

$$\delta E = -\frac{1}{128\pi^3}\int_{-\infty}^{\infty} du \int \frac{dxdy}{|\mathbf{x}-\mathbf{y}|^2}\,\psi(u, x)\,\psi(u, y). \qquad (4.13)$$

Pair correlations in this case play a dominant role and the infrared catastrophe is lacking. The fact is that the momentum acquired by the particles from the external field is so large in this case that it takes the particles out of the small-momentum region that is responsible for the collective motion.

In particular, if the system has such small dimensions L that $Lp_D \ll 1$ (or $LN^{1/3} \ll 1$) then the previous formula reduces to the estimate

$$\delta E \sim N^{7/6}. \qquad (4.14)$$

We note that the independence of δE of the density and the small role of the corrections of higher order follow directly from perturbation theory (Sec. 2). Actually, the matrix element has the order of L^{-1} in this case, while the energy gap is of the order L^{-2}, whereupon the correction of nth order amounts to $\delta_n E \sim L^{n-2}$. These questions were considered in reference 8 in application to two-electron atoms.

In conclusion, we again emphasize the impossibility of using the uniform model to find correlation effects in the range of low temperatures. If the material is in the crystalline state, then, as shown above, accounting for the non-uniformity in the particle distribution, due to the presence of the lattice, is absolutely necessary. If the same material can exist as a plasma, the effects of internuclear and electron-nuclear correlations come to the forefront. The fact is that the nucleus, having a small kinetic energy, is more sensitive to the field acting on it than is the electron. Therefore, the screening parameters are determined primarily by the nuclear mass and charge. In this case the dominant role of the nuclei appears in all temperature ranges where the electron gas is degenerate.

---

*The uniform model reduces to the expression[2] $\delta E = -0.0104\,\mathrm{N}\ln\rho + \ldots$, which has nothing in common with (4.9).

†For the derivation of (4.11) it is necessary to make use of the relation $\mu(\mathbf{x}+\mathbf{z}, \mathbf{p}) = \exp(\mathbf{z}\nabla)\,\mu(\mathbf{x}, \mathbf{p})$ [compare (3.3) and the condition (III)].

Formulation of the problem on the correlations in an inhomogeneous gas is contained only in the recent work of Hubbard,[9] where the known peculiarities of behavior of electrons in a periodic lattice field are taken into account. In the specific cases considered in the present research, it was possible to avoid the complication connected with this in the application of the approximation close to the quasi-classical.

I express my deep gratitude to V. L. Ginzburg, V. P. Silin, E. L. Fainberg and E. S. Fradkin for numerous discussions and valuable comments. I also thank L. V. Pariiskaia for the numerical computations.

---

[1] W. Macke, Z. Naturforsch, **5a**, 192 (1950); D. Pines, Solid State Physics, N. Y., **1**, 367 (1955).

[2] M. Gell-Mann and K. Brueckner, Phys. Rev. **106**, 364 (1957).

[3] K. Sawada, Phys. Rev. **106**, 372 (1957).

[4] D. A. Kirzhnits, J. Exptl. Theoret. Phys. (U.S.S.R.) **34**, 1625 (1958); Soviet Phys. JETP **7**, 1116 (1958).

[5] P. Gombas, Die statistische Theorie des Atoms, Springer, Wien, 1949 (Russian translation, IIL, 1951).

[6] D. A. Kirzhnits, J. Exptl. Theoret. Phys. (U.S.S.R.) **32**, 115 (1957); Soviet Phys. **5**, 64 (1957).

[7] C. Møller and M. Plesset, Phys. Rev. **46**, 618 (1934).

[8] D. A. Kirzhnitz, Оптика и спектроскопия (Optics and Spectroscopy) **5**, 5 (1958).

[9] J. Hubbard, Proc. Roy. Soc. (London) **A244**, 199 (1958).

Translated by R. T. Beyer
252

SOVIET PHYSICS JETP VOLUME 35(8), NUMBER 5 MAY, 1959

ON THE THEORY OF PARAMAGNETIC RESONANCE AND PARAMAGNETIC RELAXATION IN METALS

V. V. ANDREEV and V. I. GERASIMENKO

Physico-Technical Institute, Academy of Sciences, Ukrainian S.S.R.

Submitted to JETP editor May 21, 1958

J. Exptl. Theoret (U.S.S.R.) 35, 1209-1215 (November, 1958)

A kinetic equation is obtained for conduction electrons in metals, which is valid for the investigation of paramagnetic resonance. The case of uniform distribution of an alternating field in a metal is considered in detail. It is shown that for temperatures $kT \gg \mu H_0$, "longitudinal" and "transverse" spin relaxation times can be introduced, these times being practically identical.

1. The recently developed theory of paramagnetic resonance in metals is based either on the use of a representation of the diffusion of electrons from the skin depth[1] or on the use of the kinetic equation for the electron density operator,[2,3] where both the thermal and the spin collision intervals are described phenomenologically: $(f-f_0)/\tau$. In all these researches, the spin and thermal relaxation times entered as parameters. In references 2 and 3, moreover, no distinction is made between "transverse" and "longitudinal" relaxation times, although this is not evident beforehand. The spin relaxation time obtained from experiments on paramagnetic resonance (on resonance width) is "transverse," which was not computed theoretically. Existing data in the literature refer only to "longitudinal" times.[4] It would therefore be appropriate to obtain the equation for paramagnetic resonance in which the collision integral is described in microscopic fashion, and to show the possibility of introducing "longitudinal" and "transverse" spin relaxation times.

In obtaining such an equation, the problem of the choice of the mechanism according to which the perturbed spin system returns to equilibrium is of importance. In the researches of Overhauser[4] and Elliott,[5] different types of spin interactions were investigated; however, only the spin orbit coupling of the electrons with the lattice which was considered by Elliott leads to agreement with the spin relaxation times computed from the experiments. Below, therefore, we shall consider as responsible for the spin relaxation a mechanism associated with consideration of the effect of spin orbit coupling on the interaction of the electrons with the lattice vibrations.

2. To obtain the kinetic equation, we make use of the method of statistical operators for quantum systems.[6] Application of this method to obtain the kinetic equation for conduction electrons without account of their spin was made by Gurzhi.[7] We shall carry out a similar derivation with account of the spins of the electrons and spin orbit interaction of electrons with the periodic field of the lattice.

Let us consider a system of N non-interacting electrons and S phonons. The electrons are located in the periodic field of the lattice and in a constant magnetic and variable electromagnetic external fields. The complete Hamiltonian of such a system is

$$\hat{\mathscr{H}} = \sum_{k=1}^{N} \hat{\mathscr{H}}(\bar{x}_k) + \sum_{k=1}^{S} \hat{\mathscr{H}}(\bar{y}_k) + \sum_{i=1}^{N}\sum_{k=1}^{S} \hat{U}(\bar{x}_i, \bar{y}_k);$$

$$\hat{\mathscr{H}}(\bar{x}) = \frac{1}{2m}\left(\hat{\mathbf{P}} + \frac{e}{c}\mathbf{A}\right)^2 + V(\mathbf{r}) + \mu\hat{\sigma}\cdot\mathbf{H} + \frac{\mu}{2mc}[\nabla V \times \hat{\mathbf{P}}]\cdot\hat{\sigma};$$

$$\hat{\mathscr{H}}(\bar{y}) = \frac{1}{2}h\nu_{\mathbf{q}\lambda}(\hat{b}^{+}_{\mathbf{q}\lambda}\hat{b}_{\mathbf{q}\lambda} + \hat{b}_{\mathbf{q}\lambda}\hat{b}^{+}_{\mathbf{q}\lambda});$$

$$\hat{U}(\bar{x}, \bar{y}) = \left(\frac{\Delta h}{2V_0 M\nu_{\mathbf{q}\lambda}}\right)^{1/2}(\mathbf{e}_{\mathbf{q}\lambda}\cdot\nabla V)(\hat{b}^{+}_{\mathbf{q}\lambda}e^{-i\mathbf{q}\cdot\mathbf{r}/\hbar} + \hat{b}_{\mathbf{q}\lambda}e^{i\mathbf{q}\cdot\mathbf{r}/\hbar}),$$

where $\bar{x}$ and $\bar{y}$ represent, respectively, the set of coordinates and spin of the electron $(\mathbf{r}\sigma)$ and the momentum and polarization of the phonon $(\mathbf{q}\lambda)$; $e_{\mathbf{q}\lambda}$ is the polarization vector of the phonon; M is the mass of the atom; $V(\mathbf{r})$ is the periodic field of the lattice; $h\nu_{\mathbf{q}\lambda}$ is the energy of the phonon; $\mathbf{A} = \mathbf{A}_0 + \mathbf{A}_1(\mathbf{r}, t)$ is the vector potential of the external field; $\mathbf{H} = \mathbf{H}_0 + \mathbf{H}_1(\mathbf{r}, t)$, where $\mathbf{H}_0$ and $\mathbf{H}_1$ are the constant and variable magnetic field; Δ is the volume of an elementary cell; V_0 is the volume of the crystal; $\mu = |e|\hbar/2mc$;

$\hat{b}^{+}_{\mathbf{q}\lambda}$ and $\hat{b}_{\mathbf{q}\lambda}$ are the creation and annihilation operators of the phonon with momentum q and polarization λ. The state of the system is described by the statistical operator F, which satisfies the equation

$$\partial \hat{F}/\partial t = [\hat{\mathscr{H}}, \hat{F}] \equiv (1/i\hbar)(\hat{\mathscr{H}}\hat{F} - \hat{F}\,\hat{\mathscr{H}}).$$

For the single particle operator $\hat{F}(\bar{x},t)$ similar to what was done in reference 7 and under the same assumptions, we obtain the equation

$$\frac{\partial \hat{F}(\bar{x}, t)}{\partial t} = [\hat{\mathscr{H}}(\bar{x}), \hat{F}(\bar{x}, t)] + \sum_{k=1}^{S} \underset{(\bar{y}_k)}{\mathrm{Sp}} [\hat{U}(\bar{x}, \bar{y}_k), \hat{G}(\bar{x}, \bar{y}_k, t)],$$

$$\hat{G}(t) = -\int_0^\infty d\tau \cdot \exp\left\{\frac{i}{\hbar}\int_t^{t+\tau} dt' [\hat{\mathscr{H}}(\bar{x}) + \hat{\mathscr{H}}(\bar{y})]\right\} \hat{B}(t+\tau) \qquad (1)$$

$$\times \exp\left\{-\frac{i}{\hbar}\int_t^{t+\tau} dt' [\hat{\mathscr{H}}(\bar{x}) + \hat{\mathscr{H}}(\bar{y})]\right\}.$$

Here

$$\hat{B}(\bar{x}_1, \bar{y}, t) = [\hat{U}(\bar{x}_1, \bar{y}), \hat{F}(\bar{x}_1, t)\hat{F}(\bar{y})]$$
$$- N\mathrm{Sp}_{(\bar{x}_2)} [\hat{U}(\bar{x}_2, \bar{y}), \hat{P}_{12}\hat{F}(\bar{x}_1, t)\hat{F}(\bar{x}_2, t)\hat{F}(\bar{y})]$$

and it is assumed that the lattice is in thermal equilibrium:

$$(N_{\mathbf{q}\lambda} | \hat{F}(\bar{y}) | N'_{\mathbf{q}\lambda}) = \delta_{N_{\mathbf{q}\lambda}N'_{\mathbf{g}\lambda}}\delta_{N_{\mathbf{q}\lambda}\bar{N}_{\mathbf{q}\lambda}};\ \bar{N}_{\mathbf{q}\lambda} = [\exp(h\nu_{\mathbf{q}\lambda}/kT) - 1]^{-1}.$$

$\hat{P}_{12}$ is the permutation operator of the particles:

$$(n_1 n_2 | \hat{P}_{12}\hat{F}(\bar{x}_1)\hat{F}(\bar{x}_2) | n'_1 n'_2) = (n_1 | \hat{F} | n'_2)(n_2 | \hat{F} | n'_1).$$

In the collision integral, we limit ourselves to terms of zero order in the vector potential $\mathbf{A}_1(\mathbf{r},t)$. Moreover, we shall not take into consideration the effect of the constant magnetic field on the orbital motion of the electrons which, in any case, is valid if the turning radius of the electron in the magnetic field is much longer than the mean free path. Then the matrix elements of the operator $\hat{G}$ in the proper representation of the operator

$$\frac{\hat{p}^2}{2m} + V(\mathbf{r}) + \frac{\mu}{2mc}[\nabla V \times \hat{\mathbf{p}}] \cdot \hat{\sigma} + \mu\hat{\sigma} \cdot \mathbf{H}_0 + \hat{\mathscr{H}}(\bar{y}) \equiv \hat{\mathscr{H}}_0(\bar{x}) + \hat{\mathscr{H}}(\bar{y})$$

will be:

$$(\mathbf{p}\sigma N_{\mathbf{q}\lambda} | \hat{G} | \mathbf{p}'\sigma' N'_{\mathbf{q}\lambda})$$

$$= -\int_0^\infty d\tau \cdot \exp\left\{\frac{i\tau}{\hbar}[E_{\mathbf{p}\sigma} - E_{\mathbf{p}'\sigma'} + (N_{\mathbf{q}\lambda} - N'_{\mathbf{q}\lambda})h\nu_{\mathbf{q}\lambda}]\right\} \qquad (2)$$
$$\times (\mathbf{p}\sigma N_{\mathbf{q}\lambda} | \hat{B}(t+\tau) | \mathbf{p}'\sigma' N'_{\mathbf{q}\lambda}),$$

where $E_{\mathbf{p}s}$ are the eigenvalues of the operator $\hat{\mathscr{H}}_0(x)$. The eigenfunctions

$$\psi_{\mathbf{p}\sigma} = \sqrt{V_0/\Delta}\, u_{\mathbf{p}\sigma} e^{i\mathbf{p}\cdot\mathbf{r}/\hbar},$$

where $u_{\mathbf{p}s}$ are periodic with the period of the lattice. By virtue of this fact the matrix elements of the operator $\hat{U}(\bar{x}, \bar{y})$ in the representation of $\psi_{\mathbf{p}\sigma}$ will be (neglecting processes of "transfer" and transition from zone to zone):

$$(\mathbf{p}\sigma N_{\mathbf{q}\lambda} | \hat{U} | \mathbf{p}'\sigma' N'_{\mathbf{q}\lambda})$$
$$= (N_{\mathbf{q}\lambda} | \hat{b}^{+}_{\mathbf{q}\lambda} | N'_{\mathbf{p}\lambda}) A^{\mathbf{p}\sigma}_{\mathbf{p}'\sigma'}\delta_{\mathbf{p}'-\mathbf{p}-\mathbf{q}} + (N_{\mathbf{q}\lambda} | b_{\mathbf{q}\lambda} | N'_{\mathbf{q}\lambda}) A^{\mathbf{p}\sigma}_{\mathbf{p}'\sigma'}\delta_{\mathbf{p}'-\mathbf{p}+\mathbf{q}};$$
$$A^{\mathbf{p}\sigma}_{\mathbf{p}'\sigma'} = \left(\frac{\Delta h}{2V_0 M\nu_{\mathbf{q}\lambda}}\right)^{1/2} \int_{(\Delta)} u^{*}_{\mathbf{p}\sigma}(\mathbf{r})(\mathbf{e}_{\mathbf{q}\lambda} \cdot \nabla V) u_{\mathbf{p}'\sigma'}(\mathbf{r})\, d\mathbf{r}. \qquad (3)$$

We shall now obtain the kinetic equation. We shall consider the case in which the variable field inside the metal can be considered homogeneous. Such a consideration is suitable if the dimensions of the specimen d are much smaller than the skin depth. Then the matrix of the operator $\hat{F}(\bar{x})$ in the representation of the function $\psi_{\mathbf{p}\sigma}$ will be diagonal in the momentum:

$$(\mathbf{P}\sigma | \hat{F} | \mathbf{P}'\sigma') = N^{-1} f_{\sigma\sigma'}(\mathbf{P})\,\delta_{\mathbf{P}-\mathbf{P}'}. \qquad (4)$$

In the presence of an electromagnetic field, the distribution function depends upon the generalized momentum $\mathbf{P} = \mathbf{p} - e\mathbf{A}/c$. However, it is appropriate to transform to the distribution function which depends on the kinetic momentum $\mathbf{p}$. In such a transition,

$$\dot{f}(\mathbf{P}) = \dot{f}(\mathbf{p}) + \frac{e}{c}\dot{\mathbf{A}}_1(t)\frac{\partial f(\mathbf{p})}{\partial \mathbf{p}}.$$

Making use of (2) to (4) for the functions $f_{\sigma\sigma'}$ we obtain from (1) a set of four equations:

$$\frac{\partial f_{\sigma\sigma'}(\mathbf{p})}{\partial t} + \frac{e}{c}\dot{\mathbf{A}}_1(t)\frac{\partial f_{\sigma\sigma'}}{\partial \mathbf{p}} = (\mathbf{p}\sigma | \hat{\mathscr{H}}_0(\bar{x}) | \mathbf{p}\sigma'') f_{\sigma''\sigma'}(\mathbf{p})$$

$$- f_{\sigma\sigma''}(\mathbf{p})(\mathbf{p}\sigma'' | \hat{\mathscr{H}}_0(\bar{x}) | \mathbf{p}\sigma')$$

$$+ \frac{1}{\hbar^2}\int_0^\infty d\tau \sum_{\mathbf{q}}\sum_{\lambda=1}^{3}\left\{\exp\left[\frac{i\tau}{\hbar}(E_{\mathbf{p}\sigma} - E_{\mathbf{p}+\mathbf{q}\sigma''} - h\nu_{\mathbf{q}\lambda})\right]\right. \qquad (5)$$

$$\times F^{(1)}_{\sigma\sigma'} + \exp\left[\frac{i\tau}{\hbar}(E_{\mathbf{p}+\mathbf{q}\sigma''} - E_{\mathbf{p}\sigma'} + h\nu_{\mathbf{q}\lambda})\right]F^{(2)}_{\sigma\sigma'} + \exp\left[\frac{i\tau}{\hbar}(E_{\mathbf{p}\sigma}\right.$$
$$\left.\left. - E_{\mathbf{p}+\mathbf{q}\sigma''} + h\nu_{\mathbf{q}\lambda})\right]F^{(3)}_{\sigma\sigma'} + \exp\left[\frac{i\tau}{\hbar}(E_{\mathbf{p}+\mathbf{q}\sigma''} - E_{\mathbf{p}\sigma'} - h\nu_{\mathbf{q}\lambda})\right]F^{(4)}_{\sigma\sigma'}\right\},$$

where

$$F^{(1)}_{\sigma\sigma'} = N_{\mathbf{q}\lambda} A^{\mathbf{p}\sigma}_{\mathbf{p}+\mathbf{q}\sigma'''} A^{\mathbf{p}+\mathbf{q}\sigma''}_{\mathbf{p}\sigma'} f_{\sigma'''\sigma''}(\mathbf{p}+\mathbf{q}) - (N_{\mathbf{q}\lambda} + 1)$$
$$\times A^{\mathbf{p}\sigma'''}_{\mathbf{p}+\mathbf{q}\sigma''} A^{\mathbf{p}+\mathbf{q}\sigma''}_{\mathbf{p}\sigma'} f_{\sigma\sigma'''}(\mathbf{p}) + A^{\mathbf{p}\sigma_2}_{\mathbf{p}+\mathbf{q}\sigma'_2} A^{\mathbf{p}+\mathbf{q}\sigma''}_{\mathbf{p}\sigma'} f_{\sigma\sigma_2}(\mathbf{p}) f_{\sigma'_2\sigma''}(\mathbf{p}+\mathbf{q});$$

$$F^{(2)}_{\sigma\sigma'} = N_{\mathbf{q}\lambda} A^{\mathbf{p}\sigma}_{\mathbf{p}+\mathbf{q}\sigma''} A^{\mathbf{p}+\mathbf{q}\sigma'''}_{\mathbf{p}\sigma'} f_{\sigma''\sigma'''}(\mathbf{p}+\mathbf{q}) - (N_{\mathbf{q}\lambda} + 1)$$

$$\times A^{\mathbf{p}\sigma}_{\mathbf{p}+\mathbf{q}\sigma''} A^{\mathbf{p}+\mathbf{q}\sigma''}_{\mathbf{p}\sigma'''} f_{\sigma'''\sigma'}(\mathbf{p}) + A^{\mathbf{p}\sigma}_{\mathbf{p}+\mathbf{q}\sigma''} A^{\mathbf{p}+\mathbf{q}\sigma_2}_{\mathbf{p}\sigma'_2} f_{\sigma'_2\sigma'}(\mathbf{p}) f_{\sigma''\sigma_2}(\mathbf{p}+\mathbf{q}).$$

Repeated index in σ indicates summation. The expressions for $F^{(3)}_{\sigma\sigma'}$ and $F^{(4)}_{\sigma\sigma'}$ are obtained from $F^{(1)}_{\sigma\sigma'}$ and $F^{(2)}_{\sigma\sigma'}$ by the substitution $N_{\mathbf{q}\lambda} \rightleftarrows N_{\mathbf{q}\lambda} + 1$ and by change of sign for the term which is nonlinear in f.

We note that in the quasi-classical approximation on the coordinates and momenta of the electrons, the resulting equations are applicable also to the case of an inhomogeneous distribution of the variable field in the metal, i.e., in analysis of the skin effect. In this case it suffices to substitute the commutator $[\hat{\mathcal{H}}_0(\overline{\mathrm{x}}),\ \hat{\mathrm{F}}(\overline{\mathrm{x}})]$ which enters into (5) for the classical Poisson bracket:

$$\mathbf{v}\,\frac{\partial f_{\sigma\sigma'}}{\partial \mathbf{r}}+\frac{e}{c}\,[\mathbf{v}\times\mathbf{H}_0]\,\frac{\partial f_{\sigma\sigma'}}{\partial \mathbf{p}}$$

$$+(\sigma\,|\,\mu\,\hat{\sigma}\cdot\mathbf{H}\,|\,\sigma'')\,f_{\sigma''\sigma'}-f_{\sigma\sigma''}\,(\sigma''|\,\mu\,\hat{\sigma}\cdot\mathbf{H}|\sigma'),$$

while the collision integral remains as before (taking into consideration the fact that the desired functions depend on the coordinates). The collision integral remains as before because the matrix elements $(\mathrm{p}\sigma\,|\,\hat{\mathrm{F}}\,|\,\mathrm{p}'\sigma')$, which are nondiagonal in the momentum, are small since the dimensions of the inhomogeneity of the field (skin depth) are always large in comparison with the de Broglie wavelength of the electron $\hbar/\mathrm{p}$ (p extends to the limiting Fermi surface since only electrons with energies close to the limiting energy ϵ_0 make a contribution to the resonance).

3. To simplify Eq. (5), it is necessary to know the form of the matrix elements $A^{\mathrm{p}\sigma}_{\mathrm{p}'\sigma'}$. Here we limit ourselves to the alkali metals, for which the wave functions $\psi_{\mathrm{p}\sigma}$ with consideration of spin orbit coupling were computed by Yafet:[8]

$$\hbar u_{\mathbf{p}1,2}=\{\hbar u_0+i\,(\mathbf{p}\cdot\mathbf{r})\,u_1$$

$$\pm C_1\,[\mathbf{p}\cdot\mathbf{r}]_z\,u_2\}\,\chi_{1/2,-1/2}+C_2[\mathbf{p}\cdot\mathbf{r}]_{x\pm iy}u_3\chi_{-1/2,1/2},$$

where $\chi_{1/2}$ and $\chi_{-1/2}$ are the eigenfunctions of the operator $\hat{\sigma}_z$; the z axis is directed along the field H_0. It was shown in reference 5 that $u_1(r) \sim u_2(r) \sim u_3(r)$, and $C_1 \sim C_2 \sim g-2$, where g is the splitting factor of the conduction electron. The matrix elements consequently will be:

$$-(A^{\mathbf{p}2}_{\mathbf{p}'2})^*=A^{\mathbf{p}1}_{\mathbf{p}'1}=\left(\frac{\Delta}{2V_0Mh\nu_{\mathbf{q}\lambda}}\right)^{1/2}C\,\{i\ \ \mathbf{e}_{\mathbf{q}\lambda}\cdot(\mathbf{p}'-\mathbf{p})$$

$$+C_1\,[\mathbf{e}_{\mathbf{q}\lambda}\times(\mathbf{p}'+\mathbf{p})]_z\};$$

$$A^{\mathbf{p}1}_{\mathbf{p}'2}=\left(\frac{\Delta}{2V_0Mh\nu_{\mathbf{q}\lambda}}\right)^{1/2}CC_1\,\{[\mathbf{e}_{\mathbf{q}\lambda}\times(\mathbf{p}'+\mathbf{p})]_x-i\,[\mathbf{e}_{\mathbf{q}\lambda}\times(\mathbf{p}'+\mathbf{p})]_y\};$$

$$C=\int\limits_{(\Delta)}u_0\,(r)\,u_1\,(r)\,(\nabla V\cdot\mathbf{r})\,d\mathbf{r}.$$

the quantity C is of the order of the mean energy of the electron in the crystal.

In the following we shall assume a simple Debye model for the lattice vibrations, in which the vector $\mathbf{e}_{\mathrm{q}1}$ is parallel to the momentum of the phonon q while $\mathbf{e}_{\mathrm{q}2}$ and q are mutually orthogonal. We transform from a summation over q to integration:

$$\sum_{\mathbf{q}}\to\frac{V_0}{(2\pi\hbar)^3}\int\limits_{q_{\min}}^{q_{\max}}q^2dq\int d\Omega_{\mathbf{q}},\ \ q_{\max}=\frac{2\pi\hbar}{a}\left(\frac{3}{4\pi}\right)^{1/3};$$

a is the lattice constant; $q_{\min}$ is determined from the law of conservation of energy. Moreover, for simplicity, we do not distinguish between transverse and longitudinal sound velocities: $v_\perp = v_\parallel = v_s$ (i.e., the phonon energies $h\nu_{\mathrm{q}\lambda} = v_s q$, $\lambda = 1, 2, 3$). We also assume that $E_{\mathrm{p}1} = \epsilon - \mu H_0$, $E_{\mathrm{p}2} = \epsilon + \mu H_0$, $\epsilon = p^2/2m^*$, m^* is the effective mass of the electron.

It is not difficult to prove that in the equations for $2f_z = f_{11} - f_{22}$ and f_{12}, we can discard terms with $\mathrm{\AA}$. In this case the desired functions will depend only on $|\mathrm{p}|$, inasmuch as it is assumed that $\epsilon = \epsilon(|\mathrm{p}|)$. We can then show that the terms in the collision integral containing matrix elements of the type $A^{\mathrm{p}1}_{\mathrm{p}'2}A^{\mathrm{p}'1}_{\mathrm{p}2}$ and $A^{\mathrm{p}1}_{\mathrm{p}'2}A^{\mathrm{p}'1}_{\mathrm{p}2}$ disappear in the integration over p and q. The equations in this case are significantly simplified.

4. Multiplying the equations for f_{11} and f_{22} by $\mu(2\pi\hbar)^{-3}d\mathrm{p}$ and integrating over the entire momentum space, we obtain for the "longitudinal" component of the magnetization

$$M_z=\frac{\mu}{(2\pi\hbar)^3}\int(f_{11}-f_{22})\,d\,\mathbf{p}\equiv\frac{2\mu}{(2\pi\hbar)^3}\int f_z d\mathbf{p}$$

the equation

$$\frac{\partial M_z}{\partial t}=\frac{2\mu}{\hbar}\,\mathrm{Im}\,[(H_{1x}-iH_{1y})\ M^*_{12}]$$

$$+\frac{4\mu}{\hbar^2\,(2\pi\hbar)^6}\int\limits_0^\infty d\tau\int d\mathbf{p}\int\ d\mathbf{q}\ \sum_{\lambda=1}^{3}\,|\,A^{\mathbf{p}1}_{\mathbf{p}+\mathbf{q}2}\,|^2$$

$$\times\Big\{\cos\frac{\tau}{\hbar}\,(E_{\mathbf{p}1}-E_{\mathbf{p}+\mathbf{q}2}-v_s q)[N_{\mathbf{q}\lambda}f_{22}\,(\mathbf{p}+\mathbf{q})$$

$$-(N_{\mathbf{q}\lambda}+1)f_{11}(\mathbf{p})+f_{11}\,(\mathbf{p})\,f_{22}\,(\mathbf{p}+\mathbf{q})] \tag{6}$$

$$+\cos\frac{\tau}{\hbar}\,(E_{\mathbf{p}1}-E_{\mathbf{p}+\mathbf{q}2}+v_s q)\,[(N_{\mathbf{q}\lambda}+1)\,f_{22}\,(\mathbf{p}+\mathbf{q})$$

$$-N_{\mathbf{q}\lambda}f_{11}\,(\mathbf{p})-f_{11}\,(\mathbf{p})\,f_{22}(\mathbf{p}+\mathbf{q}\,)]\Big\}.$$

Here,

$$M_{12}=\frac{2\mu}{(2\pi\hbar)^3}\int f_{12}d\,\mathbf{p}\equiv\frac{\mu}{(2\pi\hbar)^3}\int(f_x-if_y)\,d\,\mathbf{p}\equiv M_x-iM_y.$$

Inasmuch as thermal equilibrium is obtained much more rapidly than spin equilibrium, we can make use of the representation of partial equilibrium, i.e., we can write the functions f_{11} and f_{22} which enter into (6) as

$$f_{11}\,(\mathbf{p})=f_0\,(\varepsilon-\mu H_0+\Delta\varepsilon);\ \ f_{22}\,(\mathbf{p})=f_0\,(\varepsilon+\mu H_0-\Delta\varepsilon);$$

$$f_0\,(x)=(e^{(x-\varepsilon_0)/kT}+1)^{-1}, \tag{7}$$

where $\Delta\epsilon \to 0$ as the system tends toward complete equilibrium; $\Delta\epsilon \lesssim \mu H_0$. We then obtain

$$M_{0z}-M_z=\Delta\varepsilon\,(\mu m^* p_0/\pi^2\hbar^3)\equiv(\chi/\mu)\,\Delta\varepsilon;\quad M_{0z}=\chi H_0. \tag{8}$$

the solutions for M_Z must be time independent if we take a rotating magnetic field: $H_{1x} - iH_{1y} = H_{10}e^{-i\omega t}$ and the solution M_{12} must be sought in the form $M_{12}e^{-i\omega t}$. Then, carrying out the integration in (6) over τ and over all angles except the angle between **p** and **q** we get after summation over λ:

$$
\begin{aligned}
&-\operatorname{Im}(H_{10}M_{12}^{*})\\
&= \frac{4(2\pi)^3 C^2 C_1^2}{3Mv_s(2\pi\hbar)^6}\int_0^{\infty} p^2 dp \int_{q_{\min}}^{q_{\max}} q\,dq \int_0^{\pi} (2\mathbf{p}+\mathbf{q})^2 \sin\theta\, d\theta\\
&\times\Big\{\delta\Big(\frac{pq}{m^*}\cos\theta + \frac{q^2}{2m^*} + 2\mu H_0 + v_s q\Big)[N_q f_{22}(\mathbf{p}+\mathbf{q})\\
&-(N_q+1)f_{11}(\mathbf{p}) + f_{11}(\mathbf{p})\times f_{22}(\mathbf{p}+\mathbf{q})] \qquad (9)\\
&+\delta\Big(\frac{pq}{m^*}\cos\theta + \frac{q^2}{2m^*} + 2\mu H_0 - v_s q\Big)[(N_q+1) f_{22}(\mathbf{p}+\mathbf{q})\\
&-N_q f_{11}(\mathbf{p}) - f_{11}(\mathbf{p}) f_{22}(\mathbf{p}+\mathbf{q})]\Big\}.
\end{aligned}
$$

After integration over θ, the right hand side of (9) reduces to a sum of two integrals in which the regions of integration of p and q are bounded by the inequalities

$$|q/2p + 2\mu H_0 m^*/pq \pm m^* v_s/p| \leqslant 1$$

by virtue of the fact that $|\cos\theta| \leq 1$. The values of p close to p_0, the limiting momentum of the electron, make the principal contribution to the integrals. Therefore the inequalities are automatically satisfied while the condition

$$q_{\min} \approx 2\mu H_0 m^*/(p_0 \pm m^* v_s)$$

applies to q. Inasmuch as $p_0 \gg m^* v_s$, we can consider the regions of integration in the two integrals to be identical. On integration over θ we obtain the expressions $4p^2 - q^2 - 8\mu H_0 m^* \pm 4m^* v_s q$ under the integral sign. These expressions we can set equal to $4p^2$, since the contribution of the other terms in the integral is significantly less than the contribution from $4p^2$. Thus Eq. (9) reduces to

$$
\begin{aligned}
&-\operatorname{Im}(H_{10}M_{12}^{*})\\
&= \frac{16(2\pi)^3 m^* C^2 C_1^2}{3Mv\ (2\pi\hbar)^6}\int_0^{\infty} p^3 dp \int_{q_{\min}}^{\max} dq\,(e^{\Delta\varepsilon/kT} - e^{-\Delta\varepsilon/kT})\\
&\times\exp\Big\{\frac{\varepsilon-\mu H_0-\varepsilon_0}{kT}\Big\} f_0(\varepsilon-\mu H_0+\Delta\varepsilon) \qquad (10)\\
&\times\{N_q f_0(\varepsilon-\mu H_0-\Delta\varepsilon-v_s q)\\
&+(N_q+1) f_0(\varepsilon-\mu H_0-\Delta\varepsilon+v_s q)\}.
\end{aligned}
$$

for $\Delta\epsilon \ll kT$ we can introduce the relaxation time. Actually, expanding the function under the integral sign in $\Delta\epsilon/kT$ and keeping only terms of the expansion that are linear in $\Delta\epsilon$ we get, after regrouping,

$$
\begin{aligned}
&\frac{2\Delta\varepsilon}{kT}\exp\Big\{\frac{\varepsilon-\mu H_0-\varepsilon_0}{kT}\Big\} f_0^{-2}(\varepsilon-\mu H_0)\{2N_q+1\\
&+f_0(\varepsilon-\mu H_0+v_s q) - f_0(\varepsilon-\mu H_0-v_s q)\}. \qquad (11)
\end{aligned}
$$

If we make use of the fact that

$$\frac{1}{kT}\exp\Big(\frac{\varepsilon-\mu H_0-\varepsilon_0}{kT}\Big)\cdot f_0^{-2}(\varepsilon-\mu H_0) \approx \delta(\varepsilon-\mu H_0-\varepsilon_0),$$

then (11) reduces to the form

$$4\Delta\varepsilon\Big(\sinh\frac{v_s q}{kT}\Big)^{-1}\delta(\varepsilon-\mu H_0-\varepsilon_0). \qquad (12)$$

Taking into account the coupling (8), substituting (12) in (10), and carrying out integration over p and q, we obtain the equation for M_Z:

$$\operatorname{Im}(\Omega_{10}M_{12}^{*}) = (M_z - M_{0z})/\tau_l; \quad \Omega_{10} = 2\mu H_{10}/\hbar.$$

Here τ_l is the "longitudinal" spin relaxation time:

$$\tau_l = \frac{\alpha}{T}\Big(\ln\frac{\tanh(T_D/T)}{\tanh(T_m/T)}\Big)^{-1}; \quad \alpha = \frac{3\mu^2\hbar\rho v_s^2}{16\pi\chi k C^2 C_1^2}, \qquad (13)$$

χ is the paramagnetic susceptibility of the metal; $\rho = M/V$ is the density of the metal: T_D is the Debye temperature; $T_m = (v_s/kv)2\mu H_0$; v_s is the sound velocity; v is the velocity of the electron on the Fermi surface. If the dimensions of the specimen being considered are such that $\hbar/d > 2\mu H_0/v$, we must take $T_m = \hbar v_s/kd$. Equation (13) is valid in the temperature region $kT \gg \mu H_0$ if the resonance is close to saturation, i.e., $M_Z \approx 0$. Far from saturation of the resonance, the region of applicability of (13) extends in the direction of lower temperatures. For $T \gg T_D$

$$\tau_l = \alpha/T \ln(T_D/T_m),$$

which for $T_m = \hbar v_s/kd$ is identical with the expression (58) of the work of Elliott[5] with accuracy to within a coefficient 3/16. However, in reference 5, $\tau_l \sim T^{-3}$ for $T \ll T_D$ while it follows from (13) that $\tau_l = \alpha/T \ln(T/T_m)$ which agrees with experiment.* The quantitative agreement of the relaxation time of (13) with that observed is also satisfactory. Thus for sodium, if we substitute in (13) $\rho = 1$ g/cm^3, $\chi = 6 \times 10^{-7}$, $C_1 = 3 \times 10^{-4}$, $C = 10^{-12}$ erg, $v_s = 10^5$ cm/sec, we have: $\alpha = 10^{-5}$. The quantity $\ln[\tanh(T_D/T)/\tanh(T_m/T)] \approx 10$ for all $kT \gg \mu H_0$ (for $H_0 = 10^4$ Oe). Thus, $\tau_l \approx 10^{-6}T^{-1}$ sec, which agrees with data of Thayer and Kip[9] for sodium.

5. We now obtain the equation for the (transverse) component of the magnetization M_{12} =

---

*It is pointed out in reference 9 that Yafet obtained the same result for τ_l: $\tau_l \sim 1/T$ if $T \ll T_D$.

$M_x - iM_y$. We seek a solution of the equation for f_{12} in the form $f_{12}e^{-i\omega t}$. In the equation for f_{12}, we complete the integration over τ. In this case the exponential functions in the integrand lead to appearance of functions of the type $\delta_+(E_{p1} - E_{p+q2} - v_s q - \hbar\omega) \times \delta_+(x) = \delta(x) + i/\pi x)$. We can show that the part of the collision integral due to the second terms in δ_+ is negligibly small. We now note that under the condition $kT \gg \mu H_0$, we can seek a solution of f_{12} in the form $f_{12}\delta(\epsilon - \epsilon_0)$. Actually, the function f_z entering into the equation can be written as $f_z\delta(\epsilon - \epsilon_0)$ for $kT \gg \mu H_0$. Furthermore, if we substitute in the equation for f_{12} the solution for the form $f_{12}(p_0)\delta(\epsilon - \epsilon_0)$ then we can show that $\delta(\epsilon - \epsilon_0)$ will be a general factor of the equation. Multiplying this equation for f_{12} by $\mu(2\pi\hbar)^{-3}dp$ (similarly to what we have done previously), we obtain:

$$i(\omega - \Omega_0)M_{12} + i\Omega_{10}M_z = \frac{2}{3}M_{12}\frac{C^2C_1^2m^*p_0}{\pi\hbar^4Mv_s}\int\limits_{q_{\min}}^{q_{\max}} dq\,\{8N_q + 4$$

$$+ f_{11}(E_{\mathbf{p}_01} + v_sq) + f_{22}(E_{\mathbf{p}_02} + v_sq)$$

$$+ f_{22}(E_{\mathbf{p}_01} + v_sq) + f_{11}(E_{\mathbf{p}_02} + v_{sq}) - f_{11}(E_{\mathbf{p}_01} - v_sq)$$

$$- f_{22}(E_{\mathbf{p}_02} - v_sq) - f_{22}(E_{\mathbf{p}_01} - v_sq) - f_{11}(E_{\mathbf{p}_02} - v_sq)\}.$$

In setting up this equation use is made of the relation $M_{12} = 8\pi m^*p_0\mu(2\pi\hbar)^{-3}f_{12}(p_0)$. Substituting in the expression under the integral the Eq. (7) we have in first approximation for $\Delta\epsilon/kT$ and $\mu H_0/kT$:

$$i(\omega - \Omega_0)M_{12} + i\Omega_{10}M_z = M_{12}/\tau_t;\ \Omega_0 = 2\mu H_0/\hbar,$$

where τ_t is the "transverse" spin relaxation time which agrees exactly with Eq. (13) for the "longitudinal" relaxation time.

In conclusion, the authors express their gratitude to Prof. I. M. Lifshitz for discussion of the results of the work.

---

[1] F. J. Dyson, Phys. Rev. **98**, 349 (1955).

[2] V. P. Silin, J. Exptl. Theoret. Phys. (U.S.S.R.) **30**, 421 (1956), Soviet Phys. JETP **3**, 305 (1957).

[3] Azbel', Gerasimenko, and Lifshitz, J. Exptl. Theoret. Phys. (U.S.S.R.) **31**, 357 (1956), **32**, 1212 (1957); Soviet Phys. JETP **4**, 276, **5**, 986 (1957). Lifshitz, Azbel', and Gerasimenko, J. Phys. Chem. Solids **1**, 164 (1956).

[4] A. W. Overhauser, Phys. Rev. **89**, 689 (1953).

[5] R. J. Elliott, Phys. Rev. **96**, 266 (1954).

[6] N. N. Bogoliubov and K. P. Gurov, J. Exptl. Theoret. Phys. (U.S.S.R.) **17**, 614 (1947).

[7] R. N. Gurzhi, J. Exptl. Theoret. Phys. (U.S.S.R.) **33**, 451 (1957, Soviet Phys. JETP **6**, 352 (1958).

[8] Y. Yafet, Phys. Rev. **85**, 478 (1952).

[9] G. Feher and A. F. Kip, Phys. Rev. **98**, 337 (1955).

Translated by R. T. Beyer
253

SOVIET PHYSICS JETP VOLUME 35(8), NUMBER 5 MAY, 1959

ON THE INTERACTION BETWEEN SMALL DISTURBANCES AND DISCONTINUITIES IN MAGNETOHYDRODYNAMICS AND ON THE STABILITY OF SHOCK WAVES

V. M. KONTOROVICH

Institute of Radiophysics and Electronics, Academy of Sciences, Ukrainian S.S.R.

Submitted to JETP editor May 28, 1958; resubmitted June 30, 1958

J. Exptl. Theoret. Phys. (U.S.S.R.) 35, 1216-1225 (November, 1958)

A simple geometrical method is presented for the construction of waves (reflected and refracted) diverging from a surface of discontinuity and produced by the incidence of a plane monochromatic wave on a plane stationary surface of discontinuity in a medium describable by the equations of magnetohydrodynamics. The case of a shock wave is considered.

On the basis of the results obtained, the stability of shock waves with respect to splitting up is investigated as regards obliquely incident disturbances. The change in frequency resulting from the interaction of small disturbances with shock waves is considered.

1. INTRODUCTION

WITHIN a stationary homogeneous flow of a fluid of infinite conductivity situated in a magnetic field, there exist several types of small disturbances with different dispersion laws $\omega = \omega(\mathbf{k})$: magnetohydrodynamic, magnetoacoustic (slow and fast), and entropy waves. In the presence of discontinuities, these disturbances can be transformed one into another; when some one disturbance (of frequency ω and propagation vector $\mathbf{k}$) falls on a discontinuity, the waves (reflected and refracted) diverging from the discontinuity will contain, generally speaking, disturbances of all types.

Because of the relatively complicated dispersion law in the case of magnetoacoustic waves, the analytic solution for the propagation vectors (phase velocities) of the divergent waves (the laws of reflection and refraction) becomes inconvenient, since the solution involves roots of a fourth-degree equation. Nevertheless, the problem admits of a simple geometric solution with respect to which the laws of reflection and refraction can be formulated. The calculation of the amplitudes of the divergent waves in terms of the amplitude of the incident disturbance is not given in the present article.

Recently Akhiezer, Liubarskii, and Polovin[1] have investigated the stability of shock waves with respect to splitting, under disturbances that depend only on the distance to the shock wave and on the time (in our treatment this corresponds to normal incidence of the disturbance on the discontinuity).

The problem considered here allows us to investigate the stability of shock waves with respect to splitting under obliquely-incident disturbances as well. Of considerable interest is the fact that within a definite angular interval the components of the phase and of the group velocities along the normal to the discontinuity have opposite signs, and to obtain the correct solution of the problem of stability we must therefore perform the division into incident and divergent waves by considering not their phase velocities but their group velocities.

In ordinary hydrodynamics the interaction of sound with shock waves has been investigated (for the case of an ideal gas) by Blokhintsev,[2] Burgers,[2] and Brillouin,[3] and (in the case of an arbitrary nonviscous fluid) by the author.[4*]

2. SMALL DISTURBANCES

We denote by δA the amplitudes of disturbances proportional to $\exp i(\mathbf{k}\cdot\mathbf{r} - \omega_0 t)$ in the coordinate system in which the fluid is at rest.

---

*In D'iakov's articles[5] the interactions between stationary discontinuities of low intensity, and also between stationary weak discontinuities and shock waves, have been studied within the framework of ordinary hydrodynamics. We note that owing to the absence of dispersion, the laws of reflection and refraction, and also the amplitudes of the divergent discontinuities, agree with the corresponding quantities for plane monochromatic waves. In magnetohydrodynamics, since the phase velocity depends only on the direction $\mathbf{k}/k$ and not on the frequency ω, the results of the present investigation must also be applicable to discontinuities interacting with shock waves. Naturally, it is not possible to derive from this the shape of the perturbed shock wave, nor the results with respect to weak discontinuities (discontinuities of the derivatives). On the other hand, an investigation of monochromatic waves enables us to determine such quantities as frequency shifts produced by reflection or refraction at a discontinuity (cf. Sec. 7).

These disturbances are therefore proportional to $\exp i(\mathbf{k}\cdot\mathbf{r} - \omega t)$ in the system in which the surface of the unperturbed discontinuity is at rest. We state here only those characteristics of small disturbances[6,7] needed for subsequent discussion, i.e., the dispersion laws $\omega_0(\mathbf{k})$.

Entropy wave. Just as in the case of hydrodynamics, the disturbance in the entropy $\delta\sigma$ and the disturbance in the density $\delta\rho$ associated with it are at rest with respect to the fluid. All the other quantities are undisturbed:

$$\omega_0(\mathbf{k}) = 0. \tag{2.1}$$

Magnetohydrodynamic waves or Alfven waves. The thermodynamic quantities are undisturbed. The velocity and the related magnetic field both oscillate:

$$\omega_0(\mathbf{k}) = \pm\mathbf{k}\cdot\mathbf{u}, \quad \mathbf{u} \equiv \mathbf{H}/\sqrt{4\pi\rho}. \tag{2.2}$$

Magnetoacoustic waves. This is an adiabatic motion $(\delta\sigma = 0)$ in which the pressure and the velocity, density, and magnetic field associated with it all oscillate:

$$\omega_0^2(\mathbf{k}) = \frac{k^2}{2}\left[s^2 + u^2 \pm \sqrt{(s^2+u^2)^2 - 4s^2u^2\cos^2\theta}\right], \tag{2.3}$$

$s^2 = (\partial p/\partial\rho)_\sigma$ is the square of the velocity of sound.

In the system of coordinates in which the discontinuity is at rest while the fluid moves with the velocity $\mathbf{v}$, the frequency ω of the disturbance has the form

$$\omega_0 = \omega - \mathbf{k}\cdot\mathbf{v}. \tag{2.4}$$

By introducing the phase velocity of the disturbance with respect to the fluid at rest, which depends in our case only on the direction of propagation,

$$\mathbf{V}(\boldsymbol{\varkappa}) = \frac{\omega_0(\mathbf{k})}{k}\boldsymbol{\varkappa}, \qquad \boldsymbol{\varkappa} \equiv \frac{\mathbf{k}}{k}, \tag{2.5}$$

we can write the relation between the frequency and the propagation vector in the form

$$\omega - \mathbf{k}\cdot\mathbf{v} = \pm kV(\boldsymbol{\varkappa}), \tag{2.6}$$

where we take V to denote the absolute value of the phase velocity. For the Alfven waves we have

$$V_A = u|\cos\theta|. \tag{2.7}$$

Magnetoacoustic waves can be separated into two branches (fast and slow waves):

$$V_\pm = \frac{1}{2}\left[s^2 + u^2 \pm \sqrt{(s^2+u^2)^2 - 4s^2u^2\cos^2\theta}\right]. \tag{2.8}$$

The plus sign corresponds to the fast waves which go over into ordinary sound when the magnetic field is removed, the minus sign corresponds to the second branch, the slow sound, which together with the Alfven waves degenerates, in going over to ordinary hydrodynamics, into a disturbance of the curl of the velocity (rotational wave) which is at rest with respect to the motionless fluid. In a moving fluid all the disturbances considered above are, in addition, carried along by the stream.

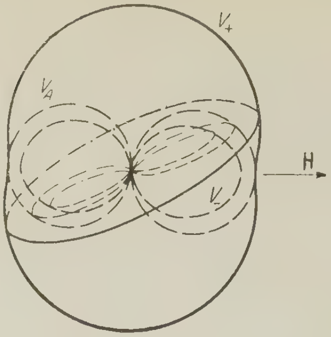

FIG. 1. The surfaces $V(\varkappa)$ and the interaction of these surfaces with the plane of incidence.

We shall make use hereinafter of velocity vector diagrams which specify V_A, V_+, V_-, in accordance with (2.7) and (2.8), as functions of the direction κ.[7] The speed of propagation of a disturbance of a given type is determined by the length of the vector drawn from the origin in the direction $\mathbf{k}$ to its intersection with the corresponding surface $V(\kappa)$ (Fig. 1). $V(\kappa)$ represent surfaces of revolution with respect to the direction of the magnetic field $\mathbf{H}$ and possess central symmetry with respect to the origin.

3. BOUNDARY CONDITIONS AT THE SURFACE OF DISCONTINUITY

At the surface of discontinuity in the coordinate system I, in which the surface of discontinuity is at rest, the system of boundary conditions which follows from the continuity of the fluxes of mass $\rho\mathbf{v}$, of energy $\mathbf{g}$, of momentum π_{ik}, of the tangential components of the electric field $-[\mathbf{v}\times\mathbf{H}]/c$, and of the normal component of the magnetic field[6,7] has the form

$$\begin{gathered}\{\rho v_n\} = 0, \quad \{g_n\} = 0, \quad \{\pi_{in}\} = 0, \\ \{[\mathbf{v}\times\mathbf{H}]_t\} = 0, \quad \{H_n\} = 0.\end{gathered} \tag{3.1}$$

Here n and t denote components normal or tangential to the discontinuity. $\{A\}$ denotes the abrupt change in the value of the quantity A at the discontinuity. In the coordinate system I we shall choose the x axis to be directed along the normal to the discontinuity in the direction of flow (for shock waves). The quantities belonging to the semi-infinite space $\overline{\text{II}}$, for which $x < 0$ (ahead of the shock wave), will be denoted by $\overline{A}$ to distinguish them from the quantities A belonging to the semi-

infinite space Π (behind the shock wave);
$\{A\} \equiv A - \bar{A}$.

When a small disturbance falls on the discontinuity it is necessary, in the approximation linear in terms of the amplitude of the incident disturbance $\delta A^{(i)}$ (or $\overline{\delta A}^{(i)}$), to take into account the deformation and the additional velocity of the surface of discontinuity. In this approximation the boundary conditions for the disturbance can be written[8] with reference to the unperturbed surface of discontinuity at $x = 0$ (cf. the cases of ordinary hydrodynamics[9] and relativistic hydrodynamics[10]).

For disturbances of the type $\sim \exp i(\mathbf{k}\cdot\mathbf{r} - \omega t)$ we must guarantee the "continuity" at the surface of discontinuity ($x = 0$) of the frequency ω and of the component $\mathbf{q}$ of the propagation vectors $\mathbf{k}^{(i)}$ and $\mathbf{k}^{(d)}$, i.e., the divergent waves will have the same frequency and component of the propagation vector as the incident wave. We note that this is not associated with the specific form of the boundary conditions (3.1), but only with the smallness of the disturbance, which allows us to reduce the perturbed boundary condition to the plane $x = 0$.[11] As a consequence of linearity, the equation of the disturbed discontinuity has the form

$$x = \eta \exp i(\mathbf{q}\cdot\mathbf{r} - \omega t) \tag{3.2}$$

and is characterized by the amplitude η. By expanding the incident and the divergent disturbances in terms of eigenwaves, we obtain from (3.1) a system of equations for the amplitudes of the divergent waves $\delta A^{(d)}$ and of the amplitude of the disturbance of the discontinuity η. When $\delta A \sim \exp i(\mathbf{k}\cdot\mathbf{r} - \omega t)$, the last perturbed equation in (3.1) is a consequence of the two preceding ones. Finally we obtain a system of seven inhomogeneous equations enabling us to find $\delta A^{(d)}$ and η in terms of given values of $\delta A^{(i)}$:

$$\sum T_{ik}\delta A_k^{(d)} + \sum T_{il}\delta \bar{A}_l^{(d)} + T_i\eta = \sum U_{im}\delta A_m^{(i)} + \sum U_{in}\delta \bar{A}_n^{(i)}, \quad i = 1, 2, \ldots, 7 \tag{3.3}$$

Here we take into account the fact that both incident and divergent waves, generally speaking, may appear in Π and in $\bar{\Pi}$. The specific form of the coefficients will be needed only for the calculation of the amplitudes, where it will be given in due course.

4. THE LAWS OF REFLECTION AND REFRACTION

The relation between the angles of incidence and reflection or refraction may be obtained by equating the frequency ω and the component $\mathbf{q}$ of the propagation vector along the surface of discontinuity for the incident and the divergent waves.

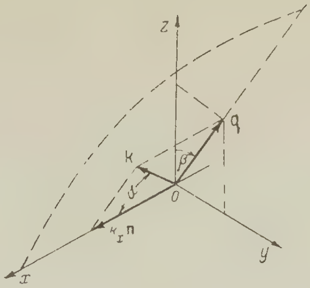

FIG. 2. The plane of incidence contains the normal to the discontinuity (0x) and the propagation vector **k**. The surface of discontinuity (zy) contains the component of the propagation vector along the discontinuity **q**.

From this it follows that the propagation vectors of all the divergent waves $\mathbf{k}^{(d)}$ lie in the plane of incidence formed by $\mathbf{k}^{(i)}$ and by the normal to the undisturbed discontinuity $\mathbf{n}$ (the x axis). In future we shall consider the intersections of the surfaces $V(\kappa)$ (Fig. 1) with the plane of incidence. We introduce the angles α and β defining the direction of κ:

$$k_i(q \cot\alpha,\quad q\sin\beta,\quad q\cos\beta). \tag{4.1}$$

The angle α between the vector $\mathbf{k}$ and the normal $\mathbf{n}$ lies in the plane of incidence. The angle β (Fig. 2) defines the position of the plane of incidence. The intersection gives the curves $V(\alpha)$ [more accurately $V(\alpha, \beta)$ for $\beta = \text{const}$]. The equations of these curves will be obtained from (2.7) and (2.8) by the substitution

$$\cos\theta = \cos\alpha \frac{H_x}{H} + \sin\alpha \frac{\mathbf{q}\cdot\mathbf{H}}{qH}. \tag{4.2}$$

We introduce the angle ψ, which plays a fundamental role in subsequent development:

$$\cot\psi \equiv (\omega - \mathbf{q}\cdot\mathbf{v})/qv_x. \tag{4.3}$$

By using the relation (2.6) we shall obtain a formula for ψ in terms of the velocity vectors

$$\cot\psi = (v_x \cos\alpha \pm V(\alpha))/v_x \sin\alpha. \tag{4.4}$$

A simple geometric meaning of the angle ψ (Fig. 2) follows from (4.4): in the system of coordinates in which the velocity of the fluid $\mathbf{v}$ has only a normal component, it is the angle between the total velocity of the disturbance $\pm V\boldsymbol{\kappa} + v_x\mathbf{n}$ (taking drift into account) and the velocity of this disturbance $\pm V\boldsymbol{\kappa}$ with respect to the fluid at rest.

The solution with the minus sign corresponds to the wave for which $\omega_0 < 0$ and for which the propagation vector and the phase velocity are therefore oppositely directed [$\delta A \sim \exp(\mathbf{k}\cdot\mathbf{r} + |\omega_0|t)$]. Such disturbances result from the fact that the flow is "supersonic" for the given disturbance.

It follows directly from (4.3) that the angle ψ is not changed on reflection. This is the content of the law of reflection

$$\psi^{(i)} = \psi^{(r)}. \tag{4.5}$$

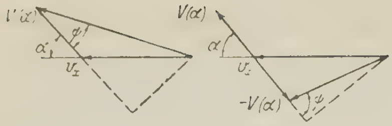

FIG. 3. The angles α and ψ for $\omega_0 > 0$ (on the left) and for $\omega_0 < 0$.

It follows from (4.3) that the law of refraction has the form

$$\{v_x \cot\psi\} + \frac{q}{q}\{v\} = 0. \tag{4.6}$$

In the case when the tangential components do not undergo a discontinuity (ordinary hydrodynamics, parallel and perpendicular shock waves in magnetohydrodynamics), $q\{v\} = 0$, and the law of refraction takes on the simple form of the "law of tangents":[4]

$$\tan\psi/\tan\bar{\psi} = v/\bar{v}. \tag{4.7}$$

We now turn to the construction of the propagation vectors κ restricted by the relation (4.5), i.e., to the construction of $\alpha^{(r)}$ in terms of the given $\alpha^{(i)}$. We see (Fig. 3) from (4.4) that the segment of the normal $-v_x$ subtends the angle ψ at the end of the vector $V = V\kappa$ [in the case of the plus sign in formula (4.4)], or subtends the angle $\pi - \psi$ at the end of the vector $V = -V\kappa$ [in the case of the minus sign in (4.4)]. It follows from the law of reflection (4.5) that if the segment subtends the angle ψ at the end of the vector $V^{(i)}$ of the incident wave, then it must subtend either the same angle ψ or the angle $\pi - \psi$ at the ends of the vectors $V^{(r)}$ for all the reflected waves. This means that the only waves that can be reflected are those for which the ends of the vectors $V^{(r)}$ lie on the circle drawn through the ends of the segment $-v_x$ and the end of the vector $V^{(i)}$. We note that in virtue of the central symmetry of the surfaces $V(\kappa)$, each point of the graph of V corresponds also to a point of the graph of $-V$. Naturally, this property is preserved also for a central section, such as the section defined by the plane of incidence. We can thus construct, with the aid of the velocity vector diagram in the plane of incidence, the phase velocity vectors satisfying the boundary condition of reflection. To do this we must draw a circle through the ends of the segment $-v_x$ and the end of the velocity vector of the incident wave $V^{(i)}$. The points of intersection of this circle with the curves $V(\alpha)$ will give the ends of the required vectors $V = V\kappa$, $V = -V\kappa$ for the intersections with the larger and the smaller circular arcs respectively (for $\psi < \pi/2$) (Fig. 4). The points of intersection of the circle with the curve $V_+(\alpha)$ will give the velocity vector (and the corresponding angle α) for fast sound. The points of intersection of the circle with the curve $V_-(\alpha)$ will give the velocity vector (and the corresponding angle) for slow sound. The points of intersection of the circle with the curve $V_A(\alpha)$ will determine the velocity vector for the Alfven wave.

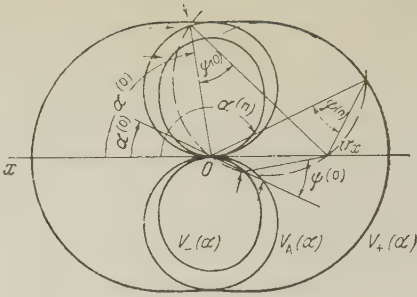

FIG. 4. Arrows indicate points of intersection of the ψ circle circle (dotted line) with the curves $V_+(\alpha)$, $V_A(\alpha)$, $V_-(\alpha)$. The vectors drawn from the center to these points are the velocities of the reflected waves behind the shock wave, which arise when the V_+ wave is incident on the discontinuity. The point at which the ψ circle is tangent to V_+ (dot-dashed line) divides the V_+-waves into incident and divergent ones.

In the drawing the magnetic field lies in the plane of the discontinuity and in the plane of incidence. This case is not in any way special for making the construction.

For a given value of v_x, each angle ψ corresponds to its own circle (ψ circle). To construct the refracted waves we must, in accordance with the law of refraction (4.6), find the angle $\bar{\psi}$ in terms of the angle ψ, and then construct the $\bar{\psi}$ circle on the segment $-\bar{v}_x$. The points of intersection with $V(\alpha)$ and $\bar{V}(\alpha)$ respectively determine the types and velocities of the disturbances which are restricted by the laws (4.5) and (4.6). For the Alfven waves, the angles α may be easily found in terms of the given angle ψ also in analytic form, by making use of formulas (4.4), (2.7), and (4.2). However, in the case of magnetoacoustic waves the analytic solution of the problem of refraction, i.e., of determining the angles α in terms of the given angle ψ, requires the solution of the complete fourth-degree equation, obtained from (4.4), (2.8), and (4.2). The graphical method given above is nothing but a graphical solution of this equation.

In the case of normal incidence, the circle degenerates into a straight line and the obvious solution is given by the points of intersection of the normal to the discontinuity with the curves $V(\alpha)$ of the diagram.

5. INCIDENT AND DIVERGENT WAVES

In accordance with the results of the preceding section, the points where the circle drawn through the ends of the vector $-\mathbf{n}v_x$ intersect the curves of the velocity diagram determine the phase velocity vectors of all the waves that are interrelated by the reflection condition.

Among these waves there are divergent ones as well as those incident on the discontinuity, and we must know how to classify them by making use of this property.

However, we have no justification for using phase velocities to separate waves into incident and divergent ones, since the phase and the group velocities may have opposite signs for certain angles of incidence. In such cases, as has already been pointed out by Mandel'shtam,[12] the physical requirement, that the energy should flow away from the boundary of the discontinuity for the reflected or for the refracted wave, must lead to the classification of waves in terms of the group velocity $\mathbf{V}^{\mathrm{gr}} = \partial\omega/\partial\mathbf{k}$. Taking into account the fact that $V(\kappa)$ is a function of $\cos\theta$ only, we shall obtain in the system of coordinates I:

$$\mathbf{V}^{\mathrm{gr}} = \pm\left(\varkappa V + \frac{dV}{d\cos\theta}\frac{[\mathbf{k}\times[\mathbf{H}\times\mathbf{k}]]}{Hk^2}\right) + \mathbf{v}. \tag{5.1}$$

For the classification of waves we need the component V_x^{gr} normal to the discontinuity. By going over to the angle α we can easily obtain

$$V_x^{\mathrm{gr}} \equiv \frac{\partial\omega}{\partial k_x} = v_x \pm \left(V(\alpha)\cos\alpha - \frac{\partial V}{\partial\alpha}\sin\alpha\right). \tag{5.2}$$

We turn once again to the ψ circles to obtain a geometrical interpretation. We now regard equation (4.4) as the equation for ψ in terms of α and we take the derivative

$$\frac{\partial\psi}{\partial\alpha} = \frac{\sin^2\psi}{v_x\sin^2\alpha}\left[v_x \pm \left(V(\alpha)\cos\alpha - \frac{\partial V}{\partial\alpha}\sin\alpha\right)\right]. \tag{5.3}$$

By comparing formulas (5.2) and (5.3) we arrive at the relation

$$\frac{\partial\psi}{\partial\alpha} = \frac{\sin^2\psi}{v_x\sin^2\alpha}V_x^{\mathrm{gr}}, \tag{5.4}$$

which is of importance to us, where the group velocity is determined in the coordinate system in which the surface of the shock wave is at rest. The divergent waves in II and $\overline{\mathrm{II}}$ must satisfy the inequalities:

$$\begin{aligned} V_x^{\mathrm{gr}} &\equiv v_x \pm \left[V(\alpha)\cos\alpha - \frac{\partial V}{\partial\alpha}\sin\alpha\right] > 0, \\ \bar{V}_x^{\mathrm{gr}} &\equiv \bar{v}_x \pm \left[\bar{V}(\bar{\alpha})\cos\bar{\alpha} - \frac{\partial\bar{V}}{\partial\bar{\alpha}}\sin\bar{\alpha}\right] < 0. \end{aligned} \tag{5.5}$$

Similarly the incident waves will be determined by the inverse inequalities. In accordance with (5.4), we need merely determine the sign of $\partial\psi/\partial\alpha$ to determine the sign of the group velocity.

As can be seen from the expression for the group velocity (5.3), its projection on the direction of the propagation vector coincides with the phase velocity in the coordinate system in which the liquid is at rest.*

Consequently, in the case of normal incidence of the disturbance, the components of the phase and of group velocities along the normal to the discontinuity coincide, and in the case of normal incidence the division into incident and divergent waves can be carried out by making use of the components of the phase velocity (taking drift into account).[1] In the diagram (Fig. 4) these components are given by the points of intersection of the curves $V(\alpha)$ with the x axis, into which the ψ circle degenerates. The end of the segment v_x separates the waves into incident and divergent ones in accordance with the inequalities:

$$v_x \pm V_x \gtrless 0, \quad \bar{v}_x \lesseqgtr \bar{V}_x\ 0, \tag{5.6}$$

where the upper sign in the inequality corresponds to divergent, and the lower sign corresponds to incident waves.

In the case of oblique incidence, the ψ circle intersects both parts of the curve $V_A(\alpha)$, since they are also circles [cf. (2.7)] and have a point common with the ψ circle at the origin. A similar assertion can be made with respect to the curve $V_-(\alpha)$, both parts of which pass through the origin and have a common tangent at that point. Two of the aforementioned four points of intersection of the ψ circle with $V_A(\alpha)$ and $V_-(\alpha)$ may lie on the smaller arc of the ψ circle and correspond in that case to $\omega_0 < 0$ (for $\psi < \pi/2$). We now turn to the intersection of the ψ circle with the curve $V_+(\alpha)$. We consider the case $v_x < V_+(\pi)$. In the case of normal incidence $(\psi = 0)$ we have two waves, one $(\alpha = 0)$ divergent and the other $(\alpha = \pi)$ incident. As ψ increases the points of intersection with the ψ circle move along the curve $V_+(\alpha)$ towards each other. At the same time the angle α for the incident wave decreases, while for the divergent (reflected) wave the angle α increases as ψ increases, i.e., in accordance with (5.4) and (5.5), the condition $\partial\psi/\partial\alpha < 0$ is fulfilled for the former and the condition $\partial\psi/\partial\alpha > 0$ is fulfilled for the latter wave. When $\partial\psi/\partial\alpha = 0$ the ψ circle is tangent to the curve $V_+(\alpha)$ and both roots α of Eq. (4.4) coincide. We denote the corresponding values of ψ and α by ψ_m and α_m. We see from (5.7) that at this point for both waves we have $V_x^{gr} = 0$.*

---

*This result depends in an essential way on the fact that the dispersion is a purely spatial one. If V depends not only on $\varkappa$, but also on ω, the component of the group velocity does not coincide with the phase velocity.

As ψ increases further, the ψ circle no longer intersects the curve V_+. The real solutions are now replaced by complex conjugate solutions, which correspond to traveling waves. One of these must be discarded since it does not satisfy the boundary conditions at ∞, while the other one represents a surface wave that is attenuated as it penetrates into the fluid. We note that while in an ordinary fluid surface waves can arise only in the case of propagation of sound,[3,4] in the present case surface V_+ waves can arise also in the case of reflection of V_- or V_A waves.

6. STABILITY OF SHOCK WAVES

In accordance with the results of Akhiezer, Liubarskii, and Polovin[1] a shock wave is stable with respect to splitting up only in the case when the problem of the incidence of an arbitrary small disturbance on the discontinuity has a unique solution.† The system of equations for the amplitudes of the divergent waves in terms of the amplitudes of the incident waves (3.3) contains (after the amplitude of the shock wave itself has been eliminated) six equations, from which it follows that six waves must diverge from a stable discontinuity. The entropy wave always gives rise to a diverging wave in Π and to an incident one in $\overline{\Pi}$. Therefore in the vector diagram a stable wave must correspond in Π and in $\overline{\Pi}$ to five divergent waves of types $V_\pm$ and V_A for aribtrary ψ. When $\psi = 0$ (normal incidence) this requirement yields the conditions of Akhiezer, Liubarskii, and Polovin,[1] leading to waves of three kinds:

$$\begin{aligned} &\text{a) } v_x < V_-, && \overline{V}_- < \overline{v}_x < \overline{V}_A \\ &\text{b) } V_- < v_x < V_A, && \overline{V}_A < \overline{v}_x < \overline{V}_+ \qquad (6.1) \\ &\text{c) } V_A < v_x < V_+, && \overline{V}_+ < \overline{v}_x. \end{aligned}$$

We shall show that the number of diverging waves for any ψ (any α) is equal to the number of divergent waves for $\psi = 0$.

The component of the group velocity along any given direction in the case of Alfven waves is equal to the phase velocity in this direction, as can be seen directly from the dispersion law $\omega_0 = \pm \mathbf{k} \cdot \mathbf{u}$. Therefore the component along the normal, $\mathbf{V}_A^{gr} \cdot \mathbf{n} = V_x^{ph}$, and the inequality that determines the divergent wave are generally independent of the angle.

In accordance with the results of the preceding section the number of divergent waves does not change when $\psi < \psi_m$ in the case of magnetoacoustic waves. As ψ increases one divergent (and one incident) wave disappears at the point ψ_m, but a surface wave appears which, from the point of view of counting up the number of unknowns in the boundary conditions, must be included among the divergent waves. Thus, the number of unknowns is, as before, equal to the number of equations, only we must now consider all quantities to be complex. [Similarly, in the case when the ψ circle for a certain value $\psi_{m'}$ is also tangent to the curve V_- in addition to intersecting two curves, then in passing through $\psi_{m'}$ the surface wave disappears, and in addition to the waves present previously two traveling V_- waves appear, one of which corresponds to $\partial\psi/\partial\alpha > 0$ and is incident, while the other, for which $\partial\psi/\partial\alpha < 0$, is diverging (the converse holds in $\overline{\Pi}$). Leaving aside the question as to when such a case can be realized, we see that it does not change the number of divergent waves.] Thus, the number of diverging waves does not depend on the angle of incidence, and in order to have stability with respect to splitting up for an arbitrary angle of incidence of the disturbance on the discontinuity (provided only that the equations are not separable) it is sufficient that the conditions (6.1) should be satisfied.

If the disturbances were classified by means of their phase velocities (taking into account the drift of the disturbance with the stream) we would have arrived at a "paradox" of the instability of shock waves in magnetohydrodynamics. Indeed, in virtue of the spatial dispersion, there will be such a range of angles $\psi_0 < \psi < \psi_m$ in which the components of the phase and of the group velocities of fast sound along the normal to the discontinuity have opposite signs. In connection with this, if a classification with respect to phase velocity is carried out, the number of diverging waves for this angular interval differs from the number of diverging waves determined according to their group velocity, i.e., from the number of diverging waves for $\psi = 0$.*

---

*We note that the ψ circle is tangent to the curve V_+ at only one point, since in the opposite case there could be four points of intersection of the ψ circle with the curve V_+, which is impossible. Indeed, the equation for the points of intersection of the ψ circle with V_+ and V_- is of the fourth degree, but two points of intersection always lie on the curve V_-.

†When the number of diverging waves can only exceed the number of equations, for example, in the case of a perpendicular shock wave, the conclusion with respect to instability also follows from the well-known argument given in the book by Landau and Lifshitz.[13]

*We note that while opposite signs for the phase and the group velocities occur very infrequently in the usual problems involving a boundary (cf. reference 12), in the case of a moving boundary three always exists such a range of velocities of this motion, that in a system of reference in which the boundary is at rest the phase and the group velocities have opposite signs (if $V^{ph} > V^{gr}$, it is sufficient, for example, that $V^{ph} > v > V^{gr}$). In spatial problems, such a difference in sign may arise for arbitrary velocities v within a definite range of angles of incidence if spatial dispersion is present, as in our case.

We now consider a parallel shock wave in which the magnetic field is directed along the normal to the surface of discontinuity. In the case of exact normal incidence the perturbed equations can be separated into those for purely acoustic and for Alfven waves. Akhiezer, Liubarskii, and Polovin,[1] in considering unidimensional disturbances, have naturally drawn the conclusion that parallel shock waves that do not satisfy the inequalities $\bar{v} > \bar{s}$, $v < s$ [type b in (6.1)] are unstable. However, since the separation of a purely acoustic wave corresponds to an isolated point in the space of propagation vectors, it is necessary to investigate obliquely-incident disturbances in order to obtain a final answer to this problem. In such an investigation the boundary equations for the Alfven wave can be separated from the equations for the magnetoacoustic waves, and in order for stability to exist it is necessary to have two diverging Alfven waves. The waves of type b are unstable in agreement with the results of Akhiezer, Liubarskii and Polovin,[1] since among the divergent waves they have only one Alfven wave.

7. FREQUENCY SHIFT

When monochromatic disturbances interact with a shock wave, the Doppler effect and the discontinuity in the propagation vector at the surface of discontinuity cause the generator frequency Ω_0 and the received frequency Ω' to be different. In the case of magnetohydrodynamics there are more possibilities in this connection than in an ordinary fluid,[4] since we can compare the frequencies of different types of disturbances, for example, the frequency shift of the reflected V_+, V_-, V_A waves with respect to the frequency of the incident V_+ wave, etc. We shall restrict ourselves to the case of normal incidence, for which there is no need to use the graphic method. We assume that the receiver and the transmitter are at rest with respect to $\overline{\mathrm{II}}$. In accordance with (2.6), we obtain for the absolute value of the propagation vector in II (limiting ourselves to the solution involving the plus sign)

$$k = \omega / (V(\alpha) + \varkappa \cdot \mathbf{v}). \qquad (7.1)$$

Here, as before, ω is the frequency in the system I. In II we should place a bar over all the quantities with the exception of ω. The relation between ω and Ω_0 and Ω' is given by:

$$\omega - k^{(i)}\bar{v}_x \cos\alpha^{(i)} = \Omega_0, \quad \omega - k^{(r)}\bar{v}_x \cos\alpha^{(r)} = \Omega'. \qquad (7.2)$$

Here $\alpha^{(i)}$ and $\alpha^{(r)}$ are equal to 0 or π, depending on the direction of the incident and the reflected waves, $\sin\alpha \equiv 0$. In $\overline{\mathrm{II}}$ we should place a bar over the quantities k and α. From (7.1) and (7.2) we obtain formulas for the relative shifts $\Delta = (\Omega_0 - \Omega')/\Omega_0$. For the sake of definiteness we shall limit ourselves to those incident waves which have a propagation vector directed towards the boundary, and to divergent waves which have a propagation vector directed away from the boundary. In II the incident wave corresponds to $\alpha = \pi$, the diverging wave corresponds to $-\alpha = 0$; the converse holds in $\overline{\mathrm{II}}$. The relative frequency shift is given by the following expressions — in the case of reflection in II:

$$\Delta = \frac{\bar{v}_x [V(0) + V(\pi)]}{[V(\pi) - \{v_x\}][V(0) + v_x]}, \qquad \{v_x\} \equiv v_x - \bar{v}_x; \quad (7.3)$$

in the case of reflection in $\overline{\mathrm{II}}$:

$$\Delta = -\frac{\bar{v}_x}{\bar{V}(0)} \frac{\bar{V}(\pi) + \bar{V}(0)}{\bar{V}(\pi) - v_x}; \qquad (7.4)$$

in the case of transmission from II into $\overline{\mathrm{II}}$:

$$\Delta = \frac{\bar{v}_x [\bar{V}(\pi) - V(\pi) + \{v_x\}]}{V(\pi) - \{v_x\}][\bar{V}(\pi) - \bar{v}_x]}; \qquad (7.5)$$

in the case of transmission from $\overline{\mathrm{II}}$ into II:

$$\Delta = \frac{\bar{v}_x}{\bar{V}(0)} \frac{\bar{V}(0) - V(0) - \{v_x\}}{V(0) + v_x}. \qquad (7.6)$$

In all the above expressions we must everywhere in place of $V(\pi)$ and $\bar{V}(0)$ substitute the velocity of the incident disturbance, in place of $V(0)$, $\bar{V}(\pi)$ we must take the velocity of the disturbance of the type with which we are concerned. By measuring the different Δ we obtain from (7.3) to (7.6) a system of equations from which $\bar{v}/v$, $\bar{V}_{(i)}/\bar{v}$, $V_{(i)}/v$, ($i = \pm, A$) may be found. If we know V_i/v, we can easily obtain s/v, u/v, and H_x/H (similarly in II and in $\overline{\mathrm{II}}$):

$$s^2 = V_+^2 V_-^2 / V_\Lambda^2, \quad u^2 = V_+^2 - V_-^2 - s^2, \quad (H_x/H)^2 = V_A^2/u^2. \quad (7.7)$$

If the values of $\bar{s}$ and $\bar{\rho}$ (or $\bar{H}$) are known, we can obtain not only the ratios, but the quantities that characterize the discontinuity themselves.

The author takes this opportunity to thank A. I. Akhiezer, G. Ia. Liubarskii, and R. V. Polovin for communicating the results of their work prior to publication, and for useful discussions.

Note added in proof (September 30, 1958). As shown by Syrovatskii [J. Exptl. Theoret. Phys. **35**, (1958), Soviet Phys. JETP **8** (in press)] because of plane motion in shock waves (in contradistinction to the essentially spatial rotational discontinuities) there always exists a special plane of incidence (which coincides with the plane of motion in the shock wave), in which the boundary conditions for the Alfven and the magnetoacoustic waves become separable. In particular, such a separation always occurs in the case of normal incidence. As a result of this shock waves of type b are unstable (cf. the case of a parallel shock wave), while rotational discontinuities which should also be included in type b, are stable with respect to splitting up.

---

[1] Akhiezer, Liubarskii, and Polovin, J. Exptl. Theoret. Phys. (U.S.S.R.) **35**, 731 (1958), Soviet Phys. JETP **8** 507 (1959).

[2] D. I. Blokhintsev, Dokl. Akad. Nauk S.S.S.R. **47**, 22 (1945); J. M. Burgers, Proc. Ned. Akad. Wet. **49**, 273 (1946).

[3] J. Brillouin, Acustica **5**, 149 (1955).

[4] V. M. Kontorovich, J. Exptl. Theoret. Phys. (U.S.S.R.) **33**, 1527 (1957), Soviet Phys. JETP **6**, 1180 (1958);Акустический журнал Acoust. Journal) (in press).

[5] S. P. D'iakov, J. Exptl. Theoret. Phys. (U.S.S.R.) **33**, 948, 962 (1957), Soviet Phys. JETP **6**, 729 (1958).

[6] L. D. Landau and E. M. Lifshitz, Электродинамика сплошных сред (The Electrodynamics of Continuous Media), Ch. VIII, Tekhteoretizdat, 1957.

[7] S. I. Syrovatskii, Usp. Fiz. Nauk **62**, 247 (1957).

[8] S. I. Syrovatskii, Труды ИФАН (Trans. Physics Institute, Academy of Sciences, U.S.S.R.) **8**, 15 (1956).

[9] S. P. D'iakov, J. Exptl. Theoret. Phys. (U.S.S.R.) **27**, 288 (1954).

[10] V. M. Kontorovich, J. Exptl. Theoret. Phys. (U.S.S.R.) **34**, 186 (1958), Soviet Phys. JETP **7**, 127 (1958).

[11] L. D. Landau and E. M. Lifshitz, Механика сплошных сред (The Mechanics of Continuous Media), Gostekhizdat, 1953, p. 311.

[12] L. I. Mandel'shtam, J. Exptl. Theoret. Phys. (U.S.S.R.) **15**, 475 (1945); Собрание трудов (Collected Works) Acad. of Sci. Press, **5**, 463-465 (1950), **2**, 334 (1948).

[13] L. D. Landau and E. M. Lifshitz, Механика сплошных сред (The Mechanics of Continuous Media), Gostekhizdat, 1953, p. 405.

Translated by G. Volkoff
254

SOVIET PHYSICS JETP VOLUME 35 (8), NUMBER 5 MAY, 1959

DOUBLE ELASTIC SCATTERING OF DEUTERONS IN A MAGNETIC FIELD

G. R. KHUTSISHVILI and O. D. CHEISHVILI

Institute of Physics, Academy of Sciences, Georgian S.S.R.

Submitted to JETP editor May 27, 1958

J. Exptl. Theoret. Phys. (U.S.S.R.) 35, 1226-1231 (November, 1958)

A treatment is given of the double elastic scattering of a beam of deuterons in a magnetic field. An expression is obtained for the angular distribution of double elastic scattering. The special cases of longitudinal and transverse fields are considered.

1. Mendlowitz and Case[1] have given a theoretical treatment of the double elastic scattering of an electron beam for the case in which the beam is acted on between the scatterers by a magnetic field which is constant in time and homogeneous. The presence of an anomalous magnetic moment of the electron brings about an additional scattering, and measurements of this provide a possibility of experimental determination of the anomalous moment.

The present paper is devoted to the theoretical study of the double elastic scattering of a beam of particles with unit spin, in a magnetic field. It turns out that in this case (unlike that of particles with spin one-half) measurement of the double scattering in a magnetic field provides additional information about the scattering amplitude.

2. The amplitude for scattering of a deuteron by a nucleus with spin zero has the form[2]

$$F(\vartheta, \varphi) = A(\vartheta) + B(\vartheta)(\mathbf{S}\cdot\mathbf{n}) + C(\vartheta)(\mathbf{S}\cdot\mathbf{n})^2 + \frac{1}{2} D(\vartheta)\{(\mathbf{S}\cdot\mathbf{k}_0)(\mathbf{S}\cdot\mathbf{k}) + (\mathbf{S}\cdot\mathbf{k})(\mathbf{S}\cdot\mathbf{k}_0)\}, \tag{1}$$

where $\mathbf{k}_0$ and $\mathbf{k}$ are unit vectors along the momenta of the deuteron before and after the scattering; $\mathbf{n} = \mathbf{k}_0 \times \mathbf{k} / \sin\vartheta$ is the unit vector perpendicular to the plane of the scattering; $\mathbf{S}$ is the spin operator of the deuteron; and A, B, C, D are functions of the scattering angle and the energy of the deuteron.

The cross section for the scattering of a polarized beam is calculated by the formula

$$I(\vartheta, \varphi) = \mathrm{Sp}\,\{F(\vartheta, \varphi)\,\rho F^+(\vartheta, \varphi)\}, \tag{2}$$

where ρ is the spin density matrix of the deuteron beam,

$$\rho = \frac{1}{3}\sum_{jM}\langle T_{jM}\rangle T_{jM}^+, \tag{3}$$

in writing which we have introduced the following operators

$$T_{1\pm1} = \mp\frac{\sqrt{3}}{2}(S_x \pm iS_y), \qquad T_{10} = \sqrt{\frac{3}{2}}\,S_z,$$
$$T_{2\pm2} = \frac{\sqrt{3}}{2}(S_x \pm iS_y)^2,$$
$$T_{2\pm1} = \mp\frac{\sqrt{3}}{2}\{(S_x \pm iS_y)S_z + S_z(S_x \pm iS_y)\},$$
$$T_{20} = (3S_z^2 - 2)/\sqrt{2}, \tag{4}$$

and $\langle T_{jM}\rangle$ means the average value of T_{jM}.

If instead of $\langle T_{jM}\rangle$ we insert the polarization obtained after the first scattering,

$$\langle T_{jM}\rangle I_0(\vartheta) = {}^1\!/_3\,\mathrm{Sp}\,\{F(\vartheta, \varphi)\,F^+(\vartheta, \varphi)\,T_{jM}\}, \tag{5}$$

and if we use a coordinate system in which the plane of the first scattering is the xz plane and that of the second scattering contains the z axis (in other words, the z direction coincides with the direction of the deuteron momentum after the first scattering), then we get for the differential cross section of the double scattering:

$$I(\vartheta_1, \vartheta, \varphi) = I_0(\vartheta)\{1 + \langle T_{20}(\vartheta_1)\rangle\langle T_{20}(\vartheta)\rangle + 2[\langle T_{11}(\vartheta_1)\rangle\langle T_{11}(\vartheta)\rangle^* + \langle T_{21}(\vartheta_1)\rangle\langle T_{21}(\vartheta)\rangle]\cos\varphi + 2\langle T_{22}(\vartheta_1)\rangle\langle T_{22}(\vartheta)\rangle\cos 2\varphi\}, \tag{6}$$

where ϑ_1 and ϑ are the angles of the first and second scatterings, φ is the angle between the planes of the two scatterings, and $I_0(\vartheta)$ is the differential cross section for the scattering of an unpolarized beam,

$$I_0(\vartheta) = |A|^2 + \frac{2}{3}(|B|^2 + |C|^2) + \frac{1}{2}\left(\cos^2\vartheta + \frac{1}{3}\right)|D|^2 + \frac{4}{3}\mathrm{Re}\,[A^*(C + \cos\vartheta D)] + \frac{2}{3}\mathrm{Re}\,(C^*D)\cos\vartheta. \tag{7}$$

The average values used in Eq. (5) are given by the formulas

$$\langle T_{11}\rangle I_0(\vartheta) = -i\frac{2}{\sqrt{3}}\operatorname{Re}\left[\left(A + C + \frac{1}{2}\cos\vartheta D\right)B^*\right],$$

$$\langle T_{20}\rangle I_0(\vartheta) = \frac{\sqrt{2}}{6}(|B|^2 + |C|^2) + \frac{\sqrt{2}}{8}\left(3\cos^2\vartheta - \frac{1}{3}\right)|D|^2$$

$$-\frac{\sqrt{2}}{3}\operatorname{Re}[(A - \cos\vartheta D)C^*] + \frac{2\sqrt{2}}{3}\cos\vartheta\operatorname{Re}(A^*D)$$

$$+\frac{\sqrt{2}}{2}\sin\vartheta\operatorname{Im}(B^*D),$$

$$\langle T_{21}\rangle I_0(\vartheta) = -\frac{\sqrt{3}}{6}\sin\vartheta\cos\vartheta|D|^2$$

$$-\frac{\sqrt{3}}{3}\sin\vartheta\operatorname{Re}[(A + C)D^*] + \frac{\sqrt{3}}{3}\cos\vartheta\operatorname{Im}(B^*D),$$

$$\langle T_{22}\rangle I_0(\vartheta) = -\frac{\sqrt{3}}{6}\Big\{|B|^2 + |C|^2 + \frac{\sin^2\vartheta}{4}|D|^2$$

$$+ 2\operatorname{Re}[(A + \cos\vartheta D)C^*] + \sin\vartheta\operatorname{Im}(B^*D)\Big\}.$$

We note that we have the following relations:

$$\langle T_{1-M}\rangle = (-1)^{M+1}\langle T_{1M}\rangle; \quad \langle T_{2-M}\rangle = (-1)^M\langle T_{2M}\rangle. \tag{8}$$

3. It is well known that owing to the existence of an anomalous magnetic moment of the electron the precession of the electron spin in a magnetic field is at a somewhat more rapid rate than that of the orbital angular momentum; therefore, generally speaking, when a polarized electron beam passes through a magnetic field there will be a change of the polarization (we deal here with the direction of the polarization relative to the direction of the beam).[1,3] We note that for particles with spin one-half there will be a change of the original polarization only in cases in which the particle has an anomalous magnetic moment (i.e., the Lande g-factor is not equal to two). In the case of a particle with spin unity, on the other hand, there will be a change of the original polarization in the magnetic field even in the case in which there is no anomalous magnetic moment (i.e., even if the Lande g-factor is equal to unity).

According to reference 1 the change of the density matrix under the action of the magnetic field is given by

$$\rho(t) = \exp[i(\omega_L\mathbf{L} + \omega_S\mathbf{S})\cdot\mathbf{h}t]\,\rho(0)\exp[-i(\omega_L\mathbf{L} + \omega_S\mathbf{S})\cdot\mathbf{h}t],$$

where $\rho(0)$ is the density matrix before the application of the magnetic field, $\rho(t)$ is the density matrix at the time t after the application of the field, $\mathbf{h}$ is the unit vector along the field, and

$$\omega_L = eH/mc, \quad \omega_S = geH/2mc. \tag{9}$$

Introducing the notations

$$\xi = (\omega_S - \omega_L)t, \quad \eta = \omega_L t, \tag{10}$$

we get

$$\rho(t) = \exp[i\mathbf{J}\cdot\mathbf{h}\eta]\exp[i\mathbf{S}\cdot\mathbf{h}\xi]\,\rho(0)\exp[-i\mathbf{S}\cdot\mathbf{h}\xi]\exp[-i\mathbf{J}\cdot\mathbf{h}\eta]$$

(where $\mathbf{J} = \mathbf{L} + \mathbf{S}$ is the total angular momentum).

It is easy to see that the differential cross section for double elastic scattering reduces to the form

$$I(\vartheta, \varphi) = Q(t)\operatorname{Sp}\{F(\vartheta, \varphi)\rho'(t)F^+(\vartheta, \varphi)\}Q^{-1}(t), \tag{11}$$

where

$$\rho'(t) = \exp[i\mathbf{S}\cdot\mathbf{h}\xi]\,\rho(0)\exp[-i\mathbf{S}\cdot\mathbf{h}\xi], \tag{12}$$

$$Q(t) = \exp[i\mathbf{L}\cdot\mathbf{h}\eta]. \tag{13}$$

Calculation gives (see Appendix)

$$\rho'(t) = \frac{1}{3} + \frac{1}{2}P_i(t)S_i + T_{ik}(t)S_iS_k, \tag{14}$$

where

$$P_i(t) = \cos\xi P_i + (1 - \cos\xi)h_ih_kP_k + \sin\xi\varepsilon_{ikn}h_nP_k, \tag{15}$$

$$T_{ik}(t) = \cos 2\xi T_{ik} + (\cos\xi - \cos 2\xi)h_l(h_iT_{kl} + h_kT_{il})$$

$$-\sin\xi(\cos\xi - 1)h_nh_m(h_i\varepsilon_{kln} + h_k\varepsilon_{iln})T_{lm}$$

$$+\sin\xi\cos\xi h_n(\varepsilon_{iln}T_{kl} + \varepsilon_{kln}T_{il}) + (\cos\xi - 1)^2h_ih_kh_lh_mT_{lm}$$

$$-\sin^2\xi\cdot\delta_{ik}h_lh_mT_{lm}, \tag{16}$$

$$P_i = \operatorname{Sp}[S_i\rho(0)] = P_i(0),$$

$$T_{ik} = \operatorname{Sp}\left\{\left[\frac{1}{2}(S_iS_k + S_kS_i) - \frac{2}{3}\delta_{ik}\right]\rho(0)\right\} = T_{ik}(0).$$

It is easy to verify that

$$T_{ik}(t) = T_{ki}(t), \qquad T_{ii}(t) = 0.$$

For the further calculations it is convenient to use the irreducible spin tensors of Racah;[4] the expressions for the average values of these quantities are as follows:

$$\langle T_{1\pm1}(t)\rangle = \mp(\sqrt{3}/2)\{P_x(t) \pm iP_y(t)\};$$

$$\langle T_{10}(t)\rangle = \sqrt{3/2}\,P_z(t);$$

$$\langle T_{2\pm2}(t)\rangle = (\sqrt{3}/2)\{T_{xx}(t) - T_{yy}(t) \pm 2iT_{xy}(t)\}; \tag{17}$$

$$\langle T_{2\pm1}(t)\rangle = \mp\sqrt{3}\{T_{xz}(t) \pm iT_{yz}(t)\};$$

$$\langle T_{20}(t)\rangle = (3/\sqrt{2})T_{zz}(t).$$

Thus by using Eqs. (15), (16), and (17) we can express $\langle T_{jM}(t)\rangle$ in terms of $\langle T_{jM}(0)\rangle$.

For $\rho'(t)$ it is easy to obtain the following formula:

$$\rho'(t) = \frac{1}{3}\sum_{jM}\langle T_{jM}(t)\rangle T_{jM}^+. \tag{18}$$

Let us consider the cases of longitudinal and transverse fields. In the case of a longitudinal field (i.e., $\mathbf{h}$ parallel to z), Eqs. (15), (16), (17), and (8) give

$$\langle T_{1\pm1}(t)\rangle = e^{\mp i\xi}\langle T_{1\pm1}\rangle, \ \langle T_{10}(t)\rangle = 0,$$

$$\langle T_{2\pm2}(t)\rangle = e^{\mp 2i\xi}\langle T_{2\pm2}\rangle;$$

$$\langle T_{2\pm1}(t)\rangle = e^{\mp i\xi}\langle T_{2\pm1}\rangle; \ \langle T_{20}(t)\rangle = \langle T_{20}\rangle.$$

For the transverse field, on the other hand (**h** parallel to y), we get

$$\langle T_{1\pm1}(t)\rangle = \langle T_{1\pm1}\rangle, \quad \langle T_{10}(t)\rangle = 0,$$

$$\langle T_{2\pm2}(t)\rangle = \frac{1}{2}(1+\cos^2\xi)\langle T_{2\pm2}\rangle$$

$$\pm\frac{1}{2}\sin 2\xi\langle T_{2\pm1}\rangle + \frac{1}{2}\sqrt{\frac{3}{2}}\sin^2\xi\langle T_{20}\rangle,$$

$$\langle T_{2\pm1}(t)\rangle = \cos 2\xi\langle T_{2\pm1}\rangle$$

$$\mp\frac{1}{2}\sin 2\xi\langle T_{2\pm2}\rangle \pm \frac{1}{2}\sqrt{\frac{3}{2}}\sin 2\xi\langle T_{20}\rangle,$$

$$\langle T_{20}(t)\rangle = \frac{1}{2}(\cos 2\xi + \cos^2\xi)\langle T_{20}\rangle$$

$$+\sqrt{\frac{3}{2}}\sin^2\xi\langle T_{22}\rangle - \sqrt{\frac{3}{2}}\sin 2\xi\langle T_{21}\rangle.$$

In the case of the longitudinal field the operator Q(t) takes the form

$$Q(t) = \exp[\eta\partial/\partial\varphi],$$

and for the differential cross section for double elastic scattering we get

$$I_\parallel(\vartheta_1, \vartheta, \varphi) = I_0(\vartheta)\{1 + \langle T_{20}(\vartheta_1)\rangle\langle T_{20}(\vartheta)\rangle$$
$$+ 2[\langle T_{11}(\vartheta_1)\rangle\langle T_{11}(\vartheta)\rangle^*$$
$$+ \langle T_{21}(\vartheta_1)\rangle\langle T_{21}(\vartheta)\rangle]\cos(\varphi+\eta+\xi) \tag{19}$$
$$+ 2\langle T_{22}(\vartheta_1)\rangle\langle T_{22}(\vartheta)\rangle\cos 2(\varphi+\eta+\xi)\}.$$

In the case of the transverse magnetic field

$$Q(t) = \exp[\eta\cos\varphi\partial/\partial\vartheta - \eta\sin\varphi\cot\vartheta\partial/\partial\varphi],$$

and the differential cross section for double elastic scattering takes the form

$$I_\perp(\vartheta_1, \vartheta, \varphi) = I_0(\vartheta)\{1 + a(\vartheta_1+\eta\cos\varphi, \vartheta)$$
$$+ b(\vartheta_1+\eta\cos\varphi, \vartheta)\cos(\varphi - \eta\sin\varphi\cot\vartheta_1)$$
$$+ c(\vartheta_1+\eta\cos\varphi, \vartheta)\cos 2(\varphi - \eta\sin\varphi\cot\vartheta_1)\}, \tag{20}$$

where

$$a(\vartheta_1, \vartheta) = \langle T_{20}(\vartheta)\rangle\Big\{\frac{1}{2}(\cos 2\xi + \cos^2\xi)\langle T_{20}(\vartheta_1)\rangle$$
$$+ \sqrt{\frac{3}{2}}\sin^2\xi\langle T_{22}(\vartheta_1)\rangle - \sqrt{\frac{3}{2}}\sin 2\xi\langle T_{21}(\vartheta_1)\rangle\Big\},$$

$$b(\vartheta_1, \vartheta) = 2\Big[\langle T_{21}(\vartheta)\rangle\Big\{\cos 2\xi\langle T_{21}(\vartheta_1)\rangle - \frac{1}{2}\sin 2\xi\langle T_{22}(\vartheta_1)\rangle$$
$$+ \frac{1}{2}\sqrt{\frac{3}{2}}\sin 2\xi\langle T_{20}(\vartheta_1)\rangle\Big\} + \langle T_{11}(\vartheta)\rangle^*\langle T_{11}(\vartheta_1)\rangle\Big],$$

$$c(\vartheta_1, \vartheta) = 2\langle T_{22}(\vartheta)\rangle\Big\{\frac{1}{2}(1+\cos^2\xi)\langle T_{22}(\vartheta_1)\rangle$$
$$+ \frac{1}{2}\sin 2\xi\langle T_{21}(\vartheta_1)\rangle + \frac{1}{2}\sqrt{\frac{3}{2}}\sin^2\xi\langle T_{20}(\vartheta_1)\rangle\Big\}. \tag{21}$$

4. Repeated scatterings are used for the determination of the scattering amplitude from experimental data. To determine the coefficients in the scattering amplitude (1) one needs seven independent relations (for the four absolute values and three phase differences). By measurement of the intensity of the scattering of an unpolarized beam of deuterons, we can obtain one relation between the coefficients A, B, C, and D.

Let us consider experiments on simple double scattering (i.e., in the absence of a magnetic field), confining ourselves to the case in which the two scatterings occur under almost identical conditions (i.e., $\vartheta \approx \theta_1$, and also the energies are approximately equal). It can be seen from (6) that experiments on simple double scattering give three relations for the coefficients of the scattering amplitude. In fact,

$$\Big(\frac{1}{2\pi}\int_0^{2\pi} I d\varphi - I_0\Big)\Big/ I_0 = \langle T_{20}(\vartheta)\rangle^2,$$
$$(I(\varphi=0) - I(\varphi=\pi))/2I_0 = 2[|\langle T_{11}(\vartheta)\rangle|^2 + \langle T_{21}(\vartheta)\rangle^2], \tag{22}$$
$$\Big[\frac{1}{2}I(\varphi=0) + \frac{1}{2}I(\varphi=\pi) - I\Big(\varphi=\frac{\pi}{2}\Big)\Big]\Big/ 2I_0 = 2\langle T_{22}(\vartheta)\rangle^2.$$

Thus experiments on simple double scattering do not allow us to determine $<T_{11}>$, that is, the degree of polarization received by the beam in the first scattering* (this situation is different from that in the case of spin one-half).

Let us consider, finally, experiments on double scattering in a transverse magnetic field (the case of the longitudinal field gives nothing new as compared with simple double scattering). From the expression (20) one can obtain

$$[I_\perp(\varphi=0) - I_\perp(\varphi=\pi)]/2I_0$$
$$= {}^1/_2\{a(\vartheta+\eta, \vartheta) - a(\vartheta-\eta, \vartheta)$$
$$+ b(\vartheta+\eta, \vartheta) + b(\vartheta-\eta, \vartheta) + c(\vartheta+\eta, \vartheta) - c(\vartheta-\eta, \vartheta)\}.$$

We shall choose the value of the magnetic field strength and the time during which the deuteron is in the field (i.e., the time interval between the scatterings) in such a way that (with n an integer)

$$\eta = 2\pi n, \text{ i.e., } Ht = 2\pi(mc/e)n. \tag{23}$$

Then

$$[I_\perp(\varphi=0) - I_\perp(\varphi=\pi)]/2I_0$$
$$= 2\Big[|\langle T_{11}(\vartheta)\rangle|^2 + \langle T_{21}(\vartheta)\rangle\Big\{\cos 2\xi\langle T_{21}(\vartheta)\rangle$$
$$- \frac{1}{2}\sin 2\xi\langle T_{22}(\vartheta)\rangle + \frac{1}{2}\sqrt{\frac{3}{2}}\sin 2\xi\langle T_{20}(\vartheta)\rangle\Big\}\Big],$$

$$[I_\perp(\varphi=0) + I_\perp(\varphi=\pi)]/2I_0$$
$$= 1 + \langle T_{20}(\vartheta)\rangle\Big\{\frac{1}{2}(\cos 2\xi + \cos^2\xi)\langle T_{20}(\vartheta)\rangle$$

---

*We note, however, that if the energy of the incident deuterons is such that only elastic scattering is possible, then one can apply the unitarity relations,[4] in virtue of which the number of quantities to be measured is reduced to four.

$$+\sqrt{\frac{3}{2}}\sin^2\xi\langle T_{22}(\vartheta)\rangle-\sqrt{\frac{3}{2}}\sin 2\xi\langle T_{21}(\vartheta)\rangle\Big\}$$

$$+2\langle T_{22}(\vartheta)\rangle\Big\{\frac{1}{2}(1+\cos^2\xi)\langle T_{22}(\vartheta)\rangle+\frac{1}{2}\sin 2\xi\langle T_{21}(\vartheta)\rangle$$

$$+\frac{1}{2}\sqrt{\frac{3}{2}}\sin^2\xi\langle T_{20}(\vartheta)\rangle\Big\}, \tag{24}$$

$$\left[\frac{1}{2}I_\perp(\varphi=0)+\frac{1}{2}I_\perp(\varphi=\pi)-I_\perp\left(\varphi=\frac{\pi}{2}\right)\right]\Big/I_0$$

$$=-(2I_0)^{-1}[I_\perp(\varphi=0)-I_\perp(\varphi=\pi)]\sin(2\pi n\cot\vartheta)$$

$$+2[1+\cos(4\pi n\cot\vartheta)]\langle T_{22}(\vartheta)\rangle\Big\{\frac{1}{2}(1+\cos^2\xi)\langle T_{22}(\vartheta)\rangle$$

$$+\frac{1}{2}\sin 2\xi\langle T_{21}(\vartheta)\rangle+\frac{1}{2}\sqrt{\frac{3}{2}}\sin^2\xi\langle T_{20}(\vartheta)\rangle\Big\}.$$

We note that with the choice of Ht indicated above we have

$$\xi=2\pi n(g/2-1). \tag{25}$$

Thus we have obtained six relations — Eqs. (22) and (24). Of course, not all these relations are independent of each other, but they are sufficient for the determination of $\langle T_{11}\rangle$, $\langle T_{20}\rangle$, $\langle T_{21}\rangle$, and $\langle T_{22}\rangle$. Having determined these quantities, and knowing also the expression $I_0(\vartheta)$, we shall have five equations for the seven unknown quantities in the scattering amplitude.

We have examined in detail the case of a field directed along the y axis. If the field is directed along the x axis, i.e., parallel to the plane of the first scattering and perpendicular to the momentum of the deuteron after the first scattering, then no new information is obtained about the scattering amplitude (beyond that obtained in the case of the field parallel to the y axis). The same is true for the case of an arbitrary direction of the field.

Thus, although measurement of the double elastic scattering in a magnetic field does give additional information about the scattering amplitude, this information is still not sufficient to determine it completely.

Accordingly we see that double elastic scattering in a magnetic field gives less information than simple triple scattering (the latter gives complete information about the scattering amplitude). This is due to the fact that the magnetic field leaves unchanged the absolute value of the polarization vector, and also the sum of the squares of the components of the tensor $\langle T_{2M}\rangle$.

APPENDIX

According to Eq. (12)

$$\rho'(t)=\exp[i\mathbf{S}\cdot\mathbf{h}\,\xi]\,\rho(0)\exp[-i\mathbf{S}\cdot\mathbf{h}\,\xi]. \tag{A.1}$$

Expanding $\exp[\pm i\mathbf{S}\cdot\mathbf{h}\xi]$ in a power series in ξ and using the formula for reduction of tensors of third rank in S_i to tensors of lower ranks,

$$S_k S_m S_n=i\varepsilon_{kml}S_l S_n+i\varepsilon_{mnl}S_k S_l+\delta_{kn}S_m-i\varepsilon_{kmn}, \tag{A.2}$$

we get

$$\exp[\pm i\mathbf{S}\cdot\mathbf{h}\xi]=1\pm i(\mathbf{S}\cdot\mathbf{h})\sin\xi+(\mathbf{S}\cdot\mathbf{h})^2(\cos\xi-1). \tag{A.3}$$

Substituting Eq. (A.3) into (A.1), applying Eq. (A.2), and recalling that[5]

$$\rho(0)={}^1/_3+{}^1/_2P_iS_i+T_{ik}S_iS_k,$$

one readily obtains Eqs. (14) to (16) of the main text.

---

[1] H. Mendlowitz and K. M. Case, Phys. Rev. **97**, 33 (1955).

[2] O. D. Cheishvili, J. Exptl. Theoret. Phys. (U.S.S.R.) 30, 1147 (1956), Soviet Phys. JETP **3**, 974 (1956).

[3] K. M. Case, Phys. Rev. **106**, 173 (1957).

[4] R. M. Ryndin and Ia. A. Smorodinskii, J. Exptl. Theoret. Phys. (U.S.S.R.) 32, 1584 (1957), Soviet Phys. JETP **5**, 1294 (1957).

[5] R. Dalitz, Proc. Phys. Soc. **A65**, 175 (1952).

Translated by W. H. Furry
255

SOVIET PHYSICS JETP VOLUME 35 (8), NUMBER 5 MAY, 1959

ON THE POSSIBLE EXISTENCE OF THE Ξ^0-HYPERON

E. O. OKONOV

Joint Institute for Nuclear Research

Submitted to JETP editor May 31, 1958

J. Exptl. Theoret. Phys. (U.S.S.R.) 35, 1232-1234 (November, 1958)

It is suggested that the appreciable difference between the mean lifetime of the Λ^0 particle as measured in cosmic ray or in accelerator work is due to the existence of the Ξ^0 hyperon. Based on this assumption a rough estimate is made of the lifetime and relative production probability for the Ξ^0 hyperon.

In spite of the large volume of phase space available, the decay $\Xi^- \rightarrow n + \pi^-$ has not as yet been observed. The absence of this decay has led Gell-Mann and Pais to suggest that decays involving strongly interacting particles are governed by the $|\Delta S| = 1$ selection rule, which forbids decays in which "strangeness" changes by two units.[1] This rule requires the "strangeness" of Ξ^- to be -2, since it decays into Λ^0 and π^- of total strangeness -1. It then follows from the well known relation $Q = I_Z + N/2 + S/2$ that the Ξ-hyperon is an isotopic doublet, i.e., that besides Ξ^- $(I_Z = -\frac{1}{2})$ there also exists Ξ^0 $(I_Z = +\frac{1}{2})$. The main mode of decay of this particle will apparently be $\Xi^0 \rightarrow \Lambda^0 + \pi^0$, which is hard to observe. However, as was already noted by Okun and Pontecorvo[2] the selection rule $|\Delta S| = 1$ is no more than a working hypothesis. The apparent validity of this rule is a natural consequence of the fact that all known strange particles (with the exception of Ξ) are assigned the values $S = \pm 1$ and consequently $|\Delta S| = 1$ is the only possible change in strangeness in the decay into "usual" particles. It should also be noted that within the framework of the Gell-Mann and Nishijima scheme the possibility exists of assigning a strangeness $S = -3$ to the cascade particle which would lead to an isotopic singlet. In such a case the selection rule would have to be changed to permit decays with $|\Delta S| = 1, 2$ and forbid $|\Delta S| = 3$.

Consequently the observation of the Ξ^0 hyperon is of particular interest since it would, in a sense, confirm the selection rule $|\Delta S| = 1$.

In connection with the possible existence of the Ξ^0 hyperon we want to call attention to the appreciable difference between the mean lifetime of the Λ^0 particle as measured in cosmic ray work: $\tau'_{\Lambda^0} = (3.5^{+0.2}_{-0.1}) \times 10^{-10}$ sec, and as measured in accelerator work: $\tau_{\Lambda^0} = (2.8 \pm 0.1) \times 10^{-10}$ sec.* In the first case it is possible that in addition to Λ^0 particles produced directly, Λ^0 particles from the invisible decay $\Xi^0 \rightarrow \Lambda^0 + \pi^0$ are also registered. Furthermore, as a rule, the primary reaction is not observed and so the two types of Λ^0 particles cannot be distinguished. It is clear that this circumstance will cause an apparent increase in the measured τ'_{Λ^0} as compared with the true lifetime, the increase depending on the relative production probabilities (followed by decay) of Ξ^0 and Λ^0 particles. At the same time, Λ^0 particles produced artificially by accelerators are "pure" since the production of Ξ^0 particles is energetically impossible. It is to be noted that in those few "cosmic" events for which the primary interaction is strongly coplanar with the Λ^0 decay as seen in the chamber, the measured τ_{Λ^0} has also turned out to be markedly smaller: $(2.14^{+0.8}_{-0.5}) \times 10^{-10}$ sec.[3] However, coplanarity cannot be used as a criterion for "purity" of the Λ^0 at high energies, since in such a case the Λ^0 from the decay of Ξ^0 will be very nearly collinear with the parent Ξ^0-hyperon.

The probability that a Λ^0 resulting from the decay of Ξ^0 will be observed in a given time interval dt_i (or in a corresponding distance dl_i) is given by

$$dp_i = f_i \, dt_i = B_i \frac{\tau_{\Lambda^0}}{\tau_{\Xi^0} - \tau_{\Lambda^0}} \left[\exp\left(-\frac{t_i}{\tau_{\Xi^0}}\right) - \exp\left(-\frac{t_i}{\tau_{\Lambda_0}}\right) \right] dt_i,$$

where τ_{Λ^0} and τ_{Ξ^0} are the mean lifetimes of the Λ^0 and Ξ^0 hyperon, respectively, and B_i is a normalization coefficient. In this manner, without going into the details of the statistical method of determination of τ_{Λ^0},[4] it can be shown that the starting probability distribution of all particles will actually be not

---

*These numbers represent a weighted average of results published in 1958: τ_{Λ^0} from 425 analyzed events, τ'_{Λ^0} from 207 events. The latter number does not include 25 events published in reference 3, for reasons given below (their inclusion would have almost no effect on our results anyhow.)

$$dP = \prod_{i=1}^{n} A_i \exp\left(-\frac{t_i}{\tau'_{\Lambda^0}}\right) dt_i,$$

as was assumed in the analysis, but rather

$$dP' = \prod_{i=1}^{n} A_i \exp\left(-\frac{t_i}{\tau_{\Lambda_0}}\right) dt_i$$

$$\times \prod_{i=1}^{m} B_i \frac{\tau_{\Lambda^0}}{\tau_{\Xi^0} - \tau_{\Lambda^0}} \left[\exp\left(-\frac{t_i}{\tau_{\Xi^0}}\right) - \exp\left(-\frac{t_i}{\tau_{\Lambda^0}}\right)\right] dt_i,$$

where n and m are the number of Λ^0's produced in the primary interaction and resulting from decays of Ξ^0, respectively.* At the same time, the mean lifetime was determined on the assumption that the time dependence of the Λ^0 decays is given by a pure exponential. Clearly, the exponent of the exponential best approximating the true distribution function will depend on the relative number of Ξ^0 particles $(q = m/n)$ and on their lifetime. A rough estimate of q and τ_{Ξ^0} can be obtained from a comparison of τ'_{Λ^0} with the true lifetime as measured in the accelerator work.

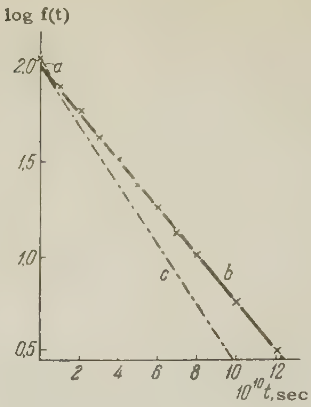

Λ^0-decay distribution function a) $f'(t)$, $q = 0.2$, $\tau_{\Xi^0} = 4 \cdot 10^{-10}$ sec b) $f(t) \sim \exp(-t/\tau') = 3.5 \cdot 10^{-10}$ sec c) $f(t) \sim \exp(-t/\Lambda^0)$, $\tau\Lambda^0 = 2.8 \cdot 10^{-10}$ sec.

For this purpose we find those values of q and τ_{Ξ^0} which make the distribution function

$$f'(t) = \exp\left(-\frac{t}{\tau_{\Lambda^0}}\right) \tag{a}$$

$$+ q \frac{\tau_{\Lambda^0}}{\tau_{\Xi^0} - \tau_{\Lambda^0}} \left[\exp\left(-\frac{t}{\tau_{\Xi^0}}\right) - \exp\left(-\frac{t}{\tau_{\Lambda^0}}\right)\right]$$

approximate as well as possible the exponential

$$f(t) \sim \exp\left(-\frac{t}{\tau'_{\Lambda^0}}\right) \tag{b}$$

(see figure) (the effect of the normalizing coefficients A_i and B_i has been ignored). The values of q and τ_{Ξ^0} obtained in this manner turn out to be reasonable: $q = 0.1$ to 0.2, and $\tau_{\Xi^0} = (4 \text{ to } 6) \times 10^{-10}$ sec. Indeed, there is at present no reason why the production cross sections of Ξ^- and Ξ^0 should differ drastically. On the other hand, it is known that the number of Ξ^- produced in cosmic rays amounts to 0.1 of the number of Λ^0 observed under similar conditions,[5] which agrees in order of magnitude with q. As regards τ_{Ξ^0}, one would expect, from an analysis of the isotopic spin states produced in the decays of Ξ^- and Ξ^0, that $\tau_{\Xi^0}/\tau_{\Xi^-} = 2$ if the decay interaction transforms in isotopic spin space as a tensor of rank $\frac{1}{2}$, or that $\tau_{\Xi^0}/\tau_{\Xi^-} = \frac{1}{2}$ if the transition is pure $|\Delta I| = 3/2$.[6] Consequently the value for τ_{Ξ^0} is reasonable since experimentally $\tau_{\Xi^-} = 4.6 \times 10^{-10}$ sec.[7] it is our opinion that the above-mentioned fact favors the existence of the neutral cascade hyperon Ξ^0, although, understandably, the possibility of some systematic error cannot be excluded.

In conclusion the author expresses his gratitude to M. I. Podgoretskii for valuable comments.

---

*We ignore the small difference in the velocities of the Ξ^0 and the Λ^0 produced in the decay.

[1] M. Gell-Mann and A. Pais, Nuovo cimento Suppl. **4**, 848 (1956).

[2] L. B. Okun' and B. Pontecorvo, J. Exptl. Theoret. Phys. (U.S.S.R.) **32**, 1587 (1957), Soviet Phys. JETP **5**, 1297 (1957).

[3] Ballario, Bizzarri, Brunelli, De Marco, Di Capua, Michelini, Moneti, Zavattini, and Zichichi, Nuovo cimento **6**, 994 (1957).

[4] M. S. Bartlett, Phil. Mag. **44**, 249 (1953).

[5] G. H. Trilling and R. B. Leighton, Phys. Rev. **104**, 1703 (1956).

[6] R. Gatto, Nuovo cimento **3**, 318 (1956).

[7] G. H. Trilling and G. Neugebauer, Phys. Rev. **104**, 1688 (1956).

Translated by A. M. Bincer
256

SOVIET PHYSICS JETP VOLUME 35(8), NUMBER 5, MAY, 1959

POLARIZATION OF INTERNAL CONVERSION ELECTRONS FOLLOWING BETA DECAY

B. V. GESHKENBEIN

Submitted to JETP editor May 31, 1958

J. Exptl. Theoret. Phys. (U.S.S.R.) 35, 1235-1242 (November, 1958)

The correlation between the polarization of conversion electrons and the direction of electron emission in the preceding β decay is treated. The entire calculation is done taking account of the electric field of the nucleus. Conversion can occur in any atomic shell. In particular, the nuclear electric field has a significant effect in K conversion. It causes the appearance of an appreciable transverse component of the polarization in magnetic transitions, and significantly increases the magnitude of the polarization for electric transitions.

BECAUSE of non-conservation of parity in β decay, the residual nucleus will be polarized in the direction of emission of the electron. The β-decaying nucleus is assumed to be unpolarized and the direction of emission of the neutrino is not recorded. Thus if the β decay is followed by internal conversion, the conversion electrons should have a definite polarization. This phenomenon, for the case of K conversion and omitting effects of the nuclear electric field, was treated by Berestetskii and Rudik.[1] The electric field of the nucleus has a marked effect on the internal conversion process and causes a large change in the conversion coefficient. The nuclear electric field should therefore also have a marked effect on the polarization of the conversion electrons.

We write the initial wave function of the electron which undergoes conversion in the form:

$$\psi_1 = \begin{pmatrix} ig_{\varkappa_1}(r) \ \Omega^{(l_1)}_{j_1 M_1}(\mathbf{r}/r) \\ f_{\varkappa_1}(r) \ .\Omega^{(l'_1)}_{j_1 M_1}(\mathbf{r}/r) \end{pmatrix}, \qquad (1)$$

where $\Omega^{(l)}_{jM}(\mathbf{n})$ is a spinor surface harmonic having components

$$[\Omega^{(l)}_{jM}(\mathbf{n})]_\mu = C^{jM}_{1/2\,\mu;\, l,\, M-\mu} Y_{l,\, M-\mu}(\mathbf{n}),$$

$$l' = 2j - l, \ \varkappa = (l - l')(j + 1/2),$$

in which $C^{c\gamma}_{a\alpha;\, b\beta}$ are Clebsch-Gordan coefficients and Y_{lm} is a spherical harmonic. Throughout the paper, we use the system of units in which $\hbar = c = 1$.

The wave function of the emitted electron is a solution of the Dirac equation which, at infinity, is a superposition of plane and outgoing spherical waves. This function was found in reference 2, and we shall write it in the form

$$\psi_2 = \frac{(2\pi)^{3/2}}{\sqrt{p_2 \varepsilon_2}} \sum_{j_2 l_2 M_2} [\Omega^{(l_2)}_{j_2 M_2}(\mathbf{n})]^*_\xi \begin{pmatrix} ig_{\varkappa_2}(r) \ \Omega^{(l_2)}_{j_2 M_2}(\mathbf{r}/r) \\ f_{\varkappa_2}(r) \ \Omega^{(l'_2)}_{j_2 M_2}(\mathbf{r}/r) \end{pmatrix} \exp\{-i\delta_{\varkappa_2}\}, \qquad (2)$$

where $\mathbf{n}$ is a unit vector in the direction of the emerging electron, ξ is the polarization of the electron; $g_{\kappa_2}(r)$ and $f_{\kappa_2}(r)$ are the radial parts of the Coulomb functions, normalized to a δ-function in the energy scale; the phase δ_{κ_2} approaches $-\pi(l_2 - 1)/2$ as $z \to 0$.

The matrix element for the conversion process can be written in the following form:[3]

$$\mathfrak{M}_{m_1 m_2} = \sum_M (I_1 m_1 \,|\, Q^{(\lambda)}_{jM} \,|\, I_2 m_2)^* \, (B^{(\lambda)}_{jM})_{21}; \qquad (3)$$

$$(B^{(\lambda)}_{jM})_{21} = \int \psi_2^* B^{(\lambda)}_{jM} \psi_1 \, dv. \qquad (3a)$$

Here $(I_1 m_1 \,|\, Q^{(\lambda)}_{jM} \,|\, I_2 m_2)$ is the nuclear matrix element for the transition, $I_1 m_1$ are the spin and spin projection of the nucleus before conversion, $I_2 m_2$ the spin and spin projection of the nucleus after the conversion, I is the nuclear spin before the β-decay, $B^{(\lambda)}_{jM}$ is the operator of the interaction of the electron with the field of the multipole. This operator has the following form:

$$B^{(0)}_{jM} = G_j(\omega r)\, \boldsymbol{\alpha} \mathbf{Y}_{jjM}(\mathbf{r}/r),$$

$$B^{(1)}_{jM} = \sqrt{\frac{j}{j+1}}\, G_j(\omega r)\, Y_{jM}(\mathbf{r}/r) \qquad (4)$$

$$+ \sqrt{\frac{2j+1}{j+1}}\, G_{j+1}(\omega r)\, \boldsymbol{\alpha} \mathbf{Y}_{j,\, j-1,\, M}(\mathbf{r}/r).$$

$\lambda = 0$ for magnetic transitions and $\lambda = 1$ for electric transitions. In addition, $\alpha = \begin{pmatrix} 0 & \sigma \\ \sigma & 0 \end{pmatrix}$, where the σ's are the Pauli matrices; ω is the energy of the transition;

$$G_j(x) = (2\pi)^{3/2} i^j H^{(1)}_{j+1/2}(x) / \sqrt{x}$$

($H^{(1)}$ is a Hankel function); $\mathbf{Y}_{jlM}$ is a vector spherical harmonic with contravariant components equal to

$$(\mathbf{Y}_{jlM})^\mu = C^{jM}_{l,\, M-\mu;\, 1\mu} Y_{l,\, M-\mu}.$$

The properties of vector spherical harmonics were studied in Ref. 3.

The density matrix with respect to the spin states of the conversion electron has the form

$$P = \sum_{\substack{m_1, m_1', m_2 \\ M, M'}} \rho_{m_1 m_1'} (I_1 m_1 | Q_{jM}^{(\lambda)} | I_2 m_2)^* \times (I_1 m_1' | Q_{jM'}^{(\lambda)} | I_2 m_2) (B_{jM}^{(\lambda)})_{21} (B_{jM'}^{(\lambda)})_{21}^*. \tag{5}$$

The expression for the matrix $\rho_{m_1 m_1'}$ which characterizes the state of polarization of the nucleus after β-decay was found in reference 1:

$$\rho_{m_1 m_1'} = \frac{1}{2I_1+1} \left\{ \delta_{m_1 m_1'} + \sqrt{\frac{I_1+1}{I_1}} \alpha \sum_{\mu} C_{I_1 m_1'; 1\mu}^{I_1 m_1} v^{\mu} \right\}, \tag{6}$$

where v^{μ} are the spherical components of the velocity vector of the β particle:

$$v^{(0)} = v_z, \quad v^{\pm 1} = \mp \frac{1}{\sqrt{2}} (v_x \mp i v_y) / \sqrt{2};$$

and α is a constant which determines the angular distribution of β particles in the decay of polarized nuclei with spin I_1 and average value $\langle I_{1z} \rangle$ for the spin projection, which make a transition to a state with spin I.

For allowed transitions, and for the S, T, A and V interactions, the value of α is:[4]

$$\alpha = [c_1 + (Ze^2/\varepsilon v) c_2] / (1 + b/\varepsilon),$$

$$c_1 \zeta = 2 \operatorname{Re} \Big\{ (C_T C_T'^* - C_A C_A'^*) | M_{\mathrm{GT}} |^2 \lambda_{I_1 I} + \sqrt{\frac{I_1}{I_1+1}} (C_T C_S'^* + C_T' C_S^* - C_A C_V'^* - C_A' C_V^*) M_{\mathrm{F}} M_{\mathrm{GT}}^* \Big\};$$

$$c_2 \zeta = 2 \operatorname{Im} \Big\{ (C_T C_A'^* + C_T' C_A^*) | M_{\mathrm{GT}} |^2 \lambda_{I_1 I} + \sqrt{\frac{I_1}{I_1+1}} (C_T C_V'^* + C_T' C_V^* - C_A C_S'^* - C_A' C_S^*) M_{\mathrm{F}} M_{\mathrm{GT}}^* \Big\};$$

$$b\zeta = 2\sqrt{1-(Ze^2)^2} \operatorname{Re} \{ (C_T C_A^* + C_T' C_A'^*) | M_{\mathrm{GT}} |^2 + (C_S C_V^* + C_S' C_V'^*) | M_{\mathrm{F}} |^2 \};$$

$$\zeta = (| C_T |^2 + | C_T' |^2 + | C_A |^2 + | C_A' |^2) | M_{\mathrm{GT}} |^2 + (| C_S |^2 + | C_S' |^2 + | C_V |^2 + | C_V' |^2) | M_{\mathrm{F}} |^2;$$

$$\lambda_{I_1 I} = \begin{cases} 1/(I+1) & \text{if } I_1 = I \\ 1 & \text{''} \quad I_1 = I+1 \\ -(I-1)/I & \text{''} \quad I_1 = I-1. \end{cases}$$

The matrix element of the multipole moment can be expressed as

$$(I_1 m_1 | Q_{jM}^{(\lambda)} | I_2 m_2) = Q^{(\lambda)} C_{I_2 m_2; jM}^{I_1 m_1}. \tag{7}$$

The general expression for the polarization vector $\langle \sigma \rangle$ of the conversion electron must have the following form:

$$\langle \sigma \rangle = a (\mathbf{v} \cdot \mathbf{n}) \mathbf{n} + b \{ \mathbf{v} - (\mathbf{v} \cdot \mathbf{n}) \mathbf{n} \}, \tag{8}$$

where a and b are constants.

We note that the matrix $\rho_{m_1 m_1'}$ can be written as in Eq. (6) and the polarization expressed in the form (8) only for allowed transitions and for first forbidden Coulomb transitions.

MAGNETIC TRANSITIONS

Substituting in (3a) the electron wave functions ψ_1 and ψ_2 from (1) and (2) and the operator $B_{jM}^{(0)}$, we get

$$(B_{jM}^{(0)})_{21} = -\frac{(2\pi)^{3/2} i}{\sqrt{p_2 \varepsilon_2}} \sum_{j_2 l_2 M_2} [\Omega_{j_2 M_2}^{(l_2)}(\mathbf{n})]_{\xi} e^{i\delta_{\varkappa_2}} \Big\{ R_{1\varkappa_2} \int \Omega_{j_2 M_2}^{(l_2')*} \left(\frac{\mathbf{r}}{r}\right) \boldsymbol{\sigma} \mathbf{Y}_{jM}^{(0)} \left(\frac{\mathbf{r}}{r}\right) \times \Omega_{j_1 M_1}^{(l_1)} \left(\frac{\mathbf{r}}{r}\right) do - R_{2\varkappa_2} \int \Omega_{j_2 M_2}^{(l_2)*} \left(\frac{\mathbf{r}}{r}\right) \boldsymbol{\sigma} \mathbf{Y}_{jM}^{(0)} \left(\frac{\mathbf{r}}{r}\right) \Omega_{j_1 M_1}^{(l_1')} \left(\frac{\mathbf{r}}{r}\right) do \Big\}. \tag{9}$$

We have introduced the following notation for the radial integrals:

$$R_{1\varkappa_2} = \int f_{\varkappa_2}(r) g_{\varkappa_1}(r) G_j(\omega r) r^2 dr, \qquad R_{2\varkappa_2} = \int g_{\varkappa_2}(r) f_{\varkappa_1}(r) G_j(\omega r) r^2 dr. \tag{10}$$

We shall use the system of mutually orthogonal vector spherical harmonics

$$\mathbf{Y}_{jM}^{(0)} = \mathbf{Y}_{jjM},$$

$$\mathbf{Y}_{jM}^{(1)} = \sqrt{\frac{j}{2j+1}} \mathbf{Y}_{j,\, j+1,\, M} + \sqrt{\frac{j+1}{2j+1}} \mathbf{Y}_{j;\, j-1,\, M}, \tag{11}$$

$$\mathbf{Y}_{jM}^{(-1)} = \mathbf{n} \mathbf{Y}_{jM}.$$

$\mathbf{Y}_{jM}^{(0)}$ and $\mathbf{Y}_{jM}^{(1)}$ are transverse vectors, so that $\mathbf{Y}_{jM}^{(0)}(\mathbf{n}) \cdot \mathbf{n} = \mathbf{Y}_{jM}^{(1)}(\mathbf{n}) \cdot \mathbf{n} = 0$. They are related to one another by

$$i \mathbf{Y}_{jM}^{(1)} = [\mathbf{n} \times \mathbf{Y}_{jM}^{(0)}]. \tag{12}$$

The following useful formula holds for $\mathbf{Y}_{jM}^{(0)}$:

$$\mathbf{Y}_{jM}^{(0)} = \mathbf{L} Y_{jM} / \sqrt{j(j+1)} \quad (\mathbf{L} = -i [\mathbf{r} \times \nabla]). \tag{13}$$

In calculating the angular integrals in (9), we make use of formula (13), the self-adjoint character of the operator $\boldsymbol{\sigma} \cdot \mathbf{L}$, and the formulas:

$$\boldsymbol{\sigma} \cdot \mathbf{L} \Omega_{jM}^{(l)} = \left\{ j(j+1) - l(l+1) - \frac{3}{4} \right\} \Omega_{jM}^{(l)}; \tag{14}$$

$$\boldsymbol{\sigma} \cdot \mathbf{n} \Omega_{jM}^{(l)}(\mathbf{n}) = \Omega_{jM}^{(l')}(\mathbf{n}); \tag{15}$$

$$Y_{l_1 m_1}(\mathbf{n}) Y_{l_2 m_2}(\mathbf{n}) = \sum_{LM} \sqrt{\frac{(2l_1+1)(2l_2+1)}{4\pi(2L+1)}} C_{l_1 0;\, l_2 0}^{L0} C_{l_1 m_1;\, l_2 m_2}^{LM} Y_{LM}(\mathbf{n}). \tag{16}$$

In carrying out the summation in (9) we use Racah's formula (cf., for example, reference 5):

$$\sum_{\beta} C_{a\alpha;\, b\beta}^{e,\, \alpha+\beta} C_{c,\, \alpha+\beta;\, d,\, \gamma-\alpha-\beta}^{c\gamma} C_{b\beta;\, d,\, \gamma-\alpha-\beta}^{f,\, \gamma-\alpha} = (2e+1)^{1/2} (2f+1)^{1/2} C_{a\alpha;\, f,\, \gamma-\alpha}^{c\gamma} W(abcd;\, ef) \tag{17}$$

in which W (abcd; ef) are Racah coefficients. After performing the integration and summation in (9), we get

$$(B^{(0)}_{jM})_{21} = \sum_{j_2 l_2 M_2} a_{\varkappa_2} W(l_2 j_2 l'_1 j_1;\ {}^1/_2\, j)$$

$$\times C^{l_2 0}_{j0,\ l'_1 0} C^{j_2 M_2}_{jM;\ j_1 M_1} C^{j_2 M_2}_{l_2,\ M_2-\xi;\ {}^1/_2\,\xi} Y_{l_2,\ M_2-\xi}(\mathbf{n}); \tag{18}$$

$$a_{\varkappa_2} = -\pi i \sqrt{\frac{2(2j+1)(2l'_1+1)(2j_1+1)}{j(j+1)\,p_2\varepsilon_2}}\, e^{i\delta_{\varkappa_2}} (R_{1\varkappa_2} + R_{2\varkappa_2}).$$

Substituting from (6), (7) and (18) into formula (5), dropping irrelevant common factors, and summing over all values of M, M′, M_1, M_2, M_3, μ, we find for the density matrix:

$$P_{\xi\xi'} = (A + 2A_1\xi)\,\delta_{\xi\xi'} + 2\sqrt{2\pi}\, A_4 C^{{}^3/_2\,\xi'}_{2,\ \xi'-\xi;\ {}^1/_2\,\xi} Y_{2,\ \xi'-\xi}(\mathbf{n}), \tag{19}$$

where

$$A = \sum_{j_2 l_2} |a_{\varkappa_2}|^2 (2j_2+1)(C^{l_2 0}_{j0;\ l'_1 0})^2 W^2(l_2 j_2 l_1 j_1;\ {}^1/_2\, j),$$

$$A_1 = \sqrt{\frac{2j+1}{6}}\,\alpha\,\frac{j(j+1) + I_1(I_1+1) - I_2(I_2+1)}{I_1\sqrt{j(j+1)}}$$

$$\times \sum_{\substack{j_2\ l_2,\ j_3\\ l_3 = l_2}} (-1)^{j_2 - j_3 - 1} \alpha_{\varkappa_2} \alpha^*_{\varkappa_3}$$

$$\times (2j_2+1)(2j_3+1)(C^{l_2 0}_{j0;\ l'_1 0})^2 W(l_2 j_2 l'_1 j_1;\ {}^1/_2\, j)$$

$$\times W(l_2 j_3 l'_1 j_1;\ {}^1/_2\, j)\, W(jjj_2 j_3;\ 1j)\, W(j_3 j_2\, {}^1/_2\, {}^1/_2;\ 1 l_2), \tag{20}$$

$$A_2 = \sqrt{\frac{2j+1}{3}}\,\alpha\,\frac{j(j+1) + I_1(I_1+1) - I_2(I_2+1)}{I_1\sqrt{j(j+1)}}$$

$$\times \sum_{j_2,\ l_2,\ j_3,\ l_3} (-1)^{j_2 - j_3 + l_2 + 1} \alpha_{\varkappa_2} \alpha^*_{\varkappa_3}$$

$$\times \sqrt{(2l_2+1)(2l_3+1)}(2j_2+1)(2j_3+1) C^{l_2 0}_{j0;\ l'_1 0} C^{l_3 0}_{j0;\ l'_1 0} C^{20}_{l_2 0;\ l_3 0}$$

$$\times W(l_2 j_2 l'_1 j_1;\ {}^1/_2\, j)\, W(l_3 j_3 l'_1 j_1;\ {}^1/_2\, j)$$

$$\times W(j_3 j_2\, {}^1/_2\, {}^3/_2;\ 1 l_3)\, W(l_2 j_2\, 2\, {}^3/_2;\ {}^1/_2\, l_3)\, W(jjj_2 j_3;\ 1 j_1).$$

We choose the z axis to be along the direction of the velocity of the β particle. Then formula (19) can be rewritten as

$$P_{\xi\xi'} = \tag{21}$$

$$\begin{pmatrix} A + A_1 - A_2(3\cos^2\theta - 1), & -3A_2 \sin\theta\cos\theta \\ -3A_2\sin\theta\cos\theta, & A - A_1 + A_2(3\cos^2\theta - 1) \end{pmatrix},$$

where θ is the angle between the directions of emergence of the β particle and the conversion electron. Knowing the density matrix $P_{\xi\xi'}$, it is easy to find the polarization of the conversion electrons:

$$\langle\sigma\rangle = \mathrm{Sp}\, P\sigma / \mathrm{Sp}\, P; \tag{22}$$

$$\langle\sigma\rangle = a(\mathbf{v}\cdot\mathbf{n})\,\mathbf{n} + b\{\mathbf{v} - (\mathbf{v}\cdot\mathbf{n})\,\mathbf{n}\},$$
$$a = (A_1 - 2A_2)/vA, \quad b = (A_1 + A_2)/vA. \tag{23}$$

For the K shell ($l_1 = 0$; $j_1 = \frac{1}{2}$, $\kappa_1 = -1$), using formulas (23) and (20) and inserting the values of the Clebsch-Gordan and Racah coefficients, we find

$$\langle\sigma\rangle = \alpha\,\frac{j(j+1) + I_1(I_1+1) - I_2(I_2+1)}{2j(j+1)\,I_2(1 + |\eta^0_k|^2)}$$

$$\times\{(\mathbf{v}\cdot\mathbf{n})\,\mathbf{n} + \sqrt{j(j+1)}\,\mathrm{Re}\,\eta^{(0)}_k(\mathbf{v} - (\mathbf{v}\cdot\mathbf{n})\,\mathbf{n})\}, \tag{24}$$

$$\eta^{(0)}_k =$$

$$\frac{\sqrt{j(j+1)}\,\{R_{1,\,-j} + R_{2,\,-j} - (R_{1,\,j+1} + R_{2,\,j+1})\exp(i(\delta_{j+1} - \delta_{-j}))\}}{(j+1)(R_{1,\,-j} + R_{2,\,-j}) + j(R_{1,\,j+1} + R_{2,\,j+1})\exp(i(\delta_{j+1} - \delta_{-j}))}.$$

Let us consider two limiting cases.

(1) Small Z. In this case the electric field of the nucleus can be neglected. Then the radial integrals are calculated explicitly and, using (24), we get the same value of the polarization as was given in reference 1.

(2) Large Z and low energy of the conversion electron, so that $p_2/mZe^2 \ll 1$. In this case, $|R_{1,\,j+1} + R_{2,\,j+1}| \ll |R_{1,\,-j} + R_{2,\,-j}|$, and we find for the polarization the expression

$$\langle\sigma\rangle = \alpha\,\frac{j(j+1) + I_1(I_1+1) - I_2(I_2+1)}{2j(2j+1)\,I_1}$$

$$\times\{(\mathbf{v}\cdot\mathbf{n})\,\mathbf{n} + j(\mathbf{v} - (\mathbf{v}\cdot\mathbf{n})\,\mathbf{n})\}. \tag{25}$$

We note that the formulas (24) are valid for any shell, so long as $\kappa_1 = -1$ for the electrons in the shell. In particular they are applicable to conversion in the LI shell. We also give the formulas for conversion in the LII shell (or in any shell with $\kappa_1 = 1$; $j_1 = \frac{1}{2}$; $l_1 = 1$):

$$\langle\sigma\rangle = \alpha\,\frac{j(j+1) + I_1(I_1+1) - I_2(I_2+1)}{2j(j+1)\,I_2(1 + |\eta^{(0)}_{L\,\mathrm{II}}|^2)}$$

$$\times\{(\mathbf{v}\cdot\mathbf{n})\,\mathbf{n} + \sqrt{j(j+1)}\,\mathrm{Re}\,\eta^{(0)}_{L\,\mathrm{II}}(\mathbf{v} - (\mathbf{v}\cdot\mathbf{n})\,\mathbf{n})\}, \tag{26}$$

$$\eta^{(0)}_{L\,\mathrm{II}} = \sqrt{j(j+1)}$$

$$\times\frac{(R_{1,\,-j-1} + R_{2,\,-j-1}) - (R_{1,\,j} + R_{2,\,j})\exp\{i(\delta_j - \delta_{-j-1})\}}{j(R_{1,\,-j-1} + R_{2,\,-j-1}) + (j+1)(R_{1,\,j} + R_{2,\,j})\exp\{i(\delta_j - \delta_{-j-1})\}}$$

ELECTRIC TRANSITIONS

Substituting the electron wave functions ψ_1 and ψ_2 from (1) and (2) and the operator $B^{(1)}_{jM}$ into (3a), we get

$$(B^{(1)}_{jM})_{21} = \frac{(2\pi)^{3/2}}{\sqrt{p_2\varepsilon_2}} \sum_{j_2 l_2 M_2} [\Omega^{(l_2)}_{j_2 M_2}(\mathbf{n})]_\xi \exp\{i\delta_{\varkappa_2}\}\cdot\Bigg\{\sqrt{\frac{j}{j+1}}$$

$$\times\Big[R_{3,\,\varkappa_2}\int \Omega^{(l_2)*}_{j_2 M_2} Y_{jM}\Omega^{(l_1)}_{j_1 M_1}\,do + R_{4,\,\varkappa_2}\int \Omega^{(l'_2)}_{j_2 M_2} Y_{jM}\Omega^{(l'_1)}_{j_1 M_1}\,do\Big]$$

$$-\sqrt{\frac{2j+1}{j+1}}\Big[R_{5,\,\varkappa_2}\int \Omega^{(l'_2)*}_{j_2 M_2}\sigma\cdot\mathbf{Y}_{j,\,j-1,\,M}\Omega^{(l_1)}_{j_1 M_1}\,do \tag{27}$$

$$-R_{6,\,\varkappa_2}\int \Omega^{(l_2)*}_{j_2 M_2}\sigma\cdot\mathbf{Y}_{j,\,j-1,\,M}\Omega^{(l'_1)}_{j_1 M_1}\,do\Big]\Bigg\}.$$

We have introduced the following notation for the radial integrals:

$$\begin{aligned} R_{3,\,\varkappa_2} &= \int G_j(\omega r)\, g_{\varkappa_2}(r)\, g_{\varkappa_1}(r)\, r^2\, dr, \\ R_{4,\,\varkappa_2} &= \int G_j(\omega r)\, f_{\varkappa_2}(r)\, f_{\varkappa_1}(r)\, r^2\, dr, \\ R_{5,\,\varkappa_2} &= -i\int G_{j-1}(\omega r)\, f_{\varkappa_2}(r)\, g_{\varkappa_1}(r)\, r^2\, dr, \\ R_{6,\varkappa_2} &= -i\int G_{j-1}(\omega r)\, g_{\varkappa_2}(r)\, f_{\varkappa_1}(r)\, r^2\, dr. \end{aligned} \tag{28}$$

Now let us calculate the angular integrals. For the first pair of integrals over angle, we get:

$$\begin{aligned} &\int \Omega^{(l_2)*}_{j_2M_2} Y_{jM} \Omega^{(l_1)}_{j_1M_1}\, do = \int \Omega^{(l_2')}_{j_2M_2} Y_{jM} \Omega^{(l_1')}_{j_1M_1}\, do \\ &\frac{1}{\sqrt{4\pi}} \sqrt{(2j+1)(2j_1+1)(2l_1+1)} \\ &\times C^{l_20}_{l_10;\, j0} C^{j_2M_2}_{j_1M_1;\, jM}\, W(jl_1j_2\,{}^1\!/_2;\; l_2j_1). \end{aligned} \tag{29}$$

To calculate the second pair of integrals over angle, we write

$$\mathbf{Y}_{j,\,j-1,\,M} = \sqrt{\frac{j}{2j+1}}\, \mathbf{Y}^{(-1)}_{jM} + \sqrt{\frac{j+1}{2j+1}}\, \mathbf{Y}^{(1)}_{jM}. \tag{30}$$

Using formula (13) and the commutation relations for the Pauli matrices, we find:

$$\begin{aligned} (\sigma\cdot\mathbf{Y}_{j,\,j-1,\,M})\left(\sigma\frac{\mathbf{r}}{r}\right) &= \sqrt{\frac{j}{2j+1}}\, Y_{jM} + \frac{1}{\sqrt{j(2j+1)}}\, \sigma\cdot\mathbf{L}Y_{jM}, \\ \left(\sigma\frac{\mathbf{r}}{r}\right)(\sigma\cdot\mathbf{Y}_{j,\,j-1,\,M}) &= \sqrt{\frac{j}{2j+1}}\, Y_{jM} - \frac{1}{\sqrt{j(2j+1)}}\, \sigma\cdot\mathbf{L}Y_{jM}. \end{aligned} \tag{31}$$

Using formulas (31), (14), (15), and (16) along with the fact that the operator $\sigma\cdot\mathbf{L}$ is self-adjoint, we find for the second pair of angle integrals:

$$\begin{aligned} &\int \Omega^{(l_2')*}_{j_2M_2} \sigma\cdot\mathbf{Y}_{j,\,j-1,\,M} \Omega^{(l_1)}_{j_1M_1}\, do \\ &= \frac{1}{\sqrt{4\pi}} \sqrt{j(2j_1+1)(2l_1+1)} \left(1+\frac{\varkappa_2-\varkappa_1}{j}\right) \\ &\times C^{l_20}_{l_10;\, j0} C^{j_2M_2}_{j_1M_1;\, jM}\, W(jl_1j_2\,{}^1\!/_2;\; l_2j_1); \\ &\int \Omega^{(l_2)*}_{j_2M_2} \sigma\cdot\mathbf{Y}_{j,\,j-1,\,M} \Omega^{(l_1')}_{j_1M_1}\, do \\ &= \frac{1}{\sqrt{4\pi}} \sqrt{j(2j_1+1)(2l_1+1)} \left(1-\frac{\varkappa_2-\varkappa_1}{j}\right) \\ &\times C^{l_20}_{l_10;\, j0} C^{j_2M_2}_{j_1M_1;\, jM}\, W(jl_1j_2\,{}^1\!/_2;\; l_2j_1). \end{aligned} \tag{32}$$

Substituting the results of the angular integrations in (27) and using the symmetry properties of the Clebsch-Gordan and Racah coefficients, we find an expression for $(B^{(1)}_{jM})_{21}$ which differs from (18) only in the replacement of l_1' by l_1 and of a_{κ_2} by

$$\begin{aligned} b_{\varkappa_2} = \pi\sqrt{\frac{2j(2j+1)(2j_1+1)(2l_1+1)}{(j+1)p_2\varepsilon_2}} \Big[&R_{3,\,\varkappa_2} + R_{4,\,\varkappa_2} \\ &- \left(1+\frac{\varkappa_2-\varkappa_1}{j}\right) R_{5,\,\varkappa_2} + \left(1-\frac{\varkappa_2-\varkappa_1}{j}\right) R_{6,\,\varkappa_2}\Big] \exp\{i\delta_{\varkappa_2}\}. \end{aligned} \tag{33}$$

We can therefore immediately write the formula for the polarization of conversion electrons in an electric transition:

$$\begin{aligned} \langle\sigma\rangle &= a(\mathbf{v}\cdot\mathbf{n})\mathbf{n} + b\{\mathbf{v} - (\mathbf{v}\cdot\mathbf{n})\mathbf{n}\}; \\ a &= (B_1 - 2B_1)/vB, \quad b = (B_1 + B_2)/vB, \end{aligned} \tag{34}$$

where the quantities B, B_1, and B_2 are gotten from A, A_1, and A_2 by making the substitution described above.

For the polarization of conversion electrons ejected from the K-shell, we get the expression

$$\begin{aligned} \langle\sigma\rangle &= \alpha\, \frac{j(j+1) + I_1(I_1+1) - I_2(I_2+1)}{2j(j+1)I_1(1+|\eta^{(1)}_k|^2)} \\ &\times \{(\mathbf{v}\cdot\mathbf{n})\mathbf{n} + \sqrt{j(j+1)}\, \mathrm{Re}\,\eta^{(1)}_k (\mathbf{v} - (\mathbf{v}\cdot\mathbf{n})\mathbf{n})\}; \end{aligned} \tag{35}$$

$$\eta^{(1)}_k = \frac{1}{\sqrt{j(j+1)}}\, \frac{(j+1)(R_{3,\,-j-1} + R_{4,\,-j-1} + 2R_{6,\,-j-1}) + j\left(R_{3,\,j} + R_{4,\,j} - \frac{2j+1}{j}R_{5,\,j} - \frac{1}{j}R_{6,\,j}\right)\exp\{i(\delta_j - \delta_{-j-1})\}}{(R_{3,\,-j-1} + R_{4,\,-j-1} + 2R_{6,\,-j-1}) - \left(R_{3,\,j} + R_{4,\,j} - \frac{2j+1}{j}R_{5,\,j} - \frac{1}{j}R_{6,\,j}\right)\exp\{i(\delta_j - \delta_{-j-1})\}}. \tag{36}$$

In the free electron approximation, the radial integrals can be calculated explicitly:

$$\begin{aligned} R_{3,\,\varkappa_2} &= (2\pi Ze^2m)^{3/2}\sqrt{\frac{2(\varepsilon_2+m)}{\omega}}\, I_j i^j; \\ R_{4,\,\varkappa_2} &= R_{6,\,\varkappa_2} = 0; \\ R_{5,\,j} &= -(2\pi Ze^2m)^{3/2}\sqrt{\frac{2(\varepsilon_2-m)}{\omega}}\, I_{j-1} i^j; \quad \delta_j - \delta_{-j-1} = 0. \end{aligned}$$

Substituting these values for the radial integrals into (36), we get

$$\eta^{(1)}_k = -\sqrt{\frac{j}{j+1}}\, \frac{2\varepsilon_2}{\varepsilon_2 - m}, \tag{37}$$

after which we find from (35) the same value for the polarization as in Ref. 1.

For high Z the radial integrals cannot be found explicitly, and must be computed numerically. We give, for Z = 80, a table of the values of $\sqrt{j(j+1)} \times \eta^{(1)}_k$, calculated using values of the radial integrals which were kindly communicated to us by L. A. Sliv.

As we see from a comparison of the table with formula (37), the electric field of the nucleus also has a significant effect on the polarization of the

j \ ω/m	0.3	0.5	0.7	1
1	4.6	3.3	2.5	2.0
2	3.7	2.5	2.0	1.4
3	3.2	2.2	1.6	1.04−0.27i

conversion electrons in the case of electric transitions. Formulas (35) and (36) are applicable to conversion in any shell with $\kappa_2 = -1$. In particular they are applicable to conversion in the LI shell, except that the radial integrals will be different. For conversion in the LII shell (or any shell with $\kappa_1 = 1$), we find for the polarization of the conversion electrons

$$\langle\sigma\rangle = \alpha \frac{j(j+1) + I_1(I_1+1) - I_2(I_2+1)}{2j(j+1)I_1(1+|\eta_{LII}^{(1)}|^2)} \times \{(\mathbf{v}\cdot\mathbf{n})\mathbf{n} + \sqrt{j(j+1)}\,\mathrm{Re}\,\eta_{LII}(\mathbf{v} - (\mathbf{v}\cdot\mathbf{n})\mathbf{n})\}; \tag{38}$$

$$\eta_{LII} = \frac{1}{\sqrt{j(j+1)}} \times \frac{j\left(R_{3,-j} + R_{4,-j} + \frac{1}{j} R_{5,-j} + \frac{2j+1}{j} R_{6,-j}\right) +}{\left(R_{3,-j} + R_{4,-j} + \frac{1}{j} R_{5,-j} + \frac{2j+1}{j} R_{6,-j}\right) -}$$

$$\rightarrow \frac{+(j+1)(R_{3,j+1} + R_{4,j+1} - 2R_{5,j+1}) \exp\{i(\delta_{j+1} - \delta_{-j})\}}{-(R_{3,j+1} + R_{4,j+1} - 2R_{5,j+1}) \exp\{i(\delta_{j+1} - \delta_{-j})\}}.$$

In conclusion I express my sincere thanks to Profs. V. B. Berestetskii and A. P. Rudik for posing the problem and for advice, to Academician A. I. Alikhanov and V. A. Liubimov for interest in the work and for discussion, and to Prof. L. A. Sliv who provided the values of the radial integrals.

---

[1] V. B. Berestetskii and A. P. Rudik, J. Exptl. Theoret. Phys. (U.S.S.R.) **35**, 159 (1958), Soviet Phys. JETP **8**, 111 (1959).

[2] Berestetsky, Ioffe, Rudik and Ter-Martirosian, Nucl. Phys. **5**, 464 (1958).

[3] A. I. Akhiezer and V. B. Berestetskii, **Квантовая электродинамика** (Quantum Electrodynamics) GTTI, Moscow, 1953; (translation by U. S. Gov't. Printing Office, 1957).

[4] I. M. Shmushkevich, J. Exptl. Theoret. Phys. (U.S.S.R.) **33**, 1477 (1957), Soviet Phys. JETP **6**, (33) 1139 (1958).

[5] Biedenharn, Blatt, and Rose, Revs. Modern Phys. **24**, 249 (1952).

Translated by M. Hamermesh
257

SOVIET PHYSICS JETP VOLUME 35(8), NUMBER 5 MAY, 1959

THE OSCILLATIONS OF A DEGENERATE ELECTRON FLUID

V. P. SILIN

P. N. Lebedev Physics Institute, Academy of Sciences, U.S.S.R.

Submitted to JETP editor May 31, 1958

J. Exptl. Theoret. Phys. (U.S.S.R.) 35, 1243-1250 (November, 1958)

The oscillations of an electron fluid are treated on the basis of the Landau theory of the Fermi fluid.[1] The oscillations reduce to longitudinal plasma waves, transverse electromagnetic waves, zeroth sound, and spin waves.

1. In treating the oscillations of a degenerate electron fluid on the basis of the usual theory of such a fluid one can deal with longitudinal plasma waves, and also with transverse electromagnetic waves.[2-4] The treatment includes the interaction between the electrons caused by the electromagnetic field. Such a treatment, however, is valid only under the condition that the interaction between the electrons is small in comparison with their kinetic energy. In the opposite case the correlation of the particles, and in particular the exchange correlation of the electrons, leads to important changes in the kinetic equations.[5]

The general theory of the degenerate Fermi fluid has been examined by Landau,[1] and the use of such a theory for the electron fluid has been discussed in an earlier paper.[6] We examine below the oscillations of a degenerate electron fluid on the basis of the Landau theory. The analogous problem for the uncharged degenerate Fermi fluid has been discussed in references 7 to 9.

2. For our study of the oscillations of a degenerate electron fluid we use the kinetic equation for the quasi-particles, which has the form[6]

$$\frac{\partial n}{\partial t} - \frac{i}{\hbar}[\varepsilon, n] + \frac{1}{2}\left(\frac{\partial \varepsilon}{\partial \mathbf{p}}\frac{\partial n}{\partial \mathbf{r}} + \frac{\partial n}{\partial \mathbf{r}}\frac{\partial \varepsilon}{\partial \mathbf{p}}\right) - \frac{1}{2}\left(\frac{\partial \varepsilon}{\partial \mathbf{r}}\frac{\partial n}{\partial \mathbf{p}} + \frac{\partial n}{\partial \mathbf{p}}\frac{\partial \varepsilon}{\partial \mathbf{r}}\right)$$
$$+ e\mathbf{E}\frac{\partial n}{\partial \mathbf{p}} + \frac{1}{2}\frac{e}{c}\left(\left[\frac{\partial \varepsilon}{\partial \mathbf{p}} \times \mathbf{H}\right]\frac{\partial n}{\partial \mathbf{p}} + \frac{\partial n}{\partial \mathbf{p}}\left[\frac{\partial \varepsilon}{\partial \mathbf{p}} \times \mathbf{H}\right]\right) = \hat{J}, \tag{1}$$

where n is the density matrix, ϵ is the Hamiltonian function of the quasiparticles, and $[\epsilon, n]$ is the commutator of these quantities; these are all matrices in the spin space. $\hat{J}$ is the collision operator. The field strengths obey the Maxwell equations:

$$\operatorname{div}\mathbf{E} = 4\pi e\,\mathrm{Sp}_\sigma \int d\mathbf{p}'\delta n,$$
$$\operatorname{curl}\mathbf{H} - \frac{1}{c}\frac{\partial \mathbf{E}}{\partial t} = \frac{4\pi e}{c}\mathrm{Sp}_\sigma \int d\mathbf{p}\frac{\partial \varepsilon}{\partial \mathbf{p}} n + 4\pi\beta \operatorname{rot}\mathrm{Sp}_\sigma \int d\mathbf{p}\hat{\sigma} n,$$
$$\operatorname{div}\mathbf{H} = 0, \operatorname{curl}\mathbf{E} + \frac{1}{c}\frac{\partial \mathbf{H}}{\partial t} = 0, \tag{2}$$

where σ are the Pauli spin matrices $(\sigma_i\sigma_k + \sigma_k\sigma_i = 2\delta_{ik})$, and δn is the nonequilibrium contribution to the density matrix. For small deviations from the equilibrium state

$$\delta\varepsilon(\mathbf{p}, \mathbf{r}) = -\beta(\hat{\sigma}\cdot\mathbf{H})$$
$$+ \mathrm{Sp}_{\sigma'}\int\{\varphi(\mathbf{p}, \mathbf{p}') + (\hat{\sigma}\cdot\hat{\sigma}')\psi(\mathbf{p}, \mathbf{p}')\}\,\delta n(\mathbf{p}', \mathbf{r})\,d\mathbf{p}'. \tag{3}$$

Here the spin-orbit interactions have been neglected.

It is convenient to use instead of n the distribution function $f = \mathrm{Sp}\, n$ of the particles in the phase space of the coordinates and momenta, and the vector function $\sigma = \mathrm{Sp}\,\hat{\sigma} n$ of the spin density in the phase space.

Then (cf. reference 7), recalling that $\epsilon_{mn} = \delta_{mn}\epsilon_1 + \hat{\sigma}_{mn}\epsilon_2$, we have:

$$\frac{\partial f}{\partial t} + \frac{\partial \varepsilon_1}{\partial \mathbf{p}}\frac{\partial f}{\partial \mathbf{r}} - \frac{\partial \varepsilon_1}{\partial \mathbf{r}}\frac{\partial f}{\partial \mathbf{p}} + \frac{\partial \varepsilon_2}{\partial p_j}\frac{\partial \sigma}{\partial r_j} - \frac{\partial \varepsilon_2}{\partial r_j}\frac{\partial \sigma}{\partial p_j}$$
$$+ e\mathbf{E}\frac{\partial f}{\partial \mathbf{p}} + \frac{e}{c}\left[\frac{\partial \varepsilon_1}{\partial \mathbf{p}} \times \mathbf{H}\right]\frac{\partial f}{\partial \mathbf{p}} + \frac{e}{c}\left[\frac{\partial \varepsilon_{2j}}{\partial p} \times \mathbf{H}\right]\frac{\partial \sigma_j}{\partial \mathbf{p}} = J, \tag{4}$$

$$\frac{\partial \sigma}{\partial t} + \left(\frac{\partial \varepsilon_1}{\partial \mathbf{p}}\cdot\frac{\partial}{\partial \mathbf{r}}\right)\sigma - \left(\frac{\partial \varepsilon_1}{\partial \mathbf{r}}\cdot\frac{\partial}{\partial \mathbf{p}}\right)\sigma + \frac{2}{\hbar}[\boldsymbol{\varepsilon}_2 \times \sigma] + \left(\frac{\partial f}{\partial \mathbf{r}}\cdot\frac{\partial}{\partial \mathbf{p}}\right)\boldsymbol{\varepsilon}_2$$
$$- \left(\frac{\partial f}{\partial \mathbf{p}}\cdot\frac{\partial}{\partial \mathbf{r}}\right)\boldsymbol{\varepsilon}_2 + e\left(\mathbf{E}\cdot\frac{\partial}{\partial \mathbf{p}}\right)\sigma$$
$$+ \frac{e}{c}\left(\left[\frac{\partial \varepsilon_1}{\partial \mathbf{p}} \times \mathbf{H}\right]\frac{\partial}{\partial \mathbf{p}}\right)\sigma - \frac{e}{c}\left(\left[\frac{\partial f}{\partial \mathbf{p}} \times \mathbf{H}\right]\frac{\partial}{\partial \mathbf{p}}\right)\boldsymbol{\varepsilon}_2 = \mathbf{J}. \tag{5}$$

In the equilibrium state, on the assumption that we can expand in powers of the constant field H_0 and keep only the first-order terms, we have:

$$\boldsymbol{\varepsilon}_{20} = -\beta\mathbf{H}_0 + \int d\mathbf{p}'\psi(\mathbf{p}, \mathbf{p}')\,\sigma_0(\mathbf{p}') \tag{6}$$

In virtue of the fact that

$$\sigma_0 = \frac{\partial f_0}{\partial \varepsilon}\boldsymbol{\varepsilon}_{20}, \tag{7}$$

Equation (6) is an integral equation for ϵ_{20}. It is easy to see that the solution of this equation has the form*

---

*It is assumed throughout that the Fermi surface has the shape of a sphere.

$$\varepsilon_{20} = -\gamma(p)\,\mathbf{H}_0,$$

where

$$\gamma(p) = \beta\left\{1 + \frac{2}{(2\pi\hbar)^3}\frac{p_0^2}{v_0}\int do'\,[\psi(\mathbf{p}_0, \mathbf{p}_0') - \psi(\mathbf{p}, \mathbf{p}_0')]\right\} \times \left\{1 + \frac{2}{(2\pi\hbar)^3}\frac{p_0^2}{v_0}\int do'\psi(\mathbf{p}_0, \mathbf{p}_0')\right\}^{-1}. \tag{8}$$

For a momentum equal to the limiting momentum p_0 of the Fermi distribution Eq. (8) gives an expression agreeing with that obtained by Landau.[1]

The oscillations of the degenerate electron fluid, regarded as small deviations from the equilibrium state, can be described by kinetic equations obtained from Eqs. (4) and (5) by neglect of terms of the order of H_0^2:

$$\frac{\partial\delta f}{\partial t} + \left(\mathbf{v}\frac{\partial}{\partial\mathbf{r}}\right)\left(\delta f - \frac{\partial f_0}{\partial\varepsilon}\delta\varepsilon_1\right) + e\mathbf{E}\frac{\partial f_0}{\partial\mathbf{p}} + \frac{e}{c}[\mathbf{v}\times\mathbf{H}_0]\frac{\partial}{\partial\mathbf{p}}\left(\delta f - \frac{\partial f_0}{\partial\varepsilon}\delta\varepsilon_1\right) = J; \tag{4'}$$

$$\frac{\partial\delta\sigma}{\partial t} + \left(\mathbf{v}\frac{\partial}{\partial\mathbf{r}}\right)\left(\delta\sigma - \frac{\partial f_0}{\partial\varepsilon}\delta\varepsilon_2\right) - \frac{2\gamma(p)}{\hbar}\left[\mathbf{H}_0, \delta\sigma - \frac{\partial f_0}{\partial\varepsilon}\delta\varepsilon_2\right] + \frac{e}{c}\left([\mathbf{v}\times\mathbf{H}_0]\frac{\partial}{\partial\mathbf{p}}\right)\left(\delta\sigma - \frac{\partial f_0}{\partial\varepsilon}\delta\varepsilon_2\right) = \mathbf{J}. \tag{5'}$$

Here*

$$\mathbf{v} = \partial\varepsilon_1/\partial\mathbf{p},$$

$$\delta\varepsilon_1(\mathbf{p}, \mathbf{r}) = \int\varphi(\mathbf{p}, \mathbf{p}')\,\delta f(\mathbf{p}', \mathbf{r})\,d\mathbf{p}',$$

$$\delta\varepsilon_2(\mathbf{p}, \mathbf{r}) = -\beta\mathbf{H} + \int\psi(\mathbf{p}, \mathbf{p}')\,\delta\sigma(\mathbf{p}', \mathbf{r})\,d\mathbf{p}'.$$

3. Of the various types, we first single out the oscillations that are not accompanied by changes of the spin distribution function. We then get the following equation for the nonequilibrium contribution δf to the distribution function, which describes such oscillations:

$$-i\omega\delta f + \left(i\,\mathbf{k}\cdot\mathbf{v} + \frac{e}{c}[\mathbf{v}\times\mathbf{H}_0]\frac{\partial}{\partial\mathbf{p}}\right)\left(\delta f - \frac{\partial f_0}{\partial\varepsilon}\delta\varepsilon_1\right) + \frac{\partial f_0}{\partial\varepsilon}\frac{4\pi i e^2c^2}{\omega^2 - c^2k^2}\left\{\mathbf{k}\cdot\mathbf{v}\int d\mathbf{p}'\delta f' - \frac{\omega}{c^2}\int d\mathbf{p}'\mathbf{v}\cdot\mathbf{v}'\left(\delta f' - \frac{\partial f_0}{\partial\varepsilon'}\delta\varepsilon_1'\right)\right\} = -\frac{1}{\tau}\left\{\delta f - \frac{\partial f_0}{\partial\varepsilon}\delta\varepsilon_1 - \int\frac{do'}{4\pi}\left(\delta f' - \delta\varepsilon_1'\frac{\partial f_0}{\partial\varepsilon}\right)\right\}. \tag{9}$$

Here it is assumed that the dependence of δf on the time and the coordinates has the form $\exp(-i\omega t + i\mathbf{k}\cdot\mathbf{r})$, and in addition it is assumed that there is no constant electric field.

When we represent δf in the form of a series of spherical harmonics (with the polar axis directed along $\mathbf{H}_0$),

$$\delta f = \frac{\partial f_0}{\partial\varepsilon}\sum_{n,m} F_{n,m}Y_n^m(\theta, \varphi),$$

$$Y_n^m(\theta, \varphi) = \sqrt{\frac{2n+1}{4\pi}\frac{(n-|m|)!}{(n+|m|)!}}\,e^{im\varphi}P_n^m(\cos\theta) \tag{10}$$

and set

$$\frac{2}{(2\pi\hbar)^3}\frac{4\pi p_0^2}{v_0}\varphi = \Phi = \sum_l A_lP_l(\cos\chi), \tag{11}$$

where χ is the angle between the vectors $\mathbf{p}$ and $\mathbf{p}'$, we get the following dispersion equation for the determination of the frequencies of the characteristic oscillations of the electron fluid:

$$\begin{aligned}
\Bigg|\,\delta_{nn'}\delta_{mm'} &- \frac{A_{n'}}{2n'+1}\Bigg\{\left(-im'\Omega + \frac{1}{\tau}\right)N_{nn'}^{mm'} \\
&- ikv_0\Bigg[\left(\sqrt{\frac{(n'+1)^2 - m'^2}{4(n'+1)^2 - 1}}\,N_{n,n'+1}^{mm'} + \sqrt{\frac{n'^2 - m'^2}{4n'^2 - 1}}\,N_{n,n'-1}^{m,m'}\right)\cos\theta_k \\
&+ \frac{1}{2}\sin\theta_k e^{-i\varphi_k}\left(\sqrt{\frac{(n'-m'-1)(n'-m')}{4n'^2 - 1}}\,N_{n,n'-1}^{m,m'+1} - \sqrt{\frac{(n'+m'+1)(n'+m'+2)}{4(n'+1)^2 - 1}}\,N_{n,n'+1}^{m,m'+1}\right) \\
&+ \frac{1}{2}\sin\theta_k e^{i\varphi_k}\left(\sqrt{\frac{(n'-m'+1)(n'-m'+2)}{4(n'+1)^2 - 1}}\,N_{n,n'+1}^{m,m'-1} - \sqrt{\frac{(n'+m')(n'+m'-1)}{4n'^2 - 1}}\,N_{n,n'-1}^{m,m'-1}\right)\Bigg]\Bigg\} - \frac{1+A_0}{\tau}\delta_{n'0}\delta_{m'0}N_{nn'}^{mm'} \\
&+ \frac{4\pi i e^2c^2}{\omega^2 - c^2k^2}\frac{8\pi p_0^2}{(2\pi\hbar)^3}\Bigg\{\frac{k}{\sqrt{3}}\delta_{n'0}\delta_{m'0} \\
&\times\left[\cos\theta_k N_{n1}^{m0} + \frac{e^{i\varphi_k}}{2}\sin\theta_k N_{n,1}^{m,-1} + \frac{e^{-i\varphi_k}}{2}\sin\theta_k N_{n1}^{m1}\right] \\
&+ \frac{\omega v_0}{3}\left(1 + \frac{A_1}{3}\right)\delta_{n'1}(\delta_{m'0} + \delta_{m'1} + \delta_{m',-1})N_{nn'}^{mm'}\Bigg\}\Bigg| = 0,
\end{aligned} \tag{12}$$

where $\Omega = evH_0/cp$, θ_k and φ_k are the angles fixing the direction of the vector $\mathbf{k}$, and, finally,

$$\begin{aligned}
N_{nn'}^{mm'} = \int do\,Y_n^m(\theta, \varphi) &\times\left\{\exp\left[-\frac{2\pi i}{\Omega}\left(\omega + \frac{i}{\tau} - kv\cos\theta_k\cos\theta\right)\right] - 1\right\}^{-1}\frac{1}{\Omega}\int_{\varphi}^{2\pi+\varphi}d\varphi' \\
&\times\exp\left\{-\frac{1}{\Omega}\left(\left[-i\omega + \frac{1}{\tau} + ikv_0\cos\theta_k\cos\theta\right](\varphi - \varphi')\right.\right. \\
&\left.\left.- ikv_0\sin\theta_k\sin\theta\,[\sin(\varphi_k - \varphi) - \sin(\varphi_k - \varphi')]\right)\right\}Y_{n'}^{m'}(\theta, \varphi').
\end{aligned} \tag{13}$$

Equation (12) has a simple solution in the long-wave region, where the condition $kv_0 \ll \Omega_0$ holds. In this case we get*

$$\omega_{nm} = m\Omega\left(1 + \frac{A_n}{2n+1}\right) + O(k^2),\quad (1 < |m| \leqslant n). \tag{14}$$

The frequencies ω_{nm} correspond to definite spherical harmonics, which are approximately independent of each other. With increasing values of kv_0, however, the different harmonics are more strongly coupled to each other, and it is then impossible to find solutions like Eq. (14).

---

*Hereafter H is the alternating magnetic field.

*In what follows we suppose τ sufficiently large and neglect the frequency of collisions. We note that the frequency corresponding to $n = 1$ is the resonance frequency of the cyclotron resonance in the region of the normal skin effect.

Let us analyze the simplest case of oscillations under the condition $H_0 = 0$. Then by orienting the polar axis parallel to **k** and taking $\tau \to \infty$, we get instead of Eq. (12)

$$\left| \delta_{nn'}\delta_{mm'} + ikv_0 \frac{A_{n'}}{2n'+1} \left[\sqrt{\frac{(n'+1)^2 - m'^2}{4(n'+1)^2 - 1}} N^{mm'}_{n,n'+1} + \sqrt{\frac{n'^2 - m'^2}{4n'^2 - 1}} N^{mm'}_{n,n'-1} \right] + \frac{4\pi i e^2 c^2}{\omega^2 - c^2k^2} \frac{8\pi p_0^2}{(2\pi\hbar)^3} \left[\frac{k}{\sqrt{3}} \delta_{n'0}\delta_{m'0} N^{m0}_{n1} + \frac{\omega v_0}{3}\left(1 + \frac{A_1}{3}\right) \delta_{n'1} (\delta_{m'0} + \delta_{m'1} + \delta_{m',-1}) N^{mm'}_{nn'} \right. \right| = 0, \qquad (15)$$

and here

$$i N^{mm'}_{nn'} = \delta_{mm'} \int \frac{do Y^{m*}_{n}(\theta, \varphi) Y^{m'}_{n'}(\theta, \varphi)}{-\omega + kv\cos\theta}. \qquad (16)$$

From this we see that the waves with different values of m are independent. Furthermore, the terms in Eq. (15) that arise from the charge of the electrons are important only for waves with $m \leq 1$ and play no part for the oscillations with $m > 1$. Therefore the theory of the zeroth sound in the electron fluid for waves with $m > 1$ is just like that for the case of He^3.[7,8] In particular, if for $i > 2$ all the A_i are zero, then the dispersion equation for the zeroth sound with $m = 2$, which determines the speed of sound $sv_0 = \omega/k$, has the form

$$\frac{4}{A_2} - \frac{1}{5} = -\frac{3}{2}(s^2 - 1)\left\{\frac{1}{3} + (s^2 - 1)\left[1 - \frac{s}{2}\ln\frac{s+1}{s-1}\right]\right\}. \qquad (17)$$

The case $m = 0$ corresponds to the plasma oscillations considered in reference 10. For them let us here look in more detail into the case in which only A_1 is different from zero. In this case we get from Eq. (15):

$$1 + \frac{A_1}{3} + \left\{A_1 s^2 + \frac{32\pi^2 e^2 p_0^2}{k^2 v_0 3 (2\pi\hbar)^3}\left(1 + \frac{A_1}{3}\right)\right\}\left[1 - \frac{s}{2}\ln\frac{s+1}{s-1}\right] = 0. \qquad (18)$$

In the region $\omega \gg kv_0$ we get from this the dispersion equation of the plasma oscillations:

$$\omega^2 = \omega_0^2 + \frac{3}{5}\left(1 + \frac{A_1}{3}\right)k^2 v_0^2, \quad \omega_0^2 = \frac{32\pi^2 e^2 p_0^2 v_0}{3(2\pi\hbar)^3}\left(1 + \frac{A_1}{3}\right). \qquad (19)$$

It is important to consider the question of the possibility of undamped longitudinal oscillations with frequency much smaller than the plasma frequency ω_0. For this purpose we can write Eq. (18) approximately in the form

$$\frac{k^2 v_0^2}{3\omega_0^2}\left(1 + \frac{A_1}{3}\right) = \frac{s}{2}\ln\frac{s+1}{s-1} - 1 \equiv \eta(s). \qquad (20)$$

Because of the fact that the left side is small and the right side can be small only in the region $s \gg 1$, where it is $\sim (1/3s^2)$, Eq. (20) has no solutions with $\omega \ll \omega_0$. Here it is supposed throughout that A_1 is not too large in comparison with unity.

Let us now consider the transverse oscillations $m = 1$, again supposing that only A_1 is different from zero and that $\tau \to \infty$. Here we have from Eq. (15):

$$1 - \frac{1}{2}A_1\left\{\frac{1}{3} - (s^2 - 1)\eta(s)\right\} - \frac{3}{2}\frac{\omega_0^2}{\omega^2 - c^2k^2}\{1 - (s^2 - 1)\eta(s)\} = 0. \qquad (21)$$

In the case in which the phase velocity considerably exceeds the speed of the electrons on the Fermi surface $(s \gg 1)$ we get $\omega^2 = \omega_0^2 + c^2k^2$, which corresponds to propagation of transverse electromagnetic waves in the electron fluid with the dielectric constant $\epsilon(\omega) = 1 - \omega_0^2/\omega^2$.

Let us now examine the possibility of propagation of waves with frequency much smaller than the plasma frequency (ω_0) and with phase velocity much smaller than the speed of light. Then Eq. (21) gives

$$(s^2 - 1)\eta(s) = 1 + \left(1 + \frac{A_1}{3}\right)\left[\frac{3}{2}\frac{v_0^2}{c^2}\frac{\omega_0^2}{\omega^2}s^2 - \frac{A_1}{2}\right]^{-1}. \qquad (22)$$

Because of the fact that the right member of Eq. (22) is positive and bounded $(\lesssim 0.3)$, undamped solutions are not always possible. In particular, there are no solutions for $\omega \ll (v_0/c)\omega_0$. The situation is particularly simple in the opposite case, in which the inequalities

$$\omega_0 \gg \omega \gg (v_0/c)\,\omega_0 A_1^{-1/2}, \qquad (23)$$

hold and Eq. (22) takes the form

$$(s^2 - 1)\eta(s) = 1/3 - 2/A_1, \qquad (24)$$

corresponding to oscillations of an uncharged fluid. Equation (24) has solutions only for $A_1 > 6$. Calculations of the coefficient A_1 for several metals,* carried out in reference 11, give $A_1 \lesssim 3$. Therefore we can suppose that for such metals a transverse zeroth sound can scarcely be possible. In principle, however, the possibility of the existence of solutions of Eq. (24) is of interest in connection with the possibility that in the range of frequencies given by the inequalities (23) there may be a band of transparency of the metal, with a real index of refraction.

If the constant magnetic field is not zero, and H_0 is parallel to k, the dispersion equation (12) can be put in the form:

---

*The quantity A given by Eq. (19) of reference 11 is connected with A_1 by the equation $A_1 = 3A$.

$$\Big|\delta_{nn'}\delta_{mm'} + i\,\frac{A_{n'}}{2n'+1}\Big\{m'\Omega N_{nn'}^{mm'} + kv_0\Big[\sqrt{\frac{(n'+1)^2-m'^2}{4(n'+1)^2-1}}\,N_{n,n'+1}^{mm'} + \sqrt{\frac{n'^2-m'^2}{4n'^2-1}}\,N_{n,n'-1}^{mm'}\Big]\Big\} + \frac{4\pi i e^2c^2}{\omega^2-c^2k^2}\,\frac{8\pi p_0^2}{(2\pi\hbar)^3}\Big[\frac{k}{\sqrt{3}}\,\delta_{n'0}\delta_{m'0}N_{n,1}^{m0} + \frac{\omega v_0}{3}\Big(1+\frac{A_1}{3}\Big)\delta_{n'1} \times (\delta_{m'0}+\delta_{m'1}+\delta_{m'-1})\,N_{nn'}^{mm'}\Big]\Big| = 0, \tag{25}$$

where

$$iN_{nn'}^{mm'} = \delta_{mm'}\int\frac{do\,Y_n^{m*}(\theta,\varphi)\,Y_{n'}^{m'}(\theta,\varphi)}{-\omega+kv_0\cos\theta+m\Omega}. \tag{26}$$

To bring out the part played by the constant magnetic field let us consider oscillations corresponding to the conditions under which the dispersion relation (17) holds in the absence of a magnetic field. Then for the oscillations with $m = 2$ we get:

$$-\frac{1}{A_2} = \frac{1}{5} + \frac{3\omega}{8kv_0}\Big\{\Big(\frac{\omega-2\Omega}{kv_0}\Big)^3 - \frac{5}{3}\Big(\frac{\omega-2\Omega}{kv_0}\Big) + \frac{1}{2}\Big[\Big(\frac{\omega-2\Omega}{kv_0}\Big)^2-1\Big]^2\ln\Big|\frac{\omega-2\Omega-kv_0}{\omega-2\Omega+kv_0}\Big|\Big\}. \tag{27}$$

In the long-wave region $(kv_0 \ll 2\Omega)$ we have from this

$$\omega = 2\Omega\Big(1+\frac{A_2}{5}\Big)\Big\{1+\frac{5}{7A_2}\Big(\frac{kv_0}{2\Omega}\Big)^2\Big\}. \tag{28}$$

In order for Eq. (27) to have undamped solutions, it is necessary that the inequality

$$|\omega-2\Omega| > |k|\,v_0 \tag{29}$$

be satisfied. From this and Eq. (27) it follows that for negative A_2, when Eq. (17) has no solutions, Eq. (27) also will have no solutions for wavelengths smaller than a critical value, which is of the order of magnitude v_0/Ω. The same assertion also holds for cases less restricted than that in which only A_2 is different from zero.

4. Let us now consider oscillations of the spin distribution function. Here we turn first to the case in which there are changes of the component of the vector function $\boldsymbol{\sigma}$ parallel to the constant magnetic field $\mathbf{H}_0$. Neglecting the collisions, we then have from Eq. (5′):

$$\frac{\partial\delta\sigma_z}{\partial t} + \Big(\mathbf{v}\,\frac{\partial}{\partial\mathbf{r}}\Big)\Big(\delta\sigma_z - \frac{\partial f_0}{\partial\varepsilon}\,\delta\varepsilon_{2z}\Big) + \frac{e}{c}\Big([\mathbf{v}\times\mathbf{H}_0]\,\frac{\partial}{\partial\mathbf{p}}\Big)\Big(\delta\sigma_z - \frac{\partial f_0}{\partial\varepsilon}\,\delta\varepsilon_{2z}\Big) = 0. \tag{30}$$

This equation is similar to Eq. (3), differing in the absence of terms coming from the alternating magnetic field, and also in the fact that $\delta\epsilon_{2Z}$ appears instead of $\delta\epsilon_1$ and δf is replaced by $\delta\sigma_Z$. Therefore it is easy to verify that Eq. (30) yields the following dispersion relation:

$$\Big|\delta_{nn'}\delta_{mm'} + i\,\frac{B_{n'}}{2n'+1}\Big\{m'\Omega N_{nn'}^{mm'} + kv_0\Big[\cos\theta_k\Big(\sqrt{\frac{(n'+1)^2-m'^2}{4(n'+1)^2-1}}\,N_{n,n'+1}^{mm'} + \sqrt{\frac{n'^2-m'^2}{4n'^2-1}}\,N_{n,n'-1}^{m,m'}\Big) + \frac{1}{2}\sin\theta_k e^{-i\varphi_k}\Big(\sqrt{\frac{(n'-m'-1)(n'-m')}{4(n'+1)^2-1}}\,N_{n,n'-1}^{m,m'+1} - \sqrt{\frac{(n'+m'+1)(n'+m'+2)}{4(n'+1)^2-1}}\,N_{n,n'+1}^{m,m'+1}\Big) + \frac{1}{2}\sin\theta_k e^{i\varphi_k}\Big(\sqrt{\frac{(n'-m'+1)(n'-m'+2)}{4(n'+1)^2-1}}\,N_{n,n'+1}^{m,m'-1} - \sqrt{\frac{(n'+m')(n'+m'-1)}{4n'^2-1}}\,N_{n,n'-1}^{m,m'-1}\Big)\Big]\Big\}\Big| = 0, \tag{31}$$

where $N_{nn'}^{mm'}$ is given by Eq. (13) for $\tau \to \infty$, and the coefficients B_n are defined by the relation

$$\frac{2}{(2\pi\hbar)^3}\,\frac{4\pi p_0^2}{v_0}\,\psi = \Psi = \sum_n B_nP_n(\cos\chi). \tag{32}$$

In the long-wave region we get from this a simple expression for the frequencies of the spin oscillations

$$\omega_{n,m} = m\Omega\Big(1+\frac{B_n}{2n+1}\Big) + O\Big(\frac{k^2v_0^2}{\Omega}\Big). \tag{33}$$

In the region of shorter waves, for example in the case in which the wave vector is parallel to the magnetic field, the dispersion relation is like that obtained for the oscillations of the distribution function, with replacement of A_n by B_n [cf. e.g., Eqs. (27) to (29)].

Let us now turn to the case in which there are vibrations of the components of $\boldsymbol{\sigma}$ perpendicular to the constant magnetic field. Writing $\sigma^{(\pm)} = \sigma_x \pm i\sigma_y$, we get the following equation:

$$\frac{\partial}{\partial t}\,\delta\sigma^{(\pm)} + \Big\{\Big(\mathbf{v}\,\frac{\partial}{\partial\mathbf{r}}\Big) + \frac{e}{c}\Big([\mathbf{v}\times\mathbf{H}_0]\,\frac{\partial}{\partial\mathbf{p}}\Big) \pm i\,\frac{2\gamma(p)}{\hbar}\,H_0\Big\} \times \Big(\delta\sigma^{(\pm)} - \frac{\partial f_0}{\partial\varepsilon}\,\delta\varepsilon_2^{(\pm)}\Big) = 0, \tag{34}$$

which leads to a dispersion relation differing from Eq. (31) only by the replacement of $m'\Omega$ by $m'\Omega \pm \Omega_0$, where $\Omega_0 = 2\gamma(p_0)H_0/\hbar$. Therefore in the special case of long waves we have at once, as in Eq. (33):*

$$\omega_{m,n} = (\pm\Omega_0 + m\Omega)\Big(1+\frac{B_n}{2n+1}\Big) + O\Big(\frac{k^2v_0^2}{\Omega}\Big). \tag{35}$$

In particular, for $m = 0$ we have $\omega_{00} = \pm 2\beta H_0/\hbar$, which corresponds to the ordinary Bloch frequency.

Let us examine in somewhat greater detail the case of short waves, on the assumption that only B_0 is different from zero and that the wave vector **k** is parallel to the direction of the constant magnetic field H_0. The dispersion equation takes the form:

---

*For $\Omega = 0$ the spectrum obtained here corresponds to the spectrum of the spin waves of a paramagnetic fluid, as treated in reference 9 in the approximation of small B_n. I take this occasion to point out that in Eq. (2.16) of that paper the coefficients α_n should be taken with the opposite signs.

$$-\frac{1}{B_0} = 1 - \frac{s}{2} \ln\left|\frac{s \mp s_0 + 1}{s \mp s_0 - 1}\right|,$$

where $s = \omega/kv_0$, $s_0 = \Omega_0/kv_0$.

In the region of small wavelengths we have from this

$$\omega = kv_0 s = \pm\Omega_0 (1 + B_0)\{1 + k^2 v_0^2/3B_0\Omega_0^2\}. \quad (36)$$

For positive B_0 the frequency increases with increasing k.

In the short-wave region $kv_0 \gg \Omega_0$ the dispersion equation takes the form $1/B_0 = \eta(s)$ and has solutions only for positive B_0. In the case of negative B_0, on the other hand, it follows from Eq. (36) that with decrease of the wavelength the absolute value of the frequency decreases. Furthermore, in the case $1 + 1/B_0 < 0$ the frequency of the spin wave goes to zero for $|k| = \Omega_0/v_0$, according to the formula

$$\omega = \pm\left\{\Omega_0 - |k| v_0\left[1 + \exp\left(\frac{1 + B_0}{B_0} \frac{2|k|v_0}{\Omega_0 - |k|v_0}\right)\right]\right\}. \quad (37)$$

5. The oscillations of a degenerate electron fluid considered here are in a certain sense similar to plasma waves, and correspond to excitations that obey Bose statistics. The same applies also in particular to the excitations of an electron fluid in a magnetic field, with the spectra given by Eqs. (14), (33), and (35). Therefore the contributions of such excitations to the partition function will be decidedly different from the contribution of the single-particle states, which obey Fermi statistics.

---

[1] L. D. Landau, J. Exptl. Theoret. Phys. (U.S.S.R.) 30, 1058 (1956), Soviet Phys. JETP 3, 920 (1956).

[2] I. I. Gol'dman, J. Exptl. Theoret. Phys. (U.S.S.R.) 17, 681 (1947).

[3] D. Bohm and D. Pines, Phys. Rev. 82, 625 (1951).

[4] Iu. L. Klimontovich and V. P. Silin, J. Exptl. Theoret. Phys. (U.S.S.R.) 23, 151 (1952). V. P. Silin, Тр. ФИАН, Изд. АН СССР (Trans. Phys. Inst. Acad. Sci., U.S.S.R.) 6, 199 (1955).

[5] V. P. Silin, Физика металлов и металловедение (Phys. of Metals and Metal Research) 3, 193 (1956).

[6] V. P. Silin, J. Exptl. Theoret. Phys. (U.S.S.R.) 33, 495 (1957), Soviet Phys. JETP 6, 387 (1958).

[7] L. D. Landau, J. Exptl. Theoret. Phys. (U.S.S.R.) 32, 59 (1957), Soviet Phys. JETP 5, 101 (1958).

[8] I. M. Khalatnikov and A. A. Abrikosov, J. Exptl. Theoret. Phys. (U.S.S.R.) 33, 110 (1957), Soviet Phys. JETP 6, 84 (1958).

[9] V. P. Silin, J. Exptl. Theoret. Phys. (U.S.S.R.) 33, 1227 (1957), Soviet Phys. JETP 6, 948 (1958).

[10] V. P. Silin, J. Exptl. Theoret. Phys. (U.S.S.R.) 34, 781 (1958), Soviet Phys. JETP 7, 538 (1958).

[11] V. P. Silin, J. Exptl. Theoret. Phys. (U.S.S.R.) 33, 1282 (1957), Soviet Phys. JETP 6, 985 (1958).

Translated by W. H. Furry
258

SOVIET PHYSICS JETP VOLUME 35(8), NUMBER 5 MAY, 1959

GALVANOMAGNETIC CHARACTERISTICS OF METALS WITH OPEN FERMI SURFACES. I

I. M. LIFSHITZ and V. G. PESCHANSKII

Physico-Technical Institute, Academy of Sciences, Ukrainian S.S.R., Khar'kov State University

Submitted to JETP editor July 10, 1958

J. Exptl. Theoret. Phys. (U.S.S.R.) **35**, 1251-1264 (November, 1958)

Galvanomagnetic phenomena in strong fields are studied for metals with open Fermi surfaces. Characteristic features of the angular dependences of galvanomagnetic parameters on the magnetic field direction are investigated and their relation to the topology of an open surface is determined. In particular, the possibility of resistivity saturation, previously established in principle[1] for certain orientations of the magnetic field relative to the crystal axes, and its quadratic increase for other directions are analyzed in detail. It is found under what conditions the resistivity can increase linearly with the field as a result of averaging over the orientations of the crystallites in polycrystalline samples.

THE theory of galvanomagnetic phenomena in metals, developed in reference 1 for an arbitrary dispersion law $\epsilon = \epsilon(\mathbf{p})$ and an arbitrary collision integral, enable us to draw certain inferences regarding the topology of the Fermi surface from the experimentally determined galvanomagnetic characteristics. When the Fermi surface is open or when it is located near open constant-energy surfaces, the asymptotic behavior of the conductivity tensor σ_{ik} in strong magnetic fields can differ essentially from its asymptotic behavior when the constant-energy surfaces are closed. Thus, for example, the asymptotic Hall coefficient for metals with an open Fermi surface can depend on the orientation of the magnetic fields with respect to the crystallographic axes, whereas for closed surfaces the Hall coefficient in strong magnetic fields is isotropic (if the number of electrons does not equal the number of holes).

An even more important distinguishing characteristic of open surfaces is the fact that for some directions of the magnetic field the resistivity can approach saturation, while for other directions it can rise without limit ($\rho \sim H^2$).

In the present paper we investigate the galvanomagnetic properties of metals with different types of open constant-energy surfaces and determine the characteristics of the angular dependences of these properties.

1. GEOMETRY OF PLANE SECTIONS OF AN OPEN FERMI SURFACE

For convenience we shall discuss only the constant-energy surfaces which have the form of an "undulating cylinder" (Fig. 1) and the surface which is represented by a three-dimensional grid of undulating cylinders (Fig. 2).

Such surfaces are of the most common type. The existence of the three-dimensional grid has been detected experimentally by Pippard[2] for copper, while Verkin[3] has found the undulating cylinder type for zinc.

Further extension to arbitrary open constant-energy surfaces is not difficult, because the sections of such surfaces by a plane $p_z = \text{const}$ may contain momentum-space trajectories ($\epsilon = \text{const}$, $p_z = \text{const}$) of all possible types — closed and open trajectories, with or without the periodicity of the reciprocal lattice.

The direction of the magnetic field will always be taken along the z axis. The set of magnetic field directions for which it is possible to have a band of open momentum-space trajectories is determined by the structure of the constant-energy surface. In the case of the undulating-cylinder type, open trajectories are encountered only when the magnetic field is perpendicular to the cylinder axis. Open trajectories are encountered much more frequently in the case of the three-dimensional grid. Figure 3 is a stereographic projection of the magnetic field directions for which open plane sections appear in the case of the three-dimensional grid type of surface. There is a two-dimensional set (solid angle) of magnetic field directions for which open trajectories are possible (regions I in Fig. 3).

When the magnetic field direction coincides with one of the crystallographic axes open trajectories are possible only for certain isolated values of p_z and do not contribute to the tensor σ_{ik}.

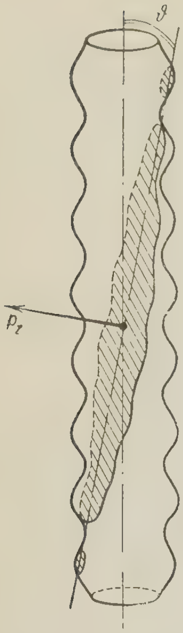

FIG. 1. Section of an "undulating cylinder" type of constant-energy surface by a plane p_z = const.

When the magnetic field is not along one of the crystallographic axes, we can have an entire band of open trajectories, integration along which contributes to σ_{ik}. A geometrical analysis shows that open trajectories appear, in particular, when the magnetic field direction is located in any principal crystallographic plane.

When the magnetic field direction is not located in any principal crystallographic plane, the condition for realization of a band of open trajectories (in the simplest case of constant-diameter tubes) is

$$b_1 \cos\varphi \tan\vartheta \leqslant d, \quad b_2 \sin\varphi \tan\vartheta \leqslant d; \qquad (1)$$

where d is the tube diameter, H, ϑ, φ are the polar coordinates of the vector H in the coordinate system where the polar axis coincides with the crystallographic axis that is closest to the magnetic field direction (axis 3 in Fig. 2), and b_1, b_2 are the periods of the reciprocal lattice in directions 1 and 2. In the general case of tubes with nonuniform diameter condition (1) is not exact and the boundaries of regions I and II (in Fig. 3) are deformed. When only one of conditions (1) is fulfilled, the closed trajectories pass through several cells of the reciprocal lattice (region III in Fig. 3).

A simple analysis shows that for a given magnetic-field direction open trajectories in all cross sections p_z = const have a common direction, which is the intersection of the xy plane perpendicular to the magnetic field with the nearest (in angle) principal crystallographic plane (open trajectories are always located in one of the principal crystallographic planes (1 0 0), (0 1 0) or (0 0 1). This direction will hereinafter be the x axis. Thus the projections of all trajectories will be of finite length along the y axis (see Fig. 4). It must always be kept in mind that for a suitable choice of axes the magnetic field direction completely determines the entire coordinate system.

2. ASYMPTOTIC BEHAVIOR OF GALVANOMAGNETIC CHARACTERISTICS IN STRONG FIELDS. TYPES OF SINGULAR MAGNETIC FIELD DIRECTIONS

In describing the motion of an electron we shall, as in reference 1, use the quantities ϵ and p_z, which are conserved in a magnetic field, as well as the dimensionless quantity $\tau = t/T_0$, which characterizes the position of the electron in the momentum-space trajectory ϵ = const and in p_z = const. Here t, the time of motion along a given trajectory, is given by $(c/eH)\int dp_x/v_y$ (see reference 1), and T_0 agrees in order of magnitude with the time required for the momentum projection (p_x or p_y) of an electron moving along a momentum-space trajectory either to return to its original value (when the trajectory is located entirely within a single cell of the reciprocal lattice) or to change by a quantity of the order of the reciprocal lattice. The latter case is possible for an electron moving along an open trajectory or along a closed trajectory which passes through a few cells of the reciprocal lattice.

To determine the conductivity tensor σ_{ik}, it is necessary to solve a kinematic equation which, after linearization for a weak electric field E, is of the form[1]

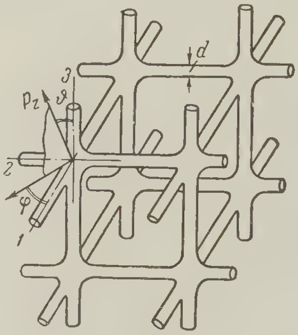

FIG. 2

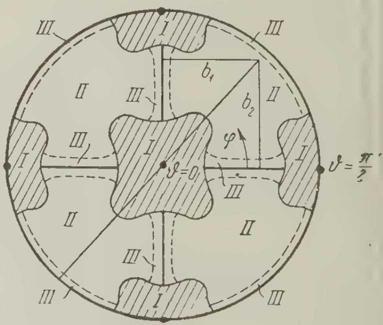

FIG. 3

FIG. 2. Constant-energy surface of the "three-dimensional grid" type.

FIG. 3. Stereographic projection of magnetic field directions. The shaded regions (I) give the field directions for which a band of open trajectories exists. Region II has no open trajectories. Region III, bounded by dashed lines, represents the field directions for which elongated closed trajectories exist (enclosing many cells).

$$\frac{t_0}{T_0}\frac{\partial \psi_i}{\partial \tau} + \widetilde{W}\{\psi_i\} = f_0'(\varepsilon)\, v_i, \tag{2}$$

where ψ_i characterizes the addition to the equilibrium function f_0 of the electron distribution:

$$f = f_0 - e t_0 \mathbf{E}\cdot\boldsymbol{\psi};$$

$\widetilde{W}\{f\}/t_0$ is the collision integral, t_0 is the mean free electron time, and $|\widetilde{W}| \sim 1$.

The electrical conductivity tensor σ_{ik} is given by[1]

$$\sigma_{ik} = -2e^2 t_0 h^{-3}\int v_i \psi_k \, d\mathbf{p}. \tag{3}$$

Strong magnetic fields are understood to be those which satisfy the condition

$$\gamma_0 = T_0/t_0 = H_0/H \ll 1. \tag{4}$$

The characteristic field H_0 is the field for which the characteristic time T_0 equals the mean free time t_0. We shall hereinafter assume that condition (4) is always fulfilled.

When all closed trajectories are located within a single cell of the reciprocal lattice and the open trajectories possess the periodicity of the reciprocal lattice, Eq. (2) can be solved by successive approximations (as in reference 1), with the following representation of ψ_i:

$$\psi_i = \sum_{l=0}^{\infty} \gamma_0^l \psi_i^{(l)}. \tag{5}$$

As will be seen below, the expansion (5) is not always permissible for open Fermi surfaces. Specifically, this can occur when the momentum-space trajectory extends over a few cells of the reciprocal lattice. This is associated with the fact that the characteristic time of electron motion in the magnetic field is the electron period of revolution along the trajectory (for a closed trajectory), which in the case of greatly extended closed trajectories that pass through a large number of reciprocal lattice cells can be comparable with or even much longer than the mean free time. Consequently, the character of the dependence of σ_{ik} on the magnetic field (that is, on $\gamma_0 = H_0/H$) varies greatly with the magnetic field orientation and near certain singular directions the expansion in powers of γ_0 is not permissible.

To simplify the following investigation, we illustrate the foregoing for the case $\widetilde{W} = 1$ (that is, for the case in which collisions can be described by introducing only the relaxation time t_0). Equation (2) then becomes

$$\frac{1}{\gamma_0}\frac{\partial \psi_i}{\partial \tau} + \psi_i = f_0'(\varepsilon)\, v_i. \tag{6}$$

For closed trajectories, as in reference 1, we use the Fourier method to obtain

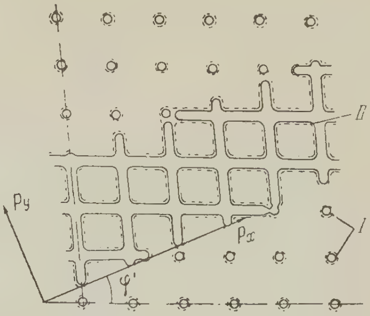

FIG. 4. Intersection of the plane $p_z = \text{const}$ and the "three-dimensional-grid" constant-energy surfaces $\epsilon = \epsilon_0$ (solid curves) and $\epsilon = \epsilon_0 + \delta\epsilon$ (dashed curves). Closed trajectories of type I correspond to energy regions $\epsilon < \epsilon_0$; trajectories of type II correspond to energy regions $\epsilon > \epsilon_0$. Accordingly, opposite directions are taken along these trajectories. These two types of curves are separated by open trajectories. The direction of an open trajectory is given by the angle φ', for which $\cos\varphi' = \cos\varphi(1 + \sin^2\varphi\tan^2\vartheta)^{-1/2}$.

$$\sigma_{il} = -2e^2 t_0 h^{-3}$$
$$\times \iint \sum_{k=1}^{\infty} f_0'(\varepsilon)\frac{cHT}{c}\frac{v_i^{-k}v_l^k + v_i^k v_l^{-k} + (ik/\gamma)(v_i^k v_l^{-k} - v_i^{-k}v_l^k)}{k^2/\gamma^2 + 1}\, d\varepsilon\, dp_z, \tag{7}$$

where $\gamma = T/t_0$, and T is the period of revolution of an electron in a closed trajectory:

$$T = (c/eH)\oint dp_x/v_y. \tag{8}$$

Near certain singular directions of the magnetic field (small ϑ in Fig. 1 and region III in Fig. 3) the trajectories are closed and greatly extended. To determine the basic angular dependence of σ_{ik} near these directions the angular dependence of γ must be taken into account explicitly. In the case of an undulating cylinder with $\vartheta \ll 1$ we have $T = \alpha T_0/\vartheta$, $\gamma = \alpha\gamma_0/\vartheta$, $\alpha \sim 1$ for most trajectories and $\gamma \sim \gamma_0$ for the remaining trajectories.

The contribution to σ_{il} from the "stretched" trajectories will be

$$\sigma_{il}' = \sum_{k=1}^{\infty}\frac{A_{il}^k\gamma_0 + B_{il}^k\vartheta}{k^2\vartheta^2 + \alpha^2\gamma_0^2}, \quad \gamma_0 = \frac{T_0}{t_0} = \frac{H_0}{H}; \tag{9}$$

where α, A^k, B^k also depend on the angles. Thus σ_{il} is a function of γ_0 and also of γ_0/ϑ. When $\vartheta \sim \gamma_0 \ll 1$ it can be seen from (9) that the following expansion is possible:

$$\sigma_{il} = \sigma_{il}(\gamma_0, \gamma_0/\vartheta) = \sum_n \gamma_0^n \sigma_{il}^{(n)}(\gamma_0/\vartheta), \tag{10}$$

whereas the expansion given in (5) is impermissible.

When $\widetilde{W} \neq 1$ the character of the angular dependence of σ_{ik} in (7) and (10) does not change qualitatively.

We have no further interest in the smooth angular dependence of σ_{ik}, which results from the specific form of the collision integral. We shall distinguish only the steep angular variation of σ_{ik} which is associated with the approach to the singular magnetic field directions.

When a two-dimensional region (solid angle) of directions of H exists for which there is a band of open trajectories, an analysis of the methods and equations of reference 1 shows that within this region it is reasonable to use the expansion of ψ_i in powers of γ_0 [expansion (5)] even when the open trajectories are aperiodic. The essential requirement for this purpose is that the mean velocities $(\overline{v}_1)_{\Delta\tau}$, during the mean free time on each portion of the trajectory (that is, in the interval $\Delta\tau \sim 1/\gamma_0$) should, to a very high degree of probability, differ very little from the mean value $\overline{v}_1$ over the entire trajectory* (it must be noted, of course, that this condition is not fulfilled for greatly extended closed trajectories).

By means of the given expansion we can see that in the most usual case when, for a given magnetic field direction, all open trajectories have a common direction (taken along the x axis) Eqs. (14), (21), (29) and (54) of reference 1 are valid and, specifically, the resistivity increases quadratically with the field, $\rho \sim H^2$. The foregoing statement refers to all surfaces considered in the present paper, for which more details are given in the following section. On the other hand, when open trajectories exist simultaneously for different directions (belonging to the same or to different surfaces if there are several of these) all components of σ_{ik} and ρ_{ik} approach saturation.

When the open trajectories have a common x direction, the asymptotic value of the transverse conductivity component σ_{yx} is of the order of $\gamma_0 \sim 1/H$ and, in virtue of Eqs. (21) and (23) of reference 1, can be written as

$$\sigma_{yx} = -2e^2h^{-3}T_0 \int \frac{\partial p_x}{\partial \tau} \left\{ C_x{}^{(1)}(p_z, \varepsilon) - \frac{c}{eHT_0} f'_0(\varepsilon)\, p_y \right\} d\tau\, dp_z\, d\varepsilon, \qquad (11)$$

where $C_x^{(1)}$ is obtained from the condition

$$\overline{\widetilde{W}\{\psi^1{}_x\}} = \overline{\widetilde{W}\left\{C^1{}_x - \frac{c}{eHT_0} f'{}_0(\varepsilon)\, p_y\right\}} = 0 \qquad (12)$$

[see Eqs. (16) to (18) of reference 1].

The second term is independent of the collision integral and is determined only by the geometry of the surface. The first term disappears for closed trajectories in virtue of the condition $\oint (\partial p_x/\partial\tau)\, d\tau = 0$. However, for open trajectories

$$\bar{v}_y \sim \lim \frac{1}{T} \int_0^T \frac{\partial p_x}{\partial \tau} d\tau \sim b_x/T_0 \neq 0.$$

Consequently σ_{yx} together with the Hall coefficient depends on the form of the collision integral and the magnetic field direction if the trajectories are not straight lines (in which case $\psi_x^{(1)} = \psi_x^{(1)}(\epsilon, p_z) = 0$). In this case the singularity in the angular dependence of the galvanomagnetic characteristics is the point where open trajectories disappear.

In accordance with the above, the special magnetic field directions can be of at least three types:

(1) Magnetic field directions for which a band of open trajectories exists form a one-dimensional set. This occurs, specifically, if there is an isolated direction of open trajectories. Examples are directions perpendicular to the axis for an undulating cylinder, and continuous curves connecting regions I in the sterographic projection of directions of H for a three-dimensional grid (Fig. 3).

(2) There exists a two-dimensional region (solid angle) of magnetic field directions corresponding to open trajectories. The singular directions of the magnetic field in this case are the boundaries of this region. An example is given by the boundaries of the shaded regions I in Fig. 3.

(3) In the open trajectory region there exists an isolated magnetic field direction for which the band of open trajectories disappears. An example is given by the directions of the principal crystallographic axes for a three-dimensional grid ($\vartheta = 0$ and similar points in Fig. 3).

As has been shown above, in case (1) a strong angular dependence of σ_{il} appears in the closed trajectory region as the singular line of magnetic field directions is approached.

In case (2) when the width of the open trajectory band vanishes on the boundary of region I, then, as will be shown, a strong angular dependence of σ_{il} appears inside this boundary (that is, in the open trajectory region). The same occurs in case (3).

A more detailed discussion with specific examples will be given in the next section.

3. INVESTIGATION OF ASYMPTOTIC BEHAVIOR FOR SOME TYPES OF FERMI SURFACE

a. Surface of the Undulating Cylinder Type

When the magnetic field is not perpendicular to the axis of a constant-energy surface of the undulating cylinder type, all trajectories $\epsilon = \text{const}$ and $p_z = \text{const}$ are closed.

---

*This requirement follows from the fact that the expansion of ψ_i in powers of γ_0 contains expressions such as $\int_0^T (v_i - \overline{v}_i)\, d\tau$ and their iterations.

When the angle ϑ between the magnetic field directions and the plane perpendicular to the cylinder axis is not small, the period T_ϑ of electron revolution through its entire momentum-space trajectory is much smaller than the characteristic mean free time t_0:

$$T_\vartheta/t_0 \approx T_0/t_0\vartheta \ll 1,$$

$\gamma_0 \ll 1$.

The conductivity tensor σ_{ik} and the resistivity tensor ρ_{ik} in strong magnetic fields have the same asymptotic form as in the case of closed constant-energy surfaces (1):

$$\sigma_{ik} = \begin{pmatrix} \gamma_0^2 a_{xx} & \gamma_0 a_{xy} & \gamma_0 a_{xz} \\ \gamma_0 a_{yx} & \gamma_0^2 a_{yy} & \gamma_0 a_{yz} \\ \gamma_0 a_{zx} & \gamma_0 a_{zy} & a_{zz} \end{pmatrix}; \tag{13}$$

$$\rho_{ik} = \begin{pmatrix} b_{xx} & \gamma_0{}^{-1}\, b_{xy} & b_{xz} \\ \gamma_0{}^{-1} b_{yx} & b_{yy} & b_{\ y} \\ b_{zx} & b_{zy} & b_{zzz} \end{pmatrix}. \tag{14}$$

For $\vartheta \gg \gamma_0$ the Hall coefficient is isotropic, independent of the form of collision integral, and inversely proportional to the volume between the cylinder surface and two adjacent crystallographic planes perpendicular to the cylinder axis.

When $\vartheta \sim \gamma_0 \ll 1$ the electron period of revolution in the largest trajectory (Fig. 1) is comparable with t_0 and σ_{ik} contains terms, which cannot be expanded in powers of γ_0 since these terms contain γ_0 in the combination γ_0/ϑ.

We shall continue to take the z axis in the direction of the magnetic field, with the x axis in the plane of the magnetic field, and cylinder axis and the y axis perpendicular to this plane.

Taking into account the angular dependence of the Fourier components of velocities v^k in different trajectories, we obtain for σ_{il}, in accordance with Sec. 2,

$$\begin{gathered} \sigma_{xx} = \sum_k \frac{A^1{}_k \vartheta^2 \gamma_0^2}{k^2\vartheta^2 + \alpha^2\gamma_0^2} + \alpha'{}_{xx}\gamma_0^2, \\ \sigma_{yy} = \sum_k \frac{B_k^1 \gamma_0^2}{k^2\vartheta^2 + \alpha^2\gamma_0^2} + a'{}_{yy}\gamma_0^2 \end{gathered} \tag{15}$$

with similar expressions for the other components (α, A_k^1, B_k^1 are coefficients independent of γ_0 and ϑ in first approximation). The second terms in (15) are associated with the trajectories which remain closed even when $\vartheta = 0$ (see Fig. 1).

For small γ_0, $\vartheta \ll 1$ but arbitrary γ_0/ϑ we can retain only the first nonvanishing terms in the expansion (10). A simple analysis then shows that the conductivity tensor can be represented asymptotically by the following general form:

$$\sigma_{il} = \begin{pmatrix} \gamma_0^2 a_{xx}(\eta) & \gamma_0 a_{xy}(\eta) & \gamma_0 a_{xz}(\eta) \\ \gamma_0 a_{yx}(\eta) & a_{yy}(\eta) & a_{yz}(\eta) \\ \gamma_0 a_{zx}(\eta) & a_{zy}(\eta) & a_{zz}(\eta) \end{pmatrix} \tag{16}$$

where $\eta = \gamma_0/\vartheta$.

When $\vartheta \ll \gamma_0$ (i.e., $\eta \to \infty$) $a_{ik}(\eta)$ tends to the finite values $a_{ik}(\infty)$; this correspond to Eqs. (29) of reference 1. On the other hand, when $\vartheta \gg \gamma_0$ the tensor $a_{ik}(\eta)$ has the form

$$a_{ik} = \begin{pmatrix} a_{xx}(0) & a_{xy}(0) & a_{xz}(0) \\ a_{yx}(0) & \alpha_1\eta^2 & \alpha_2\eta \\ a_{zx}(0) & -\alpha_2\eta & a_{zz}(0) \end{pmatrix}, \tag{17}$$

where α_1 and α_2 are constants. It is easily seen that in this case (16) reduces to (13).

Expressions of the form

$$a_{il}(\eta) = \frac{\alpha_{il}^{(0)} + \alpha_{il}^{(1)}\eta + \alpha_{il}^{(2)}\eta^2}{1 + \beta_{il}\eta^2} \tag{18}$$

furnish a good extrapolation of $a_{il}(\eta)$ corresponding to the structure of σ_{il}. Here

$$\alpha_{yy}^{(0)} = \alpha_{yy}^{(1)} = \alpha_{yz}^{(0)} = \alpha_{zy}^{(0)} = 0.$$

In the special case of a right circular cylinder, $\epsilon = (p^2 - p_3^2)/2m_0$ (p_s is the cylinder axis) and $\widetilde{W} = 1$, Eq. (18) is exact and

$$\begin{gathered} a_{xy}(\eta) = -a_{yx}(\eta) = a_{xx}(\eta) = \sigma_0/(1+\eta^2); \\ a_{zz}(\eta) = a_{yy}(\eta) = \sigma_0\eta^2/(1+\eta^2); \\ a_{yz} = a_{xz} = -a_{zy} = -a_{zx} = \sigma_0\eta/(1+\eta^2); \\ \sigma_0 = 2Vh^{-3}(e^2t_0/m_0). \end{gathered}$$

It must be noted that the singular character of $a_{il}(\eta)$ in the case of a right cylinder (specifically, the fact that $a_{zz}(0) = 0$; $a_{xx}(\infty) = a_{xy}(\infty) = 0$) is associated with the absence of undulation; then $\bar{v}_z = 0$ on each trajectory and there is no velocity component along the cylinder axis.

For the resistivity tensor ρ_{ik} we obtain

$$\rho_{ik} = (\sigma^{-1})_{ik} = \begin{pmatrix} \gamma_0^{-2} b_{xx}(\eta) & \gamma_0^{-1} b_{xy}(\eta) & \gamma_0^{-1} b_{xz}(\eta) \\ \gamma_0^{-1} b_{yx}(\eta) & b_{yy}(\eta) & b_{yz}(\eta) \\ \gamma_0^{-1} b_{zx}(\eta) & b_{zy}(\eta) & b_{zz}(\eta) \end{pmatrix}, \tag{19}$$

where $b_{ik} = (a^{-1})_{ik}$.

When $\vartheta \ll \gamma_0$ ($\eta \gg 1$), $b_{ik} \cong b_{ik}(\infty)$ are finite quantities, which are generally different from zero. In the limit $\vartheta = 0$ ($\eta = \infty$) Eq. (19) agrees with Eq. (54) of reference 1.

When $\vartheta \gg \gamma_0$ ($\eta \to 0$) the tensor $b_{ik}(\eta)$ becomes

$$b_{ik} = \begin{pmatrix} \eta^2\beta_1 & b_{xy}(0) & \eta\beta_2 \\ b_{yx}(0) & b_{yy}(0) & b_{yz}(0) \\ \eta\beta_2 & b_{zy}(0) & b_{zz}(0) \end{pmatrix}; \tag{20}$$

and the expressions for ρ_{ik} reduce to (14). In virtue of $\rho_{ik}(H) = \rho_{ki}(-H)$ we then have $b_{xy}(\eta) = -b_{yx}(\eta)$; specifically, $b_{xy}(0) = -b_{yx}(0) = 1/a_{xy}(0)$.

Equations (16) to (20) remain valid even when the Fermi surface breaks up into an undulating cylinder and an arbitrary number of closed regions. When additional open surfaces exist these equations remain valid for those magnetic field directions for which the sections of the additional surfaces are closed.

Since in the expressions for σ_{ik} and ρ_{ik} the coordinate axes were selected in a special manner, it is of interest to write the expression for the resistivity with an arbitrary direction of the current (perpendicular to the magnetic field). This gives

$$\begin{aligned}\rho &= \rho_{xx}\cos^2\alpha + \rho_{yy}\sin^2\alpha - (\rho_{xy} + \rho_{yx})\sin\alpha\cos\alpha \\ &= \gamma_0^{-2} b_{xx}(\eta)\cos^2\alpha - \gamma_0^{-1}(b_{xy}(\eta) \\ &\quad + b_{yx}(\eta))\sin\alpha\cos\alpha + b_{yy}(\eta)\sin^2\alpha,\end{aligned} \tag{21}$$

where α is the angle between the current direction and the x axis.

Taking into account the behavior of $b_{ik}(\eta)$ for $\eta \ll 1$ and $\eta \gg 1$, we represent b_{xx} in the form

$$b_{xx}(\eta) = \frac{\beta_1\eta^2}{1 + \lambda^2\eta^2}\, c(\eta),$$

and for ρ we obtain

$$\rho = \frac{\beta_1 \cos^2\alpha}{\vartheta^2 + \lambda^2\gamma_0^2}\, c(\eta) + A, \tag{22}$$

where A, β_1, λ are smooth functions of the angles and $c(\eta)$ is a smooth function of its argument $\eta = \gamma_0/\vartheta$, with $c(0) = c(\infty) = 1$.

Thus the basic dependence on angles and on the field as the singular line $\vartheta = 0$ is approached is given by (22), or explicitly

$$\rho = \frac{\beta_1 H^2 \cos^2\alpha}{\vartheta^2 H^2 + \lambda^2 H_0^2}\, c(\eta) + A. \tag{23}$$

Thus as the direction $\vartheta = 0$ is approached there appears a quadratic rise of resistivity with the field, whereas in all other directions saturation is obtained in the fields $H \sim H_0/\vartheta$. For a fixed field H there is a sharp maximum in the angular dependence of resistivity, the width of which is inversely proportional to the field:

$$\Delta\vartheta \sim \gamma_0 = H_0/H.$$

Since this maximum is very sharp in large fields, any averaging over the angles in the interval $\delta\vartheta \gg \gamma_0$ (including $\vartheta = 0$) leads to a linear rise of resistivity with the field:

$$\overline{(\rho)_{\delta\vartheta}} = \frac{\varkappa H \cos^2\alpha}{\delta\vartheta H_0} + A; \qquad \varkappa = \frac{\beta_1}{\lambda}\int_0^\infty \frac{c(\eta/\lambda)}{1+\eta^2}\, d\eta. \tag{24}$$

In particular, when the resistivity is measured in a thin polycrystalline wire with diameter of the order of the crystallite size the averaged resistivity is observed:

$$\rho = (\overline{\varkappa}/2\pi)\, H/H_0 + \overline{A} \tag{25}$$

(the bar over κ and A denotes averaging over the smooth angular dependence in the equatorial plane $\vartheta = 0$).

The linear law discovered by Kapitza[4] is possibly associated with similar averaging. It must be emphasized again that because of the narrowness of the maximum the method of averaging does not play an important part; specifically, averaging of the conductivity σ_{ik} followed by a transformation to inverse quantities yields the same result.

It must be noted that conclusions regarding the growth of resistivity near singular field directions [Eq. (23)] remain valid in the presence of few surfaces of the undulating cylinder type with differently directed axes (in view of the fact that for each of the singular field directions open sections occur for only one of these surfaces, which thus determines the behavior of ρ and σ). This can occur for cubic crystals, in which case the singular directions lie in each of the three principal crystallographic planes and the averaging again gives the linear law $\rho \sim H$.

The transverse component of the resistivity for an arbitrary current direction x' will be

$$\rho_{y'x'} = \rho_{yx}\cos^2\alpha - \rho_{xy}\sin^2\alpha + (\rho_{xx} - \rho_{yy})\sin\alpha\cos\alpha.$$

Hence for the Hall coefficient with an arbitrary current direction we obtain

$$R = \frac{\rho_{y'x'}(H) - \rho_{y'x'}(-H)}{2H} = \frac{b_{yx}(\eta) + b_{yx}(-\eta)}{2H_0} = R_0 b(\eta), \tag{26}$$

where R_0, the Hall coefficient for $\vartheta \gg \gamma_0$, is independent of the angles and the field:

$$R_0 = b_{yx}(0)/H_0 = 1/nec \tag{27}$$

(n is the number of electrons per cell) and $b(\eta)$ is a smooth function of η with

$$b(0) = 1; \quad b(\infty) = b_{yx}(\infty)/b_{yx}(0).$$

The characteristic angular dependence of the Hall coefficient on field direction for a fixed H (the rotation diagram) is shown in Fig. 5. $R = R_0$ everywhere except for a narrow region near $\vartheta = 0$, the width of which decreases with the field: $\Delta\vartheta \sim \gamma_0 = H_0/H$. In this region the asymptotic behavior of the Hall coefficient depends on the specific form of the collision integral and cannot be expressed simply.

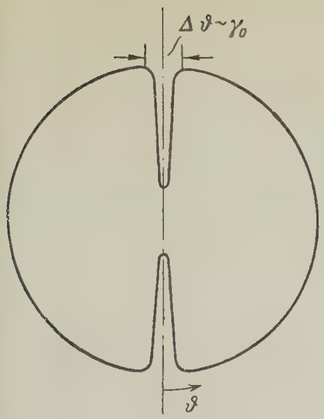

FIG. 5. Dependence of R on the angular coordinate ϑ of H (rotation diagram) for the undulating-cylinder type of surface.

b. "Three-dimensional Grid" Type of Surface

It has already been indicated that this surface (Fig. 2) possesses all of the types of singularities enumerated in Sec. 2. Specifically, the portions of the equatorial lines which do not belong to regions I in the stereographic projection of magnetic field directions (the heavy continuous lines in Fig. 3) are singular lines equivalent to the directions $\vartheta = 0$ for surfaces of the undulating cylinder type. Region III surrounding this line contains strongly stretched closed trajectories; the entire analysis and all results of the preceding section can be applied to this region. The part of ϑ is played by the angle between the magnetic field direction and the nearest principal crystallographic plane.

Singular directions of another type are found in the boundaries of regions I and II (Fig. 3) as well as the principal crystallographic axes. Before investigating these it must be noted that region II contains only closed trajectories located within the limit of a single cell while region I contains open trajectories in addition. Therefore the standard asymptotic forms (13) apply to region II up to its boundary and the steep angular dependence occurs only on the inner side of this boundary.

The asymptotic behavior of the conductivity within region I can be most conveniently investigated by considering separately the contribution to each component of the conductivity σ_{ik} (Eq. (3)) from the band of open trajectories and from all other simple closed lines. It will be remembered that the contribution from simple closed trajectories is given by (13).

To determine the contribution from the band of open trajectories we first note that the magnetic field direction (inside region I) uniquely determines the single common direction of all open trajectories (the intersection of the plane perpendicular to the magnetic field with the nearest crystallographic plane). By selecting this direction as the x axis we obtain a picture similar to the previously discussed case of an undulating cylinder with the magnetic field perpendicular to its axis ($\vartheta = 0$). Therefore the corresponding contribution to σ_{ik} is given by (16), where, however, instead of $a_{ik}(\eta)$ there are constants which are generally proportional to the width of the band of open trajectories (when this is small). The width of the band of open trajectories becomes zero on the boundary between the regions I and II and also in the directions of the principal crystallographic axes. Near these singular directions the width is generally proportional to ϑ', which is the absolute value of the angle between the magnetic field and the I-II boundary (or the direction of the nearest crystallographic axis).

Therefore near the singular directions, retaining in σ_{ik} the principal terms in the small parameters γ_0 and ϑ', we obtain

$$\sigma_{ik} = \begin{pmatrix} \gamma_0^2 a_{xx} & \gamma_0 a_{xy} & \gamma_0 a_{xz} \\ \gamma_0 a_{yx} & \gamma_0^2 a_{yy} + \vartheta' c_2 & \gamma_0 a_{yz} + \vartheta' c_3 \\ \gamma_0 a_{zx} & \gamma_0 a_{zy} + \vartheta' c_3 & a_{zz} \end{pmatrix}; \qquad (28)$$

where a_{ik}, c_i are smooth functions of the angles and are generally quantities of the same order of magnitude.

For the reciprocal tensor ρ_{ik} we have with the same accuracy

$$\rho_{ik} = \begin{pmatrix} b_{xx} + b'_{xx}\vartheta' / \gamma_0^2 & \gamma_0^{-1} b_{xy} & b_{xz} + b'_{xz}\vartheta' / \gamma_0 \\ \gamma_0^{-1} b_{yx} & b_{yy} & b_{yz} \\ b_{zx} + b'_{zx}\vartheta' / \gamma_0 & b_{zy} & b_{zz} \end{pmatrix} \qquad (29)$$

(b_{ik} are smooth functions of the angles with $b_{xy} = 1/a_{xy}$).

To determine the resistivity for an arbitrary current direction and a perpendicular field direction, the components of the tensor ρ_{ik} must again be transformed as in the preceding section [Eq. (21)]. If α is the angle between the current direction and the x direction indicated above, the resistivity ρ is given by

$$\rho = \gamma_0^{-2}\vartheta' b'_{xx} \cos^2\alpha + \gamma_0^{-1} \cos\alpha \sin\alpha \, (b_{yx} + b_{xy})$$
$$+ b_{xx} \cos^2\alpha + b_{yy} \sin^2\alpha.$$

Assuming that with accuracy to terms $\sim \gamma_0$, $b_{xy} = -b_{yx}$, we have for $H \gg H_0$ ($\gamma_0 \ll 1$)

$$\rho = \vartheta' b_{xx} (H / H_0)^2 \cos^2\alpha + A \qquad (30)$$

(A is a smooth function of the angles which is independent of H).

Thus in regions I the resistivity grows quadratically, disappearing at the boundaries and at the centers of the regions. In the current direction $\cos\alpha = 0$ (perpendicular to the direction of

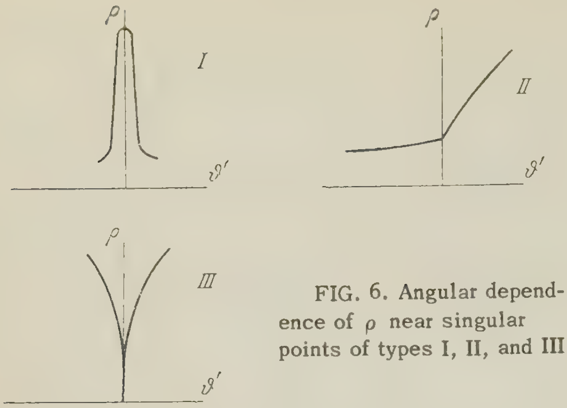

FIG. 6. Angular dependence of ρ near singular points of types I, II, and III.

open trajectories) the resistivity also tends to saturation.

It follows from Eqs. (22) and (30) that in very strong fields ($H \gg H_0$) the angular dependence of the resistivity near directions of the three singular types given at the end of the second section will have the form shown schematically in Fig. 6. A characteristic resistivity rosette containing all three types of singularities is obtained by rotating the field in a plane that passes through one of the crystallographic axes but does not lie too close to a crystallographic plane such as the (110) plane (Fig. 7). The experimental plotting of these angular dependences in different planes enables us to determine the nature of the singular points and thus to "probe" the entire Fermi surface.

We note that all the results obtained remain valid when a metal possesses an arbitrary number of closed Fermi surfaces in addition to one open surface.

As was shown in reference 1, the asymptotic behavior of σ_{yx} together with that of the Hall coefficient R in the case of simple closed trajectories is independent of the form of the collision integral and is associated only with the geometry of the Fermi surface. We are therefore able to calculate R in region II as well as close to singular points of the discussed type.

By means of Eqs. (11) and (12) and by taking into account the invariance of the distribution function under transformations associated with the translational symmetry of the lattice, we obtain for field directions close to the crystallographic axes

$$\sigma_{yx} = -\frac{2ec}{h^3 H}\left\{V - d_{\min} b_1 b_2 \left[1 - \frac{b_1 \cos\varphi + b_2 \sin\varphi}{d_{\min}} \sin\vartheta\right]\cos\vartheta + u(\vartheta, \varphi)\right\} \quad (31)$$

where V is the total volume of the tubes in one cell, $d_{\min}$ is the minimum diameter of a tube in the direction of a crystallographic axis, ϑ, φ are the angular coordinates of H (see Fig. 2), and $u(\vartheta, \varphi)$ depends on the specific form of the collision integral $\widetilde{W}$, being given by the integral

$$u(\vartheta, \varphi) = -2b_1 \int \bar{p}_y(p_z)\, dp_z,$$

taken only over open trajectories. The magnitude of $\bar{p}_y(p_z)$ is determined from the condition (12):

$$\overline{\widetilde{W}\{C_x^{(1)}\}} = \overline{\widetilde{W}\left\{f_0'(\varepsilon)\frac{c}{eHT_0}\bar{p}_y(p_z)\right\}} = \overline{\widetilde{W}\left\{f_0'(\varepsilon)\frac{c}{eHT_0}p_y(\tau)\right\}}.$$

When $\vartheta = 0$ the open trajectories disappear and $u(\vartheta, \varphi) = 0$. For small ϑ we have $u(\vartheta, \varphi) \sim \vartheta$; for constant tube diameter u decreases more rapidly than ϑ and this term in (31) can be neglected.

We can therefore make the following statements regarding the asymptotic behavior of the Hall coefficient. $R = (\rho_{y'x'}(H) - \rho_{y'x'}(-H))/2H$ is independent of H but is a function of the angles and the form of the collision integral in regions I and III (Fig. 3). In region II

$$R = 1/nec, \quad (32)$$

where $n = 2Vh^{-3}$ is the number of electrons. When the magnetic field is directed along a crystallographic axis the asymptotic Hall coefficient is also determined only by the topology of the Fermi surface and is independent of the form of collision integral. R can be written formally, by analogy with (32):

$$R = 1/n_i ec; \quad i = 1, 2, 3, \quad (33)$$

where the numbers n_i do not equal the number of electrons n and are given by

$$n_1 = n - 2h^{-3}d_1 b_2 b_3; \quad n_2 = n - 2h^{-3}d_2 b_1 b_3; \quad n_3 = n - 2h^{-3}d_3 b_1 b_2; \quad (34)$$

d_1, d_2, d_3 are here the minimum diameters of the tubes in the directions of the crystallographic axes 1, 2, 3.

An interesting fact must be noted. As shown in reference 1, the concepts of "electrons" and "holes" can be introduced only for closed surfaces. In the case of closed trajectories on open surfaces we

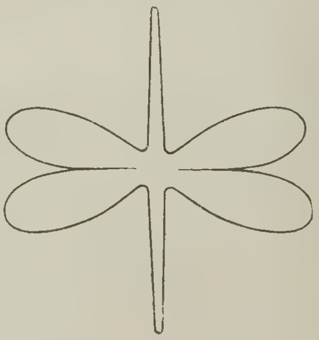

FIG. 7. Rotation diagram ($\rho = \rho(\vartheta)$) with three types of singular points.

can also speak in some sense of two types of motion depending on the direction in which a trajectory is traversed (for closed surfaces this direction differs for "electrons" and "holes"). On an open surface, however, the direction at a single point may depend on the magnetic field direction (that is, on the direction of the intersecting plane). This occurs in the case of the "three-dimensional grid" (Fig. 4). Therefore the "number of carriers" of types I and II depends on the magnetic field direction and is not invariant.

From this point of view the quantities n_1 in (33) can be interpreted formally as differences between the numbers of such carriers, in the form $n_i = n_i^{I} - n_i^{II}$, although we naturally cannot speak of any division into "holes" and "electrons".

The authors are indebted to M. I. Kaganov for valuable discussions.

Note added in proof (October 7, 1958). An angular dependence of the resistivity which becomes linear as the result of averaging, has been determined experimentally very recently by Alekseevskii and Gaidukov [J. Exptl. Theoret. Phys. (U.S.S.R.) **35**, 554 (1958), Soviet Phys. JETP **8**, 383 (1959)].

---

[1] Lifshitz, Azbel', and Kaganov, J. Exptl. Theoret. Phys. (U.S.S.R.) **31**, 63 (1956), Soviet Phys. JETP **4**, 41 (1957).

[2] A. B. Pippard, Phil. Trans. Roy. Soc. (London) **A250**, 325 (1957).

[3] B. I. Verkin, Doctoral Dissertation, Khar'kov State University, 1956.

[4] P. L. Kapitza, Proc. Roy. Soc. **A123**, 292 (1929).

Translated by I. Emin
259

SOVIET PHYSICS JETP VOLUME 35(8), NUMBER 5 MAY, 1959

CASCADE CURVES FOR COPPER

I. P. IVANENKO and B. E. SAMOSUDOV

Moscow State University

Submitted to JETP editor June 2, 1958

J. Exptl. Theoret. Phys. (U.S.S.R.) 35, 1265-1270 (November, 1958)

Electron cascade curves in copper are calculated for primary electron or photon energies $10^7 \lesssim E \lesssim 10^{12}$ ev by the method of moments. The calculation is performed with account taken of the dependence of the total photon absorption coefficient on energy and of Rutherford scattering of the charged particles. A brief analysis of the numerical results is carried out.

In experimental work on cosmic rays one uses copper or iron ionization chambers shielded by absorbers made of different materials. Thick layers of copper or iron are sometimes used as absorbers. For the purpose of analyzing the results obtained with such apparatus it is necessary to have quite accurate cascade curves in copper and iron[*] for primary electron or photon energies E_0.

Cascade curves for copper have been calculated by the method of moments.[1] In calculating the moments of the distribution function $\{N_p(E_0, 0, t)\}^{p,\Gamma}$ for electrons with energy greater than zero at depth[†] t in a shower generated by a primary electron or photon of energy E_0, by means of recursion formulas,[2] we took into account the energy dependence of the total photon absorption coefficient $\sigma(E)$ as well as Rutherford scattering of charged shower particles. $\sigma(E)$ for different E was taken from Heitler's book.[3] The expression for the "equilibrium" spectrum taking account of scattering, which served as the zero moment, was taken from the paper of Belen'kii and Maksimov.[2] The cascade unit (t-unit) in copper was taken to be 11.6 g/cm^2 with the critical energy $\beta = 16.6$ Mev. Results for the first two moments $\overline{t}(\epsilon_0, 0)$ and $\overline{t^2}(\epsilon_0, 0)$ with primary particle energies[‡] ϵ_0 from 2 to 1.4×10^5 are given in the table.

The values obtained for $\overline{t}$ and $\overline{t^2}$ were used to plot cascade curves. In earlier papers[1] a method was presented for computing cascade curves and the energy spectrum of particles generated by primary electrons or photons, for not-very-high energies in both light and heavy substances. In the present paper we shall compute cascade curves for copper over a broad energy range of the primary particles. Therefore in selecting a weighting function we must use more information regarding the behavior of the cascade curve. Cascade curves for a primary photon are approximated by means of polynomials which are orthogonal in the interval $(0, \infty)$ with the weighting function[*]

$$w(t) = \gamma^{i+1} t^i e^{-\gamma t} / \Gamma(i+1). \qquad (1)$$

Here $\gamma = 0.376$ is the minimum value of the total photon absorption coefficient in copper. We determine i by equating the first moment of the weighting function to the sought distribution function. The ordinary theory of orthogonal polynomials[4] was used to construct an orthogonal system of polynomials with weighting $w(t)$ in the interval $(0, \infty)$.

Figures 1 and 2 show the resulting curves. It may be noted that for $\epsilon_0 \sim 1$ we obtain $i < 1$. In this case $dN/dt\,|_{t=0} = \infty$, so that it is more convenient to assume $i = 1$ and to determine γ accordingly. For $\epsilon_0 = 2$, 6, 10, and 14 we obtain $\gamma = 0.64$, 0.55, 0.51, and 0.47, respectively. The series obtained in this way converges rapidly and $\{N_p\}^\Gamma$ for $\epsilon_0 = 14$ practically coincides with the value obtained with $\gamma = \sigma_{\min}$.

The cascade curves for a primary electron were approximated by means of polynomials that were orthogonal in the interval $(0, \infty)$ with the weighting function

$$w(t) = \gamma^{i+1} (a + t^i) e^{-\gamma t} / (\Gamma(i+1) + a\gamma^i). \qquad (2)$$

Here i and a are determined by equating the

---

[*] Z of copper is ~ 10% different for that of iron, so that the derived cascade curves can also be used for calculations of cascade processes in iron.

[†] In cascade theory depth is measured in the so-called "cascade unit" of length.[3]

[‡] ϵ is the particle energy measured in units of β/q, where β is the critical energy for the given material and q is a constant equal to 2.29

[*] For convenience in subsequent calculations, the weighting function w(t) will always be assumed to be normalized to unity.

ε_0	$\{\bar{t}_p(\varepsilon_0, 0)\}^p$	$\{\overline{t_p^2}(\varepsilon_0,0)\}^p$	$\{\bar{t}_p(\varepsilon_0, 0)\}^\Gamma$	$\{\overline{t_p^2}(\varepsilon_0, 0)\}^\Gamma$	ε_0	$\{\bar{t}_p(\varepsilon_0, 0)\}^p$	$\{\overline{t_p^2}(\varepsilon_0, 0)\}^p$	$\{\bar{t}_p(\varepsilon_0, 0)\}^\Gamma$	$\{\overline{t_p^2}(\varepsilon_0,0)\}^\Gamma$
2	0.96	2.99	3.13	17.8	$3.5 \cdot 10^2$	6.62	56.4	7.48	69.7
6	2.02	8.22	3.61	21.2	$5.6 \cdot 10^2$	7.10	64.0	7.92	77.1
10	2.64	12.1	3.94	23.8	$7.7 \cdot 10^2$	7.42	69.2	8.22	82.7
14	3.06	15.1	4.24	26.2	$9.8 \cdot 10^2$	7.66	73.3	8.47	87.2
35	4.13	24.9	5.16	36.3	$1.4 \cdot 10^3$	8.01	79.5	8.83	94.1
56	4.66	30.6	5.65	42.3	$7.4 \cdot 10^3$	9.68	112	10.5	129
77	5.01	34.6	5.97	46.7	$1.4 \cdot 10^4$	10.3	126	11.1	144
98	5.27	37.9	6.22	50.1	$7.4 \cdot 10^4$	12.0	166	12.8	187
$1.4 \cdot 10^2$	5.66	42.9	6.58	55.3	$1.4 \cdot 10^5$	12.6	183	13.4	205

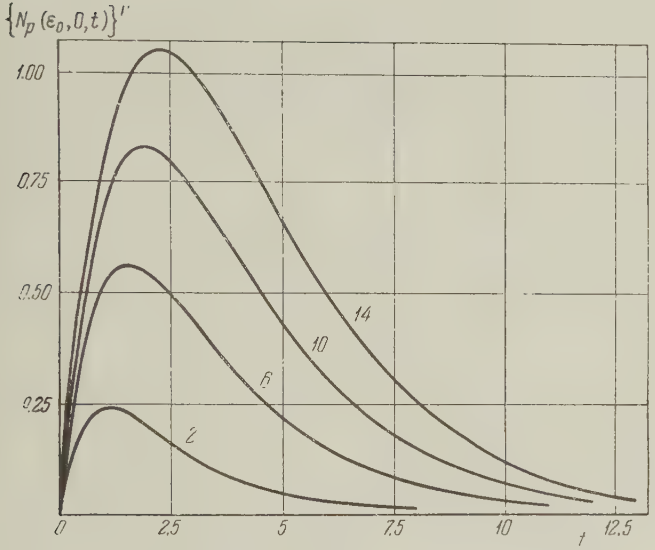

FIG. 1. Cascade curves in copper for a primary photon. The numerals over the curves denote the primary photon energy in units of β/q.

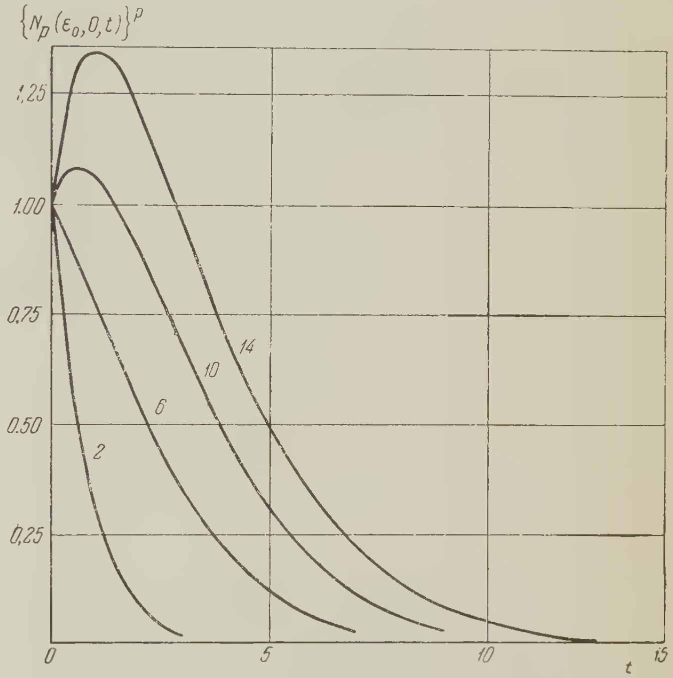

FIG. 3. Cascade curves in copper for a primary electron. The numerals over the curves denote the primary electron energy in units of β/q.

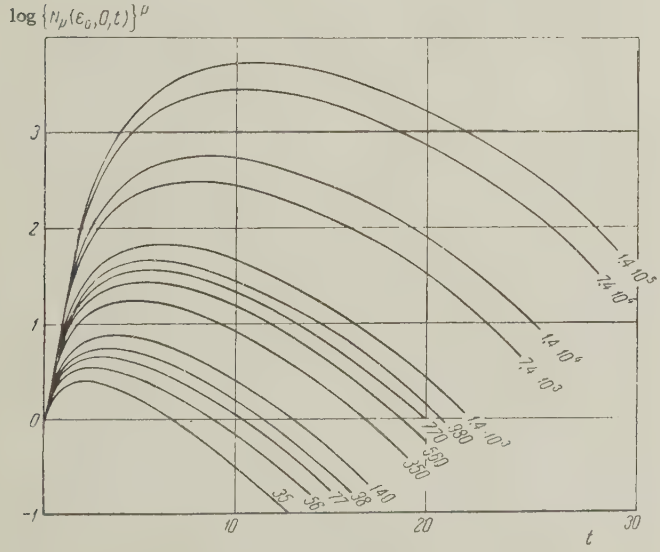

FIG. 2. The same as in Fig. 1.

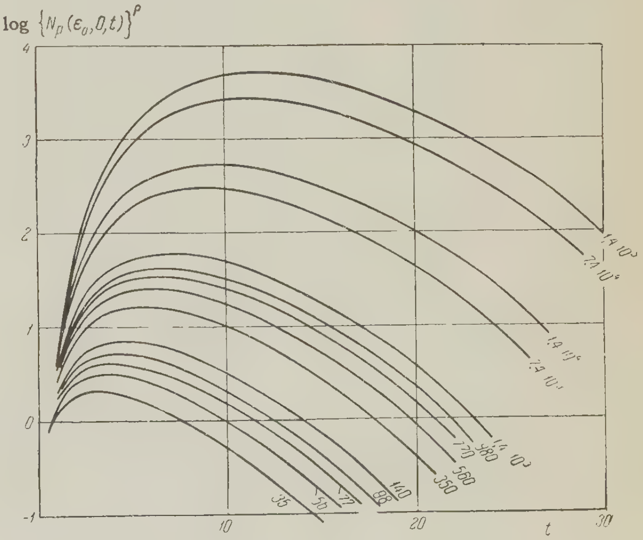

FIG. 4. The same as in Fig. 3.

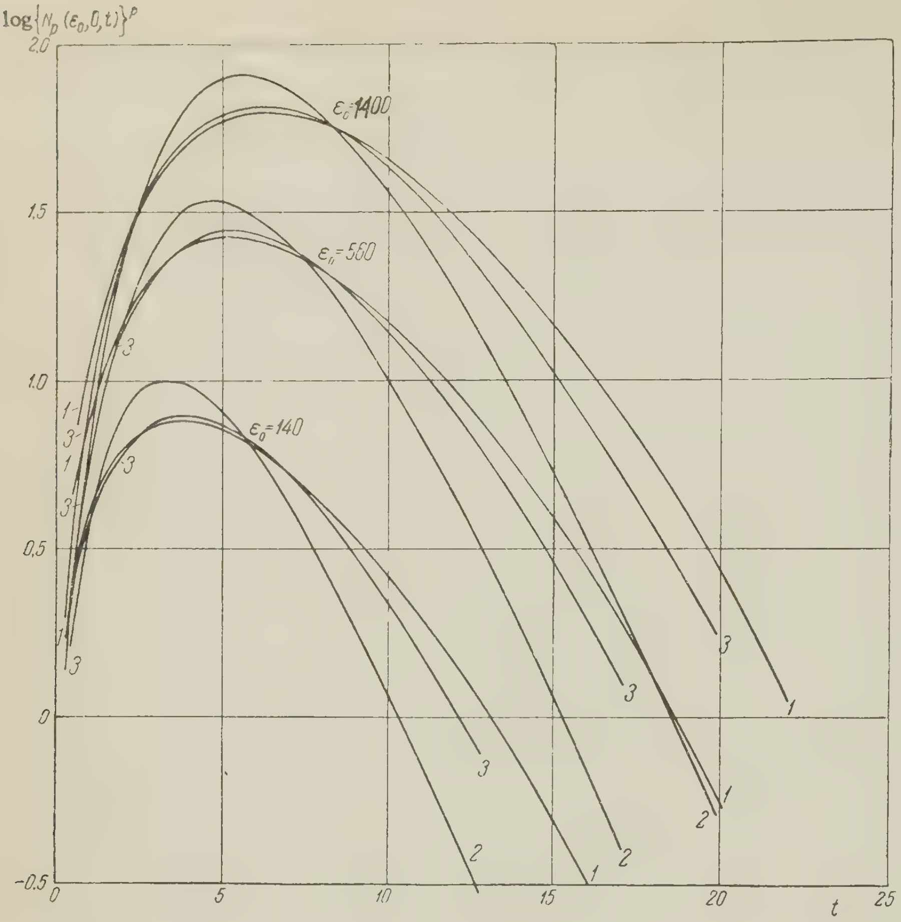

FIG. 5. Cascade curves in copper for a primary electron with several values of ε_0. Curves 1 were calculated by the method of moments, curves 2 from the equations of Belen'kii and Maksimov[2] and curves 3 from Ott's equations.[6]

first moments of the weighting function to the value $\bar{t}(\epsilon_0, 0)$ of the sought distribution function and from the boundary condition $\{N_p(\epsilon_0, 0, 0)\}^p = 1$.

The resulting curves are shown in Figs. 3 and 4. For $\epsilon_0 \sim 1$ we obtain $0 < i < 1$. To avoid obtaining an infinite derivative at $t = 0$, in the first few curves we assume i to be equal to the nearest integer, after which a is determined. As in the case of a primary photon the series converge quite rapidly, owing to the proper choice of a weighting function that provides a good representation of all essential features of the distribution function. We note that by means of only a slight complication this method can be used to obtain cascade curves that are more exact for small values of t. For this purpose it is sufficient to introduce one additional parameter into the weighting function. The values of this parameter can be determined from the boundary condition at $t = 0$ for the derivative of the cascade curve with respect to t, which can be obtained from the equations of the cascade theory. An investigation of the computed functions (see reference 1, for example, which contains a detailed analysis of similar functions) shows that in the present case over the entire interval of primary energies and depths with the exception of the first cascade unit the error in the cascade curves does not exceed 10%.

It is of interest to compare our results with the cascade curves of ordinary shower theory[5] which do not take into account the energy dependence of the total photon absorption coefficient nor Rutherford scattering, and with the cascade curves obtained for copper from the approximate formula of K. Ott (see reference 6). Figure 5 shows that curves 1 and 3 are in good agreement around the maximum, while curves 1 and 2 differ by a factor of 1.5, with the difference diminishing as ϵ_0 increases. In the first few cascade t-units the curves differ by a factor of about 1.3. The tails of curves 1 and 3 [where $N(t) \sim 1$] differ by a factor of 1.4 to 1.7. Thus Ott's approximate equation[6] satisfactorily describes the development of the cascade process in copper only in the vicinity of the shower maximum. Bernstein[7] solved the cascade equations by successive approximations, the zero approximation being that obtained by using asymptotic expressions for the cross sections of elementary processes.[5] A correction was calculated by means of Bethe and Heitler's more exact approximation for the cross sections. However the results are valid only when there is little difference between the exact and asymptotic cross sections and become incorrect when $Z \approx 30$. The tails of curves 1 and 2 differ by a factor of 2.5 to 4.5 and the difference increases with ϵ_0 as in the case of curves 1 and 3.

Belen'kii[5] obtained the following equations for the position and number of particles of a shower maximum:

$$t_m = \bar{t}, \quad N_m = (E_0/\beta)\,[2\pi(\overline{t^2} - \bar{t}^2)]^{-1/2}. \tag{3}$$

A comparison of the values of t_m and N_m for the curves of Figs. 1 to 4 with the values calculated from (3) by means of the table shows that (3) can be used for t_m when $\epsilon_0 > 10^2$ and for N_m when $\epsilon_0 > 10^3$. The accuracy of (3) is somewhat diminished for cascade curves from a primary photon.

---

[1] I. P. Ivanenko, J. Exptl. Theoret. Phys. (U.S.S.R.) **31**, 86 (1956), Soviet Phys. JETP **4**, 115 (1957); **32**, 491 (1957), Soviet Phys. JETP **5**, 413 (1957); Dokl. Akad. Nauk SSSR **107**, 819 (1956), Soviet Phys. "Doklady" **1**, 231 (1956).

[2] S. Z. Belen'kii and B. I. Maksimov, J. Exptl. Theoret. Phys. (U.S.S.R.) **22**, 102 (1952).

[3] W. Heitler, The Quantum Theory of Radiation (Oxford, 1953), (Russ. Transl. IIL, Moscow, 1956).

[4] G. Szego, Orthogonal Polynomials, Amer. Math. Soc. Coll. Publ. 23 (1939); Научное наследие П. Л. Чебышева (Scientific Heritage of P. L. Chebyshev) No. 1, Acad. Sci. Press, 1945.

[5] S. Z. Belen'kii, Лавинные процессы в космических лучах (Cascade Processes in Cosmic Radiation), Gostekhizdat, 1948.

[6] W. Heisenberg, Kosmische Strahlung, Springer, Berlin, 1953.

[7] I. B. Bernstein, Phys. Rev. **80**, 995 (1950).

Translated by I. Emin
260

CALCULATION OF THE PHONON PART OF THE MUTUAL FRICTION FORCE IN SUPERFLUID HELIUM

L. P. PITAEVSKII

Institute of Physical Problems, Academy of Sciences, U.S.S.R.

Submitted to JETP editor July 13, 1958

J. Exptl. Theoret. Phys. (U.S.S.R.) **35**, 1271-1275 (November, 1958)

The part of the mutual friction force in superfluid helium due to the scattering of phonons by vortex filaments is calculated. It is shown that the phonon part of the mutual friction force becomes comparable with the roton part at temperatures on the order of 0.5°K.

It has been shown by Hall and Vinen[1] that in rotating helium II there exists a force of mutual friction between the normal and the superfluid parts of the liquid. To calculate this force it is necessary to study the scattering of the elementary excitations that make up the normal part of the liquid, i.e., of the phonons and rotons, by the vortex filaments. At temperatures above about 0.6°K the phonon part of ρ_n is considerably smaller than the roton part. Because of this, at such temperatures the entire mutual friction force is due to the rotons. Calculations of this part of the friction force have been carried out by Hall and Vinen[2] and by Lifshitz and Pitaevskii.[3] At the very lowest temperatures, however, the number of rotons decreases sharply, and the contribution of the phonons to the mutual friction force can become important.

To calculate this contribution we must use the ordinary hydrodynamical equations to calculate the scattering of sound by a vortex line. We point out to start with that the theory given below is essentially based on the smallness of the dimensionless quantity

$$\nu = \hbar k / mc = \hbar\omega / mc^2, \tag{1}$$

where k is the wave vector of the phonon, ω is the frequency, c is the speed of sound in the helium, and m is the mass of a helium atom. The main part in all phenomena is played by the phonons for which $\hbar\omega \sim \kappa T$ (κ is Boltzmann's constant), so that we have for ν:

$$\nu \sim \kappa T / mc^2 \approx 4 \cdot 10^{-2} T, \tag{2}$$

i.e., $\nu \sim 0.02$ for $T \sim 0.5°$. Physically the quantity ν is the ratio of the distance from the axis of the vortex at which the speed would equal the speed of sound to the wavelength of the phonon.

We write out the hydrodynamical equations:

$$\partial \mathbf{v} / \partial t + (\mathbf{v} \cdot \nabla) \mathbf{v} + \nabla p / \rho = 0, \tag{3}$$

$$\partial \rho / \partial t + \operatorname{div} \rho \mathbf{v} = 0, \tag{4}$$

and take the velocity $\mathbf{v}$ in the form $\mathbf{v} = \mathbf{v}_0 + \mathbf{v}'$, where $\mathbf{v}_0$ is the velocity of the liquid around the vortex

$$\mathbf{v}_0 = (\hbar / m) [\boldsymbol{\beta} \times \mathbf{r}] / r^2 \tag{5}$$

($\boldsymbol{\beta}$ is the unit vector along the axis of the vortex), and $\mathbf{v}'$ is the velocity in the sound wave. We use similar expressions for the density ρ and the pressure p: $\rho = \rho_0 + \rho'$, $p = p_0 + p'$. Linearization of Eqs. (3) and (4) in the primed quantities leads to the equations of propagation of sound in the presence of the vortex:

$$\frac{\partial \mathbf{v}'}{\partial t} = -(\mathbf{v}_0 \cdot \nabla) \mathbf{v}' - (\mathbf{v}' \cdot \nabla) \mathbf{v}_0 - \frac{c^2}{\rho_0} \nabla \rho' + \frac{\nabla p_0}{\rho_0^2} \rho'; \tag{6}$$

$$\frac{\partial \rho'}{\partial t} + \rho_0 \operatorname{div} \mathbf{v}' + \mathbf{v}_0 \cdot \nabla \rho' + \nabla \rho_0 \cdot \mathbf{v}' = 0. \tag{7}$$

We now put $\mathbf{v}' = \mathbf{v}_1 + \mathbf{v}_2$, where $\mathbf{v}_1 = (\mathbf{k}/k) v_1 \times e^{i(\mathbf{k} \cdot \mathbf{r} - \omega t)}$ is the velocity in the incident wave,* $\mathbf{v}_2$ that in the scattered wave; and similarly we put $\rho' = \rho_1 + \rho_2$ and $p' = p_1 + p_2$.

We now make the assumption, the correctness of which will be verified later, that at all relevant distances the scattered wave is weaker than the incident wave. This enables us to treat the scattering by perturbation theory, i.e., in the Born approximation.

We further note that at all distances much larger than $\hbar/mc \approx 0.5 \times 10^{-8}$ cm the condition $v_0 \ll c$ is satisfied, so that the change of density in the vortex is relatively small, $\Delta\rho_0 \ll \rho_0$, and can be evaluated from Bernoulli's equation:

---

*Since the component of a wave propagated along the vortex is not scattered, we can confine ourselves to a discussion of waves in the plane perpendicular to the vortex line. Accordingly in all formulas $\mathbf{r}$, $\mathbf{k}$, and so on are two-dimensional vectors.

$$\Delta\rho_0 \approx c^{-2}\Delta p_0 = -\rho_0 v^2/2c^2 = \rho(\hbar/mc^2)^2. \tag{8}$$

It can be seen from Eq. (8) that near the axis of the vortex the change of the density of the liquid is quadratic in the "perturbation" $\mathbf{v}_0$, and consequently in the Born approximation we can regard ρ_0, p and c as constants in Eqs. (7) and (8). A detailed calculation shows that the terms coming from the change of density would make a contribution to the scattered wave containing an additional factor of the small parameter $\hbar k/mc$. Thus we have (from now on we shall always write ρ instead of ρ_0):

$$\frac{\partial \mathbf{v}_2}{\partial t} + \frac{c^2}{\rho}\nabla\rho_2 = -(\mathbf{v}_0\cdot\nabla)\mathbf{v}_1 - (\mathbf{v}_1\cdot\nabla)\mathbf{v}_0; \tag{9}$$

$$\frac{\partial\rho_2}{\partial t} + \rho\,\mathrm{div}\,\mathbf{v}_2 = -\mathbf{v}_0\cdot\nabla\rho_1. \tag{10}$$

Eliminating the velocity $\mathbf{v}_2$ from Eqs. (9) and (10), we get an equation for ρ_2:

$$\Delta\rho_2 + k^2\rho_2 = c^{-2}\rho\{k^2(\mathbf{v}_0\cdot\mathbf{v}_1) - i\mathbf{k}\cdot\nabla(\mathbf{v}_0\cdot\mathbf{v}_1) - \mathrm{div}[(\mathbf{v}_1\cdot\nabla)\mathbf{v}_0]\}. \tag{11}$$

As is well known, the solution of the equation

$$\Delta\rho + k^2\rho = Q(\mathbf{r}) \tag{12}$$

(Δ is the two-dimensional Laplacian operator) that contains only an outgoing wave at infinity has the form[4]

$$\rho(\mathbf{r}) = -\frac{i}{4}\int H_0^{(1)}(k|\mathbf{r}-\mathbf{r}'|)\,Q(\mathbf{r}')\,d^2\mathbf{r}' \tag{13}$$

($H_0^{(1)}$ is the Hankel function). Solving Eq. (11) by this formula and using integration by parts in the terms containing the divergence, we get:

$$\rho_2(\mathbf{r}) = \frac{i\rho}{4}\Big\{\frac{k^2}{c^2}\int H_0^{(1)}(k|\mathbf{r}-\mathbf{r}'|)(\mathbf{v}_0\cdot\mathbf{v}_1)\,d^2\mathbf{r}' \tag{14}$$
$$-\mathrm{div}\Big[\int H_0^{(1)}(k|\mathbf{r}-\mathbf{r}'|)\Big(\frac{i}{c}\mathbf{k}(\mathbf{v}_0\cdot\mathbf{v}_1) + c^{-2}(\mathbf{v}_1\cdot\nabla)\mathbf{v}_0\Big)d^2\mathbf{r}'\Big]\Big\}.$$

First let us convince ourselves that the condition for the applicability of the Born approximation, which we have used for the calculation, is actually fulfilled. For the validity of the Born approximation it is necessary that the condition

$$\rho_2 \ll \rho_1 \tag{15}$$

hold at such distances as are of importance in all the integrations. It is clear that the region $r' \sim 1/k$ is the important one for the integrals of Eq. (14). But for $r \sim 1/k$

$$\rho_2 \sim (\hbar k/mc)\rho_1 \ll \rho_1, \tag{16}$$

which indeed justifies the approximations that have been made.*

Let us now find the asymptotic expression for ρ_2 for

$$r \gg \lambda \sim 1/k$$

(λ is the wavelength of the phonon). To do this we use the asymptotic formula

$$H_0^{(1)}(kR) = \sqrt{2/\pi ikR}\,e^{ikR}, \quad R \gg 1/k. \tag{17}$$

for $r \gg 1/k$ values $r' \ll r$ are the important ones in the integrals. We have approximately

$$|\mathbf{r}-\mathbf{r}'| \approx r - \mathbf{r}'\cdot\mathbf{n}; \tag{18}$$
$$H_0^{(1)}(k|\mathbf{r}-\mathbf{r}'|) \approx \sqrt{2/\pi ikr}\exp(ikr - i\mathbf{k}'\cdot\mathbf{r}')$$

($\mathbf{k}' = k\mathbf{n}' = k\mathbf{r}/r$ is the wave vector of the scattered wave). Substituting Eq. (18) into Eq. (14), we find

$$\rho_2 = \frac{i}{4}\rho\frac{v_1}{c}\sqrt{2/\pi ikr}\,\frac{e^{i\mathbf{k}\cdot\mathbf{r}}}{c}\{k^2\mathbf{k} + (\mathbf{k}\cdot\mathbf{k}')\mathbf{k} + (\mathbf{k}\cdot\mathbf{q})\mathbf{k}'\}\cdot\frac{\mathbf{v}_\mathbf{q}}{k}. \tag{19}$$

Here $\mathbf{q} = \mathbf{k} - \mathbf{k}'$, and

$$\mathbf{v}_\mathbf{q} = \int e^{i\mathbf{q}\cdot\mathbf{r}'}\mathbf{v}_0\,d^2\mathbf{r}'. \tag{20}$$

We can calculate the integral in Eq. (20) most simply by using the fact that

$$\mathrm{div}\,\mathbf{v}_0 = 0, \qquad \mathrm{curl}\,\mathbf{v}_0 = 2\pi\frac{\hbar}{m}\beta\delta(\mathbf{r}). \tag{21}$$

By the relations (21) one can easily find $(\mathbf{v}_\mathbf{q}\cdot\mathbf{q})$ and $\mathbf{v}_\mathbf{q}\times\mathbf{q}$, and consequently also $\mathbf{v}_\mathbf{q}$. In fact,

$$(\mathbf{v}_\mathbf{q}\cdot\mathbf{q}) = \int \mathbf{q}e^{i\mathbf{q}\cdot\mathbf{r}}\cdot\mathbf{v}_0\,d^2\mathbf{r} \tag{22}$$
$$= -i\int \mathbf{v}_0\cdot\nabla e^{i\mathbf{q}\cdot\mathbf{r}}\,d^2\mathbf{r} = i\int e^{i\mathbf{q}\cdot\mathbf{r}}\,\mathrm{div}\,\mathbf{v}_0\,d^2\mathbf{r} = 0;$$

$$[\mathbf{v}_\mathbf{q}\times\mathbf{q}] = \int[\mathbf{v}_0\times\mathbf{q}]\,e^{i\mathbf{q}\cdot\mathbf{r}}\,d^2\mathbf{r} \tag{23}$$
$$= -i\int[\mathbf{v}_0\times\nabla e^{i\mathbf{q}\cdot\mathbf{r}}]\,d^2\mathbf{r} = -i\int e^{i\mathbf{q}\cdot\mathbf{r}}\ \mathrm{curl}\ \mathbf{v}_0\,d^2\mathbf{r} = -2\pi i\frac{\hbar}{m}\beta.$$

We take the vector products of the two sides of Eq. (23) by $\mathbf{q}$. Thus we get

$$2\pi i\frac{\hbar}{m}[\mathbf{q}\times\beta] = [\mathbf{q}\times[\mathbf{q}\times\mathbf{v}_\mathbf{q}]] - q^2\mathbf{v}_\mathbf{q}$$

or, using Eq. (22),

$$\mathbf{v}_\mathbf{q} = 2\pi\frac{\hbar}{m}i[\beta\times\mathbf{q}]\,q^{-2}. \tag{24}$$

---

*We note that $\rho_2 \ll 1$ also at all distances down to those between atoms. In fact, as can be seen from Eq. (14), for small r we have $\rho_2 \sim \hbar/mcr$, i.e., $\rho_2 \ll \rho_1$ for $r \sim a$.

Substituting this expression into Eq. (19), we find:

$$\rho_2 = \rho \frac{v_1}{c^2} \frac{\pi e^{ikr}}{\sqrt{2\pi ikr}} \frac{\hbar}{m} \left(1 - \frac{2k^2}{q^2}\right) \frac{(\mathbf{k}\cdot[\boldsymbol{\beta}\times\mathbf{k}'])}{k} \tag{25}$$

Differentiating, we obtain the velocity in the scattered wave

$$\mathbf{v}_2 = \mathbf{k}' \frac{v_1}{c} \frac{\pi e^{ikr}}{\sqrt{2\pi ikr}} \frac{\hbar}{m} \frac{\sin\varphi\cos\varphi}{\sin^2(\varphi/2)}, \tag{26}$$

where φ is the angle between $\mathbf{k}$ and $\mathbf{k}'$. We note that for values of φ close to zero v_2 increases as $1/\varphi$. This means that the Born approximation is not valid for small scattering angles. Such angles, however, are unimportant for the calculation of the friction force.

The effective scattering cross section for the sound, per unit length of the vortex filament, is given by:

$$d\sigma = \frac{|\mathbf{v}_2|^2}{|\mathbf{v}_1|^2} r\,d\varphi = \frac{\pi}{2}\left(\frac{\hbar}{mc}\right)^2 k \frac{\sin^2\varphi\cos^2\varphi}{\sin^4(\varphi/2)}\,d\varphi. \tag{27}$$

Let us now introduce the "transport cross section"

$$\sigma^* = \int (1 - \cos\varphi)\,d\sigma.$$

The physical meaning of this quantity lies in the fact that the momentum transferred to unit length of a vortex in unit time by a sound wave of energy density E_0 is given by

$$\sigma^* E_0 \sin^2\vartheta \tag{28}$$

(where ϑ is the angle of incidence of the sound wave on the plane perpendicular to the axis of the vortex). Integrating, we find

$$\sigma^* = (\pi^2\hbar^2/m^2c^2)\,k. \tag{29}$$

Let us now go on to the calculation of the phonon part of the mutual friction force. The energy density of the phonons of given frequency and direction of motion is $E_0 = \hbar\omega\,dN$, where dN is the number of phonons in unit volume. When the relative velocity is $\mathbf{u} = \mathbf{v}_R - \mathbf{v}_L$[2] ($\mathbf{v}_R$ is the velocity of the normal part near the vortex filament, and $\mathbf{v}_L$ is the velocity of the filament), dN has the form

$$\begin{aligned} dN &= \frac{1}{\exp\{\hbar(\omega - \mathbf{k}\cdot\mathbf{u})/\varkappa T\} - 1} \frac{d^3\mathbf{k}}{(2\pi)^3} \\ &\approx dN_0 - \frac{\hbar}{\varkappa T} \frac{(\mathbf{k}\cdot\mathbf{u})\,e^{\hbar\omega/\varkappa T}}{(e^{\hbar\omega/\varkappa T} - 1)^2} \frac{d^3\mathbf{k}}{(2\pi)^3} \end{aligned} \tag{30}$$

(dN_0 is the phonon distribution for $u = 0$).

Projecting the momentum transfer (28) onto the direction $\mathbf{u}$ and integrating over the angles, we get for the friction force:

$$F = \frac{3\pi^2}{8} \frac{\hbar^2 cu}{\varkappa T} \int \sigma^* \frac{e^{\hbar kc/\varkappa T}}{(e^{\hbar kc/\varkappa T} - 1)^2} \frac{k^4\,dk}{(2\pi)^3}.$$

Let us insert here the expression (29) for σ^* and make the change of variable $\hbar kc/\kappa T = x$. Then

$$F = \frac{3\pi^4}{8(2\pi)^3} \frac{(\varkappa T)^5 u}{\hbar^2 c^7 m^2} \int_0^\infty \frac{x^5 e^x}{(e^x - 1)^2}\,dx. \tag{31}$$

The remaining integral reduces to a Riemann zeta function. We get finally:

$$F = \frac{3\pi^4\, 5!\,\zeta(5)}{8(2\pi)^3} \frac{(\varkappa T)^5 u}{\hbar^2 c^7 m^2} = \frac{5!\,\zeta(5)\cdot 135}{128\,\pi} u\rho_{n\,\mathrm{ph}} \approx 42 \frac{\hbar\varkappa T}{c^2 m^2} \rho_{n\,\mathrm{ph}} u. \tag{32}$$

As for the lift force, it is zero in this approximation, because of the symmetry of the scattering in the Born approximation.

The effect calculated here can be important only at low temperatures, at which the free paths of the elementary excitations (and therefore also the viscosity of the normal part) are large and $\rho_n \ll \rho$. In this case we can neglect all effects associated with the viscosity and the Magnus effect (cf. reference 2), and simply assume that $\mathbf{u} = \mathbf{v}_n - \mathbf{v}_s$. Then formula (32) gives directly the coefficient B in the Hall-Vinen expression for the mutual friction force:

$$B_{\Phi} \approx 42\,\varkappa T/\pi mc^2 \approx 0.42\,T. \tag{33}$$

Noting that the phonon and roton coefficients B_{ph} and B_{r} give the total coefficient B by the formula

$$B = (B_{\mathrm{ph}}\rho_{n\,\mathrm{ph}} + B_{\mathrm{r}}\rho_{n\,\mathrm{r}})/(\rho_{n\,\mathrm{ph}} + \rho_{n\,\mathrm{r}})$$

(for $\rho_n \ll \rho$), and recalling that $B_r \sim 1$, we see that B_{ph} can be of importance only at temperatures $\lesssim 0.5°$. Such experiments are of course very difficult, but they are of interest for testing the theoretical ideas about the vortex filaments.

In conclusion the writer expresses his gratitude to Professor E. M. Lifshitz and Academician L. D. Landau for aid in the work and for a discussion.

---

[1] H. E. Hall and W. F. Vinen, Proc. Roy. Soc. **A238**, 204 (1956).

[2] H. E. Hall and W. F. Vinen, Proc. Roy. Soc. **A238**, 215 (1956).

[3] E. M. Lifshitz and L. P. Pitaevskii, J. Exptl. Theoret. Phys. (U.S.S.R.) **33**, 535 (1957), Soviet Phys. JETP **6**, 418 (1958).

[4] A. N. Tikhonov and A. A. Samarskii, Уравнения математической физики (Equations of Mathematical Physics), p. 505. Gostekhizdat 1951.

Translated by W. H. Furry
261

SOVIET PHYSICS JETP VOLUME 35(8), NUMBER 5 MAY, 1959

Letters to the Editor

ON A POSSIBLE STATISTICAL DESCRIPTION OF SYSTEMS OF PARTICLES INTERACTING WITH THE FIELD

Iu. L. KLIMONTOVICH

Moscow State University

Submitted to JETP editor April 11, 1958;
resubmitted July 3, 1958

J. Exptl. Theoret. Phys. (U.S.S.R.) 35, 1276-1277
(November, 1958)

To investigate the emission of electromagnetic waves by charged particles in dielectrics and decelerating media, we consider the kinetic equations for systems of electrons and oscillators of the transverse electromagnetic field, It is assumed that the charge of the electrons is compensated by a uniformly distributed background of positive charge.

A state of the system in question is determined by the coordinates and momenta of the electrons and the coordinates $Q_{\mathbf{k}}$ and momenta $P_{\mathbf{k}}$ of the field oscillators with the various wave numbers $\mathbf{k}$. We introduce a distribution function $f(q_1, \ldots, q_N, p_1, \ldots, p_N, Q_{\mathbf{k}}, \ldots, P_{\mathbf{k}}, \ldots, t)$ which gives the probabilities of different states of the system.[1]

To obtain the kinetic equations for the first electron distribution function $f_1(q, p; t)$ and the first field-oscillator distribution function $F_1(Q_{\mathbf{k}}, P_{\mathbf{k}}; t)$ we construct a suitable chain of equations connecting distribution functions of different orders. The approximation of the higher distribution functions in terms of the lower is carried out in the same way as in the paper of Bogoliubov and Gurov.[2]

If the initial distribution of the field oscillators is the equilibrium distribution and the electrons are in near-equilibrium state, we get for the distribution function f_1 an equation of the Fokker-Planck type in the phase space:

$$\frac{\partial f_1}{\partial t} + \frac{\mathbf{p}}{m}\frac{\partial f_1}{\partial \mathbf{q}}$$
$$-\frac{e^2 n}{c^2}\frac{\partial}{\partial t}\int \frac{1}{|\mathbf{q}-\mathbf{q}'|}\left\{\mathbf{p} f_1\left(\mathbf{q}', \mathbf{p}; t - \frac{|\mathbf{q}-\mathbf{q}'|}{c/\sqrt{\varepsilon}}\right) + \frac{1}{4\pi}\right.$$
$$\times \left.\int \frac{\operatorname{grad}_{\mathbf{q}''}\operatorname{div}_{\mathbf{q}''}[\mathbf{p} f_1(\mathbf{q}'', \mathbf{p}; t - |\mathbf{q}-\mathbf{q}'|\sqrt{\varepsilon}/c)]}{|\mathbf{q}'-\mathbf{q}''|}\,d\mathbf{q}''\right\} d\mathbf{q}'\,d\mathbf{p}\,\frac{\partial f_1}{\partial \mathbf{p}}$$
$$= \frac{\partial}{\partial p_\alpha} B_{\alpha\beta}\frac{\partial f_1}{\partial p_\beta} + \frac{\partial}{\partial \mathbf{p}}(\mathbf{A} f_1), \qquad (1)$$

where the diffusion coefficients $B_{\alpha\beta}$ and the systematic friction coefficient $\mathbf{A}$ are given by the following expressions:

$$B_{\alpha\beta} = \frac{e^2 \varkappa T}{2\pi}\int \delta\left(\omega_k - \frac{\mathbf{k}\cdot\mathbf{p}}{m}\right) a_{k\alpha} a_{k\beta}\, d\mathbf{k},$$
$$\mathbf{A} = \frac{e^2}{2\pi m}\int \delta\left(\omega_k - \frac{\mathbf{k}\cdot\mathbf{p}}{m}\right)\mathbf{a}_k(\mathbf{a}_k\cdot\mathbf{p})\, d\mathbf{k}, \quad \omega_k = \frac{c}{\sqrt{\varepsilon}}k. \qquad (2)$$

In Eq. (1), n is the number of electrons in unit volume, and ϵ is the dielectric constant of the medium. The region of integration in the last term of the left member of Eq. (1) is restricted by the condition $|q - q'| \leq c(t - t_0)/\epsilon^{1/2}$, which comes from the fact that we are considering the problem in which the distribution functions of the electrons and field oscillators are prescribed at the initial time t_0; therefore, owing to the finite speed of propagation of the interaction, the change of the distribution function f_1 at the point q at the time t can be affected only by the states of the electrons at distances less than or equal to $c(t - t_0)/\epsilon^{1/2}$ from the point q. In Eq. (1), only the interaction of the electrons with the transverse electromagnetic waves has been expressed separately.

The coefficients $B_{\alpha\beta}$ and $\mathbf{A}$ are nonvanishing only when the condition for Cerenkov radiation is satisfied. The coefficient $\mathbf{A}$ gives the deceleration of a particle with momentum $\mathbf{p}$ by the field. After integration the expression for the decelerating force takes the form

$$(e/c)^2 \int (1 - c^2 m^2/p^2 \varepsilon)\,\omega_k d\omega_k$$

and agrees with the well known expression of the theory of Cerenkov radiation.[3,4]

We note further that in the equilibrium case the Maxwell distribution satisfies Eq. (1).

Under the inverse conditions, with the electrons in equilibrium and the oscillators close to an equilibrium state at the initial time, we get for the distribution function of the oscillators an equation of the Fokker-Planck type in the phase space of the coordinates and momenta of the field oscillators. In the equilibrium case the solution of this equation has the form:

$$F_1^{(0)} = A\exp\{-P_{\mathbf{k}}^2/2\varkappa T - \omega_{\mathbf{k}}^2 Q_{\mathbf{k}}^2/2\varkappa T\}.$$

By means of this equation we get the averaged equation for the coordinates of the oscillators. For example, for a uniform distribution of the electrons this equation has the form:

$$\ddot{\bar{Q}}_{\mathbf{k}} + 2\gamma\dot{\bar{Q}}_{\mathbf{k}} + \Omega_k^2\bar{Q}_{\mathbf{k}} = 0; \quad \bar{Q}_{\mathbf{k}} = \int Q_{\mathbf{k}} F_1(dQ_{\mathbf{k}}\,dP_{\mathbf{k}}), \qquad (3)$$

where

$$\Omega_k^2 \approx \omega_L^2 + \omega_k^2; \qquad \gamma = \left(\frac{\pi m}{8\varkappa T}\right)^{1/2}\frac{\omega_L^2}{k}\exp\left\{-\frac{m\omega_k^2}{2k^2\varkappa T}\right\}.$$

We have also considered the more general case in which neither of the subsystems (electrons and electromagnetic oscillations) is in a state of thermal equilibirum. The results obtained will be applied in the study of the radiation emitted from electron beams passing through decelerating systems.

We take occasion to express our gratitude to Academician N. N. Bogoliubov for his interest in this work.

---

[1] W. E. Brittin, Phys. Rev. **106**, 843 (1957).

[2] N. N. Bogoliubov and K. P. Gurov, J. Exptl. Theoret. Phys. (U.S.S.R.) **17**, 614 (1947).

[3] B. M. Bolotovskii, Usp. Fiz. Nauk **62**, 201 (1957).

[4] L. D. Landau and E. M. Lifshitz Электродинамика сплошных сред (The Electrodynamics of Continuous Media), Gostekhizdat 1957.

Translated by W. H. Furry
262

THE SCATTERING OF SPIN 2 PARTICLES BY A COULOMB FIELD

A. I. BEDRITSKII

Vitebsk Pedagogical Institute

Submitted to JETP editor July 16, 1958

J. Exptl. Theoret. Phys. (U.S.S.R.) **35**, 1278-1280 (November, 1958)

THE effective cross section for the elastic scattering of particles with spin 2 by a heavy Coulomb center can be found by analogy with the theory for electrons (see reference 1). The relativistic wave equations for free particles with spin 2 can be written, taking into account their irreducibility to the Hamiltonian form, (see, for example, references 2 and 3)

$$(\gamma_l \nabla_l + \varkappa)\,\psi = 0, \qquad (1)$$

and in first order perturbation theory, the effective cross section for elastic scattering of particles with spin 2 and charge e from a heavy nucleus with charge ze becomes

$$\sigma = \frac{4z^2e^4k_0}{c^2h^2k}\int \frac{G\,(k_0 + k_0')}{(\mathbf{k}-\mathbf{k}')^4\,(k+k')}\,\delta\,(k'-k)\,d^3k', \qquad (2)$$

$$G = \frac{1}{5}\sum_{s}\sum_{s'} B^{+}\gamma^{+}{}_{4}B'\cdot B'^{+}\gamma_4 B \,/\, B'^{+}\gamma_4^{+}B'\cdot B'^{+}\gamma_4 B'. \qquad (3)$$

Here and in the following primed quantities refer to the final state of the particle, after scattering.

The matrix γ_4 and the matrix A of the invariant bilinear form for spin 2 particles are known;[3] they are of the thirtieth degree. The other three matrices γ_α are easily found from the "coupling" formulas found by Fedorov,[3] and the irreducible representations of the Lorentz group,[2] use being made of the relations $\gamma_\alpha = i\,[I^{0\alpha}, \gamma_4]$, where the $I^{0\alpha}$ are the infinitesimal operators of the representation.

In calculating the quantity G, it is not necessary to know the matrices γ_l explicitly. The wave functions can be classified by their spin projections and normalized by their charge, $\psi^* A\gamma_4\psi = 1$ (the normalization $\psi^* A\psi = 1$ leads to the same final result) with the help of the method proposed by Fedorov,[4] using an invariant form. In this method, we do not use the functions B_{rs}, which describe the state with rest mass m_r and projection of spin on momentum s, but use instead the matrices $T = \alpha_r\beta_s$, where $\alpha_r = \alpha_+ = P_+(\alpha)/P_+(\kappa)$, $\beta_s = Q_s(S)/Q_s(s)$ can be determined by the minimal polynomials of the operator $\alpha = ik_l\gamma_l$ and the operator $S = (i/2\,|\mathbf{k}|)\,\delta_{\alpha\beta\sigma}I^{\beta\sigma}k_\alpha$ $(\alpha, \beta, \sigma = 1, 2, 3)$ which projects the spin on the momentum of the particle:

$$P\,(\alpha) = \alpha^3\,(\alpha^2 - \varkappa^2) = (\alpha \mp \varkappa)\,P_{\pm}\,(\alpha) = 0, \qquad (4)$$

$$Q\,(S) = S\,(S^2-1)\,(S^2-4) = Q_s\,(S)\,(S-s) = 0. \qquad (5)$$

The method of reference 4 leads to the formula

$$G = (k_0'/5k_0)\sum_{s'}\mathrm{Sp}\,(\alpha_+ A\gamma_4^+\alpha'_+ A\gamma_4\beta'_{s'})/\mathrm{Sp}\,(\alpha'_+ A\gamma_4^+\alpha'_+ A\gamma_4\beta'_{s'}). \qquad (6)$$

Even with this method, the calculations involved in finding G are tedious. In calculating the traces which occur in the numerators and denominators of the terms in G, it is helpful to remember the structure of the matrices $\beta'_{s'}$ and of the other factors. The matrices $\beta'_{s'}$ are quasi-diagonal, while each of the matrices $\alpha'_+A\gamma_4^+$, $\alpha'_+A\gamma_4$, $\alpha_+A\gamma_4^+$ can be written as the sum of two matrices in such a way that each of the terms arising from multiplication have zero in the quasi-diagonal part corresponding to the quasi-diagonal part of $\beta'_{s'}$. All five denominators in the fractions of (6) turn out to be different (in the nonrelativistic case they are all equal to $5k_0$), but it is much easier to calculate them than the numerators.

Equations (2) and (6) give the following formula for the differential elastic scattering cross section:

$$\begin{aligned} d\sigma = {} & \frac{z^2r_0^2}{960\varepsilon^4\,(1-5\varepsilon^2+4\varepsilon^4)^2\,\sin^4(\theta/2)}\,\{(7-14\varepsilon^2-166\varepsilon^4 \\ & +722\varepsilon^6-41\varepsilon^8+832\varepsilon^{10}+756\varepsilon^{12}+64\varepsilon^{14})+(\varepsilon^2-1) \\ & \times(3-15\varepsilon^2+15\varepsilon^4+41\varepsilon^6+660\varepsilon^8-576\varepsilon^{10}-128\varepsilon^{12})\cos^2\theta \\ & +4\,(\varepsilon^2-1)^2\,(-1+9\varepsilon^2-28\varepsilon^4+49\varepsilon^6-45\varepsilon^8+16\varepsilon^{10}) \\ & \times\cos^4\theta+4\,(\varepsilon^2-1)\,[(1+2\varepsilon^2-44\varepsilon^4+140\varepsilon^6+211\varepsilon^8+50\varepsilon^{10}) \\ & +(\varepsilon^2-1)\,(1-9\varepsilon^2+31\varepsilon^4+27\varepsilon^6-50\varepsilon^8)\cos^2\theta]\cos\theta\}\,d\Omega, \end{aligned} \qquad (7)$$

where $\epsilon = E/E_0$, E is the initial total energy of the particle, $E_0 = mc^2$ is the rest energy, $r_0 = e^2/mc^2$ and $d\Omega = \sin\theta d\theta d\varphi$.

In the nonrelativistic case ($k \ll k_0, \kappa$) (7) gives the classical Rutherford formula, while in the extreme-relativistic case ($\kappa \ll k, k_0$) only transitions in which the final states have spin projections $s' = \pm 2$ are important and

$$d\sigma = \frac{z^2}{15} r_0^2 \varepsilon^2 \cos^4 \frac{\theta}{2} d\Omega. \tag{8}$$

The effect of the field due to the electron cloud around the nucleus can be evaluated with the Thomas-Fermi method;[1] for no screening ($qa \gg 1$) the result is

$$d\sigma = \frac{z^2 r_0^2}{960\varepsilon^4 (1 - 5\varepsilon^2 + 4\varepsilon^4)^2 \sin^4(\theta/2)} (7 - 14\varepsilon^2 - 166\varepsilon^4 + 722\varepsilon^6 - 41\varepsilon^8 + 832\varepsilon^{10} + 756\varepsilon^{12} + 64\varepsilon^{14}) d\Omega, \tag{9}$$

while for maximum screening we have

$$d\sigma = \frac{0.32 z^{2/3} \hbar^4}{r_0^2 \varepsilon^4 (1 - 4\varepsilon^2)^2 m_e^4 c^4} (7 - 14\varepsilon^2 - 166\varepsilon^4 + 722\varepsilon^6 - 41\varepsilon^8 + 832\varepsilon^{10} + 756\varepsilon^{12} + 64\varepsilon^{14}) d\Omega. \tag{10}$$

At low velocities ($p \ll \hbar z^{1/3}/2a_0$, $a_0 = \hbar^2/m_e e^2$, m_e = rest mass of the electron) there is total shielding at all scattering angles and we must use formula (10), but can neglect the small quantities ϵ:

$$d\sigma = (2.24 z^{2/3} \hbar^4 / r_0^2 \varepsilon^4 m_e^4 c^4) d\Omega. \tag{11}$$

At high velocities ($p \gg \hbar z^{1/3}/2a_0$) the screening effect is noticeable only at small angles θ, defined by[1]

$$\sin\frac{\theta}{2} < \hbar z^{1/3}/2a_0 p. \tag{12}$$

Hence for large velocities and at angles satisfying (12), formula (10) should be used, while at angles not satisfying (12) the proper formula to use is (9).

In the extreme relativistic case (when the condition $p \gg \hbar z^{1/3}/2a_0$ will be satisfied if $m \geq m_e$) we need consider only higher order terms in ϵ, and for small angles satisfying (12), Eq. (10) gives

$$d\sigma = (1.28 z^{2/3} \varepsilon^6 \hbar^4 / r_0^2 m_e^4 c^4) d\Omega, \tag{13}$$

while for angles which do not satisfy (12), Eq. (9) reduces to

$$d\sigma = \frac{z^2 r_0^2 \varepsilon^2}{240 \sin^4(\theta/2)} d\Omega. \tag{14}$$

For ϵ close to unity, Eq. (9) gives the classical Rutherford formula (for $p \gg \hbar z^{1/3}/2a$, and $\sin\theta/2 > \hbar z^{1/3}/2a_0 p$).

I am deeply grateful to Prof. F. I. Fedorov, under whose guidance this work was carried out.

---

[1] A. A. Sokolov and D. D. Ivanenko, Квантовая теория поля (Quantum Field Theory), Moscow-Leningrad, 1952.

[2] I. M. Gel'fand and A. M. Iaglom, J. Exptl. Theoret. Phys. (U.S.S.R.) **18**, 703 (1948).

[3] F. I. Fedorov, Уч. зап. Белорус. гос. ун., серия физ.-мат. (Scientific Notes, Belorussian State University, Physics-Mathematics Series) **12**, 156 (1951).

[4] F. I. Fedorov, J. Exptl. Theoret. Phys. (U.S.S.R.) **35**, 493 (1958), Soviet Phys. JETP **8**, 339 (1959).

Translated by R. Krotkov
263

HYDRODYNAMIC ANALYSIS OF THE COMPRESSION OF A RAREFIED PLASMA IN AN AXIALLY-SYMMETRIC MAGNETIC FIELD

Iu. N. BARABANENKOV

Moscow State University

Submitted to JETP editor June 3, 1958;
resubmitted July 9, 1958

J. Exptl. Theoret. Phys. (U.S.S.R.) **35**, 1280-1281
(November, 1958)

We consider a totally ionized plasma (neglecting collisions) confined in a narrow magnetic tube by an axially-symmetric magnetic field (the axis of the tube is the axis of symmetry of the magnetic field). Assuming quasi-neutral motion of the plasma along the tube, we can write the hydrodynamic equations:[1,2]

$$m\left(\frac{\partial v}{\partial t} + v\frac{\partial v}{\partial x}\right) = -\frac{W_\perp}{H}\frac{\partial H}{\partial x} - \frac{1}{n}\frac{\partial}{\partial x}(2W_\parallel n),$$

$$\frac{\partial n}{\partial t} + \frac{\partial}{\partial x}(nv) = 0, \tag{1}$$

$$m = m_e + m_i,\quad W_\perp = W_{\perp e} + W_{\perp i},\quad W_\parallel = W_{\parallel e} + W_{\parallel i}.$$

Here the subscript e refers to the electrons and the subscript i refers to the ions, $W_\perp$ and $W_\parallel$ are the mean energies due to thermal motion of the electrons (ions) (perpendicular and parallel to the tube); $n \equiv N/H$ is a quantity proportional to the number of electrons (ions) per unit length of the tube, and N is the density per unit volume. We consider two modes of longitudinal compression of the plasma along the magnetic tube.

(a) Isothermal compression. Let $W_\perp$ and $W_\parallel$ be constant in time and over the length of the tube, with $W_\perp > 2W_\parallel$ (the latter condition can be realized by using a magnetic field which increases sharply). The magnetic field is assumed to be of the form:

$$H(x) = H^* \exp(x^2/2a^2). \tag{2}$$

At a given time the density distribution is given by the expression:

$$N/N_0 = (1/\psi)\exp[-(\psi^{-2} - 1)x^2/2a^2], \tag{3}$$

where $\psi(t)$ satisfies the equation:

$$\begin{gathered}\ddot{\psi} + (W_\perp/ma^2)(\psi - 2W_\parallel/W_\perp\psi) = 0,\\ \psi(0) = 1, \quad \dot{\psi}(0) = 0.\end{gathered} \tag{4}$$

It follows from Eq. (4) that ψ is a periodic function of time (period T) which varies between the limits ψ_1 and 1. As an approximation we have:

$$T \approx \begin{cases}(W_\perp/ma^2)^{1/2} & \text{for}\quad W_\perp/2W_\parallel \sim 1,\\ \pi(W_\perp/ma^2)^{1/2} & \text{for}\quad W_\perp/2W_\parallel \gg 1;\end{cases} \tag{5}$$

$$\psi_1 \approx \begin{cases}(2W_\parallel/W_\perp)^{1/2} & \text{for}\quad W_\perp/2W_\parallel \sim 1,\\ \exp(-W_\perp/4W_\parallel) & \text{for}\quad W_\perp/2W_\parallel \gg 1.\end{cases} \tag{6}$$

According to Eqs. (3) to (6), the plasma undergoes periodic longitudinal compression at the point of minimum magnetic field and expands to a uniform distribution of density N_0.

(b) Adiabatic stratification when a magnetic gradient, which is periodic along the tube, is turned on quasi-statically. Let the magnetic field be of the form:

$$\begin{gathered}H(x, t) = H_1(t) - H_2(t)\cos(\pi x/a),\\ H_1(t) > H_2(t), \quad H_2(0) = 0.\end{gathered} \tag{7}$$

We neglect the inertia term in Eq. (1) and introduce the adiabaticity equations:[1]

$$W_\perp/H = W_{\perp 0}/H_0, \quad W_\parallel/n^2 = W_{\parallel 0}/n_0^2. \tag{8}$$

The density is:

$$\begin{gathered}(n/n_0)^2 = A + B\cos(\pi x/a), \quad B = (W_{\perp 0}/3W_{\parallel 0})H_2(t)/H_0,\\ (2/\pi)(A+B)^{1/2}E(k) = 1, \quad k^2 = 2B/(A+B),\end{gathered} \tag{9}$$

where E(k) is a complete elliptic integral of the second kind. At a given time

$$\frac{n}{n_0} = \frac{\pi}{2}\left|\cos\frac{\pi x}{2a}\right|. \tag{10}$$

According to Eq. (9) the plasma is stratified along the magnetic field, forming bunches which are concentrated about the points of minimum magnetic field.

In conclusion we wish to thank Professor Ia. P. Terletskii for his interest in this work.

---

[1] Chew, Goldberger, and Low, Proc. Roy. Soc. (London) 236, 112 (1956).

[2] A. Schlüter, Z. Naturforsch. 5a, 72 (1950).

Translated by H. Lashinsky
264

THE RADIATION FROM A CHARGED PARTICLE PASSING THROUGH A PLATE

G. M. GARIBIAN and G. A. CHALIKIAN

Physics Institute, Academy of Sciences, Armenian S.S.R.

Submitted to JETP editor June 12, 1958

J. Exptl. Theoret. Phys. (U.S.S.R.) 35, 1282-1283 (November, 1958)

LET a charged particle moving in vacuum along the positive z direction pass through a plate of thickness a made of a material with dielectric constant ϵ. We proceed as in reference 1, the only difference being that in the region $z < 0$ the radiation field will consist of reflected waves only, and the field in the region $z > a$ of waves moving in the positive z direction, while inside the plate there are both kinds of waves; we then get for the Fourier components of the radiation field in the spaces before and after the plate the formulas

$$\begin{aligned}\mathbf{E}''_{0t}(\mathbf{k}) = \frac{ei}{2\pi^2}\frac{\varkappa}{F}\Big\{\Big(\frac{\varepsilon}{\lambda} + \frac{1}{\lambda_0}\Big)^2 \alpha e^{-i\lambda a}\\ + \Big(\frac{\varepsilon}{\lambda} - \frac{1}{\lambda_0}\Big)\beta e^{i\lambda a} + \frac{2\varepsilon}{\lambda}\gamma e^{ik_z a}\Big\},\end{aligned} \tag{1}$$

$$\begin{aligned}\mathbf{E}'_{1t}(\mathbf{k}) = -\frac{ei}{2\pi^2}\frac{\varkappa}{F}\Big\{\Big(\frac{\varepsilon}{\lambda} - \frac{1}{\lambda_0}\Big)\alpha e^{i\lambda a}\\ + \Big(\frac{\varepsilon}{\lambda} + \frac{1}{\lambda_0}\Big)\beta e^{-i\lambda a} + \frac{2\varepsilon}{\lambda}\delta e^{-ik_z a}\Big\},\end{aligned} \tag{2}$$

where

$$\begin{gathered}\lambda_0^2 = \frac{\omega^2}{c^2} - \varkappa^2; \quad \lambda^2 = \frac{\omega^2}{c^2}\varepsilon - \varkappa^2;\\ F = \Big(\frac{\varepsilon}{\lambda} + \frac{1}{\lambda_0}\Big)^2 e^{-i\lambda a} - \Big(\frac{\varepsilon}{\lambda} - \frac{1}{\lambda_0}\Big)^2 e^{i\lambda a},\end{gathered} \tag{3}$$

$$\begin{gathered}\left.\begin{matrix}\alpha\\ \beta\end{matrix}\right\} = \frac{\pm\varepsilon/\lambda - v/\omega}{k^2 - \omega^2/c^2} + \frac{\mp 1/\lambda + v/\omega}{k^2 - \omega^2\varepsilon/c^2};\\ \left.\begin{matrix}\gamma\\ \delta\end{matrix}\right\} = \frac{\mp 1/\lambda_0 + v/\omega}{k^2 - \omega^2/c^2} + \frac{\pm 1/\lambda_0\varepsilon - v/\omega}{k^2 - \omega^2\varepsilon/c^2}.\end{gathered} \tag{4}$$

Taking $R \gg a$, where R is the distance from the place the particle enters the plate (or where it leaves the plate) to the point of observation, we can obtain for the radiation emitted (as has been done in reference 1) a formula agreeing with that obtained by Pafomov.[2*] We only remark that the formula given in reference 2 does not hold for $a \lesssim R$. In this case we can obtain (cf. reference 1) from Eqs. (1) and (2) a formula that has no zeroes in the denominator.

In the extreme relativistic case, setting $\lambdabar\epsilon^{-1/2} \ll a \ll R$, we get for the radiation emitted backward the expression

$$W''_{\text{Cer}} = 2\,\frac{e^2}{\pi c}\left(\ln\,\frac{2}{1-v/c}-1\right)(\omega_2-\omega_1)\left(\frac{\sqrt{\varepsilon}-1}{\sqrt{\varepsilon}+1}\right)^2, \tag{5}$$

if $\epsilon(\omega)$ is constant in the frequency interval (ω_1, ω_2) In this same case we get for the radiation emitted forward the formula (5), but without the last factor, on the assumption $\lambdabar/|\epsilon^{1/2}-1| \ll a \ll R$ ($\lambdabar$ is the wavelength of the radiation divided by 2π.

It can be seen from the formulas (1) and (2) that there will be no Cerenkov radiation if $a \ll \lambdabar$. If, on the other hand, $\lambdabar < a \lesssim R$, then in finding the paths of steepest descent one must take into account the exponents appearing in Eqs. (1) and (2), and the result is that at a given point in the field we shall have bands of Cerenkov frequencies given by the relations

$$\begin{aligned}\frac{v}{c}\sin\theta\left(1-\frac{a}{R}\,\frac{s\cos^2\theta}{\sqrt{\varepsilon(\omega)-\sin^2\theta}}\right) &\leqslant \sqrt{(v/c)^2\,\varepsilon(\omega)-1}\\ &\leqslant \frac{v}{c}\sin\theta\left(1-\frac{a}{R}\,\frac{t\cos^2\theta}{\sqrt{\varepsilon(\omega)-\sin^2\theta}}\right),\end{aligned} \tag{6}$$

where θ is the angle between R and the perpendicular to the plate, while $s = 2n + 2$, $t = 2n + 1$ for the Cerenkov radiation emitted backward, and $s = 2n + 1$, $t = 2n$ for the radiation emitted forward (n is a nonnegative whole number). The backward flux of Cerenkov radiation through the area between ρ and $\rho + d\rho$ will be given by

$$\begin{aligned}\frac{dW''_{\text{Cer}}}{d\rho} = \frac{4e^2}{v^2}\sum_{n=0}^{\infty}\int\limits_{\Delta\omega_n^{\cdot}}&\frac{\left[1-\varepsilon\sqrt{1+(v/c)^2\,(1-\varepsilon)}\right]^{4n}}{\left[1+\varepsilon\sqrt{1+(v/c)^2\,(1-\varepsilon)}\right]^{4n+4}}\\ &\times\sqrt{\left(\frac{v^2}{c^2}\varepsilon-1\right)\left(1+\frac{v^2}{c^2}(1-\varepsilon)\right)}\\ &\times\left(\sqrt{1+\frac{v^2}{c^2}(1-\varepsilon)}-1\right)^2\omega d\omega,\end{aligned} \tag{7}$$

and for the forward radiation we have

$$\begin{aligned}\frac{dW_{\text{Cer}}}{d\rho} = \frac{4e^2}{v^2}\sum_{n=0}^{\infty}\int\limits_{\Delta\omega'_n}&\frac{\left[1-\varepsilon\sqrt{1+(v/c)^2\,(1-\varepsilon)}\right]^{4n}}{\left[1+\varepsilon\sqrt{1+(v/c)^2\,(1-\varepsilon)}\right]^{4n+2}}\\ &\times\sqrt{\left(\frac{v^2}{c^2}\varepsilon-1\right)\left(1+\frac{v^2}{c^2}(1-\varepsilon)\right)}\,\omega d\omega.\end{aligned} \tag{8}$$

For $a \ll R$ the intensity of the Cerenkov radiation goes to zero.

The writers are grateful to A. Ts. Amatun' and I. I. Gol'dman for interesting discussions.

*V. E. Pafomov has informed us that there are misprints in Eq. (2) of reference 2: the exponent of the second term in square brackets should have the plus sign, and the exponent of the third term the minus sign.

---

[1] G. M. Garibian, J. Exptl. Theoret. Phys. (U.S.S.R.) **33**, 1403 (1957), Soviet Phys. JETP **6**, 1079 (1958).

[2] V. E. Pafomov, J. Exptl. Theoret. Phys. (U.S.S.R.) **33**, 1074 (1957), Soviet Phys. JETP **6**, 829 (1958).

Translated by W. H. Furry
265

RADIATIVE DECAY OF $\pi^{\pm}$ MESONS AND EFFECTS OF PARITY NONCONSERVATION

A. I. MUKHTAROV and S. A. GADZHIEV

Azerbaidzhan State University

Submitted to JETP editor June 13, 1958

J. Exptl. Theoret. Phys. (U.S.S.R.) **35**, 1283-1285 (November, 1958)

LONGITUDINAL polarization of particles is a consequence of the nonconservation of parity in weak interactions. A study of the radiative decay $\pi^{\pm} \to \mu^{\pm} + \nu + \gamma$ shows that parity is not conserved also in mixed interactions.

In the four-component-neutrino theory the equation for the decay has the form

$$D\psi_\nu = (eg/hc)\,\psi_\pi D^{-1}(\gamma_\mu A^{+}_{\mu})\,\psi_\mu. \tag{1}$$

Here ψ_μ, ψ_ν, ψ_π, A_μ are the respective wave functions of the μ meson, the neutrino, the π meson, and the γ-ray quantum, and D is the Dirac operator. The longitudinal polarization of the μ meson and the neutrino is taken into account by means of the projection operator $\hat{\sigma\mathbf{p}}/p$; its characteristic values (s_μ or s_ν) describe the longitudinal polarizations. $s_\mu = 1$ ($s_\nu = 1$) corresponds to spin in the direction of motion of the μ meson (neutrino), and $s_\mu = -1$ ($s_\nu = -1$) to the opposite spin direction. The circular polarization of the γ-ray quantum is described by means of the polarization vector

$$\mathbf{a}_l = \{\boldsymbol{\beta} + il\,[\mathbf{n}\times\boldsymbol{\beta}]\}/\sqrt{2},$$

where β is a unit vector perpendicular to $\mathbf{n} = \kappa/\kappa$;

hκ is the momentum of the quantum. $l = 1$ corresponds to right-circular polarization (spin directed parallel to the motion) and $l = -1$ to left-circular polarization (spin opposite to motion) of the γ-ray quantum.

In the case of a π meson at rest we get the following expression for the decay probability:

$$dW = \frac{e^2 g^2}{h^2 c\pi} \frac{k_\mu^2 \, dk_\mu \sin\theta \, d\theta}{k_{0\pi} K_\mu} (f_1 \pm s_\mu s_\nu f_2 \pm s_\mu l f_3 + s_\nu l f_4). \tag{2}$$

Here the upper sign is for decay occurring with the emission of a neutrino, and the lower sign is for decay with emission of an antineutrino. The notations used are:

$$\begin{aligned} f_1 &= k_\mu^2 \frac{q(1-\cos^2\theta)}{Q-K_\mu} + \frac{Q-K_\mu}{k_{0\pi}-\gamma}\gamma k_{0\pi}, \\ f_2 &= -\left\{k_\mu(1-\cos^2\theta)\left(K_\mu + \frac{k_\mu^2}{Q-K_\mu}\right)\right. \\ &\quad \left. + \frac{Q-K_\mu}{k_{0\pi}-\gamma}(k_\mu - K_\mu\cos\theta)\right\}, \\ f_3 &= -\frac{K_\mu}{k_{0\pi}-\gamma}\left\{k_\mu(1-\cos^2\theta)\left(k_{0\pi} - \frac{k_{0\mu}^2}{K_\mu}\right)\right. \\ &\quad \left. -(Q-K_\mu)k_{0\pi}\cos\theta + \frac{k_{0\pi}(Q-K_\mu)}{K_\mu(k_{0\pi}-\gamma)}k_\mu^2\cos\theta\right\}, \\ f_1 &= -\frac{k_{0\pi}}{k_{0\pi}-\gamma}\{\gamma^2 - \gamma(Q+K_\mu) + k_{0\mu}^2\}, \end{aligned} \tag{3}$$

where hk_μ is the momentum and hcK_μ the energy of the μ meson, $hck_{0\pi}$ is the rest energy of the π meson, θ is the angle between the directions of motion of the μ meson and the γ-ray quantum, and

$$Q = (k_{0\pi}^2 + k_{0\mu}^2)/2k_{0\pi}, \quad q = (k_{0\pi}^2 - k_{0\mu}^2)/2k_{0\pi},$$

$$\gamma = K_\mu - k_\mu \cos\theta.$$

In the expression (2) for the decay probability the last three terms are due to parity nonconservation, i.e., the longitudinal polarizations of the μ meson, the neutrino, and the γ-ray quantum. If in Eq. (2) we carry out a summation over the directions of polarization of the μ meson and the γ-ray quantum, we get the well known expression[1] for the decay probability of the π meson.

Summation only over the spin states of the μ meson leads to the result of Bund and Ferreira.[2]

To simplify the analysis of the formula (2) we suppose that the momentum of the μ meson is very small (close to zero); then the momenta of the γ-ray quantum and the neutrino will be antiparallel. In this limit ($k_\mu \to 0$)

$$\begin{aligned} f_1 &= f_4 = k_{0\mu}(k_{0\pi} - k_{0\mu})/2, \\ f_2 &= f_3 = {}^1\!/_2\, k_{0\mu}(k_{0\pi} - k_{0\mu})\cos\theta, \end{aligned} \tag{4}$$

where θ is the angle between the spin vector of the μ meson and the direction of motion of the γ-ray quantum. The analysis leads to the following results:

(a) if the spin of the μ meson is directed opposite to the motion of the γ-ray quantum ($s_\mu = -1$ and $\cos\theta = -1$), then the decay probability is different from zero only in the case $s_\nu = 1$ and $l = 1$, i.e., when the decay involves emission of a neutrino and the quantum emitted has right-circular polarization;

(b) if the spin of the μ meson is directed along the direction of motion of the γ-ray quantum ($s_\mu = 1$), then we must permit decay of the π meson with emission of an antineutrino ($s_\nu = -1$) and a γ-ray quantum with left-circular polarization ($l = -1$). We note that in this limit the probabilities of the two types of decay are equal.

From the above it follows that if the π meson decays with emission of a neutrino, then for small momenta of the μ meson its spin must make an angle close to 180° with the direction of the quantum. In the case of antineutrino decay this angle is close to zero. Obviously this conclusion can be checked by measurement of the μ-γ correlation.

---

[1] B. Ioffe and A. Rudik, Dokl. Akad. Nauk SSSR **82**, 359 (1952). W. A. Fry, Phys. Rev. **83**, 1268 (1951). T. Eguchi, Phys. Rev. **85**, 943 (1952). H. Primakoff, Phys. Rev. **84**, 1255 (1951).

[2] G. W. Bund and P. L. Ferreira, Nuovo cimento **7**, 246 (1958).

Translated by W. H. Furry
266

ON THE THEORY OF THE "SECOND MOMENT" IN THE NUCLEAR MODEL OF LANE, THOMAS, AND WIGNER

V. M. AGRANOVICH and V. S. STAVINSKII

Submitted to JETP editor June 23, 1958

J. Exptl. Theoret. Phys. (U.S.S.R.) **35**, 1285-1287 (November, 1958)

THE "second moment" was first introduced in a paper of Lane, Thomas, and Wigner[1] as a quantitative criterion for the error committed when the nuclear Hamiltonian is replaced by the Hamiltonian of the shell model.

Let H be the nuclear Hamiltonian and H_0 the shell model Hamiltonian. Then $H = H_0 + H_1$, where H_1 is an operator which gives rise to correlations between single-particle states of the shell model. Further, let $H\Phi_b = E_b\Phi_b$, where the Φ_b are Slater determinants describing the various nuclear states in the shell model. The wave function of the nucleus for energy E, which satisfies the equation $H\psi_E = E\psi_E$, can be represented as an expansion in the complete orthogonal function system Φ_b:

$$\psi_E = \sum_b C_b(E)\,\Phi_b. \tag{1}$$

Let us assume that the state ψ_E corresponds to a state of the compound nucleus in the Bohr model, in which the wave functions in different channels do not interfere. This is equivalent to assuming that the phases of the coefficients $C_b(E)$ are random (cf. reference 1 and 2). Thus the description of the state ψ_E in the Bohr model is incomplete, and the state can be characterized by means of a density matrix. In the state ψ_E, the average value of H_0 is

$$(\psi_E,\ H_0\psi_E) = \sum_b |C_b(E)|^2 E_b. \tag{2}$$

Since according to the assumptions of the model[1] the function $|C_b(E)|^2$ has a maximum at $E_b \approx E$,*

$$(\psi_E,\ H_0\psi_E) \approx E. \tag{3}$$

Comparing (2) and (3), we conclude that the state of the compound nucleus in the Bohr picture is a "mixed" state which can be characterized by the statistical matrix:

$$W_{bb} = |C_b(E)|^2,\quad W_{bb'} = 0,\quad b \neq b', \tag{4}$$

where, according to (3) the nuclear energy E is the average energy of the system having the Hamiltonian H_0.

In order to characterize the compound nucleus with excitation energy E by a temperature $T(E)$, as was done by N. Bohr[3] and Ya. I. Frenkel,[4] it is sufficient to assume that

$$|C_b(E)|^2 \sim \exp(-E_b/kT), \tag{5}$$

where the nuclear temperature T is related to the total energy of excitation of the nucleus, E, by the equation of state of a Fermi gas at low temperature: $E = aT^2$.

On the basis of assumption (5) it is easy to determine the "second moment" of the model,[1] which, by definition, is equal to

$$W^2(E) = \sum_b (E_b - E)^2 |C_b(E)|^2. \tag{6}$$

Going over from a sum to an integral in (6) and using for the level density $\rho(E_b)$ the expression found by Landau,[5]

$$\rho(E_b) = \lambda^{-1}(E_b)\exp(S(E_b)/k),$$

where $S(E_b)$ is the entropy of the nucleus on the shell model, and $\lambda(E_b)$ is a smoothly varying function, we get

$$W^2(E) = \int_0^\infty \frac{1}{\lambda(E_b)}(E - E_b)^2 \exp\left[\frac{S(E_b)}{k} - \frac{E_b}{kT}\right] dE_b. \tag{7}$$

Expanding the exponent in powers of $(E - E_b)$ and stopping at quadratic terms, we find†

$$W^2(E) = A\int_0^\infty (E - E_b)^2 \exp[-(E - E_b)^2/\Omega^2(E)]\,dE_b, \tag{8}$$

where

$$1/A(E) = \int_0^\infty \exp[-(E - E_b)^2/\Omega^2(E)]\,dE_b,$$

$$\Omega^2(E) = \frac{4}{\sqrt{a}}E^{3/2}.$$

Performing the integration in (8), we find

$$W^2(E) = \frac{\Omega^2(E)}{2(1 + \Phi(x))}\left\{1 + \Phi(x) - \frac{2x}{\sqrt{\pi}}e^{-x^2}\right\}, \tag{9}$$

$$x = E/\Omega(E),\qquad \Phi(x) = \frac{2}{\sqrt{\pi}}\int_0^x e^{-t^2}\,dt.$$

If $x > 1$,

$$W^2(E) \approx \Omega^2(E)/2. \tag{10}$$

Formulas (9) and (10) give the dependence of the "second moment" on the excitation energy E and the nucleon number A $(a \approx 0.07A)$.[7] Thus, for $a = 10\ \text{Mev}^{-1}$ and $E = 8$ Mev, $W(E) = 3.8$ Mev; if we take $E = 16$ Mev, $W(E) = 10.8$ Mev. It is interesting to note that the value found for the "second moment" for $E = 16$ Mev coincides with the value which had to be postulated in a paper of the authors[8] in order to give a satisfactory description of the parameters of the "giant resonance" in photonuclear reactions.

A straightforward quantum-mechanical computation of the second moment" has been made in several papers. In a paper of Vogt[9] the value $W \sim 4.5$ Mev was found, and in a paper of Brown et al.[10] the value $W \sim 7$ Mev, etc. However none of the above-mentioned papers enables one to determine the value of the excitation energy corresponding to their calculated values of the "second moment." This makes it difficult to give a quantitative comparison of the energy dependence of the "second moment" found in the present paper with the calculations of these earlier authors.

---

*Relation (3) would be exact if the equation $(\psi_E, H_1\psi_E) = 0$ were satisfied.

†The approximation in which relation (8) is valid is equivalent to the assumption that

$$|C_b|^2\rho(E_b) = A\exp[-(E - E_b)^2/\Omega^2(E)],$$

which was used in reference 6.

[1] Lane, Thomas, and Wigner, Phys. Rev. **98**, 693 (1955).
[2] T. Teichmann and E. P. Wigner, Phys. Rev. **87**, 123 (1952).
[3] N. Bohr and F. Kalckar, Kgl. Danske Videnskab. Selskab, Mat.-fys. Medd. **14**, No. 10 (1937).
[4] Ya. I. Frenkel, Sov. Phys. **9**, 533, (1936).
[5] L. D. Landau, J. Exptl. Theoret. Phys. (U.S.S.R.) **7**, 819 (1937).
[6] V. M. Agranovich and A. S. Davydov, J. Exptl. Theoret. Phys. (U.S.S.R.) **32**, 1429 (1957), Soviet Phys. JETP **5**, 1164 (1957).
[7] J. M. Blatt and V. F. Weisskopf, Theoretical Nuclear Physics, John Wiley and Sons, Inc., New York, 1952.
[8] V. M. Agranovich and V. S. Stavinskii, J. Exptl. Theoret. Phys. (U.S.S.R.) **34**, 700 (1958), Soviet Phys. JETP **34 (7)**, 481 (1958).
[9] E. Vogt, Phys. Rev. **101**, 1792 (1956).
[10] G. E. Brown and C. T. De Dominicis, Proc. Phys. Soc. **A70**, 668 (1957).

Translated by M. Hamermesh
267

ON THE LIMITS OF APPLICABILITY OF THE IMPACT-PARAMETER METHOD

M. L. TER-MIKAELIAN and B. V. KHACHATRIAN

Erevan State University

Submitted to JETP editor June 23, 1958

J. Exptl. Theoret. Phys. (U.S.S.R.) **35**, 1287-1289 (November, 1958)

IN studies of radiative processes, use is made of ordinary perturbation theory, and also of the impact-parameter method (Weizsäcker-Williams method). The opinion is sometimes expressed that the latter gives insufficiently accurate results.[1] But let us compare the results given by these methods.

We consider deceleration radiation in collisions with atoms.

Following Überall[1] we write the bremsstrahlung cross section in the form

$$\sigma_t = \frac{Z^2 r_0^2}{137}\frac{2d\varepsilon}{\varepsilon_1^2}\int_0^\infty dq_\perp^2 \int_{\delta+q_\perp^2/2\varepsilon_1}^{q} dq_z \frac{[1-F(q)]^2}{q^4}$$
$$\times\left\{-\frac{1}{(q_z-q_\perp^2/2\varepsilon_1)^2}-\frac{q_z+q_\perp^2(\varepsilon-\varepsilon_2)/2\varepsilon_1\varepsilon_2}{[(q_z-q_\perp^2/2\varepsilon_2)^2+4\delta^2 q_\perp^2]^{3/2}}\right. \quad (1)$$
$$\left.+\frac{(1+\varepsilon\delta)\,q_\perp^2+2}{(q_z-q_\perp^2/2\varepsilon_1)[(q_z-q_\perp^2/2\varepsilon_2)^2+4\delta^2 q_\perp^2]^{1/2}}\right\}.$$

Here ϵ_1, ϵ_2 are the initial and final energies of the electron, ϵ is the energy of the photon (denoted by k in reference 1), $\delta = \epsilon/2\epsilon_1\epsilon_2$, $\hbar = m = c = 1$. On the other hand, the impact-parameter method gives[2,3]

$$\sigma_t = \frac{Z^2 r_0^2}{137}\frac{d\varepsilon}{\varepsilon_1^2}\int_0^{\sim 1} dk^2 \int_\delta^{\sim 1}\frac{k^2 dk_1}{k_1^2(k_1^2+k^2+R^{-2})^2}$$
$$\times\left[\frac{\varepsilon_1}{\varepsilon_1-\varepsilon}+1-\frac{\varepsilon}{\varepsilon_1}-\frac{2\varepsilon}{k_1\varepsilon_1(\varepsilon_1-\varepsilon)}+\frac{\varepsilon^2}{k_1^2\varepsilon_1^2(\varepsilon_1-\varepsilon)^2}\right]; \quad (2)$$

here $k^2 = k_2^2 + k_3^2$ (ϵ is the energy of the photon). In Eq. (1) let us replace the variable q_z by $q_z' = q_z - q_\perp^2/2\epsilon_1$ and expand the expression in square brackets in powers of $(q_\perp/mc)^2$:

$$\frac{1}{q_z'^2}\left(1+\varepsilon\delta-\frac{2\delta}{q_z'}+\frac{2\delta^2}{q_z'^2}\right)q_\perp^2$$
$$+\left[\frac{\delta(1+\varepsilon\delta)}{q_z'^3}-\frac{9\delta^2+2\varepsilon\delta^3}{q_z'^4}+\frac{24\delta^3}{q_z'^5}-\frac{18\delta^4}{q_z'^6}\right]q_\perp^4\cdots \quad (3)$$

Comparing Eqs. (3) and (2) we see that the first term of the expansion of the exact formula gives the result of the impact-parameter method (we have here $q_z' = k_1$, $q_\perp^2 = k^2$), and the second term is only a correction if $q_\perp^2 \ll 1$. Consequently, Eq. (2) agrees with the exact formula (1) only in the region $q_\perp^2 \ll 1$ (which corresponds to values of the impact parameter larger than $\hbar/mc$). A similar treatment can be given for pair production.

Let us now turn our attention to radiation and pair production in periodic structures. In reference 1 a problem of this sort is solved for a chain of atoms [Eqs. (33) and (23)]. These formulas differ from the corresponding formulas for collisions with a single atom (for example, Eq. (1)) by the factor:

$$\frac{2\pi}{a}N\sum_h 2\Big/\sqrt{q_\perp^2\vartheta^2-\left(q_z-\frac{2\pi}{a}h\right)^2}, \quad (4)$$

which gives the effect of interference in radiation or pair production in collisions with a chain of atoms. It is easy to obtain analogous formulas by the impact-parameter method. To do this we set $\mathbf{r}_i = h\mathbf{a}$ in Eq. (4) of reference 2, where h is an integer and **a** is the direction vector of the chain of atoms. Integrating the crystalline factor with respect to ψ [Eq. (4) of reference 2] we get

$$\int d\psi\left|\sum_i e^{i(\mathbf{k}\cdot\mathbf{r}_i)}\right|^2 = \frac{2\pi}{a}N\sum_h 2\Big/\sqrt{k^2\vartheta^2-\left(k_1-\frac{2\pi}{a}h\right)^2}, \quad (5)$$

where we have set $k_1a_1 + k_2a_2 + k_3a_3 = k_1a \cos\vartheta + k \sin\vartheta \cos\varphi$. We see that the factor obtained is similar. It must be noted that after the changes of variables $q'_z = q_z - q_\perp^2/2\epsilon_1$ or $q'_z = q_z - q_\perp^2/2\epsilon$, for bremsstrahlung and pair production, respectively, the factors (4) and (5) differ somewhat, but not to any important degree if $\delta \gg q_\perp^2/2\epsilon_1$, $\delta \ll q_\perp^2/2\epsilon_2$, and $\delta \ll q_\perp^2/2\epsilon_-$, $\delta \ll q_\perp^2/2\epsilon_+$ for the two respective cases.

We remark that when one takes into account thermal vibrations in the interference factor of the radiation these make the contribution[2] $q_\perp < h/(\overline{u^2})^{1/2}$, where $\overline{u^2}$ is the mean square deviation of the atoms from their equilibrium positions. Furthermore, on inserting the factor (5) under the integral in Eq. (2) (or in the corresponding formula for the case of pair production) we arrive at a formula for radiation or pair production in collisions with a chain of atoms obtained by the impact-parameter method (when thermal vibrations are included there is an additional factor $\exp\{-(k^2 + k_1^2)\overline{u^2}\}$).

If we now compare these formulas with the formulas for the inteference radiation obtained by perturbation theory [Eqs. (41) and (42) of reference 1], we see that they are completely identical. An analogous argument can also be carried through for the case of collisions of charged particles with atomic electrons (ionization losses). Here it can be shown that the exact quantum mechanical formulas go over into those obtained by the impact-parameter method when they are expanded in powers of the parameter $q_\perp R$, where R is the radius of the atom and $q_\perp$ is the change of momentum in the direction perpendicular to the motion.

---

[1] H. Überall, Phys. Rev. **103**, 1055 (1956).

[2] M. L. Ter-Mikaelian, J. Exptl. Theoret. Phys. (U.S.S.R.) **25**, 289 (1953).

[3] M. L. Ter-Mikaelian, Izv. Akad. Nauk ArmSSR **9**, 77 (1956).

Translated by W. H. Furry
268

DIFFRACTION BREAKUP OF LIGHT NUCLEI

A. G. SITENKO and Iu. A. BEREZHNOI

Khar'kov State University

Submitted to JETP editor June 28, 1958

J. Exptl. Theoret. Phys. (U.S.S.R.) **35**, 1289-1291 (November, 1958)

REFERENCE 1 treated the processes of diffractive interaction of deuterons with nuclei. Obviously, diffraction processes (scattering, disintegration, and stripping) can also occur in the collision of other loosely bound light nuclei with heavy nuclei. The possible occurrence of diffraction phenomena must be taken into account in studying the interaction with heavy nuclei of beams of light nuclei which have been accelerated to high energy.

There are several light nuclei whose binding energies against two-particle breakup are small. Thus, for example, Li^6 may be regarded as being made up of a deuteron and an α particle (with binding energy $\epsilon = 1.53$ Mev), Li^7 is a triton plus an α particle ($\epsilon = 2.52$ Mev), Be^9 is Be^8 plus a neutron ($\epsilon = 1.64$ Mev), B^{10} is Li^6 plus an α particle ($\epsilon = 4.36$ Mev), etc. Diffraction processes in the interaction with heavy nuclei of light nuclei which are made up of two relatively weakly bound particles can obviously be described in the same way as the diffractive interaction of deuterons with nuclei. However, the results of reference 1 cannot be used without change, since it was assumed in reference 1 that the deuteron radius R_d is considerably smaller than the nuclear radius R.

In the present note we calculate the total cross sections for various processes of diffractive interaction of a deuteron with a black nucleus, assuming an arbitrary ratio of the radii R_d and R. The Coulomb interaction is neglected.

To simplify the calculations, the wave function of the deuteron ground state is chosen to be Gaussian

$$\varphi_0(r) = (2/\pi R_d)^{3/2} \exp\left\{-2r^2/\pi R_d^2\right\}, \tag{1}$$

in which the constants are determined from the conditions $\int \varphi_0^2(r)\,d\mathbf{r} = 1$ and $\int r\varphi_0^2(r)\,d\mathbf{r} = R_d$.

Using the general formulas of reference 1, one easily obtains the following expressions for the total cross section for all processes σ_t, the cross section σ_n for stripping off a neutron, the cross section σ_p for stripping off a proton, and the elastic scattering cross section σ_e:

$$\sigma_t = 4\pi R^2 \left\{1 - \int_0^\infty e^{-\xi^2/q^2} \frac{J_1^2(\xi)}{\xi}\, d\xi\right\},$$

$$\sigma_n = \sigma_p = \pi R^2 \left\{1 - 2\int_0^\infty e^{-\xi^2/q^2} \frac{J_1^2(\xi)}{\xi}\, d\xi\right\}, \tag{2}$$

$$\sigma_e = 2\pi R^2 \int_0^\infty I^2(\zeta)\,\zeta\, d\zeta,$$

where we have used the notation $q = 4R/\sqrt{\pi}\, R_d$, and the function $I(\zeta)$ which enters into σ_e is defined by

$$I(\zeta) = \begin{cases} 1 - \dfrac{2}{\pi}\displaystyle\int_0^{\pi/2} \exp\{-q^3(\cos\psi + \sqrt{1-\zeta^2\sin^2\psi})^2\}\, d\psi, \zeta < 1 \\ \dfrac{2}{\pi}\displaystyle\int_0^{\arcsin(1/\zeta)} [\exp\{-q^2(\zeta\cos\psi - \sqrt{1-\zeta^2\sin^2\psi})^2\} \\ - \exp\{-q^2(\zeta\cos\psi + \sqrt{1-\zeta^2\sin^2\psi})^2\}]\, d\psi, \zeta > 1. \end{cases}$$

The cross sections for diffraction breakup σ_d and absorption of the deuteron σ_a can be found from the relations[1]

$$\sigma_d + \sigma_e = \sigma_t/2, \qquad \sigma_a + \sigma_n + \sigma_p = \sigma_t/2. \tag{3}$$

Figure 1 shows the dependence of the various cross sections on the ratio R/R_d.

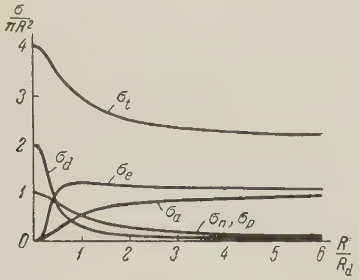

FIG. 1

In the limit of large values of the parameter q ($q \gg 1$), the following asymptotic formulas are valid:

$$\sigma_e = \pi R^2 + (1 - 1/\sqrt{2})\pi R R_d, \quad \sigma_d = {}^1/_2(\sqrt{2}-1)\pi R R_d,$$
$$\sigma_n = \sigma_p = \pi R R_d/2, \quad \sigma_a = \pi R^2 - \pi R R_d/2,$$
$$\sigma_t = 2\pi R^2 + \pi R R_d. \tag{4}$$

We note that for $R/R_d \sim 2$, the cross section values given by the asymptotic formulas (4) are already practically the same as the exact values found by numerical integration.

Relations (2) and (3) also describe processes of diffractive interaction of weakly bound light nuclei with heavy nuclei if R_d is interpreted to be the average distance between the constituents of the light nucleus.

The region $R/R_d < 1$ in Fig. 1 corresponds to the process of interaction of π mesons (or nucleons) with deuterons at high energies, to which the diffraction model is also applicable. R should then be interpreted to be the radius of interaction between the π meson and the nucleon. According to reference 2, for $E_\pi = 1.4$ Bev this radius is $R = 1.18 \times 10^{-13}$ cm, i.e., $R/R_d \approx 0.5$. Assuming that $q \ll 1$, one can get the following approximate formulas:

$$\sigma_e = 2\pi R^2 q^2, \qquad \sigma_d = 2\pi R^2(1 - {}^9/_8\, q^2),$$
$$\sigma_n = \sigma_p = \pi R^2(1 - q^2/4), \qquad \sigma_a = {}^1/_4\, \pi R^2 q^2,$$
$$\sigma_t = 4\pi R^2(1 - q^2/8). \tag{5}$$

The cross section σ_e corresponds to elastic scattering of the π meson by the deuteron, σ_d to scattering of the π meson accompanied by breakup of the deuteron, σ_n and σ_p to processes of inelastic interaction of the π meson with the neutron or the proton in the deuteron, and σ_a to the process of inelastic interaction of the π meson with the neutron and proton. As a result of the diffraction the total interaction cross section of a fast π-meson with a deuteron is less than the sum of the total cross sections for interaction of the π meson with a free neutron and proton (eclipse effect[3,4]). The diffraction also has the effect that the scattering of the π meson by the deuteron occurs mostly with simultaneous breakup of the deuteron ($\sigma_d \gg \sigma_e$).

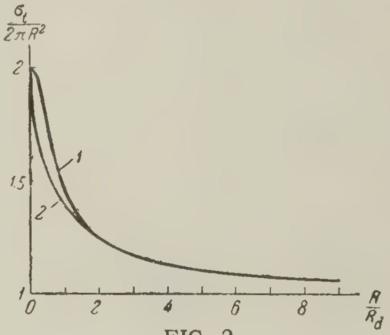

FIG. 2

It should be pointed out that the total cross sections in the region $R < R_d$ are strongly dependent on the choice of the wave function $\varphi_0(r)$ of the deuteron ground state. Figure 2 shows the total cross section σ_t for two choices of $\varphi_0(r)$. Curve 1 is for the Gaussian of Eq. (1) and curve 2 for $\varphi_0(r) = \sqrt{\alpha/2\pi}\, e^{-\alpha r}/r$, where $\alpha = 1/2R_d$. On the other hand, in the region $R > R_d$ the cross section values are practically independent of the form of the wave function of the deuteron ground state.

---

[1] A. I. Akhiezer and A. G. Sitenko, J. Exptl. Theoret. Phys. (U.S.S.R.) **32**, 794 (1957), Soviet

Phys. JETP 5, 652 (1957).

[2] Eisberg, Fowler, Lea, Shepard, Shutt, Thorndike, and Whittemore, Phys. Rev. 97, 797 (1955).

[3] R. J. Glauber, Phys. Rev. 100, 242 (1955).

[4] J. S. Blair, Nucl. Phys. 6, 348 (1958).

Translated by M. Hamermesh
269

THE SPLITTING OF A SMALL DISCONTINUITY IN MAGNETOHYDRODYNAMICS

G. Ia. LIUBARSKII and R. V. POLOVIN

Physico-Technical Institute, Academy of Sciences, Ukrainian S.S.R.

Submitted to JETP editor June 30, 1958

J. Exptl. Theoret. Phys. (U.S.S.R.) 35, 1291-1293 (November, 1958)

IN 1926 Kochin[1,2] investigated the break-up of an arbitrary hydrodynamic plane discontinuity. In doing this he made essential use of the fact that either a single shock wave or a single self-similar rarefaction wave can be propagated in each direction from the initial discontinuity.

In magnetohydrodynamics a discontinuity breaks up, generally speaking, in a considerably more complicated manner: up to three waves (shock waves or self-similar waves) can be propagated in each direction from the initial discontinuity. This is connected with the fact that in magnetohydrodynamics there exist three different types of stable shock waves[3] (fast and slow magnetoacoustic waves and magnetohydrodynamic waves) and two types of self-similar waves[4] (fast and slow magnetoacoustic waves). Because the different speeds of propagation, up to three waves of the types enumerated above may be propagated in each direction from the initial discontinuity.

We note that the initial discontinuity is characterized by seven parameters — the discontinuities in the density $\Delta\rho$, in the entropy Δs, in the velocity $\Delta \mathbf{V}$ and in the tangential component of the magnetic field $\Delta \mathbf{H}_t$. Since each wave is characterized by one parameter, the initial discontinuity breaks up into seven waves, of which three are propagated to the left, three are propagated to the right and one — a contact discontinuity — remains stationary. As has been shown by Akhiezer et al.,[3] two waves of the same type move in such a way that the wave in the rear overtakes the wave in front. Therefore waves of three different types must be propagated in each direction: in front there will be the fast magnetoacoustic (shock or self-similar) wave, followed by the Alfven shock wave, and finally, the slow magnetoacoustic (shock or self-similar) wave.

One should have in mind the fact that the self-similar wave is a rarefaction wave,[4] while the shock wave is a compression wave.[5]

The problem now consists of choosing the amplitudes of these seven waves in such a way as to make a transition from the state to the left of the initial discontinuity to the state to the right of the initial discontinuity. For the sake of simplicity, we shall restrict ourselves to the case when the initial discontinuity is very small. Then all the secondary discontinuities will also be small. The relation between the discontinuities in the magnetohydrodynamic quantities in the self-similar and the shock waves (in the case of low intensity) is the same as between the amplitudes of the corresponding linearized wave. We now state these relations:

(1) Magnetoacoustic waves (shock and self-similar waves)

$$\Delta_{\pm}^{(\varepsilon)} v_x = \varepsilon (u_{\pm} / \rho) \Delta_{\pm}^{(\varepsilon)} \rho,$$

$$\Delta_{\pm}^{(\varepsilon)} \mathbf{v}_t = -\varepsilon H_x \mathbf{H}_t u_{\pm} \Delta_{\pm}^{(\varepsilon)} \rho / 4\pi\rho^2 (u_{\pm}^2 - V_x^2),$$

$$\Delta_{\pm}^{(\varepsilon)} \mathbf{H}_t = u_{\pm}^2 \mathbf{H}_t \Delta_{\pm}^{(\varepsilon)} \rho / \rho (u_{\pm}^2 - V_x^2),$$

$$\Delta_{\pm}^{(\varepsilon)} s = 0, \qquad \Delta_{\mp}^{(\varepsilon)} p = c^2 \Delta_{\pm}^{(\varepsilon)} \rho,$$

where c is the speed of sound, $\mathbf{V}_t$ is the tangential component of the velocity of the liquid $\mathbf{V}$, and

$$\mathbf{V} = \mathbf{H} / \sqrt{4\pi\rho}, \quad u_{\pm}^2 = \tfrac{1}{2} [V^2 + c^2 \pm \sqrt{(V^2 + c^2)^2 - 4c^2 V_x^2}].$$

The plus sign corresponds to the fast magnetoacoustic wave, the minus sign corresponds to the slow one. For waves moving to the right $\epsilon = +1$; for waves moving to the left $\epsilon = -1$. The difference between the shock and the self-similar magnetoacoustic waves is that in the former the density increases, while in the latter it decreases.

(2) Alfven shock waves

$$\Delta_{\mathrm{A}}^{(\varepsilon)} \mathbf{v}_t = -\varepsilon \Delta_{\mathrm{A}}^{(\varepsilon)} \mathbf{H}_t / \sqrt{4\pi\rho},$$

$$\Delta_{\mathrm{A}}^{(\varepsilon)} v_x = \Delta_{\mathrm{A}}^{(\varepsilon)} p = \Delta_{\mathrm{A}}^{(\varepsilon)} \rho = 0, \qquad \Delta_{\mathrm{A}}^{(\varepsilon)} H_t^2 = 0.$$

(3) Contact discontinuity

$$\Delta_{\mathrm{C}} v_x = \Delta_{\mathrm{C}} v_y = \Delta_{\mathrm{C}} v_z = \Delta_{\mathrm{C}} p = \Delta_{\mathrm{C}} H_y = \Delta_{\mathrm{C}} H_z = 0,$$

$$\Delta_{\mathrm{C}} \rho = (\partial\rho / \partial s)_p \Delta_{\mathrm{C}} s, \quad H_x \neq 0.$$

The sum of the discontinuities of each magnetohydrodynamic quantity at the seven new waves is equal to the initial discontinuity. We thus obtain seven equations in seven unknowns, on solving which we obtain all the discontinuities. We give the expression for the discontinuities in the density:

$$\Delta_{\pm}^{(\varepsilon)}\rho = \frac{1}{2R}\left\{\frac{c^2V_t^2[\Delta\rho - (\partial\rho/\partial s)_p\Delta s]}{u_{\mp}^2 - V^2} - \frac{\Delta H_t^2}{8\pi} + \frac{\varepsilon\rho V_x^2}{u_{\pm}}\left[\frac{\mathbf{H}_t\Delta\mathbf{v}_t}{H_x} + \frac{V_t^2\Delta v_x}{u_{\mp}^2 - V_x^2}\right]\right\},$$

where

$$R = \sqrt{(V^2 + c^2)^2 - 4c^2V_x^2}.$$

The formulas obtained above enable us to determine the signs of $\Delta_{\pm}^{(\epsilon)}\rho$ and in this way to determine the type of wave into which the initial discontinuity breaks up.

The authors express their gratitude to Professor A. I. Akhiezer for a number of valuable suggestions.

---

[1] N. E. Kotchine, Rendiconti del Circolo Nat. di Palermo **50**, 305 (1926).

[2] L. D. Landau and E. M. Lifshitz, Механика сплошных сред (The Mechanics of Continuous Media) Gostekhizdat, Moscow, 1954.

[3] Akhiezer, Liubarskii, and Polovin, J. Exptl. Theoret. Phys. (U.S.S.R.) **35**, 731 (1958), Soviet Phys. JETP **8**, 507 (1959).

[4] G. Ia. Liubarskii and R. V. Polovin, J. Exptl. Theoret. Phys. (U.S.S.R.) **35**, 509 (1958), Soviet Phys. JETP **8**, 351 (1959).

[5] R. V. Polovin and G. Ia. Liubarskii, J. Exptl. Theoret. Phys. (U.S.S.R.) **35**, 510 (1958), Soviet Phys. JETP **8**, 351 (1959).

Translated by G. Volkoff
270

ON A METHOD FOR DETERMINING THE PARITY OF STRANGE PARTICLES

E. I. DOLINSKII

Moscow State University

Submitted to JETP editor July 5, 1958

J. Exptl. Theoret. Phys. (U.S.S.R.) 35, 1293-1294 (November, 1958)

SINCE parity is not conserved in weak interactions that are responsible for the decay of elementary particles, the intrinsic parity of particles may be determined only from strong interaction processes. On the other hand, due to strangeness conservation, only the relative parity of strange particles can be determined in strong interactions. This letter discusses an experiment by which the relative parity of K mesons and hyperons may be determined.

Consider the process of absorption of a K^- meson from an s state by a polarized proton with the production of a Y hyperon (Y stands for Λ or Σ) and π-meson:

$$K^- + p \rightarrow Y + \pi. \quad (1)$$

In the following it is assumed that the spin of the K-meson is zero and that of the hyperon is $\frac{1}{2}$. Let ξ_K be the intrinsic parity of the K meson, ξ the relative hyperon-proton parity, L the orbital angular momentum of the relative hyperon – π meson motion in their center of mass system, and P_p the degree of polarization of the proton. Conservation of parity and angular momentum in process (1) leads to the relations: $\xi_K\xi = (-)^{L+1}$ and $L = 0$ or 1. There are two possibilities: (a) $\xi_K\xi = +1$, hence $L = 1$, and (b) $\xi_K\xi = -1$, hence $L = 0$.

It is easy to show that: (1) in both cases the hyperons are emitted isotropically; (2) the degree of polarization $P_Y(\theta)$ of the hyperon emitted at an angle θ relative to the direction of polarization of the proton is $P_Y(\theta) = \cos(2\theta)\, P_p$ in case (a) and $P_Y(\theta) = P_p$ in case (b); (3) the degree of polarization $\overline{P}_Y$ of the hyperon averaged over the emission angle θ is $\overline{P}_Y = -\frac{1}{3}P_p$ in case (a) and $P_Y = P_p$ in case (b). Since parity is not conserved in the decay $Y \rightarrow N + \pi$ (N stands for nucleon), the possibilities (a) and (b) can be distinguished and the sign of $\xi_K\xi$ determined by measuring the asymmetry in the angular distribution of the decay π mesons.

The experiment described can also be performed with polarized nuclei. Let the nuclear spin j be determined entirely by one nucleon N outside a closed subshell (or by a "hole" in a subshell) and suppose that as a result of capture of a K^- meson, from an s state, a hyperon and π meson are emitted by this nucleon and the daughter nucleus suffers no recoil. Conservation of parity and angular momentum leads then to the relations $\xi_K\xi = (-)^{L+l+1}$ (l is the orbital angular momentum of the nucleon in the nucleus) and $L = j - \frac{1}{2}$ or $j + \frac{1}{2}$. A simple calculation shows that for $L = j - \frac{1}{2}$, $\overline{P}_Y = P_n$ and for $L = j + \frac{1}{2}$, $\overline{P}_Y = -P_n/(j+1)$ where P_n denotes the degree of polarization of the nucleus. Clearly, due to parity conservation, for a given j and l the two values $\xi_K\xi = +1$ and -1 will correspond to different values of L. It should be noted that the indicated values of $\overline{P}_Y$ will be decreased due to the background of unpolarized hyperons resulting from the absorption of K^- mesons by nucleons from filled shells of the nucleus, however the sign of $\overline{P}_Y$ will persist.

I am grateful to I. S. Shapiro for discussions.

Translated by A. M. Bincer
271

HEAT OF MIXING OF LIGHT AND HEAVY WATER

V. P. SKRIPOV

Ural' Polytechnical Institute

Submitted to JETP editor July 4, 1958

J. Exptl. Theoret. Phys. (U.S.S.R.) 35, 1294-1295 (November, 1958)

IT seems at first glance that the thermal effect in mixing H_2O and D_2O should be very small, since a mixture of molecules of different isotopes could be considered to a high degree of approximation as an ideal solution. But account must be taken of the chemical interaction between the molecules of the initial substances:

$$H_2O + D_2O \rightleftarrows 2HDO. \qquad (1)$$

A value K = 3.26 is usually taken[1] for the equilibrium constant of the above reaction in the liquid phase. This means that when one mole of H_2O and 1 mole of D_2O are mixed, 0.95 moles of HDO is formed.

The properties of the H_2O and D_2O molecules have been investigated in sufficient detail, but the same cannot be stated with respect to the molecules of HDO, since they always occur mixed with H_2O and D_2O. If the heat of mixing q of light and heavy water and the equilibrium constant of the reaction (1) are known, the heat of formation q′ of HDO, when H_2O and D_2O react in the condensed phase, can be determined directly, and certain conclusions can be drawn from this regarding the difference in the zero-point energies of the different isotopic forms of water molecules.

The heat of mixing of H_2O and D_2O (99.7%) was determined in a hermetically sealed reversing calorimeter provided with a heater and a thermistor. A cooling of the system (by ≈ 0.3°C) was observed on mixing (up to a molecular concentration of deuterium $n \approx 0.5$). The temperature of the external container was adjusted to the temperature of the calorimeter. The correction for heat exchange did not exceed 2.5% of the magnitude of the effect observed. The thermal capacity of the system was determined in the course of the experiment.

As the result of experiments (at 24°C) the following value for the heat of mixing (heat is absorbed) was obtained for the case $n = 0.50$, taking into account possible errors: $q = 7.92 \pm 0.25$ cal/mole.

If we assume the equilibrium constant for the reaction (1) in the liquid phase to be equal to 3.26, we shall obtain for the heat of formation of 1 mole of HDO (not taking into account the effect due to the heavy isotope of oxygen O^{18}) the value $q' = 16.7 \pm 0.5$ cal/mole. This value can be compared with the results of calculations for the gas phase. To do this, we make use of the theoretically calculated dependence of the equilibrium constant on the temperature,[2] and the well-known thermodynamic relation[3]

$$\partial \ln K / \partial T = \Delta H / RT^2, \ \Delta H = 2q'.$$

From this we obtain $q' = 34$ cal/mole. A decrease in the heat of formation of HDO in the condensed phase, compared with the gaseous phase, may be due to a strong intermolecular interaction in solution and to the associated change in the zero-point energies.

I express my gratitude to V. M. Kostin for his help in carrying out the experiments.

---

[1] A. I. Brodskii, Химия изотопов (Chemistry of Isotopes), Acad. Sci. Press, Moscow, 1957.

[2] I. Kirschenbaum, Heavy Water, IIL, Moscow, 1953.

[3] M. A. Leontovich, Введение в термодинамику (Introduction to Thermodynamics) Gostekhizdat, Moscow-Leningrad, 1952.

Translated by G. Volkoff
272

MEASUREMENT OF β-γ CORRELATION FROM ORIENTED NUCLEI

A. V. KOGAN, V. D. KUL' KOV, L. P. NIKITIN, N. M. REINOV, I. A. SOKOLOV, and M. F. STEL' MAKH

Leningrad Physico-Technical Institute, Academy of Sciences, U.S.S.R.

Submitted to JETP editor July 9, 1958

J. Exptl. Theoret. Phys. (U.S.S.R.) 35, 1295-1296 (November, 1958)

IN connection with the problem of nonconservation of parity, it has been shown by Dolginov[1] and others[2,3] that in an allowed transition the investigation of the angular correlation between the β particle and the subsequent γ quantum emitted by an oriented nucleus can give the answer to the question whether the so-called combined parity is conserved in β decay. When there is interference between the Fermi and Gamow-Teller interactions, the shape of the correlation function depends essentially on the validity of the hypothesis of conservation of combined parity which was enunciated by Landau.

One of the experimental difficulties in such measurements is the short time available for the measurements on nuclei which have been oriented at very low temperatures, because of the rapid heating up of the samples. In the first experiments on parity nonconservation[4] the asymmetry of the β radiation disappeared completely after 5 or 6 minutes, and the actual time for the measurements may have amounted to only 3 or 4 minutes.

In studying the correlation we constructed an apparatus for orienting nuclei in which measures were taken to increase the duration and statistical accuracy of the measurements.

The principal source of heat loss is heat radiation passing through the light pipe which serves to transmit the light pulses occurring in the plastic scintillator for recording the β particles (Fig. 1). To absorb this radiation, the 6-micron thick aluminum reflector over the plastic scintillator was covered by a copper foil of the same thickness. Heat absorbed by the foil was transferred to a helium dewar through the clamps and glass of the container.

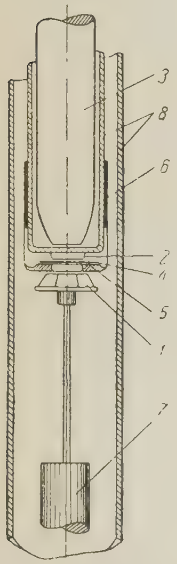

FIG. 1. 1) crystal of $2[C_e(NO_3)_3]$ $3[Mg(NO_3)_2]\cdot 24H_2O_2$; 2) plastic scintillator; 3) light pipe; 4) aluminum foil; 5) copper foil; 6) copper clamp; 7) Ballast salt; 8) vessel walls.

Measurements were made of the asymmetry of the β radiation of Co^{60} introduced into a thin surface layer of a crystal of cerium-magnesium nitrate. The polarization of the nuclei alternately in the direction toward the β detector and away from it was accomplished by means of a magnetic field along the axis of the vacuum vessel. The time during which the asymmetry of the radiation was close to its limiting value was about 20 minutes (Fig. 2). The degree of asymmetry of the β radiation in these experiments was approximately half that in the experiments of Wu et al., since the solid angle for counting of the β particles was increased by approximately a factor of 20 and was close to 2π. In measuring the correlation, the decrease of the observed effect by a factor of 2 is more than compensated by the increase in statistical accuracy of the measurements.

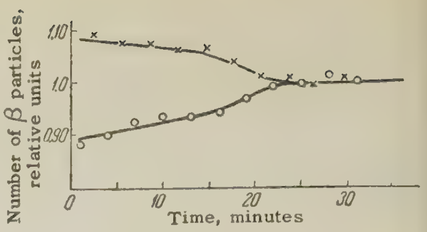

FIG. 2. Asymmetry of β radiation. Direction of polarizing magnetic field: ×) down, ○) up.

The Co^{58} isotope was first chosen for the investigation of the β-γ correlation, but before the completion of our experiments it was shown that the interference term in the β decay of Co^{58} should be small[5] and that correlation measurements on this isotope do not allow one to draw any conclusions concerning the conservation of combined parity.[6]

We have made measurements of the β-γ angular correlation for oriented Co^{60} nuclei. The preliminary data do not contradict the theoretical computations made on the assumption of conservation of combined parity. We plan to study the β-γ angular correlation for Mn^{52} and V^{48} in which, according to data in the literature, the interference term should be markedly different from zero.

The authors thank Academician A. I. Alikhanov and Prof. S. Ia. Nikitin for supplying the Co^{58}, A. Z. Dolginov for frequent valuable discussions and for preprints of his papers, and O. V. Larionov for the chemical separation of the Co^{58}.

---

[1] A. Z. Dolginov, J. Exptl. Theoret. Phys. (U.S.S.R.) **33**, 1363 (1957), Soviet Phys. JETP **6**, 1047, (1958). Nucl. Phys. **5**, 512 (1958).

[2] M. Morita and R. S. Morita, Phys. Rev. **107**, 1316 (1957).

[3] R. B. Curtis and R. R. Lewis, Phys. Rev. **107**, 1381 (1957).

[4] Wu, Ambler, Hayward, Hoppes and Hudson, Phys. Rev. **105**, 1413 (1957).

[5] F. Boehm and A. H. Wapstra, Phys. Rev. **107**, 1462 (1957).

[6] Ambler, Hayward, Hoppes and Hudson, Phys. Rev. **108**, 503 (1957).

Translated by M. Hamermesh
273

μ^+-MESON DEPOLARIZATION IN NUCLEAR EMULSIONS WITH DIFFERENT GELATIN CONTENT

Iu. M. IVANOV and A. I. FESENKO

Moscow Institute of Engineering and Physics

Submitted to JETP editor July 9, 1958

J. Exptl. Theoret. Phys. (U.S.S.R.) **35**, 1297-1298 (November, 1958)

FRIEDMAN and Telegdi[1,2] and Gurevich et al.[3] have studied the asymmetry in nuclear emulsions in the angular distribution of electrons from the μ^+-e^+ decay to verify the failure of the parity conservation law in weak interactions.[4] Their results for the asymmetry coefficient in the angular distribution had a smaller absolute value than predicted by theory. One of the reasons for this is μ^+-meson depolarization in the emulsion. The results of Chadwick et al.[5] indicate that the depolarization effect is different for the two constituents of the nuclear emulsion (silver halide and gelatin).

The present work was undertaken to clarify the dependence of μ^+-meson depolarization on the relative content of each constituent of the emulsion (by studying the "forword-backward" asymmetry in the electron distribution from μ^+-e^+ decay). To this end a chamber was used consisting of layers of the usual NIKFI type "R" emulsion and of layers of emulsion whose gelatin content by weight was 2, 3, and 4 times that of the usual emulsion. We shall refer to these emulsions as 2-, 3-, and 4-fold diluted emulsions. The chamber was exposed to the π^+-meson beam from the synchrocyclotron of the Joint Institute for Nuclear Research. The emulsion chamber was placed inside a magnetic screen (within which the field intensity did not exceed 0.08 gauss) to prevent precession of the spin of stopped μ^+ mesons due to stray magnetic fields of the synchrocyclotron.

The various emulsions were prepared at the same time and were from the same batch. The thickness of each emulsion layer was measured before and after exposure.

In the scanning process those π^+-μ^+-e^+ decays were registered for which the μ^+-meson track was entirely within one emulsion layer. The direction of electron emission was measured relative to the direction of the μ^+-meson momentum at the point where the π^+ meson decayed. The plane perpendicular to this direction served as the dividing plane for decay electrons emitted forwards and backwards.

The events in which the μ^+ meson decayed within 50 μ from the surface of the unexposed emulsion were excluded in the processing of the results. The resultant data are given in the table.

Emulsion dilution factor	Number of $\pi \to \mu \to e$ decays	Number of undetected electrons	$-A$
×1	2300	11	0.065±0.041
×2	2300	13	0.118±0.041
×3	2300	21	0.14±0.041
×4	1133	53	0.37±0.06

For each emulsion we calculated the ratio $2(N_B - N_F)/(N_B + N_F)$ (N_B, N_F is the number of electrons emitted backwards and forwards respectively), which was taken to be the asymmetry coefficient A. The statistical root-mean-square error was taken to be $2/\sqrt{N}$. It was assumed that the electron angular distribution is of the form $1 + A\cos\theta$, where θ is the angle between the initial directions of the μ-meson and electron momenta. In the first three types of emulsion the number of undetected decay electrons was less than 1%. To exclude the comparatively large number of unseen electrons in 4-fold diluted emulsions it was assumed that all these electrons were emitted forwards. Clearly, this lowers the asymmetry coefficient. Nevertheless, as can be seen from the figure, the angular asymmetry tends to rise with the increase in the gelatin weight content of the nuclear emulsion.

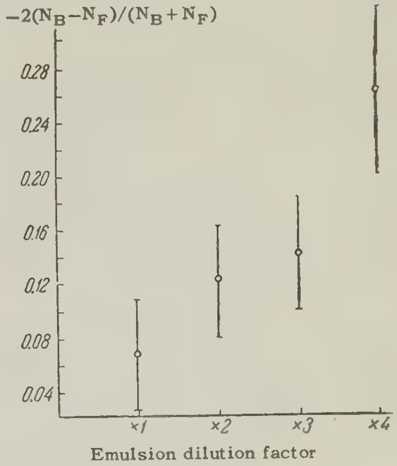

To allow definitive conclusions to be drawn on the dependence of the asymmetry on gelatin content, we are continuing the experiment to improve our statistics.

In addition we processed 1198 π^+-μ^+-e^+ decay events in 4-fold diluted emulsions containing triethanolamine $(C_2H_4OH)_3N$. The events in which the μ^+-meson stopped in the emulsion surface (the thickness of the end zones was taken as 50 μ of unexposed emulsion) were excluded. The number of unseen decay electrons was 10. In those cases the asymmetry coefficient equals 0.182 ± 0.058.

The authors are grateful to Prof. I. I. Gurevich and to V. G. Kirillov-Ugriumov for interest in this work and advice in carrying it out, and to Z. S. Galkina, G. I. Polosina and A. V. Smelianska for help in emulsion scanning.

---

[1] J. I. Friedman and V. L. Telegdi, Phys. Rev. **105**, 1681 (1957).

[2] J. I. Friedman and V. L. Telegdi, Phys. Rev. **106**, 1290 (1957).

[3] Gurevich, Kutukova, Mishakova, Nikolskii, and Surkova, J. Exptl. Theoret. Phys. (U.S.S.R.) **34**, 280 (1958), Soviet Phys. JETP **7**, 195 (1958).

[4] T. D. Lee and C. N. Yang, Phys. Rev. **105**, 1671 (1957).

[5] Chadwick, Durrani, Eisberg, Jones, Wignall, and Wilkinson, Phil. Mag. **2**, 684 (1957).

Translated by A. M. Bincer
274

OBSERVATION OF NUCLEAR-ACTIVE PARTICLES OF COSMIC RADIATION WITH ENERGY $\geq 10^{13}$ ev.

E. A. MURZINA, S. I. NIKOL'SKII, and V. I. IAKOVLEV

P. N. Lebedev Physics Institute, Academy of Sciences, U. S.S.R.

Submitted to JETP editor July 10, 1958

J. Exptl. Theoret. Phys. (U.S.S.R.) **35**, 1298-1300 (November, 1958)

In Autumn 1957 we measured the flux intensity of high-energy nuclear-active particles of cosmic radiation at 3860 m above sea level.

The detector of nuclear-active particles consisted of seven ionization chambers surrounded by lead (Fig. 1). Six chambers (1 – 6) 150 cm in length, 25 cm wide, and 15 cm high formed the upper part of the detector. This was shielded from above and below by ~ 45 g/cm² of lead. The dimensions of the lower ionization chamber (7) were 150 × 150 × 15 cm. A graphite absorber of varying thickness (40, 63, 100 g/cm²), covered by 2 cm of lead, was placed above the detector. This was intended to reduce the contribution of the electron-photon component accompanying the nuclear-active particles. Five groups of cylindrical ionization chambers were placed around the detector to record extensive air showers accompanying the high-energy nuclear-active particles in the depth of the atmosphere. The sensitivity and total area of these chanbers made it possible to detect all events in which nuclear-active particles were accompanied by extensive air showers with total number of particles $\geq 3 \times 10^3$.

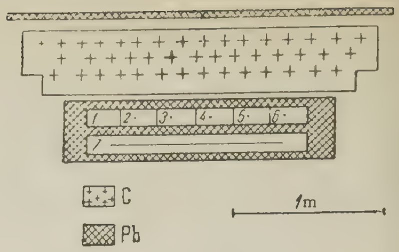

FIG. 1. Detector of nuclear-active particles. Side view.

The size of bursts in all chambers was automatically recorded whenever the ionization in both layers of the nuclear-active particle detector exceeded that due to 1000 relativistic particles. An estimate of the energy of nuclear-active particles producing the observed bursts was facilitated by the fact that we could assume, from the ratio of radiation lengths in lead and graphite, that the majority of nuclear interactions occurred in the graphite, while the electron-photon component, originating in the decay of π^0 mesons, multiplied in the layer of lead of a given thickness. Assuming that 30% of the energy of the nuclear-active particle is carried away by π^0 mesons in a single nuclear interaction and in the ensuing nuclear cascade in a slab of graphite 100 g/cm² thick, we obtain from the electromagnetic cascade theory the following relation between the energy of a nuclear-active particle E and the number of relativistic particles N detected in the ionization chamber under 90 g/cm² of lead:

$$E = N \cdot 10^9 / 0.35 \ln 0.015 N.$$

This expression is valid for $5 \times 10^{11} \leq E \leq 2 \times 10^4$ ev.

An analysis of the experimental data showed that nuclear-active particles with energy $\geq 2 \times 10^{12}$ ev are accompanied in 81 ± 3% of the cases by extensive air showers with the number of particles > 3 × 10^3. Nuclear-active particles of ≥ 1.5 × 10^{13} ev are accompanied by such showers in 83 ∓ 4% of the cases. This shows that the particles are accompanied by extensive air showers almost independently of their energy.

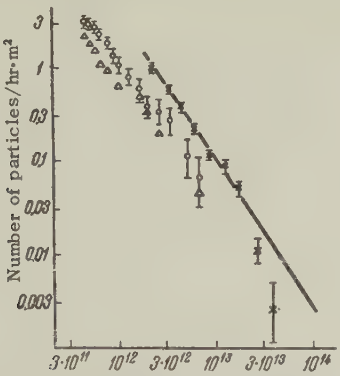

FIG. 2. Integral energy spectrum of nuclear-active particles; ○ and △ – data of reference 2. The energy of detected particles and the detection efficiency was estimated for the data of reference 1 according to reference 2, and a correction for the difference of observation levels was applied. ×) results of the present experiments.

The integral energy spectrum of nuclear-active particles observed at 3860 m above sea level is shown in Fig. 2. The energy of the particles detected in the experiment was determined according to the relation given above. The detection efficiency was found by comparing the number of ionization bursts under layers of graphite of different thickness. It can be seen from the figure that, in the energy region 10^{12} to 10^{13} ev, the energy spectrum is given by the formula $F(>E) \sim 1/E^{1.53\pm0.07}$, which is in agreement with the energy spectrum of the primary cosmic radiation in the corresponding energy range.[1]

It is interesting to note that considerably fewer particles with energy ≥ 3 × 10^{13} ev were found than it could be expected if the similarity between the spectra of nuclear-active particles and of the primary cosmic radiation were extended to that region. The probability that the discrepancy between the observed and expected number of nuclear-active particles with energy ≥ 3 × 10^{13} ev can be explained by statistical fluctuations is less than 3%. This result indicates clearly that the character of nuclear interactions changes at ~ 3 × 10^{14} ev.[3] According to this assumption, primaries of > 3 × 10^{14} ev lose their energy on the production of secondary particles in the first interaction and are absorbed in the atmosphere sooner than particles of lower energies.

In conclusion, the authors express their gratitude to Prof. N. A. Dobrotin and G. T. Zatsepin for helpful discussion of the results.

---

[1] Barrett, Bollinger, Cocconi, Eisenberg, and Greisen, Revs. Modern Phys. **24**, 133 (1952).

[2] Grigorov, Shestoperov, Sobiniakov, and Podgurskaia, J. Exptl. Theoret. Phys. (U.S.S.R.) **33**, 1099 (1957), Soviet Phys. JETP **6**, 848 (1958).

[3] Nikol'skii, Vavilov, and Batov, Dokl. Akad. Nauk SSSR **111**, 71 (1956), Soviet Phys. "Doklady" **1**, 625 (1956); S. I. Nikol'skii and A. A. Pomanskii, J. Exptl. Theoret. Phys. (U.S.S.R.) **35**, 618 (1958), Soviet Phys. JETP **8**, 430 (1959).

Translated by H. Kasha
275

ELASTIC SCATTERING OF 5 TO 22 Mev POSITIVE PIONS BY CARBON

V. G. KIRILLOV-UGRIUMOV, L. P. KOTENKO, E. P. KUZNETSOV, and F. M. SERGEEV

P. N. Lebedev Physics Institute, Academy of Sciences, U.S.S.R.

Submitted to JETP editor July 10, 1958

J. Exptl. Theoret. Phys. (U.S.S.R.) **35**, 1300-1302 (November, 1958)

THE cross sections for the elastic scattering of pions by light nuclei at energies above 30 Mev have been obtained experimentally. It was difficult to investigate the scattering of slower pions by the method previously used, although such data are required to give a complete picture of interactions between pions and nuclei. Low-energy pion scattering is naturally studied in light nuclei, where the Coulomb forces are relatively small. We have investigated the elastic scattering of 5- to 22-Mev pions in carbon, using a 750 cm^3 propane bubble chamber.[1] The chamber was irradiated by a positive pion beam from the synchrocyclotron of the Joint Institute for Nuclear Research. The investigated energy interval corresponds to residual pion ranges in propane from 0.125 to 2 g/cm^2. Pions were identified from $\pi \rightarrow \mu \rightarrow e$ decay after stopping in the working material of the chamber. We used 5675 photographs of tracks of pions stopped in the chamber in the analysis. We did not study star production by 5- to 22-Mev pions. It must be noted that the observed scattering of 5- to 22-

Mev pions is elastic. There is very little inelastic scattering of positive pions at such energies. For example, inelastic scattering on emulsion nuclei is practically zero at 30 Mev.[2-4] We also have indications that inelastic scattering diminishes with decreasing energy in carbon.[5,6]

We measured the angular projections of singly-scattered pions on the plane of the photographic film. Out of the 5675 pions, 75 were scattered in the given energy interval at an angle with a projection greater than 15°. After taking Coulomb scattering into account we found that 31 particles underwent nuclear scattering. In order to determine the nuclear scattering cross section in carbon we took into account: (1) Pion scattering (Coulomb and nuclear) by hydrogen contained in the propane; (2) possible imitation of $\pi \rightarrow \mu - e$ decay by muons (10 to 20% muon admixture in the beam); (3) transmission of the chamber (unequal probability that the chamber would register scattering at a given angle for different energies); (4) imitation of single scattering by multiple scattering, and also superposition of multiple scattering on single scattering. Special attention was devoted to determining the boundaries of the angular and energy intervals, and account was taken of the statistical transfer of particles to adjacent intervals due to inaccurate determination of angles and energies (the accuracy of measurement was 2° for angles and 10% for energies). Coulomb scattering in carbon and hydrogen was calculated by the Rutherford formula, which was projected on the plane:

$$\frac{d\sigma(\varphi)}{d\varphi} = 0.8139 \; \frac{32\, Z^2}{\pi\,(p\beta c_{\mathrm{Mev}})^2} \, \frac{\sin\varphi + (\pi - \varphi)\cos\varphi}{\sin^3\varphi} \, 10^{-26} \frac{\mathrm{cm}^2}{\mathrm{rad}},$$

where φ is the projection of the angle of pion scattering.

The table gives the cross sections for elastic nuclear scattering of pions which were obtained in the present work as well as data taken from other authors. It can be seen that at 8 to 22 Mev the cross section does not differ within the limits of error from the result obtained at 33 Mev. At 5 to 8 Mev a considerable growth of the scattering cross section is observed. It is significant that at these energies the pion wavelength already exceeds the radius of the carbon nucleus. For a 6-Mev pion $\lambda\!\!\!^{-} = 4.78 \times 10^{-13}$ cm whereas the radius of the carbon nucleus is $R = 3.2 \times 10^{-13}$ cm. We know that in the limiting case, when the particle wavelength $\lambda\!\!\!^{-} \gg R$, the elastic cross section for a sufficiently high potential $+V$ approaches 4 times the geometric cross section. (At low energies the potential is positive since repulsion occurs, as follows, for example, from work on mesic atoms.[13]) The observed increase of the cross section can evidently be attributed to this effect. However, at 5 Mev the pion wavelength is still comparable with nuclear dimensions and in our case we must consider both S and P waves, especially since the angular distribution of particles undergoing nuclear scattering is directed forward. The energy dependence of the cross section and the angular distributions will be analyzed at a later date.

Elastic scattering of pions by carbon

Energy interval, Mev	Sign of pion	Angular interval, degrees	Elastic scattering cross section, 10^{-27} cm (nucl.)	Author
5—8	+	>15	402±152	Our data
8—15	+	>15	78±45	
15—22	+	>15	56.0±32	
5—22	+	>15	97±27	
33	+	>10	96±30	[7]
46	+	> 0	182±46	[7]
35—60	+	>20	78±23	[8]
52—72	+	>20	89±10	[9]
68	+	> 0	112±20	[7]
90	—	>15	240±30	[10]
125	—	>20	179±18	[11]
230	—	>10	200±32	[12]

We may note in conclusion that for the purpose of verifying the correctness of pion energy determination from the residual range we determined the energies of decay muons in 120 instances. The muon range in propane was 3.15 ± 0.02 mm for a propane density of 4.00 ± 0.05 g/cm² (at 67°C and pressure between 5 and 6 atmos), which corresponds to the muon energy E = 4.10 ± 0.04 Mev.

We take this opportunity to thank Prof. A. I. Alikhanian for his interest and Prof. V. P. Dzhelepov for making the synchrocyclotron of the Joint Institute for Nuclear Research available.

---

[1] Kotenko, Popov, and Kuznetsov, **Приборы и техника эксперимента** (Instruments and Measurement Engineering) **1**, 36 (1957).

[2] B. Rankin and H. Bradner, Phys. Rev. **90**, 647 (1953).

[3] G. Bernardini, Phys. Rev. **84**, 610 (1951).

[4] L. Feretti and E. Manaresi, Nuovo cimento **1**, 512 (1957).

[5] V. T. Osipenko and S. S. Filippov, J. Exptl. Theoret. Phys. (U.S.S.R.) **34**, 224 (1958), Soviet Phys. JETP **7**, 154 (1958).

[6] L. M. Barkov and B. A. Nikol'skii, Usp. Fiz. Nauk **61**, 341 (1957).

[7] D. H. Stork, Phys. Rev. **93**, 868 (1954).

[8] A. M. Shapiro, Phys. Rev. **84**, 1063 (1951).

[9] Byfield, Kessler, and Lederman, Phys. Rev. **86**, 17 (1952).

[10] Isaacs, Sachs, and Steinberger, Bull. Amer. Phys. Soc. **26**, 22 (1951).

[11] J. O. Kessler and L. M. Lederman, Phys. Rev. **94**, 689 (1954).

[12] Dzhelepov, Ivanov, Kozodaev, Osipenkov, Petrov, and Rusakov, J. Exptl. Theoret. Phys. (U.S.S.R.) **31**, 923 (1956), Soviet Phys. JETP **4**, 864 (1957).

[13] M. B. Stearns, M. Stearns, DeBenedetti, and Leipuner, Phys. Rev. **96**, 804 (1954).

Translated by I. Emin
276

STATISTICAL INTERPRETATION OF EXPERIMENTAL DATA ON MULTIPLE PRODUCTION OF PARTICLES AT 1 TO 20 Bev

V. M. MAKSIMENKO

P. N. Lebedev Physics Institute, Academy of Sciences, U.S.S.R.

Submitted to JETP editor July 10, 1958

J. Exptl. Theoret. Phys. (U.S.S.R.) **35**, 1302-1304 (November, 1958)

THIS communication presents a comparison of experimental data on multiple particle production in nucleon-nucleon and pion-nucleon collisions at a few Bev with Fermi's statistical theory.[1] In the calculations two forms of this statistical theory were employed (for details see the review paper, Ref. 2), — with and without account being taken of resonant nucleon-pion interactions through the introduction of isobaric states.[3] The radius of the effective volume is taken to be $\hbar/\mu c = 1.4 \times 10^{-13}$ cm. The methods developed in Ref. 4 were used to calculate the statistical weights.

The table gives the experimental[5,6] and theoretical distributions of p-p collisions at different energies according to the number of generated pions (W_n is the percentage of cases with the production of n pions).

Maenchen et al.[7] investigated interactions between negative pions and protons at 4.5 to 5 Bev and detected 61 2-prong events, 43 4-prong events and 2 6-prong events. The "isobaric" version of the statistical theory gives 64, 39, and 3 as the corresponding numbers, while the "nonisobaric" version gives 70, 35 and 1.

The momentum spectra in the center-of-mass system which are given in Ref. 7 are also in good agreement with the isobaric version (Figs. 1 and 2).

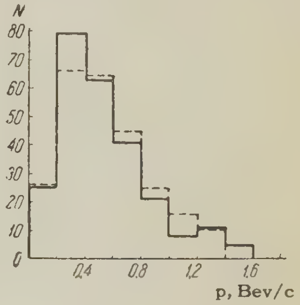

FIG. 1. Experimental[7] (solid line) and theoretical (dashed line) momentum spectra of secondary charged pions in the c. m. system from π^-–p collisions at 4.5 to 5 Bev.

$\bar{p}_{\text{exp}} = 0.54$ Bev/c; $\bar{p}_{\text{theor}} = 0.55$ Bev/c; $N_{\text{tot}} = 253$

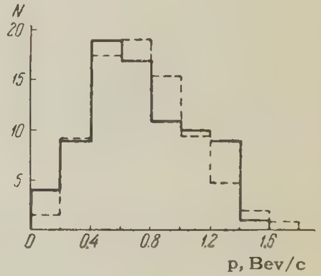

FIG. 2. Experimental[7] (solid line) and theoretical (dashed line) momentum spectra of secondary protons in the c. m. system from π^- – p collisions at 4.5 to 5 Bev.

$\bar{p}_{\text{exp}} = 0.74$ Bev/c; $\bar{p}_{\text{theor}} = 0.75$ Bev/c; $N_{\text{tot}} = 80$

We also calculated the distributions according to the number of secondary particles and the momentum spectra for nucleon-nucleon collisions at an average energy of 20 Bev, for comparison with experimental results[8] on nuclear interactions between cosmic-ray protons and Be, which in most cases can be regarded as nucleon-nucleon interactions. Unfortunately the experimental material does not permit a sufficiently reliable comparison of the experimental and theoretical secondary-particle distributions. However the momentum spectra for the experimentally observed multiplicities agree within statistical errors.

Our calculations confirm an earlier conclusion[2] (from an analysis of data on p-p, n-p and π-p collisions at energies different from those used here) that the Fermi theory including isobaric states gives a satisfactory description of multi-

Energy (lab. system), Bev	$W_1 : W_2 : W_3 : W_4$		
	Experimental	Theoretical (with isobaric states)	Theoretical (without isobaric states)
0.8 [5]	100 : 0 : 0 : 0	100 : 0 : 0 : 0	100 : 0 : 0 : 0
1.5 [5]	80 : 20 : 0 : 0	69 : 30 : 1 : 0	94 : 6 : 0 : 0
2.75 [5]	36 : 48 : 16 : 0	31 : 49 : 17 : 3	78 : 20 : 2 : 0
3.0 [6]	$(42^{+27}_{-25}) : (45^{+25}_{-29}) : (12^{+8}_{-5}) : (1^{+4}_{-0})$	25 : 46 : 25 : 4	68 : 31 : 1 : 0

plicities and momentum distributions of nucleon-nucleon and pion-nucleon collisions at a few Bev. The Fermi theory neglecting isobaric states gives poorer agreement with experiment. It must be noted, however, that angular distributions of particles in the given experiments do not agree with predictions from the Fermi theory.

In conclusion I wish to thank I. L. Rozental' and E. L. Feinberg for their interest in this work, and N. G. Birger and S. A. Slavatinskii for a discussion of the cosmic-ray data.

---

[1] E. Fermi, Progr. Theoret. Phys. 5, 570 (1950).

[2] Belen'kii, Maksimenko, Nikishov and Rozental', Usp. Mat. Nauk 62, 1 (1957).

[3] S. Z. Belen'kii and A. I. Nikishov, J. Exptl. Theoret. Phys. (U.S.S.R.) 28, 744 (1955), Soviet Phys. JETP 1, 593 (1955).

[4] V. M. Maksimenko and I. L. Rozental', J. Exptl. Theoret. Phys. (U.S.S.R.) 32, 658 (1957), Soviet Phys. 5, 546 (1957).

[5] W. B. Fowler et al., Phys. Rev. 103, 1489 (1956).

[6] Cester, Hoang and Kernan, Phys. Rev. 103, 1443 (1957).

[7] Maenchen, Fowler, Powell, and Wright, Phys. Rev. 108, 850 (1957).

[8] Birger, Grigorov, Guseva, Zhdanov, Slavatinskii and Stashkov, J. Exptl. Theoret. Phys. (U.S.S.R.) 31, 971 (1956), Soviet Phys. JETP 4, 872 (1957).

Translated by I. Emin
277

PARAMAGNETIC ABSORPTION IN PARALLEL FIELDS AT 9.3 × 10⁹ cps IN THE SALTS $Fe(NH_4)(SO_4)_2 \cdot 12H_2O$ *AND* $Fe(NO_3)_3 \cdot 9H_2O$

V. A. KUTUZOV

Kazan' State University

Submitted to JETP editor July 9, 1958

J. Exptl. Theoret. Phys. (U.S.S.R.) 35, 1304 (November, 1958)

FOR the case of paramagnetic absorption in parallel fields there exists a phenomenological theory due to Shaposhnikov.[1] Experimental curves obtained by Garif'ianov[2] and Sitnikov[3] support this theory. However, Smits et al.[4] have experimentally found a more complicated dependence of the absorption on the field at 10^6 to 10^7 cps and at 20°K. Kurushin[5] obtained similar curves for $Mn(NH_4)_2(SO_4)_2 \cdot 6H_2O$ and $Mn(NO_3)_2 \cdot 6H_2O$ at 9.3×10^9 cps and room temperature. In this note we report the results of measurements of the paramagnetic absorption in parallel fields in powdered salts $Fe(NH_4)(SO_4)_2 \cdot 12H_2O$ and $Fe(NO_3)_3 \cdot 9H_2O$ at 9.3×10^9 cps and 295°K. The measurements were made with a radiospectroscope consisting of a klystron generator connected by a waveguide to a reflecting rectangular resonator operating in the H_{01} mode.

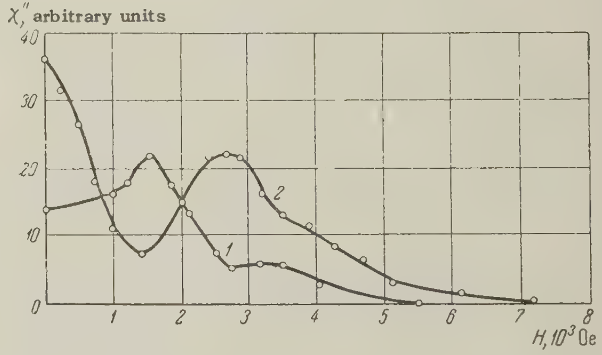

The absorption curves of $\chi''(H)$ have the following maxima: in the case of $Fe(NH_4)(SO_4)_2 \cdot 12H_2O$ (curve 1 in the figure) at a constant field of 1600 Oe, and in the case of $Fe(NO_3)_3 \cdot 9H_2O$ (curve 2) at a constant field of 2600 Oe. To explain this shape of these curves, it is apparently necessary to develop further the theory of spin-spin relaxation.

The investigation was suggested and directed by K. P. Sitnikov.

---

[1] I. G. Shaposhnikov, Doctoral Thesis, Physics Institute, Academy of Sciences, U.S.S.R., 1949.

[2] N. S. Garif'ianov, J. Exptl. Theoret. Phys. (U.S.S.R.) 25, 359 (1953).

[3] K. P. Sitnikov, Thesis, Kazan' State University, 1954.

[4] Smits, Derksen, Verstelle, and Gorter, Physica 22, 773 (1956).

[5] A. I. Kurushin, J. Exptl. Theoret. Phys. (U.S.S.R.) 32, 938 (1957), Soviet Phys. JETP 5, 766 (1957).

Translated by G. Volkoff
278

ON THE QUESTION OF ANTIGRAVITATION

Iu. A. ALEKSANDROV, V. N. ANDREEV, and
I. I. BONDARENKO

Submitted to JETP editor July 16, 1958

J. Exptl. Theoret. Phys. (U.S.S.R.) **35**, 1305-1306
(November, 1958)

IN connection with the discovery of heavy antiparticles (antiprotons and antineutrons) there have been several papers discussing the possibility that antiparticles have negative gravitational mass.[1,2,3] The attractiveness of such a hypothesis lies in the fact that it enables us to understand the absence of antiparticles in our stellar system and its vicinity,[4] since the gravitational repulsion of matter and antimatter would be a mechanism assuring their spatial separation.

It is of interest to discuss the degree of agreement between the hypothesis of antigravitation and present physical theories and experimental facts.

1. Experiments on the deflection of positrons and antiprotons in magnetic fields provide evidence that the inertial masses of antiparticles are positive (if we regard it as established by the fact of annihilation that the electric charge of the positron is positive and that of the antiproton is negative).

2. According to present ideas, physical phenomena in a set of antiparticles must go on in just the same way as in a set of ordinary particles (invariance of the laws of motion with respect to combined inversion). This leads to the result that the inertial masses of particles and antiparticles must be of the same sign, i.e., positive. In the opposite case, two antiparticles interacting gravitationally would fly apart (independently of the sign of the gravitational mass), in contrast with the behavior of ordinary particles. These same considerations require us to suppose that the gravitational masses of antiparticles are proportional in magnitude to their inertial masses, as is true for ordinary particles.

The considerations presented in these two points indicate that the inertial masses of antiparticles must be positive. If this is so, the hypothesis of negative gravitational mass for the antiparticles is in obvious contradiction with the general theory of relativity (the principle of equivalence).

3. Acceptance of the hypothesis of the negative gravitational mass of antiparticles also leads to a number of additional difficulties, connected with the existence of bosons (particles with integer spin). According to the present quantum theory there is for bosons no difference between particles and antiparticles. Remaining within the framework of this theory, we may suppose that all bosons have gravitational masses of the same sign. We then have two possibilities: either the gravitational masses of bosons are different from zero, or they are equal to zero. In the former case it is not hard to show that by using the phenomena of interconversion of bosons and fermions (creation and annihilation) in a gravitational field we can arrive at a violation of the law of conservation of energy. The second assumption contradicts the usual interpretation of the observations on the deflection of light in the gravitational field of the Sun, and the observations of the gravitational shifts of spectral lines in light coming from white dwarfs and other stars. The hypothesis that bosons are divided into particles and antiparticles with different signs of their gravitational masses does not agree with the observed angular distribution of the photons in three-photon annihilation of an electron and positron.

4. From what has been said it can be seen that acceptance of the hypothesis of negative gravitational mass of antiparticles would require radical changes in our present physical ideas. Owing to this, a direct experimental determination of the sign of the gravitational mass of antiparticles seems extremely desirable, despite the enormous difficulty of the experiments in question. One such experiment could be the observation of the "fall" of positrons in the gravitational field of the earth.

The writers are deeply grateful to Prof. D. I. Blokhintsev and F. L. Shapiro for helpful discussions.

---

[1] H. Bondi, Revs. Modern Phys. **29**, 423 (1957).

[2] F. A. Kaempffer, Canad. J. Phys. **36**, 151 (1958).

[3] G. Burbidge and F. Hoyle, Sci. Amer., April 1958, p. 34.

[4] G. Burbidge and F. Hoyle, Nuovo cimento **4**, 558 (1956).

Translated by W. H. Furry
279

RANGE OF NITROGEN AND BERYLLIUM IONS IN AIR

Iu. A. VOROB' EV

Moscow State University

Submitted to JETP editor July 26, 1958

J. Exptl. Theoret. Phys. (U.S.S.R.) **35**, 1306-1307 (November, 1958)

WE measured the range of nitrogen and beryllium ions in air in the velocity interval form 8×10^8 cm/sec to 11.5×10^8 cm/sec, using a cloud chamber filled with a mixture of air and water vapor under a pressure of 15 cm Hg before expansion. The N_{14}^{+3}, N_{14}^{+4}, N_{15}^{+3}, and Be_9^{+2} ions, accelerated by a 72 cm cyclotron, were bent by a focusing magnet and, after traversing a celluloid film 35 to 40 μg cm^{-2} thick, entered into the working volume of the cloud chamber. An electrostatic deflection scheme was used, activated by the governing system of the cloud chamber to ensure the entrance of the particles into the chamber at the exact instant of expansion.

The ion velocity was determined from laboratory data on the calibration of the focusing magnet, expressed in terms of the dependence of ME/Z^2 on I (M, E and Z are the mass, energy and charge of the ion, I is the current in the coils of the focusing magnet). The error in the velocity determination did not exceed ±3%.

Ions of molecular deuterium D_2^+ were accelerated in addition to nitrogen and beryllium. Comparison of the ranges of nitrogen and beryllium ions with the range of deuterons obtained from the decay of molecular deuterium ions allows the determination of the ranges of nitrogen and beryllium in air under normal pressure. The range of deuterons in air under normal pressure was determined from the range-energy relations in Segre's book.[1] The air equivalent of the film was taken to be 0.045 cm in agreement with the data on α particles.[2] The error in the determination of the range of nitrogen and beryllium ions does not exceed ±5% and is due, mainly, to straggling in the range of deuterons and of the ions under study. The measured values of the range in air of the N_{14}, N_{15}, and Be_9 ions are given in the table.

Ion	N_{14}				N_{15}	Be_9	
$v \times 10^{-8}$ cm/sec	8.2	9.0	10.2	11.4	8.1	8.2	8.9
R_{air}, cm	0.66	0.78	0.88	1.13	0.69	0.78	0.85

The results for N_{14}^{+3} and N_{14}^{+4} are in good agreement with the data of Reynolds and Zucker[3] on the range of N_{14} in the photoemulsion, if the emulsion stopping power is assumed to be the same for nitrogen ions and α particles of equal initial velocities.

An estimate of the ranges by the Knipp and Teller method for $\gamma = 1.15$ (γ is the ratio of electron to ion velocities at which capture and loss of a given electron have equal probabilities) shows that the range of Be_9 ions at $v = 8.5 \times 10^8$ cm/sec should be smaller by about 10% than the range of N_{14} ions with the same initial velocity.

The measured ranges of Be_9 ions at $v = 8.2$ and 8.9×10^8 cm/sec exceed the corresponding ranges for N_{14} ions by 12 to 15%. This discrepancy is apparently explained by a peculiarity in the electronic shell structure of the beryllium atom whose successive ionization potentials are 9.3, 18.1, 153 and 216 v (the corresponding values for nitrogen are 14.9, 29.4, 47.4, and 77.0 v). Due to the strong binding of the K electrons the beryllium ions will have an anomalously low effective charge through a considerable part of their range, which explains the increase in the range.

I wish to express my gratitude to the cyclotron crew consisting of Engineer-Physicist G. V. Kosheliaev and operators A. A. Danilov, V. P. Khlapov and M. S. Merkulov for their part in the completion of this work.

---

[1] E. Segre, editor, Experimental Nuclear Physics (Russ. Transl.), vol. 1, M. IIL, 1955.

[2] Barile, Webeler, and Allen, Phys. Rev. **96**, 673 (1954).

[3] H. L. Reynolds and A. Zucker, Phys. Rev. **96**, 393 (1954).

[4] J. Knipp and E. Teller, Phys. Rev. **59**, 659 (1941).

Translated by A. M. Bincer
280

HYPERFRAGMENTS FROM σ_K STARS

B. P. BANNIK and S. A. BUNIATOV

Joint Institute for Nuclear Research

Submitted to JETP editor July 26, 1958

J. Exptl. Theoret. Phys. (U.S.S.R.) 35, 1307-1308 (November, 1958)

IN the systematic scanning of a photoemulsion stack irradiated by K^- mesons (see reference 1) we found four cases of mesonic decay of hyperfragments in 619 σ_K stars, of which three could be identified. The necessary data on the tracks of the hyperfragments and particles emitted in their decay are given in the table.

Event 1. The hyperfragment comes from a star of the 2+ K^- type and decays "in flight" into two charged particles. The tracks of the hyperfragment and the secondary particles are coplanar. The decay kinematics and the measurements are in agreement with either of the decay schemes:

$$_\Lambda H^4 \rightarrow He^4 + \pi^- \quad (a), \quad _\Lambda H^3 \rightarrow He^3 + \pi^- \quad (b).$$

For either scheme we calculated the angle θ between tracks (F) and (2) from the angle between tracks (F) and (1) and from the range of (1), and compared it with the measured angle $\theta_{meas.} = 41.4° \pm 1.6°$. For scheme (a), $\theta = 38.4° \pm 4.8°$; for scheme (b), $\theta = 35.7° \pm 5.8°$. The time of flight of the hyperfragment, calculated from tables,[2] equals 2.1×10^{-11} sec for scheme (a) and 2.0×10^{-11} sec for scheme (b).

Event 2. The hyperfragment comes from a star of the 4+ 1K^- type and decays into a secondary three-pronged star with coplanar prongs. The analysis shows that the decay is according to the scheme $_\Lambda He^5 \rightarrow He^4 + p + \pi^-$. The binding energy of the Λ^0 particle is $B_\Lambda = (1.8 \pm 0.7)$ Mev.

Event 3. The hyperfragment comes from a star of the 5+ 0K^- type and decays into a two-pronged star. The presence of scattering at the end of the track indicates that the decay occurred after stopping. Detailed analysis allows determination of the decay scheme as $_\Lambda He^4 \rightarrow He^3 + \pi^- + n$. The binding energy is $B_\Lambda = (0.6 \pm 0.6)$ Mev.

In calculating the range of the particles we used the shrinkage factors determined according to reference 3: $K = 2.73 \pm 0.11$, 2.68 ± 0.11 and 2.31 ± 0.07 for events 1, 2 and 3 respectively. We used 7 protons from the decay $\Sigma^+ \rightarrow p + \pi^0$ for events 1 and 2 and 6 protons for event 3.

In calculating the particle energy and binding energy we used the range-energy relations of Barkas,[4] the decay energy of the Λ^0-particle from the work of Friedlander et al.,[5] and nuclear masses from reference 6.

Additional criteria exist for the identification of events corresponding to the nonmesonic decay of hyperfragments as follows: (1) In the formation of a Σ according to the reaction $K^- + N \rightarrow \Sigma + \pi + Q$ the energy release is $Q \simeq 100$ Mev. Hence if the energy release in a σ_K star is known to be larger than Q, the emission of a Σ is excluded (if one ignores the possibility of two-nucleon capture of the K^- meson). (2) The presence of a π meson in a σ_K star excludes the possibility of emission of another π meson, since reactions with emission of two π mesons have small probability. Taking into account these additional considerations, we found two hyperfragments undergoing nonmesonic decay among 427 σ_K stars.

The authors are grateful to Z. P. Golovin and G. S. Malyshkin for performing the measurements,

Event	Track	Range R, μ	ΔR	Range straggling, μ	β	$\Delta\beta$	φ	$\Delta\varphi$	Z	Final identification of the particle	Particle energy, in Mev (at the point of production)
1	F	757			+11.4		0			$_\Lambda H^4$ or $_\Lambda H^3$	30.1 or 27.6
	1	61			−0.9		194.7		$\leqslant 2$	He^4 or He^3	10.4 or 9.3
	2	>105			+36.6		143.4		1	π^-	62.6 or 49.4
2	F	26			−66.1		0			$_\Lambda He^5$	
	1	29	3.3	0.7	+55.8	4.5	145.1	1.2	$\leqslant 2$	He^4	6.45 ± 0.45
	2	3787	37	118	−24.5	1.2	275.2	0.7	−1	π^-	13.24 ± 0.24
	3	1184	26	16.7	−61.7	1.3	343.9	0.7		p	15.42 ± 0.23
3	F	181	1.8	7	+14	1	0			$_\Lambda H^4$	8.9 ± 0.4
	1	19	1.3	0.5	+14	7	270	2		He^3	4.36 ± 0.30
	2	14635	73	166	−23	1	90	0.7	−1	π^-	$29.0 + 0.2$

β) Inclination angle of the track to the emulsion plane in degrees. The angle is taken as positive for particles going towards the emulsion surface and as negative for particles going towards the glass. φ) Azimuth angle in degrees measured counterclockwise from the hyperfragment track. ΔR, $\Delta\beta$, $\Delta\varphi$) errors in the measurement of R, β, φ.

and thank the authors of reference 1 for making their material available.

---

[1] Buniatov, Vrublevskii, Kopylova, Korolevich, Petukhova, Sidorov, Skzhipchak, and Filipkovskii, J. Exptl. Theoret. Phys. (U.S.S.R.) **34**, 1028 (1958), Soviet Phys. JETP **7**, 711 (1958).

[2] Fay, Gottstein, and Hain, Nuovo cimento Suppl. **11**, 234 (1954).

[3] W. F. Fry and G. R. White, Phys. Rev. **90**, 207 (1953).

[4] W. H. Barkas, UCRL 3769 (1957).

[5] Friedlander, Keefe, Menon, and Merlin, Phil. Mag. **45**, 533 (1954).

[6] E. Segre, editor, Experimental Nuclear Physics (Russ. Transl.), vol. 1, M. 1955 [Wiley, N.Y., 1953].

Translated by A. M. Bincer
281

INVESTIGATION OF CONVERSION ELECTRON SPECTRA OF NEUTRON-DEFICIENT ISOTOPES OF LUTECIUM

V. M. KEL' MAN, R. Ia. METSKHVARISHVILI, B. K. PREOBRAZHENSKII, V. A. ROMANOV, and V. V. TUCHKEVICH

Leningrad Physico-Technical Institute, Academy of Sciences, U.S.S.R.

Submitted to JETP editor July 29, 1958

J. Exptl. Theoret. Phys. (U.S.S.R.) **35**, 1309-1310 (November, 1958)

THE study of the radiations from highly deformed nuclei provides material for further development of the collective model of the nucleus. The isotopes of lutecium are very interesting from this point of view. Recently a series of papers have appeared[1-4] concerning the neutron-deficient isotopes of Lu, but these data do not give a clear picture of the decay of these isotopes. Further investigations are necessary for this purpose.

We have studied the conversion spectrum of the isotopes of the lutecium fraction separated from a tantalum target irradiated with fast protons (660 Mev). The separation method was described earlier.[5] The measurements were made with a prism β spectrometer having an instrumental halfwidth of ~ 0.1% and with a double-focusing spectrometer with an instrumental halfwidth ~ 0.25 to 0.30%. The spectrum of conversion electrons contains a large number of lines belonging to Lu^{169} (half-life ~ 1.5 days), Lu^{170} (~ 2 days), Lu^{171} (~ 8 days), Lu^{172} (~ 6.7 days), and Lu^{173} (~200 days).[1,4,6] The assignment of the lines to the various isotopes was made on the basis of the half-life. Because of the small difference in lifetime, the separation of the lines of Lu^{169} and Lu^{170} is very difficult and was not completely achieved. It could be established from the measurements that the lines associated with Lu^{170} (84.19 kev, 193.3 kev) decay with a period of ~ 2 days. Lines having a lifetime less than that of the Lu^{170} lines were assigned to Lu^{169}. The comparatively small difference in the half-lives of Lu^{171} and Lu^{172} also prevented a unique assignment of transitions to one or the other of these two isotopes.

Table I gives the energies of γ transitions whose conversion lines decay with a period of ~ 1.5 or 2 days. Table II gives the energies of the γ transitions with period 6.7 to 8 days. The energy of the transitions was determined from the energy of the K and L conversion lines. The accuracy of the energy determination if ~ 0.1%. In those cases where only the K line or the L line was observed, the energy of the transition is given in parentheses.

TABLE I. Energies of γ transitions in the spectra of Lu^{169}, Lu^{170}

No.	Energy of γ transition in kev	No.	Energy of γ transition in kev	No.	Energy of γ transition in kev	No.	Energy of γ transition in kev
1	24.23	7	110.9	13	(286.5)	19	(543.8)
2	62.65	8	156.8	14	(290.9)	20	(755.1)
3	70.54	9	165.0	15	(369.2)	21	(937.7)
4	84.19	10	191.2	16	378.4	22	(1453)
5	87.30	11	193.3	17	(419.8)	23	(1481)
6	(91.83)	12	283.0	18	(457.2)		

Half-life for Nos. 1, 2, 5, 7, 8, 9, 10: < 2 days; for Nos: 4, 11:~ 2 days.

---

[1] Bobrov, Gromov, Dzhelepov, and Preobrazhenskii, Izv. Akad. Nauk SSSR, Ser. Fiz. **21**, 940 (1957) [Columbia Techn. Transl. **21**, 942 (1957)].

[2] Gromov, Dzhelepov, Dmitriev, and Preobrazhenskii, Izv. Akad. Nauk SSSR, Ser. Fiz. **21**, 1573

TABLE II. Energies of γ transitions in the spectra of Lu^{171}, Lu^{172}

No.	Energy of γ transition in kev	Identification, A	No.	Energy of γ transition in kev	Identification, A
1	(55.71)		25	(594.0)	
2	66.70	171	26	625.7	
3	72.33		27	629.6	172
4	75.85	171	28	666.9	(171)
5	78.70	172	29	(688.6)	
6	(85.55)		30	697.2	
7	90.55	172	31	712.2	171
8	91.30	171	32	739.1	171
9	112.7		33	766.7	
10	181.4	172	34	780.2	
11	203.3	172	35	809.2	172
12	269.9	172	36	838.9	171
13	279.8	172	37	(853.1)	
14	323.7	(172)	38	899.8	(172)
15	372.3		39	911.0	172
16	399.7	172	40	(927.6)	
17	410.1		41	(985.7)	
18	485.9	(171)	42	1002	172
19	490.1		43	(1020)	
20	(498.6)		44	(1071)	
21	(517.7)		45	1094	172
22	527.9	(172)	46	(1103)	
23	(535.6)		47	(1139)	
24	539.5	172			

(1957) [Columbia Techn. Transl. 21, 1562 (1957)].

[3] Gorodinskii, Murin, Pokrovskii, and Preobrazhenskii, Izv. Akad. Nauk SSSR Ser. Fiz. 21, 1004 (1957) [Columbia Techn. Transl. 21, 1005 (1957)].

[4] Mihelich, Harmatz, and Handley, Phys. Rev. 108, 989 (1957).

[5] Preobrazhenskii, Lilova, Dobronravova, and Teterin, Журн. неорг. хим. (J. of Inorg. Chem.) 1, 2294 (1956). Preobrazhenskii, Kaliamin, and Lilova, Журн. неорг. хим. (J. of Inorg. Chem.) 2, 1164 (1957).

[6] G. Wilkinson and H. G. Hicks, Phys. Rev. 81, 540 (1951).

Translated by M. Hamermesh
282

ON THE PENETRATING COMPONENT IN EXTENSIVE AIR SHOWERS

R. E. KAZAROV and R. B. LIUDVIGOV

Institute of Physics, Academy of Sciences, Georgian S.S.R.

Submitted to JETP editor July 31, 1958

J. Exptl. Theoret. Phys. (U.S.S.R.) 35, 1310-1311 (November, 1958)

In reference 1 Kazarov and Andronikashvili describe their experimental apparatus and the results obtained from their investigation of the energy spectrum of the penetrating component of extensive air showers. We give here certain additional data which, together with the results given in references 1 and 2, provide the basis for a number of conclusions.

We investigated the penetrating component at a depth of 127 m water equivalent (m.w.e.) using two detectors identical with that described in reference 1. One of the detectors was placed directly under the selecting system while the other, which had been placed at our disposal by M. F. Bibilashvili, was located 45 m from the first. The apparatus was directed in such a way that coincidences were registered between the master pulse and either of the detectors.

The data showed that out of 302 registered showers with a mean number of particles $\overline{N} = 2.85 \times 10^5$, there were 23 showers accompanied by triggering of the detector located at 45 m. We used these data to calculate the penetrating particle density ρ_μ from the formula given in reference 1. The result was $\rho_\mu = 0.077 \pm 0.018\ m^{-2}$. This density refers approximately to the distance 45 to 50 m from the shower axis. Calculations yielded only a small correction to the effective distance mainly because of the angular distribution of extensive shower axes.

In their investigation of the lateral distribution of the penetrating component at 61 m.w.e. for a shower with $\overline{N} = 3 \times 10^5$ Andronikashvili and

Bibilashvili[2] obtained $\rho_\mu = 0.77 \pm 0.027$ for the penetrating component density at 45.5 m from the shower axis.

A comparison of the densities in both cases enables us to determine the exponent γ of the penetrating component energy spectrum at ~46 m from the shower axis. Assuming that

$$\rho_\mu(>E) = A(E+1.5)^{-\gamma},$$

we obtain $\gamma = 1.15 \pm 0.41$. We note that in reference 1 for an effective distance of 28 m the energy spectrum exponent is $\gamma = 1.09 \pm 0.21$. This can serve as an indirect verification that the effective distance from the axis was obtained correctly in reference 1.

Our data also permit us to draw certain conclusions regarding the lateral distribution of the penetrating component at 127 m.w.e., at which depth we know the penetrating component density for two distances from the axis: $\rho_\mu = 0.20 \pm 0.02$ at $r = 27$ m and $\rho_\mu = 0.077 \pm 0.018$ at $r = 45$ m. Assuming that at this depth, as at 61 m.w.e.,[2] the lateral distribution obeys a law of the form $\rho_\mu(r) = a \exp[-\alpha r^2]$, we can use our data to determine the parameters a and α of this distribution. Our calculation gives $a = 0.34 \pm 0.01$ and $\alpha = 0.0074 \pm 0.00011$.

Our data give 30 ± 5 m as the half radius R of the muon distribution at 127 m.w.e. It is interesting that the data for 61 m.w.e. in reference 2 give R = 34 ± 3 m.

In conclusion we wish to thank Prof E. L. Andronikashvili and M. F. Bibilashvili for their interest and for their participation in a discussion of the results.

---

[1] G. E. Kazarov and E. L. Andronikashvili, J. Exptl. Theoret. Phys. (U.S.S.R.) **33**, 1528 (1957), Soviet Phys. JETP **6**, 1182 (1958).

[2] E. L. Andronikashvili and M. F. Bibilashvili, J. Exptl. Theoret. Phys. (U.S.S.R.) **32**, 403 (1957), Soviet Phys. JETP **5**, 341 (1957).

Translated by I. Emin
283

PECULIARITIES OF MAGNETIZATION OF THE DISORDERED Ni_3Mn *ALLOY AT LOW TEMPERATURES*

N. V. VOLKENSHTEIN, M. I. TURCHINSKAIA, and E. V. GALOSHINA

Institute of the Physics of Metals, Academy of Sciences, U.S.S.R.

Submitted to JETP editor, August 8, 1958

J. Exptl. Theoret. Phys. (U.S.S.R.) **35**, 1312-1313 (November, 1958)

IT is known[1] that, close to the stoichiometric composition Ni_3Mn, the Ni-Mn alloy become ordered with a sharp dependence of the physical properties on the degree of order in the arrangement of the atoms. Particularly remarkable is the appearance of strong ferromagnetism at the maximum degree of long range order. Thus, for example, the saturation magnetization I_s of the alloy exceeds the I_s of pure nickel by 50%.[2] According to the data of Kaya and Kussman,[1] Ni_3Mn in the disordered state is not ferromagnetic at room temperature. Our investigations show that it already becomes ferromagnetic at liquid nitrogen temperatures with $I_s = 1350$ Oe.

Determination of the Curie temperature was made from data of a precise measurement of the temperature dependence of the electrical resistivity. As is seen from Fig. 1 the Curie temperature Θ is equal to 110°K.

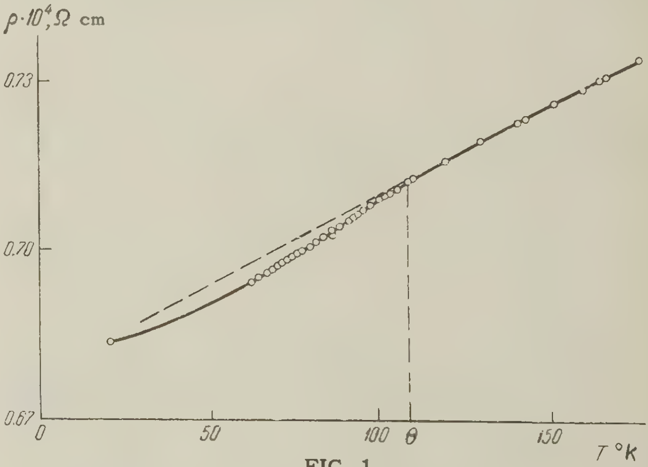

FIG. 1

A detailed examination of the magnetization curves at various temperatures down to that of liquid helium shows that the character of the magnetization has a series of peculiarities. First, the commutation magnetization curves 1a and 2a (Fig. 2), plotted at 20.4 and 4.2°K right after cooling the specimen from room temperature, run considerably below curves 1b and 2b, taken on a repeat magnetization after preliminary demagnetization by commutation from the maximum field to zero at the temperature of measurement, i.e., at 20.4

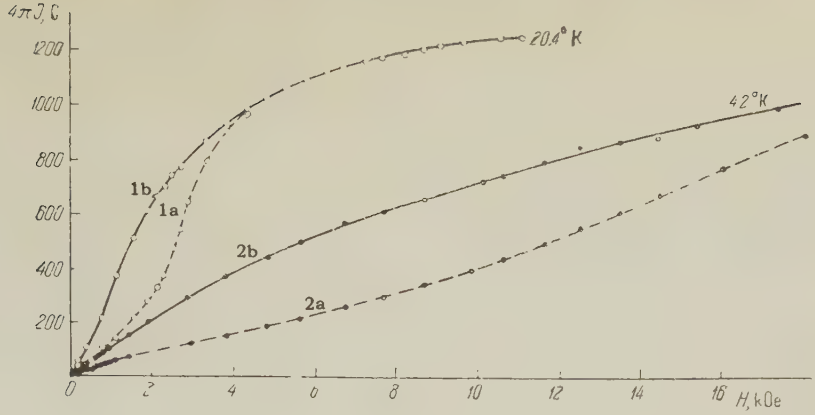

FIG. 2

and 4.2°K respectively. Such an unusual character of the curves can be explained by a large energy of magnetic anisotropy.

Repeated demagnetization and magnetization at the measurement temperature again leads to curves 1b and 2b. Secondly, the strong difference of the magnetization curves at 20.4°K from the magnetization curves at 4.2°K is remarkable. The latter run considerably below the former up to a field of 18,000 Oe and do not reach saturation there. Kouvel, Graham, and Becker[3] attribute the specific magnetic properties of these alloys to the occurrence of a ferrimagnetic structure. It seems to us that the data which they present is insufficient for such a judgement.

Measurements of the coercive force at 77.8 and 20.4°K have shown it to increase by one order of magnitude, from 140 Oe at 77.8°K to 1000 Oe at 20.4°K. Such a strong increase attests to the sharp temperature dependence of the magnetic anisotropy constant.

A final conclusion about the nature of the magnetic properties of the alloy Ni_3Mn in the disordered state can be made only after a precise determination of the magnetic anisotropy constant and after a neutron diffraction analysis to determine the character of the sublattices and to establish the antiferromagnetic interaction, if such exists.

---

[1] S. Kaya and A. Kussman, Z. Physik **72**, 293 (1931).

[2] A. P. Komar and N. V. Volkenshtein, Известия сектора физико-химического анализа ИОНХ АН СССР (Report of the section of physico-chemical analysis, Inst. Org. and Inorg. Chem. Acad. Sci. U.S.S.R.) **16**, 105 (1943).

[3] Kouvel, Graham, and Becker, J. Appl. Phys. **29**, 518 (1958).

Translated by R. Eisner
284

ALPHA DECAY OF ISOMERIC Bi^{210}

S. V. GOLENETSKII, L. I. RUSINOV, and Iu. I. FILIMONOV

Leningrad Physico-Technical Institute, Academy of Sciences, U.S.S.R.

Submitted to JETP editor July 31, 1958

J. Exptl. Theoret. Phys. (U.S.S.R.) **35**, 1313-1315 (November, 1958)

INVESTIGATIONS of the radioactivity of Bi^{210} have established that in addition to RaE ($T_{1/2}$ = 5 days, $E_{\beta\,max}$ = 1170 kev) there is a long-lived isomer of Bi^{210} which emits α particles with an energy of 4935 ± 20 kev and $T_{1/2} = 2.6 \times 10^6$ years.[1,2] In the present work we have investigated the decay of long-lived Bi^{210}.

The α-particle spectrum was studied using a pulse ionization chamber filled with a mixture of argon (90%) and CH_4 (10%) at atmospheric pressure.[3] The half-width of the line from the α particles of Pu^{239}, with energy 5150 kev, was 30 kev. We investigated an enriched and purified sample of Bi^{210} with a specific activity of 14000 α decays per min. per mg. The source area was 25 cm² and the thickness of the active layer was 10 microgram/cm².

The measured α spectrum of Bi^{210} is shown in Fig. 1. In addition to the previously observed α particles with energy 4935 ± 10 kev, we found new α-particle groups with energies of 4900 ± 10 and 4640 ± 30 kev. The relative intensities of these

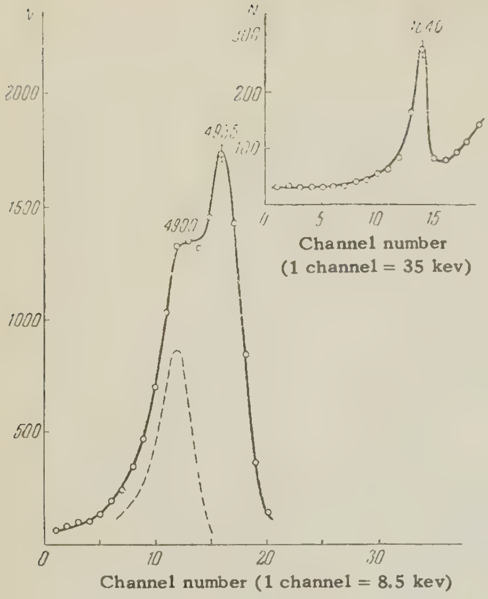

FIG. 1

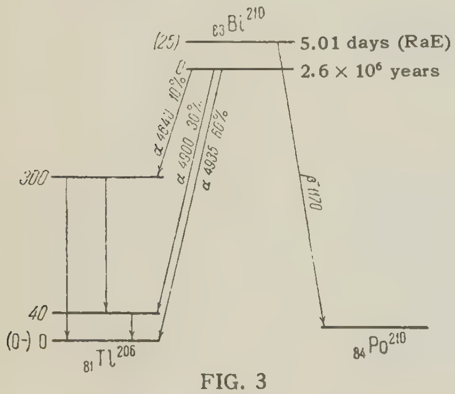

FIG. 3

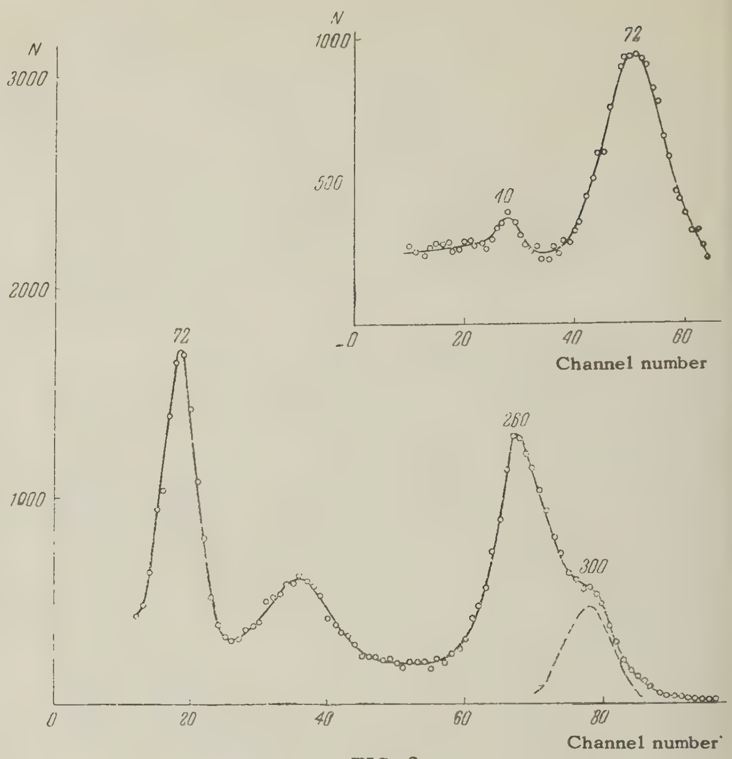

FIG. 2

three α transitions are 60, 30 and 10%, respectively.

We also found that about 10% of the α decays are accompanied by γ radiation. The γ rays were studied using a spectrometer consisting of a NaI (Tl) crystal, a FEU-13 photomultiplier and a single-channel pulse-height analyzer. The resolution of the spectrometer for the 660-kev line of Cs^{137} was 8.5%. The measured γ spectrum of Bi^{210} is shown in Fig. 2. Analysis of the curve shows the presence of γ transitions with energies of 260 ± 10 and 300 ± 10 kev, and relative intensities 1 and 0.4. The line at 72 ± 3 kev is due to the characteristic radiation of thallium. The identification of the small peak near 40 kev requires further investigation. It is possible that this maximum is due to a γ transition in Tl^{206}, which should be highly converted.

To confirm the assignment of the observed γ rays at 260 and 300 kev to transitions of the excited Tl^{206} nucleus, we studied α-γ coincidences. The α particles were detected in zinc sulphide and the γ rays in a NaI (Tl) crystal. The resolving time of the coincidence circuit was 5×10^{-8} sec. We established that the γ rays with $E_\gamma = 300$ kev and $E_\gamma = 260$ kev are in coincidence with the Bi^{210} α particles.

The results give grounds for assuming that there are excited states at 40 and 300 kev in Tl^{206}. The observed α and γ transitions can be explained on the basis of the decay scheme shown in Fig. 3.

The authors express their deep thanks to E. G. Grachev, N. B. Obel'skaia, V. K. Makhnovskaia, and L. Ia. Rudoi for radiochemical elimination of radioactive impurities from the source and for preparation of the samples.

---

[1] D. J. Hughes and H. Palevsky, Phys. Rev. **92**, 1206 (1953).

[2] H. B. Levy and I. Perlman, Phys. Rev. **94**, 152 (1954).

[3] Iu. I. Filimonov and G. A. Petrov, Izv. Akad. Nauk SSSR, Ser. Fiz. **20**, 1434 (1956) [Columbia Techn. Transl. **20**, 1311 (1956)].

Translated by M. Hamermesh

DECAY OF A PHOTON INTO TWO PHOTONS IN A HOMOGENEOUS MAGNETIC FIELD

V. G. SKOBOV

Leningrad Physical and Technological Institute, Academy of Sciences, U.S.S.R.

Submitted to JETP editor July 31, 1958

J. Exptl. Theoret. Phys. (U.S.S.R.) **35**, 1315-1317 (November, 1958)

It follows from Furry's theorem[1] that the decay of a photon into two photons in vacuum is impossible. For decay into a larger number of photons the statistical weight of the final state goes to zero (from the laws of conservation of energy and momentum it follows that the photons produced in the decay must have the same direction of motion as the original photon). Therefore an interesting question is that of the possibility of spontaneous decay of a photon in a homogeneous external field into two photons. Since such a field cannot be regarded as a perturbation, one must use the causal Green's function that takes account of its presence.

Schwinger has shown[2] that in the presence of a weak constant electromagnetic field the electron Green's function (in the system of units $h = c = 1$) is $G(x, x') = \Phi(x, x') S^c(x - x')$, where

$$S^c(x) = \frac{1}{(4\pi)^2}\int_0^\infty \frac{ds}{2s^2}\left\{m - \gamma_\alpha \frac{\partial}{\partial x_\alpha},\ 1 + \frac{ie}{2}\sigma_{ik}F_{ik}s\right\}$$

$$\times \exp\left(\frac{ix_\beta^2}{4s} - im^2 s - \varepsilon s\right), \tag{1}$$

$$\Phi(x, x') = \exp\left\{ie\int_{x'}^{x} dx''_\mu\left[A_\mu(x'') + \frac{1}{2}F_{\mu\nu}(x'' - x')_\nu\right]\right\},$$

where $\sigma_{ik} = (i/2)[\gamma_k, \gamma_i]$, $F_{ik} = \partial A_k/\partial x_i - \partial A_i/\partial x_k$ is the tensor of the external field, m is the mass of the electron, $\epsilon > 0$, γ_α are the Hermitian Dirac matrices, and $\{a, b\} = ab + ba$. The function (1) can be used under the condition $eF/m^2 \ll 1$, which is obviously always fufilled.

In the momentum representation the function (1) has the form

$$S^c(p) = \frac{1}{(2\pi)^4}\frac{m - \hat{p}}{m^2 + p^2 - i\varepsilon} + \Delta S(p), \tag{2}$$

$$\Delta S(p) = \frac{1}{(2\pi)^4}\left\{\frac{e}{4}\sigma_{ik}F_{ik},\ \frac{m - \hat{p}}{(m^2 + p^2 - i\varepsilon)^2}\right\}, \tag{3}$$

where $\hat{p} = i\gamma_\alpha p_\alpha$.

Furry's theorem will be valid also in the presence of a constant external field if under the transformation of charge conjugation

$$\gamma \rightarrow \gamma' = -\gamma^T, \text{ i.e., as } \gamma_{\alpha\beta} \rightarrow -\gamma_{\beta\alpha} \tag{4}$$

we get the relation $S^c(p) = S^{c'}(p) = S^{cT}(-p)$. It is easy to show that actually $\Delta S(p) \rightarrow \Delta S'(p) = -\Delta S^T(-p)$; that is, Furry's theorem does not apply, and we can consider the decay of a photon into two photons in a homogeneous magnetic field.

The corresponding element of the scattering matrix has the form

$$S_3 = \frac{e^3}{3!}\int d^4x_1 d^4x_2 d^4x_3 \operatorname{Sp}\hat{A}(x_1)G(x_2, x_1)$$

$$\times \hat{A}(x_2)G(x_3, x_2)\hat{A}(x_3)G(x_1, x_3), \tag{5}$$

$$A_\alpha(x_i) = (e_\alpha^{(i)}/\sqrt{2\omega_i})\exp(ik^{(i)}x_i),$$

where $A_\alpha(x_i)$ is the matrix element for the absorption or emission of the i-th photon with the four-momentum $k^{(i)}$ and the polarization vector $e^{(i)}$; ω_i is the frequency of the i-th photon.

The calculation of S_3 in the momentum representation leads to the expression

$$S_3 = \frac{\pi^2}{9}e^3\frac{\delta^4(k^{(1)} - k^{(2)} - k^{(3)})}{\sqrt{8\omega_1\omega_2\omega_3}}\frac{e}{m^2}$$

$$\times \mathbf{H}([\mathbf{k}_1\times\mathbf{e}_1] - [\mathbf{k}_2\times\mathbf{e}_2] - [\mathbf{k}_3\times\mathbf{e}_3]). \tag{6}$$

From this it is easy to calculate the total probability of decay of the photon in unit time:

$$W = \frac{5}{3(144\pi)^2}\left(\frac{e^2}{4\pi}\right)^3\left(\frac{e}{m^2}[\mathbf{H}\times\mathbf{k}_1]\right)^2\frac{1}{\omega_1}. \tag{7}$$

In relativistically covariant form and in ordinary units Eq. (7) has the form

$$W = \frac{5}{3(144\pi)^2}\alpha^3\left(\frac{\mu_0}{mc}F_{\mu\nu}k_\nu^{(1)}\right)^2\frac{1}{\omega_1}, \tag{8}$$

where μ_0 is the Bohr magneton and $\alpha = e^2/4\pi\hbar c$ is the fine structure constant.

The writer expresses his gratitude to L. E. Gurevich for suggesting the problem and for help with the work, and also to V. M. Shekhter for helpful comments.

---

[1] W. H. Furry, Phys. Rev. **51**, 125 (1937).

[2] J. Schwinger, Phys. Rev. 82, 664 (1951) (Russian translation in collection: Latest Developments in Quantum Electrodynamics, IIL 1954).

Translated by W. H. Furry
286

THE HARD γ RADIATION OF Ag^{110*}

L. V. GUSTOVA, L. P. TIMOFEEVA and O. V. CHUBINSKII

Leningrad State University

Submitted to JETP editor August 16, 1958

J. Exptl. Theoret. Phys. (U.S.S.R.) **35**, 1317-1318 (November, 1958)

DZHELEPOV and Iarytsina[1] have shown that in the β decay of Ag^{110*} ($T \sim 250$ days) γ rays with energies of 1.67 to 2.26 Mev are emitted, whose intensity is $\sim 8 \times 10^{-4}$ quanta per disintegration, if one assumes $h\nu = 1.8$ Mev. We undertook an investigation of the γ radiation of Ag^{110*} with energies greater than 1.6 Mev, using a gamma hodoscope. The method and the construction of the apparatus have been described earlier.[2,3]

The source was a neutron-activated silver powder sample (7.62 g) contained in a glass test tube. The measurements were done 4 to 9 months after the preparation of the source. The source activity at the start of the measurements was ~ 700 mCu.

The measurements were carried out at magnetic field intensities of $H = 700$, 730, 760, 810, and 865 oersteds. The data on energies and intensities of the observed γ lines, as well as the H values at which the lines are observed are given in the table. The figure shows the shape of the γ spectrum of Ag^{110*} for $H = 760$ oersteds, after subtracting the background. The resolution of the spectrum into components was done taking account of the dependence of the apparatus line shape on $h\nu$ and H. In resolving the spectrum we also took account of the contribution from bremsstrahlung (both internal and external) which is produced in the target because of the presence of a β transition with endpoint ~ 2.88 Mev. The computation of the experimental spectrum of the bremsstrahlung was made on the assumption that the hard β transition constitutes 3% of the total number of decays. In the region of 2.15 to 2.35 Mev, ($H = 865$ Oe), the bremsstrahlung contribution reaches ~ 25% of the observed effect.

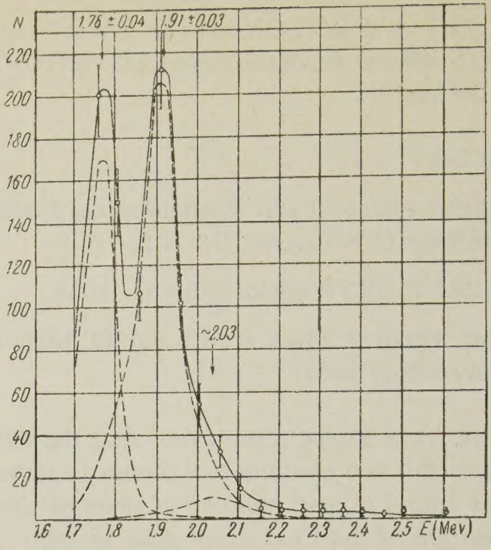

The errors in determining the relative intensities are due to inexact knowledge of the spectral sensitivity, statistical errors of the measurements, inaccuracy in resolving the spectrum into components, and in the case of the γ rays in the region 2.0 to 2.5 Mev to error in estimating the bremsstrahlung contribution. The portion of the spectrum in the region 2.05 to 2.30 Mev cannot be uniquely resolved into components because of the smallness of the effect and the relatively large statistical error of the measurements (~ ±50%). The results of one method of resolution are given in parentheses in the table.

Our measurements permit evaluation of the absolute intensity of the observed γ rays if one assumes in accordance with the data of Dzhelepov, Zhukovskii, and Kondakov[4] that the intensity of the 1.506 Mev line is 1.46×10^{-1} quanta per disintegration (cf. column 4 of the table). However this evaluation can only be done approximately, since the γ spectrum of Ag^{110*} has three close lines with energies 1.48, 1.506, and 1.56 Mev and relative in-

$h\nu$ (Mev)	H, at which the γ line is observed	Relative intensity $I/I_{1.91}$	I, quanta/disintegration	
			according to the decay scheme of Ref. 4, $I_{1.506} = 0.146$	from the efficiency of the gamma hodoscope
1.48—1.56	700	58700		
1.5—1.56	730	—		
1.76±0.04	700; 730; 760; 810	160±30	$6.0 \cdot 10^{-4}$	$5.9 \cdot 10^{-4}$
1.91±0.03	700; 730; 760; 810; 865	100	$3.7 \cdot 10^{-4}$	$3.6 \cdot 10^{-4}$
~2.03	760; 810; 865	6±3	$2.3 \cdot 10^{-5}$	$2.3 \cdot 10^{-5}$
(2.09) (2.22)	865 865	~2	$7 \cdot 10^{-6}$	$7 \cdot 10^{-6}$
2.46±0.05	810; 865	~0.85	$3.1 \cdot 10^{-6}$	$3.1 \cdot 10^{-6}$

tensities[4] of 6 : 15 : 1.3, which are not resolved in measurements with the gamma hodoscope.

The fifth column of the table contains rough values of the absolute intensities of the hard γ lines calculated starting from the known activity of the source, the coincidence counting rate for the individual lines and the efficiency of the gamma hodoscope. As one sees from the table, the intensity values obtained by the two different methods are in agreement.

Preliminary data on the results of the investigation of the hard γ radiation of Ag^{110*} were presented by us at the Seventh Annual Conference on Nuclear Spectroscopy in 1957.

The authors express their profound gratitude to V. A. Krutov for valuable advice and help in computing the bremsstrahlung spectrum of the Ag^{110*} radiation, and to N. D. Novosil'tseva for providing the source.

[1] B. S. Dzhelepov and I. A. Iarytsina, Izv. Akad. Nauk SSSR, Ser. Fiz. **20**, 343 (1956) [Columbia Techn. Transl. **20**, 314 (1956)].

[2] B. S. Dzhelepov, Izv. Akad. Nauk SSSR, Ser. Fiz. **21**, 1580 (1957) [Columbia Techn. Transl. **21**, 1569 (1957)].

[3] O. V. Chubinskii, Izv. Akad. Nauk SSSR, Ser. Fiz. **21**, 1583 (1957) [Columbia Techn. Transl. **21**, 1572 (1957)].

[4] Dzhelepov, Zhukovskii, and Kondakov, Izv. Akad. Nauk SSSR, Ser. Fiz. **21**, 973 (1957) [Columbia Techn. Transl. **21**, 975 (1957)].

Translated by M. Hamermesh
287

SOVIET PHYSICS JOURNALS

Published in English by the American Institute of Physics

Soviet Physics – JETP

A translation, beginning with the 1955 issues of the "Journal of Experimental and Theoretical Physics" of the Academy of Sciences of the USSR. The leading physics journal of the Soviet Union. Similar to "The Physical Review" in quality and range of topics. Outstanding new work is most likely to appear in this journal.

Twelve issues per year, approximately 4,000 Russian pages. Annually $75 domestic, $79 foreign. Libraries $35 domestic, $39 foreign. Back numbers, all issues, $8.*

Soviet Physics – Technical Physics

A translation, beginning with the 1956 issues of the "Journal of Technical Physics" of the Academy of Sciences of the USSR. The primary Russian vehicle for publications on semi-conductor and solid state work in general. Coverage similar to that of the A.I.P. "Journal of Applied Physics."

Twelve issues per year, approximately 3,000 Russian pages. Annually $75 domestic, $79 foreign. Libraries $35 domestic, $39 foreign. Back numbers, all issues, $8.*

Soviet Physics – Acoustics

A translation, beginning with the 1955 issues of the "Journal of Acoustics" of the Academy of Sciences of the USSR. Devoted principally to physical acoustics but includes electro, bio, and psycho acoustics. Mathematical and experimental work with emphasis on pure research.

Four issues per year, approximately 400 Russian pages. Annually $12 domestic, $14 foreign. (No library discounts) Back numbers, all issues, $4.

Soviet Physics – Doklady

A translation, beginning with the 1956 issues of the "Physics Sections" of the Proceedings of the Academy of Sciences of the USSR. An all-science journal offering four-page reports of recent research in physics and borderline subjects.

Six issues per year, approximately 1,500 Russian pages. Annually $35 domestic, $38 foreign. Libraries $15 domestic, $18 foreign. Back numbers for Vols. 1 and 2, $5 per issue; Vol. 3 and later issues, $7 per issue.*

Soviet Physics – Crystallography

A translation, beginning with the 1957 issues of the journal "Crystallography" of the Academy of Sciences of the USSR. Experimental and theoretical papers on crystal structure, lattice theory, diffraction studies, and other topics of interest to crystallographers, mineralogists, and metallurgists.

Six issues per year, approximately 1,000 Russian pages. Annually $25 domestic, $27 foreign. Libraries $10 domestic, $12 foreign. Back numbers, all issues, $5.*

Soviet Astronomy – AJ

A translation, beginning with the 1957 issues of the "Astronomical Journal" of the Academy of Sciences of the USSR. Covers various problems of interest to astronomers and astrophysicists, including solar activity, stellar studies, spectroscopic investigations of radio astronomy.

Six issues per year, approximately 1,100 Russian pages. Annually $25 domestic, $27 foreign. Libraries $10 domestic, $12 foreign. Back numbers, all issues, $5.*

**For libraries of non-profit degree-granting academic institutions.*

Please send orders and inquiries to

American Institute of Physics
335 East 45 Street, New York 17, N.Y.